Vol. 66 July, 1962 No. 7

THE JOURNAL OF PHYSICAL CHEMISTRY

(Registered in U. S. Patent Office)

CONTENTS

NOTES

COMMUNICATIONS TO THE EDITOR

THE JOURNAL OF PHYSICAL CHEMISTRY

(Registered in U. S. Patent Office)

Published monthly by the American Chemical Society at 20th and Northampton Sts., Easton, Pa. Second-class postage paid at Easton, Pa.

The *Journal of Physical Chemistry* is devoted to the publication of selected symposia in the broad field of physical chemistry and to other contributed papers.

Manuscripts originating in the British Isles, Europe, and Africa should be sent to F. C. Tompkins, The Faraday Society, 6 Gray's Inn Square, London W. C. 1, England.

Manuscripts originating elsewhere should be sent to W. Albert Noyes, Jr., Department of Chemistry, University of Rochester, Rochester 20, N. Y.

Correspondence regarding accepted copy, proofs, and reprints should be directed to Assistant Editor, Allen D. Bliss, ACS Office, Mack Printing Company, 20th and Northampton Sts., Easton, Pa.

Advertising Office: Reinhold Publishing Corporation, 430 Park Avenue, New York 22, N. Y.

Articles must be submitted in duplicate, typed, and double spaced. They should have at the beginning a brief Abstract, in no case exceeding 300 words. Original drawings should accompany the manuscript. Lettering at the sides of graphs (black on white or blue) may be pencilled in and will be typeset. Figures and tables should be held to a minimum consistent with adequate presentation of information. Photographs will not be printed on glossy paper except by special arrangement. All footnotes and references to the literature should be numbered consecutively and placed in the manuscript at the proper places. Initials of authors referred to in citations should be given. Nomenclature should conform to that used in *Chemical Abstracts*, mathematical characters be marked for italic, Greek letters carefully made or annotated, and subscripts and superscripts clearly shown. Articles should be written as briefly as possible consistent with clarity and should avoid historical background unnecessary for specialists.

Notes describe fragmentary or incomplete studies but do not otherwise differ fundamentally from articles and are subjected to the same editorial appraisal as are articles. In their preparation particular attention should be paid to brevity and conciseness. Material included in Notes must be definitive and may not be republished subsequently.

Communications to the Editor are designed to afford prompt preliminary publication of observations or discoveries whose value to science is so great that immediate publication is imperative. The appearance of related work from other laboratories is in itself not considered sufficient justification for the publication of a Communication, which must in addition meet special requirements of timeliness and significance. Their total length may in no case exceed 1000 words or their equivalent. They differ from Articles and Notes in that their subject matter may be republished.

Symposium papers should be sent in all cases to Secretaries of Divisions sponsoring the symposium, who will be responsible for their transmittal to the Editor. The Secretary of the Division by agreement with the Editor will specify a time after which symposium papers cannot be accepted. The Editor reserves the right to refuse to publish symposium articles, for valid scientific reasons. Each symposium paper may not exceed four printed pages (about sixteen double spaced typewritten pages) in length except by prior arrangement with the Editor.

Remittances and orders for subscriptions and for single copies, notices of changes of address and new professional connections, and claims for missing numbers should be sent to the Subscription Service Department, American Chemical Society, 1155 Sixteenth St., N. W., Washington 6, D. C. Changes of address for the *Journal of Physical Chemistry* must be received on or before the 30th of the preceding month. Please include an old address label with the notification.

Claims for missing numbers will not be allowed (1) if received more than sixty days from date of issue (because of delivery hazards, no claims can be honored from subscribers in Central Europe, Asia, or Pacific Islands other than Hawaii), (2) if loss was due to failure of notice of change of address to be received before the date specified in the preceding paragraph, or (3) if the reason for the claim is "missing from files."

Subscription rates (1962): members of American Chemical Society, $12.00 for 1 year; to non-members, $24.00 for 1 year. Postage to countries in the Pan-American Union $0.80; Canada, $0.40; all other countries, $1.20. Single copies, current volume, $2.50; foreign postage, $0.15; Canadian postage $0.10; Pan-American Union, $0.10. Back volumes (Vol. 56–65) $30.00 per volume; foreign postage, per volume $1.20, Canadian, $0.40; Pan-American Union, $0.80. Single copies: back issues, $3.00; for current year, $2.50; postage, single copies: foreign, $0.15; Canadian, $0.10; Pan-American Union, $0.10.

The American Chemical Society and the Editors of the *Journal of Physical Chemistry* assume no responsibility for the statements and opinions advanced by contributors to THIS JOURNAL.

The American Chemical Society also publishes *Journal of the American Chemical Society*, *Chemical Abstracts*, *Industrial and Engineering Chemistry*, International Edition of *Industrial and Engineering Chemistry*, *Chemical and Engineering News*, *Analytical Chemistry*, *Journal of Agricultural and Food Chemistry*, *Journal of Organic Chemistry*, *Journal of Chemical and Engineering Data*, *Chemical Reviews*, *Chemical Titles*, *Journal of Chemical Documentation*, *Journal of Medicinal and Pharmaceutical Chemistry*, *Inorganic Chemistry*, *Biochemistry*, and *CA — Biochemical Sections*. Rates on request.

THE JOURNAL OF PHYSICAL CHEMISTRY

(Registered in U. S. Patent Office) (© Copyright, 1962, by the American Chemical Society)

VOLUME 66 JULY 25, 1962 NUMBER 7

NON-SOAP GREASES. V. THE INFLUENCE OF *n*-HEPTYL DERIVATIVES ON SILICA–NON-POLAR LIQUID GEL STABILITY

BY JAMES P. WIGHTMAN[1] AND J. J. CHESSICK

William H. Chandler Chemistry Laboratory, Lehigh University, Bethlehem, Pennsylvania

Received April 5, 1961

At concentrations as low as 10–12 wt. % high area, polar silicas in non-polar liquids were found to form gels. Gel formation was a direct consequence of at least trace amounts of water which enhanced particle-to-particle interactions by "cementing" silica particles in a three-dimensional network structure. The influence of *n*-heptyl additives on the resulting gel structure was investigated; the additives included the acid, chloride, aldehyde, amine, and alcohol. Low concentrations (*ca.* 2 weight % of the amine and alcohol) were sufficient to fluidize the system. On the other hand, the aldehyde and acid influenced gel consistency only slightly. The chloride had no effect. Concentrations of these ineffective additives as high as 12 weight % were studied. Fundamental studies utilizing solution adsorption and heat of adsorption measurements were conducted in stringently dried systems. The results of these studies led to the development of a new mechanism to explain gel breakdown by additives. The mechanism is based on the ability of the additives to remove adsorbed water from positions between the flocculated particles. Excess additive then adsorbs onto the surfaces of the silica particles, thus preventing reflocculation when water is re-introduced into the system.

I. Introduction

Flocculation processes in multicomponent dispersions have only rarely been subjected to definitive experiment because of the complexities involved. Particle interaction theory development for such systems has suffered in proportion. Here, stability of silica–non-polar liquid gels (or dispersions) due to the presence of water or *n*-heptyl derivatives was followed by sedimentation volume and inverse yield value measurements. More fundamental measurements of the extent and energetics of additive adsorption from solution were carried out also. These combined data, complemented by a more basic knowledge of the structural characteristics of solids dispersed in pure or multicomponent organic liquids,[2] were used to develop a mechanistic picture to explain the stability characteristics of these systems.

II. Experimental

1. **Materials.**—Heptane was deolefinized using sulfuric acid prior to distillation over P_2O_5. The heptane still contained traces of water after careful distillation; this water content was determined by electrometric titration with the Karl Fischer reagent. The apparatus was carefully constructed to ensure non-contamination with atmospheric water. One ml. of the Karl Fischer reagent was equivalent to 6.32 ± 0.01 mg. of water as determined by both the wet[3] and dry[4] methods. The constancy of concentration of the reagent solution over a period of several days was taken as evidence for the maintenance of anhydrous conditions in the reagent buret.

The *n*-paraffin derivatives, heptyl chloride, heptylamine, heptyl alcohol, heptanoic acid, and heptaldehyde, C.P. decane, and paraffin oil were not distilled but kept over suitable drying agents until ready for use. Paraffin oil is a mixture of aliphatic hydrocarbons and had a molecular weight of 265 determined from the freezing point depression in benzene.[5] The refractive indices of all the liquids were measured with an Abbé refractometer. Temperature corrections were applied. The experimental value did not differ from the literature value by more than 0.5 % in any case.

The silica, Hi-Sil X303, was furnished by the Columbia-Southern Chemical Corporation. The surface area was determined from nitrogen adsorption measured at −195°. The water surface area was determined gravimetrically. The surface area and heat of immersional wetting measurements, studies of solution adsorption, as well as comprehensive company literature, were sufficient to characterize this solid as fully hydroxylated, weakly agglomerated, and homogeneous in surface characteristics in dispersions of organic liquids.

2. **Adsorption from Solution.**—A Zeiss portable laboratory interferometer was employed to determine concentra-

(1) The work reported here was used to fulfill requirements for the Ph.D. program of J. P. Wightman.

(2) J. J. Chessick, *NLGI Spokesman*, **23**, 315 (1959).

(3) J. Mitchell, Jr., and D. M. Smith, "Aquametry," Vol. 5, Interscience Publishers, New York, N. Y., 1958.

(4) J. D. Neuss, M. G. O'Brien, and H. A. Frediani, *Anal. Chem.*, **23**, 1332 (1955).

(5) D. M. Davis, M.S. Thesis, Lehigh University, 1959.

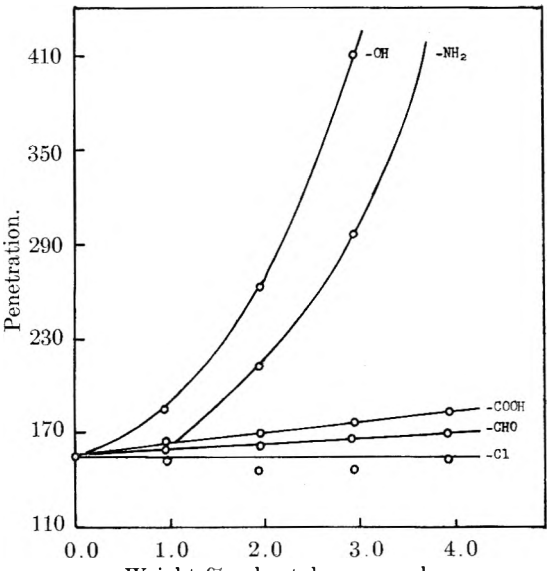

Fig. 1.—Influence of *n*-heptyl compounds on the consistency of a Hi-Sil X303–paraffin oil gel.

tion changes of solutions of the four heptyl compounds in paraffin oil due to adsorption onto Hi-Sil X303. The solutions were made up gravimetrically. The washed solid was evacuated for 12 hr. to an ultimate vacuum of 10^{-6} mm. for several hours without re-exposure to the atmosphere. In this manner, the water content of these systems is too small to influence solid–liquid interactions, a fact described fully in the text. The solutions were equilibrated with the solid for 24 hr. in a thermostated air-bath held at 26.0 ± 0.1°. The equilibrated solutions, prior to analysis, were centrifuged at 12,500 r.p.m. for 5 min. to remove the dispersed solids.

3. **Heats of Immersion.**—Heats of immersion at 26° of Hi-Sil X303 were measured in paraffin oil and in solutions of the four heptyl compounds in paraffin oil in the thermistor calorimeter previously described.[6] Trace amounts of water profoundly affected heats of immersion in those systems where the heats were less than the value for water. For solutions of the heptyl compounds in paraffin oil, a multi-bulb technique was developed to eliminate trace water; accordingly, heats of immersion were measured consecutively for a series of solid samples immersed in the same sample of wetting liquid. In order to minimize build-up of broken glass by the multi-bulb technique, wall thickness of the sample bulbs was held to a minimum. Care also was taken to avoid strains in the finished bulbs in order to minimize variations in the exothermic heat of breaking.[7]

4. **Sedimentation Volumes.**—The sedimentation volumes of Hi-Sil X303 were measured in decane and in a series of solutions of the heptyl compounds in decane. The solutions were made up gravimetrically. In one set of experiments, the solid was oven-dried and capped upon removal from the oven with self-sealing rubber caps. The liquids were introduced through the caps with a syringe. The water content of these systems is known to be intermediate between that present in large gel batches and in the liquids used for heats of immersion and solution adsorption. In another set of experiments, the solid was exposed to water vapor at several relative pressures and then capped. The liquids again were introduced by a syringe. After initial settling, the tubes were reshaken and allowed to stand prior to the measurement of final sediment heights. The volume percentage of Hi-Sil X303 used was 3.1 in all sedimentation studies.

5. **Penetrometer Measurements of Gels.**—Reproducible gels were prepared using Hi-Sil X303 (10 weight %) oven dried at 100° for 12 hr., and paraffin oil dried over P_2O_5. Pre-mixing was accomplished in a drybox containing P_2O_5 and flushed with dry nitrogen. Reproducible dispersions were prepared under atmospheric conditions on a specially designed, "floating" three-roll mill. Variables such as clearance, force on the rolls, and roll temperature could be adjusted. The introduction of water into the system during the ten passes on the mill adjusted to a pressure of 100 p.s.i. could not be avoided, however.

A precision penetrometer was employed to ensure dispersion reproducibility according to A.S.T.M. Standards, Part 5, pp. 119 ff., 1952. Essentially an inverse yield value was measured by the depth of penetration of a metallic cone into a given volume of gel. Penetrometer measurements also were employed on gels after addition of increasing amounts of heptyl additive. Gels of the same initial consistency as measured by the penetrometer were employed and the heptyl additive was milled into the system under the conditions described above except that the number of passes on the mill was reduced from ten to three.

A series of gels was prepared using paraffin oil thickened with a National Lead rutile gel (*ca.* 92 m.²/g.) and a Cabot Aerosil, now Cab-O-Sil, (*ca.* 130 m².g.). The influence of added *n*-heptyl derivatives on the consistency of these gels formulated with enough solid to yield the same initial penetration as the Hi-Sil–paraffin oil gels was investigated also.

III. Results

1. The Influence of Heptyl Additives on Gel Structure.—Changes in the consistencies of model gels (composed of *ca.* 10 weight % of silica dispersed in paraffin oil) on addition of heptyl compounds were followed using a precision penetrometer which essentially measured the inverse of the yield value of the system.[8] These data are plotted in Fig. 1. About 2 weight % of the alcohol and amine completely fluidized the gel; the systems now had rheological properties similar to the unloaded liquid itself. Only small changes in yield value were observed on addition of the acid and aldehyde even at concentrations up to 12 weight %. Dilution of the gel accounted for some degree of yield value decrease. The chloride had only a negligible influence over this same concentration range.

All the additives except the chloride caused structural breakdown of rutile (TiO_2)–paraffin oil gels.[9] The alcohol and amine also fluidized gels containing Aerosil (Cab-O-Sil), but much more additive was needed than for Hi-Sil-containing gels. The surface polarity of these solids decreases thus

rutile > Hi-Sil > Aerosil

according to adsorption and heat of wetting measurements and would appear to be an important parameter determining gel strength.

2. Adsorption from Solution.—Initially it was believed that the effect of these additives on gel structure was a *direct* consequence of strong adsorption of the compounds influential in structural breakdown. Adsorption studies were begun as a consequence. The net adsorption, ϕ_2,[10] of heptyl compounds from paraffin oil solutions onto Hi-Sil X303 as a function of the equilibrium mole fraction, X_2,

(6) A. C. Zettlemoyer, G. J. Young, J. J. Chessick, and F. H. Healey, *J. Phys. Chem.*, **57**, 649 (1953).

(7) C. M. Hollabaugh, Ph.D. Dissertation, Lehigh University, 1959.

(8) The use of a precision penetrometer might be criticized on the grounds that it has not been proved to be a quantitative instrument. The measured penetration value in arbitrary units can be converted to true yield values. Fortunately, precise yield values were not necessary here. Additive action was much of a "go"–"no go" process; an effective additive caused complete breakdown of gel structure yielding a system having rheological properties of the unloaded liquid itself. The others caused small changes in yield value.

(9) J. J. Chessick, A. C. Zettlemoyer, and G. J. Young, *J. Colloid Sci.*, **13**, 372 (1958).

(10) Subscripts 1 and 2 refer to vehicle and additive molecules, respectively.

is presented in Fig. 2. The term ϕ_2, in moles per gram of adsorbent, is the product of the number of moles of both liquids initially present and the change in mole fraction due to adsorption of the heptyl compound. This change is defined as the difference between the initial and the final equilibrium bulk mole fractions.

No adsorption of the chloride occurred from paraffin oil solutions onto Hi-Sil X303; unimolecular films of the acid, alcohol, and amine formed readily. Monolayer capacities for the adsorption of these compounds were calculated by three independent methods. Method I involved a simplification of the general equation of solution adsorption.[11] If exclusive adsorption of one component occurs, then at monolayer coverage $n_2^s = \phi_2/X_2$ where n_2^s is the monolayer capacity of the heptyl compound. Method II is the so-called graphical method of Nagy–Schay[11a] where monolayer capacities were obtained by extrapolation of the linear portions of the isotherms in Fig. 2 to $X_2 = 0$. Monolayer capacities by method III were estimated geometrically from a knowledge of the area of the adsorbate molecule and the number of adsorbent (silanol) sites capable of interacting with the adsorbate. The geometrical values were used to estimate the theoretical concentration change of the heptyl compound due to adsorption. Exclusive adsorption of the heptyl compound perpendicular to the surface (polar group down) was assumed. The calculations were made over a concentration range in excess of that required to give monolayer coverage. The fact that close agreement, within 10%, was obtained between the calculated and experimental values is offered as evidence for exclusive monolayer adsorption of the heptyl additives. It is significant also that once monolayers formed, the values for the amounts adsorbed could be used to predict accurately concentration changes on the introduction of a known amount of silica in solutions of much higher concentration.

The constancy of the heat of immersion values over a range of concentration in excess of that required to give monolayer coverage was taken as independent supporting evidence for the belief that only monolayer adsorption of the alcohol, amine, and acid occurred. If this were not the case, heats of immersion would be expected to vary continuously with concentration.

3. Calorimetric Heats.—Heats of adsorption, ΔH_a, listed in Table I were calculated from the equation

$$\Delta H_a = \Delta H_I - \Delta H_d - \Delta H_i \qquad (1)$$

where ΔH_I is the heat of immersion, ΔH_d the heat of dissolution of adsorbate molecules, and ΔH_i the enthalpy change for the formation of the adsorbate–solution interface. The application of eq. 1 assumes that mixed adsorption does not occur at monolayer coverage.[12] The heat values ΔH_I and ΔH_d were measured experimentally. Assuming monolayer coverage and orientation of the polar end of the heptyl compound toward the surface, the enthalpy of formation of the adsorbate–solution interface, ΔH_i, was estimated to be −78 ergs/cm.^{2}, which is the heat liberated when a solid covered with a monolayer of heptane is immersed in heptane at 25°.

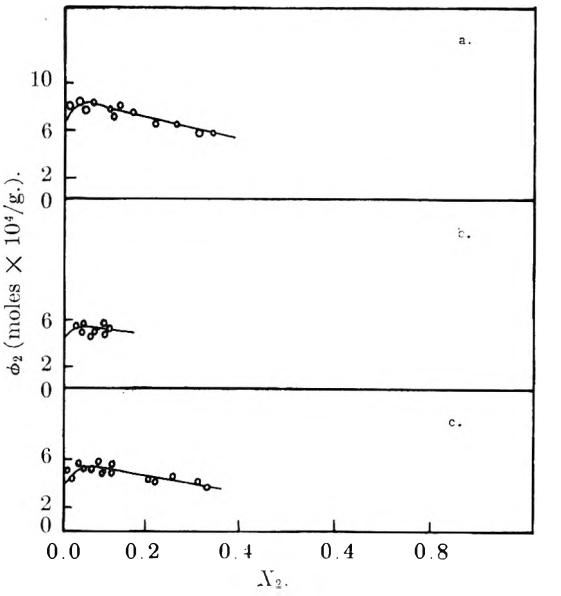

Fig. 2.—Net isotherms for the adsorption of *n*-heptyl compounds from paraffin oil solutions onto Hi-Sil X303 at 26°: a, *n*-heptyl alcohol; b, *n*-heptylamine; c, *n*-heptanoic acid.

TABLE I

HEATS OF ADSORPTION OF HEPTYL COMPOUNDS ADSORBED FROM PARAFFIN OIL SOLUTIONS ONTO Hi-Sil X303 AT 26° (MONOLAYER COVERAGE)

Liquid	$-\Delta H_I$, ergs/cm.^{2}	$-\Delta H_d$, ergs/cm.^{2}	$-\Delta H_i$, ergs/cm.^{2}	$-\Delta H_a$, ergs/cm.^{2}	$-\Delta H_a$, kcal./mole
n-Heptylamine	285	3	78	204	10.8
n-Heptyl alcohol	194	17	78	99	4.0
n-Heptanoic acid	145	2	78	65	3.6
n-Heptyl chloride	84	0	78	ca. 6	..

The immersion of Hi-Sil X303 in paraffin oil solution of the chloride gave the same heat as in paraffin oil itself; thus, the heat of adsorption of the chloride onto silica is approximately zero. The conclusion that negligible chloride adsorption occurred from solution thus is well substantiated by both heat and isotherm data.

The heat of adsorption of the alcohol was considerably less than that for the amine. The higher heat of adsorption for the amine presumably arose from the interaction of the amine with acid sites on the surface of Hi-Sil X303. In confirmation of this postulate, this solid was found to be an acidic silica with a pH of 4.5 when stirred in water. The difference between the heats of adsorption of the alcohol and acid was not significant. Further, both of these compounds were adsorbed to monolayer capacity in approximately the same concentration range.

4. Sedimentation Volumes.—Sedimentation volumes of Hi-Sil X303 in pure decane and in solutions of the heptyl compounds in decane are illustrated in Fig. 3. The sedimentation volumes

(11) Wo. Ostwald and R. de Izaguirre, *Kolloid-Z.*, **30**, 279 (1922).

(11a) L. G. Nagy and G. Schay, *Magyar Kemiai Folyoirat*, **66**, 31 (1960).

(12) J. J. Chessick and A. C. Zettlemoyer, *Advances in Catalysis*, **XI**, 263 (1959).

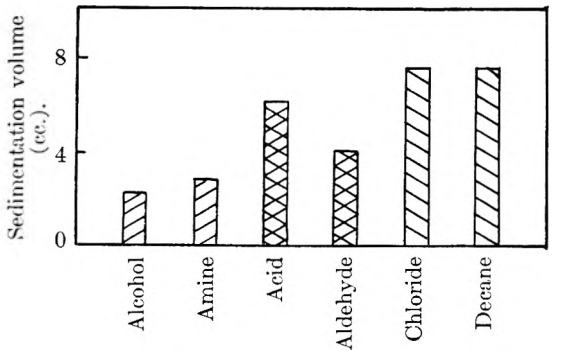

Fig. 3.—Sedimentation volumes of Hi-Sil X303 in decane solutions of *n*-heptyl compounds.

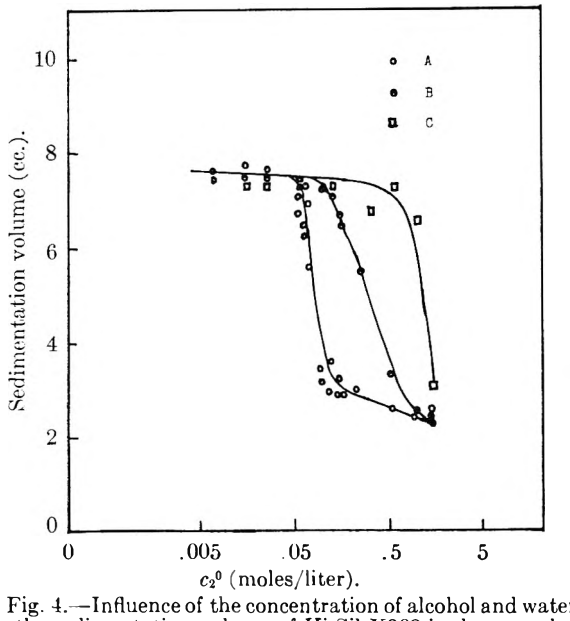

Fig. 4.—Influence of the concentration of alcohol and water on the sedimentation volume of Hi-Sil X303 in decane solutions of *n*-heptyl alcohol.

of the silica fell into three groups with significant differences between each group. The sedimentation volumes were smallest in solutions of the alcohol and the amine; the largest sedimentation volumes were found in the chloride solutions and in decane. Intermediate values were found in solutions of the acid and aldehyde.

The effect of the concentration of a heptyl compound on sedimentation volume is illustrated by curve A in Fig. 4 for the alcohol–decane–Hi-Sil X303 system. The silica was dried over P_2O_5 and was assigned a relative humidity of zero per cent. The sedimentation volume of the silica was constant and had a high value in solutions of low initial bulk alcohol concentrations. At approximately 0.05 *M*, the sedimentation volume dropped off sharply to a low value around 0.25 *M*. Thus sedimentation volume depended markedly upon alcohol concentration; a definite amount of alcohol was required for a given weight per cent solid to diminish particle–particle interaction significantly.

The marked influence of the presence of water on sedimentation volume is demonstrated by curves B and C in Fig. 4. Hi-Sil X303 was exposed to water vapor at 0.2 (curve B) and 0.9 (curve C) relative pressure, prior to the determination of sedimentation volumes. It is evident that the initial and final breaks in the sedimentation volumes are shifted to higher alcohol concentrations as the amount of preadsorbed water increases; greater amounts of alcohol are needed to diminish particle–particle interaction in systems which contained more water initially.

IV. Discussion

1. Gel Stability and Adsorption from Solution.—Gels, containing 10 to 12 weight % of a high area silica, dispersed in a non-polar liquid such as paraffin oil, form readily provided that water is present in the system. Coalescence of the adsorbed water films on adjacent particles occurs and a stable three-dimensional solid network results. Fractional monolayers of water on silica particles are effective also in gel-structure formation.[13] The gels used to study additive influence contained, as a minimum, sufficient water to form a monolayer on the surfaces of all silica particles in the dispersion.

That such adsorbed water is an attractive force in addition to and of greater magnitude than particle attractive forces of the van der Waals type in promoting flocculation is demonstrated easily. In water-free systems, a semblance of gel structure is observable but only at silica concentrations of 50 weight % or higher. Thixotropy, a characteristic of gels formulated at low silica concentrations in paraffin oil with water present (a vigorous shake of the bottled gel brought about rapid liquefaction) was not observed in water-free systems irrespective of the solid loadings employed. In addition, gels composed of small (10 to 12 wt. %) solids concentration exhibited excellent stability during storage and for periods of months also. This was demonstrated by measuring the loss of liquid from the system as a result of syneresis. Obviously, strong inter-particle bonds were produced by the "cementing" action of adsorbed water on particle surfaces; consequently redistribution of particles to achieve a more favorable junction point energy distribution did not occur to any significant extent. For this reason the kinetic aspects of these dispersions could be disregarded safely.

The "*a priori*" assumption that gel structure breakdown occurred as a result of preferential adsorption of the amine and alcohol onto the surfaces of silica particles had theoretical support. Koelmans and Overbeek[14] postulated earlier that small particles of *ca.* 0.01 μ diameter could be stabilized by just such a steric effect. The finding that monolayer adsorption of the amine, alcohol, and acid—the acid was the only additive of this group which did not fluidize the silica-based gels—occurred was initially startling. Furthermore, it was observed that monolayers formed in very nearly the same concentration range for all these components. The adsorption energies for the alcohol and acid were not much different either. The chloride was the only additive found not to

(13) G. J. Young and J. J. Chessick, *J. Colloid Sci.*, **13**, 358 (1958).
(14) H. Koelmans and J. Th. G. Overbeek, *Discussions Faraday Soc.*, **18**, 52 (1954).

adsorb onto the thickener surface; non-fluidization by this compound therefore is expected.

Parallelism between the results of sedimentation volume and penetrometer measurements provided the first clue needed to explain the divergency between these and the more fundamentally rigorous solution adsorption and heat of adsorption results. The presence of significant amounts of water in large gel samples prepared on the three-roll mill was proved easily. Knowledge that water was present in decane–silica systems used in sedimentation volume studies was obtained from Karl Fischer titration. Drying of the solid and liquid and use of a drybox during sedimentation studies were inadequate for the preparation of water-free systems. Simple addition of P_2O_5 to a silica–decane sediment which comprised the entire volume of the system revealed the presence of the flocculant, water, by causing an immediate collapse of structure. The sedimentation volume decreased as a result by approximately 60%.

On the other hand, extreme precautions were employed to maintain the water content of solution adsorption systems at a minimum. For example, the multi-bulb technique was employed to remove trace water when measuring heats of immersion of dry silica particles into paraffin oil or *n*-heptyl derivative–paraffin oil solutions. Liquids believed to be water-free after rigorous drying were proved not asceptic by this procedure since lower, constant heat values resulted. Adsorption and heat measurements were carried out for Hi-Sil X303 essentially dry systems.

2. **Proposed Mechanism for Structural Breakdown of Gels by Heptyl Additives.**—A mechanism to explain fluidization of silica–paraffin oil gels first must account for the removal of the flocculating agent, water, between particles comprising the network structure typical of such systems. Soluble water–alcohol or water–amine complexes apparently form first; thereafter, adsorption of the additive occurs, if sufficient additional amine or alcohol is added, to form a close-packed monolayer with the polar group oriented toward the surface.

The solubility of water in paraffinic compounds offers support to the view that such complexes can form in significant amounts with the amine and alcohol but not with the acid, aldehyde, or chloride. Mitchell and co-workers[3] listed these organic compounds in the following order of decreasing water solubility: amines > alcohols > acids > aldehydes >> chlorides. The same order of interaction of functional groups with water has been reported by Kakovsky[15] from a study of the influence of the functional group (or energy of its hydration) on the absolute value of solubility in water. Butler[16] also reported that the amine and alcohol groups have the highest energies of interaction with water.

The dependence of the sedimentation volumes on the amount of preadsorbed water shown in Fig. 4 supports the association mechanism; the greater the amount of water present in the gel the greater the amount of alcohol needed to effect deflocculation.

Some further results published earlier[9] corroborate or expand on the above mechanism. Gels containing Hi-Sil once fluidized by the alcohol or amine did not regain structure on subsequent addition of water up to 4 weight %. Evidently, sufficient additive was added initially to allow formation of a stable protective monolayer in addition to that needed to remove water from between adjacent, flocculated particles. Polar and non-polar attractive forces between adsorbed molecules and the silica surface as well as significant lateral interactions between molecules oriented polar group down contribute in part to films stable to replacement by added water.

Gels containing the less polar silica, Aerosil, were fluidized also by the amine and alcohol. Addition of more water, however, displaced the additive from the surface and gel structure reformed. Rutile–paraffin oil gels were fluidized not only by the amine and alcohol but also by the acid; all adsorbed films were stable to added water. Apparently, surface polarity of the solid which is least for Aerosil and greatest for rutile plays an important role in additive action. No comprehensive studies were carried out with Aerosil or rutile gels, however.

Acknowledgment.—This article is based on work performed under Air Force Contract, No. AF 33 (616)-7120, under the monitorship of Materials Central, Wright Air Development Division, Wright-Patterson Air Force Base, Ohio. Grateful appreciation for aid and encouragement are extended to Messrs. H. Schwenker and J. Christian of WADD. Prof. A. C. Zettlemoyer followed the course of this research carefully and was most generous with helpful comments and criticisms.

(15) I. A. Kakovsky, "Proc. 2nd Intern. Congr. of Surf. Act.," Vol. IV, Butterworth Scientific Publications, London, 1957, p. 310.

(16) J. A. V. Butler, "Chemical Thermodynamics," The Macmillan Co., London, 1946.

KINETICS OF HYDROGEN CHEMISORPTION ON NICKEL–MAGNESIA CATALYSTS

BY N. RAMASUBRAMANIAN* AND L. M. YEDDANAPALLI

Loyola College, Madras

Received August 29, 1961

The Elovich plots of the data obtained on the system hydrogen on nickel–magnesia show the occurrence of discontinuities. The two stages of adsorption are distinct and both the slow rates are determined only by the initial gas pressure. The rapid change in amount adsorbed, $\pm\Delta q$, occurring in gas addition or removal experiments is pressure sensitive and the presence of an initial chemisorbed state seems to be necessary to explain its occurrence.

Taylor and Thon[1] suggested that if α in the equation $dq/dt = ae^{-\alpha q}$ was characteristic of the nature of the sites involved in the adsorption process, then a break in the q *vs.* log $(t + t_0)$ plot indicated a changeover from one kind of site to another at a certain stage of the adsorption. The occurrence of discontinuities, or breaks, has been observed in quite a number of cases and is believed to be due to different types of adsorption sites. It is expected then that a study of the effect on the α values, of preadsorbed gas, and of changes in gas pressure brought about before the occurrence of the break, should provide information regarding the behavior of the different adsorption sites.

The effect of changes in the prevailing gas pressure on the slow rate of adsorption has been studied by Gundry and Tompkins[2] and Taylor, *et al.*,[3] on the system hydrogen on nickel. The latter, in particular, noted the occurrence of breaks in the q *vs.* log t plots but have confined their attention mostly to the first linear portion. Moreover, in experiments involving changes in ambient pressure there is observed a small rapid adsorption, or desorption, $\pm\Delta q$ and in order to understand the initial and ambient pressure effects more clearly, further work on this topic is considered to be necessary.[4] A preliminary study from this Laboratory of the effects of temperature and pressure on the adsorption of hydrogen on nickel–magnesia showed that breaks appeared in plotting the data. There seems to be no literature data, so far, dealing with hydrogen chemisorption kinetics on nickel–magnesia. Therefore, the system hydrogen on nickel–magnesia was chosen to carry out a systematic study of how the slow rates of adsorption are influenced by preadsorbed hydrogen and changes in the prevailing gas pressure. It is felt that such a study would add to the knowledge of the nature of the chemisorption sites and of $\pm\Delta q$, which is an experimental quantity of importance in understanding the mechanism of chemisorption.

Experimental

The rate of adsorption was followed in a constant volume system by measuring changes in pressure of hydrogen with time. The adsorbent was prepared by precipitating the mixed hydroxides from a solution of nickel nitrate (A.R. grade supplied by B.D.H.) and magnesium nitrate (Scheering Kahlbaum) in about 300 ml. of water, using 400 ml. of 1 *N* sodium hydroxide (E. Merck) solution, washing the precipitate over 2 days, drying at 100° for 12 hr., and finally reducing the dried hydroxides in a stream of pure hydrogen. A sample of the dried hydroxides was heated at 450 ± 5° and the resulting oxides were analyzed for nickel. Catalyst I: The precipitation was carried out from 10 g. of nickel nitrate and 50 g. of magnesium nitrate in solution and the dried hydroxides were reduced at 475 ± 10° for 24 hr. Catalyst II: 18 g. of nickel nitrate and 50 g. of magnesium nitrate were used and the dried hydroxides were reduced at 390 ± 5° for 60 hr.

The nickel contents of the catalysts obtained from the analysis of the oxides were 36.16 and 79.06%, respectively. Purified gases of hydrogen, oxygen, and nitrogen were used in the experiments. In between any two adsorption experiments the adsorbent was degassed for 8 hr. at 380 ± 5° by means of a cencomegavac pump coupled with a mercury diffusion pump. During an adsorption experiment the catalyst was kept at the desired temperature to within ±1° by an electrically heated furnace.

Results

The q *vs.* log t plots for a few typical runs carried out on catalyst II are shown in Fig. 1. Such runs will be referred to as the normal runs in which no interruptions by way of volume or pressure changes or preadsorbing hydrogen were made. It is evident from the linearity of the plots that t_0 or K is negligibly small. Consequently, the equation[5]

$$q_{nt} - q_{mt} = \frac{2.303}{\alpha} \log \frac{n}{m}$$

where n and m are integers and q_{nt} and q_{mt} correspond to amounts adsorbed at times nt and mt, respectively, was used to calculate α_1 and α_2, the α values of the two kinetic stages, respectively.

In Fig. 2 are presented the Elovich plots of the data obtained from a few experiments carried out on catalyst I to find out the effect of preadsorbed hydrogen on the slow rate of adsorption. The catalyst was exposed to hydrogen at 252° and 60 cm. and adsorption followed for 2 min. after which the gas phase was removed completely by pumping for 2 min. After waiting for a fixed period of time, during which there was no measurable desorption, a low pressure run was carried out at the same temperature of 252°. In Fig. 2 the plot for the normal low pressure run is included for the sake of comparison. The effect of preadsorbed undefined amounts of hydrogen is seen to be to decrease the total subsequent adsorption of hydrogen. The effect is more pronounced on the first kinetic stage than on the second as is evidenced by the α values. The second linear portion is almost parallel to that in the normal run and α_2 shows a slight increase, whereas there is a threefold increase

* Division of Applied Chemistry, National Research Council, Ottawa, Ontario.

(1) H. A. Taylor and N. Thon, *J. Am. Chem. Soc.*, **74**, 4169 (1952).

(2) P. M. Gundry and F. C. Tompkins, *Trans. Faraday Soc.*, **52**, 1609 (1956).

(3) L. Leibowitz, M. J. D. Low, and H. A. Taylor, *J. Phys. Chem.*, **62**, 471 (1958).

(4) M. J. D. Low, *Chem. Rev.*, **60**, 267 (1960).

(5) N. J. Sarmousakis and M. J. D. Low, *J. Chem. Phys.*, **25**, 178 (1956).

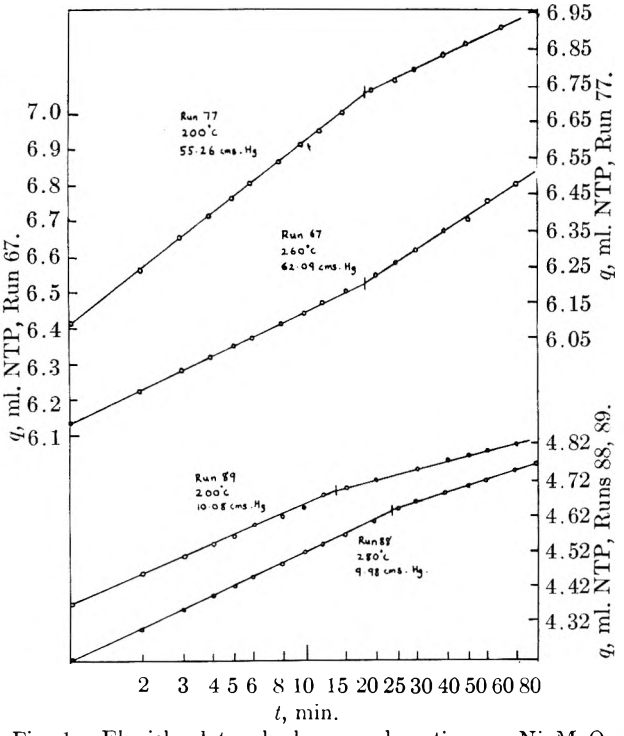

Fig. 1.—Elovich plots; hydrogen adsorption on Ni–MgO catalyst II.

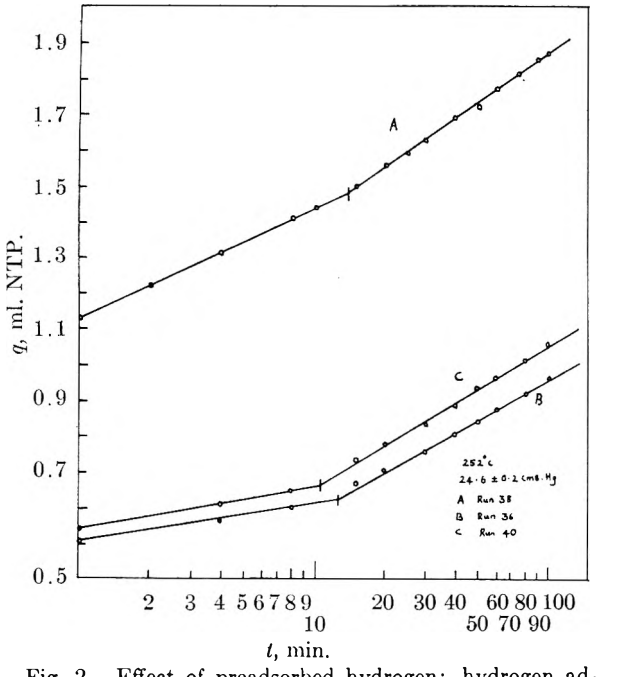

Fig. 2.—Effect of preadsorbed hydrogen; hydrogen adsorption on Ni–MgO catalyst I: A, normal run; B, preadsorbed hydrogen 1.786 ml. NTP, waiting period 2 min.; C, preadsorbed hydrogen 1.751 ml. NTP, waiting period 30 min.

in the α_1 values. It is interesting to note that the time of occurrence of the break remains almost unaffected and that the waiting period is without influence on the slow rates.

When the slow adsorption was in progress changes in the prevailing gas pressure were brought about by the addition or removal of a certain quantity of gas at a particular instant, keeping the volume of the adsorption system in the meanwhile constant. The results of the experiments carried out on catalysts I and II are given in Table I where α values for the normal runs also are included. In the table, t_c represents the time at which the pressure change was brought about, $\pm\Delta P$ the pressure change and $\pm\Delta q$ the rapid adsorption or desorption accompanying it. Taylor, *et al.*,[3] and Gundry and Tompkins[2] have reported in their work on hydrogen chemisorption on nickel that the slow rate of adsorption was unaffected by prevailing gas pressure changes. It is evident from Table I that not only is α_1 uninfluenced by pressure changes but also α_2, irrespective of the interruptions whether made before or after the break. Equally important is the quantity $\pm\Delta q$ and its dependence on pressure, temperature, and amount adsorbed. In the hydrogen–nickel work Taylor, *et al.*,[3] did not find any systematic variation of Δq, but the possibility of the small rapid adsorptions and desorptions being pressure sensitive was suggested.[4] This is found to be true in the present study. In the last column of Table I are listed the values of the ratios of ΔP to Δq and the constancy of the ratio is readily seen for gas addition or removal experiments, respectively. The initial pressure seems to have a marked influence on this ratio which is strikingly temperature independent. In the gas addition experiments where the initial pressure is around 20 cm. this ratio of ΔP to Δq is seen to be higher by a factor of more than two than in the gas removal experiments carried out at an initial pressure of 62 cm.

The data of a set of experiments on catalyst II are plotted in Fig. 3a. For a pressure change of 20 cm. and more, the amount rapidly desorbed is more than what was taken up slowly between the first minute and t_c. As a result of the gas removal, the time of occurrence of the break is shifted further and there is an interval of time Δt, only after which the interrupted runs become parallel to the normal one and during which the rate is slower. After the removal of the gas at the 12th minute, normally only 0.1 ml. should be taken up for the break to occur at the 20th minute; actually it is seen that 0.24 and 0.30 ml. are taken up and the break occurs at the 60th and 130th minutes, respectively. There is thus an indication of a slow desorption accompanying the rapid process. In all these respects, the case was similar at the other two temperatures. The plots C and E in the figure show that the rapid desorption is likely to be not characteristic of the kinetic stage and hence independent of the amount adsorbed. The phenomenon of rapid change in amount adsorbed, $\pm\Delta q$, seems to be important in understanding the mechanism of chemisorption and is discussed later.

In another type of experiment interruptions were made by cutting off a certain volume while the slow rate was in progress and reconnecting it after an interval of time. During this interval the rate could still be followed on the manometer. In such experiments the break occurred at the same time as in a normal uninterrupted run even though the buret's volume, which was more than two times the volume of the rest of the system, was cut off at

TABLE I

HYDROGEN CHEMISORPTION KINETICS ON Ni–MgO CATALYSTS; EFFECT OF PREVAILING GAS PRESSURE ON THE SLOW RATES OF ADSORPTION

Run no.	Temp., °C. $T \pm 1$	Init. press., cm.	t_c, min.	Δp, cm.	Δq, ml. NTP	α_1	α_2	$\frac{\Delta q \times 10^2}{\Delta p}$	
				Catalyst I, 36.16% Ni, 3.600 g., 21.30 M^2					
30	232	59.80	..	.....	.....	4.780	3.555	...	
31	232	59.80	10	−15.80	−0.050	...	3.555	0.316	0.279 ± 14%
34	252	60.00	..	.....	.....	3.649	2.830	...	
35	252	60.26	17	−14.40	− .035	...	2.830	0.243	
				Catalyst II, 79.06% Ni, 5.875 g., 770.2 M^2					
61	300	61.94	..	.....	.....	5.136	4.333	...	
62	300	61.90	12	−11.50	−0.213	5.333	4.473	1.852	
63	300	61.98	12	−20.00	− .434	5.333	4.473	2.170	
65	300	61.94	40	−19.60	− .460	...	4.473	2.347	
64	300	61.98	12	−28.20	− .657	5.333	...	2.330	
67	260	62.09	..	.....	.....	7.017	5.795	...	1.933 ± 11%
68	260	61.98	12	−12.05	− .203	7.017	6.060	1.685	
69	260	62.00	12	−20.40	− .435	7.017	6.060	2.132	
70	260	62.00	12	−29.15	− .655	7.017	...	2.247	
71	220	62.27	..	.....	.....	5.707	6.275	...	
72	220	62.00	12	−11.40	− .215	5.920	...	1.886	
73	220	62.20	12	−19.45	− .381	5.920	...	1.959	
117	260	20.71	..	.....	.....	5.555	4.444	...	
119	260	20.77	10	+2.900	+ .143	5.755	4.444	4.930	4.89 ± 3.5%
118	260	20.83	10	+6.200	+ .317	5.755	4.166	5.113	
120	260	20.77	10	+9.000	+ .417	5.755	4.166	4.634	

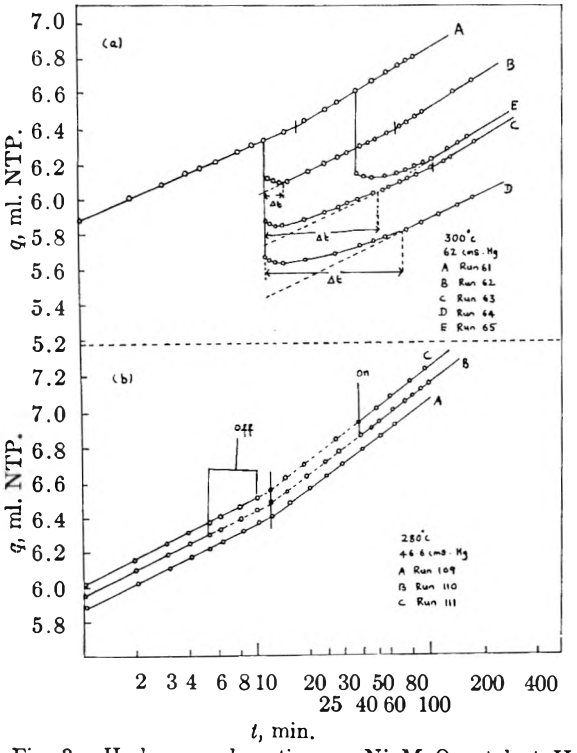

Fig. 3.—Hydrogen adsorption on Ni–MgO catalyst II: (a) effect of gas removal and (b) effect of cutting off the buret's volume.

an earlier stage and the rates of the slow adsorption remained unaffected. The Elovich plots are given in Fig. 3b.

Discussion

In the study of the effect of preadsorbed hydrogen, the observation that the two linear portions on the Elovich plot are affected to different extents shows the distinctness of the two stages of adsorption. In other words, the fact that only the first linear portion is affected means that the preadsorbed hydrogen was sufficient to cover a portion of the part of the catalyst surface that is characteristic only of the first stage adsorption. This is supported by the work of Taylor, *et al.*,[3] carried out for a different purpose on the system hydrogen on nickel–kieselguhr. An analysis of their data shows that the latter course of the adsorption is comparatively less affected than the initial part. The presence of different stages of adsorption in a system thus seems to be revealed by different linear portions on an Elovich plot and the break indicates a changeover from one kinetic stage to another.

That at a given temperature only the initial gas pressure determines the slow rate of adsorption already has been shown by Gundry and Tompkins[2] and Taylor, *et al.*[3] As the same conclusion is seen to be true for both the linear portions on the Elovich plots, it follows that the slow rates of adsorption are determined only by the initial pressure even though the adsorption stages are distinct. The observation that there is a rapid adsorption or desorption accompanying gas addition or removal is in agreement with those of the workers mentioned previously; it was reported[3] that no systematic variation of Δq with Δp was found and that no explanation of the phenomenon was available. In contrast, in the present study a definite proportionality of Δq to Δp is found in gas addition and removal experiments, respectively, and the ratio is dependent on initial pressure but independent of temperature. Furthermore, it is seen that in gas removal experiments the instantaneous desorption can be much more than what

was taken up slowly in that stage and it is not characteristic of the adsorption stage. These observations indicate every possibility of it taking place from the initial fast adsorption before onset of stage one, which is considered generally to be temperature independent and strictly proportional to initial pressure. Then the fact that for a 50% change in pressure the $-\Delta q$ forms only 10% of the amount rapidly adsorbed in the first minute points out that it is only a part of the initial fast adsorption that is likely to take part in rapid desorption. This would mean that occurrence of a weak, non-activated chemisorption, which is considered[6] to be a precursor of a strong chemisorption, appears to be an essential step. Then, to explain the effect of initial pressure on $\pm\Delta q$, one has to take into account the fraction of surface available for coverage or covered with atoms in the initial chemisorbed state.

(6) D. A. Dowden, "Chemisorption," *Proc. Symposium Keele*, 1956, Edited by W. E. Garner, Butterworths Scientific Publications, London, 1957, p. 3.

THE THERMAL DECOMPOSITION OF RUBIDIUM SUPEROXIDE[1]

BY D. L. KRAUS AND A. W. PETROCELLI

Department of Chemistry, University of Rhode Island, Kingston, R. I.

Received October 11, 1961

The thermal decomposition of rubidium superoxide has been studied in the temperature range of 280 to 360°. The studies were carried out in a Pyrex glass high vacuum system. A specially designed and constructed torsion balance for "*in situ*" vacuum weighings was employed to determine the change in composition of the decomposing superoxide. The results show conclusively that the oxide, Rb_2O_3, does not form in the course of the thermal decomposition of the superoxide, and that there is no solid solution formation between the decomposing superoxide and the peroxide product. The reaction path is, thus, established to be $RbO_2(s) = 1/2Rb_2O_3(s) + 1/2O_2(g)$. The thermodynamic properties, ΔH^0, ΔS^0, K_p, and ΔF^0 have been calculated for the above reaction. The thermal decomposition of the peroxide was studied in the temperature range of 300 to 360°. The thermodynamic properties, listed above, also have been determined for the reaction $Rb_2O_2(s) = Rb_2O(s) + 1/2O_2(g)$.

Introduction

The higher oxides of the alkali metals have been of interest to investigators since their discovery by Gay Lussac and Thenard[2] in 1810.

Of particular interest are the alkali metal superoxides. The lower molecular weight superoxides are receiving considerable attention for possible use for the revitalization of sealed breathing atmospheres. The need exists for an exact knowledge concerning the nature of the intermediate solid phases formed in the course of their thermal decomposition. In general it is known that at elevated temperatures these compounds release oxygen reversibly and form lower oxides. Many workers[3-5] have claimed that in addition to the expected peroxide, M_2O_2, and the simple oxide, M_2O, there also is formed a sesquioxide, M_2O_3. They propose that the superoxides decompose thermally in the following steps with the simultaneous liberation of oxygen

$$MO_2 \longrightarrow M_2O_3 \longrightarrow M_2O_2 \longrightarrow M_2O \qquad (1)$$

Strong evidence, however, has been uncovered supporting the view that, in the case of potassium at least, the oxide analyzing as K_2O_3 is in fact either a solid solution or a mixture of KO_2 and K_2O_2.[6-8]

(1) Based on work performed in partial fulfillment of the requirements of the Ph.D. degree of A. W. Petrocelli.

(2) J. L. Gay-Lussac and L. J. Thenard, *Recherches Physico-Chimiques*, **3**, 132 (1811).

(3) E. Rengard, *Ann. chim. phys.*, **11**, 348 (1907).

(4) R. de Forcand, *Compt. rend.*, **150**, 1399 (1910).

(5) M. Centerszwer and M. Blumenthal, *Bull. intern. acad. polon. sci. Classe sci. math. nat.*, **1933A**, 499 (1933).

(6) W. H. Schechter and J. Kleinberg, *J. Chem. Educ.*, **24**, 302 (1947).

(7) A. Klemm and H. Sodomann, *Z. anorg. allgem. Chem.*, **225**, 273 (1935).

(8) I. Kazarnovskii and S. I. Raikhshtein, *Russ. J. Phys. Chem.*, **21**, 245 (1947).

In accordance with this view the thermal decomposition would thus follow the path

$$KO_2 \longrightarrow K_2O_2 \longrightarrow K_2O \qquad (2)$$

The thermal decomposition processes of rubidium superoxide are not characterized so well as those of potassium superoxide. It is of interest to point out, however, that the same workers who argue against the existence of K_2O_3 concede the possibility that rubidium may form the sesquioxide. The picture is further complicated by the view of Brewer,[9] who states that potassium, rubidium, and cesium probably do not even form M_2O_2 solid phases.

The present investigation is concerned with the determination of the reaction path for the thermal decomposition of rubidium superoxide, and the calculation of the thermodynamic properties obtainable from such a study.

Experimental

The RbO_2 was prepared in this Laboratory by the direct oxidation of rubidium metal. The metal (99.30%) was supplied by the American Potash Company. The major impurity was cesium, 0.45%.

The metal must be handled with extreme caution because of its reactivity. In the liquid state it reacts explosively with air, and will ignite in the solid state on contact with air. It was shipped in a glass vial under argon gas. The label was scraped off the vial carefully, and the exterior of the vial washed with *n*-heptane. Then the vial was scratched with a file, broken rapidly into two halves, and submerged in *n*-heptane contained in a 1 l. beaker. The heptane was heated on a hot plate to above the melting point of the metal (38.5°) and the metal was poured out of the two vial halves. The metal was stored under heptane in the beaker, which in turn was kept in a desiccator charged with magnesium perchlorate.

Approximately 0.2–0.5 g. of metal, wet with the *n*-heptane, was transferred quickly from the beaker to a Pyrex

(9) L. Brewer, *Chem. Rev.*, **52**, 1 (1953).

reaction chamber. The reaction chamber was attached immediately to a vacuum line by means of a 24/40 standard tapered inner joint. The system was pumped down to 0.03 mm. The reaction chamber was heated to 150° with continuous pumping. Then pumping was halted and dry nitrogen was allowed to flow continuously over the sample. The flow rate was adjusted by means of the needle valve on the nitrogen tank regulator so as to maintain a positive pressure of 5 mm. over the samples.

The nitrogen was replaced very gradually by oxygen. Evidence collected in this work substantiated the observations of earlier workers[8] that with the use of more thoroughly dried oxygen the reaction is extremely slow. The rate of replacement of the nitrogen by the oxygen is governed by observations of the physical changes of the sample as described below. In two runs a too rapid addition of oxygen resulted in complete failure of the experiment. The rapid oxidation of the metal liberated enough heat to cause the formation of a molten mass of oxides and metal. The glass reaction chamber was attacked by the molten sample and became porous.

Some interesting physical changes were observed as the nitrogen was replaced gradually by the oxygen. The sample lost its metallic appearance and turned into a yellowish solid. Upon increasing the temperature to around 200° the sample changed to a molten black mass. This was swirled as the rate of flow of oxygen was increased slightly. Within 2 min. the sample became a solid black mass. At this point it was safe to cut off the nitrogen flow completely. The oxygen flow rate was adjusted so as to keep a slight positive pressure over the sample, and the temperature increased to 330°. After 72 hr. the color had become orange. Initially the reaction was thought to be complete at this point. However, analysis showed that the samples tested at the end of the above treatment contained, on the average, only 60% rubidium superoxide. It was thought that the incompleteness of the oxidation was caused by the slow rate of the reaction due to the small surface area of the sample. Accordingly, the sample was placed in a drybox and ground to a powder. Then the treatment with oxygen at 350° was resumed for an additional 36–48 hr. Analysis showed that the sample now contained 99.1% rubidium superoxide.

Rubidium superoxide is quite stable in dry air but is extremely hygroscopic. Presumably it reacts with water vapor in a manner analogous to potassium superoxide,[10] *i.e.*

$$2RbO_2 + aq = Rb_2O_2 \cdot aq + O_2 \qquad (3)$$

Thus, it is essential that all operations involving the handling of the superoxide be carried on in a drybox.

Upon heating to temperatures between 180 and 200° the rubidium superoxide changed from a yellow to an orange color. The color change is reversible and may be an indication of a phase change. Similar high temperature color changes have been observed with sodium superoxide[11] and with potassium superoxide.[12]

The vacuum system used in these studies, excepting the rubber tube connection between the oil diffusion pump and the fore pump, was constructed of Pyrex glass. The system could be pumped down to 10^{-4} mm. pressure. The leakage rate for the entire system was found to average 4 $\times$ 10^{-4} mm. per hr. Pressure readings were made with calibrated McLeod gages and a mercury manometer.

Changes in weight of the sample were followed using a specially designed torsion balance which has been described in detail elsewhere.[13] A Brown electric pyrometer was used for indicating and maintaining constant temperatures to ±3°.

Results

The Thermal Decomposition of Rubidium Superoxide.—The results of the thermal decomposition of RbO_2 are shown in Table I. Runs 1–6 were made using a sample with an original weight of 0.3419 g. Runs 7 and 8 were made with a second sample with an original weight of 0.4045 g. The sample composition was altered by pumping at 300°. Equilibrium was attained in 5–7 hr.

TABLE I

RESULTS OF THE THERMAL DECOMPOSITION OF RUBIDIUM SUPEROXIDE IN THE TEMPERATURE RANGE 280 TO 360°

Run no.	Temp., ° C. 280	320	320	340	360	Total wt. loss, mg.	Empirical formula
	Pressures, mm.						
7	0.11	0.21	0.36	0.58	0.85	4.5	$Rb_2O_{3.84}$
1	..	.20	.38	.67	1.03	10.5	$Rb_2O_{3.64}$
2	..	.20	.34	.58	0.95	12	$Rb_2O_{3.48}$
3	..	.18	.37	.49	.72	15	$Rb_2O_{3.34}$
4	..	.16	.35	.54	.87	21	$Rb_2O_{3.08}$
5	..	.20	.36	.56	.86	30	$Rb_2O_{2.70}$
8	.10	.19	.35	.53	.87	40	$Rb_2O_{2.56}$
6	..	.19	.37	.56	.88	38	$Rb_2O_{2.34}$

It is to be noted that in runs 1–3 the pressures varied more at the higher temperatures than in the later runs. The probable reason for this is that in runs 4–8 improved techniques were used in reading the pressure and temperature. The data of runs 1–3 were used, nevertheless, in computing the mean pressures for each temperature.

In Table II the mean pressure with its probable error is shown for each temperature.

TABLE II

COMPARISON OF THE EXPERIMENTALLY DETERMINED PRESSURE VALUES WITH THE PRESSURE VALUES CALCULATED USING THE RELATIONSHIP

$$\log P_{mm.} = (-4062.6/T) + 6.374$$

T, ° C.	P, mm., expt.	P, calcd.
280	0.11 ± 0.01	0.11
300	.19 ± .01	.19
320	.36 ± .01	.34
340	.56 ± .02	.56
360	.88 ± .04	.91

As can be seen, at a given temperature the dissociation pressure remains constant within experimental error over the entire composition range studied. Pressures did not begin to drop off until compositions corresponding to the peroxide were reached. This behavior is characteristic of a two-component, three-phase system. It is, therefore, univariant. The data establish quite clearly that Rb_2O_3 is not formed in the course of the thermal decomposition of RbO_2. The data in Table I may be represented by an equation of the form $\log P_{mm} = AT^{-1} + B$. The constants A and B were found from a least squares treatment of the data to have values of 4062.6 and 6.374, respectively. The comparison of the experimentally determined pressure values with those obtained from the relationship $\log P_{mm} = (-4062.6/T) + 6.374$ is given in Table II.

The thermodynamic properties obtainable from this treatment for the reaction $RbO_2(s) = {}^1/_2\ Rb_2O_2(s) + {}^1/_2\ O_2(g)$ are summarized in Table III.

The Thermal Decomposition of Rubidium Peroxide.—As was pointed out above, the decomposition pressure of RbO_2 at a given temperature remained constant until the composition of the

(10) C. A. Kraus and E. F. Parmenter, *J. Am. Chem. Soc.*, **56**, 2384 (1934).

(11) G. Carter and D. H. Templeton, *ibid.*, **75**, 5247 (1953).

(12) G. F. Carter, J. L. Margrave, and D. H. Templeton, *Acta Cryst.*, **5**, 851 (1952).

(13) D. L. Kraus, A. W. Petrocelli, and J. C. Price, *Anal. Chem.*, **33**, 479 (1961).

TABLE III

SUMMARY OF THE THERMODYNAMIC PROPERTIES DETERMINED FOR THE REACTION $RbO_2(s) = 1/2\ Rb_2O_2(s) + 1/2\ O_2(g)$

Thermodynamic property	Value of the thermodynamic property calcd. for the av. temp. of 320°
ΔH^0, kcal.	9.30
ΔS^0, cal./deg.	7.99
$K_p = P_{O_2}^{1/2}$	2.10×10^{-2}
ΔF^0, kcal.	4.55

solid phase reached Rb_2O_2. At this composition a sudden drop in pressure occurred. This new and lower pressure corresponds to the dissociation pressure of rubidium peroxide. The equilibrium pressure over the peroxide was measured at 300, 320, 340, and 360°. The measurements were made at two different compositions, $Rb_2O_{2.00}$ and $Rb_2O_{1.77}$.

TABLE IV

RESULTS OF THE THERMAL DECOMPOSITION OF RUBIDIUM PEROXIDE

Run	Sample compn.	Temp., °C. 300	320	340	360
		Pressures, mm.			
1	Rb_2O_2	0.040	0.060	0.074	0.129
2	Rb_2O_2	.042	.061	.078	.124
3	Rb_2O_2	.037	.058	.080	.128
4	$Rb_2O_{1.77}$	.038	.065	.074	.131

The thermodynamic treatment of the data is analogous to the treatment employed for the thermal decomposition of the superoxide. In Table V is given the comparison between the experimentally determined equilibrium pressures and those calculated from the relationship: $\log P_{mm} = (-2991.8/T) + 3.8118$.

The thermodynamic properties obtained for the reaction $Rb_2O_2(s) = Rb_2O(s) + {}^1/_2\ O_2(g)$ are summarized in Table VI.

TABLE V

COMPARISON BETWEEN THE EXPERIMENTALLY DETERMINED EQUILIBRIUM PRESSURE FOR THE REACTION $Rb_2O_2(s) = Rb_2O(s) + 1/2\ O_2(g)$ AND THE PRESSURE VALUES CALCULATED USING THE RELATIONSHIP

$$\log P_{mm.} = (-2991.8/T) + 3.8118$$

T, °C.	P, mm. expt.	P, mm. calcd.
300	0.039 ± 0.002	0.039
320	.061 ± .002	.059
340	.078 ± .002	.085
360	.128 ± .002	.123

TABLE VI

SUMMARY OF THE TERMODYNAMIC PROPERTIES DETERMINED FOR THE REACTION $Rb_2O_2(s) = Rb_2O(s) + 1/2\ O_2(g)$

Thermodynamic property	Value of the thermodynamic property calcd. for the av. temp. of 330°
ΔH^0, kcal.	6.85
ΔS^0, cal./degree	2.13
$K_p = P_{O_2}^{1/2}$	8.78×10^{-3}
ΔF^0, kcal.	5.58

Discussion of the Results

The results of this investigation demonstrate that during the gradual thermal decomposition of rubidium superoxide the oxide, Rb_2O_3, does not form. Nor is there any evidence of solid solution formation between the solid oxide phases present in the reaction system. It appears, therefore, that the thermal decomposition of RbO_2 is analogous to that reported for KO_2 by Kazamovskii and Raikhshtein and follows the reaction path

$$RbO_2(s) = 1/2\ Rb_2O_2(s) + 1/2\ O_2(g)$$
$$Rb_2O_2(s) = Rb_2O(s) + 1/2\ O_2(g)$$

Acknowledgments.—The authors are indebted to the American Potash Company for supplying the pure rubidium metal used in this work.

STUDIES OF THE TRANSPORT PROPERTIES OF THE SYSTEM THALLOUS SULFATE–WATER. II. SEDIMENTATION COEFFICIENTS AT 25°; A TEST OF THE "SVEDBERG EQUATION" AT FINITE CONCENTRATION[1]

BY J. M. CREETH[2]

Department of Chemistry of the University of Wisconsin, Madison 6, Wis.

Received October 11, 1961

With the purpose of testing the extended form of the Svedberg molecular weight equation: $M = RTs(1 + \mathrm{d} \ln y/\mathrm{d} \ln c)/D(1 - \bar{v}\rho)$, measurements have been made of the sedimentation coefficient of the solute in the strictly two-component system Tl_2SO_4–H_2O over the concentration range 0.8–5.0 g. dl.$^{-1}$. The Gutfreund–Ogston method was used, in a form appropriate to the Rayleigh interference optical system. It was found necessary to extend the expression relating the refractive index changes in the cell to the sedimentation coefficient to take into account the non-linearity of the relation between refractive index and concentration, and also the effects of pressure. The sources of error in the experimental procedure have been examined, and ways of minimizing the errors are demonstrated. The sedimentation coefficients obtained range between 1.0 and 1.2 S., with a positive dependence upon concentration. It is shown from previously obtained diffusion and activity coefficient data that the observed behavior agrees with that expected, the concentration-dependence being due to incomplete dissociation of the electrolyte. The significance of the findings is examined; it is concluded that a macroscopic mobility exists for the solute in a two-component system which is independent of the particular flow situation.

In a two-component system, the relation between the experimentally-measurable sedimentation coefficient, s_1, diffusion coefficient, D, solution density, ρ, and partial specific volume, $\bar{v}_1$, may be expressed as

$$M_1 = \frac{RTs_1[1 + \mathrm{d} \ln y_1/\mathrm{d} \ln c_1]}{D(1 - \bar{v}_1\rho)} \qquad (1)$$

where M_1 is the molecular weight, c_1, the concentration, and y_1, the activity coefficient of the "solute" (component 1) on, *e.g.*, the molar scale, and R and T have their usual significance. All quantities measured, with the exception of D and ρ, depend on the choice of components. In the limit of zero concentration of component 1, the expression reduces to the well known "Svedberg equation."[3]

Equation 1, which will be referred to as the extended Svedberg equation, may be derived by methods based either on the concept of frictional work,[4–5] or explicitly in terms of the thermodynamics of irreversible processes[6]; the latter derivations are less restrictive and have special importance in that the flows of solute occurring in the separate sedimentation and diffusion experiments are formulated in terms of the *same* fundamental coefficient, which has the nature of a mobility. Thus the vexed question of whether or not the frictional coefficients are identical in the two processes[7] is avoided completely,[6,8] though specification of the reference frames remains important.

An experimental demonstration that (1) applies to a system where the thermodynamic factor varies significantly with concentration would therefore constitute (at least in principle) a direct check on the propriety of the formulation, since the interpretation would then be solely in terms of macroscopic measurable properties (*cf.* the case of diffusion alone[9,10]). No such test of (1) has yet been performed on a two-component system (the various tests of the *limiting form* of (1) are discussed below), the chief difficulty being that of finding a substance whose constitution is precisely known and which possesses a sufficiently high molecular weight for the sedimentation coefficient to be measurable with the desired accuracy. A further restriction on the choice of materials arises because of the need to have the thermodynamic factor change significantly over a relatively small concentration range.

For the test of eq. 1 which forms the subject of this paper, the strictly two-component system thallous sulfate–water was studied. Although Tl_2SO_4 has a relatively low molecular weight, the partial specific volume in aqueous solution is also low, so that maximum advantage is taken of the occurrence of the factor $(1 - \bar{v}\rho)$ in the formula. The thermodynamic factor[11,12] possesses the desired attributes, and the diffusion behavior has been established.[12]

Sedimentation coefficients have now been measured over the whole accessible concentration range; it has been found that even moderately accurate determinations depend critically upon the control of several sources of error, which are accordingly discussed.

Experimental

Materials, Solutions, Partial Specific Volume Determinations.—Solutions were prepared as in the previous investigations.[11,12] Density measurements were made at 25.00° using a 25-ml. single-bulb pycnometer.

Sedimentation Coefficient Determination.—The Spinco

(1) A preliminary report of this work was presented to the Faraday Society Informal Discussion on Ultracentrifugation of Biological Macromolecules held in Birmingham, England, Sept. 14–15, 1960, an account of which has been given by D. R. Stanworth, *Nature*, **188**, 635 (1960).

(2) Lister Institute of Preventive Medicine, London, S.W.1, England.

(3) T. Svedberg and K. O. Pedersen, "The Ultracentrifuge," Oxford University Press, Oxford, 1940.

(4) R. L. Baldwin and A. G. Ogston, *Trans. Faraday Soc.*, **50**, 749 (1954).

(5) O. Lamm, *Trans. Roy. Inst. Tech.* (Stockholm), **134**, No. 3 (1959).

(6) J. W. Williams, K. E. Van Holde, R. L. Baldwin, and H. Fujita (*Chem. Rev.*, **58**, 715 (1958)) have summarized the work in this field.

(7) G. Kegeles, S. M. Klainer, and W. J. Salem, *J. Phys. Chem.*, **61**, 1286 (1957).

(8) L. Peller, *J. Chem. Phys.*, **29**, 415 (1958).

(9) H. S. Harned and B. B. Owen, "The Physical Chemistry of Electrolytic Solutions, 3rd Ed., Reinhold Publ. Corp., New York, N. Y., 1958.

(10) R. A. Robinson and R. S. Stokes, "Electrolyte Solutions," 2nd Ed., Academic Press, Inc., New York, N. Y., 1959.

(11) J. M. Creeth, *J. Phys. Chem.*, **64**, 920 (1960).

(12) J. M. Creeth and B. E. Peter, *ibid.*, **64**, 1502 (1960).

Model E analytical ultracentrifuge was employed; it was fitted with the "RTIC" temperature regulating device, and all experiments were carried out at 25.0°.

Thallous sulfate solutions do not form boundaries which separate from the meniscus at the maximum speed obtainable with the Spinco instrument. Reliable results could not be obtained with a boundary-forming cell, as diffusion was too rapid. Measurements therefore were made following the Gutfreund–Ogston[13] procedure, employing Rayleigh optics.[14,15] This method has been applied[16] to the determination of the sedimentation coefficient of a high molecular weight protein, but no application to low molecular weight systems has appeared; in principle, several advantages over schlieren optics may be anticipated.

The essential result obtained by Gutfreund and Ogston (eq. 6a of ref. 13) may be written (after the second integration has been performed)

$$\ln\left\{1 - 2\int_{r_m}^{r_X}[c(r_X) - c(r)]r\,dr/c_0 r_m^2\right\} = -2s\omega^2 t \quad (2)$$

where s is the sedimentation coefficient (assumed here to be independent of concentration; see below), ω, the angular velocity, assumed constant over the whole time, t, in which sedimentation occurs. The concentration (in g. dl.$^{-1}$) c_0 is that of the original solution (at $t = 0$), $c(r)$, the value at a point distance r from the center of rotation, and r_m and r_X are similar radial distances to the meniscus and a point in the plateau region, respectively; $r_m < r < r_X$. While c_0 is thus operationally defined, neither of the other concentrations can be directly observed, although their difference is proportional to the refractive index difference between the two points r and r_X,[18] if certain complicating factors can be ignored. The most important of these factors[17] are (i) pressure effects on the refractive index, n, and (ii) nonlinear dependence of n upon c. The following treatment takes account of these factors.

We assume that the refractive index of a solution at constant temperature is adequately represented by the equation

$$n = n_0 + Rc + ac^{3/2} + bc^2 + k_P P \quad (3)$$

where P is the pressure and c is the concentration of the solute component whose sedimentation coefficient is sought. The coefficients R, a, b, and the limiting value n_0 are assumed identical with those measured at 1 atm. (The term in $c^{3/2}$ may be expected to vanish for non-electrolytes.)

Fringes, denoted j, are counted from zero at the plateau region toward the meniscus. Since the fringes represent unit increments in the refractive index *difference* between the two compartments as a function of r,[18] we have

$$j(r_k) = -(d/\lambda)\{n_{II}(r_k) - n_I(r_k) - [n_{II}(r_X) - n_I(r_X)]\} \quad (4)$$

where d is the length of the cell along the optic axis, λ, the wave length of the light, and the subscripts I and II refer to solvent and solution compartments, respectively.

We note the relations between the solution density, the concentration, and the excess pressure at r_k, $P(r_k)$

$$P(r_k) = \int_{r_m}^{r_k}\rho\omega^2 r dr \quad (5)$$

$$\rho = \rho_0 + k_c c \quad (6)$$

It is assumed that higher order terms in the density expression are not required, and that the solution is incompressible. The values of n required in (4) are then given by

$$n = n_0 + Rc + ac^{3/2} + bc^2 + (k_P/2)\omega^2\rho_0(r_k^2 - r_m^2) + k_P k_c \omega^2 \int_{r_m}^{r_k} c(r)r\,dr \quad (7)$$

so that the expression for the fringe number becomes

$$j(r_k) = -(d/\lambda)\{R[c(r_k) - c(r_X)] + a[c(r_k)^{3/2} - c(r_X)^{3/2}] + b[c(r_k)^2 - c(r_X)^2] + k_P k_c \omega^2\left[\int_{r_m}^{r_k} c(r)r\,dr - {}^1/_2 c(r_X)(r_X^2 - r_m^2)\right]\} \quad (8)$$

Because the experiment will generally be conducted so that $c(r) - c(r_X)$ is small, the terms in $c^{3/2}$ and c^2 may be expanded, and only the first term in each series retained. We then have, after some simplification

$$(\lambda/d)j(r_k) = [c(r_X) - c(r_k)][R + 3(a/2)c(r_X)^{1/2} + 2bc(r_X)] + k_P k_c \omega^2\left[\int_{r_m}^{r_k} c(r)r\,dr - {}^1/_2 c(r_X)(r_X^2 - r_m^2)\right] + \ldots \quad (9)$$

The second bracketed term in (9) is identical with the differential refraction increment, n' (*cf.* eq. 3)

$$n' \equiv \left[\left(\frac{\partial n}{\partial c}\right)_P\right]_{c = c(r_X)} \quad (10)$$

The concentration function required in (2) is therefore given by

$$c(r_X) - c(r_k) = \lambda j(r_k)/n'd - k_P k_c \omega^2 c(r_X)(r_X^2 - r_k^2)/2n' + [k_P k_c \omega^2/(n')^2 d]\int_{r_m}^{r_k} j(r)r\,dr + \ldots \quad (11)$$

Three important conclusions implicit in this result may be summarized: (i) The differential refraction increment at the *original* concentration is a better approximation than the integral value, and its use is consistent with the other limitations on the validity of (11). (ii) The main effect of pressure, the second term on the right of (11), is due to the different densities of solution and solvent, since effects due to the differing values of the meniscus positions in the two compartments cancel. In some experiments in this series, this effect was quite large, $j(r_m)$ being reduced by 0.5 or more. However, insofar as $c(r_X)$ is independent of time, so also is this effect independent of time, and thus it may be ignored when interest lies solely in the determination of s values—that is to say, the apparent, uncorrected, j values may be used in the integration procedure. (iii) Because of the progressive loss of solute from the part of the cell centripetal to the plateau region, the density at r_k, and hence the pressure correction at this point, varies with time. This produces a time-dependent error in the apparent value of $j(r)$. When s values are to be calculated, appreciable errors may result if the effect, given by the third term on the right of (11), is ignored. However, a correction of adequate precision may be applied quite easily. The basis of the method is that the measurements of $j(r)$ are made at the *same values* of r in each exposure: thus while $j(r)$ is a function of time, r itself is not. The correction is formulated as follows.

Expanding (2) for the case of a sufficiently small, differentiating with respect to time, and substituting from (11) for the concentration-difference function, we obtain

$$s = K\cdot\frac{\mathrm{d}}{\mathrm{d}t}\left\{\int_{r_m}^{r_X}\left[j(r_k) - \frac{k_P k_c\omega^2}{n'}\int_{r_m}^{r_k} j(r)r\,dr\right]r\,dr\right\} \quad (12)$$

$$= K\cdot\left\{\frac{\mathrm{d}}{\mathrm{d}t}\left[\int_{r_m}^{r_X} j(r)r\,dr\right] - \frac{k_P k_c\omega^2}{n'}\int_{r_m}^{r_X}\left[\frac{(r_k^2 - r_m^2)}{2}\left(\frac{\mathrm{d}j}{\mathrm{d}t}\right)_{r=r_k}\right]r\,dr\right\} \quad (13)$$

where $K = \lambda/\omega^2 c_0 r_m^2 n' d$. Thus the correction term is separated from the main term and is expressed in terms of measurable quantities. The full derivation of (13) has been omitted, but it may be verified readily by writing down, from (11), the concentrations at the same point, r_k, at two different times, and then subtracting, it being realized that the sedimentation coefficient depends essentially on the quantity $\sum_{r_m}^{r_X} r_k\,(\mathrm{d}j/\mathrm{d}t)_{r=r_k}$.

(13) H. Gutfreund and A. G. Ogston, *Biochem. J.*, **44**, 163 (1949).

(14) J. S. Johnson, G. Scatchard, and K. A. Kraus, *J. Phys. Chem.*, **63**, 787 (1959).

(15) E. G. Richards and H. K. Schachman, *ibid.*, **63**, 1578 (1959).

(16) W. F. H. M. Mommaerts and B. B. Aldrich, *Biochim. Biophys. Acta*, **28**, 627 (1958).

(17) Svensson (*Optica Acta*, **1**, 25 (1954)), and Forsberg and Svensson (*ibid.*, **1**, 90 (1954)) have examined anomalies inherent in the Rayleigh method, which might also lead to error in the interpretation of experimental records. No attempt to correct for these effects will be made here, as the values of the refractive index *gradient* in the cell were always small.

(18) The two possible arrangements of the light-limiting diaphragm have been discussed by Richards and Schachman[15] and Johnson, *et al.*[14] In the experiments reported here, the offset arrangement was used.

Cell Filling and Velocity Experiments.—Standard procedures,[14,15] including the recording of a "blank" experiment, were followed; 0.43 ml. of solution and 0.46 ml. of solvent were used, to ensure that both menisci were visible. The cell was not dismantled during a series of experiments, the solution compartment only being washed, rinsed with distilled acetone, and dried between times. Speeds ranged from 29,500 r.p.m. for the more concentrated solutions, to 39,460 r.p.m. for the dilute range. Six photographs at 6–8 min. intervals were taken, using Kodak "Kodaline C.T.C." plates, after an initial period of 5–10 min. at speed; before and after this series, an exposure using the schlieren optical system (with bar angle 90°) was recorded.

Measurement of Records and Evaluation of the Integrals.—Established methods[14,15] were followed, and the following description deals only with points of detail. Capitals will be used to denote planes as recorded on the photographic plate, and lower case for the corresponding planes after conversion to true radial distances.

The cell fringe-patterns obtained were about 2.85 cm. long, and the plane R_X was taken as being 1.400 cm. from the solution meniscus; for this purpose, the position of the meniscus was assumed to be the point where the fringes ended ($(R_m)_{II}$).

After precise alignment on the stage of the toolmaker's microscope, measurements were made of the lateral displacement y (normal to the radius vector) of an intensity minimum near the center of the pattern, at the R_X plane. For this value of R, four measurements of y were obtained, reading to 0.0002 cm., while single measurements of the fringe *nearest to the original* sufficed for the other R values: these were taken at 0.1000 cm. intervals. In this way, values of y for a total of 15 R values were obtained. The blank experiment having been measured in the same way, values of $[y(R) - y(R_X)]_{cor}$ were obtained by subtraction, some being positive and others negative due to the choice of a fringe nearest to the original. Division by the fringe separation resulted in conversion to fractions of a fringe. Since $\Delta j/\Delta R$ did not exceed 1.5 mm.$^{-1}$ in these experiments, the precise $j(r)$–r relationship can readily be constructed from these data. This procedure of recording at constant r values, rather than locating r values for predetermined j's, was adopted because the blank correction can be applied very easily and accurately, and because the subsequent calculations are greatly simplified; moreover, the error in j arising from an error in the fringe separation is minimal and non-cumulative. The integrals required in (13) were approximated by Simpson's Rule, in the form of sums of $j(r_k)\cdot r_k$ products, where k is an integer running between 0 and 14; this procedure was demonstrated to be very reliable and more accurate than one employing r^2 as a variable. For the first two exposures in some experiments, it was found more accurate to make measurements of y at intervals of 0.05 cm. in R. The integrals so obtained are subject to significant errors arising from meniscus and base line locations, which will now be discussed.

Sources of Error and Corrections. (i) **Meniscus Errors.**—It is well known that considerable difficulty may be experienced in locating the true position of the meniscus in a centrifuge experiment[19,20] and indeed there is some uncertainty as to the precise meaning of the term.[21] Defining $(R_m)_I$ as the position of the *outer* end of the air-fringes and $(R_m)_{II}$ as the position of the *inner* end of the main fringe pattern, it is found that these planes may be located with a reproducibility approaching 0.001 cm. The same reproducibility has been found for the centers of the images of the menisci in a *schlieren* exposure taken at 90° bar angle, at the speeds used in this work; these images each constitute a "central shadow" as defined by Trautman.[19] If the latter meniscus images may be taken as being blurred symmetrically on the r axis (*i.e.*, that each infinitely thin meniscus records as a line where the intensity minimum is symmetrically situated) then it is clear that the planes R_m in the Rayleigh image cannot correspond to the true r_m. However, the difference $\Delta R_{Rayleigh} = (R_m)_{II} - (R_m)_I$ compared with *the corresponding quantity from a schlieren exposure* will give a precise estimate of the error attaching to the location of the meniscus in the Rayleigh exposure. Defining $\gamma = (\Delta R_{Rayleigh} - \Delta R_{schlieren})/2M$, where M is the magnification factor, it is apparent that addition of the quantity $\Delta = \gamma\cdot j(r_0)\cdot r_0$ will compensate, in the estimation of the integral, for the use of the plane $(R_m)_{II}$ as the lower limit. In practice, γ was determined separately in each experiment: values ranged from 0.005–0.009 cm.

(ii) **Base-line Errors.**—The procedure described eliminates errors arising from the time-independent pressure effect. It also follows that any *consistent* error in the base-line subtraction is eliminated in determining the time-dependence of the integral, provided that the same set of r values is used for all measurements. Thus base-line corrections of both types may be ignored, if desired. However, it has been found advantageous here to include both effects in a single correction, so that a true measure of the concentration is obtained.

The effect of random errors in locating the base-line must now be considered. An error, δj, made in locating the zeroth fringe will introduce an error $\delta j\cdot(r_X^2 - r_m^2)/2$ in the integral; in order to reduce this to 1% of the mean value of the integral in an experiment with, *e.g.*, Tl_2SO_4 at 2 g. dl.$^{-1}$, δj must not exceed 0.01. This corresponds to 3 μ in the displacement y, and it is at once clear that, as Van Holde[22] found, this source of error is likely to be serious, for experience has shown that even with the greatest care in measurement, errors of at least 5 μ are unavoidable. Fortunately, once again this error may be controlled fairly accurately, the basis of the procedure being the recognition that the lateral shift, ϵ, with time of the zeroth fringe is given in terms of j by (*cf.* ref. 14, 15)

$$\epsilon(t) = 2\omega^2 stc_0 n'd/\lambda + \ldots \qquad (14)$$

and may thus be predicted if an approximate s value is first obtained. By adding to the integral at the nth exposure the quantity

$$[\epsilon_n(\text{observed}) - \epsilon_n(\text{predicted})](r_X^2 - r_m^2)/2$$

where the predicted value is obtained from (14), the error may be almost entirely eliminated. Application of this correction was found to reduce considerably the scatter in the plots of the integral *vs.* time (*cf.* Fig. 2B); it is an illustration of the versatility and convenience of the Rayleigh optical method that this correction can so easily be made. An analogous correction is equally important in methods based on the refractive index gradient curve, but in that case there is no shift in the base line which can be used to assess, and then eliminate, the error.

The time-dependent error, arising from the changing pressure in the plateau region, was eliminated by making a correction only to the first and last exposures of an experiment. Having obtained the apparent time-dependence of the integral $\int j(r)r\,dr$, the integral $\int \Delta j(r_k)(r_X^2 - r_k^2)r\,dr$ was obtained similarly: Δj is the difference, at r_k, between the j values found in the last and the first exposure. Division by the time interval, and conversion by the appropriate constants, gave the subtraction correction to the slope term.

Results

(1) **Partial Specific Volume Factor.**—The densities, at 25°, of aqueous thallous sulfate solutions found in this work may be represented by the equation

$$\rho = \rho_0 + 9.08 \times 10^{-3} c;\ 0 < c < 5.0$$

where c is in g. dl.$^{-1}$. These values are in good agreement with the earlier, more limited data.[23] The quantity $(1 - \bar{v}_1\rho)$ was obtained directly, by the method of Kraemer.[24] The results are shown in Fig. 1; the line is for interpolation purposes only.

(2) **Refraction Increment.**—From the results reported previously,[12] the differential refraction increment (in dl. g.$^{-1}$) of Tl_2SO_4 in aqueous solution at 25.00° may be obtained as

$$n' \times 10^4 = 9.823 - 0.347c^{1/2} + 0.0233c;\ 0 < c < 5.0$$

(19) R. Trautman, *Biochim. Biophys. Acta*, **28**, 417 (1958).
(20) S. R. Erlander and G. E. Babcock, *ibid.*, **50**, 205 (1961).
(21) Ping-Yao Cheng, *J. Phys. Chem.*, **61**, 695 (1957).
(22) K. E. Van Holde, *ibid.*, **63**, 1574 (1959).
(23) "International Critical Tables," Vol. 3, McGraw-Hill Book Co., New York, N. Y., 1928, p. 64.
(24) E. O. Kraemer, ref. 3, p. 57.

The value of $(\partial n/\partial P)_c$ was taken[25] as 1.4×10^{-5} cm.^{2} kg.$^{-1}$.

(3) **Sedimentation Coefficients.**—Figure 2A illustrates both the general smoothness of the $j(r)$ *vs.* r relation always found, and the application of the time-independent pressure correction to the first and last exposures of a typical experiment. The elimination of the "tail" in the first exposure is clear.

Figure 2B shows a plot of $\int j(r) r\, dr$ (*cf.* eq. 13) *vs.* time, and the scatter is a direct indication of the precision of the resulting s value. Also shown on this group are the values of the integral *before* application of the "ϵ-correction" (see Experimental section); the smoothing effect of this correction is apparent, while the value of the slope is also significantly affected in this case.

The experimental results of the whole series of sedimentation measurements are shown as crosses in Fig. 3. A significant positive dependence of s upon c is revealed.

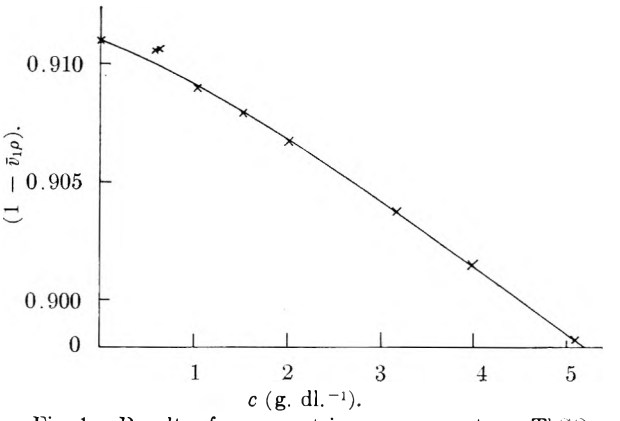

Fig. 1.—Results of pycnometric measurements on Tl_2SO_4. the quantity $(1 - \bar{v}_1\rho)$ obtained from Kraemer's equation, as a function of concentration.

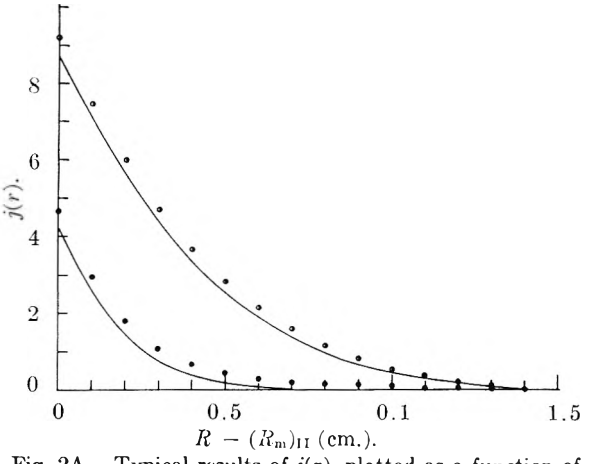

Fig. 2A.—Typical results of $j(r)$, plotted as a function of distance from the apparent meniscus position on the photographic plate. The points shown are for the first exposure (●) and last exposure (◑) in an experiment at $c = 4.101$ g. dl.$^{-1}$. After applying the correction for the *time-independent* pressure effect (see Experimental section) the j values are decreased and then fall on the curves shown. The individual corrected points have been omitted, to aid clarity, but their departure from the smooth curves may be judged from the behavior of the uncorrected points.

Discussion

Before a useful comparison may be made between the results of this study and those expected on the basis of irreversible process theory, three questions concerning the validity of the results must be examined.

(i) **Reference Frames.**—This question becomes important at moderately high concentrations. It is clear from the flow equation for the centrifuge which defines s (*e.g.*, eq. 41, p. 756 of ref. 6) that the latter is a function of the reference frame. It follows from the Gutfreund–Ogston theory and eq. 13 of this paper that the calculation procedure gives a "volume-fixed" sedimentation coefficient, as the meniscus is taken as the significant limit in the integration. Since the partial specific volume of Tl_2SO_4 is small, varies only slightly with concentration, and the concentration itself changes only to a minor extent in the experiments, the volume-fixed frame becomes identical with the "cell-fixed" frame,[26] as was the case with the diffusion coefficient values. Thus both the sedimentation and diffusion coefficients are cell-fixed values, and may be used in (1) without error, and the question of "back-flow" of solvent[27] during the sedimentation experiment does not arise. The "back-flow" is, of course, non-zero on any reference frame other than the solvent-fixed, but is identical in the sedimentation and diffusion processes provided the same reference frame is used for each.

(ii) **Effect of Pressure.**—In general, both $\bar{v}$ and y in (1) are functions of pressure; however, it follows from elementary thermodynamic relations that the pressure dependence of the thermodynamic term is directly related to the concentration-dependence of $\bar{v}$. Since the compressibility of electrolyte solutions is generally very low[9] and in this case $\bar{v}$ does not vary significantly with c, it seems very unlikely that significant errors will arise from this cause, particularly as the pressure at the rx plane was fairly low (~40 atm.). Pressure effects on the solvent, such as those producing changes in viscosity, will in principle also affect the mobility (the phenomenological coefficient in the flow equation, *cf.* ref. 6, p. 749). Since it was found (after allowance had been made for the primary effect of pressure) that a plateau region existed in these experiments, it may be concluded[28] that pressure effects of this kind were negligible. It is therefore not inconsistent to consider only the effect of pressure on the refractive index of water.

(iii) **Concentration-Dependence of Sedimentation Coefficient.**—It is assumed in the derivation of (2) that s does not vary with c.[28a] The result, however, is still valid for arbitrary dependence of s on c provided that, in the plateau region, the concentration changes so slowly with time that the s

(25) V. Raman and K. S. Venkataraman, *Proc. Roy. Soc.* (London), **A171**, 137 (1939).

(26) L. J. Gosting and R. P. Wendt, *J. Phys. Chem.*, **63**, 1287 (1959).

(27) *Cf.* H. K. Schachman, "Ultracentrifugation in Biochemistry," Academic Press, Inc., New York, N. Y., 1959, p. 92. Earlier references are also cited in this summary.

(28) H. Fujita, *J. Am. Chem. Soc.*, **78**, 3598 (1956).

(28a) It is not possible to write a simple form of the Gutfreund–Ogston equation applicable to the case where s varies with c (*cf.* ref. 7). The restriction is not important in practice.

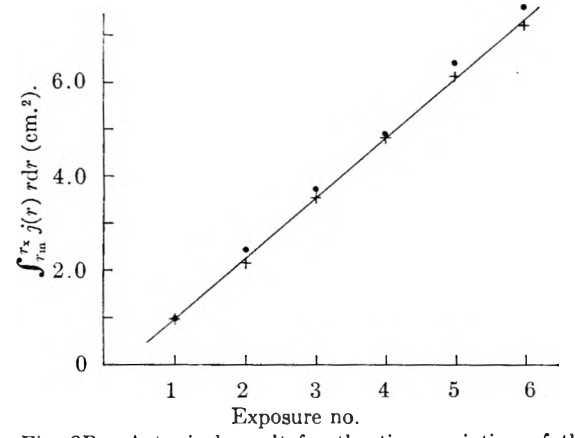

Fig. 2B.—A typical result for the time-variation of the first integral in eq. 13: the experiment was at c = 3.484 g. dl.$^{-1}$. Filled circles are values of $\int_{r_m}^{r_x} j(r)r\ dr$ (obtained by the summation procedure indicated) *before* applying the "ϵ-correction"; the crosses are the values *after* this correction has been applied. The solid line represents the best straight line through the crosses. Exposure interval was 8 min.

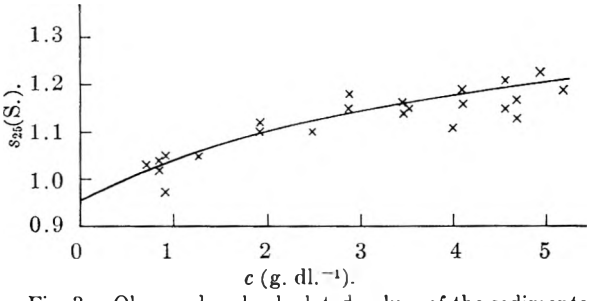

Fig. 3.—Observed and calculated values of the sedimentation coefficient of Tl_2SO_4 at 25°. Experimental points are shown as ×, while the solid line has been calculated from the known diffusion and thermodynamic characteristics, using eq. 15.

at that point can be considered constant. This condition is certainly met in these experiments, so that no error arises from this cause. It follows that the s obtained in an experiment refers closely to the original concentration of the solution.

Rewriting (1) explicitly in terms of the sedimentation coefficient of a 1:2 electrolyte we have

$$s_1 = \frac{M_1 D(1 - \bar{v}_1\rho)}{3RT(1 + \mathrm{d}\ln y_\pm/\mathrm{d}\ln c_1)} \qquad (15)$$

where M_1 is the formula weight and $y_\pm$ is the stoichiometric mean ionic activity coefficient. Values of the mobility, $D/(1 + \mathrm{d}\ln y_\pm/\mathrm{d}\ln c)$, for Tl_2SO_4, have been calculated[12] from differential values of D and the appropriate thermodynamic factors and thus refer to specific values of c. By combination with the partial specific volume factors, the prediction of s as a function of c is made possible. This relation is shown as the solid line in Fig. 3.

It is clear from this figure that the general trend of the observed concentration-dependence of the sedimentation coefficients is in good agreement with the predicted behavior. The scatter of the experimental data is quite pronounced, but is little more than must be expected from the known errors in the determination of the integrals. Applying the reasoning developed in the Experimental section one might anticipate minimum errors as follows: $0.6 < c < 1.0$, ±5%; $1.0 < c < 2.0$, ± 4%; $2.0 < c < 5.0$, ± 2%. Most of the experimental points lie within these limits, and while the mean curve drawn through the experimental points would lie some 1–2% below the predicted curve, this cannot be considered to be significant. Thus, within the limits of error, the validity of the extended Svedberg equation must be considered to be established. It may further be concluded that a single property of a solute–solvent system exists which defines its response to the application of a force, whether that force arises from a gradient of gravitational or chemical potential. The concept of a mobility (or its reciprocal, a frictional coefficient) is therefore meaningful at any concentration, and no reference need be made to the particular transport situation, provided that the force can be defined in macroscopic terms.

It might be emphasized that these conclusions are valid whatever the microscopic situation in solution may be: thus Tl_2SO_4 is certainly incompletely dissociated, and probably hydrated. Because the stoichiometric values of $\bar{v}$ and $y_\pm$ are used, the stoichiometric molecular weight will be obtained in an application of (1) to the s and D values, provided these are on the correct frame of reference. The large positive slope of the s–c curve is due to an unusual variation of the mobility (consequent upon incomplete dissociation) and is not a general property of electrolyte solutions. In general, the mobility can be expected to remain roughly constant over the range 0–0.1 molar, so that little concentration-dependence of s should occur, at least in systems where $\bar{v}$ is small. In an investigation of the system OsO_4–H_2O, Van Holde[22] found a positive slope for the dependence of s on c; this cannot be due to a similar cause, as the dissociation constant is very small, implying that little variation of the proportions of the constituents can occur.

Tests of the Svedberg equation in its limiting form for infinite dilution have been made by Baker, Lyons, and Singer[29] using silicotungstic and phosphotungstic acids in buffered solution; notably good agreement between known and calculated molecular weights was observed. It is now recognized[6,8,30] that in systems of more than two components, the appropriate form of the molecular weight equation contains cross-diffusion and cross-activity terms which do not necessarily vanish at infinite dilution of the component studied, and the reasons why this was not a source of error here have been discussed by Schonert.[31] The results of Brown, Kritchevsky, and Davies[32] on digitonin in the mixed solvent system ethanol–H_2O may well have been complicated by these effects, however, as a 6% discrepancy was reported between predicted and observed molecular weight. The present results appear to be the first on a strictly two-component system, but because of the relatively

(29) M. C. Baker, P. A. Lyons, and S. J. Singer, *J. Am. Chem. Soc.*, **77**, 2011 (1955); *J. Phys. Chem.*, **59**, 1074 (1955).

(30) R. L. Baldwin, *J. Am. Chem. Soc.*, **80**, 496 (1958).

(31) H. Schonert, *J. Phys. Chem.*, **64**, 733 (1960).

(32) R. A. Brown, D. Kritchevsky, and M. C. Davies, *J. Am. Chem. Soc.*, **76**, 3342 (1954).

low values of s found, it would still be very desirable to perform a similar test with a solute of larger molecular weight, so that the full potential accuracy of modern ultracentrifuges could be realized.

Two points which may confer advantage on the Rayleigh method of determining s by the Gutfreund–Ogston procedure must be mentioned in addition to those discussed earlier. These are: (i) the cylindrical lens magnification factor is not directly required, and errors in its equivalent, the fringe separation, are relatively unimportant; and (ii) as measurements are based on determining the positions of intensity minima, the results are independent of exposure time.

Acknowledgments.—The author is greatly indebted to Professor J. W. Williams for his interest in, and critical comments on, this work, and to Professor L. J. Gosting for many discussions. The work was supported by a grant from the National Institutes of Health, No. A3030 (C6).

OXIDATION OF *n*-OCTYL MERCAPTAN BY FERRICYANIDE IN ACETONE–WATER SOLUTION[1]

BY I. M. KOLTHOFF, E. J. MEEHAN, M. S. TSAO, AND Q. W. CHOI

School of Chemistry, University of Minnesota, Minneapolis, Minn.

Received October 16, 1961

The oxidation of *n*-octyl mercaptan (RSH) by potassium ferricyanide (Feic) in acetone–water (60–70% acetone) has been studied. The over-all reaction is first-order to Feic, RSH, and OH^-. In alkaline medium the kinetics correspond to a rate-determining bimolecular reaction between RS^- and Feic. There is a pronounced specific ion effect; potassium ion accelerates much more than Na^+, whereas the effect of tetramethylammonium ion is considerably less than that of sodium. The salt effects are accounted for on the basis of incomplete dissociation. The addition of cyanide reduces the rate markedly but the rate becomes independent of cyanide concentration above *ca.* 4×10^{-4} *M*. It is concluded that in the absence of cyanide the rate-determining step is a reversible substitution of CN^- in Feic by RS^-, followed by rapid decomposition of the substituted product to Feoc and RS·. The substitution reaction is practically suppressed in the presence of sufficient CN^-. The rate-determining step then is postulated to be Feic + RS^- → Feoc + RS·, followed by rapid oxidation by Feic of RS· to RS^+.

Introduction

As part of a study of the reactions of mercaptans with oxidizing agents, the oxidation of 2-mercaptoethanol by ferricyanide in acidic aqueous medium has been investigated in this Laboratory.[2] In the ferricyanide oxidation, both of this compound and of 3-mercaptopropionic acid,[3] complex kinetics were observed which could not be interpreted completely. The present paper describes the somewhat simpler kinetics observed in the oxidation of *n*-octyl mercaptan (RSH) by potassium ferricyanide (Feic). In order to carry out the reactions in homogeneous medium, acetone–water mixtures were used as solvent. Most of the work was carried out in 60% (by volume) acetone, which has a dielectric constant of 45. Because of the limited solubility of many inorganic compounds in this medium, the maximum ionic strength used was about 0.06.

In acid medium the reaction was found to be very complex and not to correspond to any single or a combination of two single simple mechanisms. Most of the work reported in this paper has been carried out in alkaline medium. The over-all kinetics of oxidation of RSH in alkaline medium appear to correspond to a bimolecular reaction between RS^- and Feic. There is a large salt effect which must be attributed to a specific cation effect. This effect may be related to the incomplete dissociation of potassium ferricyanide in the reaction medium. (Many of the experiments described in this paper were carried out before the magnitude of the effect was realized. Potassium ferricyanide was used in all the experiments, although it would have been preferable to use the sodium salt in the presence of sodium buffers.) There is no evidence that oxygen is directly involved in the reaction, but all the work has been carried out in the absence of oxygen to prevent oxygen-oxidation of RSH.

Experimental

Chemicals.—*n*-Octyl mercaptan was purified by vacuum distillation of commercial products at 3–4 mm. Various samples after distillation had mercaptan contents of 98.5 to 99.5% of the theoretical value, as measured by amperometric titration with silver nitrate.[4] The disulfide was prepared by oxidation with iodine. C.P. acetone was treated with sodium carbonate and calcium sulfate and distilled; the middle fraction was collected and stored over calcium sulfate. Feic and potassium ferrocyanide (Feoc) were recrystallized from analytical reagents and stored in the dark. Other chemicals were reagent grade and were used without purification. Conductivity water was used to prepare aqueous solutions and Linde "high purity" nitrogen to deaerate solutions. To prevent changes of composition during deaeration, the gas was first passed through two solvent mixtures of appropriate composition at 25°.

Experimental Procedure.—Unless otherwise specified, the reactions were run at 25° and in 60 vol. % acetone. In most experiments with an excess of RSH the following simple procedure was used. Twenty ml. of deaerated aqueous buffer solution was added to 30 ml. of deaerated acetone in a 50-ml. volumetric flask. After mixing, sufficient deaerated acetone–water mixture was added to fill up to the mark, to compensate for the volume contraction. RSH solution and Feic solution were prepared separately in 10-ml. volumetric flasks in the deaerated acetone–water buffer solution. For each experiment the solutions were

(1) This investigation was carried out under a grant from the National Science Foundation.

(2) E. J. Meehan, I. M. Kolthoff, and H. Kakiuchi, *J. Phys. Chem.*, **66**, 1238 (1962).

(3) J. J. Bohning and K. Weiss, *J. Am. Chem. Soc.*, **82**, 4724 (1960).

(4) I. M. Kolthoff and W. E. Harris, *Ind. Eng. Chem., Anal. Ed.*, **18**, 161 (1946).

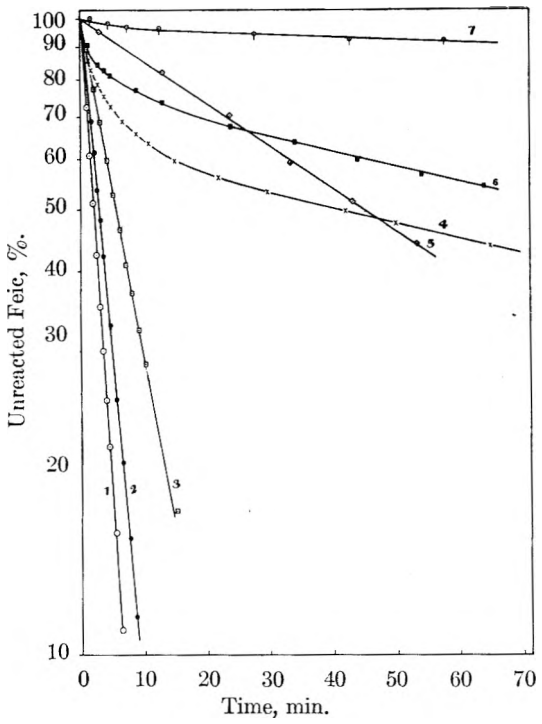

Fig. 1.—Reaction of Feic, pH 7.0–11.5, 60% acetone: (Feic) $\sim 3 \times 10^{-4}$ *M*, (RSH) 4×10^{-3} *M*. Ionic strength of buffer, 0.06; 1, carbonate, pH 11.5; 2, borate, pH 11.3; 3, carbonate, pH 10.8; 4, phosphate, pH 9.2; 5, barbiturate, pH 8.8; 6, phosphate, pH 8.8; 7, acetate, pH 7.0.

freshly prepared and were brought to 25° before being mixed. In most experiments (excess of RSH) the concentrations of RSH and Feic were about 4×10^{-3} *M* and 1–3 $\times 10^{-4}$ *M*, respectively. For relatively rapid reactions (higher pH) the solutions were mixed, quickly transferred in nitrogen atomosphere to a 1-cm. absorption cell placed in the thermostated compartment of a Beckman DU spectrophotometer, and the absorbance due to Feic was measured at 420 mμ. The maximum uncertainty in temperature was 0.5°. For slow reactions (lower pH) the solutions were mixed in a square reaction bottle with an attached 1-cm. absorption cell. This was kept in a separate thermostat and was placed in the spectrophotometer only for the actual measurement. In general this procedure gave satisfactory results. In a few experiments the reaction mixture became turbid. This appeared to be due to the formation of more than the expected amount of the disulfide. An approximate estimate of the solubility of the disulfide was carried out by adding a concentrated solution in acetone to various acetone–water mixtures until turbidity was noted, with the following results

Vol. % acetone[a]	Sol. of disulfide, $M \times 10^3$	
	Acetone–water	Acetone–buffer[b]
50	0.08	0.08
55	.16	.17
60	.21	.42
65	.68	.90
68	1.12	1.5

[a] By interpolation. [b] Aqueous part was 0.01 *M* in Na_2CO_3 and in $NaHCO_3$.

From the above results there should be no precipitation of disulfide in air-free 60% acetone at (Feic) $< 4.2 \times 10^{-4}$ *M* and 100% reaction. The occasional appearance of turbidity was due to oxidation of part of the excess of mercaptan by residual oxygen. The turbidity could be eliminated either by working in 70% acetone, which was done in a few cases, or even in 60% acetone using the following rigorous procedure. The oxygen content of the high purity nitrogen was further reduced by passage through vanadium(II) chloride. Special care was taken in deaeration by prolonged passage of nitrogen. Stock 0.01 *M* RSH was prepared in air-free acetone and the solutions were always kept protected from air. Such solutions were always used within a few days after preparation; even after 35 days of storage, the concentration never decreased more than 2%. Air-free stock solutions of Feic in water also were used within a few days. The reaction vessel with attached absorption cell was provided with a perforated metal cap and a self-sealing gasket. The vessel was flushed with nitrogen and all necessary solutions (except Feic) were added by pipet under a nitrogen atmosphere. The vessel was capped and placed in the thermostat chamber of the spectrophotometer. After reaching temperature, the Feic solution, at the same temperature, was added by syringe, the vessel was shaken vigorously for a few seconds, and replaced for measurement.

In a few experiments with either a small or no excess of RSH, the concentration of RSH was determined amperometrically.[4] Since both Feic and Feoc interfere, a 5-ml. sample was removed by syringe and extracted with 10 ml. of ether. The ether and water layers were washed with water and ether, respectively. The ether portions were combined, made up to 100 ml. with ethanol, and titrated as usual. In a few instances the combined aqueous layers were analyzed for Feoc by titration with cerium(IV) using ferrous *o*-phenanthroline as indicator.

pH measurements were made with a Beckman Model G pH meter standardized with appropriate buffers in water. The pH of dilute (*ca.* 10^{-3} *M*) solutions of hydrochloric acid and sodium hydroxide in 60% acetone indicated that the acid was completely dissociated. The difference in pH corresponded to pK_w of about 15.4 (25°). A value of 15.5 in 50% acetone has been reported.[5] Various buffers gave the following pH values in water and upon dilution to 60 vol. % acetone

Composition of aqueous buffer	pH	
	Water	Upon dilution with acetone
0.025 *M* NaAc, 0.025 *M* HAc	4.78	6.47
.025 *M* K_2HPO_4, 0.025 *M* KH_2PO_4	6.90	8.30
.046 *M* K_2HPO_4, 0.004 *M* KH_2PO_4	7.88	9.19
.002 *M* NaOH, 0.025 *M* H_3BO_3, 0.025 *M* KCl	7.95	10.37
.011 *M* NaOH, 0.025 *M* H_3BO_3, 0.025 *M* KCl	8.82	11.29
.004 *M* Na_2CO_3, 0.046 *M* $NaHCO_3$	9.00	10.79
.025 *M* Na_2CO_3, 0.025 *M* $NaHCO_3$	9.85	11.51[a]

[a] Practically the same pH in 70% acetone.

The ionic strength was adjusted by addition of sodium or potassium chloride.

A series of diethyl barbiturate (DEB) buffers was used for the pH range 8.8–10.4 in 60% acetone

	Molar composition of aqueous buffer				pH	
	NaDEB	HBEB	NaCl	KCl	Water	Upon dilution with acetone
(a)	0.01	0.03	0.03	0.035	7.40	8.8
(b)	.01	.03	.03	.11	7.38	8.8
(c)	.05	.025	.025	.075	8.18	9.5
(d)	.05	.01	.01	.09	8.58	9.9
(e)	.10	.005	.005	.045	9.18	10.4

Since the maximum (Feic) was 7×10^{-4} *M*, the capacity of even the most dilute buffer was adequate to maintain a practically constant pH during reaction. In most experiments pH was measured at the beginning and at the end of the reaction.

Ionic strengths have been calculated on the assumption of complete dissociation of electrolytes. This undoubtedly is not the case for either Feic or Feoc, but since their contribution amounts in typical cases to 0.002–0.005, any error in the calculated ionic strength due to incomplete dissociation of Feic or Feoc is minor. Complete dissociation of alkali carbonates in 60% acetone is questionable.

Results

Stoichiometry.—Reaction mixtures with a small excess of RSH were kept at 50°, pH 9.9, until reac-

(5) J. N. Pring, *Trans. Faraday Soc.*, **19**, 705 (1924).

TABLE I

EFFECT OF pH IN RANGE 7.0–10.8, μ = 0.06[a]

Buffer[b]	pH	Initial concn., M: $(K^+) \times 10^2$	$(Na^+) \times 10^2$	(Feic) $\times 10^4$	(RSH) $\times 10^3$	k_1, min.$^{-1}$[c]	k_2, l. mole^{-1} min.$^{-1}$[d]	Intercept at time = zero[e]
1	7.0	6.0	..	2.68	4.00	2.1×10^{-4}	0.052	91
2	7.5	5.6	..	2.64	4.00	6.0×10^{-4}	0.15	80
3	8.1	5.0	..	2.66	4.17	2.7×10^{-3}	0.67	76
4	8.8	3.2	..	[f]	[f]	4.1×10^{-3}	1.0	[f]
5	8.8	4.4	1.6	2.97	4.10	1.6×10^{-2}	4.0	100
6	9.2	3.9	..	2.70	3.93	5.0×10^{-3}	13	60
7	9.5	3.0	3.0	3.00	4.03	0.16	40	100
8	9.9	3.6	2.4	2.71	4.14	0.39	97	100
9	10.4	1.8	4.2	2.78	4.14	1.15	290	100
10	10.8	6.0	..	2.70	4.00	0.83	210	100
11	10.8	..	5.5	2.68	4.00	0.54	140	100

[a] Ionic strength of acetone–water buffer system. [b] Buffer compositions in reaction mixture: 1—Ac: 0.004 M HAc, 0.016 M KAc, 0.044 M KCl; 2—PO_4: 0.016 M KH_2PO_4, 0.004 M K_2HPO_4, 0.032 M KCl; 3—PO_4: 0.010 M KH_2PO_4, 0.010 M K_2HPO_4, 0.020 M KCl; 4—PO_4: 0.016 M KH_2PO_4, 0.004 M K_2HPO_4, 0.008 M KCl; 5—DEB: buffer b; 6—PO_4: 0.016 M KH_2PO_4, 0.0184 M K_2HPO_4 (μ = 0.057); 7—DEB: buffer c; 8—DEB: buffer d; 9—DEB: buffer e; 10—BO_3: 0.016 M H_3BO_3, 0.004 M KH_2BO_3, 0.056 M KCl; 11—CO_3: Na_2CO_3–$NaHCO_3$; rate extrapolated to μ = 0.06. [c] For (RSH) = 4.00×10^{-3} M. [d] Second-order rate constant. [e] Unreacted Feic, %, at time zero, by extrapolation of first-order reaction line. [f] See text.

tion was complete. The amounts of RSH consumed and Feoc formed show that the over-all reaction is

$$2RSH + 2Feic \rightleftharpoons RSSR + 2Feoc + 2H^+$$

Kinetics. A. Excess of RSH, pH Dependence and Order.—In mixtures with an excess of RSH the disappearance of Feic follows first-order kinetics at any pH above *ca.* 9 (curves 1–3, Fig. 1). (A pronounced salt effect, evident in Fig. 1, is discussed later.) In the DEB buffer, pH 8.8, the reaction is first order to Feic (curve 5). In a phosphate buffer at the same pH (curve 6) and at pH 9.2 (curve 4) and acetate buffer pH 7.0 (curve 7) there is an initially rapid reaction, higher than first order to Feic, followed by a slower reaction which appears to be first order to Feic. In acidic medium, pH <6, the behavior is much different. The initial reaction was slow, followed by a marked acceleration (Fig. 2). This pH region was not investigated further, and the subsequent discussion refers to pH $\geq$7.0.

The dependence of the pseudo first-order rate constant (excess of RSH) upon pH in the range 7.0–10.8, all in 60% acetone and ionic strength 0.062 (0.060 due to buffer), is shown in Table I. In the case of reactions with a rapid initial part, the rate of the subsequent first-order part has been used to calculate k_1, which is defined by the equation

$$\frac{-d(Feic)}{dt} = k_1(Feic)$$

Since the reaction is also first order to RSH (*vide infra*), all the values of k_1 in Table I have been referred to (RSH) = $4.00 \times 10^{-3} M$.

Over the pH range 7.0–10.8, log k_1 is linear with pH with a slope of 1.0; *i.e.*, k_1 is directly proportional to (OH^-) at constant ionic strength.

Experiments 4 and 5 of Table I were repeated at 15 and 50°, respectively. The same kinetics were observed, and the difference in rate constants corresponds to an activation energy of 24 ± 2 kcal. mole^{-1}.

Poorly reproducible results were obtained in the phosphate buffers, as compared to the other buffers. At pH 8.8, for example, in some cases

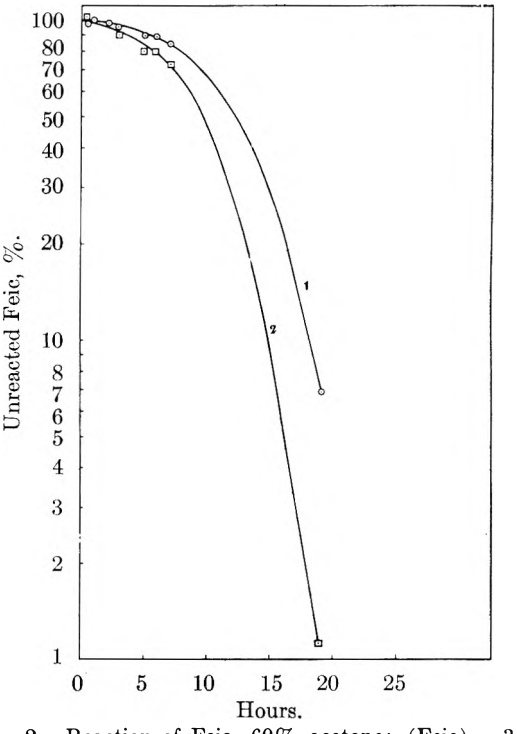

Fig. 2.—Reaction of Feic, 60% acetone; (Feic) ~3 × 10^{-4} M, (RSH) ~4 × 10^{-3} M; ionic strength 0.06: 1, HCl, pH 2.9; 2, acetate, pH 5.5.

there was an initial rapid reaction of variable extent followed by a first order; in other cases the reaction was first order throughout. The cause of the variation was not determined, but it was shown not to be due to a variable, fast reacting impurity in the mercaptan. The average value of k_1 at a total cation concentration of 0.032 M is 4.1 (± 0.9) × 10^{-3} min.$^{-1}$. In the DEB buffer at the same pH and ionic strength, but at a cation concentration of 0.060 M, first-order kinetics were observed with k_1 = 1.6 × 10^{-2} min.$^{-1}$. Both values of k_1 refer to (RSH) = $4.0 \times 10^{-3} M$.

Order with Respect to RSH.—The rate of reaction of Feic (initially *ca.* 3 × 10^{-4} M) was determined at pH 11.5, carbonate buffer, μ 0.012, in 69%

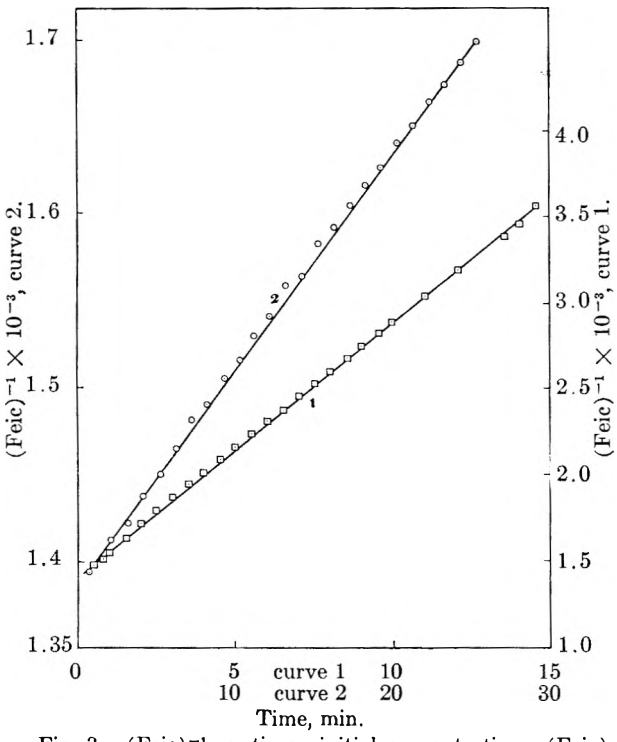

Fig. 3.—$(Feic)^{-1}$ *vs.* time; initial concentrations, (Feic) = (RSH) = 7.25×10^{-4} *M*; 60% acetone, pH 11.3: 1, no added cyanide; 2, 2.9×10^{-3} *M* KCN.

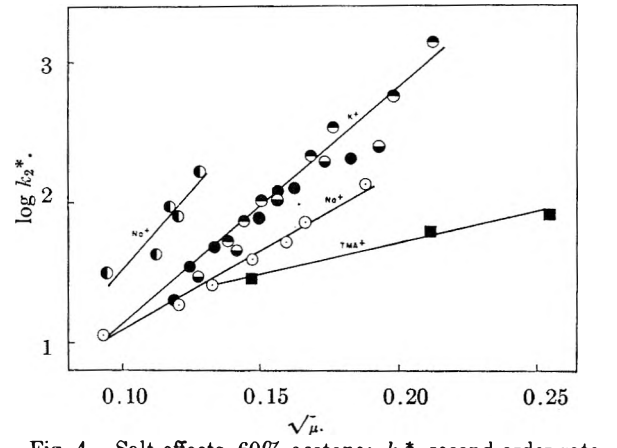

Fig. 4.—Salt effects, 60% acetone; k_2*, second-order rate constant referred to pH 11.60; initial concentrations (Feic) = (RSH) = 7.25×10^{-4} *M*: ○, sodium buffer; ◓, sodium buffer plus potassium chloride; ●, potassium buffer; ◒, potassium buffer plus potassium chloride; ■, sodium buffer plus tetramethylammonium chloride; ◐, sodium buffer in 70% acetone.

acetone in the presence of concentrations of RSH from 4×10^{-3} to 2×10^{-2} *M*. In every case Feic followed first-order disappearance and the average value of $k_1/[RSH]$ in 5 experiments was 8.3 ± 1.7 l. mole^{-1} min.$^{-1}$, showing that reaction is also first order to RSH.

The same conclusion is reached from the results of many experiments at pH 10.0–11.5 with initial equal reactant concentrations. For the sake of brevity the details are omitted but in every instance a plot of $(Feic)^{-1}$ was linear with time up to more than 70% reaction, corresponding to an over-all second-order reaction. An example is given in Fig. 3, curve 1.

B. Salt Effects.—Most of the experiments were carried out in 60% acetone with equimolar concentrations of reactants. At a given pH the bimolecular rate constant k_2 is defined by the equation

$$\frac{-\,d(Feic)}{dt} = k_2(Feic)(RSH)$$

Equimolar sodium and potassium carbonate–bicarbonate buffers were used at concentrations, respectively, 3.4×10^{-3} and 2.8×10^{-3} *M*. The maximum concentrations of potassium chloride and tetramethylammonium chloride were 0.028 and 0.054 *M*, respectively. The pH varied between 11.55 and 12.0; in most experiments the pH was 11.60. The values of k_2 referred to pH 11.60 are designated as k_2*; log k_2* is plotted against $\sqrt{\mu}$ (μ = ionic strength) in Fig. 4.

The log k_2*–$\sqrt{\mu}$ data for sodium carbonate–bicarbonate buffers (no added electrolyte) are fairly well fitted by a straight line with a slope of 11. The slopes in the presence of potassium chloride and tetramethylammonium chloride are about 18 and 4. A few experiments in 70% acetone with sodium buffers are included in Fig. 4. The slope is approximately 20. Comparing the two solvents at a buffer concentration (sodium) of 3.3×10^{-3} *M*, the values of k_2 are 30 and 170 l. mole^{-1} min.$^{-1}$ in 60 and 70% acetone, respectively (pH 11.6).

Effect of Potassium Ferrocyanide.—The experiments were carried out in 60% acetone, equimolar sodium carbonate–bicarbonate buffer, with (Feic) and (RSH) equal to 7.25×10^{-4} *M*. The results are given in Fig. 5, from which it is clear that the acceleration of potassium ferrocyanide is slightly less than that produced by potassium chloride at the same molar concentration.

Effect of Potassium Cyanide.—The experiments were carried out using equimolar reactants in potassium carbonate–bicarbonate buffer. In the presence of cyanide the reaction was followed at least to 30% completion and second-order kinetics were observed as in the absence of cyanide (curve 2, Fig. 3). The pH varied between 11.2 and 11.7; in most experiments the pH was 11.3 and the values of k_2 given in Fig. 6 are referred to pH 11.3. At the maximum concentration of cyanide used, the salt effect was practically negligible. The addition of cyanide reduces the value of k_2, but k_2 becomes practically independent of (KCN) above *ca.* 4×10^{-4} *M*.

Discussion

Assuming that the rate-determining step in all instances (*vide infra*) is a reaction involving RS^- and Feic, the effect of ionic strength upon the rate should be given by the expression

$$\frac{d \log k_2}{d\sqrt{\mu}} = 2.44 Z_A Z_A \text{ and } 2.95 Z_A Z_B$$

in 60 and 70% acetone, respectively. The dielectric constants have been interpolated from the data of Åkerlöf.[6] In the above expressions Z_A and Z_B are the charges on the reactants. The maximum $Z_A Z_B$ is 3, so the maximum slope of log k_2 *vs.* $\sqrt{\mu}$ should be 7.3 and 8.9, respectively. The

(6) G. Åkerlöf, *J. Am. Chem. Soc.*, **54**, 425 (1932).

observed slopes in 60% acetone of about 11 in sodium buffers and 18 in potassium buffers are much too great to be accounted for except by specific cation effects.[7] Even though the dielectric constant in the neighborhood of the ion in mixed solvents is unknown, it is clear that a specific cation effect must exist. Adamson[8] has mentioned a specific effect due to K^+ in the Feic oxidation of cyanide. Also, approximate measurements of the rate of reaction between Feic and iodide have shown that K^+ accelerates the reaction more than Na^+ does.[9] It is not possible to give a quantitative interpretation of the specific ion effect, but it is unmistakable that the effect of K^+ is greater than that of Na^+, and the effect of each is much greater than that of tetramethylammonium ion (slope about 4). In 60% acetone the dielectric constant is about 45 and salts of the type M_4B and M_3C (where M is K or Na) may be expected to be far from completely dissociated. Accordingly, upon the addition of K^+ or Na^+ one expects to find reactive forms of Feic in different proportions, with very little present as $Fe(CN)_6^{-3}$, more present as $MFe(CN)_6^{-2}$, and still more present as $M_2Fe(CN)_6^-$. On the other hand, tetraalkylammonium salts in general are more strongly dissociated than the alkali salts and the cation would be expected to have little or no specific effect. Indeed, the slope of 4 is of the right magnitude for an ionic strength effect on a reaction involving RS^- and $KFe(CN)_6^{-2}$.

The relatively slight effect of Feoc (Fig. 5) is in general agreement with the above interpretation. From Fig. 5 it can be concluded that in 60% acetone Feoc behaves as a uni-univalent electrolyte, and has little or no retarding effect. The latter behavior is in contrast to the pronounced effects of Feoc in the Feic oxidation (acidic aqueous medium) of 2-mercaptoethanol.

From the effect of pH it may be concluded that the rate-determining reaction involves RS^- rather than RSH.

The effect of cyanide (Fig. 6) is so pronounced that it indicates the existence of different mechanisms in the absence and presence of cyanide. Above *ca.* 4×10^{-4} *M* cyanide the rate becomes practically independent of cyanide. Thus, in the presence of sufficient cyanide (and at pH greater than 7) the main kinetic features are accounted for by a bimolecular rate-determining reaction (1) which is practically irreversible

$$\text{Feic} + RS^- \longrightarrow \text{Feoc} + RS\cdot \qquad (1)$$

(7) A. R. Olson and T. R. Simonson, *J. Chem. Phys.*, **17**, 1167 (1949).

(8) A. W. Adamson, *J. Phys. Chem.*, **56**, 858 (1952).

(9) H. B. Friedman and B. E. Anderson, *J. Am. Chem. Soc.*, **61**, 116 (1939).

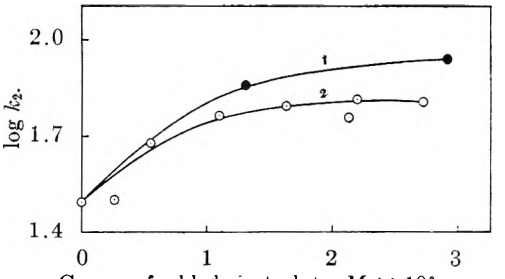

Fig. 5.—Effects of potassium chloride (curve 1) and potassium ferrocyanide (curve 2) on second-order rate constant; pH 11.6, 60% acetone, sodium carbonate–bicarbonate buffer (*ca.* $= 3.3 \times 10^{-3}$ *M*).

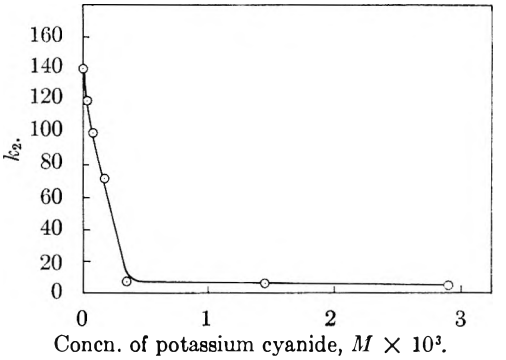

Fig. 6.—Effect of potassium cyanide on second-order rate constant; 60% acetone, pH 11.3.

followed either by a rapid dimerization of RS·, or by oxidation of RS· by Feic to RS^+ and a rapid reaction of RS^+ with RS^-. In the absence of cyanide, however, the results indicate that the rate-determining reaction is a reversible substitution

$$\text{Feic} + RS^- \rightleftharpoons \text{Feic}' + CN^- \qquad (2, -2)$$

where Feic′ represents an iron (III) cyanide with one cyanide replaced by RS^-. In the presence of more than *ca.* 4×10^{-4} *M* CN^- reaction 2 becomes of no consequence. The reaction both in the absence and presence of cyanide appears to be first order to iron(III), which indicates that Feic′ does not react directly with Feic; such a reaction, plus reactions 2, −2, would lead to an over-all order closer to 2nd than 1st order in iron(III). Instead, it is assumed that Feic′ rapidly decomposes

$$\text{Feic}' \xrightarrow{\text{rapid}} Fe(CN)_5^{-3} + RS\cdot$$

$$Fe(CN)_5^{-3} + CN^- \xrightarrow{\text{rapid}} \text{Feoc}$$

Essentially the above interpretation postulates two alternate paths for Feic and RS^- to form Feoc and RS·, the more rapid of which *via* Feic′ is suppressed upon the addition of cyanide.

REACTION BETWEEN FERRICYANIDE AND 2-MERCAPTOETHANOL[1]

BY E. J. MEEHAN, I. M. KOLTHOFF, AND H. KAKIUCHI

School of Chemistry of the University of Minnesota, Minneapolis 14, Minnesota

Received September 18, 1961

The oxidation of 2-mercaptoethanol by potassium ferricyanide has been investigated in the pH range 1.8–4.1 at 0–25°. The reaction product is the disulfide. The reaction has very complex kinetics, being in the initial stages second order to ferricyanide and becoming zero order to ferricyanide in the later stages. Addition of lead(II) makes the reaction first order to ferricyanide. Addition of small concentrations of ferrocyanide retards, but large concentrations of ferrocyanide accelerate and make the reaction zero order to ferricyanide. Two mechanisms which need further experimental substantiation have been postulated to account for the facts.

The reaction between ferricyanide and a mercaptan has been made use of for the initiation of emulsion polymerization. In order to aid in the interpretation of kinetics observed in such systems it was decided to study the kinetics of reaction between ferricyanide and a water-soluble mercaptan. For this purpose 2-mercaptoethanol was used. The reaction has a measurable speed at pH less than 4. In a subsequent paper the oxidation of a water-insoluble mercaptan by ferricyanide in acetone–water medium will be presented.

Quite generally the mechanism and kinetics of oxidations by ferricyanide are not accounted for by the simple stoichiometric reaction.[2] In our present work we have observed an effect of ferrocyanide on the kinetics of the mercaptan oxidation which is not accounted for by any simple reaction and which has not been mentioned hitherto. An attempt has been made to interpret the phenomena. Admittedly the proposed mechanisms are speculative but may serve as a guide in further work.

After completion of the present work, a study of the oxidation of 3-mercaptopropionic acid by ferricyanide was reported by Bohning and Weiss.[3] These authors also observed kinetic behavior which could not be accounted for quantitatively although some qualitative deductions could be made about the mechanism. They worked in the pH range 3.8–4.8. Since the pK_1 of 3-mercaptopropionic acid is 4.3, the effect of the varying ratio of undissociated acid and carboxylate ion must be taken into account. 2-Mercaptoethanol at pH < 4 is present virtually completely in the undissociated form, and the absence of the carboxyl group should make the reaction less complicated than with a mercaptocarboxylic acid.

Experimental

Chemicals.—2-Mercaptoethanol, denoted as ESH, was obtained from Union Carbide and Carbon Co. It was distilled under nitrogen and the fraction boiling at 69–70°, 23 mm., was collected. Results of amperometric titrations with 0.05 *M* silver nitrate corresponded to a mercaptan content of 99.3% of the theoretical value. From the measured pH after addition of known amounts of sodium hydroxide, pK_a was calculated to be 9.56 ± 0.02 at 25°, μ = 0.001. A value of 9.5 in 0.15 *N* sodium chloride, 25°, has been reported by Calvin.[4] Olcott[5] found that the rate of loss of ESH (presumably by air oxidation) in aqueous acidic medium is negligibly small compared to the reaction under consideration. The disulfide, ESSE, was prepared by oxidation with iodine.[6] Potassium ferricyanide (Feic) was recrystallized from Merck reagent, and solutions were prepared fresh as needed. Potassium ferrocyanide (Feoc) and other reagent grade chemicals were used without purification. All solutions were made up in conductivity water and were made air-free with Linde "high purity" nitrogen.

The pH, measured at 25°, was regulated in the range 1.8 to 4.1 with one of the following systems: acetic acid–sodium acetate, hydrochloric acid–potassium chloride, potassium biphthalate–potassium chloride, or phosphoric acid–potassium chloride.

Methods.—The reaction was studied at 0 and 25° in the absence of air. In most cases the rate was followed spectrophotometrically with a Beckman DU spectrophotometer, using a thermostated reaction vessel with an attached 1-cm. absorption cell. After the air-free reaction mixture, except Feic, had reached the desired temperature, an air-free solution of Feic at the same temperature was injected through a self-sealing gasket. The vessel was shaken vigorously for a few seconds and the absorbance of Feic was measured at 420 mμ, at which wave length the absorbance due to Feoc is negligible.[2] In a few experiments the rate of reaction of Feic was determined polarographically using the dropping mercury electrode at a potential at which ESSE is not reduced. The polarographic and spectrophotometric methods gave the same results for Feic concentration. ESSE formed in a completed reaction with an excess of ESH was determined polarographically in a borate buffer at pH 7.6, at −1.6 v. *vs.* s.c.e., at which potential the diffusion current is obtained by the reaction

$$\mathrm{ESSE} + 2e + 2H^+ = 2\mathrm{ESH}$$

Results

Stoichiometry.—From the amount of ESSE formed with an excess of ESH it was established that the over-all reaction is

$$2\mathrm{Feic} + 2\mathrm{ESH} = 2\mathrm{Feoc} + \mathrm{ESSE} + 2H^+$$

Separate experiments showed that ESSE does not affect the reaction rate, and that ESSE does not react to a measurable extent with Feic under the experimental conditions.

Reaction Kinetics.—The concentration of Feic was measured in the presence of an excess of ESH, at 0 and 25°, at varied pH and ionic strength, and in the presence of Feoc and lead perchlorate.

(a) In mixtures containing ESH and Feic, at any pH in the range 1.8–4.1, both at 0 and 25°, the initial rate is relatively large. Following this rapid reaction, the extent of which depends upon reactant concentrations and pH, a much slower, practically zero-order disappearance of Feic occurs. This is seen clearly from the curves of Fig. 1, which illustrate some typical results.

The ionic strength was varied with potassium chloride from 0.002 to 0.2, with no effect upon the reaction rate.

Figure 2 shows plots of $(\mathrm{Feic})^{-1}$ *vs.* time at

(1) This investigation was carried out under a grant from the National Science Foundation.

(2) See, *e.g.*, A. W. Adamson, *J. Phys. Chem.*, **56**, 858 (1952).

(3) J. J. Bohning and K. Weiss, *J. Am. Chem. Soc.*, **82**, 4724 (1960).

(4) M. Calvin, U. S. Atomic Energy Comm., UCRL-2438, 3 (1954).

(5) H. S. Olcott, *Science*, **96**, 454 (1942).

(6) I. M. Kolthoff, A. Anastasi, and B. H. Tan, *J. Am. Chem. Soc.*, **80**, 3235 (1958).

various pH. From the initial linear portion of the curves it is evident that the reaction initially is second order to Feic.

From a few experiments at 25° using concentrations of ESH between 5 and 9.5 × 10^{-3} *M* it appeared that the initial rate, as measured by extent of reaction at 1 min., is proportional to ESH. The initial rate was found to decrease with increasing acidity but no simple relation exists between rate and (H^+). Between pH 1.8 and 3.2 the rate increased only sixfold; at pH above 3.2 the rate appeared to approach inverse proportionality with (H^+).

The dependence of the rate of the zero order reaction at 25° upon (ESH) could not be established, because with increase of (ESH) the initial rapid reaction persists longer and the "final rate" becomes too small to be measured (*vide infra*, results at 0°).

Typical results at 0° are summarized in Table I. The kinetic features are the same as those discussed above. The rate constant V_f of the final zero-order reaction at 0° is approximately proportional to (ESH). The value of V_f/[ESH] at 0° is about 8 × 10^{-5} min.$^{-1}$ (pH 2.0). At 25° V_f[ESH] is about 5 × 10^{-4} min.$^{-1}$ (pH 1.76).

TABLE I

REACTION BETWEEN FEIC AND ESH, 0°, pH 2.0 ± 0.05

(Feic) × 10^{3a}	(ESH) × 10^{2a}	V_f × 10^{8b}	V_f/(ESH) × 10^5
1.10	1.89	1.4	7
1.19	2.06	1.9	9
1.66	2.06	1.8	9
1.66	11.7	10	8

[a] Initial molar concn. [b] Limiting zero-order rate constant, mole l.$^{-1}$ min.$^{-1}$.

(b) Addition of Feoc to the reaction mixture causes remarkable changes in the kinetics (Fig. 3). With increase of (Feoc) the extent of the initial rapid second-order reaction is decreased and the subsequent zero-order reaction is accelerated. As a result, the entire reaction becomes rapid and zero order to Feic in the presence of much Feoc. The final zero-order rate varies linearly with, but not in direct proportion to, (Feoc) (Table II).

TABLE II

EFFECT OF FEOC ON RATE

(Feic) = 3.91 × 10^{-4} *M*; (ESH) = 1.00 × 10^{-2} *M*; pH 1.9 (phosphoric acid); 25°

Added (Feoc) × 10^4	Initial rate[a]	Rate at 75% reaction[a]
0	22	1.3
0.76	17	1.8
2	2.4	1.3
4.59	3.2	1.7
4.92	4.4	1.8
6.45	...	2.7
40.1	6.7[b]	5.5
102	10.3[b]	10.3

[a] In % Feic per min. [b] After a brief induction period.

(c) Addition of lead perchlorate causes a pronounced acceleration (Fig. 4). While the rates are too large for exact kinetic studies it appears that the reaction becomes about first order to Feic.

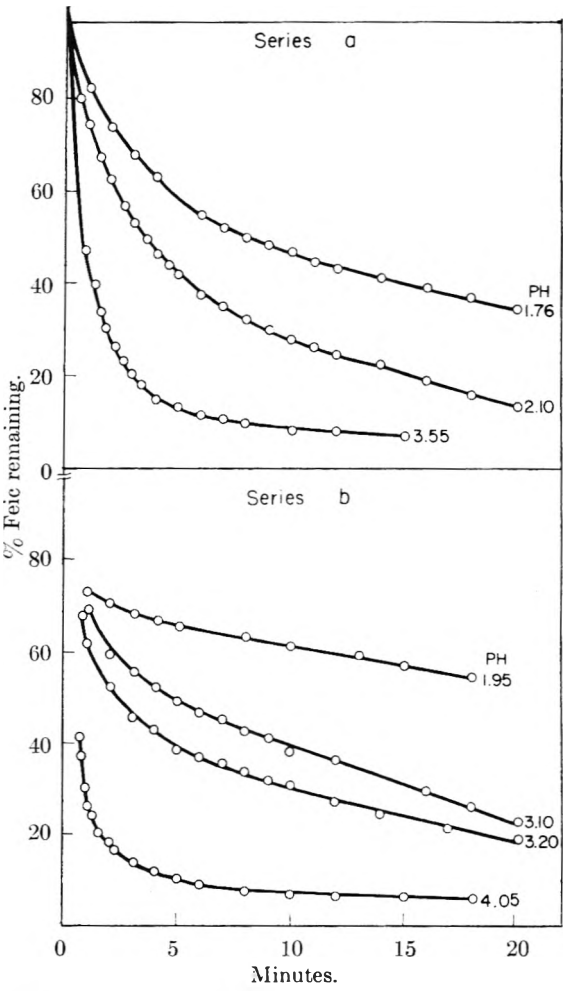

Fig. 1.—Effect of pH, 25°: (Feic) = 3.8 (± 0.1) × 10^{-4} *M* except at pH 3.55 and 4.05, in which (Feic) = 3.2 (±0.1) × 10^{-4} *M*; (ESH) = 9.0 × 10^{-3} *M* in series a and 4.0 × 10^{-3} *M* in series b. Buffers: pH 1.76, hydrochloric; pH 2.1 and 1.95, phosphoric; pH 3.10, 3.20, and 4.05, biphthalate; pH 3.55, acetic.

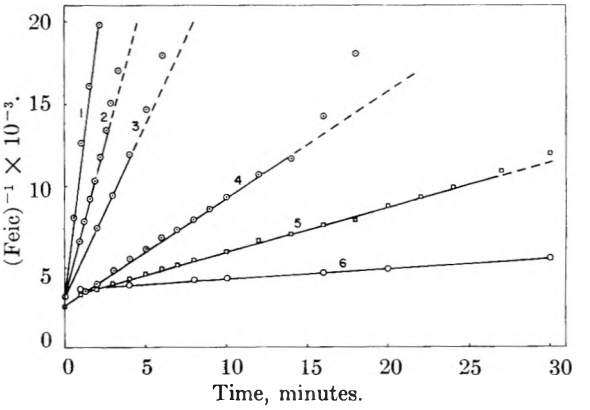

Fig. 2.—Plots of (Feic)$^{-1}$ *vs.* time: Initial (Feic), 3.5–3.9 × 10^{-4} *M*; curve 1 pH 4.05 (biphthalate), (ESH) = 3.95 × 10^{-3} *M*; curves 2 and 3 pH 3.55 (acetate), (ESH) = 9.24 × 10^{-3} *M* (2) and 6.37 × 10^{-3} *M* (3); curve 4 pH 2.10 (phosphoric), ESH = 9.65 × 10^{-3} *M*; curve 5 pH 1.80 (hydrochloric), (ESH) = 11.1 × 10^{-3} *M*; curve 6 pH 1.95 (phosphoric), (ESH) = 3.93 × 10^{-3} *M*.

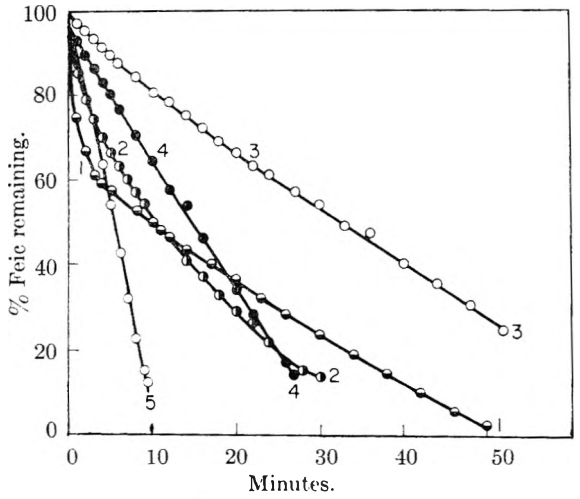

Fig. 3.—Effect of ferrocyanide; (Feic), 3.91×10^{-4} *M*; (ESH), 1.05×10^{-2} *M*; pH 1.9; 25°, and (Feoc) = curve 1, 0; curve 2, 0.76×10^{-4} *M*; curve 3, 2.00×10^{-4} *M*; curve 4, 6.45×10^{-4} *M*; curve 5, 1.02×10^{-2} *M*.

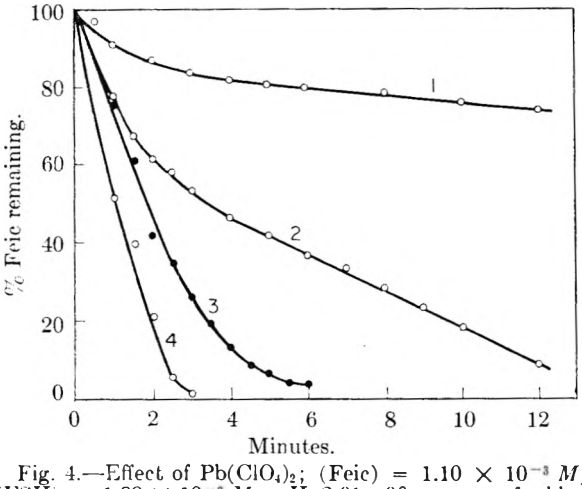

Fig. 4.—Effect of $Pb(ClO_4)_2$; (Feic) = 1.10×10^{-3} *M*; (ESH) = 1.88×10^{-2} *M*; pH, 2.01; 0°; concn. of added $Pb(ClO_4)_2$: 1, 0; 2, 0.0033 *M*; 3, 0.0065 *M*; 4, 0.0133 *M*.

Discussion

The kinetic results indicate the existence of at least two reaction mechanisms. Mechanism A, which is proposed to account for the initial reaction when no Feoc is added, has a reversible rate-determining step

$$\text{Feic} + \text{ESH} \longrightarrow \text{HFeoc} + \text{ES}^{\cdot} \quad (1, -1)$$

$$\text{Feic} + \text{ES}^{\cdot} + \text{H}^{+} \longrightarrow \text{HFeoc} + \text{ES}^{+} \quad (2)$$

$$\text{ES}^{+} + \text{ESH} \longrightarrow \text{ESSE} + \text{H}^{+} \quad (3)$$

Ferricyanic acid is a strong acid, but ferrocyanic acid is strong only for the first two hydrogens. According to Nekrasov and Zotov[7] $K_3 = 1 \times 10^{-3}$ and $K_4 = 5 \times 10^{-5}$ (values obtained at 16–18°, corrected to $\mu = 0$). Thus at pH below 4, a negligible fraction of iron(II) is present as $Fe(CN)_6^{-4}$. The major constituent is $HFe(CN)_6^{-3}$ or $H_2Fe(CN)_6^{-2}$, depending upon pH, and the maximum fraction of $HFe(CN)_6^{-3}$ occurs at about pH 3.6 ($\mu = 0$). For the sake of simplicity HFeoc in eq. (1, −1) represents the various forms in which ferrocyanide is present. The rate of reaction (−1) depends on the ferrocyanide species, and the overall rate is not a simple function of (H^+), as has been found experimentally. If ferricyanide reacted with ES^- rather than with ESH, a large ionic strength effect would be expected.

Reactions 2 and 3 are written instead of a simple dimerization of $ES^{\cdot}$ to account for observations in this Laboratory (unpublished) on the catalyzed addition of mercaptans to olefins. When persulfate, or persulfate and iron(II), is added to a solution containing mercaptan and olefin, a quantitative addition to the double bond occurs. However, when Feic is the oxidant the mercaptan is oxidized quantitatively to the disulfide and no addition to the double bond occurs. It appears that $ES^{\cdot}$ reacts more readily with Feic (reaction 2) than with an olefin.

Quantitatively mechanism A accounts for the order with respect to Feic and to ESH, and for the fact that both the rate and extent of the initial reaction are decreased upon addition of small amounts of Feoc (*vide infra*). The acceleration observed upon addition of lead(II) is accounted for by the precipitation of lead ferrocyanide, which prevents the occurrence of reaction (−1). The rate of disappearance of Feic then becomes first order to this constituent.

Because of reaction (−1), mechanism A is of no consequence when much Feoc is added. To account for a reaction zero order to Feic and accelerated by Feoc, mechanism B is postulated. (In the subsequent discussion, no distinction is made between Feoc and HFeoc.) The rate-determining step is a reversible substitution of CN^- in Feoc by ES^-

$$\text{Feoc} + \text{ESH} \rightleftharpoons \text{Feoc}' + \text{HCN} \quad (4, -4)$$

in which Feoc′ represents $Fe(CN)_5ES^{-4}$. Feoc′ is then oxidized by Feic. However, this oxidation reaction cannot occur with the direct formation of $ES^{\cdot}$; if it did so occur, $ES^{\cdot}$ would react according to reaction (−1) and no acceleration by Feoc would be observed. It is plausible that the oxidation occurs as

$$\text{Feic} + \text{Feoc}' \longrightarrow \text{Feoc} + \text{Feic}' \quad (5)$$

in which Feic′ represents $Fe(CN)_5ES^{-3}$, where the iron may be present in the divalent state and ES is uncharged, or iron in the trivalent state and ES as monovalent anion

$$\text{Feic}' + \text{Feic} \; (+ \text{CN}^-) \longrightarrow 2\text{Feoc} + \text{ES}^{+} \quad (6)$$

followed by (3). Reaction 5 undoubtedly is rapid, by analogy with the rapid electron exchange between Feic and Feoc.[8]

Apparently the ferricyanide oxidation of 2-mercaptoethanol is at least as complex as other oxidations cited by Adamson.[2] From the kinetics of the oxidation of monohydric phenols by alkaline ferricyanide, Waters[9] had already concluded that the initial stage of the oxidation is a reversible reaction. Similarly, Bohning and Weiss[3] assumed a reversible first step in the oxidation of 3-mercapto-

(7) B. V. Nekrasov and G. V. Zotov, *Zh. Prikl. Khim.*, **14**, 264 (1941).

(8) A. C. Wahl and C. F. Deck, *J. Am. Chem. Soc.*, **76**, 4054 (1954).

(9) C. G. Haynes, A. H. Turner, and W. A. Waters, *J. Chem. Soc.*, 2823 (1956).

propionic acid. In our studies on 2-mercaptoethanol, the *initial* reaction in mechanism A is explained in the same way as by Bohning and Weiss. However, they observed second-order kinetics throughout; the pronounced change in order and the remarkable effects of Feoc were not observed in the oxidation of 3-mercaptopropionic acid. The mechanism of oxidation by ferricyanide is very complex and probably involves more reactions than those in mechanisms A and B.

The complex nature of oxidation reactions with ferricyanide is encountered also in reduction reactions with ferrocyanide. In this connection it is of interest to mention that the simple mechanism postulated by Boardman[10] for the reaction of cumene hydroperoxide with ferrocyanide to form acetophenone and methanol does not account for many complex characteristics which apparently are specific for this reaction. The marked retardation by cyanide observed in this Laboratory and many other effects summarized by Reynolds[11] justify the conclusion that the mechanism cannot be accounted for by the simple stoichiometric reaction.

(10) H. Boardman, *J. Am. Chem. Soc.*, **75**, 4268 (1953).

(11) W. B. Reynolds, Ph.D. Thesis, University of Minnesota, 1955.

CATALYTIC REACTIONS ON SEMICONDUCTORS: HYDROGEN–DEUTERIUM EXCHANGE AND FORMIC ACID DECOMPOSITION ON CHEMICALLY DOPED GERMANIUM[1]

BY GEORGE E. MOORE,[2a] HILTON A. SMITH,[2b] AND ELLISON H. TAYLOR[2a]

Department of Chemistry, University of Tennessee, Knoxville, Tennessee, and Chemistry Division, Oak Ridge National Laboratory,[3] Oak Ridge, Tennessee

Received October 20, 1961

Hydrogen–deuterium exchange and the decomposition of formic acid were studied from 100 to 400° over samples of germanium doped with 10^{16} to 10^{20} atoms per cc. of n- and p-type impurities. Over these wide ranges of electronic chemical potential (Fermi level) and temperature the rate and activation energy of the exchange reaction vary definitely with the Fermi level. A minimum in the activation energy–Fermi level curve suggests a mechanism in which one step is rate-limiting on the n-type and a different one on the p-type side of intrinsic composition. Of the two paths for formic acid decomposition, only dehydrogenation seems to be markedly affected by doping.

Elemental semiconductors are well adapted to studies of the effect of electronic properties upon catalysis, since the concentration of charge carriers can be altered by many orders of magnitude by the incorporation of amounts of impurity too small to produce detectable changes in other bulk properties. Chemically doped germanium has been used for a number of such studies,[4-9] with somewhat inconclusive results from the standpoint of a general theory of catalysis. In some cases, marked differences in activity were found between n- and p-type samples, although the degree of doping was often without influence.[4,5,8,9] In the case of H_2–D_2 exchange, no dependence of activity upon doping was observed.[6,7]

The present experiments were undertaken in order to explore this important question of the catalytic behavior of doped germanium over as wide a range of doping and of temperature as possible.

Experimental

Vacuum System.—A conventional vacuum system using a mercury diffusion pump, liquid nitrogen traps, and high-vacuum stopcocks lubricated with Apiezon-N grease was employed. That portion of the apparatus accommodating the reaction vessels was separated from the rest of the system by dental gold foil and a liquid nitrogen trap.

Reaction Vessels.—Quartz reaction vessels of about 3 cc. volume (and with an additional dead space of about 3 cc. in connecting tubing) were employed. The connection to the vacuum line was through 2-mm. vacuum stopcocks and standard taper connections.

Catalysts.—Single crystals of germanium were obtained from the Bell Telephone Laboratories, Incorporated, Murray Hill, New Jersey, and from the Solid State Division of the Oak Ridge National Laboratory.[10] These crystals were doped with Al, Ga, In, As, or Sb, in concentrations varying from 10^{15} to 2×10^{20} impurity atoms per cc. (2.5×10^{-6} to 0.5 atom % impurity). The samples were washed with acetone, etched in "CP-8" (a mixture of concentrated nitric, hydrofluoric, and acetic acids in the volume ratio 5:3:3), fractured into smaller pieces, crushed, and finally mechanically ground in an agate mortar and pestle. Approximately 1 g. of the powder in a reaction vessel was heated at 675 to 700° for about 2 hr. in a stream of flowing (about 45 cc./min.) Matheson prepurified electrolytic hydrogen of 99.9% minimum purity and <20 p.p.m. oxygen (nominal), further purified by passage through a Model D Deoxo purifier (Engelhard Industries, Inc.) and a liquid nitrogen trap. The germanium was cooled in the hydrogen atmosphere and not again exposed to air.

(1) Based on a thesis presented to the University of Tennessee, Knoxville, Tennessee, by George E. Moore in partial fulfillment of the requirements for the Ph.D. degree, August, 1961. The work was carried out at the Oak Ridge National Laboratory.

(2) (a) Oak Ridge National Laboratory; (b) University of Tennessee.

(3) Operated for the United States Atomic Energy Commission by Union Carbide Corporation.

(4) (a) G. M. Schwab, in R. H. Kingston (ed.) "Semiconductor Surface Physics," University of Pennsylvania Press, Philadelphia, Pa., 1957, pp. 291–294; (b) G. M. Schwab, G. Greger, St. Krawczynski, and J. Penzkofer, *Z. physik. Chem.* (Frankfurt), **15**, 363 (1958).

(5) V. M. Frolov, O. V. Krylov, and S. Z. Roginskii, *Dokl. Akad. Nauk SSSR*, **126**, 107 (1959).

(6) V. L. Kuchaev and G. K. Boreskov, *Probl. Kinetiki i Kataliza, Akad. Nauk SSSR*, **10**, 108 (1960).

(7) V. L. Kuchaev and G. K. Boreskov, *Kinetika i Kataliz*, **1**, 356 (1960).

(8) V. M. Frolov, O. V. Krylov, and S. Z. Roginskii, *Probl. Kinetiki i Kataliza, Akad. Nauk SSSR*, **10**, 102 (1960).

(9) W. H. Watson, Jr., *J. Appl. Phys.*, **32**, 120 (1961).

(10) We are most grateful to Drs. J. W. Nielsen and C. O. Thomas (BTL) for providing us with a large assortment of highly doped specimens, and to Dr. J. H. Crawford, Jr. and Mr. John W. Cleland (ORNL) for samples of germanium of low impurity level.

At the completion of the catalytic studies, the surface area of each germanium catalyst was determined from krypton adsorption isotherms.[11] The specific surface areas for all samples were in the range 0.15 ± 0.07 m.²/g.

Gaseous Reactants.—Deuterium (Stuart Oxygen Co.) and prepurified electrolytic hydrogen (The Matheson Company, Inc.) were purified separately by passage through a heated palladium thimble and stored in reservoirs. Equal portions of each gas were mixed and similarly stored.

Formic acid of different sources and dried by two different methods showed essentially identical behavior during catalytic decompositions. First, Eastman 98+% formic acid was dried over pulverized boron oxide (B_2O_3) and vacuum distilled into a reservoir connected to the vacuum system; only about ²/₃ of the initial charge was collected. Most of the experimental data were obtained with this material. A second batch of pure formic acid was prepared by fractionating 88–90% formic acid (Baker and Adamson, Reagent Grade) in a 12-ft. Vigreux column. The first fraction of distillate contained low-boiling contaminants, while following fractions consisted of pure formic acid, since the distillation was from the formic acid side of the formic acid–water azeotrope (b.p. 107.3°, 77.5% formic acid).[12] This distillate boiled at 100.8°, and gave $n^{24}D$ 1.3693. Literature values for pure formic acid are: b.p. 100.75°,[12] and $n^{20}D$ 1.3710[13] corrected to $n^{24}D$ 1.3695.[14] When not in use, the formic acid was frozen to reduce thermal decomposition, and stored in the dark to minimize photochemical decomposition. The vapor was determined to be better than 99.7% formic acid by a cryoscopic and gas chromatographic method.

Experimental Procedure.—The hydrogen–deuterium exchange first was investigated on each catalyst, followed by the study of the formic acid vapor decomposition. The reaction vessel containing the catalyst was connected to the vacuum system and the interspace evacuated until a pressure of about 0.5 μ could be maintained without pumping for a period of time necessary for loading or sampling as described below (about 2 min.). For the hydrogen–deuterium exchange, the 1:1 gas mixture was admitted to the reaction vessel and the pressure adjusted to about 40–45 mm. by means of a Töpler pump. In the decomposition experiments the formic acid reservoir was maintained at a predetermined temperature to give the desired pressure of formic acid vapor (usually 25.0 ± 0.5° for 42 ± 1 mm.). During loading the reaction vessel was kept at a temperature somewhat higher (55–60°) than that of the formic acid reservoir and the connecting tubing in order to avoid difficulties thought due to capillary condensation of formic acid.

Each reaction was conducted at constant temperature in the range 100 to 400° (±1° for several hours and better than ±3° over several days). The gaseous products then were sampled by expansion into an evacuated 60-ml. bulb. After pumping out the reaction vessel and interspace, the system was ready for introduction of fresh reactants for the next experiment.

Reaction vessels without germanium, but otherwise identical, also were used to provide a background correction for the exchange and decomposition reactions.

Exchange Analysis.—Analysis in the exchange experiments was by mass spectrometry.[15] The unreacted exchange mixture gave a D/H ratio of 1.03 ± 0.08 and showed the presence of 3.0 ± 0.4% HD, which probably resulted from exchange of hydrogen with deuterium in the mass spectrometer. The equilibrium constants for the reaction $H_2 + D_2 \rightleftarrows 2$ HD were calculated from the equation $K = 4.24e^{-79/T}$ which gave values in agreement with literature values.[16] Reproducibility of the mass analyses over the range from 2 to 37% HD was ±0.68% HD at the 95% confidence level on the basis of analyses obtained for duplicate samples.

HCOOH Analysis.—The method of analysis took into account the two principal decomposition paths

$$\text{HCOOH} \xrightarrow{k_{CO_2}} CO_2 + H_2 \quad (1)$$

$$\text{HCOOH} \xrightarrow{k_{CO}} CO + H_2O \quad (2)$$

The analysis consisted of: (a) manometric determination of the pressures of total gas and of residual gas non-condensable at −78°; and (b) gas chromatographic determination of the relative proportions of hydrogen, carbon monoxide, and carbon dioxide.

Results

Treatment of Data.—First-order rate constants for the hydrogen–deuterium exchange showed that the reaction occurring on gallium- and indium-doped p-type and on intrinsic germanium was at least ten times faster than that occurring on the walls of the reaction vessel. However, powders of n-type and aluminum-doped germanium were much less active catalysts, and the exchange occurred predominantly on the surface of the quartz reaction vessel at the lower temperatures. Because of different activation energies for exchange on these two surfaces (found to be approximately 9 kcal./mole on quartz and 17–30 kcal./mole on n-type and aluminum-doped germanium), catalysis on the germanium began to dominate at higher temperatures (about 230–280°) and the transition of the exchange on competing catalytic surfaces gave a pronounced non-linear Arrhenius temperature dependence (Fig. 1). The over-all rate data were corrected for this catalytic exchange on quartz[17] and first-order rate constants per unit area of germanium surface were calculated.

The catalysis of the hydrogen–deuterium exchange by aluminum-doped germanium was similar not to that by germanium doped with other Group III impurity atoms, but rather to that by n-type germanium (Fig. 1). That aluminum-doped germanium should show a behavior atypical of Group III impurity atoms is not entirely unexpected, inasmuch as aluminum in silicon has been shown to produce n-type donor complexes,[18] and Schwab[4b] already has reported unique behavior of other aluminum-containing semiconductor catalysts.

For the formic acid decomposition, as with the exchange, background corrections for reaction on quartz walls were necessary. The corrected rates revealed that no significant dehydrogenation had occurred on n-type germanium. Dehydrogenation on p-type germanium did not conform to first- or second-order kinetics, but did obey zero-order kinetics (up to 30% decomposition) since the initial rate was independent of the original pressure of formic acid. Decompositions from 50 to 80% were required to obtain sufficient product for gas chromatographic analysis, and although deviations from zero-order behavior occurred in this region, the data could be empirically adjusted to yield consistent rate constants. In experiments using copper in place of germanium, activation energies,

(11) We are indebted to Mr. Paul Dake and his group at the Oak Ridge Gaseous Diffusion Plant for these measurements.

(12) L. H. Horsley, *Anal. Chem.*, **19**, 508 (1947).

(13) H. N. Barham and L. W. Clark, *J. Am. Chem. Soc.*, **73**, 4638 (1951).

(14) J. Timmermans, "Physico-Chemical Constants of Pure Organic Compounds," Elsevier Publishing Co., New York, N. Y., 1960, p. 379.

(15) We are indebted to Mr. W. D. Harman and his group of the Special Testing Department, Isotope Analysis Section, Y-12 Plant, for these analyses.

(16) Summarized by H. W. Woolley, R. B. Scott, and F. G. Brickwedde, *J. Res. Natl. Bur. Standards*, **41**, 379 (1948).

(17) The exchange rate on our quartz ampoules is given approximately by the equation $\log k = 4.7 - 2000/T$, where k is in units of hr.$^{-1}$ m.$^{-2}$ (geometric area).

(18) C. S. Fuller, *Chem. Rev.*, **59**, 83 (1959).

decomposition kinetics, and products agreed with previously reported results,[19] and thus support the validity of the experimental technique.

All data were fitted to the Arrhenius equation by the method of least squares. From the variance of the slope, the range of the activation energies at the 80% confidence level, $(E_a)_{0.8}$, was calculated.

H_2–D_2 Exchange.—The values of the constants in the Arrhenius equation, obtained by least-squares analysis of corrected rate data, are plotted in Fig. 2 *vs.* the logarithm of the concentration of impurity atom. The abscissa represents also the Fermi level, since the impurity atoms are essentially completely ionized at the temperatures used. The germanium containing 10^{15} Ga atoms/cc. behaves as an intrinsic semiconductor above about 130°.

The energy of activation of the exchange, E_a, was found to vary linearly with the logarithm of the frequency factor, A. The relative values do not result in complete compensation but produce an increase in rate constant from highly doped n-type through intrinsic to highly doped p-type germanium, as seen in Fig. 2 for the log k curve at 500°K. Rates at 450 and 550°K. show trends similar to those at 500°K., but displaced to lower and higher values, respectively.

HCOOH Decomposition.—Decomposition of formic acid according to eq. 1 produces equal amounts of H_2 and CO_2. The ratio H_2/CO_2 was observed to be unity in the gas phase for all decompositions except those on p-type germanium, where this ratio was consistently less than unity. This result probably was due to retention of some of the stoichiometric hydrogen by the p-type germanium during the process of dehydrogenation on its surface. The possibility of a simultaneous additional path of decomposition which would produce an over-all ratio $H_2/CO_2 < 1$, such as

$$2HCOOH \longrightarrow CO_2 + H_2O + HCHO \qquad (3)$$

was excluded by failure to find evidence, mass spectrometrically, for HCHO.

The ratio CO/CO_2 permitted the calculation of rate constants for both dehydrogenation and dehydration, eq. 1 and 2. Corrections for the non-stoichiometry of decomposition products in the gaseous samples and for the dimerization of formic acid vapor were made. The results are summarized in Table I. As with the exchange, a linear relationship exists between log A and E_a.

Based on the sensitivity of the analyses, it was estimated that $k_{CO_2} < 10$ μmoles hr.$^{-1}$ m.$^{-2}$ on n-type germanium at 500°K. Dehydrogenation is considerably faster (at least 20–400 times at 500°K.) on p-type germanium than on n-type; dehydration also is faster (~6–25 times). For p-type germanium, dehydrogenation, rather than dehydration, is the chief decomposition path.

Except in a few cases at high temperatures, there was no evidence for operation of the water gas equilibrium

$$CO_2(g) + H_2(g) \rightleftharpoons CO(g) + H_2O(g)$$

since experimental ratios of CO/CO_2 deviated in both directions and showed a temperature depen-

(19) K. Tamaru, *Trans. Faraday Soc.*, **55**, 1191 (1959).

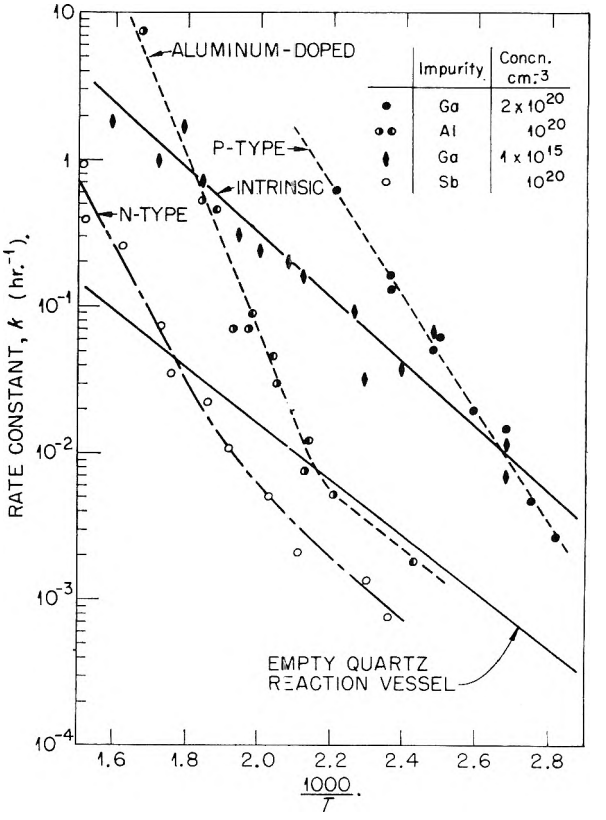

Fig. 1.—Observed rates of hydrogen–deuterium exchange on chemically doped germanium.

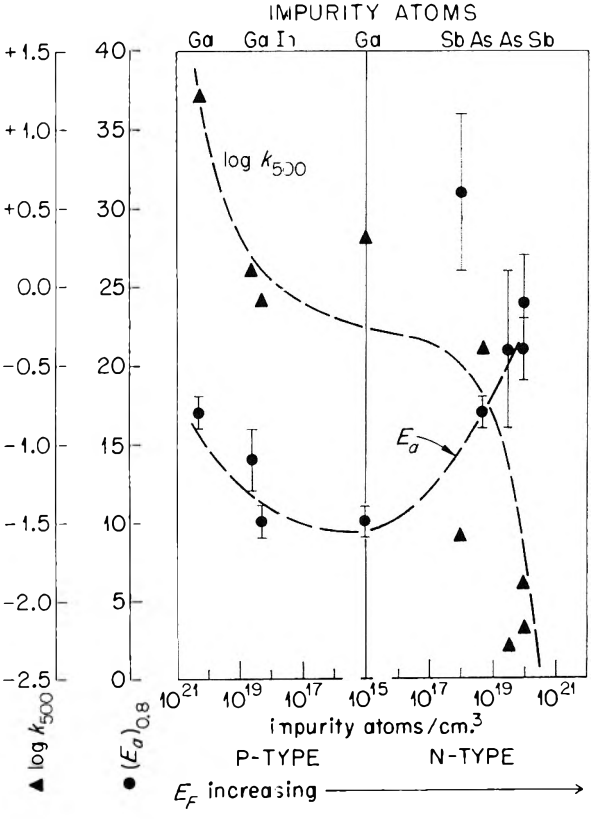

Fig. 2.—Correlation of kinetic factors of hydrogen–deuterium exchange, log k = log A − $E_a/2.3\ RT$, with Fermi level (E_F) of germanium. The rate constant at 500°K. (log k_{500}) and the limits of the values of the activation energy at the 80% confidence level ($(E_a)_{0.8}$) are shown.

TABLE I

LEAST-SQUARES VALUES FOR PARAMETERS OF THE ARRHENIUS EQUATION $\log k = \log A - E_a/2.3RT$

Semicond. type	Impurity concn. atoms/cc.		HCOOH → CO_2 + H_2			HCOOH → CO + H_2O		
			log A[a]	log k_{500}[a]	$(E_a)_{0.8}$[b]	log A[a]	log k_{500}[a]	$(E_a)_{0.8}$[b]
p	2×10^{20}	Ga	16.6	3.0	31 ± 2	10.0	1.4	20 ± 2
	4×10^{18}	Ga	15.3	2.3	30 ± 5	12.2	0.9	26 ± 5
	2×10^{18}	In	16.9	3.6	30 ± 1	11.0	1.1	23 ± 6
Intrinsic	1×10^{15}	Ga	14.2	2.3	27 ± 4	9.5	0.5	21 ± 2
n	10^{18}	Sb				9.4	.3	21 ± 3
	5×10^{18}	As		No detectable		10.1	.0	23 ± 4
	3×10^{19}	As		decomposition		8.4	− .1	20 ± 1
	10^{20}	Sb		($\log k_{500} < 1$)		7.2	.2	16 ± 2
	10^{20}	Sb				12.4	− .1	29 ± 5
Empty quartz reaction vessel			13.9	2.6	26 ± 1	11.6	1.5	23 ± 4

[a] A and k in units: μmoles hr.$^{-1}$ m.$^{-2}$. Rate data corrected for background reaction in empty quartz reaction vessel. Relative surface areas, germanium to quartz ~100. [b] In units of kcal. mole^{-1}.

dence directly opposite to that expected from the equilibrium equation. Thus, dehydrogenation and dehydration appear to be primary decomposition processes.

Discussion

The aim of these experiments was to establish whether or not the catalytic activity of germanium is affected by doping, and, hopefully, to characterize the relationship quantitatively. Such information, on the best understood semiconductor, obviously would be important to the electronic theory of catalysis, as well as a necessary preliminary to radiation experiments which we wished to carry out.

The variability of the results (shown for the activation energy in Fig. 2) is clearly too great to allow quantitative comparison with theory. This is particularly the case for n-type samples, and is a result of the very low activity in this region, and the proportionately large correction for reaction on the container. Even on the more active, p-type samples, the activity is low enough to constitute a source of imprecision.

Nevertheless, it is possible to draw the unambiguous conclusion that the activity itself is rather strongly dependent on the doping. The three points for the most p-type samples are unmistakably at much higher activity than those for the three most n-type samples. Further, each set of three involves two different doping elements, so that an influence of specific element as opposed to semiconducting character is unlikely. The points nearer to the intrinsic composition seem to scatter rather widely, but the dashed curve does not fit too badly. It is arbitrary in shape, except that the plateau is suggested by the results of Kuchaev and Boreskov,[7] who found essentially no difference in activity for p- and n-type doping up to 10^{18} atoms per cc.

Such an independence over a limited range might be explained by an insensitivity of the surface to the bulk Fermi level, a situation suggested by conductivity experiments and thought to occur in the region below 10^{18} impurity atoms per cc.[20]

The activation energy shows perhaps more clearly an influence of doping. It would be difficult to fit the data without the minimum in the curve. Here, only one point seems abnormal (10^{18} Sb atoms/cc.) and more attention to it would only accentuate the minimum. Again, as in the case of the activity itself, an independence between 10^{18} p-type and 10^{18} n-type impurity atoms can be reconciled with these data. For unexplained reasons, the Arrhenius curves from the present work (Fig. 1) are straight (after correcting for reaction on the container) rather than concave downward as found by Kuchaev and Boreskov.[7]

The minimum in activation energy implies a change from one rate-determining step to another in going from highly p-type to highly n-type samples, one step being favored by a high concentration of positive holes and the other by electrons.

HCOOH Decomposition.—Of the two paths for formic acid decomposition, the dehydration seems to be unaffected by doping, since neither the absolute activity nor the activation energy appears to vary systematically with the impurity content. The dehydrogenation is markedly sensitive to the difference between intrinsic (and p-type) germanium and n-type, but there is no large trend either of activity or of activation energy with impurity concentration on the p-side. A mechanism requiring positive holes would explain the abrupt change, since the concentration of these changes rapidly in the intrinsic region, but the lack of variation on the p-side would require some more complicated assumptions. These results agree qualitatively with those of Schwab.[4]

Acknowledgment.—The authors wish to thank Dr. James H. Crawford, Jr., of the Oak Ridge National Laboratory Solid State Division for helpful discussions.

(20) J. T. Law, in N. B. Hannay (ed.) "Semiconductors," Reinhold Publ. Corp., New York, N. Y., 1959, p. 697.

THERMAL REACTIONS OF ORGANIC NITROGEN COMPOUNDS. II. 1-*n*-BUTYLPYRROLE

BY I. A. JACOBSON, JR., AND H. B. JENSEN

Laramie Petroleum Research Center, Bureau of Mines, U.S. Department of the Interior, Laramie, Wyoming

Received November 6, 1961

Thermal reactions of 1-*n*-butylpyrrole were investigated in the 460 to 570° range by a flow method and in the 360 to 400° range by a static method. 1-*n*-Butylpyrrole isomerized to 2-*n*-butylpyrrole which then isomerized by a reversible reaction to 3-*n*-butylpyrrole. The Arrhenius equation for the isomerization of 1-*n*-butylpyrrole is $k_1 = 3.10 \times 10^{13}\, e^{-67,900 \pm 1,100/RT}$ sec.$^{-1}$. The 2- and 3-*n*-butylpyrroles decompose to form pyrrole, 2- and 3-methylpyrroles, 2- and 3-ethylpyrroles, 2- and 3-vinylpyrroles, pyridines, and hydrocarbons.

Introduction

This paper is the second resulting from a continuing study of the thermal reactions of compounds occurring in shale oil.[1] About half of the compounds in Colorado shale oil contain nitrogen, and most of these are thought to be pyridine and pyrrole types.

Only a limited amount of the literature on thermal reactions of organic nitrogen compounds deals with pyrrolic compounds,[2-7] with the majority of the pyrrole papers appearing more than 50 years ago. The only alkylpyrroles studied were methyl and ethyl substituted. The first paper of this study of shale-oil compounds described the thermal reactions of 1-methylpyrrole. To obtain information on the thermal reactions of other alkylpyrroles, 1-*n*-butylpyrrole was selected as a moderately long straight-chain alkylpyrrole.

Experimental

Material.—1-*n*-Butylpyrrole was synthesized by the thermal decomposition of the dibutylamine salt of mucic acid[8] and was purified by distillation, refluxing with calcium hydride, and redistillation. The final product had a purity of 99.5 mole %, as determined by the freezing point method. To protect the purity of the material it was kept under either vacuum or a nitrogen atmosphere.

Apparatus.—The experimental work was performed in a flow system and a static system. The equipment used for the flow studies was the same as that previously described.[1]

For the static work the heating bath was a salt mixture with a melting point of 109°; it was composed of 40% sodium nitrite, 7% sodium nitrate, and 53% potassium nitrate. The bath was heated by two electric heaters controlled so that the bath temperature was maintained within ±5° of the desired temperature. The reaction vessel was a 300-ml. round-bottom Pyrex flask. The flask had a neck 15 mm. o.d. and 5 cm. long, which was sealed on the end. A side arm, 7 mm. o.d., was attached at right angles to the neck of the flask. This sidearm ended in a "T," and one arm of the "T" was sealed to form a sample well 5 cm. long. The other arm of the "T" was used to introduce the sample and to evacuate the flask.

Procedure.—Flow studies were performed using the general procedure previously described.[1] Flow runs were made between 460 and 570°; several residence times were used at each temperature studied. Most of the runs were made in the presence of a diluent gas (purified nitrogen) and in an unpacked reaction tube. Runs also were made without the diluent gas, or in a packed reaction tube, or with added nitric oxide. For all flow runs the products were passed through a liquid nitrogen trap. The product that did not condense was collected in an evacuated gas bulb. After the completion of a run the gaseous material that was condensed in the liquid nitrogen trap was collected in another evacuated gas bulb by raising the temperature of the frozen products to room temperature.

The reaction vessel for the static work was flushed with purified nitrogen, and 0.5 g. of sample was introduced into the sample well from a hypodermic syringe. The sample then was degassed by the freeze–thaw technique, and the flask was evacuated and sealed. The flask containing the sample was immersed in the salt bath for a predetermined time. Static runs were made between 360 and 400°, with several residence times used at each of the temperatures studied.

Analysis.—For the flow work the following analytical techniques were used: (1) Unreacted 1-*n*-butylpyrrole in the liquid product was determined by infrared spectroscopy. The spectra of the products in a benzene solution were run between 7.0 and 8.5 μ, and the absorbance of the 7.9 μ peak was determined. This peak is unique to 1-*n*-butylpyrrole in these reaction products. (2) Concentration of other components in the liquid product was determined by gas–liquid chromatography from the peak areas. Emergence times and sensitivities were determined for most of the components. (3) Composition of the gaseous hydrocarbons was determined by mass spectral analyses.

The products from the static runs were analyzed only for unreacted 1-*n*-butylpyrrole. The same infrared technique was used as for the flow work.

Results

General.—Table I, a tabulation of the data from the flow runs, lists the nitrogen-compound distribution and hydrocarbon formation. The analytical results were normalized to 100% recovery.

Residence times reported in Table I were calculated as follows: The effective volume of the end elements of the reactor was determined by the method of Hillenbrand and Kilpatrick[9] and was added to the volume of the reactor at run temperature to give the total-effective volume of the reactor; the apparent residence time was calculated by dividing the total-effective volume of the reactor by the flow rate of gaseous material entering the reactor; this apparent residence time then was corrected by the method of Brinkley[10] for the increase in flow rate due to decomposition.

Table II lists the analytical results obtained from the static runs. The residence time for each of these runs was the length of time that the reaction vessel remained in the heating bath.

Isomerization.—Table I lists the nitrogen-compound distribution in the reaction products. Pre-

(1) I. A. Jacobson, Jr., H. H. Heady, and G. U. Dinneen, *J. Phys. Chem.*, **62**, 1563 (1958).

(2) G. Ciamician and P. Magnaghi, *Ber.*, **18**, 1828 (1885).

(3) G. Ciamician and P. Silber, *ibid.*, **20**, 698 (1887).

(4) P. Crespieux and A. Pictet, *ibid.*, **28**, 1904 (1895).

(5) A. Pictet, *ibid.*, **37**, 2979 (1904); **38**, 1947 (1905).

(6) A. G. Oosterhuis and J. P. Wibaut, *Rec. trav. chim.*, **55**, 348 (1936).

(7) W. Reppe, *Ann.*, **596**, 80 (1955).

(8) L. C. Craig and R. M. Hixon, *J. Am. Chem. Soc.*, **53**, 187 (1931).

(9) T. L. Hillenbrand, Jr., and M. L. Kilpatrick, *J. Chem. Phys.*, **21**, 525 (1949).

(10) S. R. Brinkley, Jr., *Ind. Eng. Chem.*, **40**, 303 (1948).

TABLE I

COMPOSITION OF PRODUCTS FROM THE THERMAL REACTIONS OF 1-*n*-BUTYLPYRROLE USING THE FLOW SYSTEM

Temp., °C.	Cor. residence times, sec.	Product analyses, wt. % *n*-Butylpyrrole 1-	2-	3-	Pyridine	Other nitrogen products[a]	Total hydrocarbon formed
462	394.8	97.1	2.1	0.03	0.1	0.5	0.2
	325.6	95.4	3.3	.3	.1	.7	.3
483	337.5	85.7	10.3	1.2	.4	1.5	.8
	265.9	85.3	10.2	1.4	.4	1.9	.9
	189.3	89.7	7.9	.8	.3	1.2	.6
	160.5	91.2	3.5	.2	.7	2.9	1.6
501	202.9	66.6	19.3	4.1	1.1	6.5	2.4
	197.2	74.7	15.4	3.5	0.9	3.8	1.8
	165.3	73.3	15.6	3.0	.9	5.3	1.9
	108.5	78.7	12.2	1.1	.6	5.8	1.6
	56.5	84.4	7.7	1.2	.2	5.4	1.1
	48.9	89.9	6.7	.6	.2	1.9	.7
	188.6[b]	74.0	15.7	4.1	.6	4.0	1.6
	49.5[b]	86.7	6.5	1.0	.2	4.4	1.3
525	186.8	44.3	27.3	9.3	3.1	10.2	5.9
	139.1	53.5	23.3	7.2	2.3	9.1	4.7
	97.7	61.5	20.0	5.6	1.7	7.6	3.6
	48.4	69.6	14.5	1.8	1.1	9.8	3.2
550	159.7	15.0	25.2	10.8	6.4	26.0	16.7
	133.9	17.7	26.6	11.6	5.4	24.3	14.4
	98.1	26.2	28.3	11.6	4.5	18.5	10.8
	51.1	44.5	19.4	9.3	2.8	11.0	13.0
	31.5	57.5	22.3	6.4	1.9	7.9	4.0
	157.8[c]	18.7	23.2	9.5	5.9	26.4	16.4
	109.7[c]	27.1	26.6	10.8	4.6	19.2	11.6
	74.4[c]	41.3	24.2	9.0	3.2	14.7	7.7
	142.7[d]	13.5	17.7	7.8	7.0	33.2	20.9
	125.0[d]	25.6	19.7	8.1	6.0	24.6	16.1
	90.0[d]	34.3	20.1	8.3	5.1	19.5	12.7
	52.2[d]	44.0	23.1	9.0	3.5	12.4	8.0
	159.6[b]	12.7	23.7	11.5	5.6	29.2	17.2
	132.8[b]	14.1	28.8	13.4	5.7	23.7	14.3
	90.1[b]	25.6	30.3	13.2	3.8	17.4	9.8
	45.0[b]	50.2	26.0	8.8	1.8	8.4	4.6
572	99.0	4.7	11.8	5.7	8.8	42.9	26.1
	70.6	12.5	17.4	8.3	7.1	34.3	20.3
	42.8	15.6	25.9	10.8	6.0	26.3	15.5
	20.3	36.9	25.8	9.2	3.7	15.7	8.8

[a] These include 2- and 3-methylpyrroles, 2- and 3-ethylpyrroles, and 2- and 3-vinylpyrroles. [b] Runs made with added nitric oxide. [c] Runs made without nitrogen diluent gas. [d] Runs made in a packed reaction tube.

TABLE II

UNREACTED 1-*n*-BUTYLPYRROLE IN THE PRODUCTS USING THE STATIC SYSTEM

Temp., ° C.	Residence time, sec. × 10^{-4}	1-*n*-Butylpyrrole in products, wt. %
360	79.5	76.7
	44.9	87.7
	29.1	92.2
	14.2	96.3
375	27.6	78.5
	15.9	87.4
	14.8	84.9
	6.06	93.9
400	5.56	78.6
	3.36	77.6
	1.44	93.2
	.63	97.0

viously reported work on 1-methylpyrroles[1] demonstrated that the isomerization of alkyl groups from the 1- to the 2-position on a pyrrole ring was irreversible and also demonstrated the reversibility of the 2- to 3-isomerization. These data indicate that the only route by which 1-*n*-butylpyrrole disappeared was by isomerization to 2-*n*-butylpyrrole.

First-order rate equations were used for the kinetic calculations of the initial isomerization reaction, based on the disappearance of 1-*n*-butylpyrrole. The first-order rate equation

$$k_i = (1/t) \ln C_0/C_a$$

was evaluated at each temperature by a least squares method using the origin as a fixed point. Table III lists the resulting specific reaction rate constants. All composition and time data were given the same weight for the calculations. The limits shown in Table III are for 95% confidence.

The izomerization of 1-*n*-butylpyrrole was not affected by changes in run conditions. Increasing the area-to-volume ratio from 2.24 to 19.88 with-

TABLE III

SPECIFIC REACTION RATE CONSTANTS FOR THE ISOMERIZATION OF 1-*n*-BUTYLPYRROLE

Temp., ° C.	Reaction rate, k_i, sec.$^{-1}$ × 10^6
By static method	
360	0.317 ± 0.042
375	0.917 ± 0.171
400	5.16 ± 2.52
By flow method	
462	103 ± 431
483	532 ± 127
501	1820 ± 300
525	4630 ± 1170
550	12700 ± 900
572	32400 ± 9100

out affecting the isomerization rate indicates that the isomerization is a homogeneous reaction. The addition of nitric oxide had no inhibiting effect on the isomerization, showing that it is not a chain reaction. The isomerization is first order and also unimolecular, as is evidenced by the fact that the presence of the diluent gas had no effect on the isomerization. The data from all of these runs were, therefore, used to calculate the specific reaction rate constants.

Two activation energies for the isomerization reaction were calculated: (1) using only the flow-method data, and (2) using only the static-method data. The energies thus calculated showed no significant difference so data from both the flow and static work were used in evaluating the Arrhenius equation. Activation energy was calculated by a least squares method weighting the specific reaction rate constants inversely to their variances. The Arrhenius equation for the isomerization of 1-*n*-butylpyrrole was evaluated to be

$$k_i = 3.10 \times 10^{13}\, e^{-57,900 \pm 1,100/RT}\ \text{sec.}^{-1}$$

Decomposition.—The butylpyrroles decompose in a complex manner to produce pyrrole, 2- and 3-methylpyrroles, 2- and 3-ethylpyrroles, 2- and 3-vinylpyrroles, pyridine, and hydrocarbons. The absence in the products of any detectable 1-substituted pyrroles, exclusive of the starting material, is indicative that decomposition takes place after isomerization. The appearance of the decomposition products is essentially a first-order process. The decomposition was, therefore, mathematically treated as a consecutive first-order reaction.

$$\text{1-}n\text{-butylpyrrole} \xrightarrow{k_i} (\text{2-}n\text{-butylpyrrole} \rightleftharpoons \text{3-}n\text{-butylpyrrole}) \xrightarrow{k_d} \text{decomposition products}$$

Two limiting conditions were imposed for these calculations: (1) both 2- and 3-*n*-butylpyrrole decompose at the same rate, and (2) all nitrogen-containing decomposition products were grouped together and treated as a single product. For the decomposition this mathematical treatment gave the following Arrhenius equation

$$k_d = 5.48 \times 10^{13}\, e^{-59,100 \pm 21,200/RT}\ \text{sec.}^{-1}$$

The decomposition is heterogeneous, as evidenced by the increase in the amount of decomposition products when the reaction tube was packed (Table I). Nitric oxide addition produced no effect.

The appearance of pyridine in the products is of interest because of the formation of a six-membered ring from a five-membered-ring starting material. It is postulated that the pyridine is formed directly from C-butylpyrroles

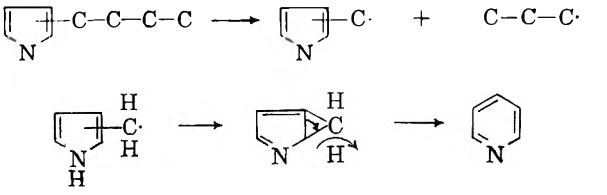

Summary.—1-*n*-Butylpyrrole isomerizes by a first-order reaction to 2-*n*-butylpyrrole, which subsequently isomerizes, by an equilibrium reaction, to 3-*n*-butylpyrrole. The isomerization reaction is not changed by packing the reactor, by eliminating the diluent gas, or by adding nitric oxide; this indicates that the reaction is unimolecular, homogeneous, and non-chain. The isomerization reaction is consistent when observed by either the flow or the static method.

The C-substituted *n*-butylpyrroles are thermally unstable and decompose to form pyrrole, 2- and 3-methylpyrroles, 2- and 3-ethylpyrroles, 2- and 3-vinylpyrroles, and pyridine. The decomposition is heterogeneous but is not affected by the addition of nitric oxide.

Acknowledgment—Thanks are extended to API Research Project 52 for the purification and purity determination of 1-*n*-butylpyrrole. The work was done under a cooperative agreement between the University of Wyoming and the Bureau of Mines, U.S. Department of the Interior.

THE CHLORIDE AND BROMIDE COMPLEXING OF SCANDIUM(III) AND YTTRIUM(III) IN AQUEOUS SOLUTION

BY ARMINE D. PAUL

Department of Chemistry, West Virginia University, Morgantown, W. Va.

Received November 16, 1961

The chloride and bromide complexing of Sc^{+3} and Y^{+3} in perchlorate solution was studied potentiometrically using concentration cells containing silver–silver halide electrodes. At 25° and an ionic strength of 0.5 *M*, the equilibrium quotients for the reactions $Sc^{+3} + Cl^- = ScCl^{+2}$, $ScCl^{+2} + Cl^- = ScCl_2^+$, $Sc^{+3} + Br^- = ScBr^{+2}$, $ScBr^{+2} + Br^- = ScBr_2^+$, $Y^{+3} + Cl^- = YCl^{+2}$, and $Y^{+3} + Br^- = YBr^{+2}$ were found to be 11.7, 10.9, 16.1, 3.3, 2.3, and 2.8, respectively. Equilibrium quotients also are given at 15 and 35°. The stability of these complexes is compared with that of other trivalent ions. The first chloride complexes of Sc^{+3} and Y^{+3} are less stable than the corresponding fluoride and bromide complexes.

The available quantitative data for the complexing of Sc^{+3} with the ligands F^-,[1] OH^-,[2] and EDTA[3] indicate that Sc^{+3} complexes are more stable than most other trivalent ions. The first fluoride complex of Sc^{+3} is more stable than that of any other trivalent ion hitherto reported.[4] The stability of the first complex of Sc^{+3} with EDTA is exceeded only by that of the corresponding complexes[5] of Co^{+3}, Fe^{+3}, In^{+3}, and V^{+3}. The first hydroxide complex of Sc^{+3} is more stable than that of the much smaller Al^{+3} ion,[4] and in addition the hydrolyzed Sc^{+3} species are polymerized.[2,6]

The unusual stability of Sc^{+3} complexes also is indicated by certain qualitative data. Vickery[7] reports the existence of $Sc(NH_3)_6^{+3}$. Pokras and Bernays,[8] upon precipitation of Sc^{+3} as the oxinate, found that the compound produced was $Sc(C_9H_6NO)_3 \cdot C_9H_7NO$ and presented evidence for the extra molecule of oxine being held by molecular forces. Kraus, Nelson, and Smith[9] report that the extraction constant of Sc^{+3} into TTA–benzene systems is larger than that of Al^{+3}, Y^{+3}, and La^{+3} by factors which range from 10^5 to 10^{11} and that the extractability of Sc^{+3} by ether from SCN^- solutions is unusually high. These authors also report that Sc^{+3} is the only element of oxidation number 3 in the series Al^{+3}, Sc^{+3}, Y^{+3}, and the rare earths which shows any adsorption on an ion-exchange resin in 12 *M* HCl and that Sc^{+3} can be separated from Y^{+3} in 12 *M* HCl by ion-exchange techniques. Fischer[10] and co-workers also observed the high solubility of $ScCl_3$ in HCl-saturated solutions of water, ether and water, and ethanol and water, and noted that this property permitted separation of Sc^{+3} from Al^{+3}, Y^{+3}, and the lanthanides.

It thus became of interest to obtain quantitative data on the chloride and bromide complexing of both Sc^{+3} and Y^{+3}. The complexing was studied potentiometrically by adding Sc^{+3} or Y^{+3} to one-half of a concentration cell, each half of which initially contained a silver–silver halide electrode and equal concentrations of $HClO_4$, $NaClO_4$, and the sodium halide.

Experimental

Solutions.—A solution of $Y(ClO_4)_3$–$HClO_4$ was prepared by dissolving 99.9% minimum purity Y_2O_3 obtained from the Fielding Chemical Co. in a known quantity of $HClO_4$. Analysis of the solution is described elsewhere.[11]

A solution of $Sc(ClO_4)_3$–$HClO_4$ was prepared by dissolving 99.9% minimum purity Sc_2O_3 obtained from the City Chemical Co. in a known quantity of $HClO_4$. Analysis of the solution is described in ref. 1.

The preparation and standardization of solutions of $HClO_4$ and $NaClO_4$ also are described in ref. 1.

Solutions of NaCl and NaBr were prepared by dissolving weighed amounts of the dried reagent grade salts in distilled water.

Electrodes.—The electrodes were prepared according to the method of Harned.[12] Both the Ag–AgCl and Ag–AgBr electrodes responded rapidly and reproducibly when tested in halide solutions of various concentrations. The Ag–AgCl electrodes were checked in 1 *M* KCl against a normal calomel electrode at 25°. E^0 for different Ag–AgCl electrodes ranged from −0.2220 to −0.2221 v.

The Ag–AgBr electrodes were compared with the Ag–AgCl electrodes in a buffered boric acid solution at 25° according to the method of Owen.[13] Using an Ag–AgCl electrode for which E^0 was −0.2220 v., E^0 for the Ag–AgBr electrodes ranged from 0.0699–0.0701 v.

Apparatus.—The cells and measuring apparatus are described in ref. 1 and 2.

Procedure.—Two half-cells were prepared, each containing the same initial concentrations of $HClO_4$ and sodium halide and enough $NaClO_4$ to make the ionic strength 0.50 *M*. The volumes of solution in each half-cell were the same. Each half-cell contained a silver–silver halide electrode. The half-cells were connected by a sodium perchlorate–agar agar salt bridge.

After the initial zero potentials (less than 0.05 mv.) became constant, a known volume of standard $Y(ClO_4)_3$–$HClO_4$ or $Sc(ClO_4)_3$–$HClO_4$ was added to one half-cell. To the other half-cell was added an equal volume of an $HClO_4$–$NaClO_4$ solution equivalent to the Y^{+3} or Sc^{+3} solution in acidity and ionic strength. The potential of the cell was measured after each addition.

Data and Calculations

Three experiments were performed at 15, 25, and 35° for each reaction. The halide concentra-

(1) J. W. Kury, A. D. Paul, L. G. Hepler, and R. E. Connick, *J. Am. Chem. Soc.*, **81**, 4185 (1959).

(2) M. Kilpatrick and L. Pokras, *J. Electrochem. Soc.*, **100**, 85 (1953).

(3) G. Schwarzenbach, R. Gut, and G. Anderegg, *Helv. Chim. Acta*, **37**, 937 (1954).

(4) J. Bjerrum, G. Schwarzenbach, and L. G. Sillén, "Stability Constants of Metal-ion Complexes, with Solubility Products of Inorganic Substances. Part II: Inorganic Ligands," The Chemical Society, London, 1958.

(5) J. Bjerrum, G. Schwarzenbach, and L. G. Sillén, "Stability Constants of Metal-ion Complexes with Solubility Products of Inorganic Substances. Part I: Organic Ligands," The Chemical Society, London, 1957.

(6) G. Biederman, M. Kilpatrick, L. Pokras, and L. G. Sillén, *Acta Chem. Scand.*, **10**, 1327 (1957).

(7) R. C. Vickery, *J. Chem. Soc.*, 255 (1955).

(8) L. Pokras and P. M. Bernays, *J. Am. Chem. Soc.*, **73**, 7 (1951).

(9) K. A. Kraus, F. Nelson, and G. W. Smith, *J. Phys. Chem.*, **58**, 11 (1954).

(10) W. Fischer, J. Wernet, and M. Zumbusch-Pfisterer, *Z. anorg. Chem.*, **258**, 157 (1949).

(11) A. D. Paul, L. S. Gallo, and J. B. VanCamp, *J. Phys. Chem.*, **65**, 441 (1961).

(12) H. S. Harned, *J. Am. Chem. Soc.*, **51**, 416 (1929).

(13) B. B. Owen, *ibid.*, **57**, 1526 (1935).

TABLE I

VOLTAGES FOR EXPERIMENT 1

Initial concn.: NaCl = 0.005085 *M*, NaBr = 0.005000 *M*, $HClO_4$ = 0.03987 *M*

Ml. $M(ClO_4)_3$–$HClO_4$ added to half-cell B	ΔE (mv.) Sc^{+3}–Cl^-			ΔE (mv.) Sc^{+3}–Br^-			ΔE (mv.) Y^{+3}–Cl^-			ΔE (mv.) Y^{+3}–Br^-		
	15°	25°	35°	15°	25°	35°	15°	25°	35°	15°	25°	35°
0.9788	0.59	0.44	0.48	0.60	0.64	0.56	0.13	0.15	0.12	0.13	0.12	0.11
1.958	1.12	0.93	0.91	1.23	1.26	1.20	.22	.24	.23	.28	.25	.22
2.936	1.62	1.45	1.31	1.86	1.86	1.81	.33	.32	.33	.43	.40	.34
3.915	2.11	1.90	1.69	2.50	2.46	2.42	.45	.42	.40	.57	.56	.45
4.894	2.60	2.34	2.05	3.17	3.03	3.01	.56	.53	.49	.70	.71	.58
5.873	3.08	2.73	2.40	3.78	3.57	3.55	.65	.65	.58	.84	.84	.70
6.852	3.53	3.10	2.76	4.31	4.14	4.05	.74	.76	.67	.98	.92	.82
7.830	3.95	3.47	3.11	4.80	4.70	4.53	.83	.85	.76	1.11	1.03	.92
8.809	4.32	3.84	3.45	5.23	5.26	4.97	.93	.95	.86	1.23	1.14	1.02
9.979	4.69	4.22	3.80	5.66	5.82	5.40	1.03	1.04	.94	1.33	1.27	1.12
10.767	5.07	4.58	4.14	6.19	6.15	5.85	1.13	1.13	1.01	1.43	1.40	1.21
11.746	5.50	4.96	4.48	6.61	6.48	6.29	1.22	1.22	1.09	1.54	1.52	1.30
12.724	5.89	5.33	4.82	7.03	6.91	6.73	1.31	1.29	1.17	1.65	1.62	1.39
13.703	6.18	5.69		7.44			1.39	1.37	1.25	1.76	1.71	1.48
14.682	6.56	6.06		7.85			1.46	1.45	1.33	1.87	1.82	1.57
15.661	6.95	6.42		8.25			1.52	1.54	1.42	1.98		1.66

TABLE II

VOLTAGES FOR EXPERIMENT 2

Initial concn.: NaCl = 0.01017 *M*, NaBr = 0.01000 *M*, $HClO_4$ = 0.09668 *M*

Ml. $M(ClO_4)_3$–$HClO_4$ added to half-cell B	ΔE (mv.) Sc^{+3}–Cl^-			ΔE (mv.) Sc^{+3}–Br^-			ΔE (mv.) Y^{+3}–Cl^-			ΔE (mv.) Y^{+3}–Br^-		
	15°	25°	35°	15°	25°	35°	15°	25°	35°	15°	25°	35°
0.9788	0.49	0.45	0.45	0.54	0.65	0.71	0.11	0.11	0.11	0.14	0.13	0.13
1.9576	0.99	0.92	0.87	1.15	1.22	1.31	.22	.21	.22	.27	.26	.25
2.9364	1.51	1.40	1.23	1.70	1.79	1.82	.33	.31	.32	.42	.40	.37
3.9152	2.02	1.75	1.57	2.32	2.34	2.35	.43	.42	.41	.56	.54	.48
4.8940	2.50	2.15	1.93	2.97	2.87	2.87	.54	.53	.50	.70	.67	.58
5.8728	2.94	2.63	2.30	3.57	3.42	3.39	.64	.63	.60	.83	.81	.69
6.8516	3.35	3.02	2.67	4.05	3.94	3.82	.74	.73	.69	.96	.93	.79
7.8304	3.77	3.43	3.05	4.51	4.44	4.26	.82	.84	.76	1.09	1.05	.89
8.8092	4.18	3.74	3.41	4.97	4.93	4.67	.92	.95	.84	1.21	1.17	1.00
9.7788	4.58	4.05	3.73	5.42	5.37	5.09	1.01	1.05	0.92	1.31	1.27	1.10
10.767	4.96	4.36	4.00	5.83	5.78	5.60	1.09	1.15	1.00	1.41	1.39	1.19
11.746	5.31	4.66	4.26	6.33	6.18	6.05	1.18	1.24	1.08	1.51	1.50	1.29
12.724	5.63	5.02	4.51		6.55	6.48	1.27	1.32	1.17	1.61	1.60	1.39
13.703					6.90	6.93	1.36	1.40	1.25	1.71	1.70	1.49
14.682					7.24	7.38	1.45	1.45	1.32	1.82	1.79	1.57
15.661					7.56	7.83	1.54	1.50	1.40	1.95	1.88	1.66

tion and the metal ion concentration were varied approximately tenfold. For a given experiment, the initial conditions were the same at 15, 25, and 35°. For all experiments the initial volume was 100.2 ml., the concentration of $Sc(ClO_4)_3$–$HClO_4$ was Sc^{+3} = 0.1796 *M*, H^+ = 0.9123 *M*, and the concentration of $Y(ClO_4)_3$–$HClO_4$ was Y^{+3} = 0.1994 *M*, H^+ = 0.1000 *M*. The experimentally determined voltages are given in Tables I, II, and III.

The initial potential of the cell before addition of M^{+3} can be represented as

$$E_i = \frac{RT}{nF} \ln \frac{(X^-)_{Ai}}{(X^-)_{Bi}} \qquad (1)$$

where $(X^-)_{Ai}$ and $(X^-)_{Bi}$ are the initial halide concentrations in moles per liter in half-cells A and B, respectively. Since the initial halide concentrations were equal, E_i should be 0, but actually was about 0.05 mv. After addition of M^{+3} to half-cell B and an equal volume of equivalent solution to half-cell A, the potential can be represented as

$$E_f = \frac{RT}{nF} \ln \frac{(X^-)_{Af}}{(X^-)_{Bf}} \qquad (2)$$

Combining eq. 1 and 2 gives

$$E_f - E_i = \Delta E = \frac{RT}{nF} \ln \frac{(X^-)_{Af}\,(X^-)_{Bi}}{(X^-)_{Ai}\,(X^-)_{Bf}} \qquad (3)$$

which upon rearrangement becomes

$$(X^-)_{Bf} = \frac{(X^-)_{Af}}{(X^-)_{Ai}} (X^-)_{Bi}\, e^{-nF\Delta E/RT} \qquad (4)$$

$(X^-)_{Af}/(X^-)_{Ai}$ can be replaced by V_i/V_f, where V_i is the initial volume in the half-cell and V_f the volume after the addition of M^{+3}, giving

$$(X^-)_{Bf} = (V_i/V_f)\,(X^-)_{Bi}\, e^{-nF\Delta E/RT} \qquad (5)$$

$(X^-)_{Bf}$ represents the uncomplexed halide ion in the half-cell containing M^{+3}. Subtraction of $(X^-)_{Bf}$ from $(X^-)_{Af}$ gives (ΔX^-), the amount of halide ion complexed. If the only complexing reaction which occurs is that given in eq. 6

TABLE III

VOLTAGES FOR EXPERIMENT 3

Initial concn.: NaCl = 0.05085 M, NaBr = 0.05000 M, $HClO_4$ = 0.09668 M

Ml. $M(ClO_4)_3$–$HClO_4$ added to half-cell B	ΔE (mv.) Sc^{+3}–Cl^-			ΔE (mv.) Sc^{+3}–Br^-			ΔE (mv.) Y^{+3}–Cl^-			ΔE (mv.) Y^{+3}–Br^-		
	15°	25°	35°	15°	25°	35°	15°	25°	35°	15°	25°	35°
0.9788	0.63	0.57	0.52	0.51	0.49	0.49	0.12	0.12	0.10	0.16	0.15	0.14
1.9576	1.26	1.13	0.99	1.00	0.98	0.97	.22	.21	.20	.27	.26	.23
2.9364	1.88	1.67	1.43	1.49	1.46	1.43	.30	.31	.29	.38	.38	.34
3.9152	2.48	2.19	1.87	1.95	1.92	1.88	.40	.40	.37	.50	.50	.45
4.8940	3.05	2.70	2.32	2.43	2.40	2.31	.48	.49	.46	.62	.61	.55
5.8728	3.58	3.20	2.70	2.88	2.78	2.74	.58	.59	.55	.75	.72	.65
6.8516	4.07	3.67	3.06	3.30	3.25	3.18	.67	.68	.63	.86	.83	.75
7.8304	4.54	4.13	3.44	3.71	3.68	3.62	.76	.78	.71	.96	.94	.83
8.8092	5.00	4.54	3.82	4.11	4.05	4.05	.86	.88	.79	1.06	1.04	.92
9.7788	5.47	4.92	4.20	4.50	4.41	4.46	.95	.97	.87	1.17	1.15	1.01
10.767	5.94	5.28	4.57	4.89	4.92	4.84	1.04	1.06	.94	1.27	1.25	1.10
11.746	6.38	5.65	4.94	5.29	5.23	5.22	1.11	1.14	1.01	1.39	1.35	1.19
12.724	6.80	6.02	5.31	5.69	5.62	5.59	1.18	1.20	1.08	1.50	1.46	1.28
13.703	7.20	6.38	5.66	6.08	6.00	5.96	1.27	1.25	1.11	1.61	1.56	1.37
14.682	7.58	6.74	6.00	6.47	6.38	6.33	1.36	1.32	1.23	1.70	1.67	1.46
15.661	7.92	7.07	6.31	6.87	6.75	6.69	1.44	1.40	1.31	1.80	1.78	1.54

TABLE IV

CALCULATED VALUES FOR EXPERIMENT 1 AT 25°

Ml. $M(ClO_4)_3$–$HClO_4$ added to half-cell B	Sc^{+3}–Cl^- $(\Delta Cl^-)/(Cl^-)$ × 10^1	Sc^{+3}–Cl^- (Sc^{+3}) × 10^2	Sc^{+3}–Br^- $(\Delta Br^-)/(Br^-)$ × 10^1	Sc^{+3}–Br^- (Sc^{+3}) × 10^2	Y^{+3}–Cl^- $(\Delta Cl^-)/(Cl^-)$ × 10^2	Y^{+3}–Cl^- (Y^{+3}) × 10^2	Y^{+3}–Br^- $(\Delta Br^-)/(Br^-)$ × 10^2	Y^{+3}–Br^- (Y^{+3}) × 10^2
0.9788	0.1683	0.1658	0.2505	0.1619	0.507	0.1917	0.4520	0.1910
1.9576	.3666	.3271	.5012	.3213	0.888	.3782	0.9353	.3781
2.9364	.5797	.4851	.7527	.4782	1.216	.5627	1.564	.5611
3.9152	.7708	.6415	1.004	.6326	1.590	.7433	2.129	.7410
4.8940	.9525	.7955	1.249	.7848	2.004	.9375	2.726	.9343
5.8728	1.120	.9475	1.492	.9346	2.481	1.094	3.194	1.091
6.8516	1.270	1.096	1.747	1.080	2.897	1.265	3.531	1.262
7.8304	1.447	1.243	2.008	1.225	3.261	1.446	3.970	1.443
8.8092	1.614	1.389	2.276	1.369	3.641	1.598	4.393	1.595
9.7788	1.784	1.530	2.545	1.508	4.001	1.757	4.915	1.754
10.767	1.956	1.670	2.705	1.649	4.356	1.919	5.426	1.915
11.746	2.130	1.807	2.839	1.747	4.684	2.074	5.893	2.069
12.724	2.305	1.942	3.086	1.921	4.981	2.229	6.301	2.224
13.703	2.538	2.075			5.276	2.380	6.668	2.374
14.682	2.659	2.206			5.605	2.528	7.108	2.523
15.661	2.839	2.333			5.981	2.673		

$$M^{+3} + X^- = MX^{+2} \quad Q_1 \qquad (6)$$

for which $Q_1 = (MX^{+2})/[(M^{+3})(X^-)]$, the concentration of uncomplexed M^{+3} can be determined from stoichiometry and Q_1 can be evaluated from a plot of $(\Delta X^-)/(X^-)$ *vs.* (M^{+3}). The symbol Q is used to represent an equilibrium quotient expressed in concentrations rather than activities.

In Table IV are shown calculated values at 25° of $(\Delta X^-)/(X^-)$ and (M^{+3}) for experiment 1 in each series.

The data were plotted in the manner described above for the reactions Y^{+3}–Cl^- and Y^{+3}–Br^-. Straight lines were obtained and the points from all three experiments for each reaction fit on the respective curves indicating that only one complex was formed.

When the data were plotted in similar fashion for the reactions Sc^{+3}–Cl^- and Sc^{+3}–Br^-, only the points from expt. 1 and 2 fit on the curve. Straight lines were obtained using these points and the plots were used to evaluate Q_1, but in order to interpret expt. 3, which was performed at low (M^{+3}) and high halide concentration, it became necessary to consider the reaction

$$ScX^{+2} + X^- = ScX_2^+ \quad Q_2 \qquad (7)$$

for which $Q_2 = (ScX_2^+)/[(ScX^{+2})(X^-)]$.

The relations

$$\Sigma Sc^{+3} = (Sc^{+3}) + (ScX^{+2}) + (ScX_2^+) \qquad (8)$$

$$(\Delta X^-) = (ScX^{+2}) + 2(ScX_2^+) \qquad (9)$$

may be combined with (6) and (7) and solved simultaneously to obtain an expression for Q_2, or may be rearranged into the form

$$\frac{(\Sigma Sc^{+3})(Q_1) + (\Delta X^-)/(X^-)}{2\Sigma Sc^{+3} - (\Delta X^-)} = Q_1 + Q_1Q_2(X^-) \qquad (10)$$

If the expression on the left, which shall be called Z, is plotted *vs.* (X^-), a straight line should be obtained whose slope is Q_1Q_2 and whose intercept is Q_1.

In Table V are shown calculated values of (X^-), $(\Delta X^-)/(X^-)$, and Z for experiment 3 at 25° in the series Sc^{+3}–Cl^- and Sc^{+3}–Br^-.

The plots of the data shown in Table V show considerable scattering of points, particularly at

TABLE V

CALCULATED VALUES FOR EXPERIMENT 3 AT 25°

Ml. $M(ClO_4)_3$–$HClO_4$ added to half-cell B	Sc^{+3}–Cl^-			Sc^{+3}–Br^-		
	$(Cl^-) \times 10^2$	$(\Delta Cl^-)/(Cl^-)$	Z	$(Br^-) \times 10^2$	$(\Delta Br^-)/(Br^-)$	Z
0.9788	4.925	0.0223	17.90	4.857	0.0194	18.68
1.9576	4.773	.0449	17.90	4.720	.0389	18.65
2.9364	4.628	.0673	17.86	4.635	.0579	18.56
3.9152	4.494	.0888	17.61	4.464	.0777	18.55
4.8940	4.363	.1110	17.55	4.341	.0980	18.62
5.8728	4.239	.1327	17.44	4.237	.1144	18.23
6.8516	4.125	.1537	17.30	4.166	.1333	18.25
7.8304	4.015	.1744	17.14	4.021	.1540	18.31
8.8092	3.917	.1933	16.89	3.924	.1709	18.10
9.7788	3.824	.2110	16.64	3.836	.1873	17.96
10.767	3.737	.2282	16.36	3.727	.2110	18.11
11.746	3.652	.2459	16.23	3.649	.2259	17.96
12.724	3.568	.2640	16.11	3.564	.2443	17.93
13.703	3.487	.2822	16.01	3.480	.2632	17.92
14.682	3.410	.3000	15.91	3.381	.2833	17.95
15.661	3.339	.3169	15.81	3.324	.3002	17.90

high halide concentrations. However, the fact that the intercept is fixed by Q_1 provides a guide in drawing the straight line through the points.

In these experiments the ionic strength, which is the same in each half-cell and which is initially 0.50 M, is constantly increasing, reaching a maximum value of approximately 0.65 M. Since the corrections at highest μ were within the limits of experimental error, no corrections were made in the calculations for this variation.

Results

Table VI lists the equilibrium quotients obtained for each reaction at 15, 25, and 35°. In the last column are listed the true equilibrium constants at $\mu = 0$. The latter values were calculated using the empirical relations for activity coefficient corrections given by Rabinowitch and Stockmayer[14] and Nasanen.[15]

TABLE VI

EQUILIBRIUM QUOTIENTS

Reaction	Q, 15°	Q, 25°	Q, 35°	K, 25° (μ = 0)
$Y^{+3} + Cl^- = YCl^{+2}$	2.4 ± 0.2	2.3 ± 0.2	2.1 ± 0.2	18
$Y^{+3} + Br^- = YBr^{+2}$	3.1 ± 0.2	2.8 ± 0.2	2.5 ± 0.2	21
$Sc^{+3} + Cl^- = ScCl^{+2}$	13.9 ± 0.5	11.7 ± 0.5	10.0 ± 0.5	90
$ScCl^{+2} + Cl^- = ScCl_2^+$	12.9 ± 1.0	10.9 ± 1.0	8.2 ± 1.0	37
$Sc^{+3} + Br^- = ScBr^{+2}$	17.2 ± 0.5	16.1 ± 0.5	15.1 ± 0.5	120
$ScBr^{+2} + Br^- = ScBr_2^+$	3.5 ± 0.3	3.3 ± 0.3	3.0 ± 0.3	10

Table VII summarizes the free energy, heat, and entropy changes for the reactions at an ionic strength of 0.5 M.

Discussion

It is of interest to compare the stability of halide complexes of other trivalent metals with those obtained for Sc^{+3} and Y^{+3}. Such a comparison may be made through use of Table VIII.

The stability of Sc^{+3} and Y^{+3} halide complexes presents an unusual pattern in several respects. The unusual stability of scandium fluoride complexes already has been discussed. One can see from Table VIII that for ions other than Y^{+3} and Sc^{+3} the stability of successive complexes decreases by a factor of approximately 10. However, the second and third fluoride complexes of Y^{+3} are of equal stability and the first and second chloride complexes of Sc^{+3} are of nearly equal stability. A change in coördination number could possibly account for the equal stability of the second and third fluoride complexes of Y^{+3},[11] but hardly could account for the nearly equal stability of the first and second chloride complexes of Sc^{+3}. Scandium shows only a coördination number of six in its

TABLE VII

THERMODYNAMIC FUNCTIONS AT $\mu = 0.5$ AND 25°

Reaction	ΔF_{298}, kcal./mole	ΔH_{298}, kcal./mole	ΔS_{298}, e.u.
$Y^{+3} + Cl^- = YCl^{+2}$	−0.49 ± 0.05	−0.3 ± 0.1	−1 ± 2
$Y^{+3} + Br^- = YBr^{+2}$	−0.61 ± .05	−0.9 ± .1	−1 ± 2
$Sc^{+3} + Cl^- = ScCl^{+2}$	−1.47 ± .1	−1.5 ± .1	0 ± 2
$ScCl^{+2} + Cl^- = ScCl_2^+$	−1.4 ± 3	−1.7 ± .7	−1 ± 4
$Sc^{+3} + Br^- = ScBr^{+2}$	−1.60 ± .1	−0.5 ± .1	4 ± 2
$ScBr^{+2} + Br^- = ScBr_2^+$	−0.7 ± .1	−0.6 ± .2	0 ± 2

TABLE VIII

EQUILIBRIUM QUOTIENTS FOR TRIVALENT METAL HALIDE COMPLEXES AT 25° AND $\mu = 0.5$

Reaction	Q(X = F)	Q (X = Cl)	Q (X = Br)	Ref.
$Sc^{+3} + X^- = ScX^{+2}$	1.55×10^6	11.7	16.1	1, This work
$ScX^{+2} + X^- = ScX_2^+$	1.89×10^5	10.9	3.3	1, This work
$ScX_2^+ + X^- = ScX_3$(aq.)	1.19×10^4			1
$Y^{+3} + X^- = YX^{+2}$	8.0×10^3	2.3	2.8	11, This work
$YX^{+2} + X^- = YX_2^+$	1.6×10^3			11
$YX_2^+ + X^- = YX_3$(aq.)	1.6×10^3			11
$Fe^{+3} + X^- = FeX^{+2}$	1.5×10^5	4	0.5	14, 16
$FeX^{+2} + X^- = FeX_2^+$	8.4×10^3	1.3		14, 16
$FeX_2^+ + X^- = FeX_3$(aq.)	8.1×10^2	0.25		14, 16
$In^{+3} + X^- = InX^{+2}$	5.6×10^3	230	100	17, 18
$InX^{+2} + X^- = InX_2^+$	4.0×10^2	18.5		17

(14) E. Rabinowitch and W. H. Stockmayer, *J. Am. Chem. Soc.*, **64**, 335 (1942).

(15) R. Nasanen, *Acta Chem. Scand.*, **4**, 140, 816 (1950).

(16) R. E. Connick, L. G. Hepler, Z. Z. Hugus, Jr., J. W. Kury, W. M. Latimer, and M. Tsao, *J. Am. Chem. Soc.*, **78**, 1827 (1956).

(17) L. G. Hepler, J. W. Kury, and Z. Z. Hugus, Jr., *J. Phys. Chem.*, **58**, 26 (1954).

(18) B. C. F. Carleson and H. Irving, *J. Chem. Soc.*, 4390 (1954).

solids[19] and the radius ratio for Sc^{+3} to Cl^- of 0.46 (assuming radius of Sc^{+3} to be 0.83 Å.[20] and Cl^- to be 1.81 Å.[20]) is well over the minimum radius ratio of 0.414 proposed by Pauling[19] for coördination number 6.

Another aspect of the unusual behavior of the halide complexes of Sc^{+3} and Y^{+3} lies in the relative stabilities of the fluoride, chloride, and bromide complexes. For predominantly ionic and relatively labile complexes the stability decreases in the order $F^- > Cl^- > Br^-$, whereas in the very stable and predominately covalent complexes such as those of Hg^{+2} and the platinum metals the stability increases in the order $F^- < Cl^- < Br^-$. However, for both Sc^{+3} and Y^{+3} the first chloride complex is less stable than the first fluoride complex and the first bromide complex. These facts seem to indicate some degree of covalent bonding in Sc^{+3} and Y^{+3}, but it is difficult to see why covalent bonding should occur in halide complexes of these metals and not in halide complexes of Fe^{+3} and In^{+3}.

The cause and explanation of these phenomena are not apparent. This work brings to light another facet of the unusual behavior of Sc^{+3} pointed out in the introduction to this paper and indicates the need for further quantitative studies of the complexing of Sc^{+3} and Y^{+3} with other ligands.

(19) L. Pauling, "The Nature of the Chemical Bond." Cornell University Press, Ithaca, N. Y., 1945.

(20) R. W. G. Wyckoff, "Crystal Structure," Interscience Publishers, Inc., New York, N. Y., 1951.

THE VAPOR PRESSURE OF ZINC SELENIDE

BY W. J. WÖSTEN AND M. G. GEERS

Physics Laboratory of the National Defence Research Organization TNO, Vlakte van Waalsdorp, The Hague, Netherlands

Received November 22, 1961

The vapor pressure of ZnSe was measured between 1060 and 1393°K. The equilibrium is described by $RT \ln p_{Zn}^2 \times p_{Se_2}$ (atm.^{3}) $= -185.000 + 99.5T$ (°K.).

Introduction

Like the other II–VI compounds, ZnSe dissociates in the gas phase, according to the reaction

$$2ZnSe(s) \rightleftarrows 2Zn(g) + Se_2(g) \qquad (1)$$

This conclusion is proved by the influence of the vapor pressure of zinc and selenium on the sublimation of this compound and more directly by mass spectroscopy.[1]

If ΔH and $\Delta S_{(p=1)}$ are the enthalpy and entropy of reaction 1, the equilibrium is described by

$$-RT \ln p_{Zn}^2 \times p_{Se_2} = \Delta H - T\Delta S_{(p=1)} \qquad (2)$$

The composition of the gas phase in equilibrium with solid ZnSe can be varied within wide limits. The total pressure $p_{tot} = p_{Zn} + p_{Se_2}$ also changes in this case. However one can easily prove that p_{tot} is a minimum for $p_{Zn} = 2p_{Se_2}$ from relation 2, $p_{Zn}^2 p_{Se_2}$ = constant.

If the vapor is stoichiometric ($p_{Zn} = 2p_{Se_2}$) the total pressure of ZnSe is

$$\log (p_{Zn} + p_{Se_2}) \text{ atm.} = -\frac{\Delta H}{13.7}\frac{1}{T(°K.)} + \frac{\Delta S_{(p=1)}}{13.7} + 0.276 \qquad (3)$$

This is the minimum vapor pressure in equilibrium with solid ZnSe.

Experimental

ZnSe was prepared from the elements (99.999% pure). The elements only react in the vapor phase.

About 45.3 g. of Zn and 54.8 g. of Se were heated in an evacuated quartz tube of 25 cm. length and 4 cm. diameter. The tube was partially heated to 1000° in an electric furnace. First the selenium evaporates to the cool part of the tube. When the zinc evaporates, the reaction between the selenium and zinc vapor proceeds rapidly.

The stoichiometry of the ZnSe samples used in our work was determined. ZnSe is converted to ZnO by oxidation in air (Table I) according to the reaction: $2ZnSe + 3O_2 \rightarrow 2ZnO + 2SeO_2$.

TABLE I

ZnSe, g.	ZnO(exp.), g.	ZnO(calcd.), g.
0.3716	0.2096	0.2095

The vapor pressure of ZnSe was measured by the gas-flow method. The same equipment was used as described in our paper on the vapor pressure of CdSe.[2]

For each component in the gas the partial pressure p_i is proportional to the number of molecules n_i and with Dalton's law

$$p_{Zn} = \frac{n_{Zn}}{n_{N_2}} \times p_{N_2}$$

The apparatus was tested with CdS. The vapor pressure of CdS was measured with various gas-flow velocities (Table II). The measurements agree well with the data of Pogorely[3] and Spandau.[4]

TABLE II

T (°K.)	N_2 gas-flow, cm.^{3}/hr.	Our measurements $p_{Cd} + p_{S_2}$ (atm.)	$(p_{Cd} + p_{S_2})$(atm.) calcd. from Pogorely[3]	Spandau[4]
1062	40	2.8×10^{-4}	2.8×10^{-4}	3.6×10^{-4}
1160	20	2.38×10^{-3}	2.1×10^{-3}	2.6×10^{-3}
1160	40	1.95×10^{-3}	2.1×10^{-3}	2.6×10^{-3}
1160	160	2.08×10^{-3}	2.1×10^{-3}	2.6×10^{-3}
1160	160	2.1×10^{-3}	2.1×10^{-3}	2.6×10^{-3}

The nitrogen must be free of oxygen, otherwise free selenium is formed by the reaction

$$2ZnSe + O_2 \longrightarrow 2ZnO + Se_2 \qquad (4)$$

and this will shift the equilibrium of reaction 1.

Chemical Analysis.—The ZnSe deposited by the nitrogen flow in the collecting tube was dissolved with a few drops of

(1) (a) P. Goldfinger, M. Ackerman, and M. Jeunehomme, Techn. Rep. AF 61 (052)-19, Univ. of Brussels, 1959; (b) M. G. Inghram and J. Drowart, "Proc. Int. Sym. High Temp. Technology," McGraw-Hill Book Co., Calif., 1959, p. 219.

(2) W. J. Wösten, *J. Phys. Chem.*, **65**, 1949 (1961).

(3) A. D. Pogorely, *Russ. J. Phys. Chem.*, **22**, 731 (1948).

(4) H. Spandau and F. Klanberg, *Z. anorg. allgem. Chem.*, **295**, 309 (1958).

10 M HNO_3. This solution was transferred to a 5-ml. beaker-glass and evaporated to dryness. Then 0.15 ml. of concd. H_2SO_4 was added and again evaporated to dryness on a hot plate (250°) to drive off SeO_2 fumes.

The residue was dissolved in 1 M KCl. The concentration of Zn was determined at 31° with a polarograph against a standard zinc solution.

Results

The method of least squares was used to express the measurements of Table III in equations 2 and 3.

TABLE III

VAPOR PRESSURE OF ZnSe

No.	T, °K.	1000/T, °K.	n_{N_2}, moles	n_{Zn} 10^6, moles	p_{N_2}, atm.	$p_{Zn} \times 10^5$, atm.	$(p_{Zn} + p_{Se_2}) \times 10^5$, atm.
1	1060	0.944	0.228	1.01	0.99	0.439	0.658
2	1100	.910	.231	2.28	1.00	0.98	1.47
3	1130	.885	.230	5.81	1.01	2.51	3.76
4	1179	.848	.232	20.8	1.01	8.9	13.4
5	1208	.829	.227	36.5	1.00	15.9	23.9
6	1286	.778	.229	180	1.00	78	117
7	1327	.754	.230	351	1.00	152	228
8	1393	.717	.160	685	0.99	424	636

$$RT \ln p_{Zn}^2 \times p_{Se_2}\,(\text{atm.}^3) = -185.000 + 99.5T(°K.) \quad (2a)$$

$$\log(p_{Zn} + p_{Se_2})\,\text{atm.} = -\frac{(13.492 \pm 204)}{T(°K.)} + (7.528 \pm 0.170) \quad (3a)$$

Evaluation of these measurements gives

$\Delta H_{1220°K} = +(185 \pm 3)$ kcal./2 moles ZnSe

$\Delta S_{1220°K} = (99.5 \pm 2.3)$ kcal./°K. per 2 moles ZnSe

From these quantities the standard heat of formation H^0_{ZnSe} and the standard entropy of ZnSe, S^0_{ZnS} are calculated.

The method of calculation has been reported in a previous paper on CdSe.[2] As C_p values of ZnSe are not known, a value $\Delta C_p = -6$ cal./°K. for reaction 1 is estimated. The thermodynamic quantities for the elements have been taken from Stull and Sinke.[5]

The result is

$H^0_{ZnSe} = 47$ kcal./mole

$S^0_{ZnSe} = 14.6$ cal./°K. mole

Discussion

(a) Korneeva[6] has measured the vapor pressure of ZnSe by an effusion method.

$$\log p'_{ZnSe}\,(\text{atm.}) = -\frac{14.200}{T(°K.)} + 8.56 (913\text{–}1039°K.) \quad (5)$$

Correcting this equation for the dissociation of ZnSe with a factor, reported by McCabe[7]

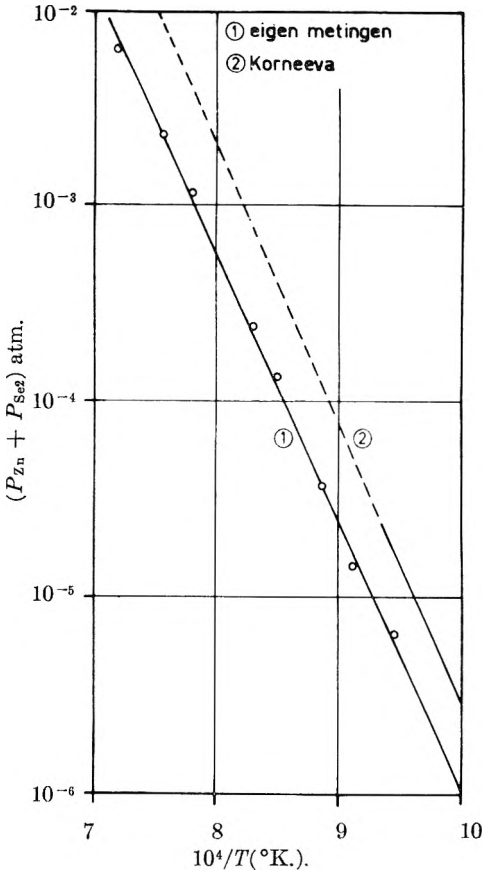

Fig. 1.—Minimum vapor pressure of ZnSe: 1, our measurements (eq. 3a); 2, corrected values of Korneeva (eq. 6).

$$\frac{3M_{Zn}^{1/6} \times M_{Se_2}^{1/6}}{2(M_{Zn} + {}^1/_2 M_{Se_2})^{1/2}}\, p'_{ZnSe} = 1.16\, p'_{ZnSe} - p_{Zn} + p_{Se_2}$$

$$\log (p_{Zn} + p_{Se_2}) = -\frac{14.200}{T(°K.)} + 8.65 \quad (6)$$

This result is plotted in Fig. 1.

The thermodynamic properties of ZnSe calculated from this equation are

$H^0_{ZnSe} = 51.1$ kcal./mole

$S^0_{ZnSe} = 9.5$ cal./°K. mole

This value of S^0_{ZnSe} is too low in comparison with the other II–VI compounds.

(b) The heat of formation calculated from our data and Korneeva's equation is much higher than the value $H^0_{ZnSe} = 34$ kcal. mentioned by Rossini.[8] Our value for $S^0_{ZnSe} = 14.6$ e.u. is reasonable in comparison with the other II–VI compounds.[8]

NOTE ADDED IN PROOF.—From eq. 3a the vapor pressure of ZnSe at the melting point (1520 ± 20°) is 1.1 atm. The melting point was determined by melting ZnSe powder in thick-walled quartz tubes.

Acknowledgment is due to the chairman of the National Defence Research Organization T.N.O. for permission to publish this paper.

(5) D. R. Stull and G. C. Sinke, "Thermodynamic Properties of the Elements," ACS Publication, 1956; see also "Thermodynamics," II Ed., by K. S. Pitzer and L. Brewer, McGraw-Hill Book Co., Inc., 1961, p. 673.

(6) J. V. Korneeva, V. V. Sokolov, and A. V. Novoselova, *Russ. J. Inorg. Chem.*, **5**, 117 (1960).

(7) C. L. McCabe, *J. Metals*, **200**, 969 (1954).

(8) F. D. Rossini, *et al.*, U. S. Bur. Stand. Circular 500, "Selected Values of Chemical Thermodynamic Constants." Series I and II.

SOLUTIONS OF ALKALI METALS IN ETHYLENEDIAMINE[1]

BY STANLEY WINDWER AND BENSON R. SUNDHEIM

Department of Chemistry, New York University, New York 3, New York

Received November 24, 1961

The electron spin resonance spectra, optical absorption spectra, and electrical conductivities of solutions of alkali metals in ethylenediamine are reported. It is concluded that the species responsible for the spin resonance is the electron (rather than the monomer), and that the light absorption is due to the monomer and dimer. Variations in line width of the spin resonance absorption reveal that the electron is not completely independent of the ionic core. The optical absorption spectrum of rubidium is distinctly different from that of sodium or potassium.

The nature of solutions of alkali metals in various liquids, such as ammonia, amines, and ethers has been a subject of continuing interest.[2] The data obtained from these systems are currently interpreted within the general framework of the Kaplan and Kittel,[3] and the Becker, Lindquist, and Alder[4] theories. Specifically, the properties of metal solutions are interpreted in terms of dynamic equilibria among various species: e^- (solvated electron), $e_2^=$ (solvated electron pair), M^+ (solvated metal ion), M (metal atom, ion pair, "monomer"), M_2 (metal dimer), and M_x (higher polymers).

It has been reported that solutions of potassium in ethylenediamine give perceptible electron spin resonance, whereas sodium solutions do not.[5] This suggests that the solvated electron is a more significant species in one solution than the other. The present work was undertaken in order to elucidate the structure of solutions of alkali metals in ethylenediamine.

I. Experimental Methods

These metal solutions resemble solutions of alkali metals in ammonia and in other amines in their metastability and sensitivity to impurities.[6] All of the steps in the preparation, handling, and measurement were carried out in scrupulously clean glass and quartz equipment under vacuum conditions. Breakseals were used in place of stopcocks and seal-offs were avoided wherever possible since the slightest outgassing has a noticeable effect in promoting the decomposition of the solutions. Even under the best of conditions, the solutions usually faded within a day or so.

A. Preparation of Materials.—The ethylenediamine (Eastman Kodak Co., 98% pure) was dried over CaO, filtered in a cellophane bag under nitrogen, refluxed with sodium overnight, and then vacuum distilled through a 10-ft. column. The middle fraction was collected, Na/K alloy introduced under vacuum conditions, and the vessel repeatedly put through a cycle of shaking, freezing, evacuating, and then remelting until a permanent blue color developed. This permanent blue color was taken as a sign of purity. The ethylenediamine was then vacuum distilled into capsules for storage.

Rubidium (MacKay Company) was received in capsules. Sodium and potassium (J. T. Baker Chemical Company) were cut in the form of cubes from the centers of large chunks. In each case the metal was melted *in vacuo*, passed through a series of capillaries to remove adhering oxide films, and then distilled into the reaction vessel for use. Lithium metal was purified using a procedure similar to that developed by Evers, Young, and Panson.[7] Reagent grade sodium iodide (Fisher Scientific Company) was dried at 55° *in vacuo*, and used as such.

B. Measurements.—For electron paramagnetic resonance measurements, each freshly prepared solution was filtered through a sintered glass disk to assure the absence of metallic particles and into a capillary which then was inserted into the cavity of a Varian Associates Model V-4500 spectrometer. The spectrum was obtained at a fixed frequency of 9.5 kMc. by scanning the magnetic field. The magnetic field strength was determined by calibration with solid DPPH and dipotassium peroxylamine disulfonate solutions. Because of the difficulties in handling conducting solutions, the spin densities were determined by affixing a weighed crystal of DPPH to the outside of the capillary. The signal from this crystal appeared on the same tracing as the solutions and the (automatically) integrated peaks then could be compared directly. As few as 2×10^{13} spins could be detected in DPPH.

In order to measure the optical absorption spectra, the solutions were prepared as above, filtered into 0.1 or 1.0 mm. quartz optical cells, and observed in a specially fabricated thermostated compartment mounted in a Cary Model 14 spectrophotometer.

An electrical conductivity cell was connected to the absorption cell so that the solutions could be passed from one to the other merely by tilting the whole assembly. Gold plated electrodes were used, since they appeared to catalyze the decomposition reaction less than tungsten or platinum. The cell was mounted in a thermostated oil bath and the conductivity determined with a Jones conductivity bridge. No effect of frequency was detected. The readings of conductivity and absorptivity were carried out as functions of time and, when necessary, adjusted to the same time by linear extrapolation.

C. Analysis.—At the conclusion of each measurement, samples were isolated in previously prepared capsules. The contents of these were mixed with water and the volume of gas evolved determined with a gas buret and manometer. By determining the initial weight of the sample, the concentration of oxidizable alkali metal in the solution could be determined.

A comprehensive description of the experimental procedures can be found in the dissertation of Windwer.[8]

II. Experimental Results

A. Electron Spin Resonance Spectra.—The sodium, potassium, and rubidium solutions gave distinct electron spin resonance absorption. Lithium and cesium solutions decomposed too rapidly to be studied. The spin resonance spectra were followed as the solutions decomposed in order to examine the effect of changing concentration. No change in the g-value or line widths were found as the spin densities decreased. The experimental results are summarized in Table I.

(1) This article is based upon a dissertation submitted by Stanley Windwer to the Graduate School of Arts and Sciences of New York University in partial fulfillment of the requirements for the degree of Doctor of Philosophy, October, 1960.

(2) (a) W. L. Jolly, "Metal Ammonia Solutions" in "Progress in Inorganic Chemistry" I. Interscience Publ., New York, N. Y., 1959, p. 235–281; (b) M. C. R. Symons, *Quart. Rev.* (London), **13**, 99 (1959); (c) E. C. Evers and R. L. Kay, "Solutions of Electrolytes" in "Annual Reviews of Physical Chemistry," Annual Reviews, Inc., Palo Alto, Cal., Vol. 11, 1960, p. 21.

(3) J. Kaplan and C. Kittel, *J. Chem. Phys.*, **25**, 1429 (1953).

(4) E. Becker, R. Lindquist, and B. Alder, *ibid.*, **25**, 971 (1956).

(5) G. W. Fowles, W. R. McGregor, and M. C. R. Symons, *J. Chem. Soc.*, 3323 (1957).

(6) C. A. Kraus, *J. Chem. Educ.*, **30**, 83 (1953).

(7) E. C. Evers, A. E. Young, and A. J. Panson, *J. Am. Chem. Soc.*, **79**, 5118 (1957).

(8) See AEC Document No. 2183; see also L. C. Card No. MIC 61–707 University Microfilms, Inc., Ann Arbor, Michigan.

TABLE I

E.P.R. RESULTS

	E.p.r.	g-value	Line width, gauss
Li			
Na	pos	2.0015 ± 0.0002	0.75
K	pos	2.0016 ± .0002	<0.15
Rb	pos	2.0013 ± .0002	approx. 6.5
Cs			

B. Absorption Spectra.—The optical absorption spectra of sodium, sodium plus sodium iodide, potassium, and rubidium solutions are given in Fig. 1. The range of the spectrum examined and the absorption maxima are recorded in Table II. A quick scan of the visible range showed a peak at 6700 Å. for lithium solutions. It was not possible under these conditions to be sure of the remainder of the spectrum. Sodium solutions showed a broad maximum extending from 6500 to 6700 Å. Addition of sodium iodide to a sodium solution produced no shift in the spectrum. Potassium solutions showed a broad maximum from 6500 to 6700 Å., similar but not identical to that of sodium. During three experiments (but not during many others), a shoulder appeared at approximately 8200 Å. In order to test whether this shoulder was associated with the decomposition process, a saturated solution (approximately 2×10^{-2} *M*) which showed only the 6500–6700 Å. band was repeatedly scanned until it was colorless. A shoulder failed to appear.

TABLE II

ABSORPTION SPECTRA

Metal	Range covered	Absorption max.
Li	....	6500–6700
Na	3000–17000	6500–6700
Na + NaI	3000–17000	6500–7600
K ($\epsilon = 2.35 \times 10^4$)	3000–17000	6500–6700
Rb	3000–17000	7000
		9000
Cs	....	....

The rubidium solution shows two absorption bands, one at 7000 Å. and the other at 9000 Å., the absorptivity of the 9000 Å. band being the greater in concentrated solutions. The fading was studied as a function of time. Although both peaks decreased linearly in optical density with time, the rate of decay of the 9000 Å. band was greater than that of the 7000 Å. one. In fact, the 9000 Å. band, which had originally been the more intense, disappeared completely while the 7000 Å. band remained.

C. Electrical Conductivities of the Potassium–Ethylenediamine Solutions.—The electrical conductivities of the potassium–ethylenediamine solutions were measured in the same experiment in which their absorption spectra were determined in order to obtain a direct correlation of conductivity with absorption. The curve of specific conductivity *vs.* absorptivity is shown in Fig. 4. The resistance of a bleached solution approached a high but finite value; that is, the products of decomposition included a small amount of conducting material. Its accumulation led to an error in the conductance attributed to the zero oxidation state. The maximum value of the relative error introduced

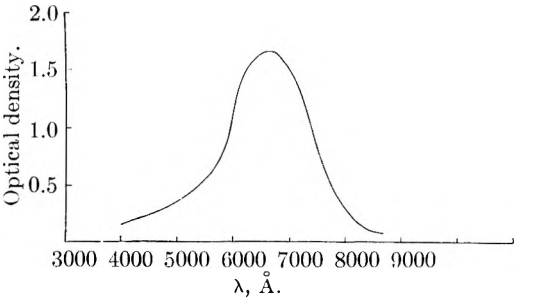

Fig. 1.—Absorption spectrum of sodium in ethylenediamine, approximately 10^{-3} *M* in a 1-mm. cell.

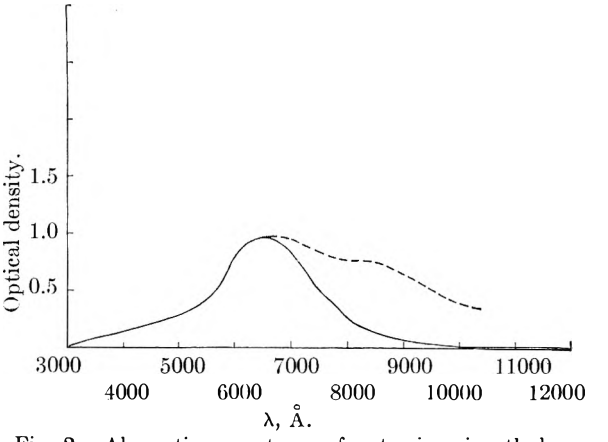

Fig. 2.—Absorption spectrum of potassium in ethylenediamine, approximately 10^{-3} *M* in a 1-mm. cell. The broken line represents absorption seen only occasionally.

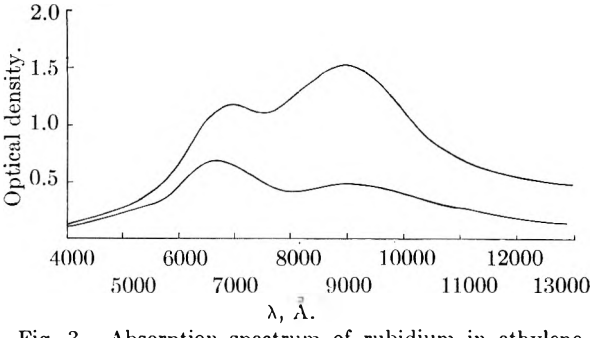

Fig. 3.—Absorption spectrum of rubidium in ethylenediamine: upper line, freshly prepared solution, approximately 10^{-3} *M* in a 1-mm. cell; lower line, after 2 hr.

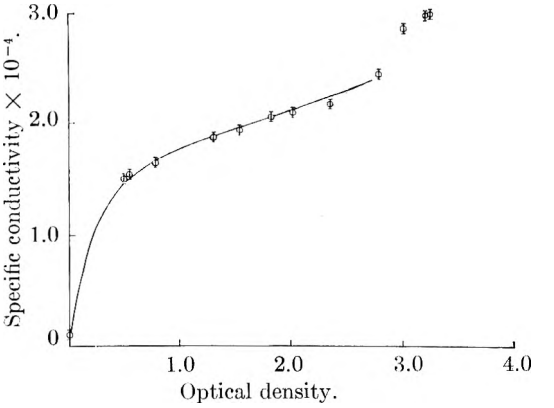

Fig. 4.—Specific conductivity of potassium in ethylenediamine *vs.* its optical density at 25°.

in this way was about 5% of the total specific conductivity in the most dilute solution studied.

III. Discussion

The magnetic data reported in this work are in conflict with those of Symons, Fowles, and McGregor.[5] They reported a weak e.p.r. signal for potassium in ethylenediamine and no e.p.r. signal for sodium solutions. We obtained a strong signal for potassium solutions and a detectable signal for sodium solutions. They did not test rubidium solutions and were unable, as we were unable, to obtain lithium solutions stable enough to observe a signal. The discrepancies between their results and ours may be attributed to a greater sensitivity of our spectrometer or perhaps to a greater purity, and hence stability, of the solutions.

The value of the spectroscopic splitting factor g found for sodium, potassium, and rubidium in ethylenediamine in this work is approximately the same as that found for potassium in liquid ammonia by Hutchinson and Pastor.[9] The values are less than the free electron value and are comparable to those found for electrons in alkali halide F centers.

Each of the line widths found for sodium, potassium, and rubidium in ethylenediamine is different. The experiment performed with sodium solutions, where the e.p.r. spectrum was scanned after different time intervals, shows that the line width is not a function of concentration. The sharpest line found in this work, that for potassium solutions, is less than 0.15 gauss in width. (This is considered to be the limit of resolution for this instrument.)

The sharpest line (0.02 gauss) ever reported for a liquid or solid is for potassium in liquid ammonia. Levy[10] explained the sharp line by "motional narrowing." This motional narrowing, which may be thought of as being due to the tumbling of the solvent molecules, would be expected to be more pronounced for symmetrical ammonia molecules than for ethylenediamine. Thus we expect the line to be somewhat broader in ethylenediamine, as indeed is the case. The different line widths (Rb > Na > K) observed for the different alkali metals in ethylenediamine presumably indicate interaction of the metal cores with the electrons.

The spin density in a 0.02 M potassium–ethylenediamine solution corresponds to approximately one free spin for every thousand metal atoms dissolved. The paramagnetic species may be either the electron or the metal atom (monomer). It is significant that only one electron spin resonance line was observed here (or indeed in any solution of this kind), and here, as elsewhere, no hyperfine splittings were seen. It would be entirely unreasonable to expect that there are in fact two lines, but that only one can be seen because they coincide exactly in their g-values. The extreme narrowness of some of the lines precludes this interpretation. The generally observed independence of line shapes and line widths of concentration and hence of ratio of monomer to electron indicates that it is not likely that there are two lines collapsed together by exchange.

In the case of moderately concentrated solutions in liquid ammonia, the high electrical conductivity[11] coupled with the high spin density[6] make certain the identification of the paramagnetic species as the electron rather than the monomer. Similar arguments apply to methylamine solutions. By analogy we conclude that the electron, rather than the monomer, is the paramagnetic species in ethylenediamine solutions and that its concentration is of the order of 0.1% of total metal concentration in the 0.02 M range.

The failure of the monomer in these systems to give detectable e.p.r. signals calls to mind the fact that no resonances are found for potassium, rubidium, and cesium metals above their melting points. The spin orbit interactions are too large in these alkali metals to produce an observable narrow line. Since the monomer is simply an expanded metal atom, a similar explanation may well apply to the absence of a detectable monomer resonance absorption.

Precise determinations of electrical conductivity as a function of concentration could not be made because of the continuous decomposition of the solutions. Instead, the conductivity was obtained as a function of optical absorptivity at the wave length of the absorption maximum.

Although the relation between conductivity and absorptivity (Fig. 4) is more or less a linear one over a considerable range, there is no doubt that a strong curvature becomes evident at very low concentrations. Onsager–Fuoss corrections to the conductance are orders of magnitude too small to be responsible for the shape of this graph. The curvature means that the concentration of the absorbing species behaves as a higher power of the stoichiometric concentration than the conducting species. In other words, the absorbing species is in a more highly associated form than the conducting species. Since there is no doubt that the conduction is due to the electron (plus unknown contribution from the positive ion), the absorbing species then may be monomer or dimer. (The e_2^- species may be ruled out because its expected contribution to the conductivity is not found.) The conclusion that the electron is involved in an associative equilibrium is strikingly reinforced by the observation, based on the e.p.r. results, that the electron is present only in small amounts in a 0.02 M solution.

Turning now to the optical absorption spectra, we note first that the absorption spectra of sodium and potassium in ethylenediamine reported in this work are in general agreement with those obtained for the same solutions by Symons, *et al.*[5] We also report the absorption spectrum of rubidium solutions.

Sodium and potassium solutions show broad maxima at 6500–6700 Å. Rubidium solutions display two maxima, one at 7000 Å., the other at 9000 Å. A shoulder near the main peak at 8200 Å. also was found in certain potassium solutions but not in others (see Fig. 2). Our considerable efforts

(9) C. A. Hutchinson and C. R. Pastor, *J. Chem. Phys.*, **21**, 1959 (1953).

(10) R. A. Levy, *Phys. Rev.*, **102**, 31 (1956).

(11) C. A. Kraus, *J. Franklin Inst.*, **212**, 537 (1931).

to establish reproducibility were unsuccessful. We have no satisfactory interpretation of this occasionally appearing additional peak. Since this shoulder was definitely absent in most cases, we consider that it does not belong to a species in dynamic equilibrium with the electron, monomer, etc., and we propose to ignore it in the discussion of the model. We note, however, that Blades and Hodgins[12] report such a shoulder at 8200 Å. for potassium solutions in methylamine and Symons, *et al.*,[5] report a similar shoulder for potassium solutions in propylenediamine. In these solvents, sodium shows only one peak at 6700 Å. Dainton, *et al.*,[13] report an infrared band at 10,000 Å. in addition to a 7000 Å. band for solutions of potassium in ethers, whereas Cafasso and Sundheim[14] only report a 7000 Å. peak for the same system.

The magnetic and optical data of both ammonia and amine solutions were interpreted by Symons, *et al.*[5] They postulated that the band near 15,000 Å. is a property of the paramagnetic species and that the visible band is a property of the diamagnetic species. Metal–ethylenediamine solutions are paramagnetic but their optical absorption spectra consist of a peak near 6700 Å. The apparent extinction coefficient of a 0.016 *M* solution of potassium in ethylenediamine is 2.35×10^4. The paramagnetic resonance results for ethylenediamine show that approximately one molecule in a thousand contributes to the spin density. The oscillator strength of this transition, if it were associated with the paramagnetic species, would have to be over 500, clearly an impossible result. Thus we may conclude that the absorption peak near 6700 A. is a property of a species which does not exhibit an e.p.r. spectrum. This result is compatible with the generalizations of Symons and co-workers, provided we postulate that the absorption spectrum of the electron is not visible for some reason.

Sodium iodide dissolves in ethylenediamine. ionizing as an electrolyte as shown by its electrical conductivity.[15] In an attempt to influence the equilibrium, sodium iodide was added to a solution of sodium in ethylenediamine and the absorption spectrum was examined for a second band. The solution did not show a marked decrease in stability and the absorption spectrum showed no second band which might be attributed to the monomer. Of course the appearance of such a band would depend on the extinction coefficient of the monomer and its dissociation constant.

The absorption spectrum of rubidium in ethylenediamine shows anomalous behavior in that a second band appeared at 9000 Å. The only other spectrum reported for rubidium in either ammonia, amines, or ethers was observed in this Laboratory in an ether.[14] This also was anomalous in that it shows one band at 9000 Å., which is displaced by 2000 Å. from the other spectra of the alkali metals in ethers.

The difference in the specific rates of decomposition of the peaks of rubidium in ethylenediamine makes it clear that at least two different species are involved. At high concentrations (see Fig. 3), the 9000 Å. band is dominant and, as the concentration decreases, it decomposes at a faster rate than the 7000 Å. peak until only the 7000 Å. peak remains at low concentrations (see Fig. 3).

It is difficult to find a reason for the unique behavior of rubidium solutions. The large magnetic moment of the rubidium nucleus might play a role in this respect. One is tempted to assign the second peak to a second species, not only here but also in methylamine. This might well be the dimer. The peak occurring infrequently in potassium solutions might be thought of as associated with the same species. The difference between rubidium and other metal solutions then would be a consequence of the somewhat different values of equilibrium constants and solubilities rather than any qualitatively different structure.

We return now to the examination of the principal peak, the one at 6500–6700 Å. A careful comparison of the various spectra leads to the conclusion that although some of the spectra are very similar, no two are really identical. The closest resemblance is between sodium and those potassium solutions which do not show a shoulder near 8000 Å. Comparison of Fig. 1 and 2 shows that the potassium spectrum has its maximum slightly to a shorter wave length than the sodium one and that its shape is slightly different. It may be argued that the difference in shape is due to a small contribution remaining from the elusive 8000 Å. peak. If this were the case, however, subtraction of the contribution from this peak would lead to more, not less, displacement of the maximum. Thus we conclude that the metal core is associated in some way with the species responsible for light absorption near 6500–6700 Å.

We note further that no absorption was detected in these solutions in the 13,000–20,000 Å. region under any circumstances. Assuming an oscillator strength near unity, any species absorbing in this region assuredly could have been detected if its concentration was as great as $^1/_{1000}$th of the stoichiometric concentration.

A comparison of the electrical conductivity of potassium in ethylenediamine with that of lithium in methylamine[16] and of sodium in liquid ammonia[6] is given in Table III. If we can assume Beer's law to hold for potassium in ethylenediamine solutions, then the equivalent conductivity calculated for potassium in ethylenediamine is similar to that for lithium in methylamine. They both are lower by an order of magnitude than that of sodium in liquid ammonia.

Evers[2c] has shown that, when one calculates the concentration of metal ions, electrons, and metals for various total metal concentrations of Li in CH_3NH_2 (using the equilibrium constants calculated from his conductivity data) in the same manner as Symons did for sodium in liquid ammonia, the electron concentration is quite low in the concentration range of 10^{-2}–10^{-3} *M*. Comparing the results obtained in amines with those in ammonia, one ob-

(12) H. Blades and J. W. Hodgins, *Can. J. Chem.*, **33**, 411 (1955).

(13) F. S. Dainton, D. M. Wiles, and A. N. Wought, *J. Chem. Soc.*, 4283 (1960).

(14) F. Cafasso and B. Sundheim, *J. Chem. Phys.*, **31**, 801 (1959).

(15) Putnam and Kolbe, *Trans. Electrochem. Soc.*, **74**, 609 (1938).

(16) D. S. Berns, E. C. Evers, and P. W. Frank, Jr., *J. Am. Chem. Soc.*, **82**, 310 (1960).

TABLE III

COMPARISON OF CONDUCTIVITY DATA

Concn. of metal, moles/l. × 10^2			Equivalent conductivity		
Ethylenediamine	Methylamine[16]	Ammonia[6]	Ethylenediamine	Methylamine[16]	Ammonia[6]
0.228	0.222	0.260	68.4	46.77	790
.654	.605	.621	29.7	32.85	699
.768	.6171	.6935	26.8	32.17	642
	.92	.9185		27.82	605
1.18	1.05		20.8	25.28	
	1.24	1.255		23.77	558

serves that the roles of the electrons and monomer have been reversed as far as being the species of prominence is concerned.

Summary

The significant results obtained in this work are in accord with the model of Becker, Lindquist, and Alder for this system.

On the basis of the magnetic data showing the similarity of g-values to those of metal–ammonia solutions, the narrowness of the line observed in potassium solutions, the independence of the line width of concentration, and the absence of hyperfine structure coupled with the arguments assigning electrons as the paramagnetic species in liquid ammonia, we conclude that the paramagnetic species in metal–ethylenediamine solutions is the electron.

The absorptivity *vs.* specific conductivity curve, the value of the extinction coefficients, and the negative result found in the sodium, sodium iodide absorption experiment show that the absorbing and conducting species are different. The absorbing species in these solutions is either the monomer or the dimer, the monomer being the most likely.

Acknowledgments.—It is a pleasure to acknowledge the generous help of Dr. Leonard Yarmus, Physics Department, N.Y.U., in making the electron spin resonance measurements. Much of this work was supported by the Atomic Energy Commission under Contract AT-30-1-1837.

THE PHOTOCHEMICAL EVOLUTION OF HYDROGEN FROM AQUEOUS SOLUTIONS OF FERROUS IONS. PART I. THE REACTION MECHANISM AT LOW pH

BY JOSHUA JORTNER AND GABRIEL STEIN

Department of Physical Chemistry, The Hebrew University, Jerusalem, Israel

Received December 6, 1961

The photochemical oxidation of ferrous ion in 0.8 N H_2SO_4 was investigated in the absence and presence of O_2. The yields of H_2 and Fe^{3+} were determined and the dependence of the quantum yield on light intensity, Fe^{2+} and Fe^{3+} concentration, and on the concentration of O_2 was investigated. The post-irradiation effect due to H_2O_2 formation was followed. The inner filter effect due to the ferric ions formed in the reaction was taken into account. As a result, a mechanism accounting for the experimental facts could be derived. The excited state resulting on light absorption yields H atoms. H atoms oxidize ferrous ions in acid solution and also react with O_2, if present. The competition between O_2 and Fe^{2+} for the H atoms formed was investigated. It appears that the direct effect of O_2 on the excited state is relatively small.

The photochemically induced oxidation of ferrous ions in aqueous solution has been the subject of several investigations, since it enables one to gain insight into the mechanism of photochemical consequences of electron transfer processes in solutions. The light absorption by the ferrous ion and the photochemical liberation of hydrogen in the absence of O_2 were investigated by Potterill, Walker, and Weiss,[1] who interpreted their results by the Franck and Haber mechanism,[2] which postulated a dissociative electron capture process by a solvent molecule. Farkas and Farkas[3] concluded that the primary absorption act involves electron transfer from the ferrous ion to a molecule of water in the primary hydration layer and as a secondary act the dissociation of the water molecule may follow. This reaction was reinvestigated by Rigg and Weiss,[4] who reported that the quantum yield was pH dependent. However, their results were not confirmed by Lefort and Douzou.[5] Recently Hayon and Weiss[6] confirmed the pH dependence. In view of these contradictions, a complete reinvestigation of this reaction appeared to be desirable.

The effect of oxygen on this reaction is of interest since it may clarify the role of H atoms formed in the system and contribute to the establishment of the complete reaction mechanism.

Experimental

Light Source.—All irradiations were carried out with a low pressure spiral mercury lamp, manufactured by Messrs. Thermal Syndicate Ltd. The lamp was run at 30–80 ma. and was fed from a stabilized a.c. supply. Variations in current to give different light output were obtained by a variable transformer in the primary circuit of a transformer feeding directly into the lamp. During irradiation small fluctuations in light intensity were corrected by manual adjustment.

Irradiation Apparatus.—A cylindrical clear fused quartz reaction vessel of 5 cm. diameter was used. The solution was stirred by a small Teflon-coated magnetic stirrer. The position of the reaction vessel which was placed inside the spiral ultraviolet lamp was kept constant by aligning a mark

(1) R. H. Potterill, O. J. Walker, and J. Weiss, *Proc. Roy. Soc.* (London), **A156**, 561 (1936).

(2) J. Franck and F. Haber, *Sitzber. Preuss. Akad. Wiss. Physik. Math. Klasse*, 250 (1941).

(3) A. Farkas and L. Farkas, *Trans. Faraday Soc.*, **34**, 1113 (1938).

(4) T. Rigg and J. Weiss, *J. Chem. Phys.*, **30**, 1194 (1952).

(5) M. Lefort and P. Douzou, *J. Chim. Phys.*, **53**, 536 (1956).

(6) E. Hayon and J. Weiss, *J. Chem. Soc.*, 3866 (1960).

on the vessel with a mark on the supporting glass tube. The distance between the lamp and reaction vessel was about 0.5 cm. The lamp and the reaction vessel were immersed in a thermostat kept at 20 ± 0.2°. As preliminary experiments indicated that light at 1850 Å. photolyzed pure 0.1 *N* sulfuric acid, the liquid in the thermostat was 0.1 *M* NaCl in triply distilled water, which cut off all light below 2000 Å. The transmittance of this filte solution at 2536 Å. did not change after 20 hr. of exposure to ultraviolet light. Light intensity was monitored by a Photovolt photomultipler unit and was held constant in the region of ±2%.

Actinometry.—The relative output of the lamp in the 2200–4000 Å. region was determined by a photoelectric cell u ing the monochromator system of a Beckman DU spectrophotometer. It was found that 90% of the total output lies at 2536 Å. Actinometry was carried out in the rea tion vessel. A 0.01 *N* uranyl oxalate actinometer solution was used.[7] The decomposition of the oxalate was held to less than 40%. The quantum yield at 2536 Å. was taken[7] as 0.60. Routine measurements of light intensity were taken after each set of experiments. It was found that the readings on the Photovolt unit were directly proportional to the lamp output as determined by chemical actinometry.

Gas Analysis.—The gas produced by photolysis was analyzed in a gas analysis instrument consisting of a modified McLeod gage. The gas ignition chamber was connected to the capillary of the gage by a stopcock. With the stopcock closed, the instrument is operated as a gage for the determination of the pressure of the gas formed. With the stopcock open, the instrument is operated as a Toepler pump to collect the gas in the ignition chamber. Hydrogen was estimated by combustion with pure oxygen on a heated platinum filament.

Procedure.—The reaction vessel was thoroughly cleaned with CrO_3–H_2SO_4, followed by nitric acid, and then finally with triply distilled water. It was stored full of triply distilled water and before irradiation it was rinsed with the solution to be irradiated. The experiments *in vacuo* were carried out when the whole system was pumped to a pressure of less than 10^{-5} mm. Twenty-five ml. of the solution was used for each irradiation. The solution was outgassed by cutting off the system from the pumps and opening the stopcock for about 30 sec. During the whole time the solution was vigorously stirred. This procedure was repeated until the uncondensable gas pressure above the solution was of the order of 10^{-5} mm. The outgassing was complete after approximately 2 hr. and losses due to evaporation were less than 0.5 ml. The reaction vessel surrounded by the lamp then was immersed in the thermostat for about 20 min. The lamp was lit preliminarily for 5 min. and afterward a metal sleeve on the vessel was lifted and the solution was irradiated. During irradiation the solution was stirred at a constant rate. After irradiation the stopcock was opened several times for about 30 sec., the water vapor was condensed in the trap, and the gas was analyzed. The reaction vessel then was disconnected and the solution analyzed.

Analysis.—Ferric ion was determined as the sulfate at 305 mμ with a Hilger Uvispek spectrophotometer. The extinction coefficient in 0.8 *N* H_2SO_4 was determined as 2175 l. mole^{-1} cm.$^{-1}$ at 24° in solutions containing less than 0.02 *M* $FeSO_4$. The temperature coefficient of the absorption was found to be 0.7% per degree, in good agreement with previous data.[8,9] The extinction coefficient depends on the total ferrous sulfate concentration and care was taken of this fact. The extinction coefficient is pH dependent. After irradiation at other acid concentrations, the final acid concentration was adjusted to 0.8 *N*.

Materials and Solutions.—Triply distilled water was prepared by redistilling distilled water from alkaline permanganate and from phosphoric acid. Ferrous ammonium sulfate, C.P., and "Analar" sulfuric acid were used without further purification. The initial ferric ion concentration of solutions containing 0.02 *M* ferrous ion did not exceed 10^{-5} *M*. Solutions at higher concentrations of ferrous ion were prepared by introducing a weighed amount of ferrous ammonium sulfate to the reaction vessel, followed by addition of the acid and immediate evacuation.

(7) E. J. Bowen, "Chemical Aspects of Light," Oxford University Press, 1946, p. 283.

(8) J. L. Haybittle, R. D. Saunders, and A. J. Swallow, *J. Chem. Phys.*, **25**, 1213 (1956).

(9) T. Rigg, W. Taylor, and J. Weiss, *ibid.*, **22**, 575 (1954).

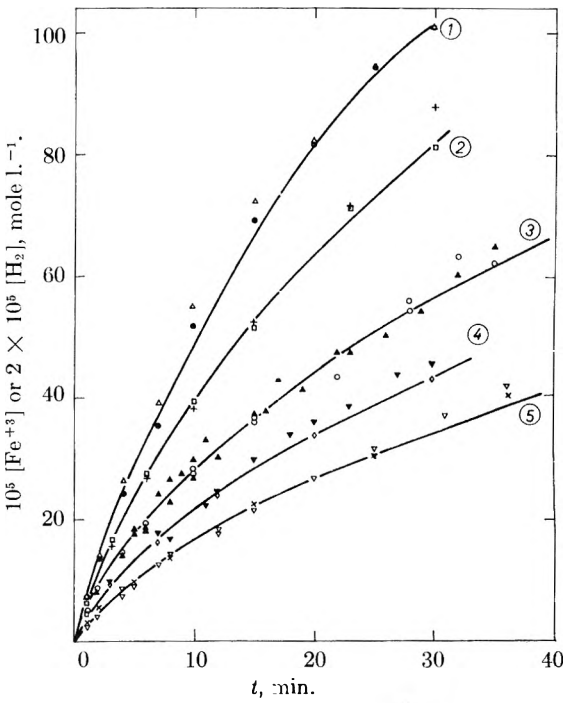

Fig. 1.—The dependence of the photooxidation yield in evacuated solutions on [Fe^{2+}] concentrations and on light intensity: [H_2SO_4] = 0.8 *N*; (1) [Fe^{2+}] = 0.102 mole l.$^{-1}$; I_0 = 4.59 × 10^{-4} einstein l.$^{-1}$ min.$^{-1}$, ●, Fe^{3+}; △, H_2. (2) [Fe^{2+}] = 0.051 mole l.$^{-1}$; I_0 = 4.59 × 10^{-4} einstein l.$^{-1}$ min.$^{-1}$, □, Fe^{3+}; +, H_2. (3) [Fe^{2+}] = 0.0204 mole l.$^{-1}$; I_0 = 4.59 × 10^{-4} einstein l.$^{-1}$ min.$^{-1}$, ○, Fe^{3+}; ▲, H_2. (4) [Fe^{2+}] = 0.0204 mole l.$^{-1}$; I_0 = 3.12 × 10^{-4} einstein l.$^{-1}$ min.$^{-1}$, ◇, Fe^{3+}; ▼, H_2. (5) [Fe^{2+}] = 0.0204 mole l.$^{-1}$; I_0 = 1.84 × 10^{-4} einstein l.$^{-1}$ min.$^{-1}$, ×, Fe^{3+}; ▽, H_2; curves calculated from eq. VI.

Results

Photochemistry in Air-Free Solutions.—The formation of ferric ion and hydrogen as a function of dose, initial ferrous ion concentration, and light intensity in 0.8 *N* H_2SO_4 solutions *in vacuo* is presented in Fig. 1. The experiments were carried out under conditions of total light absorption. The agreement with the relation $\Delta(Fe^{3+}) = 2\Delta(H_2)$ is satisfactory.

Dependence of Photochemical Yield on Irradiation Time.—The ferric yield *vs.* time plots suggest retardation by a product. As the amount of the dissolved hydrogen is negligible, the inhibition is due to Fe^{3+} ion.

The dependence of the oxidation rate on the initial ferrous ion concentration at relatively long irradiation periods (Fig. 1) suggests that a competitive reaction may be operative. In order to determine whether the rate depends on the total amount of iron oxidized or is determined by the concentration ratio of the ferrous and ferric ion, the plot of the fraction of iron oxidized against $t/[Fe^{2+}]_0$ is presented in Fig. 2, indicating that the rate depends only on the fraction of iron oxidized. It may be suggested that the fall-off of the reaction rate is due to the reduction of ferric ion by hydrogen atoms. This conclusion is not consistent with recent studies. Using ionizing radiations it was

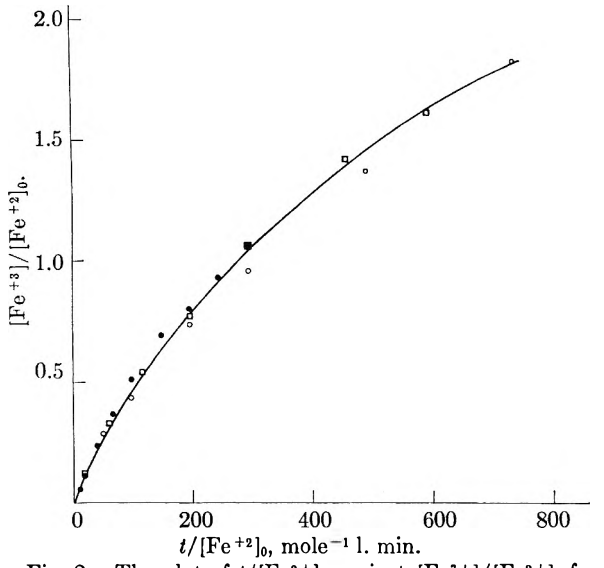

Fig. 2.—The plot of $t/[Fe^{2+}]_0$ against $[Fe^{3+}]/[Fe^{2+}]_0$ for various initial ferrous ion concentrations in evacuated solutions: ●, $[Fe^{2+}]_0 = 0.102$ mole l.$^{-1}$; □, $[Fe^{2+}]_0 = 0.051$ mole l.$^{-1}$; ○, $[Fe^{2+}]_0 = 0.0204$ mole l.$^{-1}$; curve calculated from eq. IV.

shown by Allen and Rothschild[10] that the ratio of the apparent reaction rates for reduction of ferric ion (present in various ionic forms) and oxidation of ferrous ion is 0.081 in 0.8 N H_2SO_4. Using hydrogen atoms, Czapski and Stein[11] obtained the value of 0.135 for this ratio at this pH. As in our experiments the fraction of iron oxidized did not exceed 4%, the effect of the reverse reaction is negligible in this pH region.

Since the falling off of the reaction rate is pronounced even after a relatively short irradiation period, it is very difficult to obtain reliable data for the initial photooxidation rates. This problem was solved by Rigg and Weiss[4] by drawing the limiting slopes at $t = 0$. This method is sensitive to small experimental errors in the determination of the first experimental points on the curve. We attempt to present a full calculation of the shape of the kinetic curves and to propose a more reliable method for the determination of the initial rates.

The Inner Filter Effect.—The inner filter effect is observed when more than one absorbing species is present in the photochemical system. We attribute the decrease in the oxidation rate of the ferrous ion in 0.8 N H_2SO_4 to the inner filter effect of the ferric ion. The molar extinction coefficients at 2536 Å. in 0.8 N H_2SO_4 are $\epsilon_{Fe^{2+}} = 14.8 \pm 0.15$ l. mole^{-1} cm.$^{-1}$ and $\epsilon_{Fe^{3+}} = 2850 \pm 50$ l. mole^{-1} cm.$^{-1}$; thus, this effect is appreciable.

We denote by I_0 the total absorbed light intensity and by I_a the light intensity absorbed by the ferrous ions (both in einstein l.$^{-1}$ min.$^{-1}$). Under conditions of total light absorption by the system

$$I_a = \frac{I_0}{1 + (\epsilon_{Fe^{+3}}[Fe^{+3}]/\epsilon_{Fe^{+2}}[Fe^{+2}])} \qquad (I)$$

The Reaction Mechanism.—We assume that the primary photochemical process leads to the binding of the electron in an excited state, according to

$$Fe^{+2}{}_{aq} \xrightarrow{I_a} Fe^{+2}{}_{aq}^* \qquad (1)$$

This may be followed by deactivation

$$Fe^{+2}{}_{aq}^* \xrightarrow{k_2} Fe^{+2}{}_{aq} \qquad (2)$$

or by H atom formation.

$$Fe^{+2}{}_{aq}^* \xrightarrow{k_3} Fe^{+3}{}_{aq} + OH^- + H \qquad (3)$$

Here reactions 2 and 3 are schematic only, and the actual reaction mechanism may involve dependence on ferric, ferrous, and hydrogen ions.

The hydrogen atoms formed in acid solution act as oxidizing agents for the ferrous ion. The experimental evidence from radiation chemistry[10,12-14] and from experiments on the action of hydrogen atoms on acid solutions of ferrous sulfate[11,15] in favor of this reaction is conclusive. Without considering the actual reaction mechanism and the participating species, the reaction will be schematically presented by

$$Fe^{2+}{}_{aq} + H + H^+{}_{aq} \xrightarrow{k_4} Fe^{3+}{}_{aq} + H_2 \qquad (4)$$

The hydrogen atoms formed may reduce Fe^{3+}

$$Fe^{3+}{}_{aq} + H \xrightarrow{k_5} Fe^{2+}{}_{aq} + H^+{}_{aq}^* \qquad (5)$$

or recombine

$$2H \xrightarrow{k_6} H_2 \qquad (6)$$

The possible photochemical reactions due to light absorption by the product Fe^{3+} have to be considered.[16] The amount of light absorbed by Fe^{3+} is $I_0 - I_a$

$$Fe^{3+}{}_{aq} \underset{k_7'}{\overset{I_0 - I_a}{\rightleftharpoons}} Fe^{3+}{}_{aq}^* \qquad (7)$$

followed by the possible radical formation

$$Fe^{3+}{}_{aq}^* \xrightarrow{k_8} Fe^{2+}{}_{aq} + R \qquad (8)$$

As the reaction occurs in sulfuric acid the radical R may be OH, HSO_4, and SO_4^-, which probably all act as oxidizing agents in the reaction

$$Fe^{2+}{}_{aq} + R \xrightarrow{k_9} Fe^{3+}{}_{aq} + R^- \qquad (9)$$

As the reaction was investigated at relatively high ferrous ion concentration at relatively low rate of hydrogen atom formation and at high acidity, the recombination reaction 6 can be neglected. Taking into account reactions 1–5 and 7–9 for the stationary state we obtain

$$\frac{d[Fe^{3+}]}{dt} = \frac{2k_3 I_a}{(k_2 + k_3)(1 + k_5[Fe^{3+}]/k_4[Fe^{2+}])} \qquad (II)$$

As was pointed out,[10,11] $k_5/k_4 = 0.1$ at pH 0.4; thus, at this pH the term $(k_5/k_4)[Fe^{3+}]/[Fe^{2+}]$ may be neglected under our experimental condi-

(10) A. O. Allen and W. G. Rothschild, *Radiation Res.*, **7**, 591 (1957).
(11) G. Czapski and G. Stein, *J. Phys. Chem.*, **63**, 850 (1959).
(12) T. Rigg, G. Stein, and J. Weiss, *Proc. Roy. Soc.* (London), **A211**, 375 (1952).
(13) A. O. Allen, V. D. Hogan, and W. G. Rothschild, *Radiation Res.*, **7**, 603 (1957).
(14) W. G. Rothschild and A. O. Allen, *ibid.*, **8**, 101 (1958).
(15) (a) G. Czapski and G. Stein, *Nature*, **182**, 598 (1958); (b) T. W. Davis, S. Gordon, and E. H. Hart, *J. Am. Chem. Soc.*, **80**, 4487 (1958).
(16) (a) M. G. Evans and N. Uri, *Nature*, **164**, 404 (1949); (b) J. Sadlick and A. O. Allen, *J. Am. Chem. Soc.*, **77**, 1388 (1956).

tions. For 0.8 N H_2SO_4 solution, combining eq. I and II we obtain

$$\frac{d[Fe^{3+}]}{dt} = \frac{AI_0}{1 + (\epsilon_{Fe^{3+}}[Fe^{3+}]/\epsilon_{Fe^{2+}}[Fe^{2+}])} \quad \text{(III)}$$

where $A = 2k_3/(k_2 + k_3)$

The general solution of eq. III is

$$(AI_0\, t/[Fe^{2+}]) = ([Fe^{3+}]/(Fe^{2+}]_0) - (\epsilon_{Fe^{3+}}/\epsilon_{Fe^{2+}})[([Fe^{3+}]/[Fe^{2+}]_0) + \ln (1 - [Fe^{3+}]/[Fe^{2+}]_0)] \quad \text{(IV)}$$

For low per cent of conversion, eq. IV is reduced to the form

$$AI_0t = [Fe^{3+}] + \frac{B}{2}[Fe^{3+}]^2 \quad \text{(V)}$$

where

$$B = \frac{\epsilon_{Fe^{3+}}}{\epsilon_{Fe^{2+}}[Fe^{2+}]_0}$$

The general equation for the photooxidation curve is thus

$$[Fe^{3+}] = \frac{(1 + 2BAI_0t)^{1/2} - 1}{B} \quad \text{(VI)}$$

Determination of Initial Rates.—In order to solve eq. VI, the initial rate $AI_0 = (d[Fe^{3+}]/dt)_0$ has to be determined. The determination was carried out graphically transforming eq. V to the form

$$[Fe^{+3}] = (2AI_0/B)(t/[Fe^{+3}]) - \frac{2}{B} \quad \text{(VII)}$$

The plot of the experimental results for the dependence of the photooxidation rate on the ferrous ion concentration and light intensity is presented in Fig. 3.

The linear relationship is well fulfilled within the experimental error. The intersection of the straight lines thus obtained with the $t/[Fe^{3+}]$ axis yields the value of $1/AI_0$.

Dependence of Initial Photooxidation Rate on $[Fe^{2+}]_0$.—The proposed mechanism does not include the possibility that the initial rate should be dependent on the initial ferrous concentration.

The experimental results are summarized in Table I.

TABLE I

DEPENDENCE OF INITIAL PHOTOOXIDATION RATE ON $[Fe^{2+}]_0$

Temp., 20°; $I_0 = 5.9 \times 10^{-4}$ einstein $l.^{-1}$ $min.^{-1}$

$[Fe^{2+}]_0$, mole $l.^{-1}$	B, $l.$ mole^{-1} measd. (spectroscopically)	B, $l.$ mole^{-1} calcd. from photochemical results	$AI_0 \times 10^{-4}$, mole $l.^{-1}$ $min.^{-1}$
0.0204	9450	10000	6.85 ± 0.2
.051	3780	3650	6.95 ± .2
.102	1900	1700	7.05 ± .2

A slight trend of increasing AI_0 with increasing $[Fe^{2+}]_0$ is observed. This effect may be due to the fact that the absorption of the incident light is somewhat less than 100% under our experimental conditions. These results indicate that the initial photooxidation rate does not depend greatly on the initial $[Fe^{2+}]$ concentration up to 0.1 M.

Dependence of Initial Yield on Light Intensity.—The initial quantum yield was found to be independent of the light intensity over the region 1.5–9 × 10^{-4} einstein $l.^{-1}$ $min.^{-1}$, in agreement with the theoretical considerations. The recombination reaction may indeed be neglected. We obtain for the initial quantum yield in 0.8 N H_2SO_4 *in vacuo* the value of $A = 0.148 \pm 0.010$. Our results yield that the fraction of excited ions that dissociate in 0.8 N H_2SO_4 is $k_3/(k_2 + k_3) = 0.075$, indicating the relative high efficiency of the deactivation reaction at this pH.

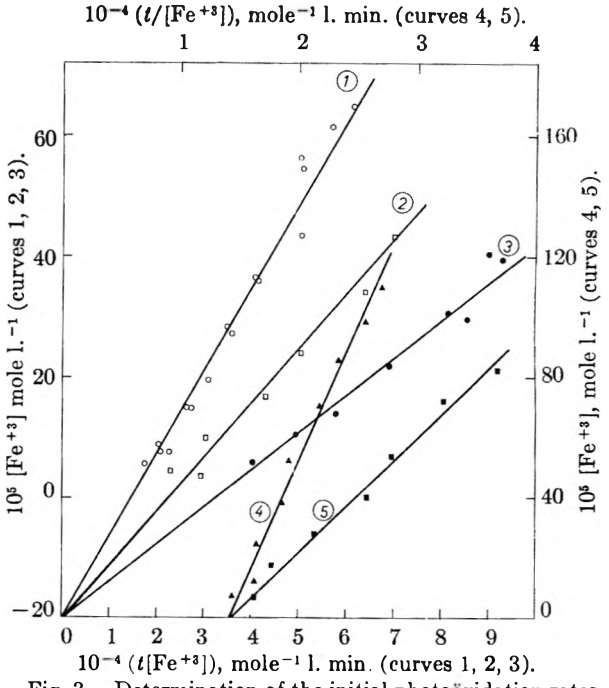

Fig. 3.—Determination of the initial photooxidation rates in evacuated solutions: H_2SO_4 = 0.8 N, according to eq. VII. (1) ○, $[Fe^{2+}]$ = 0.0204 mole $l.^{-1}$; $I_0 = 4.59 \times 10^{-4}$ einstein $l.^{-1}$ $min.^{-1}$ (2) □, $[Fe^{2+}]$ = 0.0204 mole $l.^{-1}$; $I_0 = 3.12 \times 10^{-4}$ einstein $l.^{-1}$ $min.^{-1}$. (3) ●, $[Fe^{2+}]$ = 0.0204 mole $l.^{-1}$; $I_0 = 1.84 \times 10^{-4}$ einstein $l.^{-1}$ $min.^{-1}$. (4) ▲, $[Fe^{2+}]$ = 0.102 mole $l.^{-1}$; $I_0 = 4.59 \times 10^{-4}$ einstein $l.^{-1}$ $min.^{-1}$. (5) ■, $[Fe^{2+}]$ = 0.051 mole $l.^{-1}$; $I_0 = 4.59 \times 10^{-4}$ einstein $l.^{-1}$ $min.^{-1}$.

Photochemistry in the Presence of O_2.—The plot of the experimental results for the photooxidation of aerated ferrous sulfate in 0.8 N H_2SO_4 solutions, under the conditions of total light absorption, is presented in Fig. 4. As in the case of deaerated solutions the rate depends on the fraction of iron oxidized. The results can be interpreted adequately by introduction of the correction for the inner filter effect, and can be presented by the equation

$$\frac{d[Fe^{+3}]}{dt} = \frac{A_{O_2}I_0}{1 + B[Fe^{+3}]} \quad \text{(VIII)}$$

$A_{O_2}I_0$ is the initial rate in the presence of oxygen and $B = \epsilon_{Fe^{3+}}/\epsilon_{Fe^{2+}}[Fe^{2+}]$, as before.

The initial rate was determined by the graphical method outlined above.

The Ratio of Rates of Oxidation in Air and *in vacuo*.—Some results for the observed ratio of the initial oxidation rates in the presence and absence of oxygen are presented in Table II.

TABLE II

$[Fe^{2+}]_0$	$10^4 I_0$, einstein $l.^{-1}$ $min.^{-1}$	$10^5 AI_0$ *in vacuo*	$10^5 A_{O_2}I_0$ in air	A_{O_2}/A
0.0204	4.59	6.85	13.15	1.92 ± 0.10
.051	4.59	6.95	13.15	1.89 ± .10
.0204	3.73	5.52	10.51	1.91 ± .10

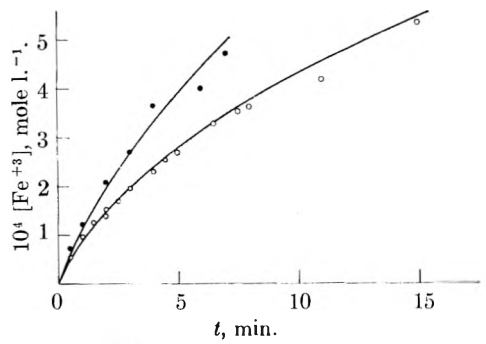

Fig. 4.—Photoöxidation curves in air saturated solutions: $[H_2SO_4] = 0.8\ N$; $I_0 = 4.59 \times 10^{-4}$ einstein l.$^{-1}$ min.$^{-1}$; O, $[Fe^{2+}] = 0.0204$ mole l.$^{-1}$; ●, $[Fe^{2+}] = 0.051$ mole l.$^{-1}$: curves calculated from eq. VIII.

We proceed now to show that this ratio of the initial yields is in agreement with the theoretical expectations.

Kinetics of Photoöxidation in Aerated Solutions.—The application of the mechanism of Rigg, Stein, and Weiss[12] to the photochemical system can be carried out assuming that the mechanism of hydrogen atom formation is identical with that *in vacuo*, including reactions 1–3 discussed above.

The hydrogen atoms formed may oxidize ferrous ions according to reaction 4 or reduce O_2

$$H + O_2 \xrightarrow{k_{10}} HO_2 \qquad (10)$$

This leads to the oxidation of three Fe^{2+} ions

$$Fe^{+2}{}_{aq} + HO_2 + H^+ \xrightarrow{k_{11}} Fe^{+3}{}_{aq} + H_2O_2 \qquad (11)$$

$$Fe^{+2}{}_{aq} + H_2O_2 \xrightarrow{k_{12}} Fe^{+3}{}_{aq} + OH^- + OH \qquad (12)$$

$$Fe^{2+}{}_{aq} + OH \xrightarrow{k_{13}} Fe^{3+}{}_{aq} + OH^- \qquad (13)$$

In this treatment reaction 5 and

$$Fe^{3+}{}_{aq} + HO_2 \xrightarrow{k_{14}} Fe^{2+}{}_{aq} + H^+{}_{aq} + O_2 \qquad (14)$$

were not included, as it appears from radiation chemical evidence[10] that in 0.8 N H_2SO_4 their influence is negligible. Steady state treatment for the intermediates Fe^{2+}*, HO_2, H_2O_2, and OH yields the result

$$\frac{d[Fe^{3+}]}{dt} = AI_a\left[1 + \frac{1}{1 + (k_1[Fe^{2+}]/k_{10}[O_2])}\right] \qquad (IX)$$

In the limiting case when the concentration ratio of ferrous ion to oxygen tends to zero the ratio of the initial rate of photoöxidation in air and *in vacuo* should approach the value of 2. The results of Table II are in agreement with this expectation.

However, it appeared that this result needed further verification. It was assumed that the presence of oxygen does not affect the mechanism of the hydrogen atom formation which is the same as *in vacuo*. The presence of oxygen may increase the yield of the hydroperoxy radicals by direct interaction of any oxygen molecule with the excited ferrous ion. Such a reaction may proceed by a charge transfer mechanism

$$Fe^{2+}{}_{aq}* + O_2 \longrightarrow Fe^{3+}{}_{aq} + O_2^- \qquad (15a)$$

or by hydrogen abstraction

$$Fe^{2+}{}_{aq}* + O_2 \longrightarrow Fe^{3+}\ OH^- + HO_2 \qquad (15b)$$

On the other hand, a deactivation process by the oxygen molecule may occur

$$Fe^{2+}{}_{aq}* + O_2 \longrightarrow Fe^{2+}{}_{aq} + O_2 \qquad (16)$$

Including these two reactions in the kinetic scheme yields the result

$$\frac{d[Fe^{3+}]}{dt} = \frac{2k_3I_a}{k_2 + k_3 + k_{16}[O_2]}\left(1 + \frac{1}{1 + (k_4[Fe^{2+}]/k_{10}[O_2])}\right) + \frac{3k_{15}I_a[O_2]}{k_2 + k_3 + k_{16}[O_2]} \qquad (X)$$

In order to investigate the contribution of these reactions it has to be established whether the oxidation rate is dependent on the ratio $[Fe^{2+}]/[O_2]$ only or also on the oxygen concentration as such.

Effect of Variable Oxygen Concentrations.—The dependence of the initial rates in oxygen-containing solutions on the ferrous and oxygen concentrations was investigated by changing $[Fe^{2+}]$ in the region 0.02–0.08 M and the oxygen concentrations in the region 0–2.3 $\times 10^{-4}$ M.

The oxygen concentration in 0.8 N H_2SO_4 solution was calculated from the solubility data[17] at 20°. A correction factor of 0.89 was introduced for solubility in 0.8 N H_2SO_4 relative to that in water.[10,17] The initial rate was obtained from the expression

$$A_{O_2}I_0 = \frac{1}{t}\left\{([Fe^{3+}]_t - [Fe^{3+}]_0) + \frac{B}{2}([Fe^{3+}]_t^2 - [Fe^{3+}]_0^2)\right\}$$

where t is the irradiation time, $[Fe^{3+}]_t$ the final ferric ion concentration, and $[Fe^{3+}]_0$ the initial Fe^{3+} concentration. The results are shown in Fig. 5 where $[Fe^{3+}]_c = A_{O_2}I_0t$, the ferric ion yield corrected for the inner filter effect.

It was found that the rate was determined solely by the concentration ratio $[Fe^{2+}]/[O_2]$. The experimental results were adequately represented by the equation

$$A_{O_2}/A = 1 + \frac{1}{1 + ([Fe^{2+}]/900[O_2])} \qquad (XI)$$

The comparison of the experimental results with the data calculated from eq. XI is in agreement within the range of ±10%. These results indicate that under the experimental conditions, the contribution of reactions 15 and 16 is negligible.

The rate constants for the competitive reactions of ferrous ion and oxygen for hydrogen atoms at 0.8 N H_2SO_4 is $k_{10}/k_4 = 900 \pm 300$. This value confirms within the range of experimental error the value of 1200 ± 300 obtained by Rothschild and Allen[14] from radiation chemical measurements in 0.8 N H_2SO_4 solution. For 0.4 M HCl solution, the results of Schwarz and Hritz[18] yield the value of $k_{10}/k_4 = 810$. There is thus agreement between the ratio of the rates obtained now from photochemistry and previously from radiation chemistry.

Post Irradiation Effect.—To verify the adequacy of the proposed mechanism we attempted to present independent evidence for the existence of H_2O_2 in solutions irradiated by ultraviolet light. At high

(17) A. Seidell, "Solubilities," D. Van Nostrand Co., New York, N. Y., 1955, p. 1355.

(18) H. A. Schwarz and J. M. Hritz, *J. Am. Chem. Soc.*, **80**, 5636 (1958).

(0.02 M) ferrous ion concentration the steady state treatment for the H_2O_2 concentration probably is justified and leads to the result for the steady state concentration of H_2O_2

$$[H_2O_2]_s = \frac{AI_a}{2k_{12}[Fe^{2+}](1 + k_4[Fe^{2+}]/k_{10}[O_2])} \quad \text{(XII)}$$

The rate constant of reaction 12 is relatively small[9,19] (k_{12} = 47 l. mole^{-1} sec.$^{-1}$, at 20°). Inserting the known values of $k_2I_a/k_2 + k_3$ and k_4/k_{10} for aerated solutions containing 0.02 M Fe^{2+}, we obtain $[H_2O_2]_s = 6 \times 10^{-7}$ M. At these high iron concentrations this amount of H_2O_2 cannot be directly identified.

The presence of hydrogen peroxide in ferrous sulfate solutions of concentration about 10^{-5} M irradiated with X-rays was demonstrated in the work of Dainton and Sutton.[20] Similar effects were observed in the present photochemical work. The experimental results were fitted to the second-order equation

$$k_{12}t = \frac{2.303}{b - a} \log \left(\frac{b}{a} \times \frac{a - x}{b - x} \right) \quad \text{(XIII)}$$

where b is the initial $[Fe^{2+}]_0$ after irradiation, $a = [Fe^{3+}]_\infty - [Fe^{3+}]_0$ = initial concentration of oxidant in eq./l., and $x = \Delta[Fe^{2+}]$.

The experimental results were in good agreement with the second-order kinetic plots. The data of Table III clearly demonstrate the kinetics of this system to be identical with that of the ferrous ion + hydrogen peroxide system.

The steady state treatment which is adequate for high ferrous ion concentrations has to be substituted by the equations

$$(d[H_2O_2]/dt) = (AI_a/2) - k_{12}[Fe^{2+}][H_2O_2] \quad \text{(XIVa)}$$

$$-(d[Fe^{2+}]/dt) = AI_a + 2k_{12}[Fe^{2+}][H_2O_2] \quad \text{(XIVb)}$$

$$\frac{d([Fe^{3+}] + 2[H_2O_2])}{dt} = 2AI_a \quad \text{(XIVc)}$$

Under the conditions of feeble light absorption, the inner filter effect can be neglected and I_a is proportional to $[Fe^{2+}]$. There is no general solution which can conveniently be applied to the experimental results and an approximate solution was used. Assuming that the ferrous ion concentration is constant, integration of eq. XIVa yields the result

$$\frac{AI_a}{2} = \frac{k_{12}[H_2O_2]_0[Fe^{2+}]}{1 - e^{-k_{12}[Fe^{2+}]t}} = [H_2O_2]_p \quad \text{(XV)}$$

where t is the irradiation time and $[Fe^{2+}]$ the mean concentration of ferrous ion during irradiation. $[H_2O_2]_p$ is the total amount in concentration units of H_2O_2 produced during irradiation, and $[H_2O_2]_0$ the amount presented at the end of the irradiation.

Hence we calculated the value of $[Fe^{3+}]_p$, the amount of Fe^{3+} produced by reactions 3 and 11

$$[Fe^{3+}]_p = [Fe^{3+}]_\infty - 2[H_2O_2]_p \quad \text{(XVI)}$$

The values of $[Fe^{3+}]_p/[H_2O_2]_p$ are presented in Table III. These results are consistent with the mechanism proposed for H_2O_2 formation from the HO_2 radical.

(19) T. J. Hardwick, *Can. J. Chem.*, **35**, 428, 437 (1957).

(20) F. S. Dainton and H. C. Sutton, *Trans. Faraday Soc.*, **49**, 1011 (1953).

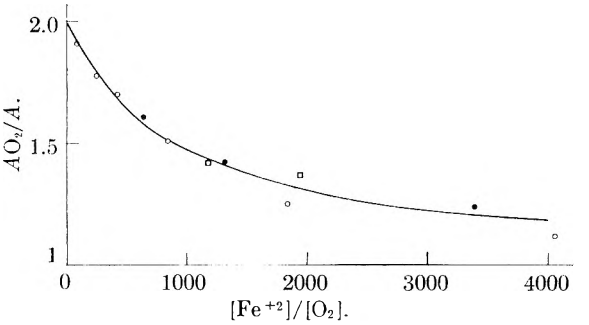

Fig. 5.—The dependence of the yield ratio AO_2/A on the concentration ratio $[Fe^{2+}]/[O_2]$; $[H_2SO_4]$ = 0.8 N: □, Fe^{2+} = 0.0816 mole l.$^{-1}$; ●, Fe^{2+} = 0.0408 mole l.$^{-1}$; ○, Fe^{2+} = 0.0204 mole l.$^{-1}$; curve calculated from eq. XI.

TABLE III

POST IRRADIATION EFFECT IN $FeSO_4$ SOLUTIONS IRRADIATED WITH ULTRAVIOLET LIGHT

Temp., °C.	t, min.	$10^5[Fe^{2+}]$ initial, M	$10^5[Fe^{2+}]$ after irradiation, M	k_{12} obsd.	k_{12} (kinetic data)	$[Fe^{3+}]_p/[H_2O_2]_p$
20°	6.0	6.0	5.02	43 ± 5	47	2.05
26°	6.0	2.4	1.81	64 ± 4	66	2.0

Throughout the whole treatment it was assumed that the light absorption by the hydrogen peroxide present can be neglected. The molar absorption coefficient of hydrogen peroxide[21,22] at 2536 Å. is ϵ = 19.6 mole^{-1} l. cm.$^{-1}$; thus, the inner filter effect of H_2O_2 will be unimportant even at low Fe^{2+} concentration.

Discussion

The results presented in this paper indicate that under our experimental conditions the major contribution to the retarding effect of the ferric ion is due to the inner filter effect. The theoretical curves, according to eq. V and VIII for evacuated and aerated solutions, were calculated using the spectroscopic values of B and the initial rates obtained by application of eq. VII. The calculated curves fit quite well with the experimental results. These conclusions are consistent with recent studies of the chemistry of hydrogen atoms in 0.8 N H_2SO_4. Another effect of the ferric ion which may be considered in the photochemical system is an electron transfer reaction from the excited ferrous ion to a ferric ion.

$$Fe^{2+}{}_{aq}{}^* + Fe^{3+}{}_{aq} \longrightarrow Fe^{3+}{}_{aq} + Fe^{2+}{}_{aq}$$

and

$$Fe^{2+}{}_{aq}{}^* + Fe^{3+}OH^- \longrightarrow Fe^{3+}OH^- + Fe^{2+}{}_{aq}$$

leading to the deactivation of the excited state. However, no evidence for such retarding effect of the ferric ion could be observed in our work.

The quantum yield is independent of the ferrous ion concentration up to 0.1 M Fe^{2+}, indicating that in this concentration region the excited state does not interact appreciably with another ferrous ion by the possible reactions

(21) R. B. Holt, C. McLane, and O. Oldenberg, *J. Chem. Phys.*, **16**, 225 (1948).

(22) J. Jortner and G. Stein, *Bull. Res. Council Israel*, **A6**, 239 (1957).

deactivation reaction: $Fe^{2+}_{aq}{}^{*} + Fe^{2+}_{aq} \longrightarrow 2Fe^{2+}_{aq}$

molecular hydrogen formation: $Fe^{2+}_{aq}{}^{*} + H^{+}_{aq} + Fe^{2+}_{aq} \longrightarrow 2\,Fe^{3+}_{aq} + H_2 + OH^-$

Besides, the reaction of the "molecular" formation of hydrogen is not consistent with the oxygen effect on the reaction mechanism.

The pronounced effect of oxygen on the rate of the photochemical oxidation is important for the elucidation of the primary photochemical process. This effect may be applied as a diagnostic criterion for hydrogen atom formation by the dissociation of the excited state. As in the case of the radiation-chemical oxidation of the ferrous ion, it appears that the photochemical system fulfills the prediction of the free radical theory where competitive scavenging reactions of the hydrogen atoms by two different solutes occur. The quantitative agreement between the photochemical and radiation-chemical results provides an additional support for the proposed mechanism. Comparison with the reactions of atomic hydrogen[11] indicates that in both systems in acid solution H atoms as such are involved.

Kinetic data derived from radiation-chemical and photochemical experiments may be compared. The application of a homogeneous kinetic treatment is justified at relatively low rates of radical formation and moderately low scavenger concentrations. This assumption is consistent with some experimental kinetic data on the reactions of hydroxyl radicals in aqueous solutions.[14,23,24]

The investigation of the photochemistry of oxygen-containing solutions yields the result that at relatively low O_2 concentrations (up to $\sim 10^{-4}$ M) the direct effect of oxygen on the excited state of the ferrous ion is negligible.

(23) T. J. Sworski, *J. Am. Chem. Soc.*, **79**, 3655 (1957).
(24) F. S. Dainton and T. J. Hardwick, *Trans. Faraday Soc.*, **53**, 333 (1957).

THE PHOTOCHEMICAL EVOLUTION OF HYDROGEN FROM AQUEOUS SOLUTIONS OF FERROUS IONS. PART II. EFFECT OF CHANGING pH

BY JOSHUA JORTNER AND GABRIEL STEIN

Department of Physical Chemistry, The Hebrew University, Jerusalem, Israel

Received December 6, 1961

The photochemistry of the ferrous ion in the presence and in the absence of oxygen was investigated in the pH region 0.35–3.0. The pH dependence of the initial quantum yield up to pH 2.5 in the presence and absence of oxygen is interpreted as arising from the dependence on H^+ ion concentration of the rate of introduction of H atoms into the bulk. This results in the dependence of the quantum yield on $\sqrt{[H^+]}$. A mechanism to account for this is proposed. Another pathway leading to the pH independent formation of H atom also is postulated. The oxidation and reduction processes of the H atoms thus formed are investigated and it is shown that the oxidation of Fe^{2+} by H atoms may proceed by way of a hydride intermediate. Specific velocity constants are derived. The results of the photochemical experiments are correlated with those obtained in radiation chemistry.

In Part I the photochemistry of aqueous Fe^{2+} solutions at a constant low pH was investigated. It was shown that the excited state of the ferrous ion yields H atoms. However, the mechanism of this photochemical formation of hydrogen atoms in ionic solution is not yet well established, and the role of H^+ ions in this process is still a matter of controversy.[1-4]

The evidence in favor of the oxidation of ions such as Fe^{2+} [5,6] or Cr^{2+} [4] by H atoms is conclusive. Again the actual oxidation mechanism is not yet finally established. The results of Rigg and Weiss[7] on the pH dependence of the quantum yield in the photooxidation of the ferrous ion were interpreted as due to the participation of the H_2^+ molecule ion in the oxidation of the ferrous ion by H atoms.[8] These results were not confirmed by Lefort and Douzou.[9] Recently the pH dependence of the initial quantum yield in the photooxidation of the chromous ion was demonstrated[4] and for Fe^{2+}, it was reconfirmed.[8]

As the basic oxidation mechanism by H atoms still is in doubt, further work on this subject appeared desirable.

(1) A. Farkas and L. Farkas, *Trans. Faraday Soc.*, **34**, 1113 (1938).
(2) J. Franck and R. L. Platzman, "Farkas Memorial Volume," Jerusalem, 1952, p. 21.
(3) J. Franck and R. L. Platzman, *Z. Physik*, **138**, 411 (1954).
(4) E. Collinson, F. S. Dainton, and M. A. Malati, *Trans. Faraday Soc.*, **55**, 209 (1959).
(5) J. Weiss, *Nature*, **165**, 728 (1950).
(6) T. Rigg, G. Stein, and J. Weiss, *Proc. Roy. Soc.* (London), **A211**, 375 (1952).
(7) T. Rigg and J. Weiss, *J. Chem. Phys.*, **30**, 1194 (1952).
(8) E. Hayon and J. Weiss, *J. Chem. Soc.*, 3866 (1960).
(9) M. Lefort and P. Douzou, *J. Chim. Phys.*, **53**, 536 (1956).

Results

The experimental technique was described in Part I. The evaluation of the initial photooxidation rates was facilitated by the introduction of the correction for the inner filter effect. The pH dependence of the molar extinction coefficient of the ferric ion and the values of B in H_2SO_4 solutions are given in Table I. The absorption of the ferrous ion was found to be independent of pH. When 0.02 M Na_2SO_4 was added to each of these solutions B remained unchanged.

Photochemistry of Aerated Solutions.—The photooxidation of aerated ferrous sulfate solutions was investigated at different values of pH. From these experimental results the values of $[Fe^{3+}]_c$—the concentrations of the ferric ion corrected for the inner filter effect—were obtained from the relation

$$[Fe^{3+}]_c = [Fe^{3+}]_t + \frac{B}{2}[Fe^{3+}]_t^2 \qquad (I)$$

These data are presented in Fig. 1. From Fig. 1

TABLE I

MOLAR ABSORPTION COEFFICIENTS OF Fe^{2+} AND Fe^{3+} IN H_2SO_4 SOLUTIONS AT 2536 Å.

Values of B calculated for $[Fe^{2+}] = 2 \times 10^{-2}$ mole^{-1} l.

$[H_2SO_4]$, N	$\epsilon_{Fe^{3+}}$ mole^{-1} l. cm.$^{-1}$	$\epsilon_{Fe^{2+}}$ mole^{-1} l. cm.$^{-1}$	B, mole^{-1} l.
0.80	2850	14.9 ± 0.2	9450
.088	2800	15.1 ± 0.2	9250
.033	2750		9000
.0088	2620	15.0 ± 0.2	8700
.0017	2300		7600

the initial yields were calculated, and are presented in Fig. 2. Inspection of these results indicates that up to pH 2.6 the photooxidation rates in aerated solutions are independent of the ferric ion concentration (after introduction of the correction for the inner filter effect). At pH 3, deviation from linearity is observed (curve 9, Fig. 1), indicating the existence of additional inhibition effect of the ferric ion.

The mechanism of the photooxidation reaction will be presented by the following scheme (keeping the notation used in Part I): excitation (1), deactivation of the excited state (2), and hydrogen atom formation (3).

The hydrogen atoms formed may react by oxidation of the ferrous ion, or by the reduction of ferric ion or oxygen (reactions 4, 5, and 10).

In these equations the nature of the actual ferric ion species reacting is not specified. It may, for example, be one of the hydrolysis products, *e.g.*, the Fe^{3+} OH^- ion pair. The hydroperoxy radical may act by the oxidation of three additional ferrous ions by the Haber–Weiss mechanism[10] as in reaction 11. HO_2 or its conjugate base O_2^- also may act as a reducing agent for the ferric ion (reaction 14).

The rate of formation of the ferric ion will be

$$\frac{d[Fe^{3+}]}{dt} = \frac{k_3 I_a}{k_2 + k_3}\left\{1 + \frac{k_4[Fe^{2+}] - k_5[Fe^{3+}]}{k_4[Fe^{2+}] + k_5[Fe^{3+}] + k_{10}[O_2]} + \frac{k_{10}[O_2](3 - k_{14}[Fe^{3+}]/k_{11}[Fe^{2+}])}{(1 + k_{14}[Fe^{3+}]/k_{11}[Fe^{2+}])(k_4[Fe^{2+}] + k_5[Fe^{3+}] + k_{10}[O_2])}\right\} \quad \text{(II)}$$

Evidence from radiation chemistry[11,12] indicates that the rate constants ratio k_{14}/k_{11} is pH dependent and at pH 2.7, $k_{14}/k_{11} = 0.3$. Thus for the initial photooxidation stages under our experimental conditions, the contribution of the competition for the HO_2 radical by the ferric ion can be neglected. Equation II then is reduced to the form

$$\frac{d[Fe^{3+}]}{dt} = AI_a\left\{\frac{2 + k_4[Fe^{2+}]/k_{10}[O_2]}{1 + (k_4[Fe^{2+}]/k_{10}[O_2]) + (k_5[Fe^{3+}]/k_{10}[O_2])}\right\} \quad \text{(III)}$$

From Fig. 1 it appears that the third term in the denominator can be neglected up to pH 2.7.

At pH 3.05, the rate constant ratio k_5/k_{10} was determined from the experimental results of curve 9 of Fig. 1. Equation III will be written in the form

$$\frac{d[Fe^{3+}]}{dt} = \frac{(1 + G)AI_0}{(1 + B[Fe^{3+}])(G + H[Fe^{3+}])} \quad \text{(IV)}$$

where

$$G = 1 + \frac{k_4[Fe^{2+}]}{k_{10}[O_2]}$$

$$H = \frac{k_5}{k_{10}[O_2]}$$

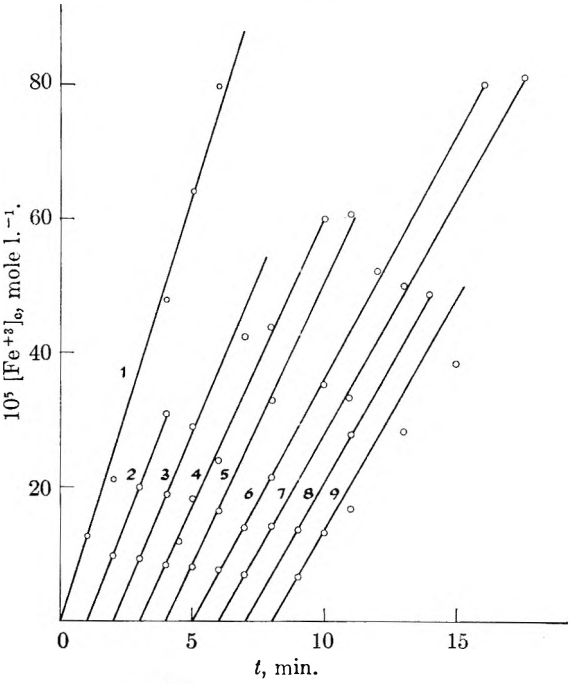

Fig. 1.—Photooxidation curves of air-saturated ferrous sulfate solutions, corrected for the inner filter effect: $[Fe^{2+}] = 0.0204$ mole l.$^{-1}$; $I_0 = 4.59 \times 10^{-4}$ einstein l.$^{-1}$ min.$^{-1}$. Curves are shifted along the time axis.

Curve	pH
1	0.60
2	0.85
3	1.20
4	1.45
5	1.55
6	1.85
7	2.35
8	2.65
9	3.05

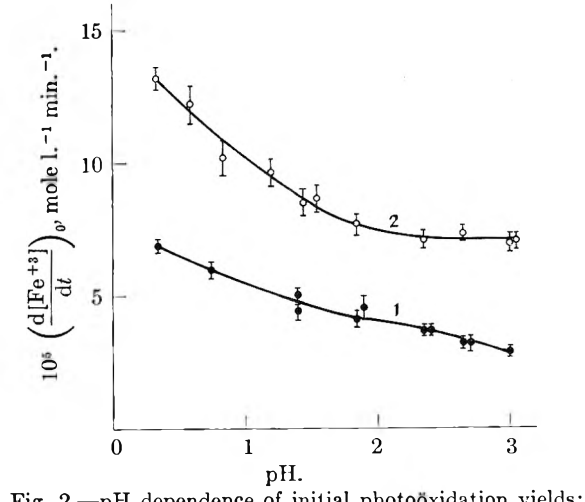

Fig. 2.—pH dependence of initial photooxidation yields: 0.0204 M Fe^{2+} solutions; $I_0 = 4.59 \times 10^{-4}$ einstein l.$^{-1}$ min.$^{-1}$: (1) evacuated solutions, (2) air-saturated solutions.

(10) F. Haber and J. Weiss, *Proc. Roy. Soc.* (London), **A147**, 332 (1934).

(11) A. O. Allen, V. D. Hogan, and W. G. Rothschild, *Radiation Res.*, **7**, 603 (1957).

(12) W. G. Rothschild and A. O. Allen, *ibid.*, **8**, 101 (1958).

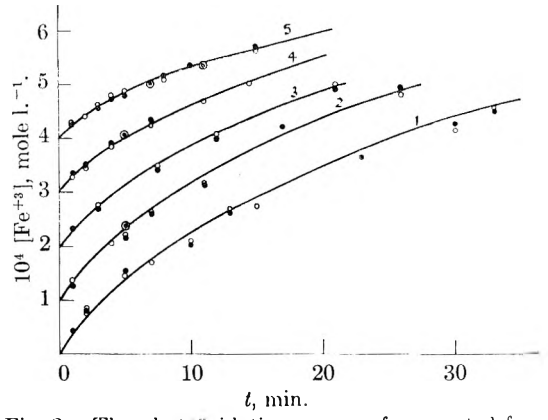

Fig. 3.—The photooxidation curves of evacuated ferrous sulfate solutions: $[Fe^{2+}] = 0.0204$ mole l.$^{-1}$; $I_0 = 4.59 \times 10^{-4}$ einstein l.$^{-1}$ min.$^{-1}$.

Curve	pH
1	1.40
2	1.85
3	2.35
4	2.65
5	3.00

Solid curves calculated from eq. VIII: ●, Fe^{3+} determination; ○, H_2 determination.

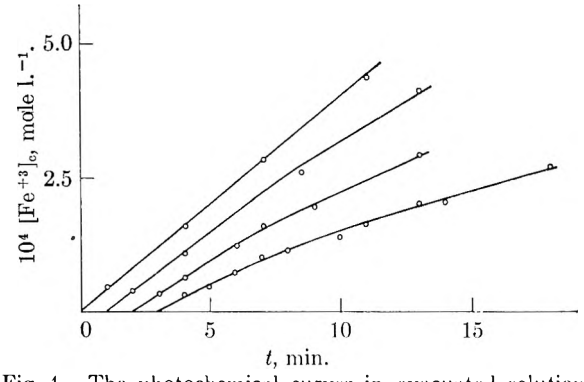

Fig. 4.—The photochemical curves in evacuated solutions corrected for the inner filter effect.

Curve	pH
1	1.85
2	2.35
3	2.65
4	3.00

Integration of eq. IV leads to the result

$$[Fe^{3+}] + \frac{B}{2}[Fe^{3+}]^2 + \frac{H}{2G}[Fe^{3+}]^2 + \frac{BH}{3G}[Fe^{3+}]^3 = AI_0\left(1 + \frac{1}{G}\right)t \quad (V)$$

Hence we calculated

$$\Delta = AI_0\left(1 + \frac{1}{G}\right)t - [Fe^{3+}] - \frac{B}{2}[Fe^{3+}]^2 \quad (VI)$$

and hence k_5/k_{10} was determined.

The results of these calculations are presented in Table II. It will be seen later that the ratio k_{10}/k_4 is only slightly pH dependent. The value of $k_{10}/k_4 = 10^3$ was used in the present calculations.

Photochemistry in Evacuated Solutions.—The photochemical oxidation curves of evacuated solutions are presented in Fig. 3. From the experimental results corrected for the inner filter effect (Fig. 4) the initial yields were obtained.

TABLE II

THE DETERMINATION OF THE RATIO k_5/k_{10} AT pH 3.05 FROM PHOTOCHEMICAL DATA IN AERATED SOLUTIONS

$[O_2] = 2.63 \times 10^{-4}$ mole l.$^{-1}$; $I_0 = 4.59 \times 10^{-4}$ einstein l.$^{-1}$ min.$^{-1}$

t, min.	$10^4[Fe^{3+}]$, mole l.$^{-1}$	$10^4[Fe^{3+}]_c$, mole l.$^{-1}$	$10^4\Delta$, mole l.$^{-1}$	H, l.$^{-1}$	$\frac{k_5}{k_{10}}$
1	0.555	0.680			
5	1.71	2.96	0.44	1780	0.5 ± 0.2
7	2.10	3.87	0.77	1750	0.5 ± 0.1

At pH values above 2.0 an additional retarding effect of the ferric ion is observed. To ascertain the extent to which the increase of the concentration of the ferric ion is responsible for the decrease of the rate, the nature of this additional inhibition effect of the ferric ion has to be considered. Attributing the retarding effects to the inner filter effect and to the reduction of the ferric ions by hydrogen atoms (reaction 5), if the recombination reaction of hydrogen atoms (reaction 6) can be neglected, the kinetic equation will be

$$\frac{d[Fe^{3+}]}{dt} = \frac{AI_0}{(1 + B[Fe^{3+}])(1 + D[Fe^{3+}])} \quad (VII)$$

where $D = k_5/k_4[Fe^{2+}]$.

Integration of eq. III, assuming that the change in $[Fe^{2+}]$ can be neglected, yields the result

$$[Fe^{3+}] + \frac{B + D}{2}[Fe^{3+}]^2 + \frac{BD}{3}[Fe^{3+}]^3 = AI_0t \quad (VIII)$$

The initial rates were calculated from initial slopes of the curves in Fig. 4 and the value of AI_0 was obtained. Using eq. I and VIII we get

$$\delta = AI_0t - [Fe^{3+}]_c = DF \quad (IX)$$

where $F = {}^1/_2[Fe^{3+}]^2 + (B/3)[Fe^{3+}]^3$.

Linear plots of δ *vs.* F were obtained and from these D was determined. Thus we obtained $k_5/k_4 = 16 \pm 4$ at pH 2.35 and 40 ± 6 at pH 2.65. At pH 3.0 agreement with the experimental results was obtained by setting $k_5/k_4 = 100$. Using these values we could calculate theoretical curves to represent the dependence of the quantum yield on pH and on $[Fe^{3+}]$. The theoretical curves drawn in Fig. 3 are in good agreement with the experimental results.

Additional experiments were carried out in the presence of 0.1 *M* sulfate. In the experiments previously described the pH was varied simultaneously with sulfate ion concentration. These photochemical results were obtained by irradiation at constant dose, and by introduction of the appropriate correction for the inner filter effect. These results are presented in Table III.

It appears that in the presence of sulfate ion, the same trend of decrease in the quantum yield with increasing pH is observed. However, in the presence of the sulfate ion, the initial quantum yield in the pH region 2–2.5 is higher than in its absence. A similar effect was observed by Rigg and Weiss.[7] Addition of 0.4 *M* Na_2SO_4 caused an increase of the oxidation yield of ferrous ion by atomic hydrogen.[13]

Our experimental results in evacuated solutions (Fig. 2) clearly indicate that the initial oxidation

(13) G. Czapski and G. Stein, *J. Phys. Chem.*, **63**, 850 (1959).

TABLE III

EFFECT OF THE SULFATE ION ON THE INITIAL PHOTOOXIDATION YIELDS

$[Fe^{2+}] = 0.204\ M$; irradiation time $t = 5$ min.

$[H_2SO_4]$, N	$[Na_2SO_4]$, mole $l.^{-1}$	pH	$10^4 I_0$, einstein $l.^{-1}$ $min.^{-1}$	$10^4[Fe^{3+}]$, mole $l.^{-1}$	$2 \times 10^4[H_2]$, mole $l.^{-1}$	$\frac{[Fe^{3+}]_c}{I_0 t}$
0.030	..	1.90	4.59	1.39	1.42	0.100
.030	0.10	2.07	3.73	1.20	1.19	.111
.008	..	2.40	4.59	1.18	1.14	.081
.015	0.10	2.42	3.73	1.18	1.15	.108
.004	..	2.70	4.59	1.07	1.05	.070
.008	0.10	2.65	3.73	1.13	1.16	.097

yield is pH dependent. This result confirms the experimental data of Rigg and Weiss,[7] who showed that a 50% drop of the initial yield at pH 2.7 relative to pH 0.35 is observed. However, our interpretation of these results is different. On the other hand, Lefort and Douzou[9] claimed that the initial yields are pH independent and that after a relatively short irradiation period a decrease of the yield of the ferric ion with increasing pH is observed. The inhibition effect of the ferric ion, observed by these workers in the pH region up to 2.2, probably is due to the inner filter effect. Inspection of eq. VIII indicates that for 1% conversion, the reduction reaction is negligible as long as $k_5/k_4 < 10$, *i.e.*, up to pH 2.2.[12] This conclusion also is confirmed by our experimental results. Thus it appears that in the pH region investigated by Lefort and Douzou the back reaction 5 is of minor importance. The decrease of the yield below 1% conversion has to be attributed only to the decrease of the initial yield. These arguments might have been invalidated if an efficient deactivation reaction of the excited state would occur by

$$Fe^{2+*} + Fe^{3+}\,OH^- \longrightarrow Fe^{2+} + Fe^{3+}\,OH^-$$

The efficiency of this reaction would increase with increasing pH, due to the increase of the fraction of the hydrolyzed ferric ion. However, our experimental results *in vacuo* do not confirm this hypothesis. The inhibition effect of the ferric ion up to pH 2.0 can be interpreted adequately by the correction for the inner filter effect. This conclusion also is consistent with the results in aerated solutions.

Effect of Variable Oxygen Concentrations.—The determination of the ratio of the rate constants for the competitive reactions between oxygen and ferrous ions for hydrogen atoms is important for the elucidation of the oxidation mechanism by hydrogen atoms. Solutions of 0.02 M ferrous sulfate were irradiated at constant dose at various O_2 concentrations. These experiments were performed at pH 2.4 ($H_2SO_4 = 0.0055\ N$). From these results corrected for the inner filter effect, the initial yields were obtained. The results were treated according to the relation

$$\frac{1}{(A_{O_2} - A)I_0} = \frac{1}{AI_0} + \frac{k_4}{k_{10}AI_0}\frac{[Fe^{2+}]}{[O_2]} \qquad (X)$$

where AI_0 and $A_{O_2}I_0$ are the initial yields *in vacuo* and in the presence of O_2. This equation can be deduced from eq. XI of part I.

The experimental results plotted according to this relation (Fig. 5) yield $AI_0 = (0.35 \pm 0.03) \times 10^{-4}$ mole $l.^{-1}$ and $k_{10}/k_4 = 1500 \pm 400$ at pH 2.4. This result indicates a relatively small pH effect

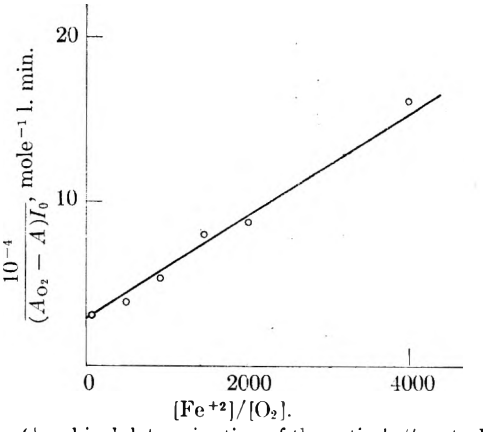

Fig. 5.—Graphical determination of the ratio k_4/k_{10} at pH 2.4 according to eq. X.

on the ratio of these rate constants, in agreement with the radiation chemical data.[12,14]

Assuming that in the pH region 2.35–2.65 k_4/k_{10} remains constant, we obtain the constants ratio presented in Table IV.

TABLE IV

THE pH DEPENDENCE OF RATE CONSTANTS RATIO FOR REACTIONS OF Fe^{2+} AND Fe^{3+} IONS

pH	$\frac{k_{H+Fe^{3+}}}{k_{H+Fe^{2+}}} = \frac{k_5}{k_4}$	$\frac{k_{H+O_2}}{k_{H+Fe^{2+}}} = \frac{k_{10}}{k_4}$	$\frac{k_{H+Fe^{3+}}}{k_{H+O_2}} = \frac{k_5}{k_{10}}$
	Photochemical Data		
0.4	...	900 ± 300	
2.35	16 ± 4		(0.01)
2.40		1500 ± 400	
2.65	40 ± 4		(0.03)
3.00	(100)		
3.05			0.5 ± 0.2
	Radiation Chemistry[11,12,15]		
0.4	0.081	1200 ± 300	
1.1[a]	0.50		
1.57	1.35		
2.10	7.2	1500 ± 200	0.007
2.70			0.10
	Reactivity of Hydrogen Atoms[13]		
0.4	0.135		
1.3	0.87		
2.3	4.75		
2.9	50		

[a] Calculated from ref. 15.

Rate Constants Ratios as a Function of pH.—Table IV contains our results for the ratio of the

(14) A. O. Allen and W. G. Rothschild, *Radiation Res.*, **7**, 591 (1957).
(15) J. H. Baxendale and G. Hughes, *Z. physik Chem.* (Frankfurt), **14**, 323 (1958).

rate constants of hydrogen atoms produced photochemically, with ferrous ions and with oxygen. The comparison of these data with the available experimental results from other sources[11-13,15] indicates that the agreement is reasonable.

Discussion

The Absorption Spectrum.—The first step in the mechanism of the photochemical evolution of hydrogen from aqueous solutions of ferrous ions is the formation of an excited state after the absorption of one quantum. The absorption spectrum of ferrous ion solutions between 2000 and 3000 Å. has been investigated by several workers.[16-18] Our measurements, in agreement with previous data, showed the band onset (for $\epsilon = 0.1$ mole^{-1} l. cm.$^{-1}$) at 2870 Å. (100 kcal.) and a shoulder at 2390 Å. (119 kcal.) with $\epsilon = 20$ mole^{-1} l. cm.$^{-1}$.

Hitherto this band has been assigned to an electron transfer from the ion to the solvent[17-19] similar to that proposed for the absorption spectra of anions in solutions.[2,3] Weiss[16] postulated a dissociative electron capture by a water molecule as the resulting primary chemical process. Farkas and Farkas[1] have shown that such a mechanism is not consistent with energetic data. The alternative proposed by Farkas and Farkas[1] involves electron transfer to a single water molecule. Theoretical[20,21] and experimental[22] evidence shows that a single water molecule cannot bind an additional electron. However Franck and Platzman[2,3] showed that in the case of anions the organized solvent medium in the neighborhood of the ion provides a potential well in which bound excited states may exist. Good agreement can be obtained between the experimental and the theoretical spectroscopic values calculated on the basis of such a theory.[23-25]

However when the spectrum of the positive ferrous ion was compared with theoretical calculations[26] based on a similar model in which the excited electron is bound in a potential well formed by the charge of the central ion screened by the polarized medium, no agreement could be obtained. The calculated binding energy of the electron in the excited state was about 1.2 e.v. The theoretical value of the Franck–Condon orientation strain, required to transfer the solvation configuration of the ion M^{Z+} to the configuration of the ion $M^{(Z+1)+}$ was quite different from the experimental one for this and similar positive ions examined. On the other hand, comparison with the energy levels of the gaseous ions indicated that the excited state may be related to the $3d^{n-1}4s$ state.[27,28] We suggest that such forbidden transitions may appear in aqueous solutions with relatively low ϵ values, as found for the 2390 Å. band. Unlike the case of anions, *e.g.*, iodide, where excited states pertaining to the ion itself alone are impossible, such excited states are possible in the case of cations, *e.g.*, ferrous ions. Therefore in this latter case the transition may be an essentially internal one, the participation of the solvent being less pronounced than in the case of iodide.

The absorption spectrum of Fe^{2+} at 2000–3000 Å. reveals two overlapping bands. Irradiation at 2536 Å. affects both bands and the quantum yields obtained are compound quantities. Investigation of the dependence of the quantum yield on wave length is desirable.

Primary Photochemical Processes.—The excited state formed in the primary absorption process may decay back to the ground state. In competition with this there occur processes leading to the net photochemical decomposition observed. Both in the presence and in the absence of O_2 the initial photoöxidation rate at constant light intensity decreases with increasing pH up to pH 2.5 in a parallel manner. Using for the initial rates the expressions ($I_a = I_0$)

$$\left(\frac{d[Fe^{3+}]}{dt}\right)_0^{evac} = 2\alpha I_a$$

$$\left(\frac{d[Fe^{3+}]}{dt}\right)_0^{O_2} = 2\alpha I_a \left[1 + \frac{1}{1 + \frac{k_4[Fe^{2+}]}{k_{10}[O_2]}}\right]$$

α, the fraction of excited centers leading to H atom formation was calculated from the experimental results in the pH range of 0.35 to 2.5 for evacuated solutions, and of 0.35 to 3.0 for aerated solutions. The values of $k_{10}/k_4 = 10^3$ was used over the whole range. Figure 6 shows that the values of α are identical for evacuated and air-saturated solutions over the whole pH range. Therefore at this concentration the effect of O_2 on the process in which H atoms are formed is negligible. The process by which H atoms appear in the bulk of the solution is facilitated by H^+ ions specifically.

A similar pH dependence of the quantum yield of hydrogen formation in the photoöxidation of chromous ion was attributed[4] to the formation of an ion-pair complex with anions. In ferrous ion solutions up to 0.8 N H_2SO_4 there is no spectroscopic evidence (Table I) for the formation of such a complex.

A molecular mechanism for the pH dependent formation of H_2 has been suggested[29] where the excited ion and H^+ would form a cluster which dissociates yielding H_2

$$Fe^{2+}\,H_2O^* + H^+ \longrightarrow Fe^{2+}\,H - OH^* \text{ —— } H^+$$

$$Fe^{2+}\,H - OH^* \text{ —— } H^+ + Fe^{2+} \longrightarrow 2Fe^{3+} + OH^- + H_2$$

However such a molecular mechanism is inconsistent with the effect of oxygen on the reaction mechanism and with the fact that the initial rates at pH 0.35 are independent of Fe^{2+} concentration between 0.02 and 0.1 M.

Of the mechanisms by which atomic hydrogen may be formed in a pH dependent process a possible one is that involving the interaction of H^+

(16) J. Weiss, *Trans. Faraday Soc.*, **37**, 463 (1941).
(17) H. L. Schlaefer, *Z. physik. Chem.* (Frankfurt) **3**, 263 (1955).
(18) F. S. Dainton and D. G. L. James, *Trans. Faraday Soc.*, **54**, 649 (1958).
(19) E. Rabinowitsch, *Rev. Mod. Phys.*, **14**, 112 (1942).
(20) J. A. Pople, *J. Chem. Phys.*, **21**, 2234 (1953).
(21) F. O. Ellison and H. Shull, *ibid.*, **23**, 2348 (1955).
(22) N. E. Bradbury and H. E. Tatel, *ibid.*, **2**, 835 (1934).
(23) G. Stein and A. Treinin, *Trans. Faraday Soc.*, **55**, 1086 (1959).
(24) G. Stein and A. Treinin, *ibid.*, **55**, 1091 (1959).
(25) G. Stein and A. Treinin, *ibid.*, **56**, 1393 (1960).
(26) J. Jortner, Ph.D. Thesis, Jerusalem, 1959.
(27) C. K. Jorgensen, *Acta Chem. Scand.*, **9**, 717 (1955).
(28) L. E. Orgel, *Disc. Solvay Conf.*, **10**, 289 (1956).
(29) L. J. Heidt and A. F. McMillan, *J. Am. Chem. Soc.*, **76**, 2135 (1954).

ions with the primary excited state, resulting in electron transfer[8]

$$Fe^{2+}{}_{aq}{}^{*} + H_3O^+ \longrightarrow Fe^{3+}{}_{aq} + H + H_2O$$

The low molar extinction coefficient of the ferrous ion absorption band is consistent with a relatively long lifetime of the excited state. However, fluorescence was not observed in this system and the degradation of electronic excitation energy proceeds by radiationless transition. Therefore the lifetime calculated from the area of the absorption band is only an upper limit. After a much shorter period the primary excited state already may have started on its process of radiationless decay back to the ground state.

During this process distinct intermediates may have formed in the Franck–Rabinowitch photochemical cage. For example the excited electron may become a separate entity undergoing a random walk process within the cage. H^+ in the bulk then may scavenge this electron. Alternatively an H atom may have been formed within the cage, and undergo random walk there before recombination within the cage with the positive ion. In this case the H atom may be scavenged by H^+ ions. The quantitative dependence on pH will be different in the case of direct interaction with the primary excited state from that in the case of scavenging of a distinct fragment undergoing a random walk process. Systems where efficient scavenging competes with secondary recombination of the type now considered were investigated by Noyes.[30,31] The quantum yield, α, for the introduction of radicals into the bulk of the solution in the presence of a scavenger in concentration [S] is given by

$$\alpha = \alpha_0 + 2a(\pi k_s[S])^{1/2} - \frac{4a^2 k_s[S]}{\beta} + \cdots \quad \text{(XI)}$$

where a is a constant specifying the reaction probability of the two original partners, k_s is the rate constant of the reaction between the scavenger and one of the fragments, α_0 is the *residual yield* of fragments escaping recombination by diffusion into the bulk in a pH independent process, and β is a constant as defined by Noyes. The theoretical relation XI holds only after a period of time corresponding to the formation of two distinct chemical entities and subsequent few diffusive displacements.[30-33]

The quantitative results (Fig. 7) show that within a range of pH values $\alpha(H^+)$, the pH dependent rate of introduction of H atoms into the bulk is a linear function of $[H^+]^{1/2}$. The results can be presented by the straight line drawn in Fig. 7, given by the relation

$$\alpha(H^+) = 0.038 + 0.063\ [H^+]^{1/2} \quad \text{(XII)}$$

The results in Fig. 7 show at higher H^+ concentration the negative deviation from the straight line expected from eq. XI. In the case of the photochemistry of the iodide ion,[34] eq. XI was obeyed very well over a wide range of pH and the results decisively favored a scavenging mechanism rather

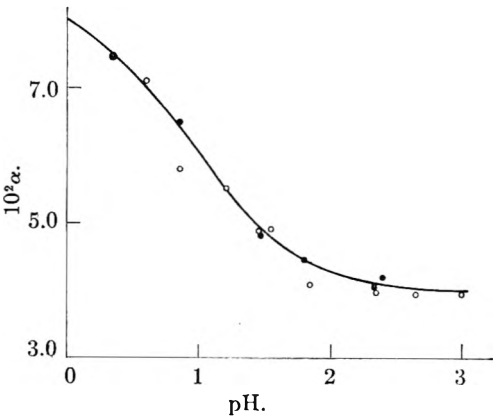

Fig. 6.—pH dependence of α: ●, evacuated solutions; O, air-saturated solutions.

than direct interaction between H^+ and the excited state. In the present case the results in evacuated solutions are in fair agreement with the theory; in aerated solutions—particularly at low pH values—the agreement is less satisfactory. We conclude that the experimental results favor the scavenging mechanism with possibly some contribution by another reaction path which is ineffective in the case of iodide, where the primary excited state is rather different.

Equation XI involves the expansion of an exponential function. A rough estimation of the scavenging rate constant may be obtained if we follow Noyes' treatment and set $4a^2 = 10^{-11}$–10^{-10} sec., which is of the order of the relaxation time of the solvent molecules. With this choice we obtain $k_s = 10^7$–10^6 l. mole^{-1} sec.$^{-1}$ for the rate constant of scavenging by the H^+ ion. One likely mechanism for the formation of dissociated fragments from the primary excited state of the hydrated ferrous ion within the cage is dissociative electron capture by a water molecule in the solvation layer. This may occur during an antisymmetric vibration of a water molecule and is facilitated by coulombic repulsion of the proton by the positive central ion. In this process an H atom will be formed within the cage. The scavenging process following on this may have involved the H atom in the cage and the H^+ ion in the bulk, forming $H_2{}^+{}_{aq}$. However it was shown[35] that the velocity of formation of $H_2{}^+{}_{aq}$ is relatively low, the rate constant being of the order of 10^3 l. mole^{-1} sec.$^{-1}$. The magnitude of the rate constant k_s now obtained indicates that another possibility, namely the charge transfer process

$$\underset{\text{cage}}{\{Fe^{3+}\,OH^-\,H\}} + \underset{\text{bulk}}{H^+} \longrightarrow \underset{\text{cage}}{\{Fe^{3+}\,OH^-\,H^+\}} + \underset{\text{bulk}}{H}$$

is more likely, in which H^+ acts as an electron scavenger. The efficiency of such electron transfer processes over relatively large distances has been pointed out.[36] This pH dependent mechanism will thus cause the appearance of H atoms in the bulk of the solution.

In addition there exists a mechanism for the appearance of H atoms in the bulk independent of pH. In the pH region above 2.0 the initial quantum

(30) R. M. Noyes, *J. Am. Chem. Soc.*, **77**, 2042 (1955).
(31) R. M. Noyes, *ibid.*, **78**, 5846 (1956).
(32) J. C. Roy, W. H. Hamill, and R. R. Williams, *ibid.*, **77**, 2953 (1955).
(33) L. Monchick, *J. Chem. Phys.*, **24**, 381 (1956).
(34) J. Jortner, R. Levine, M. Ottolenghi, and G. Stein, *J. Phys. Chem.*, **65**, 1232 (1961).
(35) G. Czapski, J. Jortner, and G. Stein, *ibid.*, **63**, 1769 (1959).
(36) W. F. Libby, *ibid.*, **56**, 863 (1952).

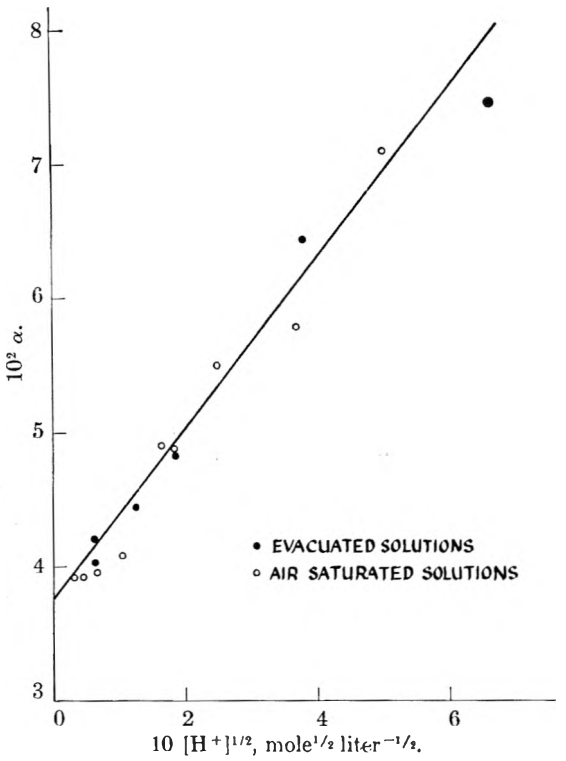

Fig. 7.—The dependence of α on $[H^+]^{1/2}$: ●, evacuated solutions; ○, air-saturated solutions.

yield in aerated solution, determined solely by the yield of H atoms, remains constant. This *residual yield* is then the fraction of H atoms which escape the back reaction by diffusion into the bulk. The full mechanism suggested for the introduction of H atoms into the bulk is therefore

$$Fe^{2+}{}_{aq} \xrightarrow{h\nu} Fe^{2+}{}_{aq}$$

$$Fe^{2+}{}_{aq}{}^{*} \longrightarrow \underbrace{\{Fe^{3+}\,OH^-\,H\}}_{\text{solvent cage}} \longrightarrow Fe^{3+}\,OH^-{}_{aq} + H_{bulk}$$

$$\{Fe^{3+}\,OH^-\,H^+\} + H^+{}_{bulk} + H_{bulk}$$

Reactions of the Hydrogen Atoms.—The atomic hydrogen appearing in the bulk of the solution as the result of the pH dependent and residual processes may recombine to give H_2 or oxidize ferrous to ferric ion. The results present in Part I provide photochemical evidence for the oxidation of ferrous ions by H atoms in agreement with other independent evidence.[5,6,13,14,37,38] Several mechanisms have been proposed for this oxidation process. Weiss[5] postulated the intermediate formation of $H_2^+{}_{aq}$. Uri[39] considered the possibility of H atom abstraction from the hydration sphere of the ferrous ion. The original suggestion of Ethier and Haber[40] was of a triple collision between H, $H^+{}_{aq}$, and $Fe^{2+}{}_{aq}$. Recently experiments with atomic hydrogen showed[41,42] that the mechanism of oxidation may be different for different acceptors. Iodide is oxidized by way of the mechanism involving intermediate $H_2^+{}_{aq}$ formation, while ferrous ions may be oxidized in a pathway involving a hydride complex intermediate between the ferrous ion and atomic hydrogen.

The photochemical results in deaerated solution show a decrease of the oxidation yield with increasing pH at pH 2.5, while in aerated solutions in this region the yield remains constant. Therefore the additional pH effect is not due to the change in the rate of introduction of H atoms into the bulk. It may well be due to a competition between a pH dependent oxidation process and recombination

$$2H \longrightarrow H_2 \qquad (6)$$

Treatment of the results according to the $H_2^+{}_{aq}$ mechanism, assuming steady state kinetics, gives for the initial photooxidation yield

$$\left(\frac{d[Fe^{3+}]}{dt}\right)_0 = \alpha I_0 + V[H^+]^2\left\{\left(1 + \frac{2\alpha I_0}{V(H^+]^2}\right)^{1/2} - 1\right\} \qquad (XIII)$$

where

$$V = \frac{k_{15}^2}{2k_6}\left(\frac{k_{17}[Fe^{2+}]}{k_{16} + k_{17}[Fe^{2+}]}\right)^2$$

involving the velocity constants of the reactions

$$H + H^+{}_{aq} \underset{k_{16}}{\overset{k_{15}}{\rightleftharpoons}} H_2^+{}_{aq}$$

$$H_2^+{}_{aq} + Fe^{2+}{}_{aq} \xrightarrow[k_{17}]{} Fe^{3+}{}_{aq} + H_2$$

Our experimental results above pH 2.5 can be represented by eq. XIII by setting the value of V = 0.1 l. mole^{-1} sec.$^{-1}$. For high Fe^{2+} concentrations $V = k_{15}/2k_6$. Introducing[13] $k_6 = 10^{10}$ l. mole^{-1} sec.$^{-1}$ yields $k_{15} = 4.5 \times 10^4$ l. mole^{-1} sec.$^{-1}$ for the lower limit of the velocity constant of $H_2^+{}_{aq}$ formation. This lower limit is higher than the value of the rate constant of $H_2^+{}_{aq}$ formation obtained in experiments using atomic hydrogen.[25]

The existence of the pH dependence rules out a pH independent mechanism as proposed by Uri.[39] The results obtained for the competition between ferrous ion and oxygen for the hydrogen atoms show that the ratio of the rate constants increases only slowly over a rather wide pH range. These results agree with those obtained for the radiation-chemical system.[12,14] They rule out a triple collision mechanism of oxidation.

Treatment of the results according to the mechanism[44,45] in which first ferrous ion and atomic hydrogen form an intermediate hydride complex, which then interacts with an H^+ ion

$$Fe^{2+}{}_{aq} + H \underset{k_{19}}{\overset{k_{18}}{\rightleftharpoons}} FeH^{2+}$$

$$FeH^{2+} + H^+ \xrightarrow[k_{20}]{} Fe^{3+}{}_{aq} + H_2$$

assuming steady state kinetics to apply, leads to the result

(37) G. Czapski and G. Stein, *Nature*, **182**, 598 (1958).
(38) T. W. Davis, S. Gordon, and E. J. Hart, *J. Am. Chem. Soc.*, **80**, 4487 (1958).
(39) N. Uri, *Chem. Rev.*, **50**, 376 (1952).
(40) J. P. Ethier and F. Haber, *Naturwiss.*, **18**, 266 (1930).
(41) G. Czapski, J. Jortner, and G. Stein, *J. Phys. Chem.*, **65**, 956 (1961).
(42) G. Czapski, J. Jortner, and G. Stein, *ibid.*, **65**, 960 (1961).
(43) H. L. Friedman and A. H. Zeltman, *J. Chem. Phys.*, **28**, 878 (1958).
(44) G. Stein, *Discussions Faraday Soc.*, **29**, 235 (1960).
(45) J. Halpern, G. Czapski, J. Jortner, and G. Stein, *Nature*, **186**, 629 (1960).

$$\left(\frac{d[Fe^{3+}]}{dt}\right)_0 = \alpha I_0 + \frac{k_{18}^2}{2k_6}[Fe^{2+}]^2\left(\frac{[H^+]}{(k_{19}/k_{20}) + [H^+]}\right)^2 \left\{\left(1 + \frac{2\alpha I_0}{k_{18}^2/2k_6[Fe^{2+}]^2[H^+]/(k_{19}/k_{20}) + [H^{2+}]}\right)^{1/2} - 1\right\} \quad \text{(XIV)}$$

Equation XIV can be transformed to the form

$$\frac{k_{18}^2}{2k_6}\left\{\frac{[H^+]}{(k_{19}/k_{20}) + [H^+]}\right\}^2 = \frac{\{(d[Fe^{3+}]/dt)_0 - \alpha I_0\}^2}{\{4\alpha I_0 - 2(d[Fe^{3+}]/dt)_0\}[Fe^{2+}]^2}$$

Analysis of the quantitative data obtained for the oxidation of ferrous ion by atomic hydrogen over a wide range of H^+ and Fe^{2+} concentrations showed[41,42] that the hydride complex mechanism gave good agreement with the experimental results, but none of the other mechanisms considered did so. This pH dependent mechanism is distinct from the triple collision mechanism over the pH range where self dissociation of the hydride complex is negligible in comparison with the interaction of the complex with H^+. According to this treatment, the value of $k_{18} = 10^5$ l. mole^{-1} sec.$^{-1}$ was obtained for the rate of formation of the ferrous–hydrogen complex. To test the consistency of the photochemical results with this mechanism, the rate constant ratio k_{19}/k_{20} is derived in Table V, using the above value of k_{18} and the value of $\alpha = 4 \times 10^{-2}$ obtained in the present series of experiments in air-saturated solutions.

TABLE V

CALCULATION OF k_{19}/k_{20} FROM PHOTOCHEMICAL DATA IN EVACUATED SOLUTION

$I_0 = 7.64 \times 10^{-6}$ einstein l.$^{-1}$ sec.$^{-1}$; $[Fe^{2+}] = 0.02$ M

pH	$10^7\,(d[Fe^{3+}]/dt)_0$, mole l.$^{-1}$ sec.$^{-1}$	k_{19}/k_{20}
2.65	5.34	0.05 ± 0.02
3.0	4.85	0.04 ± 0.02

The value of k_{19}/k_{20} obtained from the photochemical experiments is in good agreement with the values obtained in other systems.[42,46] Thus the present photochemical results are at least consistent with the assumption that the oxidation of ferrous ions by atomic hydrogen involves, in the present system, the intermediate formation of a hydride complex.

When ferric ions are present there is competition for the available H atoms between the ferric ions, which are reduced, and the ferrous ions, which are oxidized. The variation of the rate constants in Table IV shows that those involving the reduction of ferric ions are pH dependent. The pH dependence of the ratio k_5/k_4 should be due mainly to the pH dependence of reaction 5, which proceeds mainly by

$$Fe^{3+}OH^- + H \longrightarrow Fe^{2+} + H_2O \qquad (5.1)$$

rather than by the reduction of the hexaaquo ferric ion or the ferric sulfate ion pair.[44] Schwartz and Hritz[47] already have considered the effect of complexing negative groups on the reduction of ferric ions by atomic hydrogen. Their experiments on the competing reduction of ferric and oxidation of ferrous ions in irradiated solutions are not consistent with the assumption of an $H_2^+{}_{aq}$ intermediate mechanism. However, they are consistent, as are the present results, with the hydride mechanism.

The conclusion reached as the result of the present work is therefore that the main pH dependent process in the photochemical evolution of hydrogen from aqueous solutions of ferrous ions is the one in which atomic hydrogen is introduced into the bulk of the solution. The subsequent oxidation by atomic hydrogen introduces into the photochemical process only a minor additional pH dependence. The results show that this oxidation mechanism probably may be one involving a hydride intermediate. However in this respect the photochemical results may serve at most as further support for the conclusions reached by the use of atomic hydrogen in separate experiments.

Acknowledgment.—This research was sponsored by the Israel Atomic Energy Commission.

(46) G. Czapski and J. Jortner, *Nature*, **188**, 50 (1960).

(47) H. A. Schwartz and J. M. Hritz, *J. Am. Chem. Soc.*, **80**, 5636 (1958).

THE ULTRAVIOLET SPECTRUM OF POLYACRYLONITRILE AND THE IDENTIFICATION OF KETENE–IMINE STRUCTURES[1]

BY R. B. BEEVERS

Frick Chemical Laboratory, Princeton University, Princeton, New Jersey

Received December 7, 1961

The ultraviolet spectra of polyacrylonitrile and polymethacrylonitrile show an absorption band at about 270 mμ. This has been ascribed, in polymethacrylonitrile, to ketene–imine linkages in the chain. From an examination of the ultraviolet spectrum of the ketene–imine structure prepared by the photodecomposition of 2,2′-azo-bis-isobutyronitrile it is shown that the ultraviolet absorption at 270 mμ in polyacrylonitrile cannot be due to ketene–imine linkages.

During the course of an examination of the properties of acrylonitrile polymers prepared by anionic and free radical mechanisms it was observed that absorption occurred in the ultraviolet with a maximum at about 270 mμ. Absorption was most marked for the anionic polymers (Fig. 1) but some trace of a peak at this wave length was found for all polymers examined, bearing out the observations of Schurz, Bayzer, and Stübschen.[2] The origin of the absorption has so far not been determined. Some of the polymers which absorbed strongly in the ultraviolet also showed some absorption in the

(1) Experimental work carried out at Courtaulds Limited, Research Laboratory, Maidenhead, England.

(2) J. Schurz, H. Bayzer, and H. Stübschen, *Makromol. Chem.*, **23**, 152 (1957).

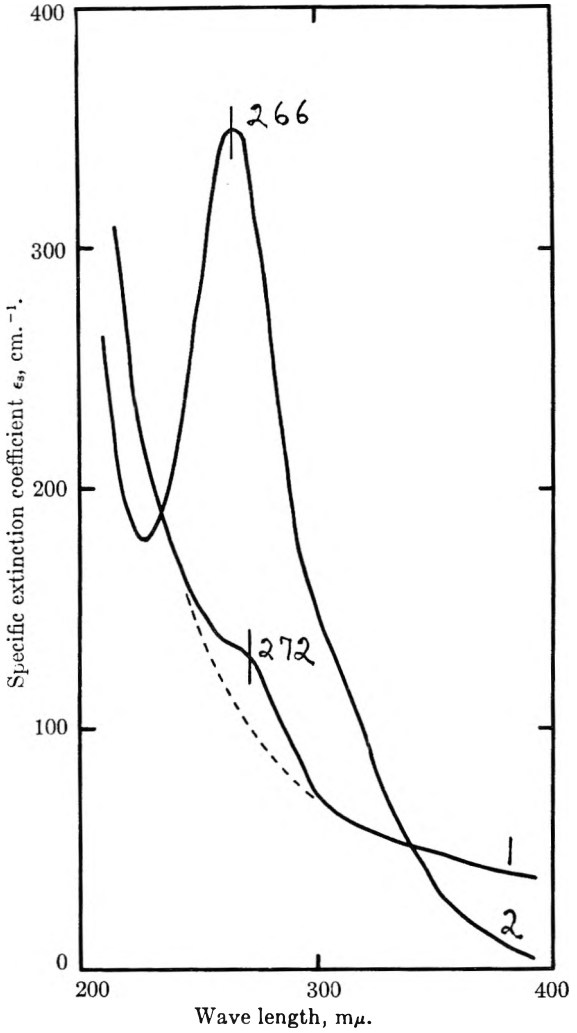

Fig. 1.—The ultraviolet spectra of polyacrylonitrile films: 1, ammonium persulfate–sodium bisulfite polymer, $[\eta]$ = 2.26 dl. g.$^{-1}$; 2, *n*-butyl lithium polymer, add 100 cm.$^{-1}$ to ordinate, $[\eta]$ = 2.45 dl. g.$^{-1}$; intrinsic viscosities measured in N,N-dimethylformamide at 25°.

infrared at about 2025 cm.$^{-1}$. Absorption near to this wave number generally is considered to be characteristic of the ketene–imine group ($R_2C{=}C{=}NR$) although the allenic group ($R_2C{=}C{=}CR_2$) (1940–2000 cm.$^{-1}$) and the imide group, occurring in carbodiimides ($RN{=}C{=}NR$) (2100 cm.$^{-1}$) also absorb in this spectral region.[3,4] The evidence so far suggests that the ultraviolet peak arises from ketene–imine structures in the polymer. Further weight is given to this view by the known occurrence of ketene–imine structures in polymethacrylonitrile which are identified by absorption at 2012 cm.$^{-1}$.[3a] Talât-Erben and Bywater[5] have shown that the ultraviolet spectrum of polymethacrylonitrile, which contains ketene–imine structures, has an ultraviolet absorption at 275 mμ, from which they conclude that this peak arises from ketene–imine structures along the polymer chain. Chen, *et al.*,[6] have shown that ketene–imine structures are formed on polymerization of acrylonitrile with X-radiation at low temperatures. Ketene–imine structures in polyacrylonitrile, as in polymethacrylonitrile, probably arise from termination by combination giving one group per molecule. Anionic polymerization most probably results in either chain branching[7] or conjugated sequences of cyclic imines which may occur either in the chain or as a result of the termination reaction.

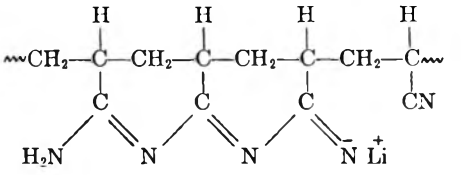

Overberger, Yuki, and Urakawa[8] have discussed this mechanism for polymethacrylonitrile. Propagation of cyclization probably is limited to an isotactic sequence and this can be clearly demonstrated with the aid of space-filling atomic models. These structures give rise to infrared absorption at 1600–1700 cm.$^{-1}$, not at 2012 cm.$^{-1}$, and also cause color formation. Models show that the conjugated sequence is planar when obtained from an isotactic group of residues. The large difference of absorption at 270 mμ (Fig. 1), however, is not easily accounted for by increase in the number of ketene–imine linkages since these can be qualitatively assessed by the ratio of the CN to C=C=N absorption in the infrared. Wide variations in the ultraviolet absorption at 270 mμ were obtained on varying the catalyst concentration without corresponding changes being observed in the weak ketene–imine absorption in the infrared. It therefore was necessary to reconsider the evidence for the assignment of the ultraviolet absorption to ketene–imine structures. The most direct method of investigating this was to determine the relative absorption of the infrared and ultraviolet peaks for a simple ketene–imine compound. This was carried out by making measurements on dimethyl-N-(2-cyano-2-propyl)-keteneimine obtained by photodecomposition of 2,2′-azo-bis-isobutyronitrile (AIBN). This compound, of the several ketene–imine compounds known, bears the greatest resemblance to the ketene–imine structure in the polymer.

Experimental

2,2′-Azo-bis-isobutyronitrile.—AIBN was purified by three recrystallizations from toluene solution at 35–40° starting with the commercial material (Genitron A.Z.D.N. 7%, Whiffen and Sons Ltd.) giving large monoclinic crystals.

Preparation of the Ketene–Imine.—The ketene–imine was prepared by irradiation of part of a solution of AIBN (0.0298 mole l.$^{-1}$) in ethanol (B.D.H. Ltd., special spectroscopic grade) with ultraviolet light of wave length 365 mμ for 136 hr. The solution was enclosed in a cylindrical fused silica cell (10 mm.) and was sealed off after degassing, under high vacuum. Irradiation was carried out using a 125-watt mercury lamp placed close to the cell with a Chance ON7 glass and $CuSO_4 \cdot 5H_2O$ solution (125 g. l.$^{-1}$) as filters.

(3) (a) N. Grassie and I. C. McNeill, *J. Polymer Sci.*, **33**, 171 (1958); (b) C. L. Stevens and J. C. French, *J. Am. Chem. Soc.*, **75**, 657 (1953); **76**, 4398 (1954).

(4) H. G. Khorana, *Chem. Rev.*, **53**, 145 (1953).

(5) M. Talât-Erben and S. C. Bywater, *Rice Sci.*, **25A**, 11 (1956).

(6) C. S. H. Chen, N. Colthup, W. Deichert, and R. L. Webb, *J. Polymer Sci.*, **45**, 247 (1960).

(7) W. M. Thomas, *Fortschr. Hochpolymer.-Forsch.*, **2**, 401 (1961).

(8) C. G. Overberger, H. Yuki, and N. Urakawa, *J. Polymer Sci.*, **45**, 127 (1960).

The ketene–imine was not isolated from solution as in the work of Stevens and French[3b] since these compounds are very unstable at room temperature and are difficult to purify. Ethanol therefore was chosen as solvent since absorption in the ultraviolet is very low and it also is free from strong absorption in the infrared at about 2000 cm.$^{-1}$.

Ultraviolet Spectra.—Spectra were obtained using a Unicam S.P. 500 spectrometer with 10 mm. and 2 mm. fused silica cells.

Infrared Spectra.—Spectra were recorded with a Perkin-Elmer Infracord spectrometer (double beam) using 1.0 mm. and 0.1 mm. NaCl cells. Compensated spectra were obtained using a variable spacing infrared cell (Research and Industrial Instruments Co. Ltd.) in the comparison beam. Cells were calibrated by standard interference fringe techniques.

Extinction Coefficients.—The molar extinction coefficient, ϵ_m, is given by $\log(I_0/I) = \epsilon_m cd$, where c is the concentration in mole l.$^{-1}$ and d is the cell thickness in cm. Ultraviolet and infrared spectra of polyacrylonitrile films are discussed in terms of the specific extinction coefficient, ϵ_s, given by $\log(I_0/I) = \epsilon_s d$.

Results and Discussion

Talât-Erben and Bywater[9] have established that the thermal decomposition of AIBN (I) at 80° gives an unstable intermediate, dimethyl-N-(2-cyano-2-propyl)-keteneimine (III), arising from combination of the two radicals (II) occurring as resonance hybrids. Pauling, Gordy, and Saylor[10] have considered similar dynamic equilibria ($R—C\equiv C—\dot{C}H_2 \rightleftarrows R—\dot{C}=C=CH_2$) as giving rise to the allenic group. Ultimately decomposition of III gives tetramethylsuccinodinitrile, isobutyronitrile, and methacrylonitrile.[11] Smith, *et al.*,[12] and Brealey[13] have established the formation of III by photochemical decomposition of I at room temperature when the rate of decay of the ketene–imine is much reduced.

$$\underset{\text{I}}{(CH_3)_2C(CN)—N=N—C(CH_3)_2CN} \longrightarrow 2(CH_3)_2C(CN)\cdot + N_2$$

$$\underset{\text{II}}{(CH_3)_2C(CN)\cdot} + (CH_3)_2C=C=N\cdot \rightleftarrows \underset{\text{III}}{(CH_3)_2C=C=N\cdot C(CH_3)_2CN}$$

Ultraviolet Spectra.—The photodecomposition of AIBN in ethanol solution was followed by changes in the ultraviolet spectrum, a typical result being given in Fig. 2. At short wave lengths the absorption rises steeply as a result of the chromophoric CN groups in I and III with λ_{max} 180 mμ. AIBN, curve 1, shows an absorption peak at λ_{max} 348 mμ, ϵ_m 13.4 l. mole^{-1} cm.$^{-1}$, in good agreement with Talât-Erben and Bywater.[9]

The relative chromophoric powers of various double bonds have been investigated. Ferguson[14] gives the sequence, C=C < C=N < N=N with λ_{max} at 200, 230, and 347 mμ, respectively. Several aliphatic azo-compounds have been prepared by Cohen and Wang,[15] azo-bis-phenylmethane having

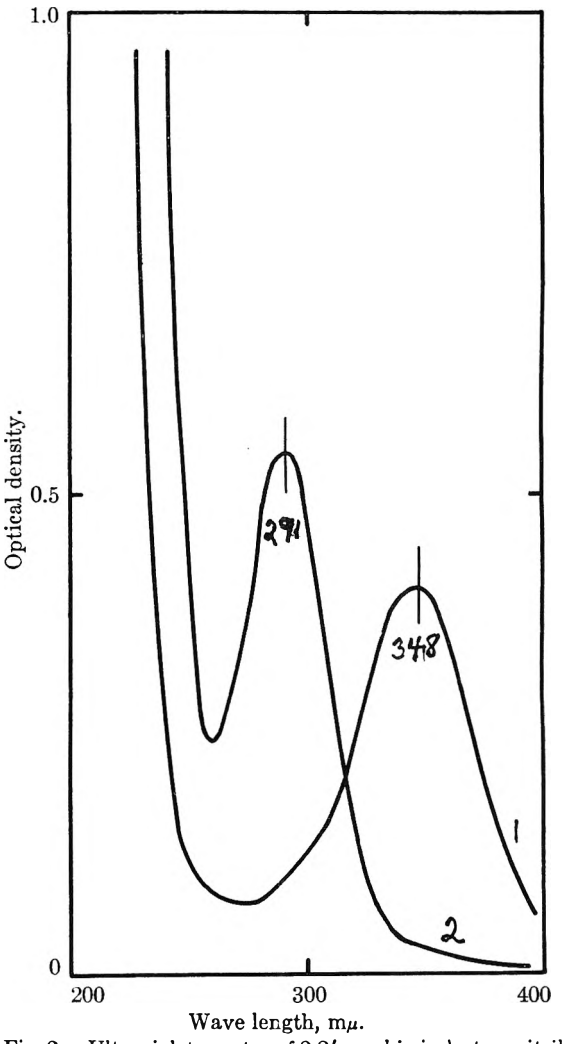

Fig. 2.—Ultraviolet spectra of 2,2′-azo-bis-isobutyronitrile in ethanol solution showing the formation of the ketene–imine structure: 1, unirradiated solution, 10-mm. cell, c = 0.0298 mole l.$^{-1}$; 2, irradiated solution, 2-mm. cell.

λ_{max} 345 mμ. Fodar and Szarvas[16] have shown that λ_{max} 355 mμ appears to be characteristic of the azo-linkage. The 348 mμ peak observed for AIBN therefore arises from the unsaturated double bond in the molecule and the disappearance of this peak on irradiation shows the scission of the azo-linkage.

Following irradiation a new band appears at 291 mμ as shown by curve 2, Fig. 2. If the assumption is made that structure III is formed (molecular weight 136) then the molar extinction coefficient at 291 mμ is ϵ_m 75.1 l. mole^{-1} cm.$^{-1}$. The further assumption is implied that all AIBN is converted to ketene–imine. Talât-Erben and Bywater[9] estimate that only 30–33 mole % of radicals II recombine to form structure III. Assuming their value of ϵ_{max} 135 at 287 mμ for the isolated ketene–imine, it is estimated that 55.6 mole % of the radicals have recombined to give the ketene–imine structure prepared photochemically in ethanol solution at room temperature. Brealey[13] has obtained yields of 54.8 and 41.6 mole %, for the ketene–imine prepared in ethanol and acetonitrile solutions, respec-

(9) M. Talât-Erben and S. C. Bywater, *J. Am. Chem. Soc.*, **77**, 3710, 3712 (1955).

(10) L. Pauling, W. Gordy, and J. H. Saylor, *ibid.*, **64**, 1753 (1942).

(11) J. C. Bevington, "Radical Polymerization," Academic Press, New York, N. Y., 1961.

(12) P. Smith and A. M. Rosenberg, *J. Am. Chem. Soc.*, **81**, 2037 (1959); P. Smith and S. Carbone, *ibid.*, **81**, 6174 (1959).

(13) G. J. Brealey, unpublished (1959).

(14) L. N. Ferguson, *Chem. Rev.*, **43**, 408 (1948).

(15) S. G. Cohen and C. H. Wang, *J. Am. Chem. Soc.*, **77**, 2457 (1955).

(16) G. Fodar and P. Szarvas, *Ber.*, **76B**, 334 (1943).

TABLE I

Ketene–imine	Infrared: cm.$^{-1}$	Infrared: log ϵ_m [b]	Ultraviolet: mμ	Ultraviolet: log ϵ_m [b]	Ref.
$(n\text{-}C_4H_9)(C_2H_5)$—C=C=N—$(CH_2)_3CH_3$	2045		294	2.06	3b
$(CH_3)_2$—C=C=N—$C_6H_4(p\text{-}CH_3)$	2020				3b
$(C_6H_5)_2$—C=C=N—CH_3	2008				3b
$(C_6H_5)_2$—C=C=N—$(CH_2)_3CH_3$	2012				3b
$(C_6H_5)_2$—C=C=N—$(C_6H_4)(p\text{-}CH_3)$	2000		286.5	4.48	3b
			357	3.14	
$(CH_3)_2$—C=C=N·$C(CH_3)_2CN$	2016		287	2.13	9
			290	2.14[a]	13
	2026[c]	2.18	291	1.88[c,a]	
	2018[c]	2.14	290	1.70[a,d]	
~~CH_2—C(CH_3)(CN)—CH_2—C=C=N~~	2020		275		5
	2012				3a
~~CH_2—C(H)(CN)—CH_2—C=C=N~~	2025		266–272		

[a] Acetonitrile. [b] Units of l. mole^{-1} cm.$^{-1}$. [c] Ethanol. [d] Assuming 100% conversion. [e] Corrected wave numbers.

tively, the isolated ketene–imine having a molar extinction coefficient ϵ_m 139 l. mole.$^{-1}$ cm.$^{-1}$ in cyclohexane.

During the course of the photochemical reaction an isosbestic point occurs at λ = 326 mμ (see ref. 12), which is a criterion for the several compounds comprising the solute to be non-interacting and in equilibrium. Provided Beer's law is obeyed the solution can be considered to be a mixture of independently absorbing substances. This enables a check to be made of the value for the molar extinction coefficient of the ketene–imine structure III. Since Beers' law was shown to be followed for these solutions, from Fig. 2 the quantity of AIBN used was 0.0186 mole l.$^{-1}$ (0.0224 mole l.$^{-1}$ of ketene–imine), which gives ϵ_m 120.4 l. mole^{-1} cm.$^{-1}$ for the ketene–imine at 291 mμ. This is in reasonable agreement with the values quoted above.

The possibility that the 291-mμ peak arises from a structure other than III is remote since the most likely alternatives do not absorb close to this region. Adjacent chromophores such as the allenic group (*e.g.*, ethylallene) absorb at λ_{max} 170 mμ and the imide group (*e.g.*, diethylcarbodiimide) absorb at λ_{max} 230 mμ. Conjugated chromophores[17] such as the enimines (—CH=CH—CH=N—) and diimines (—N=CH—CH=N—) absorb in the regions 200–220 and 220–240 mμ, respectively. Azines (—CH=N—N=CH—) absorb over the region 280–400 mμ, but they may be distinguished from the ketene–imine by the occurrence of more than one peak of comparable extinction coefficient.

Solutions of AIBN in acetonitrile (0.0302 mole l.$^{-1}$) gave similar results to Fig. 2; λ_{max} 290 mμ, ϵ_m 50.4 l. mole^{-1} cm.$^{-1}$; AIBN, λ_{max} 344 mμ, ϵ_m 18.9 l. mole^{-1} cm.$^{-1}$.

Infrared Spectra.—A compensated spectrum of the irradiated solution was obtained in the region of 2000 cm.$^{-1}$ using bands at 1754, 2128, and 2246 cm.$^{-1}$ in the ethanol spectrum to adjust the compensating cells. For a cell of spacing d = 1.004 mm., log (I_0/I) = 0.55, from which, making the same assumptions with regard to the structure and conversion as above, the molar extinction coefficient for the absorption at 2016 cm.$^{-1}$ is ϵ_m 152.4 l. mole^{-1} cm.$^{-1}$. The ratio of the two molar extinction coefficients is therefore

$$(\epsilon_m)_{2016}/(\epsilon_m)_{291} = 2.03$$

This ratio is free from considerations concerning the mole fraction of radicals which have combined to form the ketene–imine structure, since the same solution was used in both experiments.

Infrared spectra of irradiated solutions of AIBN in acetonitrile (0.0302 mole l.$^{-1}$) after a similar period of irradiation showed an absorption band at 2008 ± 5 cm.$^{-1}$, ϵ_m 175.1 l. mole^{-1} cm.$^{-1}$, making the same assumptions as above. The ratio of the molar extinction coefficients in this solution is

$$(\epsilon_m)_{2008}/(\epsilon_m)_{290} = 3.47$$

Measurements in acetonitrile enabled a check to be made on the accuracy of the wave number measurements. In acetonitrile the CN stretching mode has a double peak found here to be at 2245 ± 5 and 2283 ± 5 cm.$^{-1}$. Felton and Orr[18] obtain 2255 and 2292 cm.$^{-1}$, Kitson and Griffith[19] obtain 2254 cm.$^{-1}$, and Skinner and Thompson,[20] 2251 cm.$^{-1}$, all in close agreement. The present results are therefore too low by 10 cm.$^{-1}$.

The ultraviolet and infrared properties of other ketene–imine structures are compared with the present results in Table I. With the exception of diphenyl ketene–tolylimine and the ketene–imine structures of the polymers, the ultraviolet peak is close to 290 mμ. The absorption in the infrared appears in the region 2000–2045 cm.$^{-1}$, with the majority of results lying in the range, 2018 ± 10 cm.$^{-1}$.

(17) H. C. Baramy, E. A. Braude, and M. Pianka, *J. Chem. Soc.*, 1898 (1949).

(18) D. G. I. Felton and S. F. D. Orr, *J. Chem. Soc.*, 2170 (1955).

(19) R. E. Kitson and N. E. Griffith, *Ind. Eng. Chem., Anal. Ed.*, **24**, 334 (1954).

(20) M. W. Skinner and H. W. Thompson, *J. Chem. Soc.*, 487 (1955).

The position of the ultraviolet peaks for the polymers also given in the table shows these values to be out of line. However, this shift to shorter wave lengths by 15–25 mμ is not by itself sufficient reason to conclude that the ultraviolet peak in the polymers does not arise from ketene–imine structures, since the influence of the neighboring polymer structure is as yet an unknown factor. Use can, however, now be made of the relative extinction coefficients of the infrared and ultraviolet peaks which have been obtained above. Polyacrylonitrile films were examined in both spectral regions using, where possible, the same film (since differences in absorptivity were found to be very large, corrections for scattering were neglected). For the ketene–imine absorption at 2020 cm.$^{-1}$, ϵ_s 4 cm.$^{-1}$ and for the CN stretching mode, ϵ_s 188 cm.$^{-1}$. From the ultraviolet spectra (Fig. 1), arbitrarily subtracting the background absorption arising from the CN chromophores, ϵ_s 250 cm.$^{-1}$ (curve 2) and there is clearly no correlation between the absorption at 266 mμ in the polymer and the ketene–imine structures, since it was shown above that the infrared band should have the greater extinction coefficient. The polymer prepared by persulfate–bisulfite initiation (Fig. 1, curve I) showed no ketene–imine absorption in the infrared.

THE KINETICS OF THE IRON(II)aq–COBALT(III)aq REACTION

BY LARRY E. BENNETT[1a] AND JOHN C. SHEPPARD[1b]

Department of Chemistry, San Diego State College, San Diego, Cal.

Received December 12, 1961

The kinetics of the oxidation of iron(II) ion by cobalt(III) ion in perchloric acid have been determined. This reaction obeys the rate expression: rate = $k_0[Co^{+++}][Fe^{++}] + k_1[CoOH^{++}][Fe^{++}]$. At 0° and at μ = 1.0, k_0 and k_1 have values of 10 and 6500 M^{-1} sec.$^{-1}$, respectively. The activation energies for the unhydrolyzed and hydrolyzed paths are 9.1 and 7.9 kcal./mole. The corresponding entropies of activation are −23 and −14 e.u.

The rate of electron-transfer between the lower oxidation states of the transition metals in perchloric acid has been subject to considerable investigation.[2–8] Representative reactions of this type that have been studied are the iron(II)–iron(III)[2a] and the chromium(II)–iron(III)[7] reactions. Important characteristics of these reactions that have been observed are: (1) similar entropies and energies of activation; (2) an important inverse hydrogen ion concentration rate dependence with the implication that hydrolyzed species are involved in the reaction; (3) effective catalysis by anions which complex the reactants.

The iron(II)–cobalt(III) reaction is of interest for three reasons. The results of a study of this reaction could be compared to those obtained for the iron(II)–iron(III)[2] and cobalt(II)–cobalt(III)[8] reactions. Of particular interest would be the comparison of the relative importance of the paths involving hydrolyzed species. Furthermore, the study of the iron(II)–cobalt(III) reaction could lead to a conclusion as to whether it proceeds *via* the participation of an inert or labile aquated cobalt(III) ion.

In 1 M perchloric acid and at about 2°, with the initial reactant concentrations equal and about 5 × 10^{-3} M, visual observations indicated that the half-time of the reaction was about 4 sec. Assuming second-order kinetics, a specific rate constant of about 50 M^{-1}/sec.$^{-1}$ was calculated.[9] The progress of this reaction then was followed spectrophotometrically by the utilization of the absorbancy of cobalt(III) ion at 6100 Å. in a study which confirmed the assumption regarding the kinetics as well as the value for the rate constant.[9] This paper is a report of a more detailed investigation of the kinetics of the iron(II)–cobalt(III) reaction in perchloric acid solution.

Experimental

The cobalt(II) perchlorate stock solutions used in the preparation of the cobalt(III) perchlorate were made by reacting cobalt(II) carbonate with an excess of perchloric acid. The cobalt(III) oxide formed during this preparation was removed by filtration. The cobalt(III) perchlorate stock solutions used for the kinetic runs were prepared immediately before use by the anodic oxidation of the perchloric acid solution of cobalt(II) perchlorate at 0° to minimize the instability of cobalt(III) ion with respect to water. The iron(II) perchlorate hexahydrate used was obtained from the G. Frederick Smith Co. Sodium perchlorate solutions, used to adjust ionic strength, were prepared by the titration of perchloric acid solutions with sodium hydroxide to a pH of 7. Some sodium perchlorate solutions were made from purified, crystalline sodium perchlorate obtained from the Fisher Scientific Co. Runs conducted at the same ionic strength and hydrogen ion concentration, using either source of sodium perchlorate, gave results that agreed within the experimental error.

Cobalt(III) ion concentrations were spectrophotometrically determined using a molar absorbancy index of 36 at 6100 Å. for this ion in 1 M perchloric acid.[10] Results obtained by this method agreed within 3% of those obtained by a titration method consisting of the addition of an aliquot of the cobalt(III) ion solution to an excess of a standardized ferrous ammonium sulfate solution. The excess iron(II) then was titrated with a standardized cerium(IV) sulfate

(1) (a) National Science Foundation undergraduate research participant, 1960 and 1961; (b) to whom inquiries should be made, now with General Electric Co., Hanford Laboratories, Richland, Washington.

(2) (a) J. Silverman and R. W. Dodson, *J. Phys. Chem.*, **56**, 846 (1952); (b) J. Hudis and A. C. Wahl, *J. Am. Chem. Soc.*, **75**, 4153 (1953).

(3) K. V. Krishnamurty and A. C. Wahl, *ibid.*, **80**, 5921 (1958).

(4) A. Anderson and N. A. Bonner, *ibid.*, **76**, 3826 (1954).

(5) E. L. King and H. Taube, *ibid.*, **76**, 4053 (1954).

(6) D. L. Ball and E. L. King, *ibid.*, **80**, 1091 (1958).

(7) H. Taube and H. Myers, *ibid.*, **76**, 2103 (1954).

(8) N. A. Bonner and J. P. Hunt, *ibid.*, **82**, 3826 (1960).

(9) J. C. Sheppard and A. C. Wahl, unpublished work.

(10) G. H. Hargreaves and L. H. Sutcliffe, *Trans. Faraday Soc.*, **51**, 786 (1955).

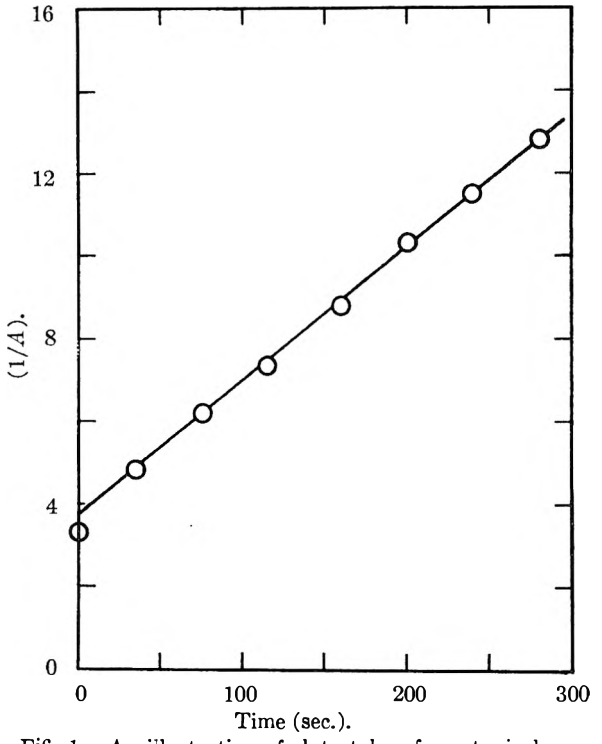

Fi6. 1.—An illustration of data taken for a typical run: $[HClO_4] = 0.285\ M$, $\mu = 1.0$, $[Fe(II)] = [Co(III)] = 1.13 \times 10^{-4}\ M$, 0°. The reciprocal absorbancy of the iron(II) tris-2,2′-bipyridyl ion at 5220 Å., a measure of the unreacted iron(II) ion, is plotted against time. The half-time is 100 ± 10 sec. and the resulting rate constant is 88 ± 9 M^{-1} sec.$^{-1}$.

solution using iron(II) tris-2,2′-phenanthroline as an indicator. Iron(II) ion concentrations were spectrophotometrically determined by the method of Moss and Mellon.[11]

The reaction vessel used in these experiments was a heart-shaped, three-necked flask. All solutions, the reaction vessel, and the pipets used for the withdrawal of aliquots of the reaction mixture were maintained at the same temperature in a refrigerated constant temperature bath, regulated to plus or minus 0.1°. The reaction was initiated by the rapid combination of the two 50-ml. reactant solutions containing either iron(II) perchlorate or cobalt(III) perchlorate and the appropriate concentrations of perchloric acid, sodium perchlorate, or any other reagent to be used. The reaction mixture was stirred by an electric motor-driven glass propellor. Seven or eight 5-ml. aliquots then were withdrawn at appropriate time intervals by means of the thermostated automatic pipets. These aliquots were injected immediately into a quench solution which in most runs consisted of 5 ml. of saturated sodium acetate, 5 ml. of 0.1% solution of 2,2′-bipyridine, and 1 or 2 ml. of concentrated ammonium hydroxide. The amount of ammonium hydroxide used depended upon the perchloric acid concentration of the reaction mixture. Other quench solutions used were ammonium hydroxide and 2,2′-bipyridine or ethyl alcohol, ammonium hydroxide, and 2,2′-bipyridine mixtures. When used, these quench solutions gave comparable but less reliable rate constants.

The absorbancy at 5220 Å. due to the iron(II) tris-2,2′-bipyridyl ion formed during the quenching reaction was used as a measure of the concentration of unreacted iron(II) ion. The absorbancies of cobalt(II) tris-2,2′-bipyridyl ion, iron(III), and cobalt(III) hydroxides are negligible at this wave length and at these concentrations.

Results

In view of the preliminary results[9] that indicated the reaction obeys the rate equation

$$\frac{-d[FeII]}{dt} = \frac{-d[Co(III)]}{dt} = {}'k'[Co(III)][Fe(II)] \quad (1)$$

all the kinetic runs were made with the reactant concentrations equal. Under these conditions the integrated rate expression, in terms of the iron(II) ion concentration, is

$$\frac{1}{[Fe(II)]_t} = {}'k't + \frac{1}{[Fe(II)]_0} \quad (2)$$

A plot of the reciprocal of the iron(II) ion concentration against time should be a straight line with slope equal to the specific rate constant, $'k'$. Each experiment obeyed this relationship and confirmed the assumption concerning the kinetics of this reaction. In most experiments the half-time, $T_{1/2}$, of the reaction was taken from the plot of the reciprocal of the iron(II) tris-2,2′-bipyridyl ion absorbancy against time and the specific rate constant was calculated from the equation

$${}'k' = \frac{1}{[Fe(II)]_0\, T_{1/2}} \quad (3)$$

Figure 1 is a plot of data obtained from a typical run and it shows that the reaction obeys second-order kinetics over a period of three half-times. Additional experiments were conducted to determine whether the reaction obeys the postulated rate law. Over a sevenfold initial concentration range the same specific rate constant was obtained, as shown by Table I. When the experiments at the lowest initial reactant concentrations are considered along with these data, this reaction obeys second-order kinetics over a sixtyfold concentration range. At least under the conditions used

TABLE I

RATE DEPENDENCE ON THE INITIAL REACTANT CONCENTRATIONS

0°, $\mu = 1.0$, 1 M perchloric acid

Initial reactant concn., $[Co(III)] = [Fe(II)] \times 10^4$, M	$'k'$, M^{-1}/sec.$^{-1}$
1.00	33
1.40	39
1.50	30
2.90	33
4.80	37
7.50	35
(av.)	34 ± 3

for these experiments there is no evidence for the reaction of polymerized species of cobalt(III)[12] with iron(II) ion. This observation is consistent with those of Bonner and Hun,t[13] who studied the cobalt(II)–cobalt(III) exchange reaction under comparable hydrogen ion but slightly higher cobalt(III) concentrations.

As seen in Fig. 1, the intercept does not coincide with the value calculated from the initial iron(II) concentration. This apparent zero-time oxidation of iron(II) is believed to be analogous to the separation-induced exchange found for many electron-transfer exchange reactions. Since it is a reproducible quantity, it does not affect the value of the specific rate constant, which is determined from

(11) M. L. Moss and M. G. Mellon, *Ind. Eng. Chem., Anal. Ed.*, **14**, 862 (1942).

(12) L. H. Sutcliffe and J. R. Weber, *J. Inorg. Nucl. Chem.*, **12**, 281 (1960).

(13) N. A. Bonner and J. P. Hunt, *J. Am. Chem. Soc.*, **74**, 1866 (1952).

the slope of the line. It is believed that this apparent zero time oxidation is due to the combination of a finite quenching time with the very rapid reaction rate involving hydrolyzed species of the reactants.

The study of reactions of this charge type has shown a marked inverse hydrogen ion dependence,[2a,3,4,7,8] which generally has been interpreted to mean that in addition to the reaction between the unhydrolyzed reactants there is another important path involving the reaction of a hydrolyzed species of one reactant with the unhydrolyzed species of the other reactant. If it is assumed that cobalt(III) ion hydrolyzes more extensively than does iron(II) ion, and therefore is the most probably hydrolyzed reactant species, the rate equation for the reaction between iron(II) and cobalt(III) is

$$\text{rate} = {}'k'\,[\text{Co(III)}][\text{Fe}^{++}] = k_0[\text{Co}^{+++}][\text{Fe}^{++}] + k_1[\text{CoOH}^{++}][\text{Fe}^{++}] \quad (4)$$

Upon expression of this equation in terms of the total cobalt(III) and iron(II) ion concentrations, eq. 5 is obtained.

$$'k' = k_0 + \frac{k_1 K_H}{[H^+]} \quad (5)$$

where K_H is the hydrolysis constant for Co^{+++} ion. A plot of the reciprocal of the hydrogen ion concentration against the formal rate constant, $'k'$, should yield a straight line with a slope of k_1K_H and an intercept of k_0. Figure 2 includes such plots at the three temperatures at which this reaction was studied and they are in agreement with the assumption that there is an important path involving the reaction of a hydrolyzed species of cobalt(III) ions with iron(II) ions.

These data were analyzed using the hydrolysis constant and heat of hydrolysis for Co^{+++} ion found by Sutcliffe and Weber.[14] Although some question has been raised concerning these values by Bonner and Hunt[8] as well as those of Sutcliffe and Weber,[12] they do, however, help to give an estimate of the specific rate constant for the path involving hydrolyzed species and should be considered tentative in nature. Table II is a summary of the rate data obtained by the use of eq. 3 and 5, data found in Fig. 2, and the hydrolysis data for cobalt(III) ion.[14]

Other experiments were conducted to determine the influence of a platinum surface, sulfate ions, and fluoride ions on the rate of the iron(II)–cobalt(III) reaction. The results of these experiments are shown in Table III.

The effect of the platinum surface and fluoride ion on the iron(II)–cobalt(III) reaction can be considered negligible; however, sulfate ion appears to be an excellent electron mediator. Assuming that the path involving sulfate ion is

$$CoSO_4^+ + Fe^{++} \xrightarrow{k_2} Co^{++} + FeSO_4^+$$

k_2 has a value of 4900 M^{-1} sec.$^{-1}$ at 0°. This calculation is based on the ionization constant of bisulfate ion found by Kerker[15] and the formation constant for $CoSO_4^+$ found by Sutcliffe and Weber.[16]

(14) L. H. Sutcliffe and J. R. Weber, *Trans. Faraday Soc.*, **52**, 1225 (1956).

(15) M. Kerker, *J. Am. Chem. Soc.*, **79**, 3664 (1957).

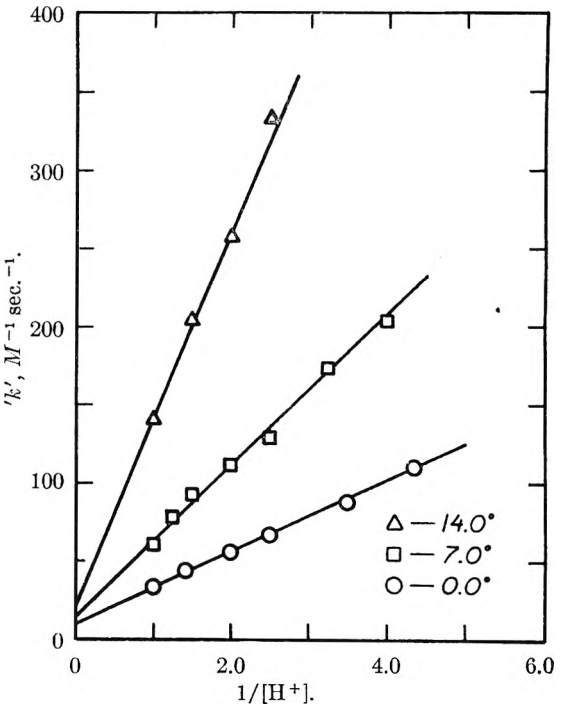

Fig. 2.—A plot of $'k'$ *vs.* the reciprocal of the hydrogen ion concentration at μ = 1.0 and at the three temperatures at which the reaction was studied. It is an illustration of the extent and nature of the hydrogen ion dependence of this reaction.

TABLE II

SUMMARY OF THE RATE DATA FOR THE IRON(II)–COBALT(III) REACTION IN PERCHLORIC ACID

μ = 1.0, adjusted with sodium perchlorate

Path	Temp., °C	k, M^{-1}/sec.$^{-1}$	E_{act}, kcal./mole
Fe^{++}–Co^{+++}	0.0	10 ± 2[b]	9.1
	7.0	15 ± 4	
	14.0	23 ± 8	
Fe^{++}–$CoOH^{++}$	0.0	(6500 ± 1200)[a,b]	7.9
	7.9	(8600 ± 1200)	
	14.0	(14000 ± 1500)	
Fe^{++}–Co(III)[c]	0.0	34 ± 3[b]	15.6
	7.0	61 ± 6	
	10.0	90 ± 15	
	14.0	140 ± 14	

[a] These values were calculated using the data of Sutcliffe and Weber,[14] for the hydrolysis of Co^{+++} ion. The hydrolysis constants for Co^{+++} ion at unit ionic strength at 0, 7, and 14° are 3.5 ± 0.5 × 10^{-3}, 5.6 ± 0.4 × 10^{-3}, and 8.7 ± 0.2 × 10^{-3}, respectively. [b] An error analysis of the data indicated that the errors, as shown in this table, are rather large. However, the excellent fit of these data with respect to the Arrhenius plot (Fig. 3) indicates that the data are possibly somewhat better. [c] These experiments were conducted in 1 M perchloric acid. This activation energy, an empirical value, is a function of the heat of hydrolysis of cobaltic ion and the activation energies for both paths listed in eq. 4.

Discussion

As shown by Fig. 2 the iron(II)–cobalt(III) reaction has a pronounced inverse hydrogen ion dependence, and these data are consistent with the rate law given by eq. 4. According to Bonner and Hunt[8] there is some question whether data of this

(16) L. H. Sutcliffe and J. R. Weber, *Trans. Faraday Soc.*, **57**, 91 (1961).

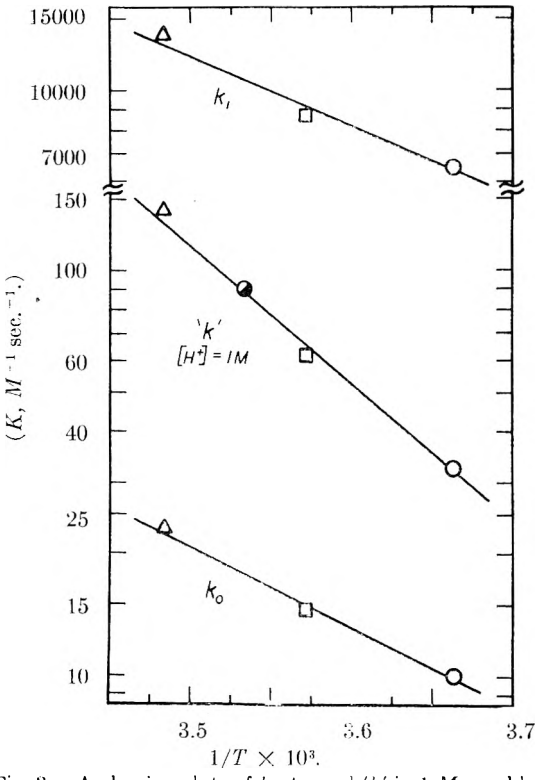

Fig. 3.—Arrhenius plots of k_0, k_1, and 'k' in 1 M perchloric acid, illustrating the good fit of the data. The activation energies reported in Table II were obtained from these plots. The half-shaded circle represents a value of 'k' found at 10.0° using one of the alternative quenching schemes. This plot was used to establish the formal activation energy in 1 M perchloric acid as well as those for the hydrogen ion concentration dependent and independent paths.

TABLE III

MISCELLANEOUS RATE DATA

0°, μ = 1.0, $[H^+]$ = 1 M

$[Co(III)] = [Fe(II)] = 1.35 \times 10^{-3}$ M

Condition	'k', M^{-1}/sec.$^{-1}$
40 cm.^{2} of Pt	
In reaction vessel	40 ± 4
1.2×10^{-3} M NaF	26 ± 3
7.0×10^{-2} M H_2SO_4	360 ± 40

type should be interpreted as a medium effect or a more intimate situation involving the reaction of hydrolyzed species. The hydrogen ion dependence data for the iron(II)–cobalt(III) and iron(II)–iron(III)[2a] reactions were analyzed using the Güntelberg[17] equation. Plots of the logarithm of the specific rate constant against perchloric acid–total perchlorate concentration ratio were found to be definite convex curves for this reaction, the iron(II)–iron(III)[2a] reaction, and to a slight extent with the cobalt(II)–cobalt(III)[8] reaction. Therefore, it was concluded that the data for these reactions are not consistent with the idea that the hydrogen ion effect is due to the reaction medium.

Although there is some question concerning the value for the hydrolysis constant for Co^{+++} ion, it was used to calculate the specific rate constant of the Fe^{++}–$CoOH^{++}$ path with the understanding that these data are only tentative in nature and subject therefore to later revision. However, it is interesting to note that the specific rate constant at 0° for the $CoOH^{++}$–Fe^{++} path is about 650 times that for the Co^{+++}–Fe^{++} path. This ratio is comparable to a ratio of 1100 for the same paths in the iron(II)–iron(III)[1] reaction. It is noteworthy that the corresponding ratio for the cobalt(II)–cobalt(III) reaction[8] is only about 40. In all of these reactions, as well as others,[3-7] the reaction between hydrolyzed species is a preferred path for the transfer of electrons.

The pronounced effect of hydroxide ion on the rate of electron transfer between cations must be due to a factor or factors other than the reduction of coulombic repulsion between reactants. If coulombic repulsion were the only factor to be considered, hydroxide ion would be expected to be about as effective as the halides and this is not what is observed.[2a,3,5] To account for the pronounced effect of hydroxide ion, an electrically symmetrical intermediate, possibly a bridge-activated complex, may be formed with the actual electron-transfer process taking place *via* some mechanism, such as hydrogen atom transfer[18,19] or electron conduction through a hydrogen-bonded intermediate.[20]

Magnetic susceptibility data have indicated that the aquated cobalt(III) ion exists predominantly in a low spin state[21] with a $(t_{2g})^6$ configuration, presumably due to the ligand field exerted by the water molecules coördinated to it. Under this circumstance it is expected that the aquated cobalt(III) ion be inert with respect to substitution. In addition, other reactions involving cobalt(III) in the low spin state are observed to be slow.[22] This is due to the structural differences between the low spin cobalt(III) and the high spin cobalt(II) complexes with the Franck-Condon restriction[23] associated with transitions between these states.

In contrast to the magnetic data,[21] aquated cobalt(III) ion behaves kinetically as though it were in the high spin state. Circumstantial evidence in support of this view is given by the following data. Friedman, Taube, and Hunt[24] found the rate of water exchange with cobalt(III) ion to be rapid. The rate of electron exchange between Co^{++} and Co^{+++} ions[8] is almost exactly that found for the corresponding path of the iron(II)–iron(III)[2] reaction under comparable conditions, indicating reaction between labile reactants. The entropy (−23 e.u.) and energy of activation (9.7 kcal./mole) for the Co^{+++}–Fe^{++} path of the cobalt(III)–iron(II) reaction are almost exactly those found for corresponding paths of the iron(II)–iron(III)[2a] reactions. All the above reactions are relatively rapid and indicate that they involve a kinetically labile

(17) E. Güntelberg, *Z. physik. Chem.*, **123**, 199 (1926).

(18) R. W. Dodson and N. Davidson, *J. Phys. Chem.*, **56**, 866 (1952).

(19) W. L. Reynolds and R. W. Lumry, *J. Chem. Phys.*, **23**, 2460 (1955).

(20) D. R. Stranks, "Modern Co-ordination Chemistry," J. Lewis and R. G. Wilkins, ed., Interscience Publishers, Inc., New York, N. Y., 1960, p. 154.

(21) H. L. Friedman, J. P. Hunt, R. A. Plane, and H. Taube, *J. Am. Chem. Soc.*, **73**, 4028 (1951).

(22) See, for example, W. B. Lewis, C. D. Coryell, and J. W. Irvine, *J. Chem. Soc. Suppl. Issue No. 2*, 5386 (1949).

(23) W. F. Libby, *J. Phys. Chem.*, **56**, 869 (1952).

(24) H. L. Friedman, H. Taube, and J. P. Hunt, *J. Chem. Phys.*, **18**, 759 (1950).

species of the aquated cobalt(III) ion, presumably in a high-spin state, and that the Franck-Condon[23] restriction is minimal for reactions involving the aquated cobalt(III) ion.

It has been suggested that the normal diamagnetic, low-spin state of cobalt(III) can be fairly easily excited to the paramagnetic high-spin state when water, with its relatively weak ligand field strength, is the ligand.[21] The rapidity of both the water exchange with the aquated cobalt(III) ion[24] and the cobalt(II)–cobalt(III)[8] exchange reactions have been explained on the basis that the reactive species of cobalt(III) is in the high-spin state, and a similar explanation could be advanced in the case of the iron(II)–cobalt(III) reaction.

In view of the preceding discussion, it is possible that the $(t_{2g})^6 \rightarrow (t_{2g})^4(eg)^2$ transition in the aquated cobalt(III) ion is the rate-determining step in the iron(II)–cobalt(II) reaction. Such a condition would require this reaction to obey zero-order kinetics with respect to the iron(II) concentration. The data for this reaction are consistent with first-order kinetics with respect to each reactant, indicating that electron-transfer is rate determining. Therefore, the possibility that the $(t_{2g})^6 \rightarrow (t_{2g})^4(eg)^2$ transition is rate determining is excluded on the basis that it is not consistent with the observed kinetics.

Another possible explanation of the rapidity of the iron(II)–cobalt(III) reaction is that it is catalyzed by the presence of cobalt(II), which always is present in these reaction mixtures. In this case it might be expected that electron-transfer between cobalt(II) and cobalt(III) could result in a labile form of cobalt(III) with the rate of electron transfer between cobalt(II) and cobalt(III) rate determining. Since the rate of the cobalt(II)–cobalt(III) reaction is slower than the iron(II)–cobalt(III) reaction under comparable conditions, the possibility of electron transfer between cobalt(II) and cobalt(III) being rate determining is excluded.

Data for additional reactions of this charge type are included in Table IV for the convenience of other investigators interested in this type of reaction.

TABLE IV

MISCELLANEOUS REACTIONS INVOLVING M(*II*) AND N(*III*) IONS IN 1 *M* PERCHLORIC ACID AT 0°

M(II)	N(III)	*k*′, M^{-1} sec.$^{-1}$
V(II)	Co(III)	>300[a]
Cr(II)	Co(III)	>300[a]
V(II)	Fe(III)	$>10^5$[b]
Eu(II)	Fe(III)	$>10^5$[b]

[a] Reaction visually observed, initial reactant concentrations were equal and about 5×10^{-3} *M*. [b] Reaction studied using a flow reactor similar to Gordon and Wahl[25] and the quenching technique used for the iron(II)–cobalt(III) reaction. The reactant concentrations were equal and about 10^{-4} *M*.

Acknowledgments.—We wish to acknowledge the support of this research by the National Science Foundation. The data found in Table IV were obtained by L. C. Brown.

(25) B. M. Gordon and A. C. Wahl, *J. Am. Chem. Soc.*, **80**, 273 (1958).

STUDIES OF ISOTHERMAL DIFFUSION AT 25° IN THE SYSTEM WATER–SODIUM SULFATE–SULFURIC ACID AND TESTS OF THE ONSAGER RELATION[1]

BY RICHARD P. WENDT[2]

Department of Chemistry and the Institute for Enzyme Research, University of Wisconsin, Madison 6, Wisconsin

Received December 15, 1961

The isothermal diffusion process at 25° in dilute solutions of the ternary system H_2O–Na_2SO_4–H_2SO_4 has been studied with the Gouy diffusiometer. Values for the four volume-fixed diffusion coefficients which may be used to describe diffusion in a ternary system were obtained at each of four compositions of the system. The cross-term diffusion coefficients responsible for the interacting-flow effect were found to be relatively large and of the same order of magnitude as the main-term coefficients. Diffusion and density measurements at two compositions of the binary systems H_2O–Na_2SO_4 and H_2O–H_2SO_4, and partial molal volumes and refractive-index derivatives for the ternary system, also are reported. Activity data in the literature were analyzed and combined with the diffusion data to test the Onsager reciprocal relation; the relation was found to be satisfied within experimental error at each composition.

Introduction

The isothermal diffusion process in a three-component system can be completely described by two flow equations[3,4] which here are written for the case of diffusion along the *x*-coördinate only

$$(J_1)_V = -(D_{11})_V \frac{\partial n_1}{\partial x} - (D_{12})_V \frac{\partial n_2}{\partial x} \quad (1)$$

$$(J_2)_V = -(D_{21})_V \frac{\partial n_1}{\partial x} - (D_{22})_V \frac{\partial n_2}{\partial x} \quad (2)$$

In these equations the flows $(J_i)_V$ are referred to the volume-fixed reference frame and have dimensions of moles/(cm.^{2} sec.), the concentrations n_i have units[5] of moles/cc., and the four volume-fixed diffusion coefficients $(D_{ij})_V$ have dimensions

(1) Portions of this work were submitted as partial requirements for the degree of Doctor of Philosophy at the University of Wisconsin. These studies were presented at the 140th National Meeting of the American Chemical Society, Chicago, Illinois, September, 1961.

(2) Institute for Molecular Physics, University of Maryland, College Park, Maryland.

(3) R. L. Baldwin, P. J. Dunlop, and L. J. Gosting, *J. Am. Chem. Soc.*, **77**, 5235 (1955).

(4) G. J. Hooyman, *Physica*, **22**, 751 (1956).

(5) The concentrations n_i in eq. 1 and 2 must have units of moles/cc. if $(J_i)_V$ and $(D_{ij})_V$ are to have the units indicated. However, the concentrations reported for all experiments in this work have units of moles/1000 cc.

of cm.^{2}/sec. The volume-fixed reference frame becomes very nearly identical with the cell-fixed (or apparatus-fixed) reference frame for the small concentration differences in the experiments described here.[6,7] In this paper we report values for the four diffusion coefficients measured with the Gouy diffusiometer at each of four compositions of the system H_2O–Na_2SO_4–H_2SO_4.

This system was particularly interesting because the solute H_2SO_4 was expected to behave approximately as it does in dilute binary aqueous solutions,[8] *i.e.*, it was expected to exhibit the properties of both a strong acid, H_2SO_4 (which dissociates completely into H^+ and HSO_4^-), and a weak acid, HSO_4^- (which only partially dissociates into H^+ and $SO_4^=$). Relatively large values were expected for the cross-term diffusion coefficients $(D_{12})_V$ and $(D_{21})_V$ because of the appreciable concentrations of very mobile H^+ in the solutions[9]; the measured values for those coefficients at some compositions in fact were found to be larger than values previously reported for any ternary system. The incomplete dissociation of the bisulfate ion was expected to cause unusual concentration dependence of certain physical properties of the system which could have invalidated assumptions in the procedure[10] used to calculate the diffusion coefficients from data obtained with the Gouy diffusiometer. However, for the small concentration differences in these experiments the calculation procedure was found to be applicable.

Available thermodynamic activity data for the system,[11–13] when combined with the diffusion coefficients and density data obtained in this work, enabled tests to be made of the Onsager reciprocal relation.[14,15] The Onsager relation was derived by Onsager by using the postulate of microscopic reversibility and is of fundamental importance to the theory of irreversible processes. Our tests of the Onsager relation for this system confirmed its validity, within experimental error, at each of the four compositions studied. The Onsager relation also has been tested and confirmed from activity and diffusion data obtained at several compositions of two other systems,[10,16,17] H_2O–NaCl–KCl and H_2O–glycine–KCl. The tests reported here are the first for a ternary system containing an incompletely-dissociated electrolyte.

(6) G. J. Hooyman, *et al.*, *Physica*, **19**, 1095 (1953).

(7) J. G. Kirkwood, *et al.*, *J. Chem. Phys.*, **33**, 1505 (1960).

(8) T. F. Young, *et al.*, in "The Structure of Electrolytic Solutions," W. J. Hamer, ed., John Wiley and Sons, Inc., New York, N. Y., 1959, pp. 48–59.

(9) L. J. Gosting in "Advances in Protein Chemistry," Vol. XI, Academic Press, Inc., New York, N. Y., 1956, p. 538. Equations 168–172 are only applicable to systems containing strong electrolytes, but by assuming the dissociation of HSO_4^- to be complete, estimates of the diffusion coefficients can be made for the system H_2O–Na_2SO_4–H_2SO_4.

(10) H. Fujita and L. J. Gosting, *J. Phys. Chem.*, **64**, 1256 (1960).

(11) H. S. Harned and R. D. Sturgis, *J. Am. Chem. Soc.*, **47**, 945 (1925).

(12) G. Åkerlöf, *ibid.*, **48**, 1160 (1926).

(13) M. Randall and C. T. Langford, *ibid.*, **49**, 1445 (1927).

(14) L. Onsager, *Phys. Rev.*, **37**, 405 (1931); **38**, 2265 (1931).

(15) S. R. de Groot, "Thermodynamics of Irreversible Processes," Interscience Publishers, Inc., New York, N. Y., 1958.

(16) P. J. Dunlop, *J. Phys. Chem.*, **63**, 612 (1959); see also corrections, *ibid.*, **63**, 2089 (1959).

(17) L. A. Woolf, D. G. Miller, and L. J. Gosting, *J. Am. Chem. Soc.*, **84**, 317 (1962).

Theoretical

Definition of Components.—The system H_2O–Na_2SO_4–H_2SO_4 is designated a three-component system because the composition at any point in the system can be specified by two independent concentration variables. For this system five constituents, designated by the subscripts[18] 0 = H_2O, 3 = Na^+, 4 = H^+, 5 = $SO_4^=$, and 6 = HSO_4^-, are hypothesized to be present at appreciable concentrations; the dissociation of H_2O produces no appreciable concentrations of OH^- in the strongly acidic solutions. There are three constraints on the concentrations of these constituents at each point in the system during the diffusion process. The concentrations C_i (in moles/1000 cc.) and the partial molal volumes $\bar{V}_i$ (in cc./mole) are related by

$$\sum_{\substack{i=0 \\ i\neq 1,2}}^{6} C_i \bar{V}_i = 1000 \qquad (3)$$

Another constraint is the condition of local electrical neutrality

$$\sum_{i=3}^{6} z_i C_i = 0 \qquad (4)$$

where z_i is the valence (including the sign) of constituent i. The condition of local chemical equilibrium for the dissociation of HSO_4^- into H^+ and $SO_4^=$ is

$$Q = C_4 C_5 / C_6 \qquad (5)$$

where Q is the dissociation quotient for the reaction. Only two of the five concentration variables related by these equations can be independent and the system therefore consists of three components.

Although the number of components is definitely fixed by eq. 3–5 the choice of components is arbitrary. Any three constituents could have been chosen as components, but the components H_2O, Na_2SO_4, and H_2SO_4 were chosen because they are neutral and can be separately weighed to prepare solutions for the experiments.

Flow Equations.—To describe the diffusion process in this system and to test the Onsager reciprocal relation it is necessary to be certain that the equations for flows of neutral components have the correct form. First the expression for the entropy production will be written to include the forces and flows of the ionic constituents; then that expression will be rewritten in terms of the forces and flows of the two neutral solutes. The forms of the linear laws are obtained by examining the final expression for the entropy production.

For the isothermal diffusion process in this system the expression for the entropy production can be written[4,6]

$$T\sigma = \sum_{i=3}^{6} (J_i)_0 \bar{X}_i \qquad (6)$$

Here T is the absolute temperature, σ is the local production of entropy per unit volume per second, $(J_i)_0$ is the flow of constituent i referred to the sol-

(18) The subscripts 1 and 2 will be used later to designate Na_2SO_4 and H_2SO_4, respectively.

vent-fixed reference frame, and $\bar{X}_i$, the thermodynamic force per mole of i, is defined by

$$\bar{X}_i = X_i + z_i F E \quad (7)$$

$$X_i = -\partial\mu_i/\partial x \quad (8)$$

In these equations μ_i is the chemical potential per mole of constituent i, F is the absolute value of the electrical charge per equivalent of electrons, and E is the local electric field strength. The solvent-fixed reference frame is used because of its mathematical convenience[19]; *i.e.*, by definition

$$(J_0)_0 = 0 \quad (9)$$

so the product $(J_0)_0 \bar{X}_0$ does not appear in eq. 6.

The required relations between the flows and forces of the neutral components and the ionic constituents now will be written. In this discussion the subscripts 1 and 2 denote Na_2SO_4 and H_2SO_4, respectively; the subscripts 0, 3, . . . , 6 were defined previously. The equations

$$X_1 = 2X_3 + X_5 \quad (10)$$

$$X_2 = X_4 + X_6 \quad (11)$$

$$2(J_1)_0 = (J_3)_0 \quad (12)$$

$$2(J_2)_0 = (J_4)_0 + (J_6)_0 \quad (13)$$

follow from the definitions of the neutral components 1 and 2. Also

$$X_6 = X_4 + X_5 \quad (14)$$

because local chemical equilibrium is considered to exist during the diffusion process. From the condition of zero electrical current density during the diffusion process

$$\sum_{i=3}^{6} z_i v_i n_i = 0 \quad (15)$$

the condition of local electrical neutrality, eq. 4, and the definition of solvent-fixed flows

$$(J_i)_0 = n_i(v_i - v_0) \quad (16)$$

we derive the constraint

$$\sum_{i=3}^{6} (J_i)_0 z_i = 0 \quad (17)$$

on the solvent-fixed flows of the ions. In eq. 15 and 16, v_i is the velocity of constituent i relative to the cell-fixed reference frame. Equations 7, 8, 10–14, and 17 are introduced into eq. 6 to obtain

$$T\sigma = \sum_{i=1}^{2} (J_i)_0 X_i \quad (18)$$

Thus eq. 6 for the entropy production can be expressed in terms of flows and forces of the two neutral solutes Na_2SO_4 and H_2SO_4.

The linear laws then have the form

$$(J_i)_0 = \sum_{j=1}^{2} (L_{ij})_0 X_j \qquad (i = 1, 2) \quad (19)$$

according to the thermodynamics of irreversible processes.[15] Furthermore, because the flows $(J_i)_0$ and the forces X_j are independent variables, the Onsager reciprocal relation for the solvent-fixed reference frame can be written

$$(L_{12})_0 = (L_{21})_0 \quad (20)$$

It has been shown by Hooyman and others[4,7] that equations such as (19) can be transformed to a pair of flow equations for the volume-fixed reference frame. The resulting independent flows $(J_1)_V$ and $(J_2)_V$ then can be related linearly to the concentration gradients of Na_2SO_4 and H_2SO_4 to obtain eq. 1 and 2, thereby justifying the description of the diffusion process in this system by those two flow equations.

(19) $T\sigma$ also can be written for flows referred to other reference frames; *cf.* eq. 31, ref. 6, and eq. 8, ref. 17.

Experimental

Reference to some earlier descriptions of studies of diffusion in ternary systems[10,17] may be helpful in reviewing standard procedures and notation. New procedures used in the present work, and other necessary information, are included here.

Materials.—H_2O, the solvent used for all experiments, was prepared by distillation of ordinary distilled H_2O from an alkaline solution of $KMnO_4$ in a Barnstead Conductance Water Still. The conductance water collected had a specific conductance of 2×10^{-6} ohm^{-1} cm.$^{-1}$ and was stored in a Pyrex carboy after being saturated with air.

Anhydrous Na_2SO_4 was prepared by dissolving Baker and Adamson reagent grade $Na_2SO_4 \cdot 10H_2O$ in conductance water at 40°. The solution was cooled to 4° and seeded; the precipitated crystals of $Na_2SO_4 \cdot 10H_2O$ then were collected by centrifugal drainage, heated in a drying oven at 115° to constant weight of the anhydrous salt, and stored in a desiccator over P_2O_5. When the Na_2SO_4 was transferred into weighing vials to prepare solutions for the diffusion experiments the desiccator was opened, and the transfer was made in a "drybox" containing an atmosphere of N_2 dried over P_2O_5.

Instead of preparing a stock solution of H_2O–H_2SO_4 and then analyzing the solution for H_2SO_4 by gravimetric or acidimetric methods, a stock solution for the diffusion experiments was prepared by weight from conductance water and 100.00% pure H_2SO_4. Kunzler[20] has concluded that the mixture H_2O–SO_3 having a maximum freezing point of 10.371° is 100.000% H_2SO_4. Two batches of H_2SO_4 were prepared at different times by mixing solutions of slightly SO_3-rich and slightly H_2O-rich distilled H_2SO_4 in an air-tight 300-ml. freezing-point cell similar to that described by Kunzler. All of the glass apparatus used in the preparation and storage of the acid was fabricated of Pyrex brand glass No. 7740, and all ground glass joints were either lubricated with concentrated H_2SO_4 or fitted with Teflon sleeves. The maximum freezing points of batches 1 and 2 were 10.358 and 10.367°, respectively, as determined by an American Instrument Co. platinum resistance thermometer and a Leeds and Northrup Type G-2 Mueller temperature bridge, both of which had been calibrated recently by the National Bureau of Standards. By assuming that SO_2 was the impurity causing the freezing point depressions of 0.013 and 0.004°, and using the cryoscopic constant[21] of 6.0 (deg. kg. solvent)/(mole solute) for solutes in the solvent H_2SO_4, the weight per cents of SO_2 in batches 1 and 2 were calculated to be 0.021 and 0.007%, respectively. These estimated amounts of impurity were so small that both of the H_2O–SO_3 mixtures were taken to be 100.00% H_2SO_4.

For each preparation the batch of H_2SO_4 was transferred from the freezing-point cell to a weighed 2-l. Florence flask through a delivery tube so that no moist air came in contact with the acid. The flask and acid were weighed and conductance water was carefully added to the acid to prepare a stock solution of moderately dilute H_2SO_4. After the flask and stock solution were weighed an automatic buret fitted with a ground-glass joint was inserted into the flask. The buret had been modified so that all air entering the flask–buret assembly first bubbled through a trap containing 30 ml. of the stock solution.

From the weights of the stock solution and the 100.00% H_2SO_4 added to the flask, the compositions of batches 1 and 2 of stock solution were calculated to be 44.873 and 48.330% H_2SO_4 by weight, respectively. A sodium carbonate analysis of batch 1 agreed, within the 0.08% relative precision of that analysis, with the calculated weight per cent of H_2SO_4 in the freshly prepared stock solution. Densities

(20) J. E. Kunzler, *Anal. Chem.*, **25**, 93 (1953).

(21) R. J. Gillespie, *Rev. Pure and Appl. Chem.*, **9**, 1 (1959).

of dilute solutions of the stock solution also were measured shortly after its preparation. Thereafter, analyses of batches 1 and 2 were made by density measurements. The relative change in the concentration of batch 1 determined from these measurements was 0.15% over a period of eight months and the relative change of batch 2 was 0.05% over a period of seven months. Because the relative precision of the density analyses was approximately the same as the changes in the stock solution concentrations, no corrections were made and the concentrations originally calculated from the weights of pure acid and stock solution were used for all experiments. The slow changes of the acid concentrations with time are not believed to have influenced the magnitudes of the diffusion coefficients reported here because those quantities showed a relatively small dependence on concentration.

Preparation of Solutions.—Two solutions A and B, having concentrations $(C_1)_A$, $(C_2)_A$, and $(C_1)_B$, $(C_2)_B$, respectively, were prepared for each diffusion experiment. Solution B, with a density $(d)_B > (d)_A$, was present in the lower portion of the diffusion cell during the siphoning process for sharpening the initial boundary, and solution A was in the upper portion of the cell. It was desirable to prepare solutions A and B so that the concentrations $\bar{C}_i$, where

$$\bar{C}_i = [(C_i)_A + (C_i)_B]/2 \qquad (21)$$

were within approximately 0.05% of the concentrations $\bar{C}_1$ and $\bar{C}_2$ which specified the compositions of the ternary solutions. The actual concentrations of the solutions were known within approximately 0.002%. Desired values for ΔC_i, where

$$\Delta C_i = (C_i)_B - (C_i)_A \qquad (22)$$

were calculated according to eq. 39 and 41 of ref. 17 for specified values of the refractometric fraction, α_1, by requiring $40 < J < 80$. The number of fringes, J, for the experiment was made as small as possible without seriously reducing the precision of the measurements, so that the effects of concentration dependence of the measured properties of the system would be minimized. From the values specified for $\bar{C}_i$ and ΔC_i the desired values for $(C_i)_A$ and $(C_i)_B$ were calculated according to eq. 21 and 22.

To determine the relative amounts of each component required for the solutions, weight per cents w_i *in vacuo* corresponding to the desired values for C_i, were calculated from

$$w_i d = C_i M_i/10 \qquad (23)$$

Here d is the solution density (in g./cc.), C_i is the concentration of component i (in moles/1000 cc.), and M_i is the molecular weight of i. No density data for the system H_2O–Na_2SO_4–H_2SO_4 are available in the literature at the concentrations required. Therefore, before performing the three-component diffusion experiments a preliminary solution at each composition was prepared as follows. From density data for the binary systems H_2O–Na_2SO_4 and H_2O–H_2SO_4 (Table V) an estimate was made of the concentration dependence of the densities of the binary systems. By assuming that this dependence on C_1 and C_2 was the same for the ternary systems an estimate was made of the density of the preliminary solution at the composition $\bar{C}_1$, $\bar{C}_2$. Equation 23 then was used to calculate the estimated values for w_1 and w_2. To prepare the solution a weighing vial containing Na_2SO_4 was emptied into a 300-ml. erlenmeyer flask. From the known weight of Na_2SO_4 and the estimated values for w_1 and w_2, the required weights of stock solution and H_2O were calculated and added to the flask. By using a weight buret it was possible to add, within approximately 4 mg., a predetermined amount of stock solution to the flask. The weights of stock solution added, and the weights of the Na_2SO_4 and of the prepared solutions, actually were known to within about 0.1 mg.

The density measured for the preliminary solution was used to estimate $d(\bar{C}_1, \bar{C}_2)$ in the density expression

$$d = d(\bar{C}_1, \bar{C}_2) + H_1(C_1 - \bar{C}_1) + H_2(C_2 - \bar{C}_2) \qquad (24)$$

for ternary solutions with small values for $C_i - \bar{C}_i$. The densities of the solutions for the diffusion experiments then could be estimated to within about 0.05%. After the densities of solutions prepared according to the above procedure had been measured for two diffusion experiments, the coefficients H_1 and H_2 in eq. 24 were sufficiently well-determined so that densities for the remaining two experiments at each composition could be predicted to within 0.005%.

Densities of the solutions were measured in triplicate in single-stem pycnometers, each holding approximately 30 ml. of solution. The percentage deviation from the average of the three densities measured for each solution was approximately 0.001%, and over a period of several months the volume of each pycnometer stayed constant within approximately 0.001%. To calibrate the pycnometers the density of water at 25° was taken to be 0.997044 g./cc.

The observed weights of solutes and solution were corrected to weights *in vacuo* by using densities of 8.4, 2.66, 1.36, and about 1.12 g./cc. for the brass weights, the anhydrous Na_2SO_4, the stock solution, and the prepared solutions, respectively.

Diffusion Experiments.—The Gouy diffusiometer described previously[22] was used for this work without modification. Two different quartz Spinco Model H electrophoresis cells were used for the diffusion experiments. Cell 1, used for experiment I, had an a distance of 2.5092 cm., and the b distance with this cell in the diffusiometer was 306.67 cm.; cell 2, used for all other experiments, had an a distance of 2.5075 cm., and the b distance corresponding to this cell was 306.64 cm.

Experiments for the binary systems H_2O–Na_2SO_4 and H_2O–H_2SO_4 were performed near the compositions $\bar{C} = 0.5$ and $\bar{C} = 1.0$ for each system. For the ternary system H_2O–Na_2SO_4–H_2SO_4 four experiments were performed near each of the composition points A ($\bar{C}_1 = 0.5$, $\bar{C}_2 = 0.5$), B ($\bar{C}_1 = 1.0$, $\bar{C}_2 = 0.5$), C ($\bar{C}_1 = 0.5$, $\bar{C}_2 = 1.0$), and D ($\bar{C}_1 = 1.0$, $\bar{C}_2 = 1.0$).

For experiment I and for the experiments at compositions A and B a stainless steel capillary, electrolytically coated with platinum to prevent chemical attack by the acidic solutions, was used to form the boundary between the two solutions in the diffusion cell. A capillary fabricated of 80% platinum–20% iridium hard-temper tubing by J. Bishop and Co. was used for the other experiments.

For all experiments in this work, monochromatic light of wave length $\lambda = 5460.7$ Å. in air, emitted from a GE H-100A4 mercury vapor lamp and transmitted by an Eastman Kodak Wratten filter 77A, illuminated the source slit of the diffusiometer. All photographs were taken on Eastman Kodak Kodaline C.T.C. Pan plates with anti-halation backing. The temperature of the water-bath in which the diffusion cell was immersed was within ±0.008° of 25.000° for all experiments and temperature variations were no greater than ± 0.005° during any experiment.

The positions of fringe maxima and minima were determined with a newly constructed photoelectric null-indicator mounted on a Gaertner Model M2001RS toolmaker's microscope. The construction of a similar device recently was reported by Bennett and Koehler.[23] Our apparatus contained a rotating glass plate having two parallel light transmitting surfaces instead of the four-surfaced plate used by those authors, and we did not find it necessary to install a light chopper as they did.[24] By using the null-indicator, positions of interference fringes on the photographic plates could be reproduced to within approximately 5 μ for fringes having broad maxima and minima and to within approximately 1 μ for fringes having narrow maxima and minima. These uncertainties are less by a factor of approximately two than the estimated uncertainties in visual determinations of fringe maxima and minima. For each of the 7 or 8 Gouy fringe photographs taken during an experiment the positions of approximately 15 fringe minima throughout the fringe pattern and 5 lower-numbered fringe maxima were measured.

Horizontal Rayleigh photographs[25] were taken during the siphoning process to find the fractional part of J, the number

(22) P. J. Dunlop and L. J. Gosting, *J. Am. Chem. Soc.*, **77**, 5238 (1955).

(23) J. M. Bennett and W. F. Koehler, *J. Opt. Soc. Am.*, **49**, 466 (1959).

(24) A more detailed description of the null-indicator is given by R. P. Wendt in his Ph.D. thesis, U. of Wisconsin, 1961 (L. C. Card No. Mic 61-680).

(25) L. J. Gosting, *et al.*, *Rev. Sci. Instr.*, **20**, 209 (1949).

of fringes for the experiment, and Rayleigh interferograms[26] were used to determine the integral part of J.

Calculations

Diffusion Coefficients.—A procedure developed by Fujita and Gosting[10] was used to calculate the four diffusion coefficients, $(D_{ij})_V$, from the Gouy diffusiometer data obtained at each composition of the system. This procedure requires data from at least two diffusion experiments at different values of α_1, the refractometric fraction of component 1. At each composition in this work data were obtained at four different values of α_1 of approximately 0, 0.15, 0.85, and 1.0 to provide checks on the internal consistency of the data and increase the accuracy of the results.

Values for the quantities required to calculate the diffusion coefficients were obtained from the data shown in Table I. Determination of the number of fringes, J, was described in the previous section, and values for ΔC_i were calculated according to eq. 22.

The reduced height–area ratio, $\mathfrak{D}_A$, is defined by eq. 35 of ref. 22. It is necessary to find preliminary values[27] $\mathfrak{D}_A'$ for $\mathfrak{D}_A$, corresponding to the times t' after the boundary sharpening process is stopped. The measured positions of the Gouy interference fringes were used to calculate $\mathfrak{D}_A'$ for each fringe photograph according to the following procedure. Except as indicated, all calculations were performed by a Bendix G-15 computer using programs written for the Intercom 1000 (double-precision) programming system.

Fringe displacements Y_j of fringes number j were calculated from measured values for the positions of the fringe minima and maxima and the corrected position of the undeviated slit image. The quantities[28] Z_j and M_j were calculated by using the appropriate equations[29] to find a_s and a_s', the zeros and turning values of the Airy integral; $f(\zeta_j)$ then was calculated from eq. 11 and 12 of ref. 28. Values for $e^{-\zeta_j^2}$ were computed by using a Newton–Rhapson iteration process. The computer then calculated and printed out values for $Y_j/e^{-\zeta_j^2}$.

A graph of $Y_j/e^{-\zeta_j^2}$ *vs.* $Z_j^{2/3}$ (or $M_j^{2/3}$) should be linear[30] for values of $Z_j^{2/3}$ (or $M_j^{2/3}$) near 0, and the intercept at $Z_j^{2/3}$ (or $M_j^{2/3}$) = 0 should equal the maximum displacement of light according to ray optics, C_t, a quantity necessary to calculate $\mathfrak{D}_A'$. We tried to use the method of least squares to determine C_t by calculating the coefficients in expressions for $Y_j/e^{-\zeta_j^2}$ as a linear function, a quadratic function, and a cubic function of $Z_j^{2/3}$. Fringe displacements Y_j for about 15 of the first 30 fringes were used for these calculations, because $Z_j^{2/3}$ and $M_j^{2/3}$ become small as $j \rightarrow 0$. Values for C_t obtained from these equations were in general significantly different from each other and were

(26) J. M. Creeth, *J. Am. Chem. Soc.*, **77**, 6428 (1955).

(27) Equation 35, ref. 17.

(28) L. J. Gosting and M. S. Morris, *J. Am. Chem. Soc.*, **71**, 1998 (1949).

(29) "The Airy Integral," British Association for the Advancement of Science Mathematical Tables, Part-Volume B, University Press, Cambridge, 1946, p. B48. The subscripts s in equations there correspond to fringe numbers $j + 1$ in our notation.

(30) See Appendix, ref. 10.

TABLE I[a]

FUNDAMENTAL DATA FOR THE SYSTEM H_2O–Na_2SO_4–H_2SO_4 AT 25°

(1 = Na_2SO_4; 2 = H_2SO_4)

		A: $\bar{C}_1 = 0.5$, $\bar{C}_2 = 0.5$			B: $\bar{C}_1 = 1.0$, $\bar{C}_2 = 0.5$			C: $\bar{C}_1 = 0.5$, $\bar{C}_2 = 1.0$			D: $\bar{C}_1 = 1.0$, $\bar{C}_2 = 1.0$		
1.	Composition[b]	1	2	3	4	5	6	7	8	9	10	11	12	13	14	15	16
2.	Experiment no.	0.50005	0.50024	0.50028	0.50009	0.99973	1.00008	1.00002	0.99996	0.50000	0.50001	0.50002	0.49996	1.00004	0.99997	0.99995	1.00000
3.	$\bar{C}_1$	.50003	.50059	.50019	0.50023	0.50062	0.50066	0.50002	.49987	1.00012	1.00002	.99991	1.00029	1.00006	.99888	.99990	1.00002
4.	$\bar{C}_2$	.50091	.49397	.45755	.44729	.95242	1.00050	.99537	.95242	.94705	0.50001	0.49204	.46347	0.45001	1.00020	.99145	0.95002
5.	$(C_1)_A$	.42442	.43304	.48533	.50108	.49240	0.42431	.43039	.49240	.50072	0.89996	0.91620	.98197	1.00014	0.90150	.90861	.98750
6.	$(C_2)_A$	1.07935	1.07899	1.07751	1.07775	1.05242	1.13470	1.13445	1.13263	1.10543	1.10551	1.10638	1.10585	1.15829	1.15774	1.15876	1.1516
7.	$(D)_A$	0.49919	0.50651	0.54302	0.55288	0.99465	1.00468	1.04750	1.05242	0.50002	0.50797	0.53644	0.55002	0.99987	1.00849	1.03750	1.04998
8.	$(C_1)_B$	0.57565	0.56815	0.51505	0.49938	0.57701	0.56964	0.50735	0.50052	1.10007	1.03401	1.01486	1.00045	1.09862	1.08915	1.01231	0.99993
9.	$(C_2)_B$	1.08732	1.03770	1.03900	1.03912	1.14200	1.14218	1.14383	1.14402	1.11673	1.11665	1.11572	1.11633	1.16814	1.16881	1.16787	1.16856
10.	$(D)_B$	58.94	58.52	72.25	75.17	39.16	42.66	70.87	73.99	82.24	78.72	57.05	61.33	64.31	69.44	54.27	61.25
11.	J	1.3110	1.2097	0.9702	0.8515	0.8063	0.7950	0.7418	0.7404	1.6929	1.5317	0.9564	0.8388	1.2569	1.1521	0.8120	0.7559
12.	$\mathfrak{D}_A \times 10^5$	180.98	155.48	.58	−44.51	61.34	46.18	−2.39	−1.60	160.65	166.65	9.48	−72.95	214.92	196.60	11.28	−33.96
13.	$Q \times 10^4$	−0.0228	0.1542	.8496	1.0033	−0.0153	0.1532	0.9451	1.0007	0.0001	0.1239	0.7844	0.9979	−0.0031	0.1504	0.8503	1.0010
14.	α_1[c]																

[a] Units: concentrations, $\bar{C}_i$, moles/1000 cc.; densities, d, g./cc.; reduced height–area ratios, $\mathfrak{D}_A$, cm.²/sec. [b] Solutions for experiments at compositions A and B were prepared from batch 1 of stock solution; batch 2 was used for the experiments at compositions C and D (see Materials in text). [c] Calculated from values for R_i in Table II according to eq. 39, ref. 17.

found to differ by 1% or more from values for C_t obtained by the graphical method of extrapolation to $Z_j^{2/3} = 0$. The differences between the graphical and calculated values for C_t were especially large for experiments with large values for the area of the fringe deviation graph for each experiment, Q, probably because the limiting slopes of the graphs of $Y_j/e^{-\zeta_j^2}$ *vs.* $Z_j^{2/3}$ also were large for these experiments. Because the graphs were visually judged not to behave as lower-order polynomials in $Z_j^{2/3}$ except for small values of j, we decided not to use the method of least squares to determine C_t for any experiments in this work. Values for C_t obtained by the graphical method were entered into the computer along with the corresponding values for t', and the method of least squares was used to calculate the coefficients[31,32] $\mathcal{D}_A$ and Δt in the linear equation for $\mathcal{D}_A'$ *vs.* $1/t'$. Values for Δt were less than 20 sec. for all experiments except 9, where $t = 114.68$ sec. This large Δt apparently produced no unusual uncertainty in $\mathcal{D}_A$. For every experiment the average deviation of the observed values for $\mathcal{D}_A'$ from the values calculated from the linear equation containing $\mathcal{D}_A$ and Δt was less than 0.2% of $\mathcal{D}_A$. Values obtained for $\mathcal{D}_A$ at the temperature of the experiment were corrected to 25.000° by using a series form of the Stokes–Einstein relation.[33]

TABLE II[a,b]

REFRACTIVE INDEX DERIVATIVES, PARTIAL MOLAL VOLUMES, AND OTHER PHYSICAL PROPERTIES OF THE SYSTEM H_2O–Na_2SO_4–H_2SO_4 AT 25°

(0 = H_2O, 1 = Na_2SO_4, 2 = H_2SO_4)

Composition	A	B	C	D
$\bar{C}_1$	0.50000	1.00000	0.50000	1.00000
$\bar{C}_2$	0.50000	0.50000	1.00000	1.00000
$R_1 \times 10^3$	15.63_7	15.31_9	13.33_7	13.36_5
$R_2 \times 10^3$	7.96_2	5.66_1	8.95_1	7.12_3
I_A	277.71	352.37	242.92	282.34
S_A	63.87	15.37	102.55	81.04
E_0	4.94074	2.04391	3.90942	6.08065
E_1	−2.38804	−1.97630	3.70018	−1.35689
E_2	3.96671	0.21178	10.29267	6.06297
$d(\bar{C}_1, \bar{C}_2)$	1.08331	1.13829	1.11107	1.16334
H_1	0.1116_4	0.1094_2	0.1046_4	0.1041_4
H_2	0.0540_9	0.0483_0	0.0564_4	0.0516_1
V_0	18.008_0	17.931_4	17.974_5	17.880_2
V_1	30.4_0	32.4_8	37.3_2	37.6_2
V_2	43.97	49.54	41.54	46.12
m_{11}	0.51908	1.05574	0.53081	1.08318
m_{12}	0.51908	0.52787	1.06161	1.08318
m_{21}	1.05455	1.09211	1.08269	1.12764
m_{22}	0.02370	0.05548	0.02347	0.05453
m_{31}	0.01639	0.01819	0.04216	0.04447
m_{32}	1.06186	1.08349	1.10854	1.13770

[a] Units: concentrations C_i, moles/1000 cc.; refractive index derivatives R_i, 1000 cc./mole; partial molal volumes $\bar{V}_i$, cc./mole; molalities m_i, moles/1000 g. H_2O. [b] Molecular weights used: $M_0 = 18.0160$, $M_1 = 142.0480$, $M_2 = 98.0820$.

The area, Q, of the fringe deviation graph for each experiment is a measure of the deviation from gaussian shape of the diffusing boundary; it was calculated by using Simpson's rule to integrate numerically a smoothed graph of the relative fringe deviation Ω_j *vs.* $f(\zeta_j)$, according to eq. 9 of ref. 10. To perform the numerical integrations the fringe deviation graphs were divided into 40 evenly-spaced segments from $f(\zeta_j) = 0$ to $f(\zeta_j) = 1$.

Refractive index derivatives R_i in Table II are defined by the equation

$$n = n(\bar{C}_1, \bar{C}_2) + R_1(C_1 - \bar{C}_1) + R_2(\bar{C}_2 - \bar{C}_2) \quad (25)$$

where n is the refractive index of the solution at composition C_1, C_2 and $n(\bar{C}_1, \bar{C}_2)$ is the refractive index of a solution at composition $\bar{C}_1$, $\bar{C}_2$. The derivatives were computed by the method of least squares according to eq. 41 of ref. 17. Values for the refractometric fraction, α_1, were calculated from eq. 39, ref. 17; the method of least squares then was used to calculate I_A and S_A in Table II from values of $\mathcal{D}_A$ and α_1 in Table I according to eq. 15, ref. 10. The coefficients E_0, E_1, and E_2 in Table II were calculated from eq. 22, ref. 10, by the method of least squares, during the iteration process used to calculate the diffusion coefficients. The quantity P which appears in the iteration process was computed directly from eq. 20, ref. 10. This equation was found to be as accurate as the equation in footnote *a* of Table I, ref. 10, for finding P when $p < 0.9999$. The entire computation was stopped when two successive iteration cycles produced values for each diffusion coefficient that differed by less than 0.000001×10^{-5}.

Chemical Potential Derivatives.—Values of these derivatives, of the $(D_{ij})_V$, and of the partial molal volumes $\bar{V}_i$ are required to calculate the phenomenological coefficients $(L_{ij})_0$ and to test the Onsager reciprocal relation at each composition.[34] For these computations the derivatives

$$\Gamma_{ik} = [\partial \log (\gamma_\pm)_i / \partial m_k]_{T,P,m_{q \neq k}} \quad (i, k = 1, 2) \quad (26)$$

of the activity coefficients $(\gamma_\pm)_i$ with respect to molality m_k, at constant temperature T and pressure P, were needed to calculate the quantities

$$A_{ik} = (\partial \mu_i / \partial m_k)_{T,P,m_{q \neq k}} \quad (27)$$

where μ_i is the chemical potential of component i. Values for the derivatives were found by using eq.

$$m_{kj} = (\partial m_k / \partial C_j)_{T,P,C_{q \neq j},0} \quad (k, j = 1, 2) \quad (28)$$

8, ref. 34, and the density data were obtained in conjunction with the diffusion experiments. The chemical potential derivatives μ_{ij} then were calculated from

$$\mu_{ij} = (\partial \mu_i / \partial C_j)_{T,P,C_{q \neq j},0} = \sum_{k=1}^{2} A_{ik} m_{kj} \quad (29)$$

E.m.f. measurements for the cell

$$H_2 | H_2SO_4(m_2), Na_2SO_4(m_1) | Hg_2SO_4 - Hg \quad (30)$$

were used by Baes[35] to calculate values for $\log(\gamma_\pm)_2$ from the equation

$$\log (\gamma_\pm)_2 = (E^0 - E)/0.088725 - (1/3) \log (4m_2^2 m) \quad (31)$$

where $E^0 = 0.61515$ volt and $m = m_1 + m_2$. He obtained an empirical expression for $\log(\gamma_\pm)_2$ as a function of m_1 and m_2 which we have rewritten as

(31) L. G. Longsworth, *J. Am. Chem. Soc.*, **69**, 2510 (1947).
(32) H. Fujita, *J. Phys. Soc. Japan*, **11**, 1018 (1956).
(33) Equation 37, ref. 17.
(34) P. J. Dunlop and L. J. Gosting, *J. Phys. Chem.*, **63**, 86 (1959).
(35) C. F. Baes, Jr., *J. Am. Chem. Soc.*, **79**, 5611 (1957).

$$\log (\gamma_\pm)_2 = \log (\gamma_\pm)_2^* - m^{0.6233} [0.2305 - 0.3355(m_2/m) + 0.1050(m_2/m)^3] \quad (32)$$

Here $\log (\gamma_\pm)_2$ is the value of $\log (\gamma_\pm)_2$ for the binary system H_2O–H_2SO_4 at a concentration m of H_2SO_4. By differentiating eq. 32 three of the required derivatives Γ_{ij} are obtained

$$\Gamma_{22}(\tilde{m}_1, \tilde{m}_2) = \Gamma_{22}^*(\tilde{m}) + \tilde{m}^{-0.3767}[0.1918 - 0.1264(\tilde{m}_2/\tilde{m}) - 0.3150(\tilde{m}_2/\tilde{m})^2 + 0.2496(m_2/m)^3] \quad (33)$$

$$\Gamma_{21}(\tilde{m}_1, \tilde{m}_2) = \Gamma_{22}^*(\tilde{m}) - \tilde{m}^{-0.3767} \times [0.1437 + 0.1264(\tilde{m}_2/\tilde{m}) - 0.2496(\tilde{m}_2/\tilde{m})^3] \quad (34)$$

$$\Gamma_{12}(\tilde{m}_1, \tilde{m}_2) = \Gamma_{21}(\tilde{m}_1, \tilde{m}_2) \quad (35)$$

In these equations we have used the identities

$$\Gamma_{22}^* = [\partial \log (\gamma_\pm)_2^*/\partial m]_{T,P} = [\partial \log (\gamma_\pm)_2^*/\partial m_2]_{T,P} = [\partial \log (\gamma_\pm)_2^*/\partial m_1]_{T,P} \quad (36)$$

which follow from the definition of $\log (\gamma_\pm)_2^*$. Equation 35 is derived from the equations defining the activity coefficients

$$\mu_i = \mu_i^0 + RT \ln [4m_i^2 m(\gamma_\pm)_i^3] \qquad (i = 1, 2) \quad (37)$$

where R is the gas constant in ergs/mole-deg., and from the cross-differentiation rule

$$A_{12} = A_{21} \quad (38)$$

The derivatives Γ_{ij} are evaluated at the molalities $\tilde{m}_1$ and $\tilde{m}_2$ corresponding to the composition-point concentrations $\tilde{C}_1$ and $\tilde{C}_2$, as calculated from eq. 7 of ref. 34. Equation 35 is integrated with respect to m_2 and differentiated with respect to m_1 to find the fourth required derivative

$$\Gamma_{11}(\tilde{m}_1, \tilde{m}_2) = \left[\partial \left(\int_0^{\tilde{m}_2} \Gamma_{21} dm_2\right) \Big/ \partial m_1\right]_{\substack{m_1 = \tilde{m}_1 \\ m_2 = \tilde{m}_2}} + \Gamma_{11}^*(\tilde{m}_1) \quad (39)$$

In this equation

$$\Gamma_{11}^* = [\partial \log (\gamma_\pm)_1^*/\partial m_1]_{T,P} \quad (40)$$

where $\log (\gamma_\pm)_1^*$ is the value of $\log (\gamma_\pm)_1$ for the binary system H_2O–Na_2SO_4 at a concentration m_1 of Na_2SO_4. Equation 34 is inserted into (39), and by using a table of integrals[36] and identity (36) we obtain

$$\Gamma_{11}(\tilde{m}_1, \tilde{m}_2) = \Gamma_{22}^*(\tilde{m}) - \Gamma_{22}^*(\tilde{m}_1) + \Gamma_{11}^*(\tilde{m}_1) - 0.7356 m_1^{-0.3767} + \tilde{m}^{-0.3767}[1.6314 - 1.7099(\tilde{m}_1/\tilde{m}) + 1.0637(\tilde{m}_1/\tilde{m})^2 - 0.2496(\tilde{m}_1/\tilde{m})^3] \quad (41)$$

The derivatives Γ_{11}^* and Γ_{22}^* were obtained by differentiating the Taylor series

$$\log (\gamma_\pm)_1^* = \sum_{r=0}^{4} a_r(m_1 - \tilde{m}_1)^r \qquad (m_1 - 0.3) \leqslant m_1 \leqslant (\tilde{m}_1 + 0.3) \quad (42)$$

$$\log (\gamma_\pm)_2^* = \sum_{r=0}^{4} b_r(m_2 - \tilde{m})^r \qquad (\tilde{m} - 0.3) \leqslant m_2 \leqslant (\tilde{m} + 0.3) \quad (43)$$

$$\log (\gamma_\pm)_2^* = \sum_{r=0}^{4} c_r(m_2 - \tilde{m}_1)^r \qquad (\tilde{m}_1 - 0.3) \leqslant m_2 \leqslant (\tilde{m}_1 + 0.3) \quad (44)$$

Values for a_r, b_r, and c_r were calculated by the method of least squares from activity data in the literature[37,38] for the binary systems H_2O–Na_2SO_4 and H_2O–H_2SO_4. The concentrations m_1 and m_2 in eq. 42–44 refer to solute concentrations in the respective binary systems, and $\tilde{m}_1$ and $\tilde{m}$ are *numbers* corresponding to each composition of the ternary system. Values calculated for Γ_{ii}^* and Γ_{ij} from eq. 33, 34, and 39–44 are shown in lines 4–6, 7C, 8C, and 9C of Table III.

TABLE III[a]

ACTIVITY COEFFICIENT DERIVATIVES FOR THE SYSTEM H_2O–Na_2SO_4–H_2SO_4 AT 25°

(1 = Na_2SO_4, 2 = H_2SO_4)

	Composition	A	B	C	D
1.					
2.	$\tilde{m}_1$	0.51908	1.05574	0.53081	1.08318
3.	$\tilde{m}_2$	0.51908	0.52787	1.06161	1.08318
4.	$\Gamma_{11}^*(\tilde{m}_1)$	-0.3153	-0.1681	-0.3105	-0.1631
5.	$\Gamma_{22}^*(\tilde{m})$	-0.0635	-0.0072	-0.0068	0.0341
6.	$\Gamma_{22}^*(\tilde{m}_1)$	-0.2405	-0.0606	-0.2329	-0.0566
7A.	Γ_{11}	*−0.0860*	*−0.0386*	*−0.1053*	*0.0175*
7B.	Γ_{11}	*−0.1996*	*−0.0742*	*−0.3386*	*−0.0621*
8C.	Γ_{11}	*−0.0830*	*−0.0867*	*−0.0361*	*−0.0306*
7D.	Γ_{11}	-0.0830	-0.0867	-0.0361	-0.0305
8A.	Γ_{12} (= Γ_{21})	*−0.2527*	*−0.1648*	*−0.1336*	*−0.0880*
8B.	Γ_{12} (= Γ_{21})	*−0.2553*	*−0.1619*	*−0.1435*	*−0.1019*
8C.	Γ_{12} (= Γ_{21})	*−0.2368*	*−0.1557*	*−0.1360*	*−0.0972*
8D.	Γ_{12} (= Γ_{21})	-0.2483	-0.1575	-0.1377	-0.0957
9A.	Γ_{22}	*−0.0032*	*0.1080*	*0.0302*	*0.1117*
9B.	Γ_{22}	*−0.0009*	*0.1048*	*0.0239*	*0.1098*
9C.	Γ_{22}	*0.0163*	*0.0970*	*0.0281*	*0.0947*
9D.	Γ_{22}	0.0041	0.1033	0.0274	0.1054

[a] The letters A and B designate values for Γ_{ij} calculated from eq. 47–49 with $n = 3$ and $n = 4$, respectively; C designates values for Γ_{ij} calculated from eq. 33, 34, and 41; D designates accepted values for Γ_{ij}.

To confirm Baes' eq. 32 and obtain estimates of the accuracy of the activity coefficient derivatives calculated from his equation we performed a separate analysis of the e.m.f. data reported[11–13] for the cell in eq. 30. Values calculated for $\log (\gamma_\pm)_2$ from eq. 31 were graphically interpolated to obtain 168 evenly spaced points on the m_1, m_2 plane in the region bounded by $0.2 \leqslant m_1 \leqslant 1.3$ and $0 \leqslant m_2 \leqslant 1.3$. The coefficients $(d_{rs})_n$ and $(e_{rs})_n$ in the following four Taylor series then were calculated by the method of least squares at each of the four compositions $\tilde{m}_1$, $\tilde{m}_2$ for which diffusion data had been obtained

$$\log (\gamma_\pm)_2 = \sum_{\substack{r=0 \\ 0 \leqslant (r+s) \leqslant n}}^{n} \sum_{s=0}^{n} (d_{rs})_n (m_1 - \tilde{m}_1)^r (m_2 - \tilde{m}_2)^s \qquad (n = 3, 4) \quad (45)$$

where $(\tilde{m}_1 - 0.3) \leqslant m_1 \leqslant (\tilde{m}_1 + 0.3)$ and $(\tilde{m}_2 - 0.3) \leqslant m_2 \leqslant (\tilde{m}_2 + 0.3)$; and

$$\log (\gamma_\pm)_2 = \sum_{\substack{r=0 \\ 0 \leqslant (r+s) \leqslant n}}^{n} \sum_{s=0}^{n} (e_{rs})_n (m_1 - \tilde{m}_1)^r (m_2 - \tilde{m}_2)^s \qquad (n = 3, 4) \quad (46)$$

where $(\tilde{m}_1 - 0.3) \leqslant \tilde{m}_1 \leqslant (\tilde{m}_1 + 0.3)$ and $0 \leqslant m_2 \leqslant (\tilde{m}_2 + 0.3)$. An IBM 704 computer calculated the 16 sets of coefficients in these equations for the four compositions of the system by using an available SHARE least-squares subroutine.[39] Standard deviations of the data from the curves determined by eq. 45 and 46 ranged from 0.002 to 0.006. The expressions for calculating Γ_{ij} from the coefficients in these equations are

(36) H. B. Dwight, "Tables of Integrals and other Mathematical Data," The Macmillan Co., New York, N. Y., 1957, p. 17.

(37) H. S. Harned and B. B. Owen, "The Physical Chemistry of Electrolytic Solutions," Reinhold Publ. Corp., New York, N. Y., 1958.

(38) R. A. Robinson and R. H. Stokes, "Electrolyte Solutions," Academic Press, Inc., New York, N. Y., 1959.

(39) L. C. Hounsel and S. W. Wilson, "Three-Dimensional Least-Squares Polynomial Fit," SHARE Distribution No. 533.

$$\Gamma_{11}(\tilde{m}_1, \tilde{m}_2) = \Gamma_{11}^*(\tilde{m}_1) + 2(e_{20})_n\tilde{m}_2 - (e_{21})_n\tilde{m}_2^2 + (2/3)(e_{22})_n\tilde{m}_2^3 \quad (47)$$

$$\Gamma_{21}(\tilde{m}_1, \tilde{m}_2) = (d_{10})_n \quad (48)$$

$$\Gamma_{22}(\tilde{m}_1, \tilde{m}_2) = (d_{01})_n \quad (49)$$

The coefficients $(e_{rs})_n$ were required for the region of the m_1, m_2 plane indicated for eq. 46 because of the integration limits in eq. 39. In eq. 47 the coefficient $(e_{22})_3$ should be set equal to zero because $(r + s) > 3$.

Values for Γ_{ij} calculated from eq. 47–49 with $n = 3$ are shown in lines 7A, 8A, and 9A of Table III; values found by using the equations with $n = 4$ are shown in lines 7B, 8B, and 9B. Because of the relatively large uncertainties[40] in the higher order coefficients $(e_{20})_n$, $(e_{21})_n$, and $(e_{22})_4$, the appreciable differences at each composition between values of Γ_{11} in lines 7A–7C found from eq. 47 and 41 are not surprising. For this derivative the accepted values in line 7D were taken to be those calculated according to eq. 41. For the derivatives Γ_{21} and Γ_{22} in Table III the accepted values in lines 8D and 9D were taken to be the averages of the values calculated from eq. 48 and 34, and 49 and 33, respectively. The equations

$$A_{ij}(\tilde{m}_1, \tilde{m}_2) = RT[3\Gamma_{ij} \ln (10) + 2\delta_{ij}/\tilde{m}_j + 1/\tilde{m}_c] \quad (i, j = 1, 2) \quad (50)$$

where δ_{ij} is the Kronecker delta, were used to calculate values for A_{ij} in Table IV from the accepted values for Γ_{ij}. Values for μ_{ij} shown in Table IV were calculated from values for m_{ij} (Table II) and A_{ij} using eq. 29.

TABLE IV[a,b]

CHEMICAL POTENTIAL DERIVATIVES FOR THE SYSTEM H_2O–Na_2SO_4–H_2SO_4 AT 25°

(1 = Na_2SO_4; 2 = H_2SO_4)

Composition	A	B	C	D
$\tilde{C}_1$	0.50000	1.00000	0.50000	1.00000
$\tilde{C}_2$	0.50000	0.50000	1.00000	1.00000
$A_{11} \times 10^{-11}$	1.05_{13}	0.47_{75}	1.02_{74}	0.51_{97}
$A_{12} (= A_{21}) \times 10^{-11}$	-0.18_{63}	-0.11_{31}	-0.08_{05}	-0.04_{94}
$A_{22} \times 10^{-11}$	1.20_{03}	1.27_{19}	0.66_{93}	0.75_{22}
$\mu_{11} \times 10^{-11}$	1.10_{56}	0.51_{95}	1.10_{90}	0.58_{38}
$\mu_{12} \times 10^{-11}$	-0.17_{29}	-0.09_{60}	-0.06_{46}	-0.02_{79}
$\mu_{21} \times 10^{-11}$	-0.17_{67}	-0.10_{04}	-0.05_{85}	-0.02_{23}
$\mu_{22} \times 10^{-11}$	1.27_{01}	1.37_{19}	0.74_{01}	0.85_{31}

[a] Units: concentrations C_i, moles/1000 cc.; chemical potential derivatives μ_{ij}, 1000 cc. ergs/mole.[2] [b] A_{ij} calculated from eq. 50 by using $R = 8.3144 \times 10^7$ ergs/(deg. mole) and $T = 298.15°$ K.

Phenomenological Coefficients and Probable Errors.—The phenomenological coefficients $(L_{ij})_0$ were calculated[41] from data in Tables IV and VI by using eq. 1d–1g of ref. 34.

Probable errors in $(L_{ij})_0$ were calculated according to the general equation[42]

$$\delta f = \sqrt{[(\partial f/\partial x)\delta x]^2 + [(\partial f/\partial y)\delta y]^2 + \ldots} \quad (51)$$

for the probable error δf in a function $f(x,y, \ldots)$. Expressions of this form for $\delta(L_{ij})_0$ were obtained by differentiating eq. 1d–1g, ref. 34, with respect to the quantities μ_{ij} and $(D_{ij})_0$, where the $(D_{ij})_0$ are diffusion coefficients for the solvent-fixed frame of reference.[43] Expressions for the probable errors $\delta\mu_{ij}$ were derived from eq. 6 of ref. 34 by considering uncertainties only in the four derivatives Γ_{ij}. The uncertainties $\delta\Gamma_{ij} = \pm 0.010$ were estimated from deviations from the accepted values for Γ_{ij} in Table III. Probable errors $\delta(D_{ij})_0$ were calculated from equations of the form of (51) by using eq. 2, ref. 34 and assuming uncertainties only in the volume-fixed coefficients $(D_{ij})_V$. Values for $\delta(D_{ij})_V$ were obtained by adding[44] the number 1×10^{-4} to values for Q at each composition and calculating new values for each $(D_{ij})_V$. The uncertainties $\delta(D_{ij})_V$ were set equal to the differences between these recalculated values for $(D_{ij})_V$ and the values originally calculated.

Results

Two-Component Systems.—Data for the binary systems H_2O–Na_2SO_4 and H_2O–H_2SO_4 are shown in Table V. For the small values of ΔC_i used in these experiments $\mathfrak{D}_A$ can be identified with D_V, the volume-fixed diffusion coefficient for a binary system. None of the values for Q listed in this table are significantly different from zero. However, if Q had differed from zero by more than approximately 3×10^{-4} then optical imperfections in the diffusion apparatus or a non-gaussian diffusing boundary, possibly caused by the flow of an impurity, would have been implied. Except for the densities of H_2O–Na_2SC_4 solutions,[45] no precise data were available in the literature at

TABLE V[a]

DATA FOR THE BINARY SYSTEMS H_2O–Na_2SO_4 AND H_2O–H_2SO_4 AT 25°

Expt. no.[b]	I	III	II	IV
Solute	Na_2SO_4	Na_2SO_4	H_2SO_4	H_2SO_4
$\bar{C}$	0.49953	0.99954	0.49899	0.99776
C_A	0.44077	0.94557	0.39943	0.89809
$(d)_A$[c]	1.05109	1.10930	1.02281	1.05244
C_B	0.55829	1.05350	0.59856	1.09743
$(d)_B$[c]	1.06491	1.12138	1.03434	1.06441
J	98.95	81.21	97.02	94.09
$(\Delta n/\Delta C) \times 10^3$	18.32_5	16.38_6	10.61_0	10.27_9
$\mathfrak{D}_A \times 10^5$	0.792_5	0.653_9	1.827_3	1.961_8
$Q \times 10^4$	−0.5	−2.9	0.2	−3.0

[a] Units: concentrations C, moles/1000 cc.; densities d, g./cc.; reduced height-area ratios $\mathfrak{D}_A$, cm.²/sec. [b] Solutions for experiments II and IV prepared from stock solution batches 1 and 2, respectively. [c] Densities measured for all H_2O–Na_2SO_4 solutions agreed, within 0.001% of d, with values for d calculated according to the density equation in Table 87, ref. 45.

(40) By assuming an uncertainty of ±0.001 in log $(\gamma_\pm)_2$ caused by an uncertainty $\delta(e_{rs})_n$ in one coefficient, and letting $(m_1 - \tilde{m}_1) = 0.3$, we have

$$\delta \log (\gamma_\pm)_2 = 0.001 = (0.3)^{r+s}\delta(e_{rs})_n$$

Thus $\delta(e_{20})_n = \pm 0.011$, $\delta(e_{21})_n = \pm 0.038$, and $\delta(e_{22})_4 = \pm 0.123$, which could account for the different values for Γ_{11} in lines 7A–7C of Table III.

(41) The ratio r in eq. 1d–1g, ref. 34, was set equal to unity for our calculations because units of moles/1000 cc. were used for the concentrations C_i.

(42) H. Margenau and G. M. Murphy, "The Mathematics of Physics and Chemistry," D. Van Nostrand Co., Inc., Princeton, N. J., 1956, p. 515.

(43) Solvent-fixed diffusion coefficients are defined by equations of the form 1 and 2 written for solvent-fixed flows $(J_1)_0$; *cf.* eq. 17, ref. 4.

(44) The number 1×10^{-4} corresponds to uncertainties of approximately $\pm 1 \times 10^{-4}$ cm. in measuring fringe positions on the Gouy fringe patterns.

(45) Landolt-Börnstein, "Physikalisch-Chemische Tabellen," 5. Auflage, 3. Erg., 1. Teil, Julius Springer, Berlin, 1935, p. 364.

the desired concentrations which could be compared with the data in Table V.

For the binary system H_2O–Na_2SO_4, D_V can be identified with the main-term diffusion coefficient $(D_{11})_V$ for the ternary system H_2O–Na_2SO_4–H_2SO_4, at corresponding compositions C_1, where $C_2 \rightarrow 0$ for the latter system. Similarly, D_V for the system H_2O–H_2SO_4 can be identified with $(D_{22})_V$ at corresponding compositions C_2 of the system H_2O–Na_2SO_4–H_2SO_4 as $C_1 \rightarrow 0$.

Diffusion Coefficients for the Ternary System.—Values obtained for the four diffusion coefficients at each composition of the system H_2O–Na_2SO_4–H_2SO_4 are shown in Table VI. The cross-term coefficients $(D_{12})_V$ and $(D_{21})_V$ were found to be generally larger than values previously reported for any ternary system.[46] From the approximate equations derived by Gosting[9] for systems of strong electrolytes we may qualitatively infer that the large values for $(D_{12})_V$ and $(D_{21})_V$ result from a coupling of the flows of Na^+, $SO_4^=$, HSO_4^-, with the flow of the relatively mobile ion, H^+. Any ternary system of electrolytes containing a strong acid as one solute, or in general, any multicomponent system of electrolytes containing at least two ions of considerably different mobilities would be expected to have a large value for at least one cross-term coefficient $(D_{ij})_V$, $i \neq j$.

TABLE VI[a]

DIFFUSION COEFFICIENTS FOR THE SYSTEM H_2O–Na_2SO_4–H_2SO_4 AT 25°

Composition	A	B	C	D
$\bar{C}_1$	0.50000	1.00000	0.50000	1.00000
$\bar{C}_2$	0.50000	0.50000	1.00000	1.00000
$(D_{11}v) \times 10^5$	1.09_{32}	0.84_{84}	1.04_{20}	0.90_{55}
$(D_{12})v \times 10^5$	-0.55_{01}	-0.60_{45}	-0.33_{38}	-0.51_{19}
$(D_{21})v \times 10^5$	-0.62_{01}	-0.31_{23}	-0.50_{87}	-0.39_{69}
$(D_{22})v \times 10^5$	2.73_{17}	2.53_{84}	2.50_{78}	2.61_{22}

[a] Units: C_i, moles/1000 cc.; $(D_{ij})_V$, cm.²/sec., corresponding to volume-fixed flows $(J_i)_V$ having units of moles/(cm.² sec.), and gradients of concentrations n_i, where n_i has units of moles/cc.

At a given composition, $1/\sqrt{\mathfrak{D}_A}$ should be linear in α_1, Q should be a quadratic function of α_1, and J should be linear in ΔC_1 and ΔC_2, if the procedure previously described for calculating the coefficients $(D_{ij})_V$ is to be used. The average deviations of measured values for $1/\sqrt{\mathfrak{D}_A}$, Q, and J from values calculated by using the appropriate coefficients in Table II were found to be approximately the same as the estimated experimental error in the measurements of those quantities. Thus the bisulfate dissociation reaction for this system did not produce any unusual concentration dependence effects which might have invalidated the calculation procedure.

An estimate of the influence on $\mathfrak{D}_A$ and Q of concentration dependence of $(D_{ij})_V$, R_i, and $\bar{V}_i$, was obtained from an additional experiment at composition A performed with approximately the same value for α_1 as expt. 1 (see Table I) but at different values for ΔC_1 and ΔC_2 than that experiment.

(46) Values for $(D_{12})_V$ and $(D_{21})_V$ of 0.102×10^{-5} and 0.327×10^{-5}, respectively, were reported by Dunlop (ref. 16) for the system H_2O–NaCl–KCl at concentrations of 1.5 M for each solute. F. J. Kelly (ref. 48) reported values of 0.013×10^{-5} and 0.456×10^{-5} for $(D_{12})_V$ and $(D_{21})_V$, respectively, for the system H_2O–mannitol–NaCl at $C_1 = 0.2$ M $C_2 = 3.0$ M.

For this additional experiment $\alpha_1 = -0.0217$, $\Delta C_1 = -0.00326$, $\Delta C_2 = 0.30174$, $J = 107.46$, $\mathfrak{D}_A = 1.2970 \times 10^{-5}$, and $Q = 171.50 \times 10^{-4}$. No theory for the dependence of $\mathfrak{D}_A$ and Q on ΔC_1 and ΔC_2 has been developed, but by analogy with the skewness theory for binary systems[47] we may assume they each vary linearly with $(\Delta C_1 + \Delta C_2)^2$. From the results of the additional experiment we infer that $\mathfrak{D}_A$ and Q for expt. 1 and for all the experiments in this work have approximately the same values, within experimental error, as would be obtained by allowing ΔC_1 and ΔC_2 to approach zero while holding α_1 constant.

Further evidence of the "normal" behavior of this system was obtained from the density measurements. Values for d calculated from eq. 24 by using the coefficients $d(\bar{C}_1,\bar{C}_2)$, H_1, and H_2 in Table II differed from measured values for d in Table I by approximately 0.002% of d at all compositions, thereby indicating no unusual dependence of the densities on concentration.

The relatively large uncertainty in $(D_{21})_V$ at composition B shown in Table VII is due to difficulties inherent in the Gouy method for studying

TABLE VII

PROBABLE ERRORS IN QUANTITIES USED TO TEST THE ONSAGER RECIPROCAL RELATION

Composition	A	B	C	D
$\delta(D_{11})_V \times 10^5$	±0.005	±0.028	±0.002	±0.004
$\delta(D_{12})_V \times 10^5$	.003	.011	.002	.003
$\delta(D_{21})_V \times 10^5$	.014	.080	.006	.010
$\delta(D_{22})_V \times 10^5$	.009	.032	.006	.008
$\delta\Gamma_{ij}$	.010	.010	.010	.010
$\delta(L_{11})_0 \times 10^{19}$	.027	.089	.038	.076
$\delta(L_{12})_0 \times 10^{19}$	.017	.030	.027	.044
$\delta(L_{21})_0 \times 10^{19}$	.039	.174	.061	.113
$\delta(L_{22})_0 \times 10^{19}$	.060	.105	.123	.172

diffusion in certain ternary systems. Essentially, the Gouy method detects the presence of two solute flows by determining the deviation of the refractive index gradient curve from a gaussian shape; Q, the area of the fringe deviation graph for each experiment, is a measure of this deviation. If there is an appreciable flow $(J_2)_V$ for experiments where $\Delta C_2 = 0$, then the measured value for Q, which usually would be non-zero, contributes to the accuracy in determining $(D_{21})_V$. This is seen from eq. 1 and 2 which, if initially $\Delta C_2 = 0$ but $\Delta C_1 \neq 0$, become

$$(J_1)_V = -(D_{11})_V \frac{\partial n_1}{\partial x} \qquad (52)$$

$$(J_2)_V = -(D_{21})_V \frac{\partial n_1}{\partial x} \qquad (53)$$

However, for experiments where $\Delta C_2 = 0$ (and hence $\alpha_1 = 1$) it can be shown, from eq. 13 and 14 of ref. 10, that $Q = 0$ if the equation

$$(R_2/R_1)(D_{21})_V[(D_{11})_V + (R_2/R_1)(D_{21})_V - (R_1/R_2)(D_{12})_V - (D_{22})_V] = 0 \qquad (54)$$

is satisfied for a given composition of a ternary system. For this system at composition B the values for $(D_{ij})_V$ and R_i are such that the quantity in brackets in eq. 54 is nearly zero, and $Q \cong 0$ for

(47) L. J. Gosting and H. Fujita, *J. Am. Chem. Soc.*, **79**, 1359 (1957).

experiments where $\alpha_1 \cong 1$, even though $(D_{21})_V \neq 0$. Thus, for expt. 5, where $\alpha_1 \cong 1$ (see Table I), the value $Q \times 10^4 = -1.60 \pm 1.0$ is nearly zero and causes a relative large uncertainty in the determination of $(D_{21})_V$ at that composition. It would be interesting to determine $(D_{21})_V$ at composition B by the diaphragm cell method developed by Stokes and Kelly,[48] which measures solute flows in a somewhat more direct manner than the Gouy method.

TABLE VIII[a,b]

PHENOMENOLOGICAL COEFFICIENTS AND TESTS OF THE ONSAGER RECIPROCAL RELATION FOR THE SYSTEM H_2O-Na_2SO_4-H_2SO_4 AT 25°

Composition	A	B	C	D
$\bar{C}_1$	0.50000	1.00000	0.50000	1.00000
$\bar{C}_2$	0.50000	0.50000	1.00000	1.00000
$(L_{11})_0 \times 10^{19}$	0.9498	1.6104	0.9321	1.5644
$(L_{12})_0 \times 10^{19}$	−0.2616	−0.2458	−0.3037	−0.4194
$(L_{21})_0 \times 10^{19}$	−0.2121	−0.2265	−0.2573	−0.5291
$(L_{22})_0 \times 10^{19}$	2.1641	1.8755	3.4980	3.1742
$(L)_0 \times 10^{19}$	0.049	0.019	0.046	−0.110
$\delta(L)_0 \times 10^{19}$	±0.043	±0.177	±0.067	±0.121

[a] Units: C_i, moles/1000 cc.; $(L_{ij})_0$ and $(L)_0$, moles²/(erg cm. sec.), calculated by using $R = 8.3144 \times 10^7$ ergs/(deg. mole) and $T = 298.15°$ K. [b] $(L)_0 = (L_{21})_0 - (L_{12})_0$.

Tests of the Onsager Reciprocal Relations.—Values for the phenomenological coefficients $(L_{ij})_0$ and for the difference

$$(L)_0 = (L_{21})_0 - (L_{12})_0 \qquad (55)$$

are shown in Table VIII. According to the Onsager reciprocal relation, eq. 20, $(L)_0$ should be exactly zero. The probable errors $\delta(L)_0$ for testing the Onsager relation were calculated from values for $\delta(L_{12})_0$ and $\delta(L_{21})_0$ in Table VII by using[49]

$$\delta(L)_0 = \sqrt{\delta(L_{12})_0^2 + \delta(L_{21})_0^2} \qquad (56)$$

The values for $(L)_0$ and $\delta(L)_0$ in Table VIII imply that the Onsager reciprocal relation is satisfied within experimental error at the compositions studied for this system.

Acknowledgments.—I am indebted to Professor L. J. Gosting for his interest and stimulating suggestions throughout the course of this work. I also wish to thank Mrs. R. A. Carhart and Dr. S. E. Lovell of the Theoretical Chemistry Laboratory, and Mr. L. F. Thompson of the Department of Chemistry, for their generous assistance in programming the calculations for this work. Mr. J. G. Albright and Mr. R. C. Riley (and Professor Gosting) collaborated in the construction of the photoelectric null-indicator described here. This research was supported in part by research grants from the National Science Foundation (G-7401) and the National Institute of Arthritis and Metabolic Diseases (U.S.P.H.S.) (A-5177) and from the Research Committee of the University of Wisconsin Graduate School from funds supplied by the Wisconsin Alumni Research Foundation. The author is grateful to the Ethyl Corporation for a graduate fellowship during the academic year 1959–1960.

(48) F. J. Kelly, Ph.D. Thesis, University of New England, Armidale, New South Wales, Australia.

(49) Probable errors in (L_0) calculated from this equation may be slightly greater than errors in $(L)_0$ calculated from the necessary and sufficient condition for the Onsager reciprocal relation, eq. 20 of ref. 4.

INFRARED SPECTRA OF SULFUR COMPOUNDS ADSORBED ON SILICA-SUPPORTED NICKEL

BY GEORGE BLYHOLDER AND DAVID O. BOWEN

Department of Chemistry, University of Arkansas, Fayetteville, Ark.

Received December 21, 1961

The infrared spectra of H_2S, CH_3SH, EtSH, Et_2S, and thiophene adsorbed on silica-supported nickel are presented in the 1350 to 2000 cm.$^{-1}$ region. Although adsorption of sulfur compounds by coördination of the sulfur atom with the surface, as generally proposed in the literature, may occur, these data indicate the adsorption on clean silica-supported nickel is a much more varied and complicated process involving frequent bond rupture in the adsorbing compound even at room temperature. The chemisorption of H_2S at room temperature was too small to detect.

Introduction

The measurement of infrared spectra has proven to be one of the most powerful tools for the determination of molecular structure. Recently, techniques have been published[1] on the application of this tool to the determination of the structure of adsorbed molecules. In this paper, the infrared spectra in the 1350 to 5000 cm.$^{-1}$ range of H_2S, CH_3SH, EtSH, thiophene, and Et_2S adsorbed on silica-supported nickel are examined. This series of compounds is interesting for several reasons. Most of the studies published to date on the infrared spectra of chemisorbed molecules have dealt with CO and light hydrocarbons. We felt it would be interesting to look at the spectra of some different types of adsorbed molecules. One point of interest about this series of sulfur compounds is that they contain unshared pairs of electrons. It has been proposed[2] that molecules in general and sulfur compounds in particular that contain unshared electron pairs chemisorb on transition metals by forming coördination links where the previously unshared electron pair from the adsorbate is shared in the d-orbitals of the metal. This view is not universally held as Emmett[3–6] and co-workers have

(1) R. P. Eischens and W. A. Pliskin, *Advan. Catalysis*, **10**, 1 (1958).

(2) E. B. Maxted, *ibid.*, **3**, 133 (1951).

(3) J. T. Kummer, H. H. Podgurski, W. B. Spencer, and P. H. Emmett, *J. Am. Chem. Soc.*, **73**, 564 (1951).

(4) J. T. Kummer and P. H. Emmett, *ibid.*, **75**, 5177 (1953).

(5) W. K. Hall, R. J. Kokes, and P. H. Emmett, *ibid.*, **79**, 2983 (1957).

proposed that alcohols adsorbed on promoted iron and cobalt Fischer–Tropsch catalysts are held to the surface by iron–carbon and cobalt–carbon bonds rather than oxygen–metal coördinate links. It is possible, perhaps even likely, that the same type of adsorbate will behave differently on different metals or even on the same metal under different conditions.

As well as the intrinsic interest in the structure of the adsorbed sulfur compounds, the structure is interesting because of the light it can shed on the poisoning of catalysts. The poisoning of catalysts by sulfur compounds has been reported by Maxted[2,7-10] and co-workers. Garland[11] has studied the effect of CS_2 poisoning on the infrared spectrum of CO adsorbed on nickel, but no peaks in the region studied were found for adsorbed CS_2.

In this study, the sulfur compounds were adsorbed on freshly reduced silica-supported nickel at room temperature except where otherwise noted. The infrared spectra were recorded with several millimeters of adsorbate in the cell and then after the gas phase had been removed.

Experimental

A specially constructed cell 10 cm. in length and having rock salt windows was employed in this experiment. The cell windows were held in place with high vacuum silicone stopcock grease with silica added for extra support. A heating element was wound around the outside of the cell and was insulated with asbestos paper and "liquid porcelain." The cell windows were cooled by means of copper coils at each end of the cell through which water was circulated.

A sample container was constructed to hold the sample disk in place inside the cell, and was held in place by a spring wedged between the container and the cell wall.

A Perkin–Elmer Model 21 infrared spectrophotometer equipped with NaCl optics was used in this work.

The samples were prepared in the following manner: $Ni(NO_3)_2 \cdot 6H_2O$ and Cab-O-Sil were weighed and mixed so that after reduction the mixture would contain 20% nickel. Water was added to make a fine slurry, and the mixture was stirred until homogenous. The mixture then was evaporated to dryness and ground to a fine texture with an agate mortar and pestle. Duplicate samples of 150 mg. each were weighed and pressed into disks 25 mm. in diameter with a hydraulic press at a pressure of 8,000 p.s.i.

The samples then were placed in the cell and the cell was assembled. The samples then were degassed for 15–20 min. at a pressure of 10^{-5} mm.

Reduction of the samples was carried out by passing purified hydrogen over the samples at one atmosphere pressure and gradually increasing the temperature of the cells to 360° over the period of 1 hr. The reduction then was continued for 5 hr. The hydrogen was purified by passage over hot copper and through a Dry Ice-cooled trap to remove oxygen and water.

The samples then were cooled to room temperature and pumped at 10^{-5} mm. pressure for 30 min. to remove hydrogen and reduction products.

The reagent grade sulfur compounds, which had been further purified by trapping several times with liquid air and pumping on while melting, then were passed into the sample cell.

The spectral region between 1350 and 5000 cm.$^{-1}$ was investigated, using a clean disk in an evacuated cell as a reference in the back beam of the instrument. Programmed slit openings were used.

Spectral Results and Assignments

The frequencies of observed bands together with group assignments for H_2S, CH_3SH, EtSH, Et_2S, and thiophene adsorbed on silica-supported nickel are shown in Table I. The frequencies given are for bands that remain after the gas phase is removed and the cell has been evacuated at 10^{-5} mm. for at least 5 min. These bands remain unchanged during further pumping, addition of CO gas, and evacuation of the CO. The assignments and changes in spectra when the gas phase is removed will be discussed on an individual basis.

H_2S.—Both while 4 mm. of H_2S is present in the cell and when the gas phase is removed, there are no bands observed. This is true both with the cell at 20 and at 165°. The suggestion of these negative results is that H_2S does not chemisorb on silica-supported nickel by the coördination of the lone pair electrons of the sulfur atom with retention of the H_2S configuration. After exposure of the nickel surface to 4 mm. of H_2S at 20° and evacuation at 10^{-5} mm. for 5 min., the surface was exposed to 4 mm. of CO. The infrared spectrum taken after evacuation of the gaseous CO indicated chemisorbed CO to the extent usually found on a freshly reduced nickel surface. This indicates that at 20° either H_2S does not chemisorb at all on a silica-supported nickel surface or that if it does adsorb, the surface bond is so weak that upon evacuation of the gas phase all of the adsorbed H_2S desorbs.

TABLE I

FREQUENCIES OF OBSERVED BANDS FOR H_2S, CH_3SH, EtSH, Et_2S, AND THIOPHENE ADSORBED ON SILICA-SUPPORTED NICKEL

Compound	Frequencies, cm.$^{-1}$ [a]	Group assignment
H_2S	No bands	
CH_3SH	2910	CH_2
EtSH	2960sh	CH_3
	2915	CH_2
	2870	CH_2 and CH_3
	1447	CH_2 and CH_3
	1406w	M–S–CH_2
	1371	CH_3
Et_2S	2960sh	CH_3
	2915	CH_2
	2870	CH_2 and CH_3
	1453	CH_2 and CH_3
	1425	M–S–CH_2
	1376	CH_3
Thiophene	2940	CH_2
	2885sh	CH and CH_2
	1610w	
	1460	CH_2 or CH_3

[a] sh—shoulder; w—weak.

When the surface which has been previously exposed to H_2S at 165° is exposed to 10 mm. of CO at 20°, only a small peak for chemisorbed CO appears on evacuation of the gas phase CO. This indicates that the surface has been poisoned by exposure to H_2S at 165°. Under these conditions Ni is reported[12] to form nickel sulfide. We presume this is the mechanism of the poisoning.

(6) R. J. Kokes, W. K. Hall, and P. H. Emmett, *J. Am. Chem. Soc.*, **79**, 2989 (1957).
(7) E. B. Maxted and H. C. Evans, *J. Chem. Soc.*, 603 (1937).
(8) E. B. Maxted and H. C. Evans, *ibid.*, 1004 (1937).
(9) E. B. Maxted and M. Josephs, *ibid.*, 2635 (1956).
(10) E. B. Maxted and H. C. Evans, *ibid.*, 455 (1938).
(11) C. W. Garland, *J. Phys. Chem.*, **63**, 1423 (1954).
(12) W. J. Kirkpatrick, *Advan. Catalysis*, **3**, 329 (1951).

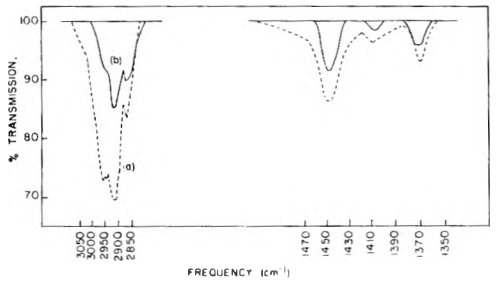

Fig. 1.—Spectra of EtSH adsorbed on silica-supported nickel at 20° recorded with a Perkin–Elmer Model 21 spectrophotometer, programmed slits 970 × 2, gain 8: curve (a) (dashed line) is with 7 mm. of EtSH in cell; curve (b) (solid line) is with cell evacuated.

CH_3SH.—While 10 mm. of CH_3SH is in the cell and after evacuation of the gas phase, the only band recorded occurred at 2910 cm.$^{-1}$. This is clearly at a lower frequency thar the 2967 cm.$^{-1}$ band[13] for the CH_3 group in CH_3SH. Comparison with the assignments of Bellamy[14] of CH_3 bands at 2962 and 2872 cm.$^{-1}$ and CH_2 bands at 2926 and 2853 cm.$^{-1}$ leads to an assignment of the 2910 cm.$^{-1}$ band for the chemisorbed species to a CH_2 group in which the carbon atom is saturated. The absence of a band for the S–H group[14] around 2600 cm.$^{-1}$ is not significant, since a comparison of the relative intensities of the S–H and CH_3 bands for CH_3SH reveals that were an S–H band present for the chemisorbed species, its intensity would be no greater than the noise level of the instrument. The following structures are consistent with the observed spectrum.

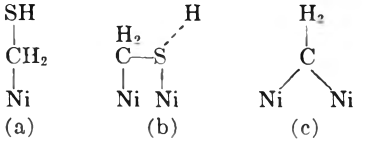

The dotted line is drawn between the sulfur and hydrogen atoms in (b) to indicate that the hydrogen might or might not be there. In view of the fact that H_2S shows no tendency to coördinate its lone pair electrons, we believe if the hydrogen remains attached to the sulfur, (a) would be more likely than (b).

EtSH.—The spectrum obtained with 7 mm. of EtSH in the cell is shown as curve (a) of Fig. 1. Upon evacuation for 5 min. at 10^{-5} mm., curve (b) is obtained. The appearance of curve (a) leaves very little room for doubt in assigning the 2915 and 2960 cm.$^{-1}$ bands to CH_2 and CH_3 group vibrations. Bellamy[14] gives the CH_3 bands as 2962 and 2853 cm.$^{-1}$. For the chemisorbed species shown in spectrum (b) it is seen that the CH_3 band is much reduced relative to the CH_2 band. This indicates that a large percentage of the adsorbed species no longer contains a CH_3 group. Since some of the adsorbed species still has a CH_3 group and the original molecule contains only one CH_3 group, there must be at least two different adsorbed species on the surface. Examination of the spectra in the region of 1400 cm.$^{-1}$ leads to the same conclusions.

(13) Am. Petroleum Institute Research Project 44, Spectrum No. 1687.

(14) L. J. Bellamy, "Infrared Spectra of Complex Molecules," Methuen, London, 1958.

Bellamy[14] lists a strong band at about 1370 cm.$^{-1}$ and a medium band around 1450 cm.$^{-1}$ for a bending motion in the C–CH_3 group. For the CH_2 group, Bellamy lists the CH bending motion at 1456 ± 20 cm.$^{-1}$. Therefore, the 1371 cm.$^{-1}$ band is assigned to a –CH_3 group frequency. Since the 1450 cm.$^{-1}$ band for CH_3 is less intense than the 1370 cm.$^{-1}$ band for CH_3, the band observed at 1447 is assumed to be largely due to a CH_2 group. The very weak band at 1406 cm.$^{-1}$ does not correspond to any observed band for EtSH or any other sulfur compound in this study. We therefore presume it to be due to a CH_2 bending motion of the chemisorbed species. Eischens[1] in studying the adsorption of hydrocarbons on silica-supported nickel has assigned C–H bending bands in Ni–CH_2– and Ni–CH_3 to 1450 ± 10 and 1380 cm.$^{-1}$, respectively. In view of all these assignments, we propose to assign the 1406 cm.$^{-1}$ band to a CH_2 group bonded to a sulfur atom in a group where either the sulfur atom or the carbon atom or both are bonded to the nickel surface. For the surface species containing no CH_3 groups, the spectrum is consistent with the structures

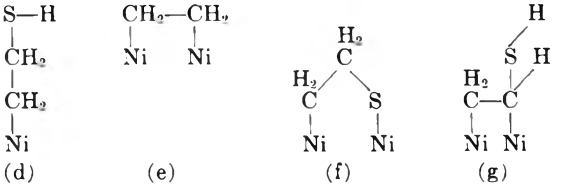

For the species containing a CH_3 group, which is present in relatively small amounts, the following structures are consistent with the spectrum

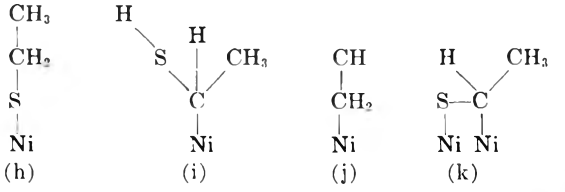

Any of the structures, (f), (g), or (h) could be responsible for the 1406 cm.$^{-1}$ band.

Et_2S.—Curve (a) of Fig. 2 shows the spectrum obtained with 9 mm. of Et_2S in the cell while curve (b) shows the spectrum obtained after evacuation of the cell. The frequency assignments identically follow the assignments for chemisorbed EtSH. Again in the C–H stretching region around 3000 cm.$^{-1}$, the intensity of the CH_3 band relative to the CH_2 band decreases for the adsorbed species relative to the spectra obtained with gas in the cell. The decrease does not appear to be as great in this case at it is for adsorbed EtSH. The 1425 cm.$^{-1}$ band, which corresponds to the 1406 cm.$^{-1}$ band of adsorbed EtSH, apparently is due to a structure as prevalent as any other on the surface. If carbon–sulfur bond rupture occurs on adsorption, all of the structures (d) through (k) are possible. In addition, a number of structures in which bond rupture does not occur and in which a sulfur atom or a carbon atom, or both, are bonded to the surface are consistent with the spectra. In view of the lack of an appreciable change in frequency of the CH_2 group bending band for changing a carbon atom to a sulfur atom to a nickel atom attached

to the CH_2, we favor the structure (f) being responsible for the 1406 and 1425 cm.$^{-1}$ bands.

Thiophene.—The spectrum obtained with 8 mm. of thiophene in the cell is shown as curve (a) of Fig. 3. The result of pumping on the cell for 5 min. at 10^{-5} mm. pressure is recorded as curve (b) of Fig. 3. Comparison of Fig. 3 with A.P.I. Spectra Numbers 364 and 740 for pure thiophene reveals a number of interesting facts. The carbon–hydrogen stretching frequency for thiophene is reported at 3096 cm.$^{-1}$,[15] 3110 cm.$^{-1}$,[16] and 3125 cm.$^{-1}$,[17] all of which are in agreement with the expected[14] C–H stretching frequency for a hydrogen atom attached to an unsaturated carbon atom. From Fig. 3 it is seen that while gas phase thiophene is in the cell, there is a band at 3095 cm.$^{-1}$ corresponding to pure thiophene, whereas for the chemisorbed complex, *i.e.*, the material not removed by pumping, the 3095 cm.$^{-1}$ band is absent and a new band with a maximum at 2940 cm.$^{-1}$ and a shoulder at 2885 cm.$^{-1}$ is present. This band due to chemisorbed material is, of course, also present while the gas phase thiophene is in the cell. In accordance with the previous assignments, this band is attributed to a carbon–hydrogen stretch of a saturated carbon atom. This suggests that in the course of chemisorbing, the double bonds in thiophene become saturated by interaction with the surface. This idea is supported by a consideration of the 1590 cm.$^{-1}$ band of thiophene, which Thompson and Temple[16] have assigned to a ring vibration. This band is present while gas phase thiophene is in the cell but is absent for the chemisorbed material. This behavior of the ring frequency is consistent with interaction of the double bonds upon chemisorption.

We have no proposed assignment for the very weak 1610 cm.$^{-1}$ band of the chemisorbed complex. While this band is not resolved in the A.P.I. spectra, it could easily be present in the low wave length side of the 1590 cm.$^{-1}$ band.

Again by analogy to the previous assignments, the band at 1460 cm.$^{-1}$ is assigned to a CH_2 or CH_3 bending vibration. According to the A.P.I. spectra, thiophene has no adsorptions at this frequency. It would be convenient if this band could be assigned to a tertiary C–H bending mode, but Bellamy[14] lists this mode at about 1340 cm.$^{-1}$. In view of the excellent agreement found for the carbon–hydrogen stretching frequencies of the other adsorbed complexes with Bellamy's list of frequencies for alkanes, a shift from 1340 to 1460 cm.$^{-1}$ is too great even for our convenience. A tertiary C–H bending frequency may exist, but 1340 cm.$^{-1}$ is beyond the transmission range of our samples.

The simplest structure that can be proposed for chemisorbed thiophene is one in which the double bonds are opened to form four carbon–nickel bonds with the surface. This structure is not inconsistent with the data.

(15) Am. Petroleum Institute Research Project 44, Spectrum No. 740.

(16) H. W. Thompson and R. B. Temple, *Trans. Faraday Soc.*, **41**, 27 (1945).

(17) Am. Petroleum Institute Research Project 44, Spectrum No. 364

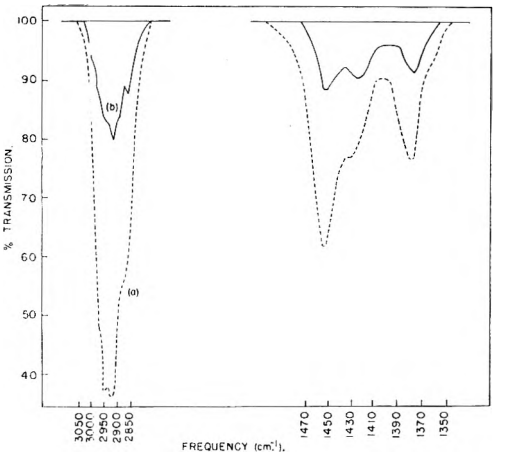

Fig. 2.—Spectra of adsorbed Et_2S at 20° recorded with a Perkin–Elmer Model 21 spectrophotometer, programmed slits 970 × 2, gain 8: curve (a) (dashed line) is with 9 mm. of Et_2S in cell; curve (b) (solid line) is with cell evacuated.

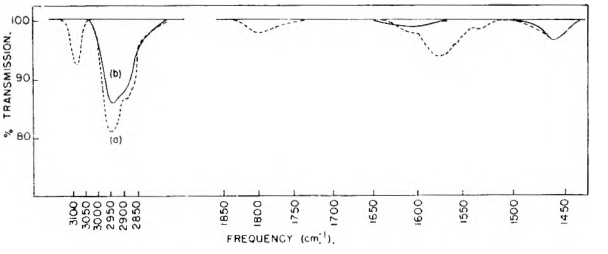

Fig. 3.—Spectra of Adsorbed Thiophene at 20° recorded with a Perkin–Elmer Model 21 spectrophotometer, programmed slits 970 × 2, gain 8: curve (a) (dashed line) is with 8 mm. of thiophene in cell; curve (b) (solid line) is with cell evacuated.

However, a close look at the spectra in the C–H stretching region and the presence of the band at 1460 cm.$^{-1}$ indicates that even if the structure of the previous paragraph exists, another structure makes a major contribution to the spectra. The C–H stretching frequency for a tertiary C–H is at[14] about 2890 cm.$^{-1}$ and should be only a single band. In the carbon–hydrogen stretching region of Fig. 3 there are observed to be at least two bands, one at 2940 cm.$^{-1}$ and a shoulder at 2885 cm.$^{-1}$. While it is possible for there to be more than one type of tertiary C–H group on the surface and hence more than one frequency for this group, the fact that surface complexing does not appear to shift CH_2 and CH_3 stretching frequencies an appeciable amount argues against this interpretation. These bands appear similar in shape and are located at the same position as bands previously ascribed to the symmetric and asymmetric stretching frequencies of CH_3 and CH_2 groups. Unfortunately, the largest band is centered at 2940 cm.$^{-1}$, which is just midway between the bands assigned to CH_3 and CH_2. In view of the low ratio of hydrogen to carbon in the parent compound, we favor a CH_2 assignment. The appearance of the band at 1460 cm.$^{-1}$, which is ascribed to CH_3 or CH_2, is consistent with this treatment of the carbon–hydrogen stretching region. Since thiophene is the only source of hydrogen atoms on the surface, the presence of CH_2 groups requires carbon–hydrogen bond rupture on adsorption. This means there also must be carbon

atoms which are bonded only to the surface, and carbon or sulfur atoms, or both. On the basis of these data, proposal of surface fragments is sheer speculation, although formation of chemisorbed carbon monosulfide would release a hydrogen to form a CH_2 group.

Discussion

Although adsorption of sulfur compounds by coördination of the sulfur atom with the surface may occur, our data certainly indicate that the adsorption of sulfur compounds on clean silica-supported nickel is a much more varied and complicated process than this. Our data indicate that H_2S can have at most only weak interaction at room temperature with the surface. On our silica-supported nickel, it certainly does not form a strong coördination bond. Common to all of the other sulfur compounds studied is the fact that a major portion of the chemisorbed molecules were dissociatively adsorbed in the sense that all underwent carbon–hydrogen bond rupture. This fact, together with the behavior of H_2S, suggests that metal–carbon bonds may be primarily responsible for the tightly held chemisorbed species. This suggestion can only be regarded as tentative on the basis of these data.

In the past, it generally has been assumed[2,7-10] that poisoning by sulfur compounds is great, due to the sulfur atom forming a strong chemisorption bond. While this may be true for some systems, our data suggest that for our system carbon–metal bonds rather than sulfur–metal bonds are responsible for the primary strong chemisorption. At higher temperatures than those employed here, the poisoning process might be envisioned as starting first with adsorption of the sulfur compound by carbon–metal bond formation and then dissociation to sulfide the catalyst surface. The sulfiding of the surface by decomposition after the primary chemisorption would be responsible for the long term poisoning of the surface. This view is consistent with the observation that while H_2S did not poison the surface at room temperature, when the temperature was raised high enough to decompose the H_2S, the surface was poisoned.

Acknowledgment.—This work was supported in part by a grant from the National Science Foundation for an Undergraduate Research Participation Program. Acknowledgment is made to the donors of the Petroleum Research Fund, administered by the American Chemical Society, for partial support of this research.

PROTON MAGNETIC RESONANCE OF SOME SYNTHETIC POLYPEPTIDES[1]

BY J. A. E. KAIL, J. A. SAUER, AND A. E. WOODWARD

Department of Physics, The Pennsylvania State University, University Park, Pennsylvania

Received December 23, 1961

Nuclear magnetic resonance spectra have been obtained for five synthetic poly-(α-amino acids) in the 77–470°K. temperature range. It is found that the temperature dependence of the n.m.r. second moment depends markedly on the side chain substituent, and that the processes occurring in the accessible temperature range can be accounted for wholly in terms of side chain motion. At 77°K. poly-(phenyl-L-alanine) and poly-(γ-benzyl-L-glutamate) are in the rigid lattice while for poly-(L-alanine) and poly-(L-leucine) some methyl group rotation is taking place. For the latter two polymers complete methyl rotation is taking place at about 120°K. and above. The gradual second moment decrease for poly-(L-leucine) and poly-(phenyl-L-alanine) in the 120–400°K. region is attributed to an increasing mean amplitude of isobutyl and benzyl group oscillation, respectively, with increasing temperature, a state of complete rotation being reached at ~400°K. For poly-(γ-benzyl-L-glutamate) the n.m.r. line narrows rapidly in the 280–370°K. region to values <1 gauss, this process being explained in terms of considerable side-chain reorientations.

Introduction

Numerous studies of the proton magnetic resonance, n.m.r., spectra of partially crystalline and glassy high polymers have been published to date[2] and it is found that even at temperatures as low as 77°K. a number of these materials are not in their rigid state but that some motion, principally side group rotation (frequencies $>10^4$ c.p.s.), is occurring. An important series of high polymers for which studies of motional processes in the solid state have not been reported to date are the synthetic poly-(L-α-amino acids) with the repeat unit $-[NH-CH(R)-CO]-_n$.

To obtain such information n.m.r. spectra have been obtained recently from 77 to 410–480°K. for the following five poly-(L-α-amino acids): poly-(L-alanine) [PLA; R = CH_3], poly-(phenyl-L-alanine) [PPLA; R = $CH_2C_6H_5$], poly-(L-leucine) [PLL; R = $-CH_2-CH(CH_3)_2$], poly-(γ-benzyl-L-glutamate) [PγBLG; R = $-CH_2-CH_2-C(=O)-O-CH_2C_6H_5$] and poly-(sodium α-L-glutamate) [PSαLG; R = $-CH_2-CH_2-C(=O)-O^-Na^+$]. The results are presented and discussed herein.

(1) Supported in part by the U. S. Atomic Energy Commission under Contract AT (30-1-)1858 and by a Research Grant (A2704) from the National Institute of Arthritis and Metabolic Diseases, Public Health Service.

(2) For references see the bibliographies in: A. E. Woodward, *SPE Trans.*, **2**, 86 (1962), and J. G. Powles, *Polymer* **1**, 219 (1960).

Experimental

The n.m.r. measurements were made using equipment and procedures described previously.[3,4]

The samples of the five polymers were obtained from Pilot Chemicals Co. All but the PSαLG were prepared from the corresponding N-carboxyl anhydride by initiation with sodium methoxide at anhydride/initiator ratios of 200/1, in benzene in the case of L-leucine, and in dioxane for the other three. The PSαLG was obtained from a PγBLG by saponification. The PγBLG and PSαLG were reported to have weight average molecular weights from viscosity measurements of 2.6×10^5 and 1.0×10^5, respectively. The PLA was found to be soluble in dichloroacetic acid and therefore is believed to be in the α form.[5]

For the n.m.r. measurements a pellet of each material was prepared by compressing the vacuum dried polymer for 3–4 min. at room temperature. The pressures used were 750–1000 p.s.i. for PLA, 1500–2000 p.s.i. for PγBLG, and 8000 p.s.i. for PPLA and PLL. Prior to pressing, PLL was dissolved in benzene at ~70° (0.8 g./100 ml.), the polymer freeze dried, and then dried further at 95° for 36 hr. in the vacuum oven. PSαLG was dissolved in water, precipitated twice in 50:50 ether:ethanol, and freeze dried prior to pressing at 1500 p.s.i. Before measurement the sample was dried at 60° under vacuum for nine days to constant weight.

Results

From 77 to 100°K. the derivative line shapes for PLA and PLL are complex, the two peaks being more evident for the former than for the latter, as is evident in Fig. 1 where line shapes at 77°K. are shown for the two polymers. At 77°K. the peak widths for PLA are 17.6 and 7.3 gauss, respectively, while for PLL the width of the narrower component was 8.5 gauss. As the temperature is increased from 77°K. the broad component narrows appreciably and disappears at ~100°K. In the temperature region from ~100–470°K. only one component is found, which slowly narrows with increasing temperature to a value of 5.8 gauss at 467°K. for PLA and 2.7 gauss at 440°K. for PLL.

The second moments for PLA and PLL, shown in Fig. 2, exhibit marked decreases in the 77–120°K. region as a consequence of the loss of the broad component of the derivative line. The gradual decrease which follows at temperatures >120°K. is seen to be more pronounced for PLL than for PLA. There is also some indication in the data that the two regions for PLL are separated by a step in the 120–160°K. range of lesser slope. For PLA there is some indication of a somewhat more rapid change in slope in the 310–380°K. range.

In the line width–temperature plot given in Fig. 3 for PγBLG a region of slow narrowing (150–270°K.) and one of precipitous narrowing (270–330°K.) are evident, with the line shape being composed of only the one component at all temperatures employed. As observed in Fig. 4 the second moment temperature plot for PγBLG also has two regions of narrowing.

PPLA showed single component line shapes over the 82–423°K. range, the width being 8.3 and 1.9 gauss at the temperature extremes, respectively. The second moment for PPLA, given in Fig. 4, appears to decrease essentially linearly in the 125–400°K. range.

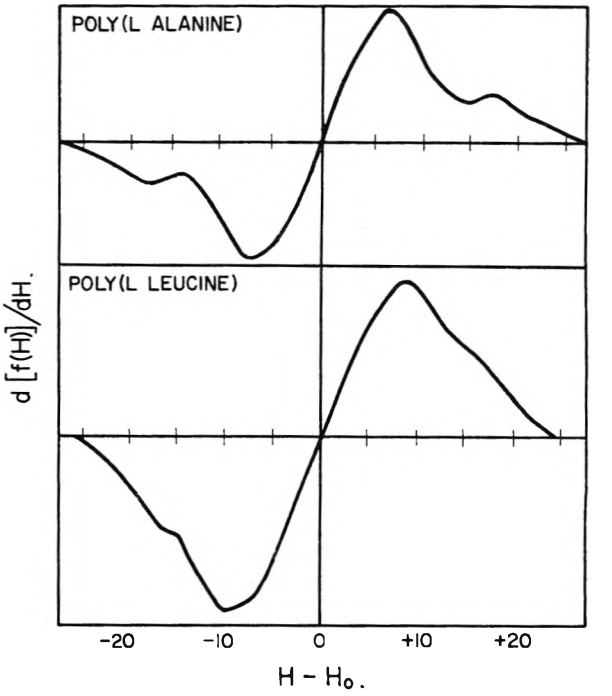

Fig. 1.—Derivative line shapes at 77°K. for poly-(L-alanine) and poly-(L-leucine) (one-half of the trace being shown).

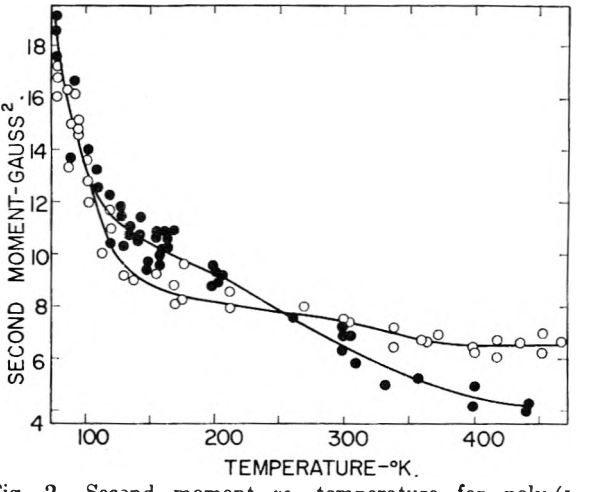

Fig. 2.—Second moment *vs.* temperature for poly-(L-alanine) (○) and poly-(L-leucine) (●).

For PSαLG single component line shapes were found with a width of 12.5 gauss from 77 to 220°K. At temperatures from 220 to 351°K. a gradual narrowing of the width to a value of 12 gauss occurred. However, due to a low signal intensity and the possibility of saturation broadening, these values are considered approximate only. A sample of PSαLG, which had not received as thorough a drying treatment, exhibited a liquid-like narrow line, in addition to the broad component, at temperatures as low as 260°K.

Discussion

In order to obtain further information as to the amount of motion occurring in the polymers studied, estimates of second moments for the rigid lat-

(3) A. Odajima, A. E. Woodward and J. A. Sauer, *J. Polymer Sci.*, **55**, 181 (1961).

(4) A. Odajima, J. A. Sauer, and A. E. Woodward, *ibid.*, **56**, in Press (1962).

(5) C. H. Bamford, A. Elliott, and W. E. Hanby, "Synthetic Polypeptides," Academic Press, New York, N. Y., 1956.

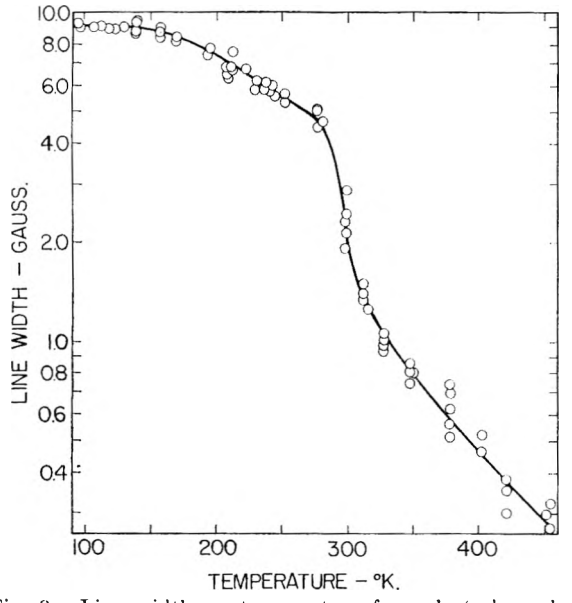

Fig. 3.—Line width *vs.* temperature for poly-(γ-benzyl-L-glutamate).

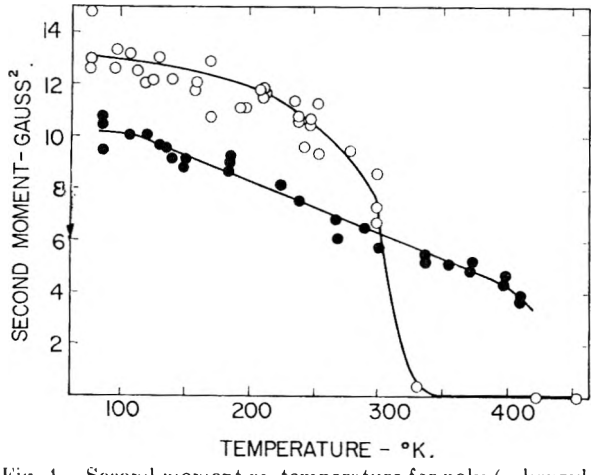

Fig. 4.—Second moment *vs.* temperature for poly-(γ-benzyl-L-glutamate) (○) and poly-(phenyl-L-alanine) (●).

tice and for cases in which rotation of certain groups around the C_3 axis takes place have been made. The intramolecular portions of the rigid lattice values were obtained using the Van Vleck equation,[6] with the assumption that the chains are in a right handed alpha helix[5]; reasonable estimates of the intermolecular contributions were made taking into account effective shielding by large side groups. Rotation around a C_3 axis was assumed to reduce the contribution of the rotating group to one-fourth the rigid lattice value.[7]

The intramolecular and intermolecular contributions to the rigid lattice second moment for PLA are found to be 20 and 4 gauss², respectively. Methyl group rotation leads to a reduction of the 24 gauss² total to 6 gauss². Therefore, it is concluded that the motional process in the $\leq$77–120°K. region for PLA is the onset of methyl rotation. This assignment is in agreement with that for a similar process exhibited by polypropylene.[8] Upon comparison of the experimental data for these two polymers it is found that the nature of the backbone has little, if any, effect on the temperature position of this process.

For PLL, intra- and intermolecular contributions to the rigid lattice second moment of 22 and 4 gauss² are obtained. Methyl rotation is expected to reduce the total value to 11 gauss², while isobutyl group rotation would cause a decrease to 7 gauss². In keeping with these calculations the process occurring below 120°K. is attributed to the onset of methyl rotation, while that starting at about 160°K. involves isobutyl group motion. Since the temperature span over which this system appears to go from a state where all methyl groups are rotating (160°K.) to one in which all isobutyl groups rotate (~400°K.) is so large, it is believed that oscillation of all isobutyl units occurs at an amplitude which increases with increasing temperature starting from essentially zero at ~160°K. Two processes, such as those found herein for PLL, were reported previously[5] for poly-(4-methylpentene-1), both occurring below the glass transformation region.

A rigid lattice second moment of 11 gauss² is calculated (9 + 2 gauss²) for PPLA with this being reduced to 7 and 3 gauss² for total phenyl rotation and total benzyl rotation, respectively, around the C_3 axis. It appears from the experimental data (Fig. 4) that PPLA is in the rigid lattice at 77°K. and in a state of complete benzyl rotation at 409°K. Since the transformation from the one state to the other is a gradual one, it is concluded, as was the case for PLL, that oscillation of all the side chains at a mean amplitude which increases with increasing temperature takes place until complete rotation is occurring. Limited oscillational motion of the phenyl units in polystyrene previously was invoked to explain the slow decrease in second moment over a wide temperature range.[4]

PγBLG is found to have a rigid lattice second moment of 13 gauss² (10 + 3 gauss²), in agreement with the experimental values at ~110°K. and below. Rotation of all phenyl groups would reduce this to 10 gauss²; rotation of all benzyl groups would lead to a value of 9 gauss²; and finally, rotation of the complete side-chain about the C_3 axis would give a value of 3 gauss². Assuming such motions to be invoked separately in the order given, it appears that the experimental second moment decrease in the 110– ~280°K. region is due to the onset of motion which includes benzyl oscillations of increasing amplitude, as for PPLA. The abrupt drop of experimental values at temperatures >280°K. cannot be explained entirely as due to onset of C_3 axis side-chain rotation alone but must include further side-chain motion which might also involve motion of the helix as a unit. It should be pointed out that the contribution of the main chain protons to the total intramolecular contribution in the rigid lattice is 0.2 gauss², which is of the order of the experimental values at high temperatures.

A dynamic mechanical loss maximum at 290°K.

(6) J. A. Van Vleck, *Phys. Rev.*, **74**, 1164 (1948).

(7) J. G. Powles and H. S. Gutowsky, *J. Chem. Phys.*, **21**, 1695 (1953).

(8) A. E. Woodward, J. A. Sauer, and A. Odajima, *J. Phys. Chem.*, **65**, 1384 (1961).

(0.2 c.p.s.) has been found[9] for a PγBLG sample similar to the one studied herein. This probably is also a consequence of the same or a closely related process which brings about the precipitous n.m.r. narrowing. The somewhat higher temperature for the latter can be attributed to the higher frequency of the n.m.r. measurement ($\geq 10^4$ c.p.s.).

A plot of the log of the correlation frequency[10] (ν_c) *vs.* $1/T$ in the 170–320°K. region for PγBLG gives a curve which appears to have two straight line portions for temperatures above and below 290°K., leading to "activation energies" of 7.9 and 1.3 kcal./mole, respectively.

(9) R. G. Saba, J. A. Sauer, and A. E. Woodward, *J. Polymer Sci.* in press.

(10) H. S. Gutowsky and G. E. Pake, *J. Chem. Phys.*, **18**, 163 (1950).

ELECTROSTATIC INTERACTIONS BETWEEN SIMPLE IONS AND HIGHLY SWOLLEN POLYELECTROLYTE GELS. SELECTIVITY IN THE ALKALI ION SERIES

By Jehuda Feitelson

Department of Physical Chemistry, The Hebrew University, Jerusalem, Israel

Received December 27, 1961

The purely electrostatic interactions between a highly swollen ionized gel and simple counterions are discussed. The Fuoss, Katchalsky, and Lifson polyelectrolyte theory, as adapted by Gregor and Kagawa to counterions of different sizes, is used to describe the electrostatic potential in the gel. It is shown how the activity ratio for counterions between gel and ambient solution should be affected by the distance of closest approach of ion to polyelectrolyte. The selectivity of highly swollen ion exchange resins for different counterions is explained in terms of electrostatic interactions. Furthermore, the preference of one ion over another in ion exchange depends upon the composition of the resin; it appears also that this dependence might be explained, at least in part, on purely electrostatic grounds. Our experimental data yield reasonable parameters for the distance of closest approach of an ion to the polymer backbone. Selectivities as determined by Myers and Boyd agree comparatively well with our calculated data.

A polyelectrolyte gel in equilibrium with its surrounding solution is a two-phase system. Because of the fixed charges imbedded in the matrix of the polymer and their movable counterions, an electric potential difference results between the phases. Although uncharged species are unaffected by this potential, the distribution of ions is governed by its influence as described by Donnan and Guggenheim.[1] The Donnan potential difference represents, however, an average quantity since the electrical potential within the gel is by no means uniform. It varies depending on the location of a test charge with respect to the highly ionized polymer chains.

There are locations in which the influences of different chains cancel one another, *i.e.*, there occur potential minima where no influence of the internal polymer electric field is experienced.

Although the interactions of simple ions with the gel should be predominantly electrostatic in nature, specific effects between organic polymer networks and organic ions also must be taken into consideration. Highly swollen ionized gels are likely to behave similarly to dilute polyelectrolyte solutions. The latter have been treated theoretically, assuming purely electrostatic interactions in a medium which consists primarily of ordinary solvent (the dielectric constant of the solvent is used).[2-4] Since these conditions apply also to a dilute gel, we have tried to implement one of the polyelectrolyte theories[5,6] in a gel–solution system. The distribution of dipolar molecules between the phases has been described in a previous paper[7] and here we shall discuss the purely electrostatic interactions of ions.

The gels described here are ion exchange resins of low degree of crosslinkage. Their behavior toward small ions has been studied extensively from a thermodynamic point of view and also has been determined experimentally.[8,9] Lately, a number of attempts have been made to describe the behavior of ion-exchange resins in terms of molecular models.[8] We feel that the understanding of purely electrostatic interactions in dilute gels should precede a comprehensive treatment of ion exchange. It is proposed to show here that the selectivities found in ion-exchange resins of very low crosslinkage can be explained by simple polyelectrolyte–ion interactions.

Symbols

ψ	electrostatic potential
ϵ	elementary charge
a	radius of polymer cylinder
b	distance of nearest approach of an ion center to polymer cylinder surface
h	polymer chain length
R	half the average distance between two centers of cylinders
f	activity coefficient
$\bar{a}$	activity
c	concentration

Subscript 0 denotes a quantity at a point where $\psi = 0$. Other subscripts indicate distances from the cylinder

(1) F. G. Donnan and E. A. Guggenheim, *Z. physik. Chem.*, **162A**, 346 (1932).

(2) R. A. Marcus, *J. Chem. Phys.*, **23**, 1057 (1955); see also for further references.

(3) N. Ise and M. Hosono, *J. Polymer Sci.*, **39**, 389 (1959).

(4) N. Imai *J. Phys. Soc. Japan*, **16**, 746 (1961).

(5) R. M. Fuoss, A. Katchalsky, and S. Lifson, *Proc. Natl. Acad. Sci.*, **37**, 579 (1951); S. Lifson and A. Katchalsky, *J. Polymer Sci.*, **13**, 43 (1954).

(6) J. Kagawa and H. P. Gregor, *ibid.*, **23**, 477 (1957).

(7) J. Feitelson, *J. Phys. Chem.*, **65**, 965 (1961).

(8) Reviewed by F. Helfferich, *Adv. Polymer Sci.*, **1**, 329 (1959).

(9) G. E. Myers and G. E. Boyd, *J. Phys. Chem.*, **60**, 521 (1956).

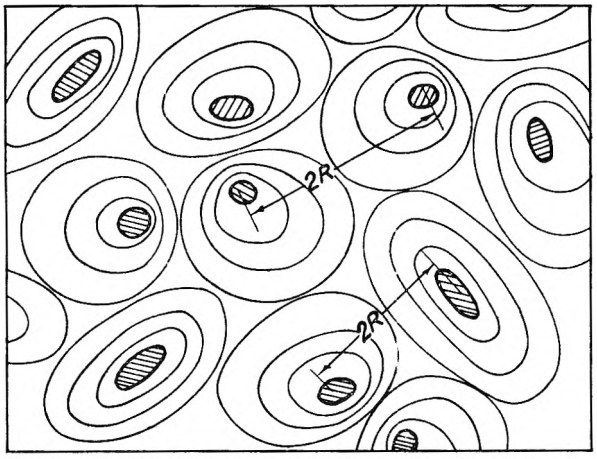

Fig. 1.—Cross-section through ionized polymer gel showing equipotential surfaces.

center. Superscripts denote the kind of species, *i.e.*, c^+ = concentration of positive ions. Prime and double prime refer to the gel and solution phases, respectively.

The Model.—Osmotic forces exert a high swelling pressure in polyelectrolyte gels. With few cross-linking points present, the polymer chains therefore will exist in a highly extended form. In order to describe the potential distribution in such a system, the theory of Fuoss, Katchalsky, and Lifson[5] was used as described earlier.[7]

Briefly, the model of the gel consists of parallel cylindrical polyions carrying evenly distributed fixed charges, while the movable counterions are distributed in accordance with the electrostatic field in the vicinity of the polymer chains. It is assumed that a very small amount of free salt does not appreciably alter the potential in the gel and the changes in solvent content for similar gels with different counterions will not influence the linear dimensions in the gel.

The concentration of a counterion at a distance r from the cylinder axis is given by

$$C_r' = C_0' \exp(-\epsilon\psi'/kT) \qquad (1)$$

The zero point of the potential ψ' is defined so that C_0' is the average concentration of counterions in the gel. The difference between ψ_0' in the gel and the potential in the ambient solution $\psi_0' - \psi''$ therefore yields the ideal Donnan potential. This is the potential difference to be expected if the counterions in the gel would not experience any interactions, and therefore would behave as in an ideal solution.

Activity Coefficients of Counterions in Gels.—The true Donnan potential determined by the activity ratio of the counterions can be evaluated theoretically. At the midpoint between the polyelectrolyte chains $(d\psi/dr)_R = 0$, meaning that the electrical forces acting on an ion in the potential trough are zero. Thus, ignoring the interactions between mobile ions as compared to those with the polyions, it follows that at $r = R$ the activity of a counterion equals its concentration $C_R' = \bar{a}'$.[2] This is, of course, smaller than the average counterion concentration in the gel C_0'.

The potential in the gel ψ' is given by[5]

$$\frac{\epsilon\psi'}{kT} = \ln\left\{\frac{2\lambda}{\beta^2}\frac{r^2}{R^2 - a^2}\sin^2(|\beta|\ln Ar)\right\} \qquad (2)$$

where λ is determined by the linear charge density and β and A are constants depending on λ and R/a. From eq. 1 for $r = R$

$$C_R' = C_0'\left\{\frac{|\beta|^2}{2\lambda}\frac{R^2 - a^2}{R^2}\frac{1}{\sin^2(|\beta|\ln AR)}\right\} \qquad (3)$$

By differentiating eq. 2 and from the condition $(d\psi'/dr)_R = 0$, it follows that $\cot(|\beta|\ln AR) = -1/|\beta|$. Also

$$1/\sin^2(|\beta|\ln AR) = 1 + \cot^2(|\beta|\ln AR)$$

and by substituting into (3) the counterion activity is obtained.[2,10]

$$\bar{a}' = C_R' = C_0'\left\{\frac{1 - (a/R)^2}{2\lambda}[|\beta|^2 + 1]\right\} \qquad (4)$$

The quantity which is of interest here and which at least in principle can be measured experimentally, is the activity ratio $\bar{a}'/\bar{a}''$. For the counterions in dilute gel and solution, it is obtained by dividing eq. 4 by the mean activity of the salt in solution.

The theory so far used treats the mobile ions as point charges and we therefore are unable to distinguish between similar gels carrying different counterions. Kagawa and Gregor[6] introduced a refinement into the theory by calculating the electrostatic potential in a polyelectrolyte solution containing counterions of finite radius. When this theory is used, expression 4 becomes

$$C_R' = C_0'\{[1 - (a + b)^2/R^2](|\beta|^2 + 1)/2\lambda\} \qquad (4')$$

where b is the distance of nearest approach of an ion center to the polymer cylinder surface. The main difference between the two equations is due to β which, being a function of $(a + b)/R$, also influences ψ'. Equation 4′ enables us to calculate how the interaction with the polyelectrolyte gel depends upon the size of the counterion. The greater the value of b the less the number of ions capable of screening the polymer charges in the immediate vicinity of the cylinder. The surface potential ψ_a' increases therefore with b.

Figure 2 shows that in spite of the higher ψ_a' values for large counteractions, they are still less strongly absorbed than smaller ions (as expressed by the $\exp(-\epsilon\psi'_{a+b}/kT)$ factor). Their distribution in the gel therefore should be more uniform and the calculated activity coefficients are somewhat larger.

The interactions between polyelectrolytes and simple ions, particularly in protein systems, often are determined by e.m.f. measurements.[11,12] The measured activity of a mobile ion in polymer solution is compared to its concentration. The ratio is considered to indicate the extent to which it is free or bound in this phase. Equation 4′ enables us to estimate, at least approximately, the degree of binding in a gel due to purely electrostatic interactions.

Selectivity in the Univalent Counterion Series.—We are now also in a position to evaluate the interaction of a particular ion, denoted ion (i), with a polyelectrolyte gel whose thermodynamic properties are wholly determined by another ion—

(10) Z. Alexandrowicz, *J. Polymer Sci.*, in press.

(11) C. W. Carr and L. Topol, *J. Phys. Chem.*, **54**, 776 (1950).

(12) G. Scatchard, J. H. Scheinberg, and S. H. Armstrong, *J. Am. Chem. Soc.*, **72**, 535 (1950).

(j). The average concentration of a counterion in the gel can be written

$$C^{i\prime} = 2\pi h C_0{}^{i\prime} \int_{a+b^i}^{R} \exp(-\epsilon\psi'/kT) r dr / 2\pi h \int_a^R r dr \quad (5)$$

Where $2\pi h r dr$ is the volume element and the integration in the denominator is carried out over the whole gel volume, except for the space occupied by the polymer matrix. From the definition of ψ_0' it follows that the ratio of the two integrals is unity for ion (j). For ion (i) present in the gel in a minute amount, however, the ratio has a different value, since in this instance the boundaries of integration in the numerator are from $a + b^i$ to R while the zero potential is determined by ion (j).

Take, for example, the case of $b^i > b^j$. In the region between b^i and R the distribution of both ions between gel and solution will be equal, since the same electrical potential difference acts on both. It follows that, neglecting mobile ion interactions, the activity ratios of ions i and j are the same

$$C_R{}^{i\prime}/C^{i\prime\prime} = C_R{}^{j\prime}/C^{j\prime\prime} = \bar{a}'/\bar{a}'' \quad (6)$$

The average concentration ratios, however, differ for the two ions. Since ion j is able to penetrate into the region between b^j and b^i, a region of particularly high electrical potential, it follows that

$$C^{j\prime}/C^{j\prime\prime} > C^{i\prime}/C^{i\prime\prime} \quad (7)$$

This means that on purely electrostatic grounds a given gel absorbs preferentially the smaller counterions.

For simplicity let us assume that in the dilute outside solution all the activity coefficients are unity. If required, the mean activity coefficients of the salt can be employed.

Assume $C^{i\prime\prime} = C^{j\prime\prime}/n$. Then, since the surface $\psi_r' = \psi_0'$ lies well within the range $b < r < R$ also $C_0{}^{i\prime} = C_0{}^{j\prime}/n$ and from eq. 5

$$\frac{C^{i\prime}}{C^{i\prime\prime}} = \frac{C_0{}^{i\prime}/n \int_{a+b^i}^{R} [\exp(-\epsilon\psi'/kT)] r dr}{C^{i\prime\prime}/n \int_a^R r dr}$$

The selectivity coefficient as defined in ion exchange

$$D = \frac{C^{i\prime}\, C^{j\prime\prime}}{C^{i\prime\prime}\, C^{j\prime}} = \frac{\int_{(a+b^i)}^{R} [\exp(-\epsilon\psi'/kT)] r dr}{\int_{(a+b^j)}^{R} [\exp(-\epsilon\psi'/kT)] r dr} =$$

$$\frac{\cot[|\beta|(\ln A + \ln R)] - \cot[|\beta|(\ln A + \ln(a + b^i))]}{\cot[|\beta|(\ln A + \ln R)] - \cot[|\beta|(\ln A + \ln(a + b^j))]} \quad (8)^{13}$$

(13) From eq. 1 as corrected by Kagawa and Gregor

$$\int_{a+b}^{R} [\exp(-\epsilon\psi/kT)] r dr = \int_{a+b}^{R} \frac{|\beta|^2}{2\lambda} \times \frac{[R^2 - (a + b^2)] r dr}{r^2 \sin^2(|\beta| \ln Ar)} = M \int_{a+b}^{R} \frac{d \ln r}{\sin^2(|\beta| \ln Ar)}$$

where $[R^2 - (a + b)^2]\,|\beta|^2/2\lambda = M$

By substituting $u = |\beta| \ln Ar$ the expression becomes

$$\frac{M}{|\beta|} \int_{|\beta| \ln A(a+b)}^{|\beta| \ln Ar} du/\sin^2 u = -\text{const} \times \cot u \Big|_{|\beta| \ln (a+b)A}^{|\beta| \ln Ar}$$

In case the potential determining ion has the greater b value a different expression should be used for ψ in the range b^i to b^j (ref. 6, eq. 5-2). Calculations have, however, shown that no significant changes in D result when the same expression for ψ is used for b^i to R.

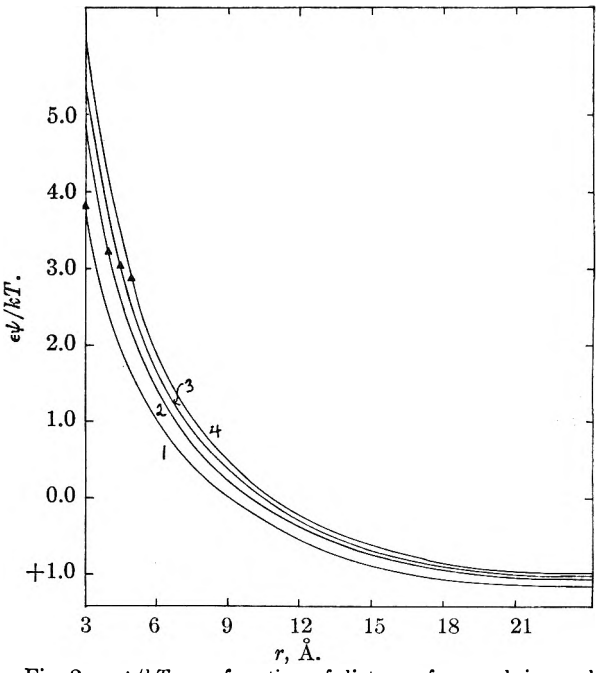

Fig. 2.—$\epsilon\psi/kT$ as a function of distance from polyion rod center for $b = 0$ (curve 1), $b = 1.0$ (curve 2), $b = 1.5$ (curve 3), $b = 2.0$ (curve 4) in Å. Triangles indicate the $\epsilon\psi_{(a+b)}/kT$ values.

It must be remembered that the potential ψ' and therefore also β throughout the expression are determined by ion (j).

Experimental

A polystyrene sulfonate resin, Zeokarb 225, of 1% nominal divinylbenzene content was used. It was washed thoroughly with HCl and NaOH and then rinsed with triple-distilled water. After removal of both the very fine and the very coarse resin particles, beads of 200–300 mesh size were left. The capacity of the resin and void volume fractions of the columns were determined as described earlier[7] and found to be 0.36 meq./ml. (swollen NH_4^+ form) and δ = 0.39, respectively. The water content of resin particles in equilibrium with solution was 92–93%. The NH_4^+-resin was thoroughly equilibrated with 0.02 N NH_4Cl eluent and Li^+, Na^+, K^+, Rb^+, and Cs^+ salts each were chromatographed separately on columns about 7 cm. high and 0.9 cm. in diameter. About 0.1 ml. of 0.1% chloride salt solutions were introduced as a sharp band at the top of the column. The cations were slowly (5 ml./hr./cm.^{2} column cross-section) eluted by the above mentioned 0.02 N NH_4Cl solution. They were determined in the eluent with an EEL flame photometer. The maxima of the somewhat diffuse elution peaks were taken to measure the elution volume. The results were reproducible with an error not greater than ±2.5%.

Results and Discussion

A cation exchange resin of nominally 1% divinylbenzene content in equilibrium with 0.02 N NH_4Cl was used as the gel–solution system so that the potential in the gel was determined by the NH_4^+ counterion. From the resin capacity, R was calculated to be 23.6 Å. A value of 3 Å. was assumed for a and since the distance between two charges along the stretched polymer axis is about 2.54 Å., λ was found to equal 2.83. β and ln A were calculated from the theory for every counterion.

The distribution of the univalent cations Li^+, Na^+, K^+, Rb^+, and Cs^+ between the two phases was found by elution chromatography. The distribution coefficient $C^{+\prime}/C^{+\prime\prime}$ is given by[7]

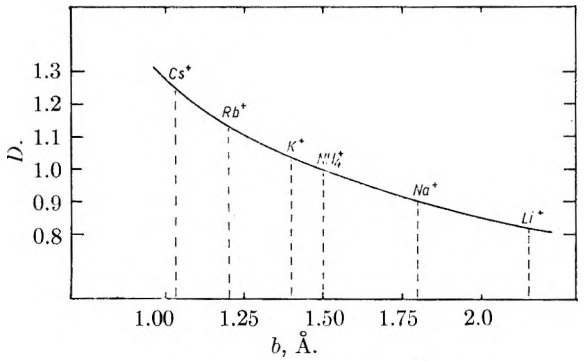

Fig. 3.—Selectivity as a function of b^i. Curve shows calculated D. Experimental values for different M^+–NH_4^+ systems are indicated by broken lines.

$$K^+ = \frac{C^{+\prime}}{C^{+\prime\prime}} = \frac{\Delta V/\Delta X - \delta}{1 - \delta - \delta^*}$$

where ΔV and ΔX are the elution and column volumes, respectively.

δ is the column void volume fraction, and δ^* the fraction taken up by the polymer-matrix. δ^* was assumed to equal 0.025. D, the selectivity coefficient, was calculated from eq. 7 for different values of b^i. b^i was assumed to be equal to 1.5 Å., which seemed reasonable for the NH_4^+ ion. The dependence of D on b^i as calculated is shown by the curve in Fig. 3. The values of b^i for the different ions, corresponding to the experimentally measured D values, are indicated in the figure.

These b^i values calculated from the experimental selectivities are not considered to represent the true hydrated ion radii in the resin. A certain amount of interpenetration of fixed resin groups and movable ion hydration shells can be assumed. The b^i values could more correctly be compared to the "a" parameter employed in the later version of the Debye–Hückel Theory.[14] It is a parameter accounting for the differences in ability of various ions to approach the resin backbone and fixed charges.

Our calculated selectivity coefficients also are capable of accounting in part for the selectivity behavior encountered in ion exchange—especially in low crosslinkage resins. The distribution of ions between resin and solution depends both on the kind of ion encountered and upon the composition of the resin. In general, ions with small hydrated radius are more readily taken up by the resin than large ions. Furthermore, at least in low crosslinked resins, the uptake of the preferred ion is greater when the majority of the resin counterions are of a different kind. Myers and Boyd[9] have evaluated the thermodynamic quantities in ion exchange resins and compared them to experimental selectivities. The above-mentioned behavior is found in their tables showing ion exchange selectivity and its dependence on resin composition. The purely electrostatic interactions denoted by them as γ_i^*/γ_0^* are derived from selectivity measurements in resins of 0.5% divinylbenzene content. Unfortunately, the water content of these resins, when in equilibrium with solution, is not given. We therefore could not recalculate their data from our theory but compared our calculated D values with their selectivity coefficients in 0.5 and 2% crosslinked resins. Assuming that R for their highly swollen resin is not very much greater than our value, some agreement might be expected.

In our calculations, as already mentioned, PV terms and changes in linear dimensions due to different moisture contents for different resin forms were not taken into account.

(14) R. A. Robinson and R. H. Stokes, "Electrolyte Solutions," Butterworth & Co., Ltd., London, 1959, p. 235.

TABLE I

CALCULATED AND MEASURED SELECTIVITY COEFFICIENTS IN ION EXCHANGE RESINS OF DIFFERENT COMPOSITIONS

Exchange	Resin form	D from Myers and Boyd's data γ_i^*/γ_0^*	2% DVB resin	Caled. from eq. 8
Li^+–Na^+	$X_{Na^+} = 1$	1.03	1.08	1.11
	$= 0$	1.06	1.12	1.14
Na^+–K^+	$X_{K^+} = 1$	1.11	1.17	1.12
	$= 0$	1.22	1.30	1.17
Na^+–Cs^+	$X_{Cs^+} = 1$	1.28	1.31	1.26
	$= 0$	1.61	1.70	1.44

It is seen that the values found by Myers and Boyd agree comparatively well with our calculations. In the Na^+–Li^+ system, our D values are somewhat greater than γ_i^*/γ_0^*. It seems that in this case factors in addition to pure resin ion interactions have to be taken into account. This also is indicated by Myers and Boyd, who attribute the selectivity in this system mainly to counterion interaction in the resin. The Na^+–K^+ exchange shows good agreement while for Cs^+–Na^+ the discrepancy might be due to the great sensitivity of our calculation to the exact value assigned to b^{Cs^+}.

Qualitatively our model explains the preference for, say, Cs^+ over Na^+ ions in the Na^+ or Cs^+ resin forms in the following way: Na^+ ions determine the potential in the first instance but Cs^+ ions also are to be found in the cylindrical shell contained between b^{Cs^+} and b^{Na^+}. Their amount will be determined by $\epsilon\psi'/kT$ in this region. In the Cs^+ resin the potential is determined by the Cs^+ ions, and since $b^{Cs^+} < b^{Na^+}$ the polyion charges are more strongly screened than in the Na^+ resin. Therefore ψ_a' and the whole ψ' *vs.* r curve lies lower in this case and the $\exp(-\epsilon\psi_r/kT)$ values are smaller (see Fig. 2). This causes the Cs^+ ion concentration to become more uniform and Cs^+ ions are therefore less preferred in their own environment.

It might seem that the picture of parallel stretched polymer chains and the diverse assumptions we made render the whole treatment unrealistic. We think, however, that the main features of the model are correct. The concentration of counterions will in any event fall off very rapidly according to their distance from the polyelectrolyte and between different chains there must exist potential minima. Also when comparing counterions of different size, the screening effect probably will influence the potential in the manner indicated above. We think, therefore, that the selectivity of one ion over another is pictured correctly even for systems where the Fuoss–Katchalsky–Lifson theory is no longer applicable.

COMPLEX STRUCTURES IN AQUEOUS BINARY SALT SOLUTIONS

BY P. M. DUELL[1] AND J. L. LAMBERT

Department of Chemistry, Kansas State University, Manhattan, Kansas

Received January 2, 1962

The solutions investigated contained varying amounts of $ThCl_4$ in given concentrations of LiCl, NaCl, or KCl. Some evidence for complex formation was obtained from apparent molal and partial molal volumes determined as a function of concentration of $ThCl_4$. Diamagnetic susceptibilities had little usefulness in clarifying the nature of the solutions.

Introduction

Efforts to clarify solvent–solute interactions in aqueous solutions have resulted in a structural approach to the characterization of aqueous electrolyte solutions. Bernal and Fowler[2] present X-ray diffraction data as evidence of an extended tetrahedral arrangement of water molecules in concentrated electrolyte solutions, the orderly arrangement being enhanced by increased surface charge of dissolved ions. Brindley and Hoare[3] describe inorganic complex formation in terms of partial dehydration of cations and changes in diamagnetic susceptibility resulting when water molecules are released from the distorting influence of the electrostatic field surrounding dissolved ions. Gurney[4] interprets ionic hydration and mobility in terms of the polarizing effect of solute ions on water molecules, the result being a more extensive arrangement of tetrahedral water structures. The use of diamagnetic susceptibilities in the detection of complex compounds between lead and alkali nitrates has been reported by Srivastava and co-workers.[5]

The purpose of this investigation was to determine the applicability of (1) apparent and partial molal volumes and (2) diamagnetic susceptibilities to the detection of inorganic complex structures in aqueous solutions. The thorium(IV) ion was selected because of its relatively high surface charge. The chlorides of lithium, sodium, or potassium (MCl) were present in constant concentrations in the three series of solutions, while the $ThCl_4$ concentration was varied to give MCl/$ThCl_4$ molar ratios from 5:1 to 1:1.

Experimental

Reagents.—The alkali metal chlorides used were Fisher Certified reagents. The thorium chloride, labeled "Fisher Laboratory Chemical," contained appreciable quantities of iron and was purified by the method outlined by Kremer.[6] Test solutions were prepared by taking a given volume of 2 *M* alkali chloride stock solution, adding a quantity of 2 *M* $ThCl_4$ solution to give the desired concentration ratios, and diluting to volume.

Experimental Measurements.—Diamagnetic susceptibilities per unit volume were measured by the Gouy method,[7] using a compensation sample tube, the lower compartment of which was filled with 2.5% agar. The pole pieces of the electromagnet were in the shape of truncated cones, the pole faces being 3.18 cm. in diameter and spaced 1.3 cm. apart. When operated at an optimum current of 8 amperes, the electromagnet developed a field strength of approximately 10,000 oersteds.

Density values necessary for converting measured values to mass susceptibilities were obtained to four significant figures at 25° by means of a Westphal balance. Densities so determined were within the range of ±0.001 of the values in the International Critical Tables.[8] Apparent and partial molal volumes of $ThCl_4$ were calculated from the measured densities.

Results and Discussion

Molal Volumes.—Apparent molal volumes of $ThCl_4$ were calculated from the relationship[9]

$$\phi = \frac{1000}{c} - \frac{1}{d_1}\left[\frac{1000\,d}{c} - M_2\right]$$

where ϕ is the apparent molal volume, c is the concentration of $ThCl_4$ in moles per liter, d_1 is the density of the solvent (0.952 *M* MCl soln.), d is the density of the solution, and M_2 is the formula weight of $ThCl_4$. Figure 1 shows the curves for the

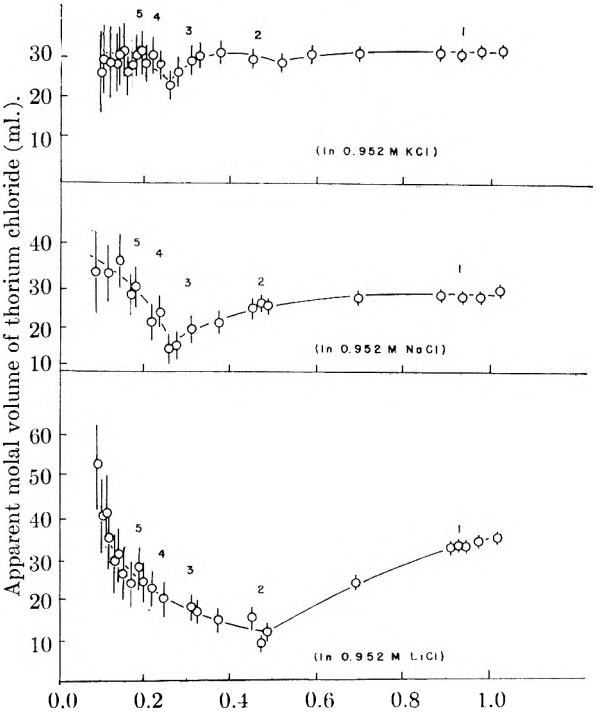

Fig. 1.—Apparent molal volume of thorium chloride as a function of concentration. Numbers above curves represent moles of alkali metal chloride per mole of thorium chloride.

three systems. In the $ThCl_4$–KCl system the apparent molal volumes remain relatively constant, with slight tendency toward decreasing volume up

(1) Chem. Dept., Willamette Univ., Salem, Oregon.

(2) J. D. Bernal and R. H. Fowler, *J. Chem. Phys.*, **1**, 515 (1933).

(3) G. W. Brindley and F. E. Hoare, *Trans. Faraday Soc.*, **33**, 268 (1937).

(4) R. W. Gurney, "Ionic Processes in Solution," McGraw-Hill Book Co., New York, N. Y., 1953, Chap. 16.

(5) S. S. Srivastava, C. S. Pande, and M. R. Nayar, *Current Sci.*, **16**, 225 (1947).

(6) C. B. Kremer, *J. Am. Chem. Soc.*, **64**, 1009 (1942).

(7) L. F. Bates, "Modern Magnetism," 3rd Ed., Cambridge Univ. Press, London, 1951.

(8) E. W. Washburn, Ed., "International Critical Tables," McGraw-Hill Book Co., New York, N. Y., 1929, Vol. 3, p. 24.

(9) H. S. Harned and B. B. Owen, "The Physical Chemistry of Electrolytic Solutions," Reinhold Publ. Corp., New York, N. Y., 1959.

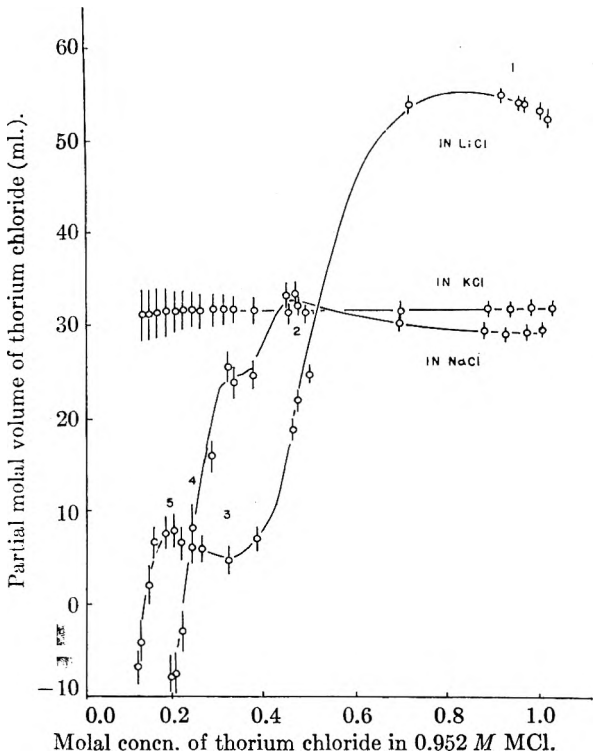

Fig. 2.—Partial molal volume of thorium chloride as a function of concentration. Numbers above curves represent moles of MCl per mole of $ThCl_4$.

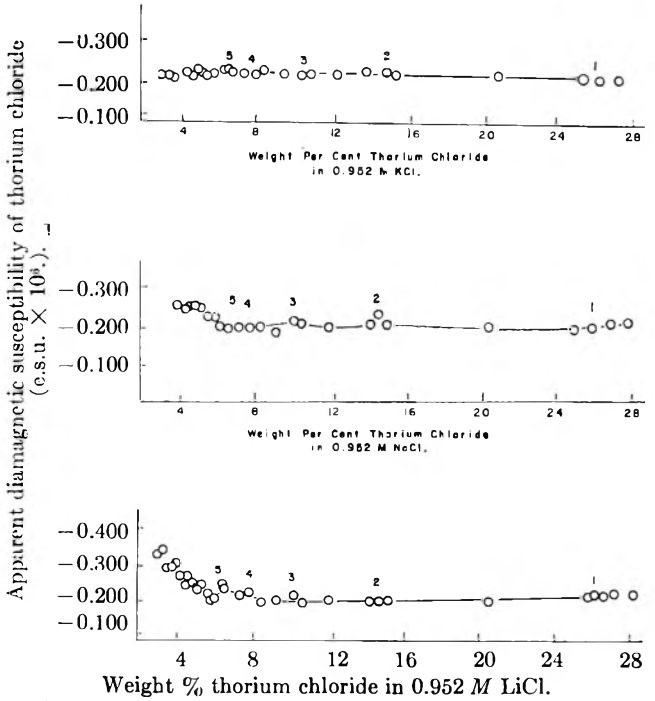

Fig. 3.—Apparent diamagnetic susceptibility of $ThCl_4$ as a function of concentration. Numbers above curves represent moles of alkali metal halide per mole of $ThCl_4$.

to approximately 0.25 *M* $ThCl_4$. Definite minima occur in the NaCl and LiCl systems, with the minimum points shifting toward higher concentrations of thorium chloride for the lighter metals. The general shape of the curves suggests that at low concentrations of $ThCl_4$ a larger volume is required to accommodate the structure surrounding each thorium ion than at higher concentrations. The trend toward small structures (and fewer displaced water molecules from the hydrated ions) continues until the minimum is reached, after which the curves rise to a relatively constant value in each case. Apparently the solutions are most alike at high $ThCl_4$ concentrations where the predominant influence is that of the thorium(IV) ion.

Partial Molal Volumes.—Partial molal volumes were determined by the method of tangents, using the familiar equation

$$\bar{V}_2 = \phi + \frac{s}{2.303}$$

where $\bar{V}_2$ is the partial molal volume of $ThCl_4$, ϕ has the same significance as before, and s is the slope at a given concentration of the curve which plots ϕ *vs.* the molal concentration of $ThCl_4$. In Fig. 2 the partial molal volumes of $ThCl_4$ are shown as a function of the molal concentration of $ThCl_4$. In the LiCl–$ThCl_4$ system there is a rapid increase in the partial molal volume of $ThCl_4$ until a concentration ratio of $LiCl/ThCl_4 = 5$ is reached. This is representative of the building up of polynuclear structures. Apparently the addition of more $ThCl_4$ has a disruptive influence on the structures and, beyond the 5:1 ratio, $\bar{V}_2$ decreases. Beyond a concentration ratio of 3:1 the rate of change again increases, then tends to level off at a 1:1 ratio. Probably some of the disruptive influence at higher concentrations of $ThCl_4$ can be attributed to the increased concentration of chloride ion, which has been described by Brady and Krause as an "order-destroying" ion in aqueous solution.[10]

Similar tendencies are indicated in the NaCl system, with diminishing rates of increase of volume appearing at $NaCl/ThCl_4$ concentration ratios of 3:1 and 2:1. At higher concentrations of $ThCl_4$ the trend seems to be toward smaller and simpler structures. The KCl system showed no apparent changes of partial molal volume of $ThCl_4$ with changes in concentration.

Diamagnetic Susceptibilities.—Insignificant deviations from linearity were observed when specific susceptibility of the solutions was plotted against $ThCl_4$ concentration. If there are no changes in the hydration spheres of the ions, and therefore no net change in the over-all influence on the solvent with the addition of $ThCl_4$, the contribution of the solution components to magnetic susceptibility would be additive and no change would be observed in the apparent diamagnetic susceptibility of $ThCl_4$ in solution. Calculations of the apparent susceptibility of $ThCl_4$ were made from the usual relationship

$$X(\text{solution}) = c_1X_1 + c_2X_2 + c_3X_3 + \ldots$$

where X is specific susceptibility and c is the fraction by weight of each component in the solution. The calculated apparent susceptibilities of $ThCl_4$ are summarized in Fig. 3. At low concentrations

(10) G. W. Brady and J. T. Krause, *Norelco Reporter*, **V**, No. 5, 6, 111 (1958).

of $ThCl_4$ where the $MCl/ThCl_4$ ratio is large, the apparent susceptibility of $ThCl_4$ shows a tendency to increase numerically. This would be true if greater numbers of water molecules were displaced per thorium ion during complex formation, thus releasing the molecules from the deforming influence of the electrostatic field of dissolved ions. As the concentration ratio becomes smaller, the value of "x" in the formula $ThCl_4 \cdot xMCl$ becomes smaller, resulting in fewer water molecules being displaced per thorium ion and a decrease in the apparent susceptibility of $ThCl_4$. This view is consistent with the apparent and partial molal volume data.

Conclusion

Apparent and partial molal volumes of $ThCl_4$ were plotted as a function of $ThCl_4$ concentrations in aqueous LiCl, NaCl, and KCl solutions. Variations in the curves suggest the formation of polynuclear structures, the complexity of which depends upon the concentration ratio of the two dissolved salts. This technique shows promise as a sensitive means of detecting changes in complex structures in solution. It is hoped that densities measured with greater precision will provide more detailed information regarding such structures.

A TEST OF GENERALIZED QUASI-LATTICE THEORY. CALCULATIONS OF THERMODYNAMIC PROPERTIES OF SOLUTIONS OF ALCOHOLS IN AROMATIC HYDROCARBONS

By J. R. Goates, R. L. Snow, and J. B. Ott

Department of Chemistry, Brigham Young University, Provo, Utah

Received January 8, 1962

Heats and excess free energies of mixing were calculated by means of a generalized quasi-lattice theory for alcohol–hydrocarbon systems and compared with experimental values from the literature. The various lattice parameters of the theory were deduced from the geometry of the molecules. A reasonable and consistent set of energy parameters was obtained from a study of the experimental results of fifteen alcohol–aromatic hydrocarbon systems. The same set of parameters was used to calculate excess free energy data, which were compared with three sets of experimental results. The theory appears to have value in interpreting and, to some extent, predicting thermodynamic properties of solutions.

The use of the generalized quasi-lattice theory described by Barker[1,2] to calculate the thermodynamic properties of mixing of solutions appears to have value in interpreting thermodynamic data for systems of associated liquids.[3,4] In a previous paper[5] we reported some success in describing the heats of mixing of ethanol with cyclohexane and both methanol and ethanol with benzene through the use of a consistent and reasonable set of energy parameters.

Recently an extensive set of heat of mixing measurements on alcohol–hydrocarbon systems has been completed by Mrazek and Van Ness.[6] That study includes measurements at three temperatures on the fifteen binary systems that can be formed from methanol, ethanol, propanol, butanol, and pentanol, each with benzene, toluene, and ethylbenzene. These data, together with the free energy of mixing data of Scatchard and Ticknor,[7] Brown and Smith,[8] and Kretchmer and Wiebe[9] now make it possible to conduct a rather exacting test of quasi-lattice theory in associated solutions.

(1) J. A. Barker, *J. Chem. Phys.*, **20**, 1526 (1952).
(2) J. A. Barker, *ibid.*, **21**, 1391 (1953).
(3) J. A. Barker, I. Brown, and F. Smith, *Discussions Faraday Soc.*, **15**, 142 (1953).
(4) J. A. Barker and F. Smith, *J. Chem. Phys.*, **22**, 375 (1954).
(5) J. R. Goates, R. L. Snow, and M. R. James, *J. Phys. Chem.*, **65**, 335 (1961).
(6) R. V. Mrazek and H. C. Van Ness, *Am. Inst. Chem. Engrs. Paper*, **72**, 190 (1961).
(7) G. Scatchard and L. B. Ticknor, *J. Am. Chem. Soc.*, **74**, 3724 (1952).
(8) I. Brown and F. Smith, *Australian J. Chem.*, **7**, 264 (1954).
(9) C. B. Kretchmer and R. Wiebe, *J. Am. Chem. Soc.*, **71**, 1793 (1949).

Quasi-lattice Theory

Lattice Parameters.—The theory described by Barker[1,2] is based on a quasi-lattice model that has been generalized by recognizing different types of contact sites on a molecule. For example, an alcohol is considered to have three types of sites—hydrocarbon type (designated as type I), hydroxyl hydrogen (H), and oxygen (O) type sites. Toluene and ethylbenzene are considered to have two types, an aromatic hydrocarbon type (S) on the benzene ring, and an aliphatic type (S′) on the alkyl substituents. Benzene is treated as having only the S type site.

The theory requires a knowledge of the number and type of sites on each molecule and the energies for all possible interactions of these sites. The number of sites present on the alcohol molecules was calculated on the assumption that each carbon and each oxygen atom occupied one position in a fourfold coördinated lattice. Some of the four nearest neighbors of each carbon or oxygen atom are atoms within the same molecule. The remainder, the number of those sites available for contact with another molecule, are designated by the letter Q, with a superscript A for alcohol and B for the other component of the solution. Subscripts to Q (H, O, I, S, and S′) refer to the type of site. Table I gives the values of the Q's used in this study.

The number of contact sites for both the alcohols and aromatic compounds was deduced directly from the structural formulas of the compounds.

Energy Parameters.—For the system containing

TABLE I

NUMBER AND TYPE OF CONTACT SITES

	$Q_H{}^A$	$Q_O{}^A$	$Q_I{}^A$	$Q_S{}^B$	$Q_{S'}{}^B$
CH_3OH	1	2	3	..	..
C_2H_5OH	1	2	5	..	..
C_3H_7OH	1	2	7	..	..
C_4H_9OH	1	2	9	..	..
$C_5H_{11}OH$	1	2	11	..	..
C_6H_5	..	..	..	12	..
$C_6H_5CH_3$	..	..	..	11	3
$C_6H_5C_2H_5$	..	..	..	11	5

benzene and an alcohol four types of sites are present, resulting in the following ten interactions: H–H, H–O, H–I, H–S, O–O, O–I, O–S, I–I, I–S, and S–S. The energy of interaction of the four of these that are between like sites is zero by definition, since U_{i-j} is defined as the energy change of the quasi-chemical process $\frac{1}{2}$ (i–i) + $\frac{1}{2}$ (j–j) = (i–j), with i and j representing any of the five types of contact sites.

Of the remaining six interactions, four (H–O, H–S, O–S, and I–S) were singled out as the most significant, either because the energy of interaction was expected to be relatively high (H–O, H–S, and O–S) or the number of such interactions of that type is large (I–S). The energy terms for the remaining two (H–I and O–I) were set equal to zero. Since both H and O sites might be expected to be preferentially involved in the more energetic interactions (H–O, H–S, and O–S), the contributions of H–I and O–I were expected, and are in fact found, to be small.

For the systems containing toluene and ethylbenzene, one additional type of contact site (S′ for the aliphatic part of the solvent molecule) and, therefore, five additional types of interactions (H–S′, O–S′, I–S′, S–S′, and S′–S′) had to be considered. Since the interaction S–S′ is similar to that of I–S, *i.e.*, each is an aliphatic–aromatic hydrocarbon interaction, the value of $U_{S-S'}$ was assigned the same value as U_{I-S}. The other four, considered to be less significant parameters, were set equal to zero. $U_{H-S'}$, $U_{O-S'}$, and $U_{I-S'}$ would be expected to be similar to U_{H-I}, U_{O-I}, and U_{I-I}, which were assigned a value of zero in the benzene systems. $U_{S'-S'}$ is zero by definition.

Values for U_{O-H}, U_{H-S}, U_{O-S}, and U_{I-S} that apply to the benzene systems had been determined in a previous study.[5] The same values, with small changes in U_{I-S}, were used for the benzene systems of this study. U_{O-H} had been fixed from a study of the relatively simple system ethanol–cyclohexane, for which only two energy parameters are required. The values of U_{H-S} and U_{O-S} were those necessary to give the correct shape to the heat of mixing–composition curves of benzene with methanol and ethanol, and U_{I-S} had been fixed at a value that gave the correct difference in height between the methanol–benzene and ethanol–benzene systems. In the present study, the value of U_{I-S} was adjusted independently for each system to give the correct height to each curve at 0.4 mole fraction alcohol, which is near the maximum heat of mixing value for these systems.

Inasmuch as the presence of an alkyl substituent in the benzene ring influences the electron density of the ring, and will, therefore, affect the H–S and O–S (and to some extent even the I–S) interactions, a new set of values for the energies associated with these interactions was needed for the toluene and ethylbenzene systems. Since the alkyl substituents increase the electron density of the ring, and the effect of the ethyl group is greater than that of the methyl, one would expect from a consideration of purely coulombic forces that in going from benzene to toluene to ethylbenzene systems, U_{H-S} should decrease and U_{O-S} should increase. The values of these parameters that produced the best fit of the experimental data did, in fact, follow the predicted change.

Computations.—The general equations for calculating the excess thermodynamic properties have been given by Barker[1,2] in terms of a function designated by X. For the toluene and ethylbenzene systems the X functions are defined by the set of five quadratic equations

$$X_H[X_H + X_O\eta_{H-O} + X_I + X_S\eta_{H-S} + X_{S'}] = Q_H x_A/2 \quad (1)$$

$$X_O[X_H\eta_{H-O} + X_O + X_I + X_S\eta_{O-S} + X_{S'}] = Q_O x_A/2 \quad (2)$$

$$X_I[X_H + X_O + X_I + X_S\eta_{I-S} + X_{S'}] = Q_I x_A/2 \quad (3)$$

$$X_S[X_H\eta_{H-S} + X_O\eta_{O-S} + X_I\eta_{I-S} + X_S + X_{S'}\eta_{S-S'}] = Q_S x_B/2 \quad (4)$$

$$X_{S'}[X_H + X_O + X_I + X_S + X_S\eta_{S-S'} + X_{S'}] = Q_{S'} x_B/2 \quad (5)$$

For the benzene systems, eq. 5 and the last term of the left-hand side of eq. 1–4 drop out. In the above equations, component A is the alcohol; component B, the hydrocarbon; x is mole fraction; $\eta = e^{-U/RT}$.

Equations 1–5 were solved by an extended form of Newton's method, the first approximation of the X's being taken as their values in the pure components. Satisfactory accuracy ($\Delta H_x{}^M$ to 0.01 cal.) was generally attained after 8–10 iterations. The computations were programmed in Fortransit language and processed on an IBM-650 computer.

Results

Heats of Mixing.—Table II lists the values of the energy parameters that resulted in the "best fit" of the experimental heat of mixing data, the "best fit" being the one that gave the lowest mean absolute value of the deviations from the nine experimental points taken at 0.1 mole fraction intervals. The procedure for fitting the experimental data consisted of establishing the general shape of the heat of mixing–composition curve by varying U_{H-S} and U_{O-S}, which are important in determining the extent of asymmetry of the curves, and then varying U_{I-S}, which has its greatest effect on the height of the curves, to produce the nearest fit of the experimental data. As shown in Table II, the same value of U_{H-O} was used throughout all fifteen systems, and the values of U_{H-S} and U_{O-S} were maintained constant for the C_2–C_5 alcohols in any given hydrocarbon system. In the methanol systems, U_{H-S}, U_{O-S}, and U_{I-S} were all three arbitrarily varied. Representative examples of the extent of agreement between theory and experi-

ment are shown in Fig. 1 and 2, in which the theory is represented by a solid line and the experimental data are plotted as circles. Considering the crudeness of the model and the assumptions involved in assigning values to the numerous parameters, the extent of agreement between theory and experiment seems fairly good.

Table II

Interaction Energies Obtained from Quasi-lattice Theory

	U_{H-O}	U_{H-S}	U_{O-S}	U_{I-S}	$U_{S-S'}$
Benzene systems					
CH_3OH	−3200	−410	−210	82	..
C_2H_5OH	−3200	−545	−300	81	..
C_3H_7OH	−3200	−545	−300	87	..
C_4H_9OH	−3200	−545	−300	82	..
$C_5H_{11}OH$	−3200	−545	−300	75	..
			Av.	81	
Toluene systems					
CH_3OH	−3200	−430	−155	82	82
C_2H_5OH	−3200	−615	−215	75	75
C_3H_7OH	−3200	−615	−215	92	92
C_4H_9OH	−3200	−615	−215	89	89
$C_5H_{11}OH$	−3200	−615	−215	72	72
			Av.	82	82
Ethylbenzene systems					
CH_3OH	−3200	−450	−110	82	82
C_2H_5OH	−3200	−670	−185	75	75
C_3H_7OH	−3200	−670	−185	95	95
C_4H_9OH	−3200	−670	−185	89	89
$C_5H_{11}OH$	−3200	−670	−185	75	75
			Av.	83	83

The prediction of the theory falls below the experimental results in each one of the fifteen systems at the low alcohol concentrations. Attempts to get better fits in this region included adjusting the values of U_{H-O}, U_{H-S}, and U_{O-S}, changing the number and types of contact sites on benzene, and considering the effect of reasonable values for the two interactions (H–I and O–I) that were previously neglected. U_{H-O}, U_{H-S}, and U_{O-S} produced the same qualitative effect on the shape of the curve, and no improvement in the fit was obtained on the use of any different combination of values for these variables. Decreasing the number of contact sites on benzene from 12 to 10 results in an 11% lowering of the maximum value, but no significant change in the composition at the maximum value. Introducing terms for two different types of sites on benzene did not improve the fit. The effects of H–I were found as predicted to be negligible; the effects of O–I though small were measurable, but O–I affects the shape of the curve qualitatively in the same way as H–O and H–S do, and so no advantage could be gained from adjusting that parameter. It appears that failure to fit the left side of Fig. 1 and 2 is a defect of the model itself rather than a failure to find a correct set of energy values.

The right sides of the figures, however, could all have been made to fit very well by making adjustments in the values assigned to U_{H-S} and U_{O-S}. There are, of course, good reasons to believe that

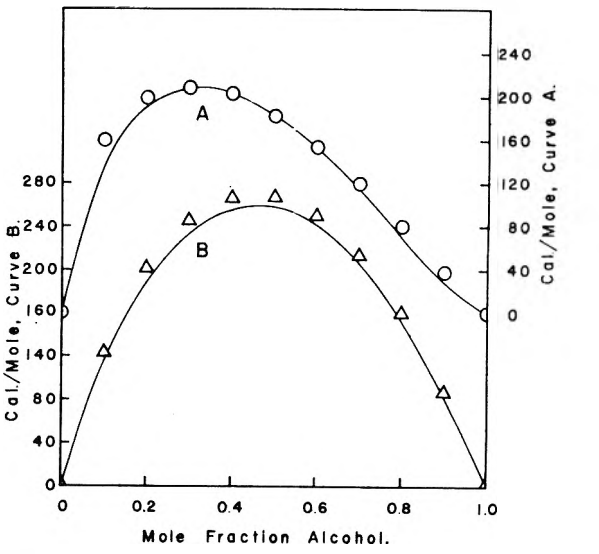

Fig. 1.—Heats (A) and free energies (B) of mixing of C_2H_5OH–C_6H_6 at 25 and 45°, respectively. The circles and triangles are experimental values; the lines are from quasi-lattice theory.

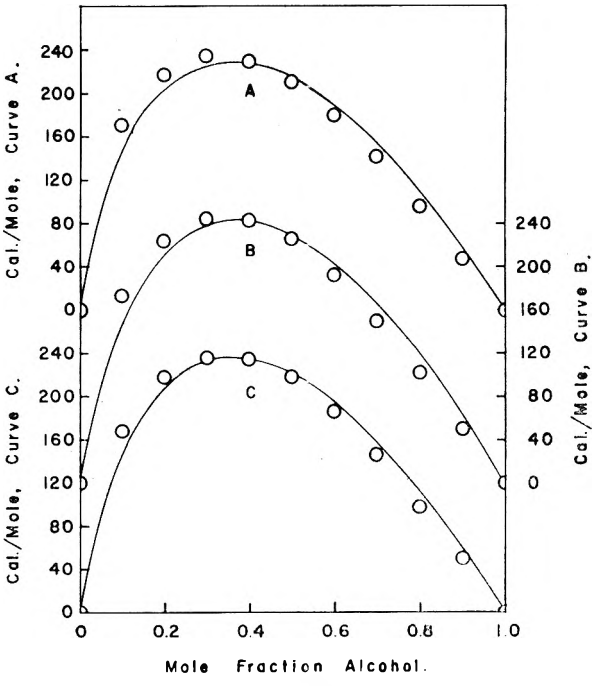

Fig. 2.—Heats of mixing of n-C_3H_7OH (A), n-C_4H_9OH (B), n-$C_5H_{11}OH$ (C) with $C_6H_5CH_3$ at 25°. The circles are experimental values; the lines are from quasi-lattice theory.

U_{H-O}, U_{H-S}, and U_{O-S} should differ slightly from one alcohol to another. In the interest of simplicity, however, we chose to hold those three parameters constant in the four systems containing the C_2 to C_5 alcohols and made whatever adjustment was necessary to give the correct height to the curve in the relatively sensitive I–S interaction.

The methanol systems, however, were fit so much better by using a different set of U_{H-S} and U_{O-S} values that in these three systems we assigned a separate set of values. From considerations of the inductive effect of the alkyl groups of the alcohols, it is reasonable to expect that there

would be a greater difference between the interaction energies involving methanol and ethanol than between ethanol and any of the other three alcohols of this series.

To test the effect of using the same value for U_{I-S} in all systems, an average (82 cal.) of the fifteen U_{I-S} values in Table II was used to calculate ΔH_x^M at the 0.5 mole fraction composition for each of the 15 systems. For the toluene and ethylbenzene systems the relationship $U_{I-S} = U_{S-S'} = 82$ cal. was used. The other parameters were as given in Table II. The average of the percentage deviations (absolute values) of the theoretical from the experimental results was 3.2%, and the maximum was 9.4%.

Excess Free Energies of Mixing.—After the values of the parameters listed in Table II had been established from the heat of mixing study, they were used to calculate the excess free energies of the three systems for which we had experimental data. Representative results can be seen in Fig. 1, the experimental data being represented by triangles. The theoretical results were calculated at 25° for methanol–benzene and are compared with data calculated at 25° from an equation by Scatchard and Ticknor[7] that summarized their experimental data from 25–55°. The theoretical results for ethanol–benzene were calculated at 45° and compared with the 45° experimental results of Brown and Smith.[8] The ethanol–toluene calculations were made at 35° and are compared with 35° measurements of Kretchmer and Wiebe.[9]

The theoretical results, while low in all three systems, reproduce the experimental results within 4–7%, which seems to be a satisfactory check inasmuch as no consideration was given to the free energy data in establishing the values of the constants in Table II.

Because one has so many parameters that he can, within reasonable limits, arbitrarily adjust, it is possible to fit a single set of ΔH_x^M experimental data with several combinations of energy values. To fit more than one system and yet maintain consistency among the constants used limits very appreciably the number of ways of producing a satisfactory fit. Calculation of free energies as well as heats places a further strain on the freedom of choice of energy values. It is interesting to note that the set of constants $U_{H-O} = -3200$, $U_{H-S} = -545$, $U_{O-S} = -300$, $U_{I-S} = 82$, and $U_{S-S'} = -45$, which are not reasonable because of the discrepancy in the last two values, nevertheless produces a fairly good fit of the heat of mixing data of ethanol–toluene and ethanol–ethylbenzene. When these values of the energy parameters are used to calculate the free energy, however, very poor results are obtained.

Temperature Effect.—In order to test the extent to which the energy parameters are temperature dependent, ΔH_x^M values were calculated at $x_A = 0.4$ from the 25° data of Table II for temperatures of 35 and 45°. The experimental ΔH_x^M data increase with an increase in temperature. The theoretical calculations, made on the assumption that the energy parameters are independent of temperature, account for 40–45% of this increase. The remainder can be accounted for by assuming a 2–3% change in the U's for each 10° change in temperature.

Since ΔF_x^E is quite insensitive to second-order changes in ΔH_x^M, the temperature dependence of the energy parameters is of much less significance in the calculation of ΔF_x^E than it is for ΔH_x^M.

Conclusions.—It appears from this study of 15 systems that the generalized quasi-lattice model is useful for interpreting, and to some extent predicting *a priori*, thermodynamic data of mixing in alcohol–hydrocarbon systems.

By assigning values to the lattice parameters that are based solely on the geometry of the molecules and making only rough estimates of reasonable values of the energy parameters, one can get qualitative information about the height and shape of the thermodynamic property–composition curves. By having access to a set of parameters such as those in Table II, one can make semi-quantitative ($\pm 10\%$) estimates.

Acknowledgment.—The authors gratefully acknowledge the support given this project by the National Science Foundation.

ADAPTATION OF LATTICE VACANCY THEORY TO GAS ADSORPTION PHENOMENA

BY J. M. HONIG

Lincoln Laboratory,[1] Massachusetts Institute of Technology, Lexington 73, Massachusetts

AND C. R. MUELLER

Department of Chemistry, Purdue University, Lafayette, Indiana

Received January 10, 1962

The Flory–Huggins polymer–monomer solution theory is adapted to obtain a lattice theory of gas adsorption in which the fractional hole size concept is utilized. Expressions for the zero-order isotherm and for the partial molecular configurational entropy are derived, in which the hole size parameter r makes its appearance. It is pointed out that certain symmetry properties of the lattice theory no longer obtain when $r > 1$. The theory is compared with experimental work on certain types of adsorbent–adsorbate systems, and experiments for providing further checks against the theory are suggested.

Introduction

In the lattice vacancy theory proposed by Mueller and Stupegia[2] the liquid is regarded as a quasi-binary lattice assembly of particles and of fractional sized holes. Despite its simplicity, the theory is quite successful in reproducing such quantities as the critical constants, vapor pressure curves, and rectilinear diameter plots for a variety of simple liquid–vapor systems. Moreover, the usefulness of this lattice model extends well into the gaseous region, and in the limit of low particle density, the perfect gas law is predicted.

The versatility of this approach suggests that it could be usefully adapted to a description of monolayer adsorption processes. In general, one deals with an adsorbate which behaves like a perfect two-dimensional gas at low coverage, and like a liquid or solid as monolayer coverage is approached ($\theta \rightarrow 1$). Furthermore, close packing of the adsorbate may not be realized if the spacing between potential minima on the surface differs from the diameter of the adsorbate atoms or molecular units; in that event, fractional holes remain on the surface even when $\theta = 1$.

We test the utility of the fractional-sized vacancy model by deriving both the isotherm equation and the partial configurational entropy for a surface phase consisting of particles and fractional-size holes. As a prerequisite, an expression for the free energy of such an assembly will be set up; the required expressions for the entropy and energy of the system are discussed in the next section.[3]

Thermodynamic Properties for a Binary Mixture in which the Components Differ in Size.— Consider the configurational entropy of a system of N_r molecules of an r-mer, built up from r monomer units, and N_1 molecules of a monomer, distributed on a lattice of L_r sites in such a manner that each monomer or r-mer segment occupies one lattice site. Then

$$L_r = N_1 + rN_r \qquad (1)$$

Moreover, Flory[4] and Guggenheim[5] have shown that the configurational entropy of mixing for the components in the solution is given by

$$\Delta S_c = -kL_r \{(1 - \phi) \ln (1 - \phi) + (\phi/r) \ln \phi\} \qquad (2)$$

where the fraction of lattice sites occupied by r-mer and monomer is $\phi = rN_r/L_r$ and $1 - \phi = N_1/L_r$, respectively. Equation 2 holds in the limit where the coördination number of the lattice is very large.

In the present situation we consider the r-mer to be analogous to an adsorbed atom or molecule and the monomer analogous to a hole. Since an adsorbed atom is far more symmetric than an r-mer, it is physically more palatable to consider the particle as occupying one surface site of area σ_a and the hole as occupying an area $\sigma_h = (1/r)\sigma_a$. To see the implication in this shift of viewpoint, we can write the area A of the surface as $A = N_a\sigma_a + N_h\sigma_h$, where N_a and N_h are the total number of each species. Then

$$N_a + N_h/r = A/\sigma_a \equiv L_a \qquad (3)$$

which leads to the following expressions for the fractional surface coverage: $\theta = N_a/L_a$ and $1 - \theta = N_h/rL_a$. It is seen that the substitution of rL_a for L_r and of θ for ϕ will convert eq. 2 to the form

$$S_c = -kL_a\{\theta \ln \theta + r(1 - \theta) \ln (1 - \theta)\} \qquad (4)$$

where $\Delta S_c \equiv S_c$ in the present case, since a lattice devoid of atoms or completely filled with atoms has zero configurational entropy. To S_c we must later adjoin the contribution of the thermal degrees of freedom to the entropy, S_T, of the adsorbed particles.

The configurational energy of the system is found by noting that, neglecting edge effects, the maximum number of nearest neighbor pairs in a lattice of L_a sites is $ZL_a/2$, where Z is the coordination number. In a purely random distribution the probability of encountering an occupied pair of nearest neighbor sites is θ^2. If now the lateral energy of interaction associated with

(1) Operated with support from the U. S. Army, Navy, and Air Force.

(2) C. R. Mueller and D. C. Stupegia, *J. Chem. Phys.*, **26**, 1522 (1957).

(3) A more detailed set of derivations and discussion of the remainder of this paper has been given by J. M. Honig in M.I.T. Lincoln Laboratory Technical Report No. 252. Copies available on request.

(4) P. Flory, *J. Chem. Phys.*, **10**, 51 (1942).

(5) E. A. Guggenheim, "Mixtures," Clarendon Press, Oxford, 1952.

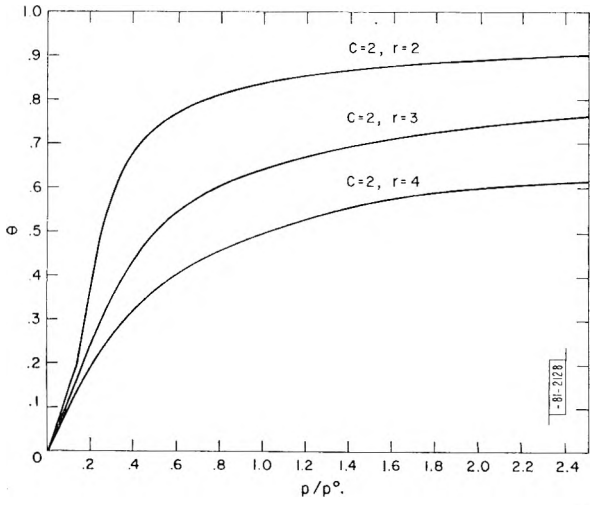

Fig. 1.—Isotherms calculated according to eq. 11, with $C = 2$, $Z = 6$, and various values of r.

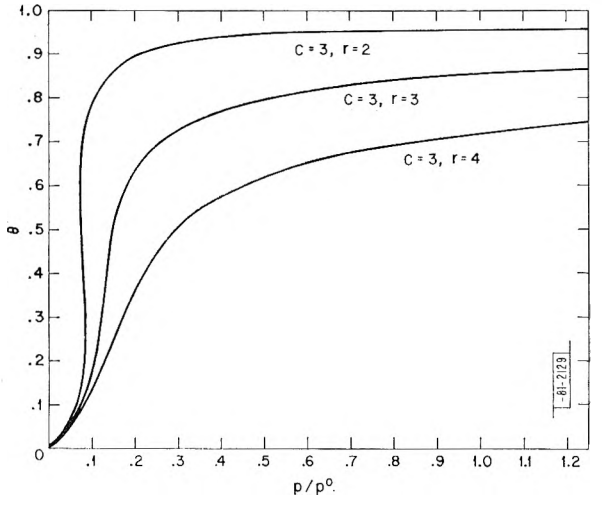

Fig. 2.—Isotherms calculated according to eq. 11, with $C = 3$, $Z = 6$, and various values of r.

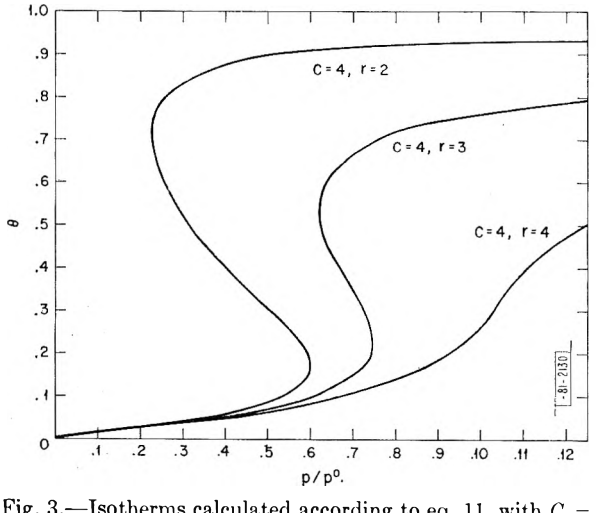

Fig. 3.—Isotherms calculated according to eq. 11, with $C = 4$, $Z = 6$, and various values of r.

such a pair is w, then

$$E_c = L_a(Z/2)w\theta^2 \qquad (5)$$

Note that the probability factor θ^2 and eq. 4 are based on the assumption of a random distribution, which can only occur if $w = 0$. However, it can be shown[5] that eq. 4 and 5 are the limiting cases for $Zw/2 << kT$ of a self-consistent approach (the so-called quasi-chemical approximation) in which the inconsistency is eliminated.

To eq. 5 we must adjoin the thermal energy

$$E_T = L_a\theta(\epsilon_T - \epsilon) \qquad (6)$$

where ϵ_T is the average energy due to the internal degrees of freedom of an adsorbed atom and $-\epsilon$ the adsorption energy.

On combining S_T with (4), (5), and (6) one obtains for the free energy of the system

$$F_s = L_a\theta\mu_s^0 + kTL_a\{\theta \ln \theta + r(1 - \theta) \ln (1 - \theta)\} + L_aZw\theta^2/2 - L_a\theta\epsilon \qquad (7)$$

where $L_a\theta\mu_s^0 = E_T - TS_T$.

Let us differentiate F with respect to $N_a = L_a\theta$, keeping T fixed. This yields the chemical potential of the adsorbed phase μ_s which at equilibrium is equal to that of the gas phase $\mu_g = -kT \ln (2\pi mkT/h^2)^{3/2} j_g kT/p \equiv -kT \ln p^*/p$, j_g being the partition function for the internal degrees of freedom. One thus finds

$$\ln \frac{p}{p^*} = \frac{\mu_s^0}{kT} + \frac{Zw\theta}{kT} + (1 - r) - \frac{\epsilon}{kT} + \ln \frac{\theta}{(1 - \theta)^r} \qquad (8)$$

which may be rewritten as

$$p/p^0 = [\theta/(1 - \theta)^r]C^{-Z\theta} \qquad (9)$$

where

$$p^0 \equiv p^* e^{-\epsilon/kT} e^{(1-r)}/j_s \; ; \; C \equiv e^{-w/kT} \qquad (10)$$

The partial molecular configurational entropy of adsorption is given by

$$S_c = -\frac{\partial}{\partial T}(\mu_s - \mu_s^0)]_{L_a,\theta} = -k\{\ln [\theta/(1 - \theta)^r] - (r - 1)\} \qquad (11)$$

Discussion

Isotherms calculated according to eq. 9 for various values of C and r are depicted in Fig. 1–3; the function $-\log [\theta/(1 - \theta)]^r$ is plotted *vs.* θ in Fig. 4.

Several points are worthy of note: (1) The theory presented above is able to take account of two-dimensional condensation, as indicated by the presence of loops in the isotherm for sufficiently large C values. These values require that $w < 0$, *i.e.*, that the interactions among neighboring molecules on the surface be attractive. The critical pressure p_{cr} at which condensation phenomena set in occurs at a value such that the vertical line $p(\theta)$ divides the loop into two equal areas. It can be shown[6] that when $r = 1$, $p_{cr} = p(1/2)$. As is evident by inspection of Fig. 2 and

(6) R. H. Fowler and E. A. Guggenheim, "Statistical Thermodynamics," Cambridge University Press, 1939.

3, when $r > 1$, $p_{cr} < p(1/2)$. (2) The effect of lateral interactions is offset to some degree by increasing the value of r. Thus, it is seen from Fig. 2 that the isotherm corresponding to $C = 3$ and $r = 2$ exhibits loops, whereas those for which $r > 2$ do not. Similarly, in Fig. 3, the curves for $C = 4$ and $r = 2,3$ indicate the onset of condensation, whereas the curve for $C = 4$ and $r = 4$ does not. Also, the various diagrams show that it requires progressively higher pressures to reach a given value of θ as r is increased. All of the above is a reflection of the fact that E_c is independent of r while S_c changes so as to make it more difficult to fill the surface completely when r becomes large. (3) One of the most interesting findings is that the configurational partial molal entropy $\bar{S}_c$ is no longer antisymmetric about the point $\theta = 1/2$ when $r > 1$. Recently, it has been shown by Kleiner[7] that when the lateral interaction energies are assumed to be pairwise additive and localized adsorption prevails, $\bar{S}_c$ will always exhibit the inversion symmetry about $\theta = 1/2$, so long as $r = 1$. Figure 4, in which $S_1 \equiv -\log [\theta/(1-\theta)^r] = \bar{S}_c/2.303k - (r-1)/2.303$ is plotted *vs.* θ, shows the progressive departure from this situation; the partial molal entropies obtained for a given θ become more negative as r is increased. (4) Figures 1–3 are very similar to those obtained from isotherms based on the two-dimensional van der Waals equation of state.[8] Mere examination of adsorption data thus does not suffice to distinguish between the two theories pertaining to localized and mobile adsorption. The model discussed here should be used primarily in the interpretation of data taken at very low temperature, and is competitive with the van der Waals isotherm equation in the intermediate region between 77 and 90°K. Where the present theory is applicable, deviations from the symmetry properties discussed in (1)–(3) may be considered to arise because of the mismatch between the extent of an adsorption site (minimum in the adsorption potential) and the dimensions of the adsorbate.

We will conclude with a brief discussion comparing theory and experiment. One of the important aspects of prior theories[6,9] dealing with monolayer adsorption of gases on energetically homogeneous surfaces and with the situation where $r = 1$ is that the point of inflection in the sigmoidal isotherms or in the loop occurs at $\theta = 1/2$. Moreover, letting θ' and θ'' represent the two fractions of occupied sites at which two-dimensional condensation sets in and terminates, it can be shown[6] that $\theta'' - 1/2 = 1/2 - \theta'$; *i.e.*, that θ' and θ'' are equidistant from the inflection point when $r = 1$.

It is not a simple matter to find experimental data against which the theory can be checked; for, to bring out the features discussed earlier, it is necessary to employ homogeneous adsorbents, adsorbates that display a high degree of molecular symmetry, and systems where the formation of

(7) W. H. Kleiner, *J. Chem. Phys.*, **36**, 76 (1962).

(8) J. H. de Boer, "The Dynamical Character of Adsorption," Oxford, 1953, Chap. VIII.

(9) S. Bumble and J. M. Honig, *J. Chem. Phys.*, **33**, 424 (1960).

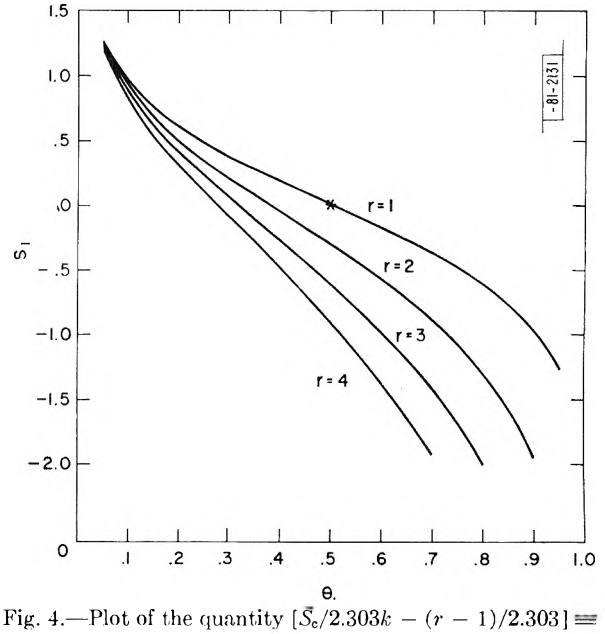

Fig. 4.—Plot of the quantity $[\bar{S}_c/2.303k - (r-1)/2.303] \equiv S_1$ *vs.* θ.

higher layers does not begin until after a monolayer has been deposited. Nevertheless, there exist data that conform to the requirements of the present theory. As an example, one may cite the measurements by Prenzlow and Halsey[10]; their adsorption isotherms for argon on graphitized carbon black covered by a preadsorbed layer of xenon are sigmoidal in character, and the inflection point occurs at $\theta \backsimeq 0.4$. Moreover, by extrapolating the results to temperatures slightly lower than the range covered in the measurements, one can see that θ' and θ'' will not be equidistant from the inflection point. The parameters $C = 3$ and $r = 3$ are roughly in accord with the data by Prenzlow and Halsey for temperatures near 65°K.[11]

A similar situation is encountered in the adsorption of argon at 77°K. on graphitized carbon black,[12] argon on one layer of xenon preadsorbed on graphitized black (77°K.),[13] krypton on graphitized carbon black, (77.8°K.),[14] and xenon, CH_4, C_2H_6 on {100} surfaces of NaCl[15] (103–113°K., 77–93°K., 123–140°K.). The list is not exhaustive, but sufficient to show that there are cases where a lattice theory in which $r = 1$ fails to apply to experimental data.

The second important aspect of the theory developed here, concerning the asymmetry of $\bar{S}_c$ about the point $\theta = 1/2$, is not checked as readily, since there is a real paucity of suitable experi-

(10) C. F. Prenzlow and G. D. Halsey, Jr., *J. Phys. Chem.*, **61**, 1158 (1957).

(11) W. Steele (personal communication) has attempted to reinterpret these data by lowering the numerical value for the number of atoms required for monolayer coverage of the surface. This does bring the inflection point of the sigmoidal isotherms closer to $\theta = 1/2$, but the thermodynamic functions nevertheless do not exhibit the symmetry associated with the value $r = 1$.

(12) J. H. Singleton and G. D. Halsey, Jr., *J. Phys. Chem.*, **58**, 1101 (1954).

(13) J. H. Singleton and G. D. Halsey, Jr., *ibid.*, **58**, 330 (1954).

(14) S. Ross and W. Winkler, *J. Colloid Sci.*, **10**, 330 (1955).

(15) S. Ross and H. Clark, *J. Am. Chem. Soc.*, **76**, 4291 (1954).

mental data. In a review by Everett and Young,[16] $\bar{S}_c$ was computed from experimental data for a large number of different adsorbent–adsorbate systems. In almost all cases calculated, $\bar{S}_c$ *vs.* θ curves deviated from the "ideal" curve (eq. 11 with $r = 1$), but for $\theta > 1/2$ the experimental values fell above the ideal curve rather than below, as in Fig. 4. This is attributed to two effects. In the particular cases cited by Everett and Young, the surfaces were energetically heterogeneous, and multilayer formation set in long before the first layer was completed. Both of these phenomena contribute to the above mentioned effect.[16,17] The only instance that has come to the writers' attention where the deviation of the experimental from the ideal $\bar{S}_c$ *vs.* θ curves is as indicated in Fig. 4 is the work by Hill, Emmett, and Joyner[18] for the adsorption of nitrogen on graphon. The $\bar{S}_c$ *vs.* θ curve cited in the above reference roughly matches the curve in Fig. 4 for which $r = 3$.

Summarizing, it may be said that the theory involving holes of fractional size, as presented in this paper, is a convenient extension of prior theories[6,9] to which it reduces in the limit $r = 1$. Subject to the assumptions inherent in the theoretical development, the theory specifies adsorption isotherms and other thermodynamic quantities for the adsorbed phase in terms of an additional parameter r. For reasonable numerical values of the latter, the theory is in better accord with a variety of experimental data than the earlier formulations for which $r = 1$.

To obtain further checks on the theory discussed above it is highly desirable to have data which are taken with the specific objective of testing the results cited here. In particular, the data should be amenable to the determination of $\bar{S}_c$. If systematic deviations from the above theory are noted, it may be necessary to resort to a more sophisticated derivation in which the self-contradictory assumptions concerning the random distribution coupled with a non-zero configurational energy are eliminated.

Acknowledgment.—The authors are very greatly indebted to Dr. Walter H. Kleiner for his unstinting assistance in the preparation of this manuscript and for many fruitful discussions.

(16) D. H. Everett and D. M. Young, *Trans. Faraday Soc.*, **48**, 1164 (1952).

(17) L. E. Drain and J. A. Morrison, *ibid.*, **48**, 316 (1952); **49**, 654 (1953).

(18) T. L. Hill, P. H. Emmett, and L. G. Joyner, *J. Am. Chem. Soc.*, **73**, 5102 (1951).

DIFFUSION OF NICKEL IN SINGLE CRYSTALS OF NICKEL OXIDE[1]

BY JAE SHI CHOI AND WALTER J. MOORE

Chemical Laboratory, Indiana University, Bloomington, Indiana

Received January 12, 1962

The diffusion of ^{63}Ni in single crystals of NiO has been measured by a sectioning method. From 1000 to 1470° for NiO in air, $D(\mathrm{Ni}) = 1.83 \times 10^{-3} \exp(-45.6 \text{ kcal.}/RT)$. The D was almost the same in crystals containing 4×10^{-4} atom fraction trivalent impurities as in those containing 60×10^{-4} cobalt. A mechanism based on singly ionized cationic vacancies gives a quantitative interpretation of the ΔH^* and ΔS^* for the diffusion.

Previous studies of the diffusion of ^{63}Ni in NiO have yielded discordant results. Shim and Moore[2] reported $D_{\mathrm{Ni}} = 4.4 \times 10^{-4} \exp(-44.2 \text{ kcal.}/RT)$ cm.^{2} sec.$^{-1}$, whereas Lindner and Åkerström,[3] using similar techniques and in some cases crystals from the same boule, found $D_{\mathrm{Ni}} = 1.72 \times 10^{-2} \exp(-56.0 \text{ kcal.}/RT)$. We have undertaken the further measurements described in this paper in an effort to resolve this discrepancy. Both earlier studies were made by the method of decline in surface activity. The isotope ^{63}Ni is not well suited to this method since it emits a soft (63 kv.) β, and consequently very thin layers of the nickel oxide suffice to absorb most of the radiation. We therefore used in the present measurement of D a different method, which is more suitable for this soft tracer radiation. This is the method of surface activity after sectioning.[4] We also made some special tests of the activation energy of D by the method of Zhoukhovitzky,[5] which is independent of the value of the absorption coefficient. A further improvement in technique was the annealing of the crystals before the diffusion run. Recent work[6] has emphasized the necessity of such preannealing of crystals made by the Verneuil method. All our new results support the lower value of the activation energy. From 1000 to 1400° for monocrystalline NiO in air, $D = 1.83 \times 10^{-3} \exp(-45.9 \pm 2.0 \text{ kcal.}/RT)$. The activation energy by the Russian method was $E = 41$ kcal. for polycrystalline specimens.

Experimental Methods

The single crystals of nickel oxide were cut as 4 to 5 mm. squares, 2 to 2.5 mm. thick. Crystals were used from two sources: Tochigi Chemical Industry Company, Osaka, Japan, and General Electric Company, Schenectady, New York. Spectrographic analyses were made of these materials. The Japanese NiO contained 0.6% cobalt and 0.1% Mg, with traces of other elements. The G.E. crystals contained less than 10 p.p.m. cobalt.[7] Both square faces of a specimen were polished flat on a precision grinder, using silicon carbide paper of grades 1/0 to 4/0. The specimens then were pre-annealed in a stream of dry tank

(1) Work assisted by the U. S. Atomic Energy Commission, Contract AT-(11-1)-250.

(2) M. T. Shim and W. J. Moore, *J. Chem. Phys.*, **26**, 802 (1957).

(3) R. Lindner and A. Åkerström, *Discussions Faraday Soc.*, **23**, 133 (1957).

(4) R. H. Condit and C. E. Birchenall, *J. Metals*, **8**, 1341 (1956).

(5) A. A. Zhoukhovitzky, *J. Appl. Rad. and Isotopes*, **5**, 159 (1959).

(6) Y. Oishi and W. D. Kingery, *J. Chem. Phys.*, **33**, 480 (1960).

(7) Analysis %: Al 0.003, Co <0.001, Cr 0.025, Cu <0.005, Fe 0.009, Mg 0.001, Mn <0.001, Si 0.004, Ti 0.001. We thank R. K. Leininger of the Indiana Geological Survey Laboratories for his cooperation in providing these analyses.

nitrogen for 40 hr. at the temperature of the run. They were cooled and cleaned with nitric acid and distilled water before use.

The radioactive nickel was obtained from Oak Ridge as $NiCl_2$ in 0.22 N HCl, with a specific activity of 38.79 mc./g. This was diluted with a buffer solution containing 250 μg./ml. of inactive nickel. About 100,000 c.p.m. was electroplated onto a tantalum strip, from which about 20,000 c.p.m. could be evaporated onto the surface of the NiO crystals, which corresponds to <0.1 μ thickness of nickel. The homogeneity of the deposit always was verified by microscopic examination before use of a specimen. After the edges were ground away, the crystal was heated 15 min. in air at 500° to fix the active deposit.

The diffusion anneals were done in air in a platinum resistance furnace controlled to ±2°. Temperatures were checked against N.B.S. thermocouples. The sample was placed in a platinum boat and the active surface was covered with an inactive crystal at a separation of 0.5 mm. provided by a small platinum ring. No appreciable activity was ever detected on the upper crystal after an anneal.

After the anneal, the edges of the specimen were ground away slightly to reduce any effects due to surface diffusion. The crystal was mounted on an aluminum holder with Araldite 6060 and sectioning was carried out on the precision grinder, with special care taken to ensure parallel sections. The mass of each section was determined by weighing the mounted disk on a Mettler single pan microbalance to an accuracy of ±2 μg. The thickness of each section was calculated from the known density of NiO and the area of the crystal face. The thickness ranged from 10 to 30 μ. After each section, the crystal was counted in a 2π geometry gas flow counter.

In the method of Zhoukhovitzky, large numbers of points are taken to determine curves of surface activity *vs.* time at different temperatures. The crystal was removed quickly from the furnace every five minutes and its surface activity measured. The half time required to achieve temperature equilibrium is estimated as about 10 sec.

Experimental Results

The solution of the one-dimensional diffusion equation for the initial condition of a plane radioactive source of activity A at the surface of the specimen is

$$c = A(\pi Dt)^{-1/2} \exp(-x^2/4Dt) \qquad (1)$$

where c is the concentration of tracer at a depth x from the surface. The actual data are summarized in Table I. We measure the activity at the surface, remove a layer of thickness δ_j, and measure the surface activity again, and so on. If the absorption coefficient of a homogeneous tracer radiation is μ, the initial surface activity is

$$A_0 = \int_0^\infty c(x) \exp(-\mu x)\, dx \qquad (2)$$

After removal of the j'th layer, or a total thickness x_j, the activity will be

$$A_j = A(\pi Dt)^{-1/2} \exp \mu x_j \times \int_{x_j}^\infty \exp(-x^2/4Dt) \exp(-\mu x)\, dx \qquad (3)$$

This expression can be rewritten as

$$A_j = A \exp(\mu^2 Dt + \mu x_j) \times \left\{1 - \mathrm{Erf}\left[\frac{1}{2\sqrt{Dt}}(x_j + 2\mu Dt)\right]\right\} \qquad (4)$$

The value of the argument of Erf is such that we can use the asymptotic expression

$$1 - \mathrm{Erf}\, y = (\pi^{1/2} y)^{-1} \exp(-y^2) \qquad (5)$$

In this case, eq. 3 for the surface activity becomes

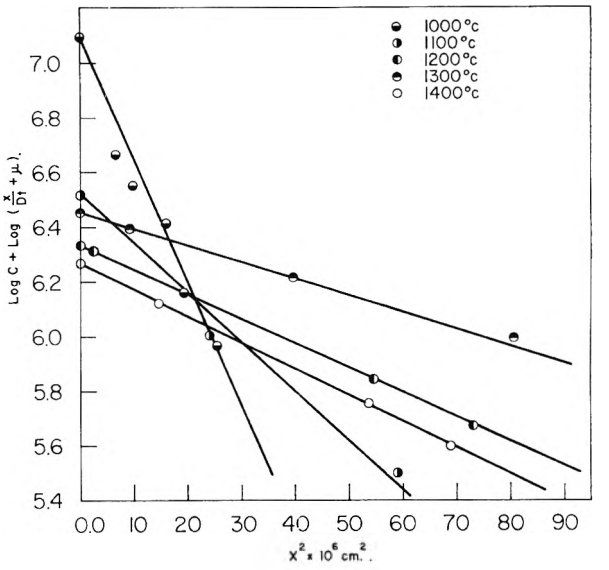

Fig. 1.—Plot of eq. 6 to evaluate the diffusion coefficient.

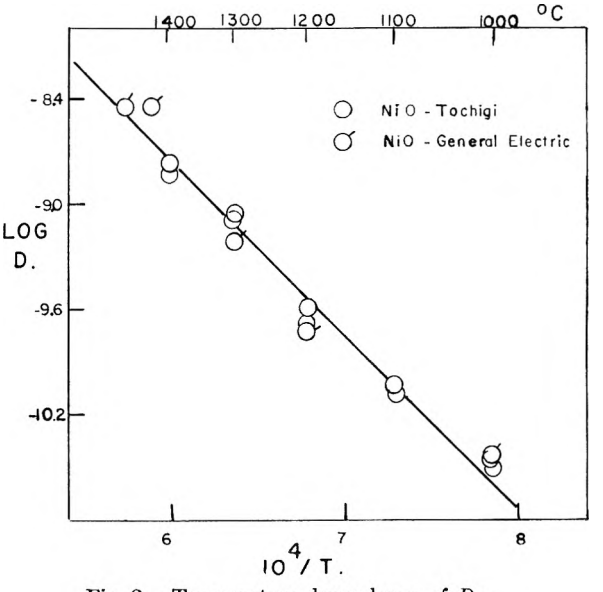

Fig. 2.—Temperature dependence of D_{Ni}.

$$A_j = A(\pi Dt)^{-1/2} (x_j/2Dt + \mu)^{-1} \times \exp(-x_j^2/4Dt) \qquad (6)$$

We note that this expression has a form identical with eq. 1 except for the factor $(x_j/2Dt + \mu)^{-1}$. Since $\mu > (x_j/2Dt)$ this term varies slowly from section to section. We can therefore first calculate an approximate value D' for D by ignoring this term, and then obtain a precise value of D by plotting log $(x_j/2D't + \mu)A_j$ against x_j^2. These plots are shown in Fig. 1 for several typical runs. The value of μ is 1.118×10^4 cm.$^{-1}$.

In Fig. 2 we have plotted log D *vs.* T^{-1} for all the diffusion runs. We have determined the constants of the best straight line by the method of least squares, including the runs on both crystals.

The application of the method of Zhoukhovitzky was limited to runs at 1000, 1100, and 1200°. The curves of surface activity *vs.* time are shown in Fig. 3. The times corresponding to $I/I_0 =$

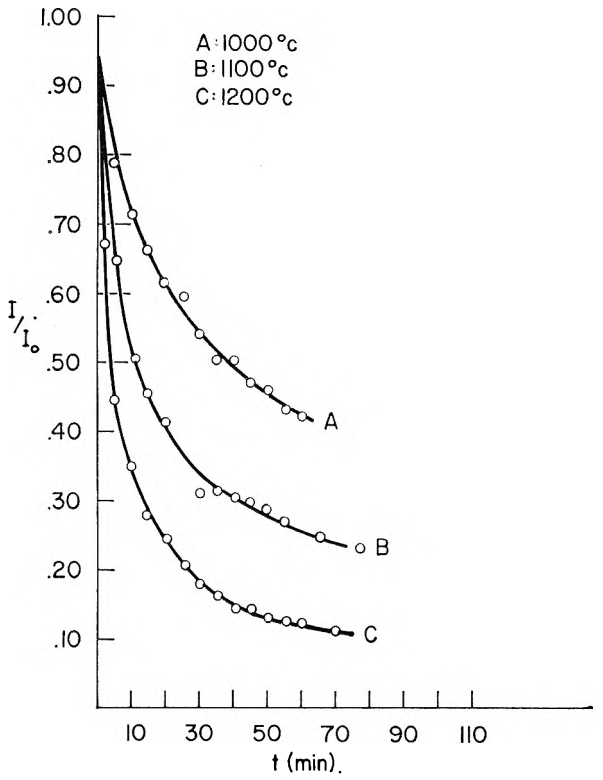

Fig. 3.—The method of Zhoukhovitzky—surface activity *vs.* time.

TABLE I

DATA ON DIFFUSION OF RADIOACTIVE NICKEL INTO CRYSTALS OF NICKEL OXIDE

Run no.[a]	Temp., °C.	Time, hr.	Depth, cm. × 10³	Activity,[b] c.p.m.
RG 4	1000	95	0.000	734
			1.083	603
			2.559	537
			4.140	274
			5.057	194
RG 1	1200	60	0.000	907
			3.337	754
			5.788	563
			7.853	396
			9.753	236
			11.237	195
			12.240	140
RG 2	1300	21	0.000	749
			2.872	638
			6.160	428
			8.252	308
			9.514	235
			10.970	171
RG 3	1430	15	0.000	475
			7.892	403
			9.932	346
			12.720	334
			15.979	227
RG 5	1470	20	0.000	889
			2.919	814
			7.936	765
			10.340	663
			12.772	607
RT 4	1000	50	0.000	1126
			2.600	406
			3.152	312
			4.024	224
			4.388	125
			5.046	80
RT 1	1000	50	0.000	2086
			5.09	350
			6.36	152
			7.61	23
RT 2C	1100	50	0.000	293
			4.787	104
			7.700	28
			11.35	7
RT 2A	1100	50	0.000	663
			5.329	240
			9.668	36
			13.220	11
RT 8	1200	30	0.000	193
			1.553	187
			5.110	100
			7.385	62
			8.565	42
RT 3	1200	20	0.000	247
			1.920	194
			3.851	125
			4.680	95
			5.51	63
RT 5	1300	14	0.000	256
			3.060	225
			6.303	145
			8.973	94
			11.19	44
RT 6	1300	14	0.000	207
			3.050	148
			7.920	93
			12.44	73
RT 9	1400	5	0.000	167
			3.850	119
			7.330	51
			8.312	36
RT 7	1400	15	0.000	317
			7.520	228
			11.32	131
			14.49	82
			16.23	60

[a] G refers to General Electric and T to Tochigi crystals [b] Corrected for background; statistical error ±2%.

0.6, 0.55, 0.50, 0.45, and 0.40 are read from the curves and the activation energies determined from

$$\frac{t_2}{t_1} = \exp\left[-\frac{E}{R}\left(\frac{1}{T_1} - \frac{1}{T_2}\right)\right]$$

The average value of E obtained by this method was $E = 40.9$ kcal. with a probable error of ±2.9 kcal.

Discussion

We can now recalculate the parameters of the transition-state expression for D as

$$D = \frac{kT}{h} a^2 \exp(\Delta S^*/R) \exp(-\Delta H^*/RT) \quad (7)$$

With a = 2.96 Å., the nearest Ni–Ni separation in NiO, we find at 1500°K. ΔH^* = 42.6 kcal. and ΔS^* = − 7.4 cal. deg.$^{-1}$. As previously pointed out,[8] these quantities are composites of the thermodynamic ΔS^0 and ΔH^0 for the formation of the defect responsible for diffusion and the kinetic ΔH_i^* and ΔS_i^* for the mobility of the defects.

There is good evidence that in these oxides with the rocksalt structure cations diffuse by a vacancy mechanism.[9] Excess oxygen dissolves in NiO by the reaction

$$\tfrac{1}{2}O_2 + Ni^{+2} \longrightarrow O^= + Ni^{+3} + V_{Ni}^{+} \quad (8)$$

[Mitoff[9b] assumes that the vacancy is doubly ionized, but his data are in better accord with the more reasonable assumption of eq. 8.] From eq. 8

$$[V_{Ni}^{+}] = K^{1/2} P_{O_2}^{1/4}$$

We then have

$$\Delta H^* = \Delta H_i^* + \tfrac{1}{2}H^8$$

$$\Delta S^* = \Delta S_i^* + \tfrac{1}{2}\Delta S^8$$

where ΔH^8 and ΔS^8 are the enthalpy and entropy of reaction 8. The data of Mitoff and of Carter and Richardson[10] yield $\Delta H^8 \simeq 30$ kcal. and $\Delta S^8 \simeq -12$ cal. deg.$^{-1}$. Therefore, for the step in which a nickel jumps into a neighboring vacancy $\Delta H_i^* = 27.6$ and $\Delta S_i^* = -1.4$.

In the case of pure CoO,[10] $\Delta H_i^* = 30$ and $\Delta H^8 = 10$. It is not surprising to find the value of ΔH_i^* as much as 2.4 kcal lower in the case of NiO. The concentration of trivalent impurities in the General Electric NiO was about 3.8×10^{-4}, which is comparable with the total concentration of vacancies. It might at first seem likely, therefore, that the ΔH^8 in the NiO samples had been lowered by the traces of impurities. Yet it would not assist the D of Ni^{+2} to have a vacancy tied to a Cr^{+3} site. Therefore the impurities may not have any marked effect on the D. This view is supported by the fact that the diffusion coefficients in the crystals containing 60×10^{-4} cobalt were not significantly different from those in the purer crystal. The ionic radii according to Pauling are Fe^{+2}, 0.75; Co^{+2}, 0.72; Ni^{+2}, 0.69. Thus we would expect Ni^{+2} to have a somewhat lower ΔH_i^* for this reason. The most consistent interpretation therefore appears to be the one given, which neglects the effect of trivalent impurities.

It is quite clear from all the data on FeO, CoO, and NiO that the activation energy for D in NiO should be close to the value of 45 kcal. The higher value of 56 kcal. given by Lindner,[3] even with $\Delta H_i^* = 30$, would require $\Delta H^8 = 52$. Such a value would be inconsistent with the observed excess oxygen concentration in NiO, which at 1350° is only about $1/20$ as large as the value in CoO. Such a factor corresponds to a difference in ΔH^8 of 18 kcal., so that with Richardson's[10] accurate value of ΔH^8 (CoO) = 10, the ΔH^8 (NiO) should be about 28 kcal.

(8) W. J. Moore and J. K. Lee, *Trans. Faraday Soc.*, **48**, 916 (1952).

(9) (a) C. E. Birchenall, *Met. Rev.*, **3**, 256 (1958), reviews the subject; (b) S. P. Mitoff, *J. Chem. Phys.*, **35**, 882 (1961).

(10) R. E. Carter and F. D. Richardson, *Trans. AIME*, **194**, 1244 (1954).

OXIDATION OF METALS IN MOLTEN SALTS. SILVER IN SODIUM CHLORIDE[1]

By Kurt H. Stern

Electrochemistry Section, National Bureau of Standards, Washington, D. C.

Received January 13, 1962

The rate of oxidation of silver in sodium chloride near 900° has been determined under a variety of conditions. When the rate of O_2 transport to the Ag–NaCl interface is low, the reaction is zero order; when it is high, the rate varies as $\sqrt{\text{time}}$, indicating a rate controlled by the diffusion of products away from the reaction site. Under all conditions the $Ag^+/O^=$ ratio is greater than can be accounted for by the formation of Ag_2O. The results can be accounted for by hypothesizing two simultaneous reactions, (a) $2Ag + 1/2O_2 = 2Ag^+ + O^=$, (b) $Ag^0 + Na^+ \rightarrow Ag^+ + Na^0$, which produce ionic silver, the relative contributions to total Ag^+ of the reactions depending on conditions. The equilibrium constant for (a) is 8.3×10^{-7} on the mole fraction scale.

Introduction

The oxidation of metals in and by molten salts is of interest from several points of view. In a molten salt, electron transfers not possible in aqueous solution may occur, the subject has practical applications in the field of corrosion, and the particular system discussed here is relevant to the Ag–AgCl reference electrodes commonly used for electrochemical measurements in fused salts.

That silver is oxidized in molten sodium chloride has been known for a long time.[2] Suggestions that the reaction proceeds, in the presence of air, by the formation of metallic sodium which then is oxidized to Na_2O, are likewise old.[3] Recently, this idea has been formulated more precisely[4,5] by suggesting

(1) Presented in part at the 137th National Meeting of the American Chemical Society, Cleveland, April, 1960.

(2) K. A. Winkler, "Europäische Amalgation der Silbererze und silberhaltigen Hüttenprodukte," Freiberg, 1846.

(3) H. Rose, *Pogg. Ann.*, **68**, 286 (1846).

(4) K. Smrjek, I. Sekerka, and V. Seifert, *Chem. Listy*, **50**, 721 (1956).

(5) K. H. Stern, *J. Phys. Chem.*, **62**, 385 (1958).

that, although the equilibrium for the reaction Ag + NaCl = AgCl + Na lies very far to the left ($K = 1.07 \times 10^{-10}$ at 900°) the reaction may be driven by the vaporization of metallic sodium from the system. One interesting feature of this mechanism[5] is that it does not require the presence of oxygen, which would presumably lead to the formation of oxide ion. Thus, an experiment in the absence of oxygen would clearly distinguish between two mechanisms possible in the *presence* of oxygen; the sequence

$$Ag^0 + Na^+ = Ag^+ + Na^0 \quad (1)$$
$$2\,Na^0 + {}^1/_2O_2 = Na_2O \quad (2)$$

and the reaction sequence which is probably analogous to that in the aqueous system,[6] *viz.*

$$2Ag + {}^1/_2O_2 = Ag_2O$$
$$Ag_2O + 2NaCl = 2AgCl + Na_2O$$

$$2Ag + {}^1/_2O_2 + 2NaCl = 2AgCl + Na_2O$$

which is equivalent to the net reaction

$$2Ag(s) + {}^1/_2O_2(g) = (2Ag^+ + O^=)_{in\ NaCl} \quad (3)$$

Although, in the presence of oxygen, both mechanisms lead to the same products, the second mechanism might be expected to lead to an equilibrium since all products remain in the system, whereas the first need not if $Na^0(g)$ continually distils out of the system. In that case no definite stoichiometric relation between Ag^+ and $O^=$ need exist, except that more Ag^+ should be in the system than is expected from the formula Ag_2O. From another viewpoint the presence of Ag_2O in the molten salt would be interesting since the pure compound itself is unstable at this temperature.

In order to suppress reaction 3 altogether it would be necessary to reduce the oxygen partial pressure in this system to zero. Since this is virtually impossible we have restricted ourselves to comparing the rate of oxidation at 1 atm., in air, and in argon in which the O_2 pressure is $\sim 10^{-4}$ atm.

In addition, an attempt was made to measure synthetically the quasi-solubility product $[Ag^+]^2[O^=]$ which might be expected to apply to reaction 3, *i.e.*

$$K = [Ag^+]^2[O^=]/p_{O_2}{}^{1/2} \quad (4)$$

by additions of AgCl and Na_2O to NaCl melts.

Experimental

In order to avoid possible reactions with containers, none of which is truly inert over long periods of time, the silver to be reacted was made into a container for most of the kinetic studies. Other reactions, described below, were carried out in alumina and mullite tubes.

Materials.—Silver crucibles, 6 in. long, 1 in. o.d., approximately ${}^1/_8$ in. thick, and weighing ~400 g. were prepared by electrodeposition onto a stainless steel mandril. For runs in oxygen the tubes were washed in NH_4OH and H_2O and dried. For runs in argon they were additionally pumped out as described below. For some experiments (see below) 1 in. long capsules with caps were made from ${}^3/_4$ in. silver rods. Spectroscopic analysis of the silver crucibles gave the following impurities (weight %): Al 0.0005, Cu 0.0005, Fe 0.005, Mg 0.001, Pb 0.0005, Si 0.001. For miscellaneous experiments silver wire and sheet of mint quality were used. Merck Reagent NaCl was dried by heating under continuous pumping at 500° for several days using a diffusion pump. Some batches also were treated with HCl gas after drying and again pumped down to ~0.1 μ. No significant difference in the reactions (with Ag) produced by the HCl treatment was noted. Results of spectroscopic analysis of a typical batch of NaCl before and after reactions with silver are shown in Table I.

TABLE I

ANALYSIS OF NaCl (WEIGHT %)

	Al	Cu	Fe	Mg	Ni	Si	Ag
Before	0.0001	0.001	0.0001	0.00005	0.0001	0.0001	0.0001
After	0.0005	0.001	0.002	0.0001	0.0001	0.005	>1

Fisher C.P. Ag_2O, Baker Reagent Na_2O_2, and Mackay Na_2O were also used in some experiments. The latter is not pure but contains some Na_2O_2.

Apparatus.—The apparatus used in most of the experiments carried out under controlled atmosphere is shown in Fig. 1. The lower part, of Vycor, containing the silver tube, had to be renewed after nearly every run because of extensive attack, which results in transition to crystalline trymidite as the container is cooled. The upper part, having the male standard taper joint, was equipped with three stopcocks as shown to permit a variety of operations. Since the thermal expansion of Pyrex is greater than that of Vycor, the system becomes self-sealing at high temperatures. Stopcocks A and B serve for entrance and exit of gases or for attachment to a vacuum pump while the brass assembly rests on O-rings on the glass tubing projecting above the stopcock C. The stirrer is introduced into the upper end of the tube through O-rings before C is opened. Similarly, on withdrawing the stirrer, C is closed after the lower end of the stirrer has just passed it. This arrangement permits stirring of the melt without having air leak past the stirrer. The melt can be sampled by dipping a cold porcelain rod into it and quickly withdrawing it. Such porcelain rods also served as stirrers.

Furnace and Temperature Regulation.—Most experiments were carried out in a 10 in. Marshall furnace, appropriately shunted to minimize temperature gradients, regulated by a Marshall control panel. Temperatures were generally measured by dipping a Chromel–Alumel thermocouple into the melt at the end of a run. After it was found that changes of 50° had only a slight effect on the reaction rate, subsequent runs were only made at a single temperature, 900°, which lies conveniently between the melting points of NaCl (800°) and Ag (960°).

Chemical Analysis.—Most of the analysis for silver in NaCl was carried out colorimetrically.[7] The method gives good results for ionic silver down to 0.05 mole %. For concentrations near or below this a spectroscopic method was used. Good agreement between the methods near 0.05% makes it clear that the silver in NaCl melts is ionic and places the upper limit for atomically dissolved Ag near this value. More decisive evidence is provided by the electron spin resonance spectrum of the quenched melt (see below). Some melts having high silver concentrations were analyzed by electrodeposition.

Melts were analyzed for oxide ions by titration with 0.01 *N* HCl to pH 4.5, blanks being run for the NaCl and for the H_2O used to dissolve the samples.

Rate Studies. A. In O_2 Atmospheres.—A large number of experiments using the Ag crucibles and Vycor apparatus was carried out. The effects of O_2 pressure, rate of O_2 transport to the metal, and temperature were studied. In these experiments 40–60 g. of dried NaCl was used and samples of a few tenths of a gram were taken at intervals by dipping a cold porcelain rod into the melt and quickly withdrawing it. The O_2, previously dried by passing over $CaCl_2$, $MgClO_4$, and freed of CO_2 by Ascarite, was slowly leaked through the stopcock into the vessel.

A number of runs also were carried out with undried NaCl and in crucibles open to the atmosphere. In still others, O_2 was bubbled through the melt to provide maximum O_2 concentration throughout the melt.

Runs in "Oxygen-Free" Environment.—A number of experiments were carried out to determine if oxygen is required for the oxidation of silver. None of these was entirely successful as the system is inordinately sensitive to O_2 and concentrations of O_2 below 0.01% are difficult to measure in a (thermodynamically) open system. In a

(6) In aqueous NaCl silver is oxidized only in the presence of oxygen: J. C. Pariaud and P. Archinard, *Bull. soc. chim.* France, 454 (1952).

(7) S. Siggia, *Anal. Chem.*, **19**, 922 (1947).

typical experiment a silver crucible was outgassed in the reaction vessel at 800° using an oil diffusion pump and liquid N_2 trap (10^{-6} mm.) for a week and then cooled under vacuum. This procedure removes O_2 dissolved in the metal.[8,9] The crucible then was filled with previously dried NaCl and again pumped down for a week, the temperature being raised gradually to 600°. After cooling, the entire assembly was transferred to an argon filled drybox[10] in which the O_2 partial pressure could be maintained between 10^{-4} and 10^{-5} atm. indefinitely. (The dew point is near −60°, corresponding to 10^{-4} atm. H_2O.) The apparatus was placed in a furnace and the temperature raised to 900°. Stopcocks were opened and the porcelain stirrer introduced. At intervals, the melt was sampled as described previously. Mass transfer in this case was nearly as extensive, though slower, as in pure O_2. As a variation on this procedure, the temperature of the assembly, after a week of salt drying at 500°, was raised to 900° under continuous pumping. In this case, since the total pressure is only $\sim 10^{-6}$ atm., the partial pressure of O_2 is $\sim 10^{-7}$. The method does not permit sampling the melt at intervals, however. The salt vaporized within a day and deposited on the cool parts of the apparatus. It contained appreciable quantities of Ag^+ and O^- ions.

Determination of Ag_2O Solubility Product.—Solutions of AgCl in NaCl were prepared by melting the components together in an alundum tube in the drybox at 900°. The melt was poured out to cool into an enamel tray. Solutions of Na_2O in NaCl were prepared in similar tubes, but in air, since the Na_2O_2 contained in the starting material decomposes with O_2 evolution. A test for peroxide in the resulting cooled melt showed that ~1% of the oxide concentration was present as peroxide.

Various portions of the AgCl and Na_2O solutions were melted together until precipitation of metallic silver occurred —(qualitative description below). Samples of the supernatant liquid were taken for analysis. These experiments were carried out both in air and in the drybox.

Evaporation of AgCl and Na_2O from Melts.—Since the composition of reaction melts may be altered by preferential evaporation of some components, this was determined separately. Heating of a 2 mole % Na_2O–NaCl solution at 900° in air showed that the composition of the melt remained unchanged for 6 days. However, a similar study of an AgCl–NaCl melt showed that the preferential evaporation of AgCl is considerable; *e.g.*, a melt initially of 1.6 mole % AgCl decreased to 1.3% in 21 hr.

"Closed-System" Experiment.—In an attempt to obtain equilibrium data small Ag capsules 1 in. long and machined from $^5/_8$ in. diameter rods were filled with molten NaCl, closed by welding on silver covers, and each tube sealed into a separate Vycor envelope under vacuum. The tubes were placed in a muffle furnace at 880° and removed at intervals for analysis. After a day or so molten NaCl could be seen outside the capsules (but inside the Vycor). Careful examination revealed no imperfections in the capsules. It must be concluded that the NaCl diffused through the metal. For most of the run, then, the capsules lay in a pool of molten salt. The concentrations of Ag^+ in the salt increased from 0.19 mole % at 51 hr. to 0.47% at 284 hr., considerably slower than in systems open to O_2.

Analysis of Silver for Sodium.—In order to investigate the possibility that any metallic sodium might, instead of vaporizing, alloy with the silver, some pieces of silver sheet were heated in NaCl at 900° in an alumina crucible under drybox conditions. After one day the melt and metal were poured out onto a tray. As soon as the hot silver became exposed to the atmosphere, although the latter is very low in O_2, yellow flames burst from the metal and continued burning for several minutes. Several pieces of the cooled metal were subsequently freed of adherent salt mechanically, washed briefly in dilute NH_4OH, and separately dissolved in HNO_3. The resulting solutions were analyzed for sodium by flame photometry, and for chloride ion. Both Na^+ and Cl^- ions were found, indicating diffusion of salt into the metal, but the results on different pieces fluctuated considerably. All were near 10^{-4} mole fraction in the ions, however. For example, one piece washed in dilute NH_4OH to remove adherent AgCl gave $[Na^+] = 2.4 \times 10^{-4}$, $[Cl^-] = 0.9 \times 10^{-4}$, or $[Na^+]/[Cl^-] = 2.6$, whereas another piece washed only in H_2O gave $[Na^+] = 1.5 \times 10^{-4}$, $[Cl^-] = 1.1 \times 10^{-4}$, $[Na^+]/[Cl^-] = 1.4$.

(8) E. W. R. Steacie and F. M. G. Johnson, *Proc. Roy. Soc.* (London), **A112**, 542 (1926).

(9) D. N. Craig, J. I. Hoffman, C. A. Law, and W. J. Hamer, *J. Res. Natl. Bur. Std.*, **64A**, 381 (1960).

(10) J. M. Sherfey, *Ind. Eng. Chem.*, **46**, 435 (1954).

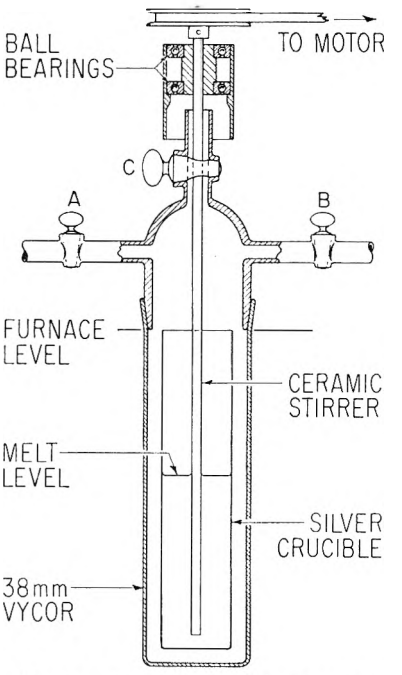

Fig. 1.—Apparatus for kinetic runs.

Results

A. Qualitative Description.—All experiments in which NaCl was fused in Ag containers as described above exhibited certain features, irrespective of quantitative differences. These are briefly described.

After about an hour the melt becomes pale yellow, while quenched samples are light gray. With time the quenched melt looks almost black although the same material when molten is quite homogeneous and yellow. A microscopic examination of the black material shows that the (macroscopic) color is produced by a very small number of black, opaque crystals in a matrix of clear transparent ones.

If oxygen transport to the melt is restricted, the first color in the quenched melt is a faint brown. Under the microscope this is seen to result from a very few ($\ll 1\%$) yellowish crystals.

If the oxygen supply is cut off from a melt which, if quenched, would be black, the color gradually lightens over a period of several hours, quenched samples eventually being colorless. The analytically determined concentration of ionic silver remains fairly constant or increases slightly. If the reaction is carried out so that the total surface area of the melt remains small, *e.g.*, by putting a small piece of silver into a salt-filled test-tube, the melt remains clear on quenching and has a faint bluish cast. In previously published work,[5] this color was taken to be evidence for the formation of sodium metal. To test this hypothesis a sample of such salt was analyzed by electron spin resonance. In this system the only possible species with unpaired electrons are Ag and Na atoms.

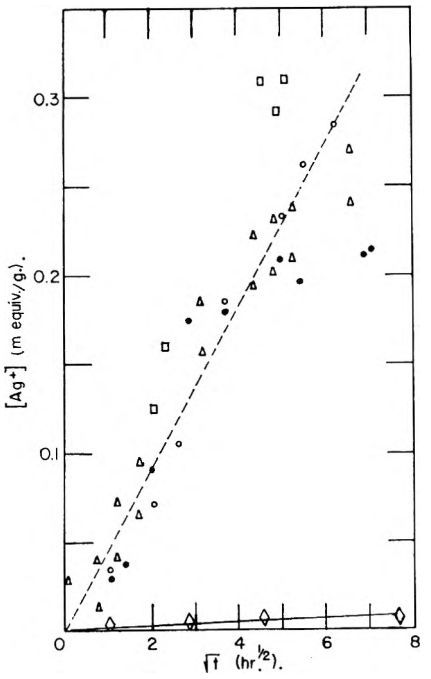

Fig. 2.—Kinetic runs under various conditions: ●, 1000 r.p.m., 900°, air; ○, 300 r.p.m., 850°, air; △, O_2 bubbling, 820°; □, O_2 bubbling, 875°; ◇, 1000 r.p.m., 835°, argon.

The total concentration of such species was found to be 1×10^{-3} mole %. This is lower than the previously referred to upper limit for atomically dissolved silver of 0.05% and must, as will be shown later by a thermodynamic argument, represent the solubility of silver alone.

After long periods of time, extensive regrowth of the silver as a mass of crystals takes place which may eventually fill the entire crucible below the surface of the melt.

Relevant here is the observation that if a mixture of NaCl and Ag_2O is heated in a test-tube, most of the Ag_2O has been decomposed to Ag metal by the time (~ 10 minutes) the NaCl has melted. A small amount of silver is dissolved in the melt. The dissolved Ag^+ concentration increases the more intimate the original mixture. Similar results are obtained if the components are sealed into Vycor capsules before heating.

The color changes which occur in the system were reproduced synthetically as follows: To AgCl–NaCl solutions containing a few mole per cent AgCl, successive small increments of Na_2O were added. The initial addition produced a faintly yellow color in the quenched melt. (The same color could be produced by reacting metallic silver with a NaCl–Na_2O solution under argon.) Further additions of Na_2O produced immediately a gray or black quenched melt. After a few minutes this cleared and some metallic silver precipitated. After several additions of AgCl and Na_2O, the clear, yellow melt was poured into a crucible where it turned gray on solidifying.

B. Rate Studies.—A number of preliminary runs were carried out in silver crucibles using the apparatus shown in Fig. 1 to assess the effect of temperature, stirring speed, and rate of oxygen transport to the melt, on the rate of silver oxidation. The results are summarized in Fig. 2 which shows the concentration of silver ions in the melt as a function of $\sqrt{\text{time}}$. The data scatter considerably since in these early experiments it proved difficult to maintain uniform conditions over long periods of time. For all of these runs the slopes, calculated by a least-square procedure, are near 0.04; all values of k, defined by $[Ag^+] = kt^{1/2}$, fall between 0.038 and 0.062 when the units of $[Ag^+]$ and t are those of Fig. 2.

The results of these kinetic runs may be summarized as follows.

1. The effect of temperature is very minor. Changes of nearly 100° increase the rate by only 10–20%. This is also in agreement with the results of previous work.[5]

2. The effect of oxygen pressure on the rate of Ag^+ increase was not studied in great detail. However, a change from pure O_2 (1 atm.) to air (0.2 atm.) produced no appreciable change. On the other hand, at very low partial pressures (~ 10^{-4} atm.) the rate was distinctly less. This effect is similar to that observed by Halpern[11–13] for the oxidation of copper in aqueous ammonia and amines.

3. Studies of the effect of rate of O_2 transport to the metal were carried out by stirring at different rates and stirring by O_2 bubbling through the salt. No significant change was observed on changing from 300 to 1000 r.p.m. and on bubbling. In one experiment a silver-plated ceramic stirrer rotating in the salt showed complete loss of plate only near the air–salt interface, the same area in which crucibles were also most attacked.

4. The effect of surface area cannot be studied rigorously because it does not remain constant during the experiment. Particularly if O_2 is bubbled through the melt, fine Ag crystals appear throughout the body of the melt and, after 60–70 hr., make stirring and sampling impossible. When O_2 is introduced only above the melt, this growth appears primarily near the surface where it eventually covers nearly the whole surface.

5. The length of time for which a run can be carried out depends on both the factors above and on the tiny holes which form in the Ag after 50–100 hr. through which the melt leaks into the outer Vycor jacket.

Similar conclusions apply to the run in O_2, except that the rates are higher and the curves are not linear. When these data (Fig. 3) are plotted *vs.* $t^{1/2}$ (Fig. 4) they appear much more nearly linear. The curvature of the Ag^+ curve can be accounted for by the preferential evaporation of AgCl but that of $O^=$ cannot be thus explained. Perhaps an approach to equilibrium is involved. (Further evidence for this is described below.) The approximate square-root dependence for all three curves suggests a diffusion controlled process.

The results for a somewhat different experimental arrangement are shown in Fig. 5. Several No. 10 Ag wires were stacked tightly into an alundum

(11) J. Halpern, *J. Electrochem. Soc.*, **100**, 421 (1953).
(12) J. I. Fisher and J. Halpern, *ibid.*, **103**, 282 (1956).
(13) J. Halpern, H. Milents, and D. R. Wiles, *ibid.*, **106**, 647 (1959).

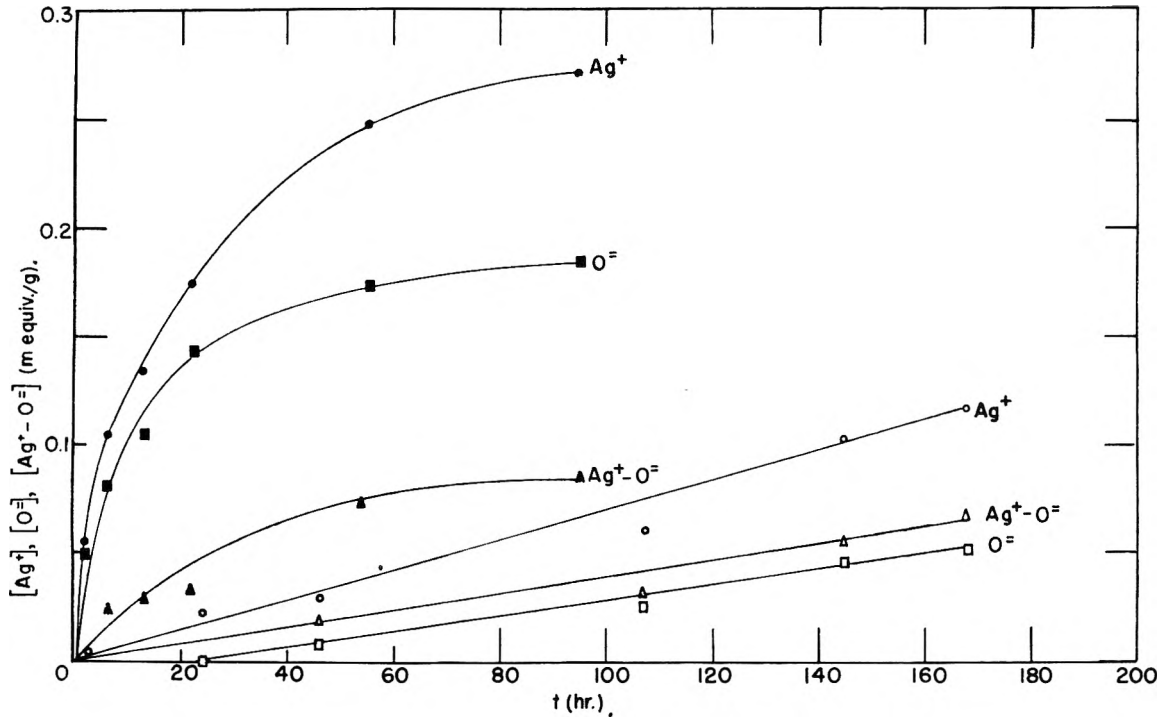

Fig. 3.—Kinetic runs in O_2 (upper curves) and argon (lower curves) atmospheres, 900°, 1000 r.p.m. stirring.

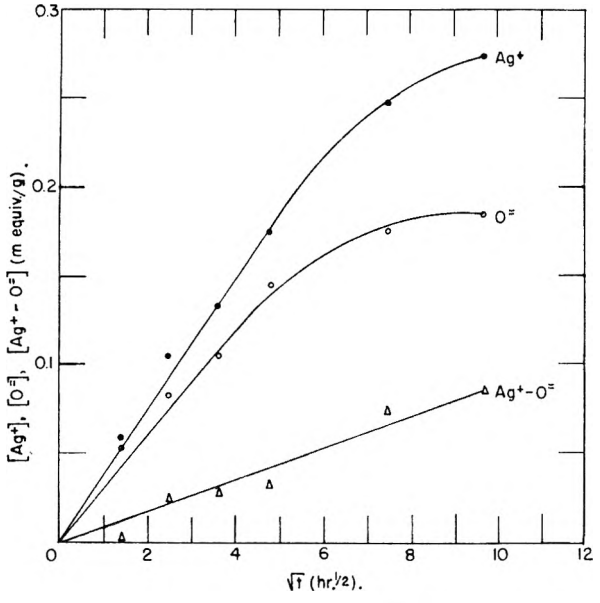

Fig. 4.—Kinetic run in O_2, 900°, 1000 r.p.m. stirring. Dependence on $\sqrt{t}$.

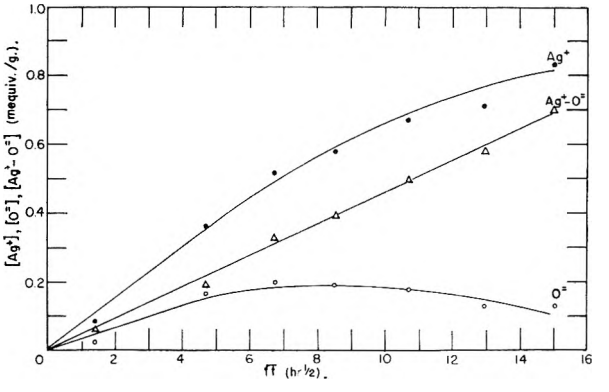

Fig. 5.—Kinetic run in O_2, 900°, no stirring; see text for description of system.

tube and NaCl added so as to form an Ag–O_2–NaCl interface. Here the metal/salt ratio is greater than in the crucibles. The tube was placed in the apparatus of Fig. 1 and a slow leak of dry and CO_2-free O_2 passed through it. Samples were taken at intervals. The results are similar to those of Fig. 4 with respect to the approximate linearity of $[Ag^+]$ and $[Ag^+]-[O^=]$ in $t^{1/2}$, but considerably higher concentrations of $[Ag^+]$ are reached in a shorter time. This suggests that the rate-controlling step in the oxidation occurs at the metal surface since there is less access of O_2 to the metal below the surface of the unstirred melt than for the system of Fig. 4, but the total volume of salt is smaller. $[O^=]$ reaches a maximum and then decreases while $[Ag^+]$ increases, suggesting the operation of an equilibrium. Indeed, for $\sqrt{t} \geq 8$ the product $[Ag^+]^2[O^=]$ remains nearly constant at 1.7×10^{-6} on the mole fraction scale, which agrees fairly well with the synthetically determined quantity of 3.8×10^{-6} (*cf.* below).

Notable is the linearity of $[Ag^+]-[O^=]=\Delta[Ag^+]$ in all three plots. It is instructive to compare the ratio $\Delta[Ag^+]/[Ag^+]$, *i.e.*, the fraction of total silver not accounted for by the reaction with oxygen, obtained in the three systems. This is shown in Fig. 6. The similarity between runs B and C and their contrast with A is striking; A and B are alike in all respects except O_2 pressure. In A nearly all the Ag^+ produced initially can be accounted for by reaction 3. After ~40 hr., 70% can be accounted for by this reaction. In B the situation is reversed. Initially none of the Ag^+ is accounted for by (3), but about 50% can be

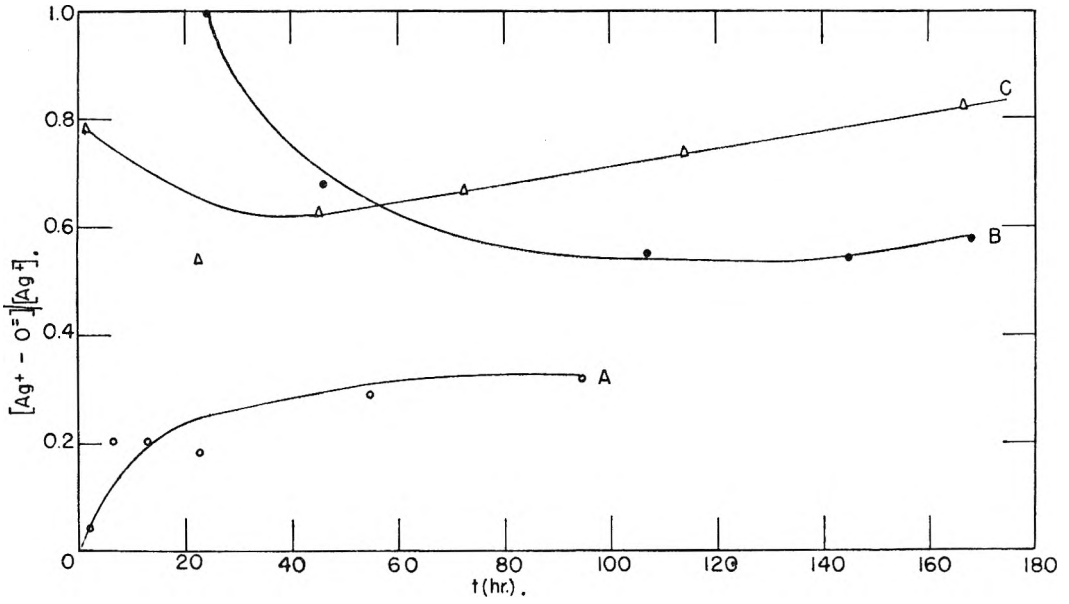

Fig. 6.—Fraction of total $[Ag^+]$ not produced by reaction 3 for systems shown in Fig. 3–5: A, O_2, stirring; B, argon, stirring; C, O_2, no stirring.

accounted for after long periods of time. In C initially 20% of the Ag^+ is due to (3). This ratio $(1-\Delta[Ag^+]/[Ag^+])$ rises slightly at first and falls slowly. It seems reasonable to suppose that in both B and C the rate of O_2-transport into the melt is slow, in B because the partial pressure of O_2 is low, in C because the melt is unstirred and transport of O_2 into the melt must be by diffusion.

C. Determination of Equilibrium Constant for Reaction 3.—One set of experiments each in air and in the drybox was carried out as indicated above. To a solution initially 5% AgCl in NaCl small increments of a melt 5% Na_2O in NaCl were added and samples taken at intervals over a period of two days. Analytical results fluctuated considerably, probably because very finely divided metallic Ag precipitates only slowly and also dissolves in the NH_4OH used during analysis. For nine samples in air, the product $[Ag^+]^2[O^=]$ was 3.8×10^{-7} (on the mole fraction scale) with an average deviation of 1.4×10^{-7}. Using $p_{O_2} = 0.21$ gives for $K = [Ag^+]^2[O^=]/p_{O_2}^{1/2} = 8.3 \times 10^{-7}$. Under drybox conditions $[Ag^+]^2[O^=] = (1.5 \pm 0.6) \times 10^{-7}$. If the partial pressure of O_2 normally obtaining in the drybox is used (*e.g.*, $p = 10^{-5}$), a much larger value of K, 4.7×10^{-5}, results. Conversely, if K for the air run is used, p_{O_2} is calculated to be near 0.01, which seems rather high. Such a value of p_{O_2} would be possible, however, if the O_2 evolved during the precipitation remained dissolved in the melt or remained in the reaction vessel above the melt, diffusing out of the container only very slowly.

Discussion

To account for the results obtained in this work we consider the hypothesis that silver is oxidized by at least two separate reactions in fused NaCl.

$$Ag^0 + Na^+ \longrightarrow (Ag^+ + Na^0)_{NaCl} \quad (1)$$

$$2Ag^0 + {}^1/_2O_2 \longrightarrow (2Ag^+ + O^=)_{NaCl} \quad (2)$$

The relative contributions of the two reactions to the total Ag^+ concentration depend on the particular experimental conditions. When O_2-transport to the silver–salt interface is rapid, *e.g.*, at higher O_2-pressures and good mixing, (2) predominates. In this case the rate is controlled by the diffusion of products away from the reaction site. Thus, since $Ag_2O(s)$ is unstable, any high local concentration of Ag^+ and $O^=$, *e.g.*, near the metal surface, which exceeds the product $K = [Ag^+]^2[O^-]/p^{1/2}$ will drive (2) to the left and result in the precipitation of metallic silver. This agrees also with the observation that crystal growth is most extensive near the salt–air interface in unstirred melts but occurs throughout the medium when oxygen is bubbled through the melt. At low oxygen pressures or poor oxygen transport through the liquid, reaction 1 is relatively more important. The data also imply that whenever the rate of Ag^+ production by (2) is diffusion controlled, that of (1) is also. This can be accounted for by observing that both reactions produce the same product, *i.e.*, silver ion, and that if its local concentration is too high its buildup in the melt will be reduced by driving (2) to the left.

The relative insensitivity of silver ion concentrations observed (*cf.* Fig. 3) under widely different O_2 pressures can be accounted for by the form of the equilibrium constant for reaction 2; *i.e.*, since $K = [Ag^+]^2[O^=]/p_{O_2}^{1/2}$ it follows that $[Ag^+]$ is proportional to $p^{1/6}$ and thus at equilibrium a reduction of O_2 pressure by a factor of 10^{+6} would only lower $[Ag^+]$ by a factor of 10. Therefore it would be virtually impossible to inhibit corrosion significantly by reducing O_2 pressure.

The thermodynamics of corrosion in fused chlorides has recently been discussed in detail by Edeleanu and Littlewood.[14] Their method permits the calculation of equilibrium constants for both reactions 1 and 2. Using their method and

(14) C. Edeleanu and R. Littlewood, *Electrochim. Acta*, 3, 195 (1960).

free energies of formation compiled by Glassner[15] the quasi-solubility product of Ag_2O in NaCl in terms of activities on the mole fraction scale at 900° is 1.9×10^{-7}. Since these dilute solutions are nearly ideal, activities can be replaced by concentrations. This value is somewhat lower than the experimentally determined one, but in view of the difficulties of determining low concentrations a factor of five in K is not too serious a disagreement. Therefore, since p_{O_2} over the melt is better known, K values obtained in air are probably more reliable.

The Ag^+ concentration resulting from reaction 1 can be calculated since all the oxidation–reduction systems involved must be at the same potential. For nearly pure NaCl at 900° the vapor pressure of sodium metal available from the thermal dissociation of the salt itself is 2.72×10^{-9} atm. Using the published E^0 values[16] of NaCl (3.130 v.) and AgCl (0.805 v.) gives for Na in NaCl

$$E_{Na} = -3.130 - 0.232 \log (2.72 \times 10^{-9}) = -1.144 \text{ v.}$$

Then for Ag in NaCl

$$-1.144 = -0.805 + 0.232 \log a_{Ag^+}$$

from which $a_{Ag^+} = 3.46 \times 10^{-2}$. This is then the silver ion concentration to be expected in this system after long periods of time based on reaction 1 alone. It is also close to the experimental values actually determined. However, it follows from the experimentally determined equilibrium constant for reaction 2 —the argument differs only slightly quantitatively if the theoretical value is used— that the concentration of oxide ion permitted in the melt is then 2.44×10^{-4}, giving a ratio of $Ag^+/O^=$ equivalents of 81, much greater than is observed experimentally; *i.e.*, the equilibrium properties of the system are subject to two restraining conditions

$$K_1 \cong [Ag^+]\, p_{Na}{}^0 \cong 1.0 \times 10^{-10}$$

$$K_2 = [Ag^+]^2[O^=] = 3.8 \times 10^{-7} \text{ (in air)}$$

Thus an $O^=$ ion concentration greater than 2.44×10^{-4} and Ag^+ ion concentrations of several mole per cent can only result from the decrease in $p_{Na}{}^0$ below the value already available from the thermal dissociation of NaCl alone. Therefore, as silver is oxidized and oxygen is reduced, the sodium metal partial pressure in the melt must be repressed below the value normally obtaining from the thermal dissociation of pure NaCl alone. This is consistent with the observation that no hydrogen evolution was ever observed when reaction melts were dissolved in water and implies that even the very low concentration of unpaired electrons found by e.s.r. must result from atomically dissolved silver.

However, thermodynamically no restrictions are imposed on the production of metallic sodium which is suggested by the material balance and kinetic experiments. There remain, then, only two possible destinations for this sodium: vaporization or alloying with the silver. Evidence for the first case was obtained previously[5] when silver and NaCl were sealed into Vycor capsules. The second case is theoretically possible since, according to the published phase diagrams of the Ag–Na system,[17,18] the solubility of sodium in silver is 8 mole % at 900°. One would then expect the sodium to be adsorbed on the surface of the silver at first and then diffuse into the solid metal. The observation of light flashes frequently emitted from silver immersed in NaCl as well as the experiment reported above supports this mechanism which, by the formation of a solid Ag–Na solution, would greatly reduce the sodium metal activity.

In galvanic cell studies of fused salts the Ag–AgCl electrode has been used extensively as reference. In order to minimize liquid-junction potentials some workers have used very dilute solutions of AgCl in alkali halides. For example, Flengas and Ingraham[19] report using 1×10^{-3} to 6×10^{-2} mole fraction in KCl–NaCl melts. However, their silver electrodes were immersed in the melts for only short periods of time.[20] The results of this work suggest that such reference electrodes may not maintain constant potential if the concentration of AgCl is much below 10 mole % and if the silver is immersed for long periods in the melt, particularly in the presence of oxygen.

Acknowledgments.—The author would like to thank Mr. E. R. Deardorff for the chemical analyses, Mrs. Martha Darr for the spectrochemical determinations, Dr. R. E. Florin for the e.s.r. measurement, Mr. R. Paulson for the sodium determination, and Mr. J. P. Young for the preparation of the silver crucibles. Miss M. Parish, a student at Wellesley College, performed some of the experiments for the determinations of Ag_2O solubility. Helpful discussions with Dr. R. E. Wood are gratefully acknowledged.

Some preliminary experiments were done by Mr. E. A. Richardson at the University of Arkansas; this part of the work was supported by the Air Force Office of Scientific Research, Air Research and Development Command, under contract AF 49(638)-653.

(15) A. Glassner, "The Thermochemical Properties of the Oxides, Fluorides, and Chlorides to 2500°K.," ANL-5750.

(16) W. J. Hamer, M. S. Malmberg, and B. Rubin, *J. Electrochem. Soc.*, **103**, 8 (1956).

(17) C. H. Mathewson, *Z. Metallk.*, **1**, 51 (1911).

(18) E. Quercigh, *Z. anorg. Chem.*, **68**, 301 (1910).

(19) S. N. Flengas and T. R. Ingraham, *Can. J. Chem.*, **35**, 1139 (1957).

(20) S. N. Flengas, private communication.

PREPARATION, STRUCTURE, AND PROPERTIES OF K_2NbO_3F

BY FRANCIS GALASSO AND WILDA DARBY

United Aircraft Corporation, Research Laboratories, East Hartford, Connecticut

Received January 22, 1962

An oxyfluoride, K_2NbO_3F with the K_2NiF_4 structure, has been prepared. Unlike most compounds with this structure, K_2NbO_3F was found to have a c/a ratio greater than the calculated 3.41 value which satisfies the geometrical conditions of touching spheres. From a study of interatomic distances (obtained from single crystals), it was found that the high c/a ratio was related to an elongation of the anion octahedra in the "c" direction. The thermal coefficient of expansion for K_2NbO_3F was found to be more than twice as large in the "c" direction as in the "a" direction, a fact which may be responsible for the positive temperature coefficient of resistance exhibited by this material.

Introduction

In 1955 Balz and Plieth described the K_2NiF_4 structure and showed its relation to the perovskite structure.[1] Since that time several ternary oxides and fluorides having the K_2NiF_4 structure have been reported in the literature and results of a survey of these compounds (presented in Table I with their cell data) revealed that there was a tendency for compounds with the K_2NiF_4 structure to exhibit a smaller c/a ratio than the calculated 3.41 value which satisfies the geometrical conditions of touching spheres. Recently, however, the oxyfluoride K_2NbO_3F, of the K_2NiF_4 type, was prepared at the Research Laboratories and was shown to have a c/a ratio of 3.46. As a consequence of this interesting observation, a study was initiated to investigate in more detail the interatomic distances and the properties observed for K_2NbO_3F.

TABLE I

LATTICE CONSTANTS FOR COMPOUNDS WITH THE K_2NiF_4 STRUCTURE

	a(Å.)	c(Å.)	c/a	Ref.
K_2UO_4	4.34	13.10	3.02	2
Ba_2PbO_4	4.30	13.30	3.10	3
Sr_2SnO_4	4.04	12.53	3.10	3
Rb_2UO_4	4.34	13.83	3.18	2
Ba_2SnO_4	4.13	13.27	3.21	3
Rb_2ZnF_4	4.10	13.25	3.24	4
Sr_2TiO_4	3.88	12.60	3.24	5, 6
K_2ZnF_4	4.01	13.02	3.25	4
K_2NiF_4	4.01	13.08	3.26	1
La_2NiO_4	3.86	12.65	3.28	7
Sr_2MnO_4	3.79	12.43	3.28	1
Sr_2MoO_4	3.92	12.84	3.28	1
Ca_2MnO_4	3.67	12.08	3.29	5
Sr_2RuO_4	3.87	12.74	3.29	8
K_2MgF_4	3.98	13.16	3.31	9
Sr_2IrO_4	3.89	12.92	3.32	10
$SrLaAlO_4$	3.75	12.50	3.33	5
Sr_2RhO_4	3.85	12.90	3.35	8
Cs_2UO_4	4.38	14.79	3.38	2
K_2NbO_3F	3.96	13.67	3.46	

(1) D. Balz and K. Plieth, *Z. Elektrochem.*, **59**, 6, 545 (1955).
(2) L. M. Kovba, E. A. Ippolitova, Yu. P. Simanov, and Vikt. A. Spitsyn, *Dokl. Akad. Nauk USSR*, **120**, 5, 1042 (1958).
(3) R. Weiss and R. Faivre, *Compt. rend.*, **248**, 106 (1959).
(4) O. Schmitz-Dumont and H. Bornefeld, *Z. anorg. allgem. Chem.*, **287**, 120 (1956).
(5) S. N. Ruddlesden and P. Popper, *Acta Cryst.*, **10**, 538 (1957).
(6) K. Lukaszewicz, *Roczniki Chem.*, **33**, 239 (1959).
(7) V. A. Rabenau and P. Eckerlin, *Acta Cryst.*, **11**, 304 (1958).
(8) J. J. Randall and R. Ward, *J. Am. Chem. Soc.*, **81**, 2629 (1959).
(9) B. Brehler and H. G. F. Winkler, *Heidelberger Beitr. Mineral. Petrog.*, **4**, 6 (1954).
(10) J. J. Randall, L. Katz, and R. Ward, *J. Am. Chem. Soc.*, **79**, 266 (1957).

Experimental Investigations

Preparation of K_2NbO_3F.—Powder samples of K_2NbO_3F were prepared by heating mixtures of potassium carbonate and niobium pentoxide in a 1:1 molar ratio with a large excess of potassium fluoride in a platinum crucible at 750° for 24 hr. After the reaction, excess potassium fluoride was removed by washing the product with water. Single crystals of K_2NbO_3F were obtained when the same mixtures used to prepare powder samples were heated to 1000° and then slowly cooled to 600° at a rate of 30°/hr. When the product was washed with water, small crystals in the shape of thin rectangular plates remained.

Chemical Analysis and Density.—The fluorescent X-ray spectrographic method using a borax bead matrix[11] was em-

TABLE II

POWDER X-RAY DIFFRACTION DATA FOR K_2NbO_3F

hkl	d/n (obsd.)	d/n (calcd.)	I (obsd.)
002	6.79	6.84	S
101	3.78	3.80	S−
004	3.42	3.42	W−
103	2.98	2.97	S+
110	2.80	2.80	S
112	2.58	2.59	W−
006	2.276	2.278	M
105	2.248	2.250	M−
114	2.162	2.164	W−
200	1.974	1.978	S−
202	1.898	1.900	W+
116	1.768	1.767	M
211	1.751	1.754	M−
107		1.751	
204	1.712	1.712	W−
008		1.709	
213	1.648	1.649	M+
206	1.494	1.494	M
215		1.485	
118	1.459	1.458	W+
109	1.418	1.418	W
220	1.397	1.398	W+
222	1.370	1.370	W−
0010		1.367	
301	1.314	1.313	W−
217		1.311	
224	1.295	1.294	W+
208		1.293	
303	1.267	1.267	W
310	1.251	1.251	W+
312	1.233	1.230	W−−
11, 10		1.228	
226	1.193	1.192	W+

(11) D. F. Fornwalt and J. Komisarek, "Analytical Chem. in Nuclear Reactor Technology," TID-7568, PT. 1, U.S.A.E.C. (1959).

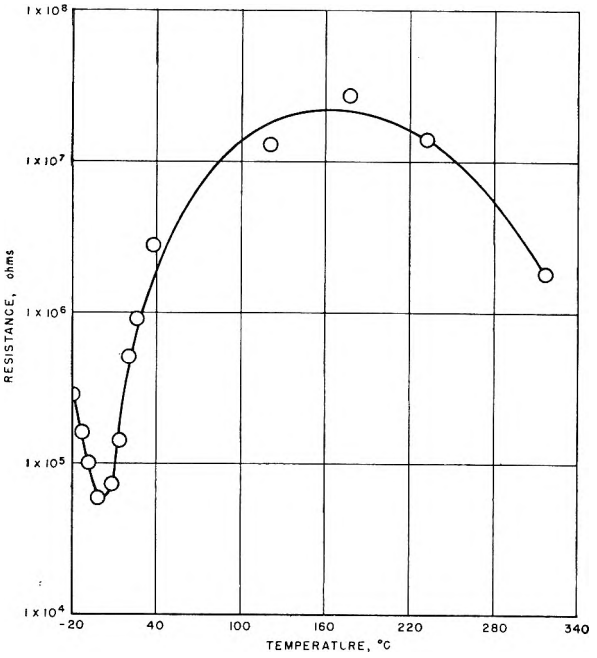

Fig. 1.—Alternating current resistance of K_2NbO_3F, 50 c.p.s.

$a = 3.956$, $c = 13.670$. Table II presents the indexing data for K_2NbO_3F.

For single crystal X-ray analysis, a long thin rectangular crystal plate was mounted on a Buerger precession camera and molybdenum Kα was used as the source of radiation. A diffraction pattern obtained when the X-ray beam entered perpendicular to the crystal plate revealed the fourfold symmetry expected in the *hk*0 net. The crystal then was rotated 90° and *h*0*l* data obtained. Intensities for the *hk*0 and *h*0*l* reflections were visually estimated using a multiple film technique and a calibrated film strip.

The similarities in lattice parameters, reflections observed, and the sizes of the constituent atoms for K_2NbO_3F and K_2NiF_4 resulted in the adoption of the space group I-4/mmm and the atomic positions found in the K_2NiF_4 structure for the initial calculations. These atomic position parameters were used in the structure factor calculations for K_2NbO_3F to determine the signs that would be placed before the observed structure factors in order to obtain an *h*0*l* Fourier projection. The electron density map was calculated using the Sly and Shoemaker program written for the IBM 704 computer. Using the atomic parameters taken from the Fourier projection peaks, the structure factors were recalculated, and it was found that the signs obtained for these structure factors were the same as those obtained from the previous calculation. The atomic positions from the Fourier analysis were, therefore, corrected for series-termination effects and used for subsequent refinement calculations which involve minimizing the reliability factor by a trial and error method. The atomic positions adopted in space group I-4/mmm (No. 139) are the following: two niobium ions are at

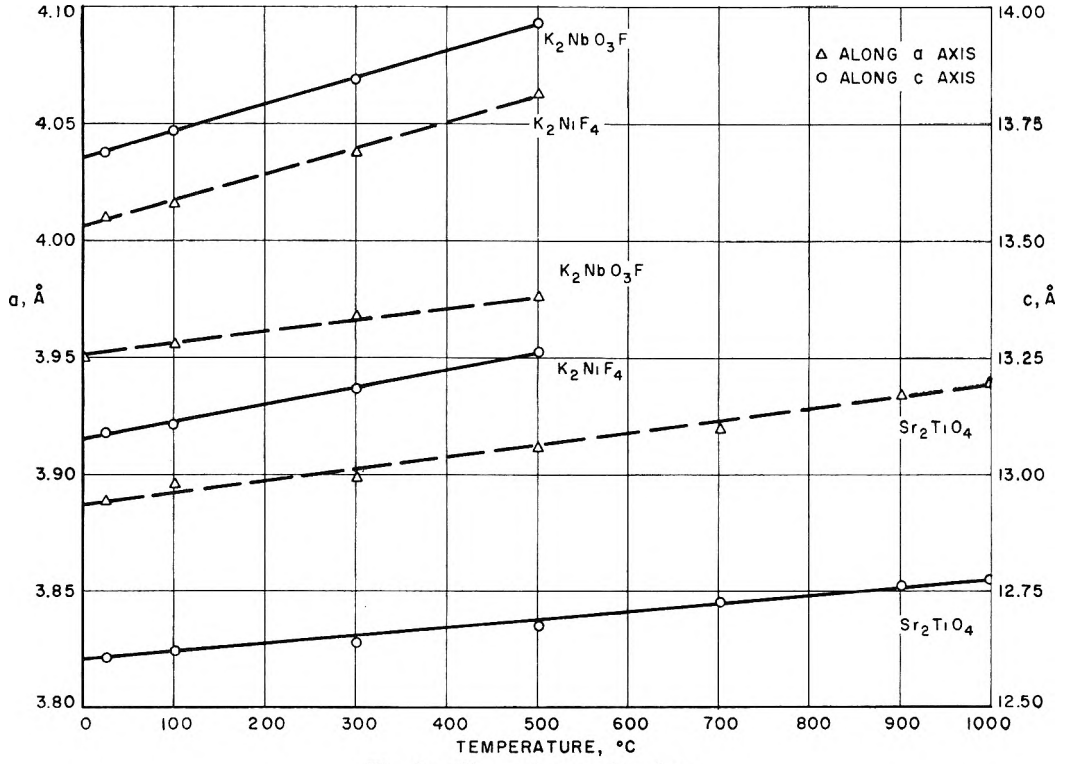

Fig. 2.—Thermal expansion data.

ployed to determine potassium content, while wet chemical analysis was used to determine the niobium and fluoride content. Results of these analyses indicated the presence of 33.52% K, 38.03% Nb, and 7.70% F; the theoretical values for K_2NbO_3F are 32.8% K, 39.05% Nb, and 7.98% F. Density was determined pycnometrically and found to be 3.64 g./cc. as compared to 3.68 g./cc. as calculated from the formula.

X-Ray Analysis.—Powder X-ray diffraction photographs were taken using a 57.3 mm. radius Phillips powder camera with copper Kα radiation. The X-ray patterns of powder samples and ground crystals, which were found to be the same, were indexed on the basis of a tetragonal unit cell of 0,0,0 and $^1/_2,^1/_2,^1/_2$; four potassium ions are at $0,0,z_K$; $0,0,\bar{z}_K$; $^1/_2,^1/_2,^1/_2 + z_K$; and $^1/_2,^1/_2,^1/_2 - z_K$ with $z_K = 0.350$; two fluorine and two oxygen ions are at $0,0,z_F$; $0,0,\bar{z}_F$; $^1/_2,^1/_2,^1/_2 + z_F$; $^1/_2,^1/_2,^1/_2 - z_F$ where $z_F = 0.151$ and four more oxygen ions are at $^1/_2,0,0$; $0,^1/_2,0$; $0,^1/_2,^1/_2$; $^1/_2,0,^1/_2$. For these calculations the fluoride ions were considered to be randomly distributed only in the 0,0,*z*, etc., positions after considering the thermal expansion data for K_2NbO_3F in the "*a*" and "*c*" axial directions. It is possible that there is an ordering of the fluoride ions existing even within the 0,0,*z* positions, but this could not be determined from the present data. Table III, which contains the observed and calculated structure factors, will be deposited with

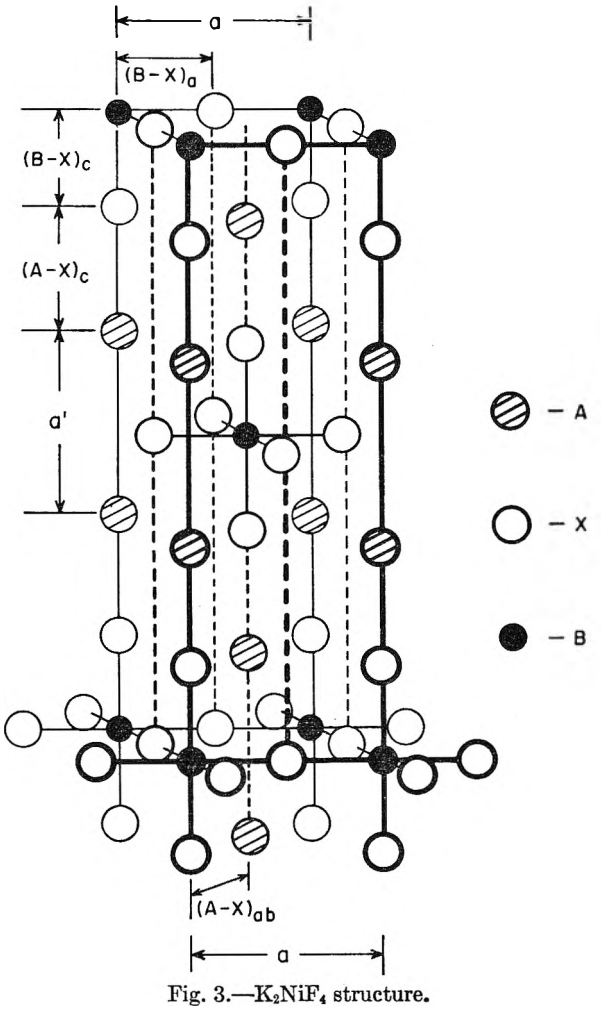

Fig. 3.—K_2NiF_4 structure.

the Library of Congress. The over-all reliability factor calculated for these reflections was found to be 0.097.

Property Measurements. Electrical Resistance.—Pellets for resistance measurements were prepared by pressing 1.5 g. of powdered K_2NbO_3F in a $^5/_8$ in. diameter die under 10,000 p.s.i. followed by sintering at 500°. The pellets were sanded to flatten the surface and then plated with evaporated gold. Powder X-ray patterns of the sanded material corresponded with the standard K_2NbO_3F pattern, thus indicating that the sintering temperature was not high enough to cause dissociation of the material.

Alternating current resistance *vs.* temperature measurements were obtained using a partial parallel substitution method utilizing a General Radio type 715 capacitance bridge. A standard capacitor in parallel with a decade resistor is placed in one arm of the bridge; the sample capacitor, the bridge capacitor, and a decade box were placed in parallel in the opposing arm of the bridge. Measurements were taken at 50 c.p.s. over a temperature range from approximately −18 to 316°. The data curve (Fig. 1) shows a drop in resistance from $3.0(10)^6$ ohms at −18° to $0.6(10)^6$ at −1.0°, followed by an increase in resistance with temperature up to approximately 180° and then a drop in resistance at higher temperatures. The curve resembles those obtained for barium titanate thermistor materials which are doped with rare earth ions.

Thermal Expansion.—High temperature X-ray diffractometer tracings were made of K_2NiF_4, Sr_2TiO_4, and K_2NbO_3F powders using a Norelco diffractometer with an attached Tem-Pres heater. Tracings were obtained at room temperature, 100, 300, and 500° for the three compounds, and also at 700, 900, and 1000° for Sr_2TiO_4. Due to dissociation of these compounds, tracings for K_2NiF_4 and K_2NbO_3F were not obtained at high temperatures. Figure 2 presents the "*a*" and "*c*" axis expansion for these three compounds.

It was found that the "*a*" direction thermal coefficient of expansion was nearly the same as the coefficient in the "c" direction for both K_2NiF_4 and Sr_2TiO_4 and that the coefficients in both directions are larger for the fluoride than for the oxide, (for K_2NiF_4 $\alpha_a = 2.87 \times 10^{-5}$ and $\alpha_c = 2.91 \times 10^{-5}$ while for Sr_2TiO_4 $\alpha_a = 1.46 \times 10^{-5}$ and $\alpha_c = 1.44 \times 10^{-5}$). On the other hand, the thermal coefficient of expansion for K_2NbO_3F in the "*c*" direction is 3.77×10^{-5}, which is more than twice the value in the "*a*" direction, 1.52×10^{-5}.

Discussion of Results

From Fig. 3 it can be seen that the central cube with cell edge a' in the K_2NiF_4 structure is the perovskite structure with the A position taken as the origin. Thus, for an ideal structure with touching spheres, a' should equal "*a*" of the K_2NiF_4 structure. Using the same reasoning of touching spheres, $(B\text{–}X)_c = (B\text{–}X)_a = a/2$ and $(A\text{–}X)_c = (A\text{–}X)_{ab} = a/\sqrt{2}$ so that the distance along the K_2NiF_4 "*c*" axis should be $a(2 + \sqrt{2})$ or c/a should equal 3.41. Results from this study show that the c/a ratio for K_2NbO_3F is greater than this ideal value, whereas all other compounds in this category have a c/a value less than 3.41.

In an attempt to understand the difference between K_2NbO_3F and the other compounds with this structure, the interatomic distances marked in Fig. 3 were calculated. The results are $a = 3.96$, $a' = 4.10$, $(A\text{–}X)_c = 2.72$, $(A\text{–}X)_{ab} = 2.80$, and $(B\text{–}X)_c = 2.06$, $(B\text{–}X)_a = 1.98$. It can be noted that the large c/a ratio for this compound is due to a' being longer than a and the elongated octahedra in the "*c*" direction, $(B\text{–}X)_c/(B\text{–}X)_a = 1.04$. If the other compounds presented in Table I have elongated octahedra, it could only be at the expense of a shortening of other bonds in the "*c*" direction. From consideration of these facts, it is highly probable that K_2NbO_3F differs from other compounds with the K_2NiF_4 structure, because it contains fluoride ions which are preferentially situated in the apical (unshared) positions in the octahedra, while the oxygen ions bridge the octahedra to give a two-dimensional layer. This conclusion is substantiated by the thermal expansion data which are so markedly anisotropic.

It is felt that the rapid change of unit cell dimensions with temperature also may cause a change of contact resistance between crystallites in the sintered pellet, which in turn produces the positive temperature coefficient of resistance exhibited by this material. It is noted that similar reasoning was applied by Peria, Bratschun, and Fenity to explain the PTC effect in semiconducting alkaline earth titanates.[12]

(12) W. T. Peria, W. R. Bratschun, and R. D. Fenity, *J. Am. Ceram. Soc.*, **44**, 249 (1961).

ACTIVITY COEFFICIENTS IN MIXED AQUEOUS CADMIUM CHLORIDE–HYDROGEN CHLORIDE SOLUTIONS AT 25° BY THE ELECTROMOTIVE FORCE METHOD

BY LESLIE LEIFER,[1] WILLIAM J. ARGERSINGER, JR., AND ARTHUR W. DAVIDSON

Department of Chemistry, The University of Kansas, Lawrence, Kansas

Received January 22, 1962

Activity coefficients of aqueous mixtures of cadmium chloride and hydrochloric acid have been measured at 25° by means of the electromotive force method. Measurements were made at total ionic strengths of 1.0, 0.5, and 0.2 molal, and at ten ionic strength fractions at each total ionic strength. The variation of the logarithm of the activity coefficient of each of the solute species with ionic strength fraction was found to be non-linear. These measurements comprise one of the few cases so far reported of experimental determinations of activity coefficients of both electrolytes in a mixture. The thermodynamic consistency of the results was checked by application in two different ways of the cross-differentiation relationship $(\partial \ln a_2/\partial m_1)_{m_2} = (\partial \ln a_1/\partial m_2)_{m_1}$ (1), in which the subscript 1 refers to hydrochloric acid and 2 to cadmium chloride. It was found that, within the limits imposed by the paucity of the data, agreement obtained was satisfactory.

Introduction

The recent attempts of numerous investigators from this as well as from other laboratories to apply the concepts of classical thermodynamics to ion-exchange processes have emphasized the paucity of available data on activity coefficients in mixed electrolyte solutions.

Prior to 1949 there were primarily two methods used for the determination of the activity coefficient of one electrolyte in a solution also containing another. They were (a) determination of the solubility of salts in salt solutions, and (b) electromotive force measurements on cells without liquid junction containing a mixture of electrolytes. In the case of aqueous solutions of metal halides and the corresponding acids, the mean activity coefficient of the acid in the mixed solutions was determined experimentally at various concentrations from electromotive force measurements.[2,3] For many of these aqueous systems at constant total ionic strength, the logarithm of the activity coefficient of the acid was found to be a linear function of the ionic strength of the other solute. The activity coefficient of the salt was then computed from the osmotic coefficients of the solvent in the separate pure solutions at the total ionic strength in question, on the assumption of a similar linear variation of the logarithm of the activity coefficient of the salt with the ionic strength of the acid. This principle of linear variation has come to be known as the Harned rule. However, since the application of the Harned rule to *both* solute species was admittedly based upon an assumption, it was thought desirable to test the validity of the Harned rule by direct measurements on both electrolytes in their mixed aqueous solutions at constant total ionic strength. A series of measurements of the activity coefficient of hydrochloric acid in its aqueous mixtures with cadmium chloride at constant total ionic strength of 5.0 molal has been previously reported[4]; in this instance, approximate agreement with the Harned rule of linearity was again observed.

In order that the individual activity coefficients in a mixed electrolyte system with a common ion may be determined by means of electromotive force measurements, reversible electrodes must be found for all ions present. In our measurements an Ag–AgCl electrode served as a reversible chloride electrode, so that by use of such an electrode together with a hydrogen electrode and a saturated cadmium amalgam electrode for the cations present we could in principle measure the activity coefficients of cadmium chloride and hydrogen chloride in their mixed aqueous solutions at various total ionic strengths.

It should be noted that in the present investigation some difficulties might be expected from direct chemical action of cadmium metal and hydrogen ion at the cadmium amalgam electrode, without the passage of any current, and from the tendency of hydrogen electrodes to become poisoned in solutions containing cadmium, first pointed out in a qualitative statement by Glasstone.[5] The results obtained indicated that at least the second possible difficulty did not interfere with the experimental measurements, and it was hoped that the first did not occur to a sufficient extent to constitute a serious source of error. This point is tested and discussed later.

In this work cells of the following types were used

$$CdHg_x \mid CdCl_2(m_2),\ HCl(m_1) \mid AgCl\text{–}Ag$$

$$Pt\text{–}H_2 \mid CdCl_2(m_2),\ HCl(m_1) \mid AgCl\text{–}Ag$$

and

$$CdHg_x \mid CdCl_2(m_2),\ HCl(m_1) \mid H_2\text{–}Pt$$

The expressions for the electromotive force of these cells are, respectively

$$E_1 = E_1^0 - 2.3026\,\frac{RT}{2F}\log\,[m_2(m_1 + 2m_2)^2] - 2.3026\,\frac{3RT}{2F}\log\,\gamma_2 \quad (2)$$

(1) From part of a thesis submitted by L. Leifer in partial fulfillment of the requirements for the degree of Doctor of Philosophy, University of Kansas, 1959. Presented before the Division of Physical Chemistry, 138th National Meeting of the American Chemical Society, New York, N. Y., September, 1960.

(2) H. S. Harned and B. B. Owen, "The Physical Chemistry of Electrolytic Solutions," 3rd ed., Reinhold Publ. Corp., New York, N. Y., 1958, p. 600.

(3) H. S. Harned and R. Gary, *J. Am. Chem. Soc.*, **76**, 5924 (1954); **77**, 1994, 4695 (1955).

(4) H. S. Harned and R. Gary, *J. Phys. Chem.*, **63**, 2086 (1959).

(5) S. Glasstone, "An Introduction to Electrochemistry," D. Van Nostrand Co., New York, N. Y., 1942, p. 352.

$$E_2 = E_2^0 - 2.3026\frac{RT}{F}\log\left[m_1(m_1 + 2m_2)\right] - 2.3026\frac{2RT}{F}\log\gamma_1 \quad (3)$$

and

$$E_3 = E_3^0 - 2.3026\frac{RT}{2F}\log\frac{m_2}{m_1^2} - 2.3026\frac{RT}{2F}\log\frac{\gamma_2^3}{\gamma_1^4} \quad (4)$$

In these equations, γ represents the stoichiometric mean ionic molal activity coefficient. Equations 2, 3, and 4 are not all independent because

$$E_3 = E_1 - E_2 \text{ and } E_3^0 = E_1^0 - E_2^0 \quad (5)$$

Experimental Methods

Solutions.—All solutions used in these investigations were prepared from demineralized water and Baker's Analyzed reagent grade cadmium chloride and hydrochloric acid. In order to ensure stoichiometric cadmium chloride, the stock solution of cadmium chloride was analyzed for both cadmium (by gravimetric determination as the sulfate) and chloride (by precipitation with silver nitrate solution). The mixed electrolyte solutions were prepared by weight from stock solutions, the 0.5 and 0.2 molal solutions being obtained by dilution of the 1.0 molal solution. Prior to actual measurement, the solutions were deoxygenated by boiling under reduced pressure and bubbling hydrogen through the solution, also under reduced pressure. The original concentrations were corrected for loss of water in this process.

Electrodes.—The hydrogen electrodes were prepared by the following procedure. Each platinum electrode was cleaned electrolytically by making it the anode in a concentrated HCl solution (new electrodes were cleaned in hot alkali). The electrodes were then made the cathode in the electrolysis for about 5 min., at a current density of 1.35 amp./dm.^{2}, of a 3% solution of chloroplatinic acid containing 0.5 ml. of 0.1 N lead acetate in 100 ml. The electrodes were then rinsed with water, made the cathode in the electrolysis of a dilute sodium hydroxide solution for a few seconds, washed, made the cathode in the electrolysis of a dilute sulfuric acid solution for one minute, again washed, and stored in deionized water until ready for use.

The silver–silver chloride electrodes were prepared by the thermal method used by Rule and LaMer,[6] Keston,[7] and Owen[8] in the preparation of Ag–AgCl, Ag–AgBr, and Ag–AgI electrodes, respectively.

The cadmium amalgam electrodes, containing 6–8 weight % (10.7–14.3 atom %) of cadmium, were prepared from Baker and Adamson reagent grade mercury and Mallinckrodt reagent grade cadmium metal. The cadmium, scraped virtually free of any oxide film, was placed in a 60-ml. Squibb separatory funnel and the air was evacuated. Mercury was introduced and, after re-evacuation, hydrogen was added. By means of successive evacuations and hydrogen additions, the space was freed of oxygen and then filled with oxygen-free hydrogen at approximately 0.5 atm. pressure. The funnel was then warmed in a water bath at 60–80°, and agitated until complete solution of the cadmium had taken place. The assembly was then cooled, during which process some solid crystallized out and could be seen floating on the surface, and hydrogen was added to atmospheric pressure. Amalgams prepared in this way remained bright and oxide-free over long periods of time.

The electrodes were checked by means both of measurements on cells containing the individual electrolytes and of internal comparisons during the course of each measurement. Where discrepancies greater than 0.1 mv. occurred, the faulty electrode was discarded.

(6) C. K. Rule and V. K. LaMer, *J. Am. Chem. Soc.*, **58**, 2339 (1936).

(7) A. S. Keston, *ibid.*, **57**, 1671 (1935).

(8) B. B. Owen, *ibid.*, **57**, 1526 (1935).

Apparatus and Procedure.—The e.m.f. cell, except for the tungsten wire lead, was constructed of Pyrex glass. It was designed to exclude air, to facilitate flushing by both solution and hydrogen, and to provide space for two Ag–AgCl and two hydrogen electrodes.

The hydrogen gas used in these experiments was freed of oxygen by passing over copper at 450° in a tube furnace. A Leeds and Northrup Type K2 potentiometer connected to a Leeds and Northrup No. 2430 galvanometer was used for the potential measurements. The potentiometer was calibrated with a Weston standard cell recently certified in the laboratories of the National Bureau of Standards. The cell apparatus was immersed in a constant temperature bath maintained at 25 ± 0.5°.

After the apparatus had been assembled, the amalgam reservoir and the electrodes were put into place and the cell was flushed with hydrogen. The cell then was evacuated, and about 30 ml. of solution, under hydrogen pressure, was allowed to flow into it. The amalgam was introduced into the cell and then hydrogen was admitted. The pressure was regulated by means of a screw clamp and a bubbler, so that there was no more than a negligible pressure differential between the interior of the cell and the surrounding atmosphere. All e.m.f. values were corrected to 1 atm. pressure. After a series of measurements had been obtained on a given solution, the amalgam and the solution were transferred, without opening the cell to the atmosphere, to a waste reservoir. The cell was then partially evacuated, a fresh portion of solution and fresh amalgam were added, and the measurements were repeated. At least three separate results were recorded for each solution.

It should be noted that a period of 15–30 min. was required to reach equilibrium (*i.e.*, before a constant potential was obtained) for solutions for which the ionic strength fraction of cadmium chloride, X_2, was less than 0.5. For ionic strength fractions of cadmium chloride between 0.5 and 1.0 an even longer contact time (40 min.–2 hr.) was necessary.

All data are recorded in absolute volts. The standard potential values used were −0.22246 absolute volt for the silver–silver chloride electrode, as given by Harned and Ehlers,[9] and 0.35163 absolute volt for the saturated cadmium amalgam electrode, as given by Harned and Owen.[2] The latter value was calculated from the E^0 value for the cell $CdHg_x$(satd.) | $CdCl_2(m)$ | AgCl–Ag, as determined by Harned and Fitzgerald.[10,11] The value of 2.3026 RT/F at 25° used in the calculations below was 0.059158 volt.

Results

The initial e.m.f. measurements were made on cells containing the individual electrolytes at unit ionic strength. Values of the activity coefficient of hydrochloric acid and of cadmium chloride obtained here were in good agreement with some of the values reported in the literature.[9,12] It should be noted that for cadmium chloride molalities above 0.1 there is a progressive divergence between the values reported by Harned and Fitzgerald,[10] who used an e.m.f. technique, and those reported by Robinson,[12] who used an isopiestic method. The values reported here agree well with those obtained by Robinson.

Data for total ionic strengths of 1.0, 0.5, and 0.2 molal, at ten ionic strength fractions for each given ionic strength, are recorded in Tables, I, II, and III. In the case of the most concentrated solutions the electromotive force measurements were performed on solutions whose total ionic strength was slightly different from unity. However, by means of a short interpolation, the activity coefficients were corrected to unit total ionic strength and reported as described below.

(9) H. S. Harned and R. W. Ehlers, *ibid.*, **55**, 2179 (1933).

(10) H. S. Harned and M. E. Fitzgerald, *ibid.*, **58**, 2624 (1936).

(11) The values reported in references 2, 9, and 10 are in international volts. Conversion to absolute volts yields the values given above.

(12) R. A. Robinson, *Trans. Faraday Soc.*, **36**, 1135 (1940).

TABLE I

ELECTROMOTIVE FORCE MEASUREMENTS ON CELLS CONTAINING AQUEOUS $CdCl_2$–HCl SOLUTIONS AT 25°

$CdHg_x$(satd.)$|\ CdCl_2(m_2),\ HCl(m_1)\ |$AgCl–Ag (1)

Pt–$H_2|\ CdCl_2(m_2),\ HCl(m_1)\ |$AgCl–Ag (2)

$CdHg_x$(satd.)$|\ CdCl_2(m_2),\ HCl(m_1)\ |\ H_2$–Pt (3)

Total ionic strength $\mu = 3m_2 + m_1$	Ionic strength fraction of $CdCl_2$ $X_2 = 3m_2/\mu$	Measured potentials of cells (1), (2), and (3) in abs. volts E_1	E_2	E_3
1.0044	0.0000		0.23312	
1.0022	.04982	0.70440	.23617	0.46829
1.0047	.12458	.69495	.24035	.45464
0.9866	.24927	.68737	.24953	.43784
1.0113	.37406	.68247	.25738	.42511
1.0146	.4991	.67939	.26729	.41207
1.0152	.6241	.67783	.27940	.39824
1.0174	.7493	.67745	.29500	.38237
1.0219	.8745	.67702	.31695	.36007
1.0062	.9498	.67759	.34613	.33151
1.0245	1.0000	.67800		

TABLE II

ELECTROMOTIVE FORCE MEASUREMENTS ON CELLS CONTAINING AQUEOUS $CdCl_2$–HCl SOLUTIONS AT 25°

$CdHg_x$(satd.)$|\ CdCl_2(m_2),\ HCl(m_1)\ |$AgCl–Ag (1)

Pt–$H_2|\ CdCl_2(m_2),\ HCl(m_1)\ |$AgCl–Ag (2)

$CdHg_x$(satd.)$|\ CdCl_2(m_2),\ HCl(m_1)\ |\ H_2$–Pt (3)

Total ionic strength $\mu = 3m_2 + m_1$	Ionic strength fraction of $CdCl_2$ $X_2 = 3m_2/\mu$	Measured potentials of cells (1), (2), and (3) in abs. volts E_1	E_2	E_3
0.5002	0.00000		0.27238	
.4994	.04982	0.71788	.27494	0.44267
.4999	.12458	.70771	.27860	.42895
.4998	.24927	.69978	.28555	.41426
.5007	.37406	.69590	.29341	.40257
.4996	.4991	.69419	.30287	.39134
.4997	.6241	.69203	.31394	.38710
.5001	.7493	.69125	.32834	.36292
.4997	.8745	.69115	.35058	.34058
.4994	.9498	.69129	.37697	.31435
.4998	1.0000	.69166		

TABLE III

ELECTROMOTIVE FORCE MEASUREMENTS ON CELLS CONTAINING AQUEOUS $CdCl_2$–HCl SOLUTIONS AT 25°

$CdHg_x$(satd.)$|\ CdCl_2(m_2),\ HCl(m_1)\ |$AgCl–Ag (1)

Pt–$H_2|\ CdCl_2(m_2),\ HCl(m_1)\ |$AgCl–Ag (2)

$CdHg_x$(satd.)$|\ CdCl_2(m_2),\ HCl(m_1)\ |\ H_2$–Pt (3)

Total ionic strength $\mu = 3m_2 + m_1$	Ionic strength fraction of $CdCl_2$ $X_2 = 3m_2/\mu$	Measured potentials of cells (1), (2), and (3) in abs. volts E_1	E_2	E_3
0.2000	0.0000		0.31899	
.1999	.04982	0.73824	.32126	0.41700
.1996	.12458	.72714	.32471	.40244
.1999	.24927	.71952	.33092	.38841
.1997	.37406	.71567	.33810	.37745
.1999	.4991	.71391	.34650	.36723
.1999	.6241	.71218	.35672	.35530
.1999	.7493	.71120	.37035	.34072
.1998	.8745	.71054	.39143	.31891
.2000	.9498	.71074	.41743	.29314
.2000	1.0000	.71107		

In general when values of E_1, E_2, and E_3 were not in complete agreement, E_1 and E_2 were used for the computation of γ_2 and γ_1, respectively. The determination of E_3, thus, was in essence but an attempt at an experimental check of the e.m.f. measurements.

The variation of the logarithm of the activity coefficient of hydrochloric acid and of cadmium chloride with the ionic strength fraction of cadmium chloride, at constant total ionic strength, is shown in Fig. 1 and 2.

The nearly linear variation of log γ_1 with solute composition is in qualitative agreement with the results obtained by Harned and Gary at 5.0 molal ionic strength.[4] The slope of their curve is of the same sign and its magnitude is consistent with the trend observed for the three lower ionic strengths studied in this investigation. It is interesting to note that the departure from linearity increases with decreasing total ionic strength. Although this general phenomenon has been observed previously, no satisfactory explanation for it has been offered. Equations describing the variation of log γ_1 with μ_2, the ionic strength of cadmium chloride, were obtained by the method of least squares for each of the total ionic strengths investigated.[13] These equations, together with their corresponding standard deviations, are

μ = 1.0 molal

$$\log \gamma_1 = -0.0928 - 0.1805\mu_2 - 0.0502\mu_2^2 \qquad \text{Std. dev.} = \pm 0.0015 \quad (6)$$

μ = 0.5 molal

$$\log \gamma_2 = -0.1213 - 0.2122\mu_2 - 0.220\mu_2^2 \qquad \text{Std. dev.} = \pm 0.0004 \quad (7)$$

μ = 0.2 molal

$$\log \gamma_1 = -0.1176 - 0.3110\mu_2 - 1.06\mu_2^2 \qquad \text{Std. dev.} = \pm 0.0008 \quad (8)$$

Values of the activity coefficients of hydrogen chloride in its pure aqueous solution as computed from the constants in these equations, 0.808, 0.756, and 0.763 for 1.0, 0.5, and 0.2 molal solutions, respectively, are in good agreement with the accepted values,[14] namely 0.809, 0.757, and 0.767.

The variation of log γ_2 with solute composition is more complex, and no attempt was made to fit the results to empirical expressions. The experimental results for log γ_2 will be compared later with calculated results based on the application of the cross-differentiation relation to the data for log γ_1.

Consistency Tests.—From the data shown in Fig. 1 and 2 and listed in Tables I, II, and III, it is clear that for neither electrolyte component does the logarithm of the activity coefficient, at constant total ionic strength, vary linearly with the ionic strength fraction of the other. The maximum

(13) It was demonstrated that a linear equation gave a standard deviation outside the limits of experimental error, whereas a cubic equation gave a standard deviation approximately the same as the experimental error, but not sensibly different from that given by the quadratic expression.

(14) R. A. Robinson and R. H. Stokes, "Electrolyte Solutions," Academic Press, Inc., New York, N. Y., 1955.

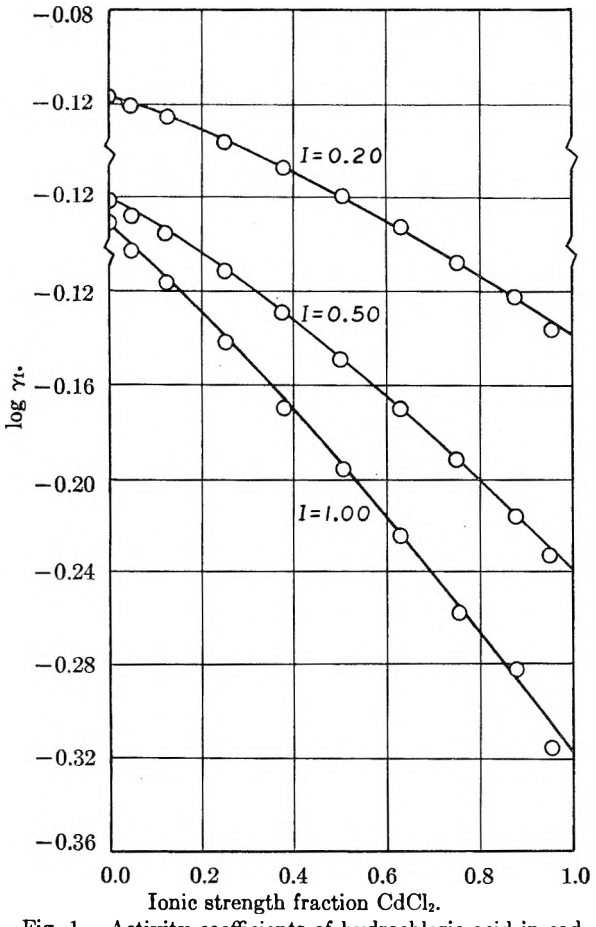

Fig. 1.—Activity coefficients of hydrochloric acid in cadmium chloride–hydrochloric acid mixtures at three ionic strengths. The curves are successively displaced vertically as indicated.

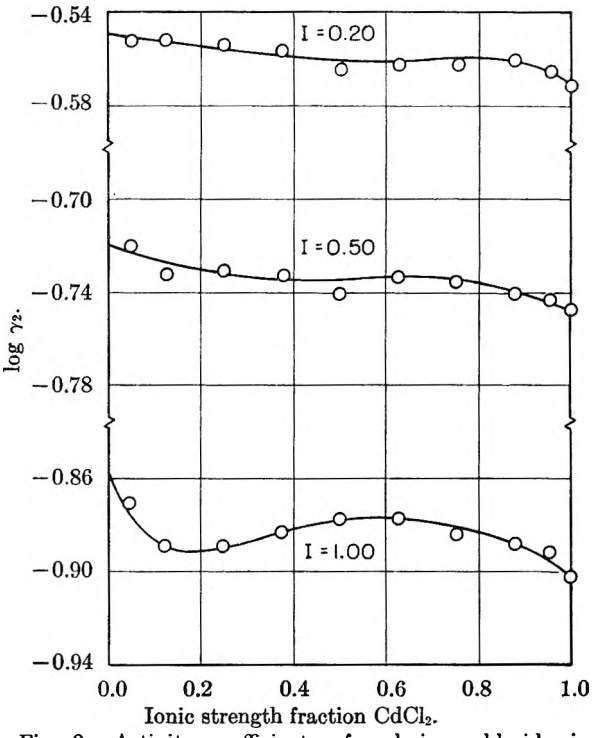

Fig. 2.—Activity coefficients of cadmium chloride in cadmium chloride–hydrochloric acid mixtures at three ionic strengths. The curves are successively displaced vertically as indicated.

probable error in the logarithm of the activity coefficient is estimated to be ±0.0017 for the acid component and ±0.003 for the salt component. These values are based upon the assumption that no irreversible electrode processes occurred during the course of our measurements. In order to verify this assumption, and specifically because of the possibility of an attack of the cadmium electrode by hydrogen ion, we applied to our data two tests, both based upon the cross-differentiation relations which were first applied to vapor pressure data by McKay[15] and McKay and Perring.[16] In the first method (A) the experimental activity coefficient data for both cadmium chloride and hydrochloric acid are used, while in the second method (B) only the experimental hydrochloric acid activity coefficients in the mixed electrolyte solutions are used.

Method A.—The cross-differentiation relation applied to this system may be written

$$3\left(\frac{\partial \ln \gamma_2}{\partial m_1}\right)_{m_2} = 2\left(\frac{\partial \ln \gamma_1}{\partial m_2}\right)_{m_1} \qquad (9)$$

If we express the composition of the solution in terms of the variables μ (the total ionic strength of the solution) and X_2 (the ionic strength fraction of cadmium chloride), given by

$$\mu = m_1 + 3m_2 \quad X_2 = 3m_2/\mu \qquad (10)$$

then eq. 9 assumes the following more convenient form

$$\frac{\partial}{\partial \mu}\left[\mu \log \gamma_2/\gamma_1^2\right] = \frac{\partial}{\partial X_2}\left[X_2 \log \gamma_2 + (1 - X_2) \log \gamma_1^2\right] \qquad (11)$$

Thus the slope of a curve of $A \equiv \mu \log \gamma_2/\gamma_1^2$ *vs.* μ must be equal to the slope of a curve of $B \equiv X_2 \log \gamma_2 + (1 - X_2) \log \gamma_1^2$ *vs.* X_2. Table IV gives a comparison of the slopes obtained from plots of A *vs.* μ and B *vs.* X_2, A and B having been computed from the experimental values of log γ_1 and log γ_2 shown in Fig. 1 and 2. Because only three

TABLE IV

COMPARISON OF SLOPES OF CURVES OF $A \equiv \mu \log \gamma_2/\gamma_1^2$ *vs.* μ AND $B \equiv X_2 \log \gamma_2 + (1 - X_2) \log \gamma_1^2$ *vs.* X_2, AT TOTAL IONIC STRENGTHS OF μ = 1.0, 0.5, AND 0.2 MOLAL

	μ = 1.0		μ = 0.5		μ = 0.2	
X_2	$-\partial A/\partial \mu$	$-\partial B/\partial X_2$	$-\partial A/\partial \mu$	$-\partial B/\partial X_2$	$-\partial A/\partial \mu$	$-\partial B/\partial X_2$
0.050	1.04	1.04	0.66	0.69	0.50	0.45
.125	1.01	1.02	.68	.66	.48	.43
.294	0.92	0.94	.60	.61	.42	.41
.374	.78	.78	.60	.58	.42	.40
.499	.73	.70	.51	.52	.43	.36
.624	.60	.59	.43	.43	.35	.29
.749	.55	.53	.36	.39	.31	.26
.874	.48	.47	.31	.31	.24	.23
.950	.39	.43	.27	.29	.23	.23

(15) H. A. C. McKay, *Nature*, **169**, 464 (1952).

(16) H. A. C. McKay and J. K. Perring, *Trans. Faraday Soc.*, **49**, 163 (1953).

values of μ were included in the study, there is of course considerable uncertainty in the slopes of A *vs.* μ.

Method B.—Should any irreversible process have occurred at the cadmium amalgam electrode, the measured activity coefficients of cadmium chloride would have been in error. The second method used to check our experimental results involved only the mixed electrolyte solution results for the activity coefficient of hydrochloric acid, in the determination of which irreversible electrode processes would be expected to interfere minimally, and allowed us to calculate the activity coefficient of cadmium chloride for limited concentration ranges.

The experimental results for hydrochloric acid satisfy expressions of the form

$$\log \gamma_1 = \log \gamma_{1(0)} - \alpha_{12}\mu_2 - \beta_{12}\mu_2^2 \quad (12)$$

in which $\gamma_{1(0)}$, the activity coefficient of hydrochloric acid at the total ionic strength in question, α_{12}, and β_{12} are functions of the total ionic strength μ only.

Upon substituting eq. 12 into 9 we obtain

$$\left(\frac{\partial \log \gamma_2}{\partial m_1}\right)_{m_2} = 2\left[\frac{d \log \gamma_{1(0)}}{d\mu} - \alpha_{12} - \mu_2 \frac{d\alpha_{12}}{d\mu} - 2\beta_{12}\mu_2 - \mu_2^2 \frac{d\beta_{12}}{d\mu}\right]_{m_1} \quad (13)$$

Equation 13 is to be integrated at constant m_2 from a lower limit $\mu = 3m_2$ to an upper limit $\mu = m_1 + 3m_2$, the molality of hydrochloric acid thus being varied from zero to m_1. The result is

$$\log \gamma_2/\gamma_{2(0)} = 2\left[\log \gamma_{1(0)}'/\gamma_{1(0)} - \int_{\mu_2}^{\mu} \alpha_{12}\, d\mu - \mu_2(\alpha_{12}' - \alpha_{12}) - 2\mu_2 \int_{\mu_2}^{\mu} \beta_{12}\, d\mu - \mu_2^2(\beta_{12}' - \beta_{12})\right] \quad (14)$$

In eq. 14 γ_2 is the activity coefficient of cadmium chloride in the mixed solution, and $\gamma_{2(0)}$ that of cadmium chloride at molality m_2 (ionic strength $3m_2$) in the absence of acid. The quantities $\gamma_{1(0)}'$ and $\gamma_{1(0)}$ represent the activity coefficient of hydrochloric acid in the absence of salt, the former at molality (*i.e.*, ionic strength) $m_1 + 3m_2$, the latter at molality $3m_2$. Similarly α_{12}' and β_{12}' refer to ionic strength $\mu = m_1 + 3m_2$, and α_{12} and β_{12} to ionic strength $\mu = 3m_2$.

In our computations the required values of $\gamma_{1(0)}$ and $\gamma_{2(0)}$ were obtained by interpolation of values reported in the literature.[2,12,14] The values of α_{12} and β_{12} were obtained from our data for hydrochloric acid and were incorporated into empirical expressions of the form

$$\alpha_{12} = \frac{A}{\sqrt{\mu}} + B + C\sqrt{\mu} \quad (15)$$

$$\beta_{12} = \frac{a}{\sqrt{\mu}} + b + c\sqrt{\mu} \quad (16)$$

This arbitrary choice was dictated by convenience and the general shape of α_{12} *vs.* μ curves for acid–salt systems. The computed values of γ_2, however, are not very sensitive to the particular choice among reasonably smooth functions. The equations for α_{12} and β_{12} as functions of μ and the results of our calculations are given in Table V. The range of values of X_2 at given μ is limited by the range of total ionic strength for which α_{12} and β_{12} are known, for we do not wish to extrapolate the relations of eq. 15 and 16. For the same reason it is impossible to compute γ_2 at $\mu = 0.2$. It should be noted that the methods used here are analogous to those applied to other systems by Argersinger and Mohilner[17]; the equations used here, however, contain additional terms due to the non-linear nature of the results for hydrochloric acid.

TABLE V

ACTIVITY COEFFICIENTS OF CADMIUM CHLORIDE IN HCl–$CdCl_2$–H_2O MIXTURES AT 25°

$$\alpha_{12} = \frac{0.1568}{\sqrt{\mu}} - 0.0902 + 0.1139\sqrt{\mu}$$

$$\beta_{12} = \frac{1.522}{\sqrt{\mu}} - 3.045 + 1.573\sqrt{\mu}$$

	μ = 1.0		μ = 0.5	
X_2	$-\log \gamma_2$ (exptl.)	$-\log \gamma_2$ (calcd.)	$-\log \gamma_2$ (exptl.)	$-\log \gamma_2$ (calcd.)
1.0	0.902	0.902	0.747	0.747
0.9	.890	.908	.741	.737
.8	.881	.904	.734	.731
.7	.879	.887	.732	.729
.6	.876	.870	.732	.730
.5	.878	.860	.734	.734
.4	.883	.862	.735	.745
.3	.887	.870		
.2	.891	.889		

Discussion

The results here presented constitute one of the very few experimental tests of the Harned rule wherein measurements were made on both solute components. Both the experimental and the calculated data clearly indicate that the cadmium chloride–hydrochloric acid–water system at ionic strengths 1.0, 0.5, and 0.2 molal does not behave in accordance with the Harned rule. Maximum experimental errors are well within the deviations from linearity. The values of log γ_2 calculated by means of method B differ from those determined experimentally by no more than 3%, and for most of the values the agreement is within 1–2%. In view of the drastic approximations involved in computation of the log γ_2 values from values of the corresponding quantity for hydrochloric acid, the agreement between calculated and experimental values is believed to be satisfactory. Further, such agreement affords strong evidence for the conclusion that, in our measurements, interference from irreversible electrode reactions was either negligible or at worst only slight.

Since a rather large degree of complex formation is to be expected in aqueous cadmium chloride–hydrochloric acid mixtures, it is not surprising that in this system the hypothesis of simple linear variation of the logarithm of the mean activity coefficient with ionic strength fraction is found to be inappli-

(17) W. J. Argersinger, Jr., and D. M. Mohilner, *J. Phys. Chem.*, **61**, 99 (1957).

cable. In the case of aqueous barium chloride–hydrochloric acid, strontium chloride–hydrochloric acid, aluminum chloride–hydrochloric acid, and ceric chloride–hydrochloric acid mixtures, the work of Harned and Gary[3] indicated a linear variation of log γ_{HCl} with the ionic strength of the salt at fixed values of μ, and these authors calculated the activity coefficients for the salt component in each mixture on the assumption of a similar simple linear variation of log γ_{salt}. However, calculations based on the cross-differentiation relationship by Argersinger and Mohilner[17] indicated small deviations from linearity in the case of the salt component, becoming slightly greater at the higher values of the total ionic strength. In the case of mixtures of calcium chloride and zinc chloride, Robinson and Farrelly[18] found significant deviations from linear variation, once again increasing with increasing total ionic strength. They attributed these deviations to chemical interaction, with the possible formation of species such as $Ca(ZnCl_4)$.

In the system studied here also, the departure from linearity of the variation of the logarithm of the activity coefficient of cadmium chloride was found to increase with increasing total ionic strength. It is of interest to note further that at all ionic strengths the activity of the hydrogen chloride was found to decrease rather markedly upon the addition of even small amounts of cadmium chloride. This decrease may be due to the formation of species such as $HCdCl_3$ and H_2CdCl_4.

Acknowledgment.—This work was supported by grants from the General Research Fund of the University of Kansas and the Office of Ordnance Research of the U. S. Army.

(18) R. A. Robinson and R. O. Farrelly, *J. Phys. Chem.*, **51**, 704 (1947).

MICELLAR STRUCTURE OF NON-IONIC DETERGENTS[1]

BY M. J. SCHICK, S. M. ATLAS, AND F. R. EIRICH

Lever Brothers Company, Research Center, Edgewater, New Jersey, and Polytechnic Institute of Brooklyn, Brooklyn, New York

Received January 22, 1962

The factors determining the micellar structure of non-ionic detergents in aqueous solutions have been investigated by means of light scattering, specific viscosity, sedimentation velocity, and partial specific volume measurements. The non-ionic detergents used, *viz.*, ethylene oxide condensates of nonylphenol, *n*-dodecanol, and *n*-octadecanol, have been characterized by analytical as well as surface chemical methods. The critical micelle concentration of non-ionic detergents is much lower than that of ionic detergents with comparable hydrophobic groups; consequently, the aggregate molecular weights are much larger than those of ionic detergents. Variations in aggregation number from 19 to 370 have been observed. These aggregation numbers depend on the length of both the hydrophobic and the hydrophilic groups. They increase with increasing length of the hydrophobic group, but decrease with increasing length of the hydrophilic group. Addition of electrolyte increases the aggregation number of the nonylphenol + 50 EO micelles. This increase is proportional to the electrolyte concentration, but is inversely proportional to the lyotropic number of the ions. The effect of variations in the lyotropic number of the anions is more pronounced than that of the cations. Whereas with ionic detergents micelle formation is ascribed to a balance between hydrocarbon-chain attractions and ionic repulsions, with non-ionic detergents the hydrocarbon-chain attractions are opposed by the hydration and space requirement of the ethylene oxide chains. For the aggregate molecular weight region of 45,000 to 100,000, spheres appear to be the most probable shape, and for larger micelles, disks or rods.

Introduction

Relatively few papers on the micellar structure of non-ionic detergents have appeared so far in the literature,[2-15] in contrast to the numerous papers published on the micellar structure of ionic detergents, of which some of the more recent ones are listed below.[16-23] General theories of micelle formation have been published by Debye,[16] Ooshika,[24] Reich,[25] and Hoeve and Benson.[26] These theories intended to explain why micelles do not grow indefinitely and do not lead to phase separation. The object of this investigation was a study to increase our experimental knowledge of the factors determining the aggregate size in aqueous solutions of non-ionic detergents. In addition, determinations of aggregate shape also were made.

(1) Paper presented at the 139th National Meeting of the American Chemical Society in St. Louis, Missouri, March 21–30, 1961.

(2) L. M. Kushner and W. D. Hubbard, *J. Phys. Chem.*, **58**, 1163 (1954).

(3) L. M. Kushner, W. D. Hubbard, and A. S. Doan, *ibid.*, **61**, 371 (1957).

(4) L. Hsiao, H. N. Dunning, and P. B. Lorenz, *ibid.*, **60**, 657 (1956).

(5) J. Stauff and J. Rasper, *Kolloid-Z.*, **151**, 148 (1957).

(6) P. Debye and W. Prins, *J. Colloid Sci.*, **13**, 86 (1958).

(7) P. Becher, *J. Phys. Chem.*, **63**, 1675 (1959).

(8) P. Becher and N. K. Clifton, *J. Colloid Sci.*, **14**, 519 (1959).

(9) P. Becher, *J. Phys. Chem.*, **64**, 1221 (1960).

(10) P. Becher, *J. Colloid Sci.*, **16**, 49 (1961).

(11) T. Nakagawa, K. Kuriyama, and H. Inoue, *ibid.*, **15**, 268 (1960).

(12) C. W. Dwiggins, R. J. Bolen, and H. N. Dunning, *J. Phys. Chem.*, **64**, 1175 (1960).

(13) A. F. Sirianni and B. A. Gingras, *Can. J. Chem.*, **39**, 331 (1961).

(14) J. M. Corkill, J. F. Goodman, and R. H. Ottewill, *Trans. Faraday Soc.*, **57**, 1627 (1961).

(15) C. W. Dwiggins and R. J. Bolen, *J. Phys. Chem.*, **65**, 1787 (1961).

(16) P. Debye, *ibid.*, **53**, 1 (1949).

(17) P. Debye and E. Anacker, *ibid.*, **55**, 644 (1951).

(18) J. N. Phillips and K. J. Mysels, *ibid.*, **59**, 325 (1955).

(19) K. J. Mysels and L. H. Princen, *ibid.*, **63**, 1696 (1959).

(20) K. J. Mysels, *J. Colloid Sci.*, **10**, 507 (1955).

(21) L. H. Princen and K. J. Mysels, *ibid.*, **12**, 594 (1957).

(22) L. M. Kushner and W. D. Hubbard, *ibid.*, **10**, 428 (1955).

(23) H. V. Tartar, *ibid.*, **14**, 115 (1959).

(24) Y. Ooshika, *ibid.*, **9**, 254 (1954).

(25) I. Reich, *J. Phys. Chem.*, **60**, 257 (1956).

(26) C. A. J. Hoeve and G. C. Benson, *ibid.*, **61**, 1149 (1957).

Experimental

Materials.—Molecularly distilled ethylene oxide (EO) condensates of branched nonylphenol, *n*-dodecanol, and *n*-octadecanol have been obtained from General Aniline and Film Corporation. The average chain length of the ethylene oxide adducts has been determined from their hydroxyl values. For a control, ultraviolet absorption spectra have been utilized for the ethylene oxide condensates of nonylphenol in 1% ethanol solutions. The molar absorbency index and the wave length of maximum absorption, 276 mμ, did not change when the assigned ethylene oxide content varied from 1 to 30.[27] The accuracy of the spectrophotometric procedure can be inferred from its demonstrated conformity to Beer's law. Thus molecular weights of the homologous series of nonylphenol + *n* EO, with *n* in the region of 1 to 30, are in close agreement when determined by either method. Nonylphenol + 50 EO dimerized in 1% ethanol solution. The homogeneity of the non-ionic detergents has been assessed from the observed sharp breaks in the surface tension *vs.* logarithm of concentration plots; only samples exhibiting sharp breaks have been used. The water was redistilled from alkaline permanganate and the electrolytes were of C.P. grade.

Methods.—The surface tensions were determined by means of a Wilhelmy balance with a sand blasted platinum plate at 25.0 ± 0.1° on 50-ml. solutions in 100-ml. crystallizing dishes. Measurements were taken 1 hr. after cleaning the solution surface by suction with a fine glass capillary. The specific refractive index increments were determined in a Brice–Phoenix[28] differential refractometer with blue light of λ 436 mμ at 25.0 ± 0.1° (see Table III). The refractometer was calibrated with sucrose and KCl solutions using sodium light. The turbidities were determined in a Brice–Phoenix[29] Universal light scattering photometer with blue light of λ 436 mμ at 25.0 ± 1.0° in a standard 40 × 40 × 120 semi-octagonal cell. The photometer was calibrated against an opal glass diffusor as a primary reference standard. For redistilled benzene the observed Rayleigh ratio at λ 436 mμ was 48.7 × 10^{-6} cm.$^{-1}$, in good agreement with the value reported by others.[29] The turbidity of the water was τ_0 = 2 to 4 × 10^{-5} cm.$^{-1}$. The usual precautions to exclude dust and other extraneous matter were taken by clarifying solvent or solutions by pressure filtration under nitrogen through a Corning UF (ultrafine) sintered glass filter. The solutions were in the concentration region of 1 to 8 × 10^{-3} g./cc. The solution method was used to avoid errors due to solubilization of impurities, *i.e.*, all solutions were made up by weighing the amount of non-ionic detergent into the volumetric flask, adding the solvent, and filtering the solution directly into the light scattering cell. The procedure was as follows: first filtration of solution into the cell, first turbidity measurement, second filtration of cell content, and second turbidity measurement.[8] Results are reported only if the reproducibility of the first and second turbidity measurements was within ±2%. Dissymmetries, $z = R_{45°}/R_{135°}$, were determined on all solutions and z was extrapolated to zero micellar concentration. The specific viscosities were determined in a 100-sec. Ubbelohde viscometer and the partial specific volumes in a 25-ml. pycnometer at 25.0 ± 0.1°. The sedimentation constants were determined in a model E Spinco ultracentrifuge using a synthetic boundary cell at 25.0 ± 0.1°. A phase plate was used in the schlieren optical system. Temperature control was achieved by automatic radiation control. All runs were performed at 60,000 r.p.m. and exposure intervals of 10 and 15 min. Single sharp peaks were observed in the schlieren patterns.

Results

Critical Micelle Concentration (c.m.c.).—The curves of surface tension *vs.* logarithm of concentration of four ethylene oxide condensates of nonylphenol in aqueous solution are given in Fig. 1. The sharp breaks in these curves are indicative of the c.m.c., *i.e.*, the maximum concentration of molecular dispersion. In order to justify the contention that these sharp breaks also serve as criteria of homogeneity of our materials, the curves of the surface tension *vs.* logarithm of concentration of equimolar mixtures of nonylphenol + 10 EO with 20 EO or 50 EO are included in Fig. 1. These mixtures exhibit no sharp breaks in the curves. Thus our non-ionic detergents appear to be reasonably homogeneous.

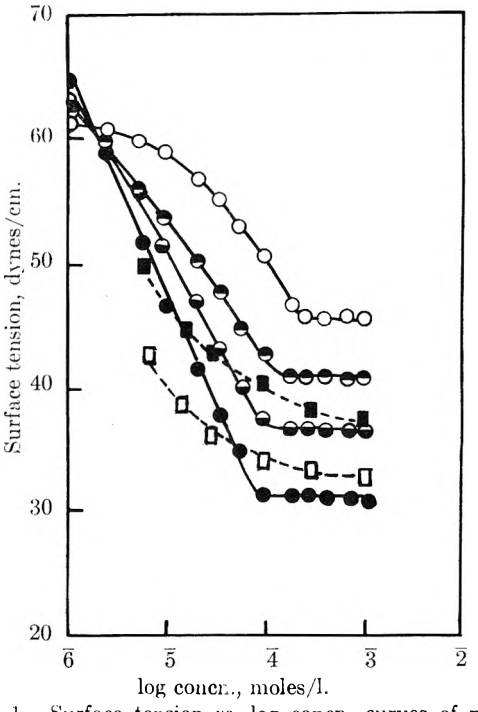

Fig. 1.—Surface tension *vs.* log concn. curves of nonylphenol + *n* EO: ●, *n* = 10; ◒, *n* = 15; ◓, *n* = 30; ○, *n* = 50; □, *n* = 10 + 20; ■, *n* = 10 + 50.

The c.m.c. values of three homologous series used in this investigation are given in Table I and are seen to be considerably lower than those of ionic detergents with comparable hydrophobic groups. This may be attributed to the absence of electrical forces which resist the growth of ionic micelles at a smaller size level. For comparison, the c.m.c. values of ionic detergents are given as sodium lauryl sulfate, 8100 μmole/l.[16,19] and *n*-dodecyltrimethylammonium bromide, 14,400 μmole/l.[16] The c.m.c. values in the two homologous series of non-ionic detergents approximately follow the relation ln c.m.c. = $A + Bn$.[4] For the relatively short chain of the nonylphenyl and *n*-dodecyl hydrophobic groups the c.m.c. values increase with increasing ethylene oxide chain length as shown in Table I. Increased hydration or solubility resists the aggregation of non-ionic detergents. The effect of the chain length of the hydrophobic group on the c.m.c. of non-ionic detergents with comparable ethylene oxide chain length of 14 or 15 units also is shown in Table I. In line with other results reported on ionic detergents,[16,23] the c.m.c. values decrease with increasing hydrophobic chain length. The hydrocarbon-chain attraction rises at constant hydration of the ethylene oxide chain and enhances aggregation. The slopes of the ln c.m.c. *vs.* *n* EO plots decrease with increasing length of the hydrophobic group. Thus the effect of hydration

(27) J. Kelly and H. L. Greenwald, *J. Phys. Chem.*, **62**, 1096 (1958).
(28) Phoenix Precision Instrument Co., Philadelphia, Pa.
(29) B. A. Brice, M. Halwer, and R. Speiser, *J. Opt. Soc. Am.*, **40**, 768 (1950).

on aggregation diminishes with increasing hydrophobic chain length. Related results were found by Becher.[7] The low c.m.c. value observed for *n*-octadecanol + 100 EO as compared to *n*-octadecanol + 14 EO may be attributed to decreasing solubility of the ethylene oxide portion with increasing molecular weight.[30]

TABLE I

C.M.C. AND AGGREGATE MOLECULAR WEIGHT OF NON-IONIC DETERGENTS IN AQUEOUS SOLUTIONS

Hydrophobic group	*n* EO	No. of C atoms in hydrophobic chain	C.m.c. μmole/l.	Agg. mol. wt.	Agg. no.
Nonylphenol (branched)	10	10.5	75	182,000	276
Nonylphenol (branched)	15		110	70,000	80
Nonylphenol (branched)	20		140	68,000	62
Nonylphenol (branched)	30		185	67,000	44
Nonylphenol (branched)	50		280	48,000	20
n-Dodecanol	7	12	50		
n-Dodecanol	14		55	100,000	125
n-Dodecanol	23		60		
n-Dodecanol	30		80	82,000	55
n-Octadecanol	14	18	60	330,000	370
n-Octadecanol	100		20	465,000	100

The effect of electrolyte or urea on the c.m.c. of non-ionic detergents is shown in Table II. A salting out of the hydrated ethylene oxide condensates of nonylphenol is shown by a decrease of the c.m.c. with increasing NaCl concentration.[4] The lowering of the c.m.c. of nonylphenol + 50 EO is affected by both the cation and the anion of the electrolyte, when added in equivalent quantities. This lowering increases with decreasing lyotropic number of the ions and is more pronounced with changes in the lyotropic number of the anions than of the cations.[31]

Aggregate Molecular Weights in Aqueous Solution.—The weight average aggregate molecular weights, M, of non-ionic detergents have been determined from light scattering data at 90° scattering angle by extrapolating the Debye function[16] $H(c - \text{c.m.c.})/(\tau - \tau_0)$ to zero micellar concentration, the intercept being equal to $1/M$ according to the equation

$$\frac{H(c - \text{c.m.c.})}{\tau - \tau_0} = 1/M + 2B(c - \text{c.m.c.}) \quad (1)$$

where H is a constant taking into account refractive index and geometrical factors, τ is the turbidity of a solution of concentration c in cm.$^{-1}$, $(c - \text{c.m.c.})$ is the micellar concentration in g./cc., and B represents the deviation from van't Hoff behavior as given by the slope of eq. 1. This is based on the assumption that the micelles behave as independent colloidal particles and the amount of light scattered by the molecularly dispersed detergent is independent of the detergent concentration above the c.m.c. This constant value is equated to the solvent blank τ_0. The observed linear nature of the Debye plots at low concentrations demonstrates the independence of aggregate molecular weights on micellar concentration in the region of $(c -$ c.m.c.) from 0 to 5×10^{-3} g./cc. The necessary corrections for internal interference were made in the aggregate molecular weights, when z exceeded 1.1.[32]

The degree of association, or the aggregation number, is defined as the ratio of the aggregate molecular weight to the molecular weight of the monomeric detergent. Water of hydration in the micelle, which is unknown, has not been taken into account. In a homologous series of a non-ionic detergent the aggregation numbers m_0 and the aggregate molecular weights M follow an intricate pattern. This is due to the fact that m_0 decreases as a result of increasing hydrophilicity, while M rises relatively, because of the increasing molecular weight of the monomeric detergent. Thus, we see for example in Table I that M increases for *n*-octadecanol + n EO, while m_0 falls.

Results for aqueous solutions are given in Tables I and III. The aggregate molecular weights and the aggregation numbers increase together with increasing chain length of the hydrophobic group from 10.5 to 18 carbon atoms at a comparable ethylene oxide chain length of 14 or 15 units as listed in Table I. These results show that the hydrocarbon-chain attraction rises at constant hydration of the ethylene oxide chain.[14] It is worth noting that a low c.m.c. value corresponds to a high aggregate molecular weight, and *vice versa*, a phenomenon generally observed with micellar solutions.[16-23]

The effect of ethylene oxide chain length on micelle formation for homologous series of non-ionic detergents is given in Table I. Here the hydrocarbon-chain length, and therefore the attraction, is maintained constant while the length of the ethylene oxide chain increases. Let us first consider the non-ionic detergents with short hydrophobic groups, *i.e.*, nonylphenol + n EO and *n*-dodecanol + n EO. Increasing the length of the ethylene oxide chain results in decreased aggregation numbers.[10] The same is true for *n*-octadecanol + n EO, but here on increasing the length of the ethylene oxide chain the aggregate molecular weight increases, in contrast to nonylphenol + n EO and *n*-dodecanol + n EO, because of the large molecular weight of the monomeric unit.

Finally, from the values of the coefficient B in Table III (which have been calculated from the slopes in the Debye plots), it can be seen that the deviation from van't Hoff behavior in eq. 1 increases with increasing ethylene oxide chain length, reflecting over-all increased solubility of the amphipathic molecule. However, the ethylene oxide portion of the molecule by itself decreases in solubility with molecular weight,[30] so that B eventually will pass through a maximum.

(30) F. E. Bailey and R. W. Callard, *J. Appl. Polymer Sci.*, **1**, 56 (1959).

(31) A. Voet, *Chem. Rev.*, **20**, 169 (1937).

(32) P. Doty and R. F. Steiner, *J. Chem. Phys.*, **18**, 1211 (1950).

TABLE II

EFFECT OF ELECTROLYTE OR UREA ON C.M.C. AND AGGREGATE MOLECULAR WEIGHT OF NON-IONIC DETERGENTS

Hydrophobic group	*n* EO	Solvent	Lyotropic no. (C)	Lyotropic no. (A)	C.m.c., μmole/l.	Agg. mol. wt.	Agg. no.
Nonylphenol	15	H_2O			110	70,000	80
Nonylphenol	15	0.5 *M* Urea			90	72,000	82
Nonylphenol	15	.43 *M* NaCl			65		
Nonylphenol	15	.86 *M* NaCl			55	73,000	83
Nonylphenol	15	1.29 *M* NaCl			45		
Nonylphenol	50	H_2O			280	48,000	20
Nonylphenol	50	0.43 *M* NaCl			200	46,000	19
Nonylphenol	50	.86 *M* NaCNS		13.3	225	46,000	19
Nonylphenol	50	.86 *M* LiCl	115		200	46,000	19
Nonylphenol	50	.86 *M* NaCl	100	10	150	62,000	26
Nonylphenol	50	.86 *M* TMACl[a]	<75		100	59,000	24
Nonylphenol	50	.86 *M* $\frac{1}{2}Na_2SO_4$		2	7	77,000	32
Nonylphenol	50	1.29 *M* NaCl			100	62,000	26
n-Octadecanol	100	H_2O			20	465,000	100
n-Octadecanol	100	0.86 *M* NaCl			~20	125,000	27
n-Octadecanol	100	1.72 *M* NaCl			~20	97,000	21

[a] Tetramethylammonium chloride.

TABLE III

LIGHT SCATTERING DATA OF MICELLES OF NON-IONIC DETERGENTS

Hydrophobic group	*n* EO	Solvent	$\Delta n/\Delta$ (c − c.m.c.), ml./g.	$B \times 10^4$
Nonylphenol	10	H_2O	0.155	−1.0
Nonylphenol	15	H_2O	.1517	2.0
Nonylphenol	20	H_2O	.150	2.0
Nonylphenol	30	H_2O	.144	2.0
Nonylphenol	50	H_2O	.136	10.0
Nonylphenol	50	0.43 *M* NaCl	.133	1.0
Nonylphenol	50	0.86 *M* NaCl	.125	0
Nonylphenol	50	1.29 *M* NaCl	.123	0
n-Octadecanol	14	H_2O	.1356	−1.5
n-Octadecanol	100	H_2O	.1362	5.0
n-Octadecanol	100	0.86 *M* NaCl	.127	2.5
n-Octadecanol	100	1.72 *M* NaCl	.122	0

$\Delta n/\Delta(c - \text{c.m.c.}) = 0.159 - n \times 0.00046$ for nonylphenol + n EO

$\Delta n/\Delta(c - \text{c.m.c.}) = 0.136 - m \times 0.01$ for nonylphenol + 50 EO in mmole/l. NaCl

This is not noticeable within our range of EO units, though the trend is indicated by the relatively low values for B for *n*-octadecanol + 100 EO and by the reversal in slope of nonylphenol + 50 EO at higher detergent concentrations.

Effect of Electrolyte on Aggregate Molecular Weight.—The results given so far show that the length of the EO portion of the monomeric detergent determines the aggregation in aqueous solution. This indicates hydration as an important stabilizing influence. To check this further, the effect of electrolyte or urea on the aggregate molecular weights and aggregation numbers was studied and is given in Table II. The aggregate molecular weight and the aggregation number increase only moderately for nonylphenol + 15 EO on addition of NaCl or urea, but both these quantities increase considerably for the more hydrophilic nonylphenol + 50 EO with increasing NaCl concentration. This behavior reverses for *n*-octadecanol + 100 EO, where a decrease in the aggregate molecular weight and aggregation number was observed with increasing NaCl concentration. It is further evident from the coefficients B in Table III that the deviation from van't Hoff behavior in eq. 1 decreases with increasing NaCl content, or in other words the interaction with the solvent diminishes generally with addition of electrolyte.

The specific effects of ions on the aggregate molecular weight and aggregation number of nonylphenol + 50 EO are given in Table II. In equivalent electrolyte solutions the aggregate molecular weights and the aggregation numbers increase with decreasing lyotropic number of the cation or anion, respectively, *i.e.*, decreasing hydration of the ions.[31] This phenomenon is more pronounced with changes in the lyotropic number of the anions than of the cations.

Aggregate Shape.—The results of measurements required to define the micellar shape of non-ionic detergents are listed in Table IV. The data are organized into three groups to show (a) the effect of ethylene oxide chain length, (b) the effect of hydrophobic group chain length, and (c) the effect of electrolyte or urea. The aggregate molecular weights are included in the first column. For blue light, λ 436 mμ, the absence of a measurable dissymmetry, *i.e.*, $z = 1$, indicates a maximum dimension of the aggregates below 330 Å.[17,32,33] Only the ethylene oxide condensates of *n*-octadecanol of aggregate molecular weights in excess of 300,000 show appreciable dissymmetries. Hence their linear dimension exceeds 330 Å., and a specific value may be assigned to them by assuming a model.

The intrinsic viscosities and sedimentation constants likewise are functions of size and shape. Both these quantities have been obtained by extrapolation to zero micellar concentration. For a given molecular weight, a low intrinsic viscosity and high sedimentation constant signify a spheroidal shape; the reverse applies for a rod shape. Thus, an unambiguous shape can be determined

(33) W. Beattie and C. Booth, *J. Phys. Chem.*, **64**, 696 (1960).

TABLE IV

DETERMINATION OF MICELLAR SHAPE OF NON-IONIC DETERGENTS

Hydrophobic group	n EO	Solvent	Agg. mol. wt., M	Dissymmetry, z	$[\eta]$, dl./g.	$s_0 \times 10^{13}$, c.g.s. units	$\bar{V}$, ml./g.
Nonylphenol	15	H_2O	70,000	1.0	0.04–0.06	1.4	0.9715
Nonylphenol	50	H_2O	48,000	1.0	.04– .06	0.83	.9573
n-Octadecanol	14	H_2O	330,000	1.05	.08	1.0	.9852
n-Octadecanol	100	H_2O	465,000	1.4	.12	2.3	.9604
Nonylphenol	15	H_2O	70,000	1.0	.04– .06	1.4	.9715
n-Dodecanol	14	H_2O	100,000	1.0	.04– .06	1.0	.9811
n-Octadecanol	14	H_2O	330,000	1.05	.08	1.0	.9852
Nonylphenol	15	H_2O	70,000	1.0	.04– .06	1.4	.9715
Nonylphenol	15	0.86 M NaCl	73,000	1.0	.04– .06	1.3	.9652
Nonylphenol	15	0.5 M Urea	72,000	1.0	.04– .06	1.3	.9822

only by combination of two or three of the methods listed in Table IV. The intrinsic viscosities, $[\eta]$, of the micelles of non-ionic detergents with the exception of the ethylene oxide condensates of n-octadecanol are moderately higher than those of rigid spheres, $[\eta] = 0.025$.[2] Hence a swollen spheroid appears to be the most probable shape for the former micelles and an ellipsoidal shape for the latter.

The sedimentation constants, s_0, are small in comparison to those of macromolecules of comparable molecular weight. This is in line with the partial specific volumes, $\bar{V}$, of the hydrated micelles, which are close to one.[12] Thus only a small density difference between the aggregates and solvent exists. In general the sedimentation constants follow the order of the aggregate molecular weights, with the exception again of the ethylene oxide condensates of n-octadecanol; these are lower than anticipated from the aggregate molecular weights. Hence a change in shape from a swollen spheroid to an ellipsoid is indicated from these data also.

The three models most frequently referred to for micellar aggregates are a sphere, disk, or rod. It generally is believed that small micelles of ionic detergents with aggregate molecular weights in the region of 10,000 to 50,000 are spherical,[23] whereas large micelles with aggregate molecular weights in excess of 500,000 are rod-shaped.[17] In view of the data given in Table IV, similar models are suggested for micelles of non-ionic detergents. For the aggregate molecular weight region of 45,000 to 100,000, spheres appear to be the most probable models, while for the larger micelles of the ethylene oxide condensates of n-octadecanol, the intrinsic viscosity numbers, sedimentation constants, and light scattering dissymmetry ratios indicate disks or rods.

The dimensions of the micelles of lower aggregate molecular weight therefore have been expressed in terms of radii of spheres, which follow the order of the aggregate molecular weights. These radii were obtained from M and $\bar{V}$, or from s_0 and $\bar{V}$ by means of Stokes' law. For the higher molecular weight aggregates of ethylene oxide condensates of n-octadecanol, presumably possessing elongated shapes, the axis ratios of the solvent penetrated ellipsoids were calculated from M, s_0, $[\eta]$, and $\bar{V}$ by means of the Scheraga–Mandelkern equation[34]

$$\beta = \frac{M s_0 [\eta]^{1/3} \eta \bar{V}_0}{M^{2/3}(1 - \bar{V}\rho_0)} \qquad (2)$$

From the β values in the region of 2.12×10^6 to 3.6×10^6, a specific axis ratio may be assigned to a prolate ellipsoid. The half axes are obtained from the volume of the ellipsoid $M\bar{V}/N = 4/3\ \pi ab^2$. The corresponding diameter of a rod of equal hydrodynamic volume is obtained by multiplying the minor axis by $\sqrt{2/3}$.[35] The pertinent data are listed in Table V.

The spherical micelles are visualized as consisting of a hydrocarbon chain core with the ethylene oxide coils at the periphery, and if the radius of the hydrocarbon core is assumed to be that of the maximum length of the hydrocarbon chains,[36] *i.e.*, 14 Å. for the branched nonylphenyl and 16 Å. for the n-dodecyl groups, sufficient space seems to be available for the ethylene oxide coils as shown by the radii for the spherical models given in Table V. The dimensions of the ellipsoidal model for the micelles of the ethylene oxide condensates of n-octadecanol may conform either to a disk or rod. Both models are cylindrical, but differ in the orientation of the molecules. In a disk the height, and in a rod the diameter, are twice the length of the molecule. For the maximum length of the hydrocarbon chains, *i.e.*, 23.6 Å. for n-octadecyl, little space seems to be available in either model for the ethylene oxide coils. However, the hydrocarbon chains may be curled up and thus form a densely packed core leaving more room for the outer shell of the ethylene oxide coils. Another possibility is that the axis ratios are too large. From the observed dimensions one cannot distinguish between a disk or rod shape; both shapes appear to be equally probable.

Discussion

The object of this investigation was a study to increase our experimental knowledge of the factors determining the aggregate size in aqueous solutions of non-ionic detergents. Comparing briefly the findings of this investigation with results reported before on ionic micelles,[16–23] the aggregation numbers of non-ionic micelles depend on the length of both the hydrophobic and hydrophilic

(34) H. Scheraga and L. Mandelkern, *J. Am. Chem. Soc.*, **75**, 179 (1953).

(35) T. Nishihara and P. Doty, *Proc. Natl. Acad. Sci.*, **44**, 411 (1958).

(36) CH_2 = 1.27 Å., CH_3 = 2.00 Å.

TABLE V

DIMENSIONS OF MICELLAR MODELS OF NON-IONIC DETERGENTS

Hydrophobic group	n EO	Solvent	Sphere r, Å. (light scat.)	Sphere r, Å. (sed. vel.)	Ellipsoid $\beta \times 10^{-6}$	Ellipsoid a/b	Ellipsoid a[a]	Ellipsoid b[a]	Rod (diam.), Å.
Nonylphenol	15	H_2O	30	42					
Nonylphenol	50	H_2O	26	27					
n-Octadecanol	14	H_2O			2.44	11	250	23	37
n-Octadecanol	100	H_2O			2.35	8	224	28	46
Nonylphenol	15	H_2O	30	42					
n-Dodecanol	14	H_2O	34	44					
n-Octadecanol	14	H_2O			2.44	11	250	23	37
Nonylphenol	15	H_2O	30	42					
Nonylphenol	15	0.86 M NaCl	30	37					
Nonylphenol	15	0.5 M Urea	30	48					

[a] a major half axis; b minor half axis.

groups, whereas those of ionic micelles depend on the length of the hydrophobic group and the state of charge. Differences due to variations of the nature of the ionic groups are insignificant in ionic micelles.[23] At constant hydrophilic group, the aggregation numbers of non-ionic as well as ionic micelles increase with increasing length of the hydrophobic group. At constant hydrophobic group the aggregation number of non-ionic micelles increases with decreasing ethylene oxide chain length, whereas the corresponding change in aggregation number of ionic micelles is brought about by addition of electrolyte. Thus, reducing the hydrophilic group of non-ionic detergents has the same effect as reducing the ionic repulsion of the polar groups in ionic detergents. However, addition of electrolyte also leads to an increased aggregation number for non-ionic micelles, suggesting that the ethylene oxide chains undergo a salting out process. This increase of the aggregation number due to extraneous electrolyte for ionic and non-ionic micelles depends inversely on the lyotropic number of the "counter" ions.[19]

Referring, after these general remarks, to the problem of why micelles do not grow indefinitely and do not lead to phase separation,[16,24-26] the theory of any aggregative colloidal system must explain why in the course of aggregation with increasing concentration there is a temporary trough or inflection point of the free energy of the total system, which halts the formation of the new phase at a given aggregate size level. Wherever there is a minimum of the total free energy in such a system, there must be an equilibrium size distribution of the micellar aggregates. A simple explanation has been given for ionic micelles[16]; as the number of long-chain ions aggregate to form a droplet or core of the hydrophobic tails, the number of charges per aggregate increases. Since the surfaces increase only with $^2/_3$ power of the aggregate volume, the charge density at the periphery increases and with it the electrostatic free energy of the growing aggregates. An equilibrium is reached at the c.m.c., where the drop in ΔF due to aggregation of hydrophobic groups is balanced by the rise in ΔF due to electrostatic repulsion.

It is evident, however, from the data on micelle formation of non-ionic detergents that other factors also must be at work. These factors may be operational for micelles of ionic and non-ionic detergents, and may play a large part besides the more readily understood electrostatic repulsion. Such additional factors stabilizing an equilibrium size distribution of micellar aggregates must be of the nature of forces resisting the decline in particle–solvent contact and the concomitant dehydration and entropy changes.

The necessity of looking for additional opposing factors, which could balance the drop in ΔF due to aggregation of hydrophobic groups, and thus the need of looking at the behavior of all other components in the system, has been stressed by Reich,[25] who calculated the equilibrium micellar size from the energy and entropy changes taking place during micelle formation. The calculation was based on a simple model of coalescence of hydrocarbon tails to a liquid droplet and fitting the ethylene oxide chains over their surfaces. Hoeve and Benson,[26] in a very extensive statistical mechanical treatment, have improved on the above approach, and point out that dehydration phenomena have to be taken into account, and that the simple shielding of the hydrocarbon tails from the water by the ethylene oxide chains accounts only for "complete micelles," *i.e.*, the micellar size for which the surface of the hydrocarbon core is entirely covered by the ethylene oxide chains. Unfortunately, their theory contained undefined parameters, which do not allow a comparison with our data at this time.

There is agreement, experimentally and with respect to deductions, between our results and those of Reich[25] in the following points: (a) micelle formation of non-ionic detergents occurs at a distinct c.m.c., (b) the c.m.c. decreases with increasing hydrocarbon chain length, and (c) for a given hydrophobic group, the c.m.c. increases with increasing length of the ethylene oxide chain. It also can be shown that the observed dependence of the aggregation number, m_0, on the length of the hydrophobic chain follows from Reich's[25] theory, if with Debye[6] one sets $m_0^{1/3} = 4\pi r^2/S$, where S is the fraction of one oil droplet covered by the ethylene oxide chain and r is the radius of the oil droplets. If, at constant m_0, the latter is set proportional to $N^{1/3}$ (N = number of C atoms in straight chain hydrophobic group), then in the Debye–Reich[6] equation $m_0 \sim N^2 \sim M^2_{HC}$ in agreement with our data, which follow a linear relation when the aggregation number, m_0, is plotted

TABLE VI

MICELLAR MODELS OF NON-IONIC DETERGENTS

Hydrophobic group	n EO	Agg. no., m_0	Surface area/m_0, Å.^{2} Periphery of oil droplet (a)	(b)	Periphery of micelle (c)	Cross sectional area of ethylene oxide coil, Å.^{2} (d)	Vol. of ethylene oxide unit, Å.^{3c} (e)	(g)
Nonylphenol	10	276	9	38		101	21	64
Nonylphenol	15	80	31	57	141	152	68	102
Nonylphenol	20	62	40	62		202	84	113
Nonylphenol	30	44	56	70		303	114	130
Nonylphenol	50	20	123	90	426	505	244	214
n-Dodecanol	14	125	26	44	117	142	52	76
n-Dodecanol	30	55	59	58		303	107	106

[a] Radius of oil droplet taken as length of nonylphenol 14 A. and n-dodecyl 16 A. (micellar core). [b] Radius of oil droplet taken as cube root of $^3/_4\pi \times$ volume of one hydrocarbon chain $\times m_0$ (micellar core). [c] Radius of micelle, r Å. (light scat.), taken from Table V. [d] Random walk with tetrahedral angle.[38] [e] Volume of ethylene oxide shell/$m_0n = 4/3\pi\ (r^3_{\text{total}} - r^3_{\text{oil droplet}})/m_0n$. [f] $r_{\text{total}} = \sqrt{r^2}$ random walk of EO chain with tetrahedral angle + r of oil droplet from (a). [g] $r_{\text{total}} = \sqrt{r^2}$ random walk of EO chain with tetrahedral angle + r of oil droplet from (b).

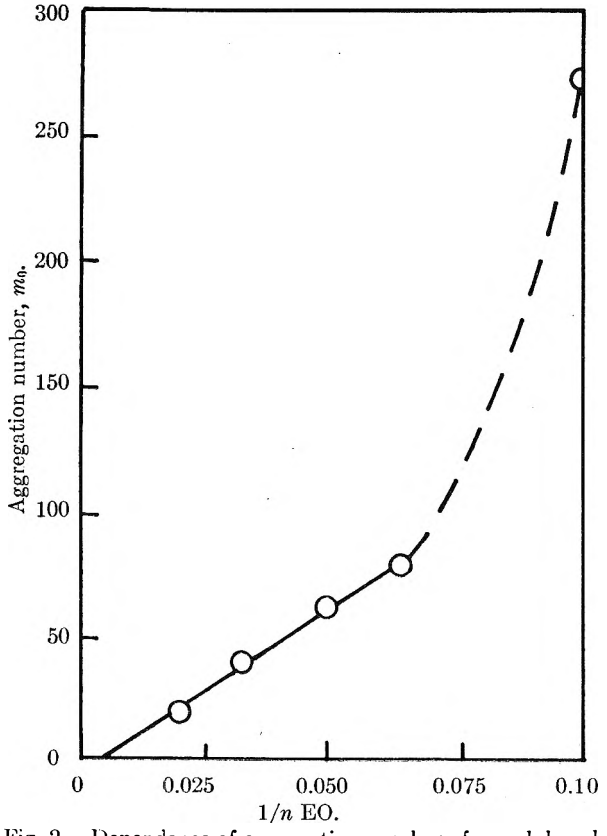

Fig. 2.—Dependence of aggregation number of nonylphenol + n EO micelles on ethylene oxide chain length.

vs. the square of the molecular weight of the straight chain hydrophobic group, M^2_{HC}, at constant (14) ethylene oxide chain length. This relation follows the equation

$$m_0 = 0.00684M^2_{HC} - 68 \pm 1 \qquad (3)$$

If a similar reasoning is applied to the Debye–Reich[6] equation with respect to S, which may be set proportional to nl^2 (n = number of EO units, l = length of EO unit), then one obtains $m_0 \sim 1/n^3$, which does not agree with the data in Fig. 2[37] or with related data of Becher.[10] Thus the existing model cannot explain the experimental dependence as shown in Fig. 2. In order to obtain it, a study of micelle formation in more detail would be necessary. Some basic data with respect to this can be found in Table VI and a corresponding attempt will be made elsewhere.

In line with the argument of the constant volume of the hydrocarbon chain within the micellar core irrespective of the aggregation number, it is interesting to calculate, from our data, the actual areas available to an ethylene oxide chain at the periphery of the micellar core, an area which plays such an important part in Reich's[25] theory. As a first instance, the radii of spherical micelles in Table V, which have been calculated from light scattering data and also from sedimentation velocity data, show that sufficient space for an outer shell of ethylene oxide coils is available, assuming densely packed extended hydrocarbon chains in the core. Table VI shows the mode of packing of the ethylene oxide chains in the outer shell more clearly. A comparison of the experimental area available to one ethylene oxide chain at the periphery of the oil droplet, as shown in columns a and b, with that at the micellar periphery, column c, indicates that the volume encompassed between is that of a truncated cone. Consequently, the mean area of this truncated cone (half height) or its volume must be compared with the corresponding requirements for the undistorted ethylene oxide chain. Taking the random walk of an undistorted polymer coil as a model, column d (even granting that for the shorter chains of 30 to 60 atoms this is not quite permissible),[38] it is seen that the ethylene oxide chains will have to be either appreciably compressed or interpenetrating. This discrepancy is larger when the experimental areas are calculated for extended hydrocarbon chains in the core, column a, than if calculated from an oil droplet assuming a density of one, column b. The latter represents the more probable packing in the core. These conclusions are supported by the volumes of the ethylene oxide unit in the outer shell listed in Table VI, columns f and g.

(37) $m_0 = 1$ for $N = 7$ and $n = 108$ from eq. 3 and Fig. 2. The sharp break in Fig. 2 at $1/n = 0.075$ may be attributed to the onset of coacervation. In the Debye–Reich[6] eq., one oil droplet signifies one hydrocarbon chain.

(38) P. J. Flory, "Principles of Polymer Chemistry," Chapter X, Cornell Univ. Press, Ithaca, N. Y., 1953.

These volumes increase with increasing ethylene oxide chain length of the non-ionic detergents, as anticipated from the increased hydration. For comparison, we refer to the molecular volumes of the ethylene oxide unit, 73 Å.^{3}, and of water, 30 Å.^{3} Likewise it is seen that the ethylene oxide chains deviate from the random walk model, and that the configurational entropy of the ethylene oxide chains in the outer shell must be reduced as compared with that of the free detergent molecules. The degree of hydration also must be affected, although how much cannot be said.

Addition of electrolyte to aqueous solutions of neutral molecules is known to change the activity coefficients of the molecules. "Salting out" and "salting in" may be found and though a complete theory has not been developed, the treatment of Debye and McAuley[39] serves as a good approximation for dilute solutions. Their derivation shows that changes in activity coefficients of the neutral molecules depend on the concentration and ionic radii of the electrolyte, and on the dielectric constant of the non-electrolyte. Small hydrated ions should be more effective in "salting out" neutral molecules; low dielectric constants of the non-electrolyte lead to "salting out," whereas high dielectric constants give rise to "salting in." The salts thus should affect the solubility of the ethylene oxide portions of the non-ionic detergents.

This can be seen in the results of Table II. They show that for non-ionic detergents with short or intermediate ethylene oxide chains, *i.e.*, nonylphenol + 15 or 50 EO, the c.m.c. values decrease and the aggregation numbers increase on addition of NaCl, which indicates an increase in the activity of the ethylene oxide chain. In contrast for the non-ionic detergents with a long ethylene oxide chain, *n*-octadecanol + 100 EO, the aggregation number decreases on addition of NaCl. The c.m.c. values are too low for observing any significant changes. One might postulate here that the increased length and lower solubility of the ethylene oxide chain enhances the adsorption of Na^+ to such an extent that it increases the over-all solubility of the non-ionic detergent.

It is well known that for cations as well as anions of electrolytes, a decrease in the lyotropic number corresponds to reduced hydration of the ions or a decrease in hydrated ionic radii. Therefore, as shown in Table II, the decrease in c.m.c. or the increase in aggregation number of nonylphenol + 50 EO on decreasing the lyotropic number of either cations or anions of the added electrolytes is attributed to reduced ion hydration. In this the hydration of the "counter" anions is more effective than that of the cations. Such a possibility has been foreshadowed by the results of Hsiao, *et al.*,[4] and Bailey and Callard.[30] These more complete investigations indicate also that the ion effects follow the Hofmeister series.

The following mechanism for this "salting out" of non-ionic detergents is suggested. First, there is the removal of hydrogen-bonded water molecules from the ether oxygens of the ethylene oxide chain by the increased ion concentration. The extent of the dehydration of the ethylene oxide chain then is determined by the closeness of the approach of the cations to the ether oxygens of the ethylene oxide chains, but is partially counteracted by the tendency of the "counter" anions to be hydrated. Applying Bailey and Callard's[30] observation of the collapse of a poly-(ethylene oxide) coil on addition of electrolyte, the ethylene oxide portion of our non-ionic detergents also will collapse on addition of electrolyte, from which qualitatively a decrease in c.m.c. or an increase in the aggregation number can be deduced.

Acknowledgment.—The authors wish to express their gratitude to Lever Brothers Co. for financial support of this investigation and to Dr. H. Keily of Lever Brothers Company for carrying out the spectrophotometric measurements.

(39) H. S. Harned and B. B. Owen, "The Physical Chemistry of Electroytic Solutions," Reinhold Publ. Corp., New York, N. Y., 1950, pp. 397–400.

2-METHYL-2-BUTANETHIOL: CHEMICAL THERMODYNAMIC PROPERTIES AND ROTATIONAL ISOMERISM[1]

BY D. W. SCOTT, D. R. DOUSLIN, H. L. FINKE, W. N. HUBBARD, J. F. MESSERLY, I. A. HOSSENLOPP, AND J. P. MCCULLOUGH

Contribution No. 113 from the Thermodynamics Laboratory of the Bartlesville Petroleum Research Center, Bureau of Mines, U.S. Department of the Interior, Bartlesville, Okla.

Received February 5, 1962

Thermodynamic and spectroscopic properties of 2-methyl-2-butanethiol (*t*-amyl mercaptan) were measured, and the results were used for calculating the chemical thermodynamic properties in the ideal gas state (0 to 1000°K.) and for studying the rotational isomerism of the compound. Experimental thermodynamic studies provided the following information: values of heat capacity for the solid (12°K. to the triple point), the liquid (triple point to 347°K.), and the vapor (360 to 500°K.); the triple point and transition temperatures; the heats of fusion and transition; thermodynamic functions for the solid and liquid (0 to 350°K.); heat of vaporization (330 to 372°K.); parameters of the equation of state; vapor pressure (324 to 411°K.); and the standard heat of formation at 298.15°K. The infrared spectrum of the crystals and relative intensity *vs.* temperature data for a pair of infrared bands of the liquid were determined.

Thermodynamic studies of 2-methyl-2-butanethiol (*t*-amyl mercaptan)

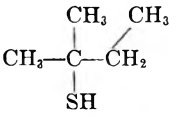

were made as part of continuing research on organic sulfur compounds. The experimental work consisted of low temperature calorimetry, vapor flow calorimetry, combustion calorimetry, and comparative ebulliometry, supplemented with special infrared spectroscopic studies. Experimental values of the entropy and heat capacity in the ideal gas state, obtained as described in the Experimental section, were interpreted by methods of statistical mechanics. The results were used to calculate a table of thermodynamic functions and, with an experimental value of the heat of formation, also the heat, free energy, and equilibrium constant of formation for temperatures of interest. The energy difference between the rotational isomers of the compound was determined from the spectroscopic studies.

Analysis by Methods of Statistical Mechanics.—The analysis by methods of statistical mechanics will be discussed first. All 54 degrees of freedom of the molecule had to be accounted for. These degrees of freedom may be classified as 3 translations, 3 over-all rotations, 43 vibrations, and 5 internal rotations. One of the internal rotations, that of the ethyl group relative to the rest of the molecule, involves three stable conformations or rotational isomers, as illustrated in Fig. 1. (Strictly, rotation of the thiol group also involves rotational isomers but, because of the small mass of the off-axis hydrogen atom, these isomers do not differ significantly in their spectroscopic or thermodynamic properties and need not be considered.) The most direct evidence for rotational isomerism in 2-methyl-2-butanethiol comes from interpretation of the molecular spectra, which will be considered next.

Spectra and Interpretation.—The molecular spectra from various sources,[2-4] including a low temperature infrared spectrum of the crystals from this research, are collected in Table I. Two moderately intense Raman and infrared bands of the liquid, 577 and 628 cm.$^{-1}$, appear in the region in which only C–S stretching fundamentals are expected. Arguments for assigning the lower frequency to the C_1 conformations (which are optical isomers and have identical spectra) and the higher frequency to the C_s conformation have been given by Brown and Sheppard[5] for the analogous *t*-amyl chloride. As only the lower frequency persists in the infrared spectrum of the crystals, 2-methyl-2-butanethiol crystallizes as the C_1 conformation, and all frequencies observed in the spectrum of the crystals must be assigned to the C_1 conformation. The spectrum of the crystals in the sodium chloride and potassium bromide regions, 400 to 5000 cm.$^{-1}$, differs from that of the liquid by the absence of a few bands peculiar to the C_s conformation and by a general sharpening of the bands and improved resolution. However, these differences are not very striking. In the cesium bromide region, 285 to 400 cm.$^{-1}$, on the other hand, the differences between the spectra of crystals and liquid are so striking that the spectra are scarcely recognizable as belonging to the same substance. In the spectrum of the crystals, each band of the liquid is split into two components by interactions with the crystal lattice, and these components are relatively sharp and intense, whereas the corresponding bands of the liquid are broad and weak. One fundamental not even detected in the spectra of the liquid appears plainly as the doublet 336–348 cm.$^{-1}$ in the spectrum of the crystals.

The description of the vibrational modes in Table I is somewhat schematic and is intended merely to show that the expected number of frequencies is assigned in each region of the spectrum. The CH_3 and CH_2 bending and C–H stretching frequencies are not all resolved, and average values had to be selected for thermodynamic calculations. Two frequencies, a CH_3 rocking and a C–C stretch-

(1) This investigation was part of American Petroleum Institute Research Project 48A on the "Production, Isolation and Purification of Sulfur Compounds and Measurement of Their Properties," which the Bureau of Mines conducts at Bartlesville, Okla., and Laramie, Wyo.

(2) K. W. F. Kohlrausch and F. Köppl, *Monatsh.*, **63**, 255 (1933).

(3) American Petroleum Institute Research Project 44 at the Carnegie Institute of Technology, Catalog of Raman Spectral Data, Serial No. 350.

(4) Ref. 3, Catalog of Infrared Spectral Data, Serial No. 1723, 1724, and 2194.

(5) J. K. Brown and N. Sheppard, *Trans. Faraday Soc.*, **50**, 1164 (1954).

TABLE I

MOLECULAR SPECTRA OF 2-METHYL-2-BUTANETHIOL IN CM.$^{-1}$ AND INTERPRETATION

Raman (with intensity[a]) liquid (ref. 2)	Raman (with intensity[a]) liquid (ref. 3)	Infrared (with intensity[a]) liquid (ref. 4)	Infrared (with intensity[a]) crystals II (−190°)	Interpretation (description of modes for C_1 fundamentals)
232 (1b.)	236 (2.5)	Not investigated		C–C–C bending
298 (1)	300 (3.5)	299 w	299 m 308 m	C–C–S bending
326 (1)	(332)[b]	324 vw	322 m 330 w	C–C–S bending
			336 m 348 m	C–C–C bending
370 (4)	370 (11.4)	369 w	367 m 370 m	C–C–C bending
	(393)[b]	391 w	382 w 399 m	C–C–C bending
413 (2)	414 (4.4)	414 vw		Other isomer
474 (1)	480 (2.4)	476 w	478 m	2 × 236 = 472
575 (10)	576 (40.7)	578 s	573 s	C–S stretching
627 (3)	629 (11.8)	627 m		Other isomer
776 (3)	778 (5.1)	778 sh	772 m	CH_2 rocking
		787 w		Other isomer
808 (3)	808 (9.7)	810 s	806 s	C–C stretching
860 (2)	860 (6.0)	864 m	*ca.* 867 sh 877 m	C–S–H bending & 300 + 577 = 877
923 (2sb)	920 (5.0)	922 m	918 m 929 m	CH_3 rocking & 342 + 577 = 919
	(941)[b]	942 sh	*ca.* 937 sh	CH_3 rocking
		999 sh		Other isomer
1007 (2sb)	1011 (2.7)	1013 m	1003 s	CH_3 rocking
1057 (2)	1060 (4.5)	1063 m	1062 m	CH_3 rocking
1135 (2)	1139) (4.9)	1142 s	1144 m	CH_3 rocking &
1160 (2)	1163 (7.6)	1167 s	1170 s	2 × 577 = 1154
	(1184)[b]	1190 sh	*ca.* 1194 sh	328 + 862 = 1190
1215 (1)	1220 (3.5)	1222 w	1215 w	C–C stretching
			1225 m	C–C stretching
1284 (1)	1288 (2.6)	1292 m	1285 m	CH_2 wagging
	(1334)[b]	1342 sh	1337 w	CH_2 twisting
	(1385)[b]	1379 s	1376 m	CH_3 sym. bending
1442 (5b)	1441 (16.1)	1464 s	1451 m	CH_3 unsym. bending & CH_2 bending
		Region 1500–2500 cm.$^{-1}$ omitted		
2571 (3b)	2575 (34.4)	2591 w	2520 m	S–H stretching
2884 (3b)	2889 (38.6)			
2898 (5)	2903 (48.1)			
2923 (6b)	2925 (54)	2924 s	2880 s	C–H stretching
	2937 (52)			
2967 (8sb)	2967 (54)			

[a] Raman intensities are given as in the original reference. Infrared intensities are given by the abbreviations: s, strong; m, medium; w, weak; vw, very weak; sh, shoulder; *ca.*, about. [b] Parentheses denote very weak Raman bands read off of the published tracing.

ing according to the schematic description, cannot be assigned from the observed spectra. As will be discussed later, the two unobserved frequencies were given an average value of 1290 cm.$^{-1}$ to fit the calorimetric data. The complete set of frequencies selected for the C_1 conformation, with the two unobserved values in brackets, is: skeletal bending, 236, 300, 328, 342, 370, and 392; C–S stretching, 577; CH_2 rocking, 778; C–S–H bending, 862; C–C stretching, 809, 1221 (2), and [1290]; CH_3 rocking, 921, 942, 1012, 1062, 1153, and [1290]; CH_2 wagging, 1290; CH_2 twisting, 1342; CH_3 and CH_2 bending, 1380 (3) and 1450 (7); S–H stretching, 2575; and C–H stretching, 2950 (11) cm.$^{-1}$.

Moments of Inertia and Internal Rotation.—Values of moments of inertia needed for treating the contributions of over-all and internal rotation to the thermodynamic functions were computed for the C_1 conformation with the thiol hydrogen atom in one of the three stable positions. Bond distances and angles were taken to be: C–C, 1.54 Å.; C–H, 1.09 Å.; C–S, 1.819 Å.; S–H, 1.336 Å.; C–S–H angle, 96° 30′, all other angles tetrahedral. These values are partly the usual ones for paraffin

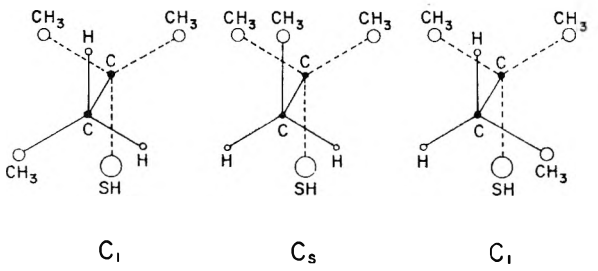

Fig. 1.—Rotational isomers of 2-methyl-2-butanethiol.

hydrocarbons; the rest are transferred from methanethiol.[6] The calculations were made by the general method of Kilpatrick and Pitzer.[7] The product of the principal moments of inertia for the assumed structure is 3.966×10^{-113} g.^{3} cm.^{6}. The "effective" reduced moments of inertia, taken so their product over all internal rotations equals $[D]$, the determinant of the internal rotational kinetic energy matrix, are 38.06×10^{-40} and 5.068×10^{-40} g. cm.^{2} for the ethyl group and its methyl group, respectively; 5.223×10^{-40} and 5.202×10^{-40} g. cm.^{2} for the other two methyl groups; and 2.833×10^{-40} g. cm.^{2} for the thiol group. The symmetry number is 3 for each of the methyl rotations and one for the other internal rotations and for over-all rotation.

Simple threefold cosine-type barriers to internal rotation were assumed for the thiol and methyl groups. Values of the barrier height were taken to be 1.5 kcal. mole^{-1} for the thiol group, as in other alkanethiols[8]; 3.4 kcal. mole^{-1} for the methyl group of the ethyl group, as in propane[9]; and 5.0 kcal. mole^{-1} for the other two methyl groups, the average of the values 5.1 kcal. mole^{-1} in 2-methyl-2-propanethiol[10] and 4.9 kcal. mole^{-1} in 3,3-dimethyl-2-thiabutane.[11] The analogy to 2-methyl-2-propanethiol and 3,3-dimethyl-2-thiabutane also was used to estimate the height of the lower barrier for rotation of the ethyl group as 5.0 kcal. mole^{-1}.

For the energy difference between the C_s and C_l conformations, the observed value of 0.25 ($\pm$0.25) kcal. mole^{-1}, determined from spectroscopic data as described in the Experimental section, was used. This value is reasonable in terms of the steric interactions involved. The C_l conformation involves one *gauche* *n*-butane interaction and one *gauche* 1-propanethiol interaction, whereas the C_s conformation involves two *gauche* *n*-butane interactions. A rough approximation to the energy difference would be the difference between a *gauche* *n*-butane interaction, 0.8 kcal. mole^{-1},[12] and a *gauche* 1-propanethiol interaction, 0.4 kcal. mole^{-1}.[13] This rough approximation to the energy difference, 0.4 kcal. mole^{-1}, lies within the limits set by the experimental observations.

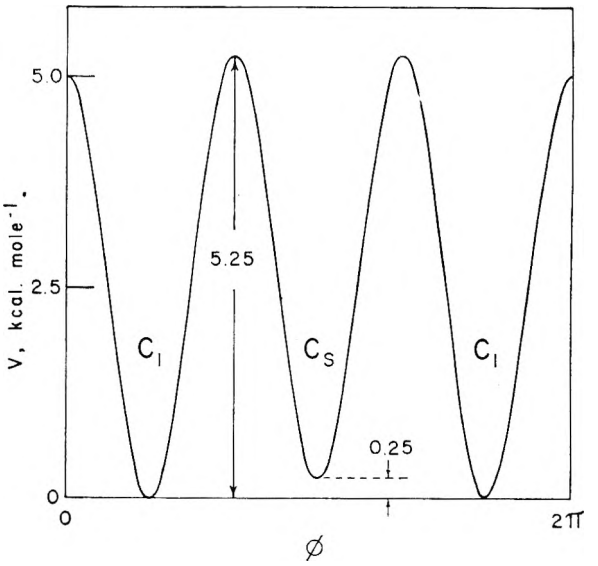

Fig. 2.—Potential energy function for internal rotation of the ethyl group in 2-methyl-2-butanethiol.

The complete potential energy function assumed for the ethyl rotation is illustrated in Fig. 2. The contributions to the thermodynamic functions were obtained from recently published tables for potential energy functions of this type.[14]

With the assumed potential barriers to internal rotation, all contributions to the entropy and heat capacity could be calculated except those of two vibrations and of vibrational anharmonicity. When an average value of 1290 cm.$^{-1}$ was taken for the two unobserved frequencies and no correction was made for vibrational anharmonicity, excellent agreement was obtained with the experimental values of entropy and heat capacity, as shown in Table II. As 1290 cm.$^{-1}$ is a reasonable value for the average of the two unobserved frequencies, the excellent agreement with the calorimetric data is evidence of the general correctness of the assumed potential barriers to internal rotation.

TABLE II

OBSERVED AND CALCULATED THERMODYNAMIC PROPERTIES OF 2-METHYL-2-BUTANETHIOL

	Entropy, $S°$, cal. deg.$^{-1}$ mole^{-1}			Heat capacity, $C_p°$, cal. deg.$^{-1}$ mole^{-1}	
T,°K.	Obsd.	Calcd.	T,°K.	Obsd.	Calcd.
330.22	96.11	96.12	360.25	39.54	39.54
349.77	98.28	98.30	381.20	41.25	41.27
372.29	100.73	100.77	410.20	43.59	43.60
			451.20	46.75	46.76
			500.20	50.31	50.29

Chemical Thermodynamic Properties.—The molecular parameters discussed in the previous sections were used in calculating the thermodynamic functions of 2-methyl-2-butanethiol for

(6) T. Kojima and T. Nishikawa, *J. Phys. Soc. Japan*, **12**, 680 (1957).

(7) J. E. Kilpatrick and K. S. Pitzer, *J. Chem. Phys.*, **17**, 1064 (1949).

(8) J. P. McCullough, H. L. Finke, D. W. Scott, M. A. Gross, J. F. Messerly, R. E. Pennington, and G. Waddington, *J. Am. Chem. Soc.*, **76**, 4796 (1954).

(9) K. S. Pitzer, *J. Chem. Phys.*, **12**, 310 (1944).

(10) J. P. McCullough, D. W. Scott, H. L. Finke, W. N. Hubbard, M. E. Gross, C. Katz, R. E. Pennington, J. F. Messerly, and G. Waddington, *J. Am. Chem. Soc.*, **75**, 1818 (1953).

(11) D. W. Scott, W. D. Good, S. S. Todd, J. F. Messerly, W. T. Berg, I. A. Hossenlopp, J. L. Lacina, A. Osborn, and J. P. McCullough, *J. Chem. Phys.*, **36**, 406 (1962).

(12) S. Mizushima, "Structure of Molecules and Internal Rotation," Academic Press, Inc., New York, N. Y., 1954, p. 98.

(13) R. E. Pennington, D. W. Scott, H. L. Finke, J. P. McCullough, J. F. Messerly, I. A. Hossenlopp, and G. Waddington, *J. Am. Chem. Soc.*, **78**, 3266 (1956).

(14) D. W. Scott and J. P. McCullough, Bureau of Mines Report of Investigation No. 5930 (1961).

TABLE III

THE MOLAL THERMODYNAMIC PROPERTIES OF 2-METHYL-2-BUTANETHIOL IN THE IDEAL GAS STATE[a]

T, °K.	$(F^\circ - H^\circ_0)/T$, cal. deg.$^{-1}$	$(H^\circ - H^\circ_0)/T$, cal. deg.$^{-1}$	$H^\circ - H^\circ_0$, kcal.	S°, cal. deg.$^{-1}$	C_p°, cal. deg.$^{-1}$	ΔHf°,[b] kcal.	ΔFf°,[b] kcal.	log Kf [b]
0	0	0	0	0	0	−37.59	−37.59	Infinite
273.15	69.49	20.07	5.483	89.56	32.21	−45.21	−10.53	8.42
298.15	71.30	21.18	6.316	92.48	34.30	−45.75	− 7.33	5.38
300	71.43	21.26	6.379	92.69	34.46	−45.79	− 7.10	5.17
400	78.15	25.60	10.24	103.75	42.79	−47.73	+ 6.10	− 3.33
500	84.32	29.81	14.91	114.13	50.28	−49.26	19.74	− 8.63
600	90.10	33.76	20.26	123.86	56.58	−50.42	33.66	−12.26
700	95.59	37.41	26.19	133.00	61.84	−51.25	47.74	−14.91
800	100.81	40.75	32.60	141.56	66.28	−51.81	61.92	−16.91
900	105.79	43.79	39.42	149.58	70.05	−52.13	76.16	−18.49
1000	110.55	46.59	46.59	157.14	73.30	−52.23	90.43	−19.76

[a] To retain internal consistency, some values in this table are given to one more decimal place than is justified by the absolute accuracy. [b] The standard heat, standard free energy, and common logarithm of the equilibrium constant for the formation of 2-methyl-2-butanethiol by the reaction, $5C(c, \text{graphite}) + 6H_2(g) + 1/2\,S_2(g) = C_5H_{12}S(g)$.

selected temperatures up to 1000°K.[15] The results are in columns 2–6 of Table III.

The calculated values of the thermodynamic functions, the experimental value of $\Delta Hf^\circ_{298.15}$ (−45.75 ± 0.23 kcal. mole^{-1}), and values of the thermodynamic functions of C(c, graphite),[16] $H_2(g)$,[16] and $S_2(g)$[17] were used in computing values of ΔHf°, ΔFf°, and log Kf. The results are in columns 7–9 of Table III.

Experimental

The basic experimental techniques used for 2-methyl-2-butanethiol are described in published accounts of apparatus and methods for low temperature calorimetry,[18] vapor flow calorimetry,[19] comparative ebulliometry,[20] and combustion calorimetry.[21] The reported values are based on a molecular weight of 104.212 g. mole^{-1} (1951 International Atomic Weights[22]), the 1951 values of the fundamental physical constants,[23] and the relations: 0° = 273.15°K.[24] and 1 cal. = 4.184 j. (exactly). Measurements of temperature were made with platinum resistance thermometers calibrated in terms of the International Temperature Scale[25] between 90 and 500°K. and the provisional scale[26] of the National Bureau of Standards between 11 an 90°K. All electrical and mass measurements were referred to standard devices calibrated at the National Bureau of Standards. The energy equivalent of the combustion calorimetric system, ε(Calor.), was determined by combustion of benzoic acid (NBS Sample 39g certified to evolve 26.4338 ± 0.0026 kj. per gram mass under specified conditions).

Material.—The sample of 2-methyl-2-butanethiol was part of the Standard Sample of Organic Sulfur Compound API–USBM 26, prepared at the Laramie (Wyo.) Petroleum Research Center of the Bureau of Mines.[27] The purity, determined by calorimetric studies of melting point as a function of fraction melted, was 99.89 ± 0.05 mole %.

Heat Capacity in the Solid and Liquid States.—The observed values of heat capacity, C_s, are listed in Table IV. Above 30°K., the accuracy uncertainty is estimated to be no greater than 0.2%. The crystals undergo an isothermal transition about 10° below the melting point, and the low temperature crystals (Crystals II) have a λ-like anomaly in the heat capacity that reaches a maximum at 145°K. Hysteresis in the thermal behavior was observed in the temperature region of the anomaly. The heat capacity of the liquid varies regularly with temperature and may be represented within 0.03% between 200 and 350°K. by the empirical equation

$$C_s(\text{liq}) = 53.373 - 0.14093T + 5.425 \times 10^{-4}T^2 - 4.6094 \times 10^{-7}T^3 \text{ cal. deg.}^{-1} \text{ mole}^{-1} \quad (1)$$

Heats and Temperatures of Fusion and Transition.—Two determinations of the heat of fusion, ΔHm, gave the values 145.25 and 145.51 cal. mole^{-1}; the accepted value is 145.4 ± 0.2 cal. mole^{-1}. Three determinations of the heat of transition, ΔHt, gave the values 1907.3, 1907.0, and 1907.0 cal. mole^{-1}; the accepted value is 1907.1 ± 0.2 cal. mole^{-1}. 2-Methyl-2-butanethiol is seen to belong to the class of substances with globular molecules for which the heat of transition is large and the heat of fusion small. The energy associated with the anomaly at 145°K. is only about 8 cal. mole^{-1}.

The results of two separate studies of the melting temperature, T_F, as a function of fraction of total sample melted, F, are reported in Table V. These results, which indicate that the impurity forms a solid solution with the major component, were treated by the method of Mastrangelo and Dornte.[28] Listed in Table V are the values obtained for the triple point temperature, T_{tp}; the mole fraction of impurity in the sample, N_2^*; the Henry's law constant for distribution of the impurity between the solid and liquid phases, K; and the cryoscopic constants,[29] $A = \Delta Hm/RT_{tp}^2$ and $B = 1/T_{tp} - \Delta Cm/2\Delta Hm$, calculated from the observed values of T_{tp}, ΔHm, and ΔCm (1.28 cal. deg.$^{-1}$ mole^{-1}).

The temperature for equilibrium between crystals I and II was studied as a function of per cent of total sample in the high temperature form (Crystals I) with the results: 20.42%,

(15) The vibrational contributions were computed by the Bureau of Mines Electronic Computer Service, Pittsburgh, Pa., and no corrections for vibrational anharmonicity were applied; the contributions of the methyl and thiol internal rotations were computed by Denver Electronic Computing Service, Inc., by two-way curvilinear interpolation in the tables of K. S. Pitzer and W. D. Gwinn, *J. Chem. Phys.*, **10**, 428 (1942).

(16) D. D. Wagman, J. E. Kilpatrick, W. J. Taylor, K. S. Pitzer, and F. D. Rossini, *J. Res. Natl. Bur. Std.*, **34**, 143 (1945).

(17) W. H. Evans and D. D. Wagman, *ibid.*, **49**, 141 (1952).

(18) H. M. Huffman, *Chem. Rev.*, **40**, 1 (1947); H. M. Huffman, S. S. Todd, and G. D. Oliver, *J. Am. Chem. Soc.*, **71**, 584 (1949); D. W. Scott, D. R. Douslin, M. E. Gross, G. D. Oliver, and H. M. Huffman, *ibid.*, **74**, 883 (1952).

(19) G. Waddington, S. S. Todd, and H. M. Huffman, *ibid.*, **69**, 22 (1947); J. P. McCullough, D. W. Scott, R. E. Pennington, I. A. Hossenlopp, and G. Waddington, *ibid.*, **76**, 4791 (1954).

(20) G. Waddington, J. W. Knowlton, D. W. Scott, G. D. Oliver, S. S. Todd, W. N. Hubbard, J. C. Smith, and H. M. Huffman, *ibid.*, **71**, 797 (1949).

(21) W. N. Hubbard, C. Katz, and G. Waddington, *J. Phys. Chem.*, **58**, 142 (1954).

(22) E. Wichers, *J. Am. Chem. Soc.*, **74**, 2447 (1952).

(23) F. D. Rossini, F. T. Gucker, Jr., H. L. Johnston, L. Pauling, and G. W. Vinal, *ibid.*, **74**, 2699 (1952).

(24) Some of the results originally were computed with constants and temperatures in terms of the relation 0° = 273.16°K. Only results affected significantly by the new definition of the absolute temperature scale [H. F. Stimson, *Am. J. Phys.*, **23**, 614 (1955)] were recalculated. Therefore, numerical inconsistencies, much smaller than the accuracy uncertainty, may be noted in some of the reported data.

(25) H. F. Stimson, *J. Res. Natl. Bur. Std.*, **42**, 209 (1949).

(26) H. J. Hoge and F. G. Brickwedde, *ibid.*, **22**, 351 (1939).

(27) J. C. Morris, W. J. Lanum, R. V. Helm, W. E. Haines, G. L. Cook, and John S. Ball, *J. Chem. Eng. Data*, **5**, 112 (1960).

(28) S. V. R. Mastrangelo and R. W. Dornte, *J. Am. Chem. Soc.*, **77**, 6200 (1955).

(29) A. R. Glasgow, A. J. Streiff, and F. D. Rossini, *J. Res. Natl. Bur. Std.*, **35**, 355 (1945).

TABLE IV

MOLAL HEAT CAPACITY OF 2-METHYL-2-BUTANETHIOL IN CAL. DEG.$^{-1}$

T, °K.[a]	C_s[c]	T, °K.[a]	ΔT[b]	C_s[c]	T, °K.[d]	ΔT[b]	C_s[c]
Crystals II		100.57	5.551	18.791	149.47	3.940	32.485[e]
		102.02	5.379	19.060	149.92	2.057	33.020[e]
12.43	1.075	103.01	5.401	19.226	151.92	1.956	35.161[e]
12.95	1.199	104.96	6.102	19.556	152.54	2.222	36.138[e]
13.69	1.398	106.00	5.317	19.747	153.80	1.815	38.624[d,e]
14.50	1.620	110.93	5.829	20.633			
15.06	1.786	116.64	5.586	21.715		Crystals I	
16.02	2.062	117.23	5.546	21.835			
16.47	2.204	122.11	5.362	22.816	160.73	2.083	40.696[d,e]
17.57	2.532	122.66	5.318	22.943	162.34	1.075	40.789[d,e]
17.96	2.653	127.37	5.151	23.972[e]	162.81	2.073	40.937[d,e]
19.30	3.062	127.87	5.106	24.110[e]	163.88	2.003	40.967[d,e]
19.67	3.170	131.19	4.879	24.917[e]	164.87	2.066	41.028[d,e]
21.17	3.635	131.41	4.966	24.969[e]	165.87	1.995	41.065[d,e]
21.58	3.763	132.90	5.909	25.341[e]			
23.23	4.236	135.97	4.675	26.279[e]		Liquid	
23.73	4.397	136.27	4.755	26.346[e]			
26.23	5.119	137.37	3.388	26.711[e]	171.53	3.905	42.671
26.32	5.147	138.64	5.582	27.213[e]	176.72	6.481	42.753
28.69	5.778	140.09	2.042	27.811[e]	179.50	10.501	42.809
31.47	6.498	140.79	4.533	28.144[e]	183.19	6.453	42.858
34.74	7.249	140.96	2.045	28.209[e]	189.62	6.419	42.982
38.56	8.034	141.69	2.047	28.185[e]	189.96	10.420	42.984
42.83	8.861	142.09	1.983	28.900[e]	200.54	10.404	43.206
47.48	9.705	142.89	1.952	29.517[e]	210.89	10.317	43.454
53.24	10.703	143.27	1.126	28.925[e]	221.16	10.229	43.744
54.10	10.841	144.02	1.896	30.543[e]	231.34	10.134	44.095
54.27	10.881	144.31	.953	29.384[e]	241.43	10.037	44.466
57.34	11.398	144.80	1.875	31.033[e]	251.91	10.922	44 922
59.81	11.816	144.88	1.901	31.012[e]	262.77	10.804	45.436
60.00	11.849	144.95	1.399	29.641[e]	273.51	10.667	45.990
61.74	12.155	145.25	.938	29.978[e]	274.54	9.608	46.039
65.74	12.828	145.41	.901	31.176[e]	280.21	10.365	46.332
71.48	13.768	145.79	1.940	30.205[e]	290.51	10.238	46.921
77.25	14.740	146.17	.924	30.550[e]	300.69	10.116	47.508
83.04	15.769	146.32	1.371	30.406[e]	301.23	9.326	47.552
88.91	16.790	146.79	2.148	30.913[e]	305.73	9.996	47.800
89.19	16.858	146.92	2.145	30.951[e]	310.96	10.126	48.164
91.67	17.258	147.70	2.147	31.285[e]	315.67	9.872	48.452
94.88	17.807	147.80	1.605	31.348[e]	325.92	10.636	49.118
96.51	18.085	147.83	2.145	31.347[e]	336.48	10.486	49.812
97.48	18.249	148.82	2.100	31.930[e]	346.89	10.335	50.534

[a] T is the mean temperature of each heat capacity measurement. [b] ΔT is the temperature increment of each heat capacity measurement. [c] C_s is the heat capacity of the condensed phase at saturation pressure. [d] Results for the solid are not corrected for the effect of premelting due to the presence of impurities. [e] Correction applied to mean heat capacity for curvature.

158.79°K.; 46.52%, 158.98°K.; and 77.78%, 159.06°K. The transition temperature was taken to be 159.1 ± 0.1°K.

Thermodynamic Properties in the Solid and Liquid States.—Values of thermodynamic functions for the condensed phases were computed from the calorimetric data for selected temperatures between 10 and 350°K. The results are in Table VI. The values at 10°K. were computed from a Debye function for 5.5 degrees of freedom with $\theta = 112.7°$; these parameters were evaluated from the heat capacity data between 12 and 20°K. Corrections for the effects of premelting have been applied to the "smoothed" data in Table VI.

Vapor Pressure.—Values of vapor pressure determined by comparative ebulliometry with water as the reference substance are in Table VII. These values were obtained in the second of two attempts to measure the vapor pressure. The first attempt was abandoned when the compound started to decompose with formation of highly volatile impurity, but the second attempt with a fresh sample was carried through without any detectable decomposition.

The different stability of the 2 samples is not understood. Intermittent tests for decomposition of the second sample were made by repeating measurements at the lowest pressure after each measurement at a higher pressure. In 14 such replicate determinations, the observed boiling points deviated from the mean at most 0.005° and seldom more than 0.002°. The difference between the ebullition and condensation temperatures of the sample at 1 atm. pressure was less than 0.001°. The Antoine and Cox equations selected to represent the results are

$$\log p = 6.82837 - 1254.885/(t + 218.759) \quad (2)$$

$$\log (p/760) = A(1 - 372.280/T) \quad (3)$$

$$\log A = 0.841629 - 7.4895 \times 10^{-4}T + 7.3565 \times 10^{-7}T^2$$

In these equations, p is in mm., t is in °C., and T is in °K. Observed and calculated vapor pressures for both equations are compared in Table VII. The normal boiling point calculated from either equation is 99.13° (372.28°K.).

Heat of Vaporization, Vapor Heat Capacity, and Effects of Gas Imperfection.—The experimental values of heat of vaporization and vapor heat capacity are in Tables VIII and

IX. The estimated accuracy uncertainty of the values of ΔHv and $C_p°$ are 0.1 and 0.2%, respectively. These values were obtained in the second of two attempts to do vapor flow calorimetry of 2-methyl-2-butanethiol. The first attempt, like the first attempt to study the vapor pressure, was abandoned because of decomposition of the sample. The sample used for the first attempt was somewhat less pure than the one used for the second, successful attempt, but the decomposition of the first sample was not necessarily related to the impurity. Tests for effects of any decomposition of the second sample were made from time to time during the vapor flow calorimetry. Although evolution of minute traces of H_2S was detected as measurements were made at progressively higher temperatures, no other evidence of decomposition was observed until the heat capacity was determined at the highest temperature, 500.2°K. During the heat capacity measurements at 500.2°K., the vapor pressure of the sample in the vaporizer increased significantly (7 mm. at 760 mm. total pressure) as if a decomposition product of higher volatility than 2-methyl-2-butanethiol was being formed. Tests for vapor phase decomposition in the flow calorimeter, made as described previously,[19] showed that decomposition was affecting slightly the results at 500.2°K. Afterwards, similar tests showed no detectable decomposition occurred at 381.2°K. A repeat measurement of the heat capacity at 381.2°K. gave results that agreed within 0.1% with those obtained before the high temperature measurements had been made. The results at 500.2°K. in Table IX were obtained after all the other reported results and so are the only ones possibly affected by decomposition. The value of $C_p°$ at 500.2°K. was not used in selecting the molecular parameters used in calculating thermodynamic functions. Nevertheless, the experimental value at that temperature agrees well enough with the calculated value to indicate that the effect of decomposition was small even under the most severe conditions.

The equation selected to represent the heat of vaporization as a function of temperature is

$$\Delta Hv = 11052 - 4.368T - 1.292 \times 10^{-2}T^2 \text{ cal. mole}^{-1} \quad (330\text{–}373°\text{K.}) \quad (4)$$

The effects of gas imperfection were correlated by the procedure described in an earlier paper.[30] The empirical

TABLE V

2-METHYL-2-BUTANETHIOL: MELTING POINT SUMMARY

T_{tp} = 169.37 ± 0.10°K.; N_2* = 0.0011 ± 0.0005 mole fraction; K = 0.221; A = 0.002552 deg.$^{-1}$; B = 0.001490 deg.$^{-1}$

Series	F	$[F + K/(1 - K)]^{-1}$	T_F, °K.	T_{calcd}, °K.
I	0.0999	2.607	168.260	168.264
I	.1735	2.187	168.439	168.441
II	.3227	1.649	168.673	168.668
I	.3843	1.497	168.729	168.733
II	.4298	1.402	168.773	168.773
II	.5834	1.153	168.877	168.878
I	.6333	1.091	168.901	168.904
II	.7459	.971	168.955	168.955
I	.8650	.871	168.998	168.997
II	.9472	.812	169.032	169.022
	1.0000	.779		169.036
	Pure			169.365

TABLE VI

THE MOLAL THERMODYNAMIC PROPERTIES OF 2-METHYL-2-BUTANETHIOL IN THE SOLID AND LIQUID STATES[a]

T, °K.	$-(F_s - H°_0)/T$, cal. deg.$^{-1}$	$(H_s - H°)/T$, cal. deg.$^{-1}$	$H_s - H°_0$, cal.	S_s, cal. deg.$^{-1}$	C_s, cal. deg.$^{-1}$
		Crystals I			
10	0.050	0.148	1.480	0.198	0.588
15	.164	.471	7.066	.635	1.764
20	.366	.982	19.630	1.348	3.273
25	.649	1.591	39.77	2.240	4.764
30	.996	2.235	67.04	3.231	6.123
35	1.389	2.877	100.70	4.266	7.304
40	1.814	3.495	139.80	5.309	8.321
45	2.260	4.084	183.79	6.344	9.262
50	2.720	4.646	232.31	7.366	10.142
60	3.661	5.705	342.3	9.366	11.848
70	4.617	6.703	469.2	11.320	13.524
80	5.575	7.660	612.8	13.235	15.220
90	6.531	8.598	773.8	15.129	16.973
100	7.485	9.521	952.1	17.006	18.690
110	8.435	10.435	1147.8	18.870	20.470
120	9.382	11.349	1361.9	20.731	22.378
130	10.327	12.280	1596.4	22.607	24.614
140	11.273	13.262	1856.7	24.535	27.760
145	11.748	13.837	2006.4	25.585	37.5
145	11.748	13.837	2005.4	25.585	29.74
150	12.226	14.417	2162.6	26.643	33.04
155	12.710	15.108	2341.8	27.818	38.92
159.1	13.112	15.791	2512.3	28.903	44.20
		Crystals II			
159.1	13.11	27.775	4419	40.89	40.56
160	13.27	27.850	4455	41.12	40.64
169.3	14.87	28.571	4837	43.44	41.36
		Liquid			
169.3	14.87	29.427	4982	44.30	42.64
170	14.99	29.482	5012	44.47	42.65
180	16.69	30.22	5440	46.91	42.81
190	18.34	30.89	5869	49.23	42.99
200	19.94	31.50	6299	51.44	43.20
210	21.49	32.06	6733	53.55	43.43
220	23.00	32.58	7168	55.58	43.72
230	24.46	33.07	7607	57.53	44.05
240	25.87	33.54	8049	59.41	44.42
250	27.25	33.98	8496	61.24	44.84
260	28.59	34.41	8946	63.00	45.31
270	29.90	34.82	9402	64.72	45.80
273.15	30.31	34.95	9547	65.26	45.96
280	31.18	35.22	9862	66.40	46.33
290	32.41	35.62	10,329	68.03	46.88
298.15	33.41	35.93	10,713	69.34	47.36
300	33.63	36.00	10,800	69.63	47.48
310	34.82	36.38	11,278	71.20	48.09
320	35.98	36.76	11,762	72.74	48.74
330	37.11	37.13	12,253	74.24	49.38
340	38.23	37.50	12,750	75.73	50.05
350	39.32	37.87	13,254	77.19	50.75

[a] The values tabulated are the free energy function, heat content function, heat content, entropy, and heat capacity of the condensed phases at saturation pressure.

TABLE VII

VAPOR PRESSURE OF 2-METHYL-2-BUTANETHIOL

Boiling point, °C. Water	2-Methyl-2-butanethiol	p(obsd.),[a] mm.	p(obsd.) − p(calcd.), mm. Antoine eq. 2	Cox eq. 3
60.000	50.888	149.41	−0.01	0.00
65	56.725	187.57	.00	.00
70	62.625	233.72	+ .01	+ .01
75	68.578	289.13	.01	− .01
80	74.579	355.22	.05	+ .02
85	80.638	433.56	.04	− .01
90	86.749	525.86	.04	− .02
95	92.914	633.99	.00	− .05
100	99.132	760.00	− .03	− .04
105	105.401	906.06	− .05	+ .01
110	111.728	1074.6	− .1	.0
115	118.106	1268.0	− .2	.0
120	124.537	1489.1	− .2	.0
125	131.021	1740.8	+ .1	+ .1
130	137.559	2026.0	+ .4	.0

[a] From the vapor pressure data for water given by N. S. Osborne, H. F. Stimson, and D. C. Ginnings, *J. Res. Natl. Bur. Std.*, **23**, 261 (1939).

(30) J. P. McCullough, H. L. Finke, J. F. Messerly, R. E. Pennington, I. A. Hossenlopp, and G. Waddington, *J. Am. Chem. Soc.*, **77**, 6119 (1955).

TABLE VIII

THE MOLAL HEAT OF VAPORIZATION AND SECOND VIRIAL COEFFICIENT OF 2-METHYL-2-BUTANETHIOL

T, °K.	P, atm.	ΔHv, cal.	B(obsd.), cc.	B(calcd.), cc.[a]
330.21	0.250	8092 ± 1[b]	−1705	−1722
349.76	.500	7821 ± 2[b]	−1478	−1479
372.28	1.000	7497 ± 2[b]	−1263	−1259

[a] Calculated from eq. 5. [b] Maximum deviation from the mean of three determinations.

TABLE IX

THE MOLAL VAPOR HEAT CAPACITY OF 2-METHYL-2-BUTANETHIOL IN CAL. DEG.$^{-1}$

T, °K.	360.20	381.20	410.20	451.20	500.20
C_p(1.000 atm.)		42.069	44.171	47.145	50.563
C_p(0.500 atm.)	40.026	41.628			
C_p(0.250 atm.)	39.779	41.445	43.732	46.848	50.373
$C_p°$	39.54	41.25	43.59	46.75	50.31
$-TB''$ (obsd.)[a]	0.92	0.76	0.54	0.38	0.24
$-TB''$ (calcd.)[b]	0.94	0.73	0.54	0.36	0.24

[a] $-TB'' = -T(d^2B/dT^2)$, cal. deg.$^{-1}$ mole^{-1} atm.$^{-1}$. [b] Calculated from eq. 5.

equation for B, the second virial coefficient in the equation of state, $PV = RT(1 + B/V)$, is

$$B = 453 - 261.2 \exp(700/T) \text{ cc. mole}^{-1} \quad (330\text{–}500°\text{K.}) \quad (5)$$

"Observed" values of B and $-T(d^2B/dT^2) = \lim_{P\to 0}(\partial C_p/\partial P)_T$ and those calculated from eq. 5 are compared in Tables VIII and IX.

The heat of vaporization at 298.15°K. was calculated by extrapolation with eq. 4 (8.51 kcal. mole^{-1}), by using the Clapeyron equation with eq. 3 and 5 (8.52 kcal. mole^{-1}) and by use of a thermodynamic network with the thermodynamic functions of Table III (8.53 kcal. mole^{-1}). From the last value, selected as the most reliable, and eq. 5, the standard heat of vaporization was calculated, $\Delta Hv°_{298.15} = 8.54$ kcal. mole^{-1}.

Entropy in the Ideal Gas State.—The entropy in the ideal gas state at 1 atm. pressure was calculated as shown in Table X.

TABLE X

THE MOLAL ENTROPY OF 2-METHYL-2-BUTANETHIOL IN THE IDEAL GAS STATE IN CAL. MOLE^{-1}

	T, °K. 330.22	349.77	372.29
S_s(liq.)	74.28[a]	77.16[a]	80.37[b]
$\Delta Hv/T$	24.50	22.36	20.14
S(ideal) − S(real)[c]	0.09	0.14	0.22
$R \ln P$[d]	−2.76	−1.38	0.00
$S°$(obsd.) ± 0.20[e]	96.11	98.28	100.73

[a] By interpolation in Table VI. [b] Extrapolated by use of eq. 1. [c] The entropy in the ideal gas state less than in the real gas state, calculated from eq. 5. [d] Entropy of compression, calculated from eq. 3. [e] Estimated accuracy uncertainty.

Heat of Combustion and Formation.—Results of a typical determination of the heat of combustion of 2-methyl-2-butanethiol are given in detail in Table XI. The symbols and abbreviations are those of Hubbard, Scott, and Waddington,[31] except as noted. The results of all experiments are summarized in Table XII.

The derived results in Table XIII were computed by use of the values of $\Delta Hc°$, $\Delta Hv°$, S_s, and $S°$ for 2-methyl-2-butanethiol and literature values of the standard heat of formation of CO_2(g),[32] H_2O(liq),[16] $H_2SO_4 \cdot 80H_2O$(liq) [−212.07 kcal. mole^{-1}],[33] and S_2(g)[17] and of the standard entropy of graphite,[16] hydrogen gas,[16] rhombic sulfur,[17] and diatomic sulfur gas,[17] all at 298.15°K.

TABLE XI

SUMMARY OF A TYPICAL COMBUSTION CALORIMETRIC EXPERIMENT WITH 2-METHYL-2-BUTANETHIOL[a]

m' (2-methyl-2-butanethiol), g.	0.77067
$\Delta t_c = t_f - t_i - \Delta t_{corr.}$, deg.	1.99550
$\mathcal{E}$(Calor.) $(-\Delta t_c)$, cal.	−7800.63
$\mathcal{E}$(Cont.) $(-\Delta t_c)$,[b] cal.	− 27.66
$\Delta E_{ign.}$, cal.	1.35
$\Delta E'_{decomp.}$ (HNO_3 + HNO_2), cal.	10.94
ΔE, corr. to st. states,[c] cal.	2.52
$-m''\ \Delta Ec°/M$ (auxiliary oil), cal.	533.48
$-m'''\ \Delta Ec°/M$ (fuse), cal.	15.26
$m'\ \Delta Ec°/M$ (2-methyl-2-butanethiol), cal. g.$^{-1}$	−7264.74
$\Delta Ec°/M$ (2-methyl-2-butanethiol), cal. g.$^{-1}$	−9426.52

[a] Auxiliary data: $\mathcal{E}$(Calor.) = 3909.11 cal. deg.$^{-1}$; V (Bomb) = 0.347 l.; $\Delta Ec°/M$ (auxiliary oil) = 10983.8 cal. g.$^{-1}$; $\Delta Ec°/M$ (fuse) = 3923 cal. g.$^{-1}$; physical properties at 25° of 2-methyl-2-butanethiol, ρ = 0.82119 g. ml.$^{-1}$,[27] $(\partial E/\partial P)_T = -0.011$ cal. g.$^{-1}$ atm.$^{-1}$, and C_p = 0.454 cal. deg.$^{-1}$ g.$^{-1}$. [b] $\mathcal{E}'$(Cont.)$(t_i - 25°) + \mathcal{E}'$(Cont.)$(25° - t_f + \Delta t_{corr.})$. [c] Items 81–85, incl., 87–91, incl., 93, and 94 of the computation form of ref. 31.

TABLE XII

SUMMARY OF RESULTS OF COMBUSTION CALORIMETRY AT 298.15°K.[a]

$\Delta Ec°/M$, cal. g.$^{-1}$	−9429.13, −9425.56, −9428.01, −9426.52, −9423.47, −9425.90, −9428.17
Mean and std. dev.	−9426.68 ± 0.73 cal. g.$^{-1}$
$\Delta Ec°_{298.15}$	−982.37 ± 0.19[b] kcal. mole^{-1}
$\Delta Hc°_{298.15}$	−985.04 ± 0.19[b] kcal. mole^{-1}

[a] These results apply to the idealized combustion reaction: $C_5H_{12}S$(liq) + $19/2O_2$(g) + $75H_2O$(liq) = $5CO_2$(g) + $H_2SO_4 \cdot 80H_2O$(liq). [b] The uncertainty interval equal to twice the final "over-all" standard deviation [F. D. Rossini, "Experimental Thermochemistry," Interscience Publishers, Inc., New York, N. Y., 1956, Chapter 14, pp. 297–320].

TABLE XIII

MOLAL THERMODYNAMIC PROPERTIES OF FORMATION OF 2-METHYL-2-BUTANETHIOL AT 298.15°K.[a]

Reference state	Ref. state of sulfur	$\Delta Hf°$, kcal.	$\Delta Sf°$, cal. deg.$^{-1}$	$\Delta Ff°$, kcal.	log Kf
Liquid	S(c, rhombic)	−38.87 ± 0.21	−132.35	0.59	−0.43
Gas	S(c, rhombic)	−30.33 ± 0.22	−109.21	2.23	−1.64
Gas	S_2(g)	−45.75 ± 0.23	−128.85	−7.33	5.38

[a] For the reaction:

$$5C(c, \text{ graphite}) + 6H_2(g) + \begin{matrix}\text{S(c, rhombic)}\\ \text{or}\\ 1/2\ S_2(g)\end{matrix} = C_5H_{12}S \text{ (liq or g).}$$

Special Infrared Spectroscopic Studies.—The spectrum of crystalline 2-methyl-2-butanethiol at liquid nitrogen temperature was determined in a low temperature infrared cell similar to the one described by Bürer.[34] However, cesium bromide windows were used so that spectra could be observed to 35 μ. The spectrum was determined from 2 to 15 μ with a Perkin–Elmer Model 21 spectrometer with sodium chloride optics and from 15 to 35 μ with a Perkin–Elmer Model 112 spectrometer with cesium bromide optics.[35]

The energy difference between the rotational isomers was

(31) W. N. Hubbard, D. W. Scott, and G. Waddington, "Experimental Thermochemistry," F. D. Rossini, Editor, Interscience Publishers, Inc., New York, N. Y., 1956, Chapter 5, pp. 75–128.

(32) E. J. Prosen, R. S. Jessup, and F. D. Rossini, *J. Res. Natl. Bur. Std.*, **33**, 447 (1944).

(33) W. D. Good, J. L. Lacina, and J. P. McCullough, *J. Am. Chem. Soc.*, **82**, 5589 (1960).

(34) T. Bürer, thesis, "Infrarot-Spektren von Cyclanonen," Eidg. Tech. Hochschule, Zürich, Switzerland, 1958.

(35) C. A Frenzel, D. W. Scott, and J. P. McCullough, Bureau of Mines Report of Investigation No. 5658 (1960).

studied by determining the ratio of intensity of the infrared bands of the liquid at 577 cm.$^{-1}$ (C_l) and 628 cm.$^{-1}$ (C_s) as a function of temperature. The low temperature cell also was used in these studies of the temperature dependence of the liquid state spectrum. Determinations were made at the temperatures obtained with solid carbon dioxide and with nearly boiling water as well as at room temperature. Values found for the ratio of the integrated intensities of the 577 and 628 cm.$^{-1}$ bands are 3.6 at about 195°K., 2.6 at about 298°K., and 2.9 at about 368°K. The variation with temperature is scarcely more than the experimental uncertainty and indicates that the rotational isomers have nearly the same energy. The value taken for the energy difference was 0.25 ± 0.25 kcal. mole^{-1} with the C_l isomer more stable. This value was determined for the liquid state but, as the rotational isomers must have small and nearly equal dipole moments, the energy difference is nearly the same in the gaseous state.

Acknowledgments.—The assistance of F. R. Frow and C. A. Frenzel in some of these experiments is gratefully acknowledged.

EQUIVALENT CONDUCTANCE AND IONIC ASSOCIATION IN AQUEOUS THALLOUS HYDROXIDE SOLUTIONS AT 25°

BY W. T. LINDSAY, JR.

Chemistry Department, Westinghouse Research Laboratories, Pittsburgh 35, Pennsylvania

Received February 8, 1962

Previous measurements on thallous hydroxide solutions by Ostwald (1887) and Hlasko and Salitowna (1935) appear to be in error, probably because of carbon dioxide difficulties. By exclusion of CO_2, it has been possible to determine the equivalent conductance at 25° with reasonable precision from 10^{-3} to 10^{-2} *M*. The phoreogram is catabatic in this range. Application of the Fuoss-Onsager equation, with an assumed value of 3.0 Å. for the ion size parameter, gives 273.0 ± 0.3 for Λ_0 and 3.0 ± 0.3 for K_a (95% confidence limits). The Λ_0 value is in good agreement with that obtained from limiting ionic conductance data. The association constant is close to that obtained by Bell and Prue from reaction kinetic measurements, but is about one-half that derived by Bell and George from solubility equilibria and by Bell and Panckhurst from other kinetic measurements.

Introduction

Ionic association in thallous hydroxide solutions is of some interest because of the unreasonably small values obtained for the "distance of closest approach" when experimental values of the association constant are used in the standard Bjerrum treatment.[1] The discrepancy originally was ascribed to covalent bonding, but n.m.r.[2] and Raman[3,4] spectra studies seem to indicate that only electrostatic interactions occur. There also are discrepancies among values of the association constant obtained by various experimental methods. The reaction-kinetic measurements of Bell and Prue[5] gave 2.63, solubility equilibria results of Bell and George[6] gave 6.7, and other reaction-kinetic experiments by Bell and Panckhurst[7] gave 7.1, all at 25°.

Conductivity data can be used to determine the association constant, but previous measurements on thallous hydroxide by Ostwald[8] and Hlasko and Salitowna[9] appear to be in error. As shown in Fig. 1, the trend of the Ostwald data is symptomatic of carbon dioxide interference. Although Hlasko and Salitowna attempted to eliminate this interference by precipitation of $BaCO_3$, their results evidently contain a systematic error, as indicated by the anomalous slope and curvature of the phoreogram and by comparison with the sum of ionic conductances at infinite dilution. There is a corresponding systematic error in the Hlasko and Salitowna data on sodium hydroxide, potassium hydroxide, and lithium hydroxide, where comparison can be made with the more accurate results of Darken and Meier[10] and Sivertz, Reitmeier, and Tartar.[11]

The purpose of the present work was to obtain more accurate values for the equivalent conductance of dilute thallous hydroxide solutions at 25° by attempting to exclude carbon dioxide, and to determine the association constant from the results.

Experimental

Two series of experiments were undertaken. For each series, fresh thallous hydroxide stock solutions, approximately 0.075 *M*, were prepared by bubbling carbon dioxide-free oxygen through de-ionized water in a closed system containing subdivided thallium metal which previously had been washed repeatedly with boiling de-ionized water. Spectrographic analyses of the subdivided metal showed the absence of any substantial concentrations of impurities. After dissolution of a major part of the metal, the resulting solution was decanted by gas pressure into a purged polyethylene storage bottle, where it was kept in the dark under carbon dioxide-free nitrogen pressure. Provision was made for withdrawal of solution from the storage bottle by hypodermic syringe. The stock solutions were analyzed at several intervals during their use by weight potentiometric titrations of triplicate samples against potassium acid phthalate primary standard. The TlOH solution was added from a hypodermic syringe which could be weighed rapidly and repeatedly by a projection-type analytical balance, while a stream of nitrogen was used to keep carbon dioxide

(1) C. W. Davies, *Discussions Faraday Soc.*, **24**, 83 (1957); C. W. Davies in "The Structure of Electrolytic Solutions," W. J. Hamer, Ed., John Wiley and Sons, New York, N. Y., 1959, p. 31; R. P. Bell and M. H. Panckhurst, *Rec. trav. chim.*, **75**, 725 (1956).

(2) R. Freeman, R. P. H. Gasser, R. E. Richards, and D. H. Wheeler, *Mol. Phys.*, **2**, 75 (1959); R. P. H. Gasser and R. E. Richards, *ibid.*, **2**, 357 (1959); R. Freeman, R. P. H. Gasser, and R. E. Richards, *ibid.*, **2**, 301 (1959).

(3) J. H. B. George, J. A. Rolfe, and L. A. Woodward, *Trans. Faraday Soc.*, **49**, 375 (1953).

(4) P. L. Goggins and L. A. Woodward, *ibid.*, **56**, 1591 (1960).

(5) R. P. Bell and J. E. Prue, *J. Chem. Soc.*, 362 (1949).

(6) R. P. Bell and J. H. B. George, *Trans. Faraday Soc.*, **49**, 619 (1953).

(7) R. P. Bell and M. H. Panckhurst, *J. Chem. Soc.*, 2836 (1956).

(8) W. Ostwald, "Lehrbuch der Allgemeinen Chemie," Engelman, Leipzig, 1891.

(9) M. Hlasko and A. Salitowna, *Roczniki Chem.*, **14**, 1038 (1934); **15**, 273 (1935).

(10) L. S. Darken and H. F. Meier, *J. Am. Chem. Soc.*, **64**, 621 (1942).

(11) V. Sivertz, R. E. Reitmeier, and H. V. Tartar, *ibid.*, **62**, 1379 (1940).

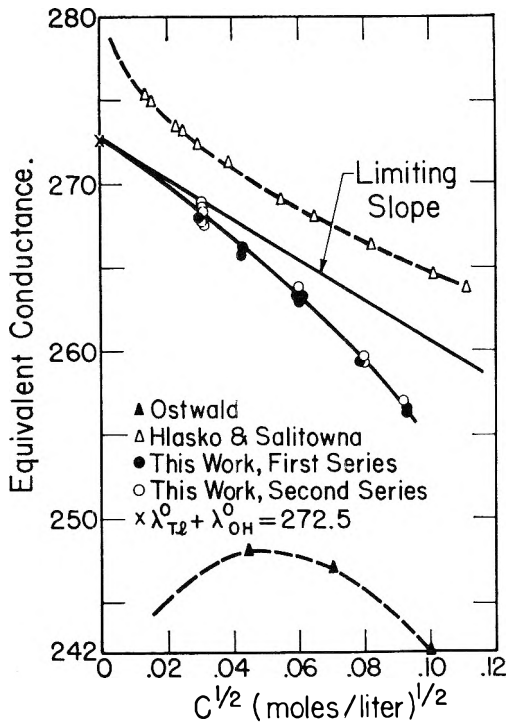

Fig. 1.—Equivalent conductance of TlOH at 25°.

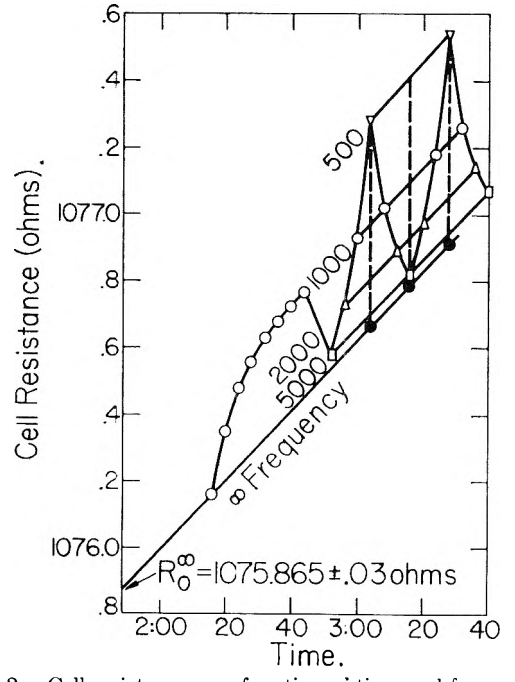

Fig. 2.—Cell resistance as a function of time and frequency. Run no. 7-C-2

from the surface of the solution being titrated. The average deviation for a typical set of triplicate samples was about 1 part in 5000.

Immediately before use, diluted solutions ranging from 10^{-4} to 10^{-2} M were prepared on a weight basis by injecting an appropriate amount of stock solution into a sealed, nitrogen-purged, polyethylene bottle, containing a known weight of de-ionized water. (All polyethylene ware was pretreated by steaming at 80° in 1 N NaOH for several days, followed by repeated rinsing and extended storage while soaking in de-ionized water.) The diluted solutions were transferred to the conductivity cell by a simple closed system using a three-way stopcock which allowed the following operations to be carried out in sequence with minimum delay: (1) purging of the cell with carbon dioxide-free nitrogen, (2) pressurization of the sealed solution bottle by injection of nitrogen, and (3) transfer of solution from the pressurized bottle to the cell with overflow of about two cell volumes. The cell then was isolated in the usual manner and immersed in an oil bath held at 25.00° to a constancy of a few thousandths of a degree. Temperatures were determined by a platinum resistance thermometer which had been calibrated against the laboratory standard.

The conductivity cell was of the Jones type[12] with a cell constant nominally 1.0. A Jones-type conductivity bridge[13,14] (Leeds and Northrup Model 4636) was used for all measurements, in connection with a variable frequency oscillator, a General Radio Model 1231-BRF amplifier and tuned filter, and an oscilloscope detector. The conductivity cell was calibrated with KCl solutions in the same conductance range as the thallous hydroxide solutions, using identical procedures. The equation of Lind, Zwolenick, and Fuoss[15] for the conductance of dilute KCl solutions was used as the basis of the calibration.

Preliminary experiments with platinized electrodes gave an excessive rate of rise of cell resistance, presumably due in part to adsorption on the electrodes. All subsequent measurements were made with bright platinum electrodes, resulting in a considerable reduction of this effect, but not in its elimination. However, the use of bright electrodes introduced a frequency effect. Consequently, the experimental sequence illustrated in Fig. 2 was adopted for these measurements. The equilibration of the cell at the thermostat temperature was followed by a series of initial measurements at 1000 c.p.s. When equilibration was complete, as indicated by a continuing linear rise of resistance at a rate expected for the concentration range, measurements were made at equally spaced time intervals in a planned sequence among frequencies of 500, 1000, 2000, and 5000 c.p.s. Since previous experience had shown that the resistance rise continued linearly for a period of time very much longer than required for the measurement sequence, the results were averaged, as indicated in Fig. 2, to give interpolated resistance values for each frequency at each of three reference times. These values were extrapolated to infinite frequency, as described below, and then extrapolated back to the time of filling of the cell. The error indicated in Fig. 2 for R_0^∞, the infinite frequency, zero-time resistance, is an estimate of the uncertainty introduced by the double extrapolation procedure and is not otherwise related to the accuracy or precision of the results.

The frequency dependence of cell resistance ranged from a linear function of f^{-1} at the higher concentrations to a linear function of $f^{-1/2}$ at the lower concentrations. Consequently, neither function was used for extrapolation. Instead, an equation of the form

$$R = R^\infty + A/(1 + Bf^{\frac{1}{2}}) \qquad (1)$$

was used, where R is the cell resistance at some frequency f, R^∞ is the resistance at infinite frequency, and A and B are constants for a given electrode condition and solution composition and concentration. Feates, Ives, and Pryor[16] have discussed the application of this equation to electrolytic conductance cells. It is based on an electrode model proposed by Grahame,[17] and, according to Grahame's discussion, should be applicable to TlOH in the concentration range covered in these measurements. All measurements at about the same concentration were combined to calculate an average value of B. Plots of R against $1/(1 + B_{av}f^{\frac{1}{2}})$ for each run showed that the 5000, 2000, and 1000 c.p.s. points fell quite accurately on a straight line, but that the 500 c.p.s. points generally fell somewhat above the line determined by the other three points. Accordingly, the value of R^∞ was determined by a least squares treatment of the data for the three higher frequencies only. Values of faradaic resistance and electrode capacitance estimated from the constants A

(12) G. Jones and G. M. Bollinger, *J. Am. Chem. Soc.*, **53**, 411 (1931).
(13) G. Jones and R. C. Josephs, *ibid.*, **50**, 1049 (1928).
(14) P. H. Dike, *Rev. Sci. Instr.*, **2**, 379 (1931).
(15) J. E. Lind, Jr., J. J. Zwolenick, and R. M. Fuoss, *J. Am. Chem. Soc.*, **81**, 1557 (1959).
(16) F. S. Feates, D. J. G. Ives, and J. H. Pryor, *J. Electrochem. Soc.*, **103**, 580 (1956).
(17) D. C. Grahame, *ibid.*, **99**, 370C (1952).

and B varied with concentration, but fell in the range indicated as reasonable by Feates, Ives, and Pryor.

Blank runs were made by following exactly the same procedure used for the solution runs, with the exception that an equivalent quantity of de-ionized water (rather than stock solution) was injected into the dilution bottles. The average conductance found for the blank runs was 0.27 μmho. When compared with a reading of 0.065 μmho obtained when the cell was filled directly from the source of de-ionized water, this result indicates that there was some pick-up of ionized contamination in the purging, dilution, or transfer procedures. It was assumed that the blank run conductance was due primarily to carbon dioxide, and correction was made according to the method of Jeffrey and Vogel.[18] This correction amounted to 1 part in 500 at 10^{-3} M and 1 part in 5000 at 9×10^{-3} M. All results at less than 10^{-3} M were eliminated from further consideration by the large correction at lower concentrations.

Results

The equivalent conductances were calculated in the usual way from the corrected, extrapolated resistance values, assuming that the density of the solutions could be estimated with sufficient accuracy by the approximate relation

$$d = d_0 + M_2 m/1000 \qquad (2)$$

where d is the density of the solution, d_0 is the density of pure water, M_2 is the molecular weight of TlOH, and m is the TlOH concentration in moles/kg. H_2O. The results from a total of 30 runs at concentrations from about 10^{-3} to about 9×10^{-3} M, 9 in the first series and 21 in the second series of measurements, are given in Table I. The phoreogram is plotted in Fig. 1. Although the experimental precision is not as good as can be achieved for solutions of acids or neutral salts, the results are a considerable improvement over previous measurements on TlOH solutions. The curve approaches the correct limiting slope and extrapolates to infinite dilution at a value very close to that indicated for the sum of limiting ionic conductances. The phoreogram is catabatic, as would be expected for a slightly associating solute.

TABLE I

EQUIVALENT CONDUCTANCES OF THALLOUS HYDROXIDE SOLUTIONS AT 25°

10^4c (moles/l.)	Λ (mho-cm.^{2}/eq.)	10^4c (moles/l.)	Λ (mho-cm.^{2}/eq.)
	First series		
9.203	267.87	63.402	259.29
18.766	265.72	63.974	259.39
18.974	266.18	87.190	256.38
37.052	262.94	87.377	256.24
37.217	263.11		
	Second series		
9.651	267.71	37.344	263.22
9.898	268.89	37.345	263.26
9.915	268.47	37.442	262.92
10.015	268.50	63.903	259.57
10.175	268.70	64.067	259.59
10.192	267.54	64.205	259.20
36.645	263.35	64.571	259.23
36.904	263.76	87.484	256.41
36.915	263.17	87.712	256.85
36.981	263.29	87.715	256.89
37.336	263.28		

(18) G. H. Jeffrey and A. I. Vogel, *Phil. Mag.*, **15**, 395 (1933); **16**, 64 (1933); **17**, 582 (1934).

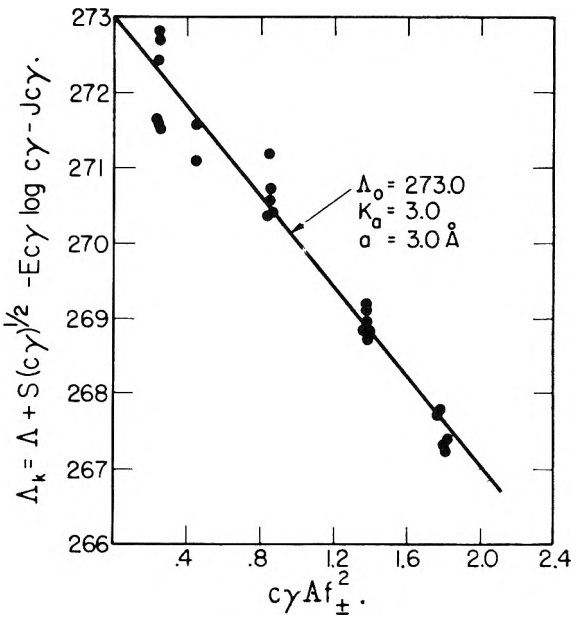

Fig. 3.—Solution of conductance equations by the Λ_k method.

The Fuoss–Onsager conductance equation[19,20] was used to derive values of Λ_0 and K_a (the association constant) from the results. The experimental precision is not sufficient to allow the simultaneous determination of all three parameters, Λ_0, K_a, and a (the ion-size parameter), appearing in these equations. Consequently, the Λ_k method[19] was used, with a value of 3.0 Å. assumed for the ion-size parameter, a. The values of Λ_0 and K_a determined by this method are relatively insensitive to the value assumed for a. Variation of a from 2.5 to 3.5 Å. does not change the calculated results by an amount greater than the spread between 95% confidence limits.

According to the conductance equations, a plot of Λ_k *vs.* $C\gamma Af_\pm^2$ should be a straight line, with the intercept on the ordinate equal to Λ_0 and the slope equal to $-K_a$. The variable Λ_k is given by

$$\Lambda_k = \Lambda + S(c\gamma)^{1/2} - Ec\gamma \log c\gamma - Jc\gamma \qquad (3)$$

Λ is equivalent conductance at concentration c; S, E, and J are functions of Λ_0, as defined by Fuoss[19,20]; γ is the degree of dissociation, given by Λ/Λ_e, where Λ_e is the equivalent conductance of a completely ionized solute at the same ionic concentration, given by

$$\Lambda_e = \Lambda_0 + \Lambda - \Lambda_k \qquad (4)$$

and $f_\pm$ is the mean activity coefficient calculated from the Debye–Hückel equation, using in the denominator of this equation a value of 3.57 Å. for the distance of closest approach between "free" ions.[21,22] Figure 3 shows the final solution of the equations after a series of successive approximations. Least squares treatment gives 273.0

(19) R. M. Fuoss, *J. Am. Chem. Soc.*, **81**, 2659 (1959).

(20) R. M. Fuoss and F. Accascina, "Electrolytic Conductance," Interscience Publishers, Inc., New York, N. Y., 1959.

(21) J. E. Prue, *Discussions Faraday Soc.*, **24**, 123 (1957).

(22) R. M. Fuoss and L. Onsager, *Proc. Natl. Acad. Sci.*, **47**, 818 (1961).

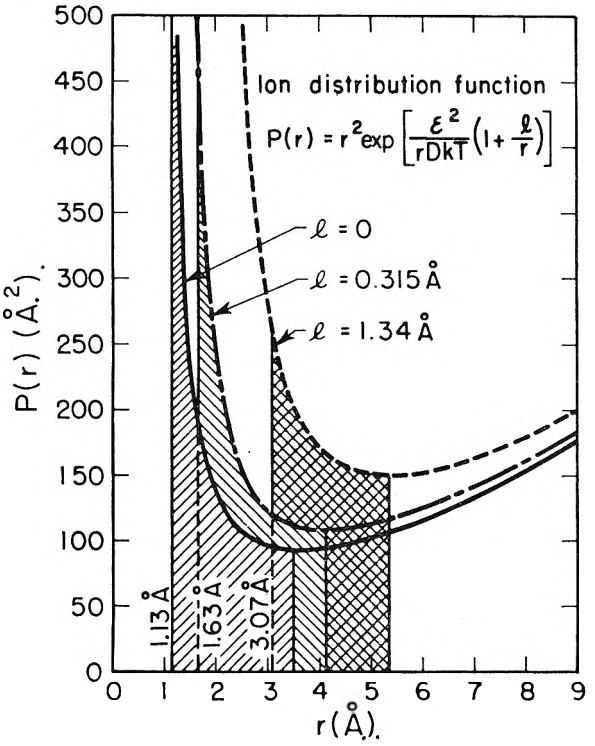

Fig. 4.—Effect of hydroxyl ion dipole on ion distribution function.

± 0.3 for Λ_0 and 3.0 ± 0.3 for K_a, where the 95% confidence limits are indicated.

Discussion

The result for Λ_0 may be compared with values of 272.5 and 273.0 for the sum of limiting ionic conductances of Tl^+ and OH^-, as tabulated by Harned and Owen[23] and Robinson and Stokes,[24] repectively. The agreement is as good as can be expected, in view of the possible sources of error both in this work and in other conductance measurements on hydroxides.

The result for K_a is close to the value originally determined by Bell and Prue[5] from reaction-kinetic measurements on the decomposition of diacetone alcohol, but it is about one-half the values later obtained by Bell and George[6] from solubility equilibria and by Bell and Panckhurst[7] from kinetic measurements on neutralization of nitroethane. Values of K_a approaching those of the last two sets of authors are inconsistent with the experimental results of this work.

Association in thallous hydroxide solutions probably is by outward transfer of a proton from a water molecule adjacent to the cation to form a pair of ions essentially in contact

$$Tl^+..OH_2 + OH^- \longrightarrow Tl^+..OH^- + HOH \quad (5)$$

The applicability to this case of the Bjerrum treatment of ion association[25] is questionable, since this treatment assumes a distribution of ions in a dielectric continuum having the macroscopic value of the dielectric constant. Nevertheless, it was considered interesting to explore the effect of inclusion of ion, dipole and ion, induced-dipole terms in a Bjerrum-type calculation of the distance of closest approach between the paired ions. The hydroxyl ion, in close association with a cation, at least, must have a permanent dipole moment. Its magnitude is unknown, but it is possible to determine by graphical calculations the value of the dipole moment that would bring the calculated distance of closest approach into agreement with the sum of crystallographic ionic radii, 2.79 Å.[26] When one of the ions is an oriented dipole, the interaction energy is

$$U(r) = -(1 + l/r)\epsilon^2/Dr \quad (6)$$

where r is the distance between electrostatic centers of the ions, l is given by μ/ϵ, μ is the dipole moment, ϵ is the electronic charge, and D is the dielectric constant of the medium. The ion distribution function

$$P(r) = r^2 \exp -[U(r)/kT] \quad (7)$$

is plotted in Fig. 4 for values of l equal to 0, 0.315, and 1.34 Å. The shaded area under each curve is equal to $10^{27}K_a/4\pi N$, where N is Avogadro's number and $K_a = 3.0$. The macroscopic value of the dielectric constant was used in calculation of the curves. For $l = 0$, the ordinary Bjerrum calculation gives a distance of closest approach of 1.13 Å., very much less than the sum of ionic radii. Increasing l has the effect of shifting the minimum of the curve to the right, as well as raising the magnitude of $P(r)$ at small values of r. However, taking $l = 0.315$ Å. (from the dipole moment assigned to the O–H bond by Pauling[27]) still results in a too-small calculated minimum distance. It would be necessary to assume a value of l slightly less than 1.34 Å. to have a calculated distance equal to 2.79 Å. This would correspond to a dipole moment that probably is unrealistically high.

The electronic structure of the thallous ion suggests that it should have a rather high polarizability. Tessman, Kahn, and Shockley[28] have estimated polarizabilities averaging 5.2 Å.^{3} for Tl^+ in crystals of TlCl, TlBr, and TlI, and a value of 1.22 Å.^{3} for OH^- in crystalline NaOH. When these values are substituted into the expression for the interaction energy including ion, induced-dipole terms

$$U(r) = -\{1 + [l + (\alpha_{Tl} + \alpha_{OH})/2Dr^2]/r\}\,\epsilon^2/Dr \quad (8)$$

where α_{Tl} and α_{OH} are the polarizabilities of the thallous and hydroxyl ions; it is easy to see that there is a negligible effect on the calculation if the

(23) H. Harned and B. B. Owen, "The Physical Chemistry of Electrolytic Solutions," Third Edition, Reinhold Publ. Corp., New York, N. Y., 1958, p. 231.

(24) R. A. Robinson and R. H. Stokes, "Electrolyte Solutions," Second Edition, Academic Press, New York, N. Y., 1959, p. 463.

(25) N. Bjerrum, *Kgl. Danske Videnskab. Selskab.*, **7**, No. 9 (1926).

(26) R. Parsons, "Handbook of Electrochemical Constants," Butterworth & Co. Ltd., London, 1959 (taking the radius of OH^- to be equal to the radius of O^{-2}).

(27) L. Pauling, "The Nature of the Chemical Bond," Second Edition, Cornell University Press, Ithaca, N. Y., 1948.

(28) J. R. Tessman, A. H. Kahn, and W. Shockley, *Phys. Rev.*, **92**, 890 (1953).

macroscopic value of the dielectric constant is used throughout. On the other hand, it is interesting to note that substitution of a very low value for the dielectric constant D in the inner brackets of (8), while retaining the macroscopic value in the outer factor, allows the use of a more believable value of hydroxyl ion dipole moment to make the calculated distance of closest approach equal the sum of ionic radii. This procedure perhaps could be justified by viewing the outer D as containing a factor correcting for changes in the solvent that otherwise are ignored in the calculation. The inner term, however, should make use of the proper local value of the dielectric constant, which may be very much less than the macroscopic value because of dielectric saturation effects.

A more realistic appraisal may be that dielectric saturation must be explicitly taken into account for *all* interactions when the ions can readily approach each other very closely, as by a proton transfer step. Although Schellman's[29] calculations suggest that the dielectric saturation effect is slight even at very small distances, it seems unlikely that the macroscopic dielectric constant would apply when the ions are adjacent with no intervening water molecules. With dielectric saturation, all contributions to the interaction energy are enhanced, and it is not necessary to suppose that any other than the simplest electrostatic interactions occur. Yet, if covalent bonding is excluded from consideration, comparison with Cs^+ or Rb^+ (which are about the same size as Tl^+) would seem to point to the higher polarizability of the thallous ion as a principal reason for its tendency toward association in solution, a property not shared by Rb^+ and Cs^+. It is possible that the artifice of assigning different values to D in the inner and outer terms of (8) may have some merit, for in this way contributions of the polarizability terms are increased in significance.

Acknowledgments.—The author wishes to acknowledge the valuable assistance of Mr. T. S. Bulischeck with the experimental work.

(29) J. A. Schellman, *J. Chem. Phys.*, **26**, 1225 (1957).

FLUORINE BOMB CALORIMETRY. IV. THE HEATS OF FORMATION OF TITANIUM AND HAFNIUM TETRAFLUORIDES[1,2]

By Elliott Greenberg, Jack L. Settle, and Ward N. Hubbard

Chemical Engineering Division, Argonne National Laboratory, Argonne, Illinois

Received February 12, 1962

The heats of formation of titanium and hafnium tetrafluorides were measured by direct combination of the elements in a combustion bomb calorimeter. The standard heats of formation, $\Delta Hf°_{298.15}$, of titanium and hafnium tetrafluorides were found to be -394.19 ± 0.35 and -461.40 ± 0.85 kcal. mole^{-1}, respectively.

Introduction

The determination of the heats of formation of the tetrafluorides of titanium and hafnium is part of a continuing program[3-5] to obtain precise thermochemical data by fluorine bomb calorimetry. This investigation completes the measurements of the heats of formation of the tetrafluorides of the group IVA elements, the heat of formation of zirconium tetrafluoride having been reported previously.[3]

Experimental

Calorimetric System.—The calorimeter, laboratory designation ANL-R1, and combustion bomb, laboratory desig nation Ni-T, already have been described[3] except for a modification of the gasket which sealed the cap to the body of the bomb. An annular U-shaped groove was cut in the gold gasket and filled with a Teflon ring in order to facilitate sealing of the bomb. In effect, the gold gasket was itself gasketed with Teflon.

Eight calibration experiments with National Bureau of Standards standard samples of benzoic acid (39g and 39h), some preceding and some following the fluorine combustions, yielded an average value for $\mathcal{E}$(calor.), the energy equivalent of the calorimetric system, of 3565.41 cal. deg.$^{-1}$, with a standard deviation of the mean of 0.4 cal. deg.$^{-1}$, or 0.01%.

Materials.—Titanium and hafnium were obtained in the form of iodide-deposited crystal bars. These were arc-melted, cast, and rolled to 0.1 × 0.1 in. rods and 0.005 in. foil. The outer portion of the rods was removed by taking surface cuts with a milling machine. Several rods, each of which was analyzed, were required for the calorimetric combustions. Table I summarizes the impurities found in the samples. No other metallic impurities were detected. The chemical state of the impurities was unknown.

Table I

Impurities in the Samples

Element	Mean values, parts per million: Ti	Hf
	Spectrochemical analysis	
Cr	1200	....
Al	200	....
Fe	300	20
Si	..	25
Zr	..	1.43×10^4
	Chemical analysis	
C	140	60
O	360	160
H	25	15
N	30	50

Because of the unavailability of hafnium wire, high-purity zirconium wire, 0.010 in. in diameter, was used as fuse

(1) This work was performed under the auspices of the U. S. Atomic Energy Commission.

(2) Presented in part at the International Calorimetry Conference in Ottawa, Canada, August, 1961.

(3) E. Greenberg, J. L. Settle, H. M. Feder, and W. N. Hubbard, *J. Phys. Chem.*, **65**, 1168 (1961).

(4) J. L. Settle, H. M. Feder, and W. N. Hubbard, *ibid.*, **65**, 1337 (1961).

(5) S. S. Wise, J. L. Margrave, H. M. Feder, and W. N. Hubbard, *ibid.*, **65**, 2157 (1961).

TABLE II

RESULTS OF TITANIUM COMBUSTION EXPERIMENTS[a]

1.	mass, g.	0.85599	0.85713	0.86908	0.86279	0.85550	0.85799	0.84818
2.	Δt_c, deg.	1.96360	1.96510	1.99219	1.97826	1.96405	1.96927	1.94545
3.	ε(calor.)$(-\Delta t_c)$, cal.	−7001.04	−7006.39	−7102.97	−7053.31	−7002.64	−7021.25	−6936.33
4.	$\Delta E_{\text{contents}}$, cal.[b,c]	−15.13	−15.16	−15.34	−15.25	−15.16	−15.18	−14.96
5.	$\Delta E_{\text{ignition}}$, cal.	1.15	1.04	1.30	1.10	0.97	1.02	1.23
6.	$\Delta E_{\text{gas.}}$, cal.[d]	−1.26	−1.26	−1.28	−1.27	−1.26	−1.26	−1.25
7.	ΔE_{fuse}, cal.	No correction necessary						
8.	$\Delta E_{\text{impurities}}$, cal.	−9.10	−9.11	−9.24	−9.17	−5.02	−5.04	−4.98
9.	$\Delta Ec°/M$, cal. g.$^{-1}$	−8207.32	−8202.82	−8201.24	−8203.50	−8209.36	−8207.22	−8201.43

Av. $\Delta Ec°/M$ = −8204.7 cal. g.$^{-1}$

Std. dev. of mean = ±1.2 cal. g.$^{-1}$

[a] The symbols employed are explained in ref. 8. [b] $\Delta E_{\text{contents}} = \varepsilon^i(\text{cont.})\,(t_i - 25) + \varepsilon^f(\text{cont.})\,(25 - t_f + \Delta t_{\text{cor.}})$ in which t_i was approximately 22.78°. [c] The bomb contents included 65.42 g. of nickel and 0.09 g. of Teflon. [d] $\Delta E\text{gas.} = [\Delta E^i(\text{gas.})]_0{}^{Pi(\text{gas.})} + [\Delta E^f(\text{gas.})]_0{}^{Pf(\text{gas.})}$.

TABLE III

RESULTS OF HAFNIUM COMBUSTION EXPERIMENTS[a]

1.	mass, g.	1.85729	2.05689	1.82159	2.05485	1.87393	1.98066	2.99433	2.43775	3.11682
2.	Δt_c, deg.	1.37236	1.51552	1.34466	1.51349	1.38410	1.46073	2.20270	1.79775	2.29126
3.	ε(calor.)$(-\Delta t_c)$, cal.	−4893.04	−5403.47	−4794.28	−5396.23	−4934.90	−5208.12	−7853.55	−6409.73	−8169.30
4.	$\Delta E_{\text{contents}}$, cal.[b,c]	−10.58	−11.72	−10.37	−11.70	−10.68	−11.28	−17.18	−13.93	−17.83
5.	$\Delta E_{\text{ignition}}$, cal.	1.35	1.38	1.28	1.35	1.25	1.21	1.58	1.55	1.47
6.	$\Delta E_{\text{gas.}}$, cal.[d]	−0.78	−0.86	−0.76	−0.85	−0.78	−0.83	−1.20	−1.00	−1.24
7.	$\Delta E_{\text{Zr fuse}}$, cal.	55.74	45.35	47.30	35.91	46.85	43.25	46.40	54.19	38.91
8.	$\Delta E_{\text{impurities}}$, cal.	60.36	66.85	59.20	71.28	65.00	68.71	105.13	85.59	109.43
9.	$\Delta Ec°/M$, cal. g.$^{-1}$	−2577.38	−2577.91	−2578.86[e]	−2579.38[e]	−2579.21[e]	−2578.46	−2577.81	−2577.51	−2579.09

Average $\Delta Ec°/M$ = −2578.4 cal. g.$^{-1}$

Std. dev. of mean = ±0.3 cal. g.$^{-1}$

[a] The symbols employed are explained in ref. 8. [b] $\Delta E_{\text{contents}} = \varepsilon^i(\text{cont.})\,(t_i - 25) + \varepsilon^f(\text{cont.})\,(25 - t_f + \Delta t_{\text{cor.}})$. Because of varying sample size t_i varied from 22.6 to 23.4°. [c] The bomb contents included 66.01 g. of nickel and 0.09 g. of Teflon. [d] ΔE gas. $= [\Delta E^i(\text{gas.})]_0{}^{Pi(\text{gas.})} + [\Delta E^f(\text{gas.})]_0{}^{Pf(\text{gas.})}$. [e] These combustions were carried out with high-purity commercial fluorine.

material for the hafnium combustions. For the titanium experiments, the fuse consisted of a 0.01 in. wide strip of 0.005 in. titanium foil.

Purified fluorine (99.94%) was prepared by distillation of commercial fluorine in a low temperature still.[3,6]

High-purity argon (99.9%) was obtained commercially.

Combustion Technique.—Trial exposures of weighed samples to fluorine indicated the absence of any reaction prior to ignition. The sample arrangement and combustion technique were the same as described[3] for the combustion of zirconium in fluorine. The gas mixture consisted of 2000 mm. fluorine for the titanium experiments, 2500 mm. fluorine for the hafnium experiments, and, in each case, sufficient argon to raise the total pressure to 12.0 atm. Argon diluent was substituted for the helium used in the zirconium experiments because of handling convenience in the high pressure manifold. The assembled bomb always was pretreated with several atmospheres pressure of fluorine for a few minutes before final evacuation and charging. The calorimetric measurements were made in the usual manner.

Analysis of Combustion Products.—After the completion of each calorimetric measurement the bomb gas was discharged and the unburned metal was recovered and weighed. The unburned hafnium was soaked in water to loosen adhering tetrafluoride, scrubbed with nylon tweezers, and scraped clean with a razor blade. The remnants of the zirconium fuse wire were isolated and weighed separately. The washing procedure for titanium was modified to avoid possible attack by concentrated solutions of titanium tetrafluoride on titanium metal.

The product of the hafnium combustions was determined to be monoclinic hafnium tetrafluoride by comparison of the X-ray powder pattern with the pattern previously obtained and verified to be that of β-(monoclinic) zirconium tetrafluoride.[3] The two powder patterns were identical except for slight shifts in line locations due to cell size differences.

The product of the titanium combustions, which was a white solid, gave an X-ray powder diffraction pattern that showed only a few diffuse bands. After the sample was annealed at about 300° for approximately half an hour, a diffraction pattern was obtained which was in general agreement with that reported for titanium tetrafluoride.[7] Electron microscopic examination of the combustion product showed spherical particles of the order of 1 μ in diameter, which are large enough particles to have given a satisfactory X-ray diffraction pattern if the particles were crystalline. Proof that the product was titanium tetrafluoride uncontaminated by lower fluorides was furnished by chemical analysis for fluorine, which showed 61.4 ± 0.3% of the product as fluorine compared to 61.3% fluorine in TiF_4.

After several of the calorimetric experiments, a portion of the gas in the bomb was reacted with mercury to remove fluorine, and then was analyzed mass spectrometrically. The bomb atmosphere after combustion was thus shown to contain 0.09% nitrogen and 0.2% oxygen. The remainder of the gas was cooled with liquid nitrogen, fluorine and other non-condensables were pumped off, and the residue was evaporated into an infrared cell equipped with silver chloride windows. All the observed absorption bands could be attributed to fluorides or oxyfluorides of carbon and to silicon tetrafluoride. The gaseous impurities found can all be attributed to contaminants in the metal sample and in the fluorine charge.

Results

Experimental Results.—Tables II and III summarize the results of the titanium and hafnium combustion experiments, expressed in terms of the defined calorie equal to (exactly) 4.184 absolute joules. The corrections to standard states were applied in accordance with the procedure illustrated for molybdenum hexafluoride.[8]

(6) L. Stein, E. Rudzitis, and J. L. Settle, "Purification of Fluorine by Distillation," Argonne National Laboratory, ANL-6364 (1961). (Available from Office of Technical Services, U. S. Dept. of Commerce, Washington 25, D. C.)

(7) K. S. Vorres and F. B. Dutton, *J. Am. Chem. Soc.*, **77**, 2019 (1955).

The entries in the tables are: (1) The mass *in vacuo* of the sample reacted, which was determined by subtracting the mass of unburned metal recovered after combustion from the mass of sample originally introduced into the bomb; (2) the observed increase in the calorimeter temperature, corrected for heat exchanged between the calorimeter and its surroundings, $\Delta t_c = t_f - t_i - \Delta t_{cor.}$; (3) the energy equivalent of the calorimetric system, multiplied by Δt_c; (4) the energy equivalents of the initial and final contents of the bomb each multiplied by its appropriate portion of $-\Delta t_c$ to correct to the hypothetical isothermal process at 25°; (5) the measured electrical energy input for ignition of the fuse; (6) the net correction for the hypothetical compression and decompression of the bomb gas; (7) the energy supplied by combustion of the fuse wire; (8) the net correction for impurities in the sample; and (9) the energy change per gram of metal for the reactions

$$\mathrm{Ti(c) + 2F_2(g) \longrightarrow TiF_4(s,\ amorph.)} \quad (1)$$
$$\mathrm{Hf(c) + 2F_2(g) \longrightarrow HfF_4(c)} \quad (2)$$

in which equations the reactants and products are in their standard states at 25°.

For calculation of item 4 the following values were used; heat capacities at constant pressure were 0.1061, 0.28, 0.1248, 0.2204, 0.0342, and 0.100 cal. deg.$^{-1}$ g.$^{-1}$ for Ni,[9] Teflon,[10] Ti,[11] TiF_4,[12] Hf,[13] and HfF_4,[14] respectively; heat capacities at constant volume were 5.50 and 2.981 cal. deg.$^{-1}$ mole^{-1} for F_2[15] and Ar,[16] respectively.

The coefficients $(\partial E/\partial P)_T$ and μ (in the equation $PV = nRT(1 - \mu P)$), which were required for calculation of item 6, were estimated by the method of Hirschfelder, *et al.*,[17] from the force constants for F_2[18] and Ar.[17] The coefficients as functions of composition at 25° were

$$\mu = 2.86 \times 10^{-6}(281 - 55.2x + x^2)\ \mathrm{atm.^{-1}} \quad (3)$$
$$(\partial E/\partial P)_T = -3.147 \times 10^{-3}(565.9 - 98.32x + x^2)\ \mathrm{cal.\ atm.^{-1}\ mole^{-1}} \quad (4)$$

in which equations x represents the mole fraction of argon in the mixture. For estimation of the internal volume of the bomb in the initial and final states, the densities used were: 8.907, 2.24, 4.51, 2.780, 13.36, and 7.13 g. ml.$^{-1}$ for Ni,[19] Teflon,[10] Ti,[20] TiF_4,[21] Hf,[22] and HfF_4,[23] respectively. The internal volume of the empty bomb was 0.358 l.

The previously reported[3] value for the heat of formation of zirconium tetrafluoride was used for calculation of item 7.

For calculation of item 8 these assumptions were made regarding the states of combination of the impurities: carbon, oxygen, and nitrogen were assumed to be present as TiC, HfC, TiO, HfO_2, TiN, and HfN, respectively; hydrogen was assumed to be present in solid solution; silicon was assumed to be present in the hafnium sample as Hf_4Si. The remaining impurities were assumed to be present in the sample as elements, and to form their most stable fluorides during combustion. The required heats of formation were taken from the following sources: TiC and TiN,[24] TiO,[25] Ti–H system,[26] HfC,[27] HfO_2 and HfN,[28] Hf–H system,[29] Hf_4Si,[30] CF_4,[31] HF,[32] ZrF_4,[3] SiF_4,[33] FeF_3,[34] and reference 16 for CrF_3 and AlF_3. The approximate corrections to the measured heat for the titanium sample were: oxygen, −0.07%; chromium, −0.05%; iron, −0.02%; hydrogen, +0.01%; carbon, +0.01%; aluminum, +0.007%; nitrogen, −0.005%; and, for the hafnium sample: zirconium, +1.34%; oxygen, −0.07%; hydrogen, +0.03%; carbon, +0.02%; nitrogen, −0.02%; and silicon, +0.01%; other impurity corrections were negligible. The net correction made for all impurities (item 8) was (−0.11 ± 0.06)% for the titanium sample and (+1.32 ± 0.18)% for the

(8) W. N. Hubbard, "Experimental Thermochemistry," Vol. II, H. A. Skinner, Ed., Interscience Publishers, Ltd., London, 1962, Ch. 6, pp. 95–127.

(9) R. H. Busey and W. F. Giauque, *J. Am. Chem. Soc.*, **74**, 3157 (1952).

(10) W. D. Good, D. W. Scott, and G. Waddington, *J. Phys. Chem.*, **60**, 1080 (1956).

(11) C. W. Kothen and H. L. Johnston, *J. Am. Chem. Soc.*, **75**, 3101 (1953).

(12) R. D. Euler and E. F. Westrum, Jr., *J. Phys. Chem.*, **65**, 132 (1961).

(13) D. R. Stull and G. C. Sinke, "Thermodynamic Properties of the Elements," American Chemical Society, Washington 6, D. C., 1956.

(14) K. K. Kelley, "Contributions to the Data on Theoretical Metallurgy, XIII. High-Temperature Heat-Content, Heat-Capacity, and Entropy Data for the Elements and Inorganic Compounds," Bureau of Mines Bulletin 584, U. S. Govt. Printing Office, Washington, D. C., 1960.

(15) W. H. Evans, T. R. Munson, and D. D. Wagman, *J. Res. Natl. Bur. Std.*, **55**, 147 (1955).

(16) "Selected Values of Chemical Thermodynamic Properties," National Bureau of Standards Circular 500, U. S. Govt. Printing Office, Washington, D. C., 1952.

(17) J. O. Hirschfelder, C. F. Curtiss, and R. B. Bird, "Molecular Theory of Gases and Liquids," John Wiley and Sons, New York, N. Y., 1954.

(18) D. White, J. H. Hu, and H. L. Johnston, *J. Chem. Phys.*, **21**, 1149 (1953).

(19) H. E. Swanson and E. Tatge, "Standard X-ray Diffraction Powder Patterns," Vol. I, National Bureau of Standards Circular 539, U. S. Govt. Printing Office, Washington, D. C., 1953.

(20) G. Skinner, H. L. Johnston, and C. Beckett, "Titanium and Its Compounds," Herrick L. Johnston Enterprises, Columbus, Ohio, 1954, p. 3.

(21) F. D. Rossini, P. A. Cowie, F. O. Ellison, and C. C. Browne, "Properties of Titanium Compounds and Related Substances," Office of Naval Research Report ACR-17, Department of the Navy, Washington, D. C., 1956.

(22) L. B. Prus, "Reactor Handbook," Vol. I, C. R. Tipton, Jr., Ed., Second Edition, Interscience Publishers, Inc., New York, N. Y., 1960, Ch. 36, p. 784.

(23) Calculated from the data of W. H. Zachariasen, *Acta Cryst.*, **2**, 388 (1949).

(24) G. L. Humphrey, *J. Am. Chem. Soc.*, **73**, 2261 (1951).

(25) A. D. Mah, K. K. Kelley, N. L. Gellert, E. G. King, and C. J. O'Brien, "Thermodynamic Properties of Titanium–Oxygen Solutions and Compounds," Bureau of Mines Report of Investigations 5316 (1957).

(26) A. D. McQuillan, *Proc. Roy. Soc.* (London), **A204**, 309 (1950).

(27) K. K. Kelley, unpublished data.

(28) G. L. Humphrey, *J. Am. Chem. Soc.*, **75**, 2806 (1953).

(29) R. K. Edwards and E. Veleckis, to be published.

(30) Assumed to be the same as the value for Zr_4Si given by L. Brewer and O. Krikorian, "Heats of Formation of Refractory Silicides," University of California Radiation Laboratory, UCRL-3352 (1956).

(31) D. W. Scott, W. D. Good, and G. Waddington, *J. Am. Chem. Soc.*, **77**, 245 (1955).

(32) G. T. Armstrong and R. S. Jessup, *J. Res. Natl. Bur. Std.*, **64A**, 49 (1960).

(33) S. S. Wise, J. L. Margrave, H. M. Feder, and W. N. Hubbard, *J. Phys. Chem.*, **66**, 381 (1962).

(34) L. Brewer, L. A. Bromley, P. W. Gilles, and N. L. Lofgren, Paper 6, "The Chemistry and Metallurgy of Miscellaneous Materials: Thermodynamics," L. L. Quill, Ed., McGraw-Hill Book Co., Inc., New York, 1950, pp. 76–192.

hafnium sample. The large uncertainties attached to the impurity corrections arise in part from analytical uncertainties and in part from a generous allowance for the possibility that the elements existed in states of combination other than those assumed.

The remaining corrections to standard states were all negligible. $\Delta Ec°/M$ is just the sum of items 3 through 8 divided by the mass of metal reacted.

It was estimated[3] previously that the *maximum* heat effect due to the formation of nickel fluoride on the bomb surfaces during combustion is a quarter of a calorie per experiment. The possibility of nickel fluoride formation during the combustion period was further investigated during the course of this work. Selected internal nickel components were weighed before and after a series of calorimetric combustions. The weight loss per combustion was found to be comparable to the average weight loss per experiment in a series of control experiments in which the bomb was charged, discharged, and washed as in the calorimetric combustions. This observation supports the view that the formation of nickel fluoride occurs during the prefluorination period, with no significant additional fluorination during the combustion period.

In the hafnium combustion experiments the mass of metal burned varied by almost a factor of two. No significant trend in the data was observed as a result of this variation.

Three of the hafnium combustions were carried out with a high-purity commercial fluorine made available to us by the General Chemical Co. The purity of the commercial fluorine was about 99.75% as compared to 99.94% for the fluorine purified in this Laboratory and used for all of the other combustion experiments. Although the data are somewhat limited, there appears to be no significant difference in the results obtained with the two grades of fluorine.

Derived Data.—Table IV presents derived standard thermal data for reactions 1 and 2 for the formation of titanium and hafnium tetrafluorides at 25°. The atomic weights[35] of titanium and hafnium were taken as 47.90 and 178.49, respectively. The entropies, $S°$, at 25°, of Ti(c),[11] TiF_4(s),[12] F_2(g),[15] and Hf(c)[13] were taken as 7.33, 32.02, 48.45, and 10.91 cal. deg.$^{-1}$ mole^{-1}, respectively. The entropy of HfF_4(c) was estimated to be 26.5 cal. deg.$^{-1}$ mole^{-1}. The estimated uncertainties given are uncertainty intervals[36] equal to twice the combined standard deviations arising from known sources. The uncertainties in the results are due primarily to the uncertainties in the impurity corrections, and more specifically in the case of hafnium, to the uncertainty in the analysis for the zirconium content of the hafnium.

TABLE IV

DERIVED DATA AT 25°

	TiF_4 (s, amorph.)	HfF_4(c)
Energy of formation, $\Delta Ef° = \Delta Ec°$, kcal. mole^{-1}	-393.01 ± 0.35	-460.22 ± 0.85
Heat of formation, $\Delta Hf°$, kcal. mole^{-1}	-394.19 ± 0.35	-461.40 ± 0.85
Entropy of formation, $\Delta Sf°$, cal. deg.$^{-1}$ mole^{-1}	-72.21	-81.3
(Gibbs) energy of formation, $\Delta Gf° = \Delta Hf° - T\Delta Sf°$, kcal. mole^{-1}	-372.66 ± 0.35	-437.16 ± 0.85

Conclusion

The standard heats of formation of titanium and hafnium tetrafluorides have been determined to be -394.19 ± 0.35 and -461.40 ± 0.85, respectively. The value for TiF_4 is in good agreement with that of Gross, Hayman, and Levi.[37] For hafnium tetrafluoride the literature contains only the estimate[34] of -435 ± 40 kcal. mole^{-1}. It should be noted that this estimated value was 10 kcal. mole^{-1} less negative than the corresponding estimate for zirconium tetrafluoride. The value reported herein for the heat of formation of HfF_4 is 5 kcal. mole^{-1} more negative than that for ZrF_4,[3] in agreement with experimental data for the chlorides,[38] oxides, carbides, and nitrides, and estimated data for the tetrabromides and tetraiodides of hafnium and zirconium.

Acknowledgment.—The performance of special analyses by R. W. Bane, J. P. Faris, J. A. Goleb, R. K. Hart, B. D. Holt, R. P. Larsen, and R. V. Schablaske, and the fabrication by F. J. Karasek of the rods and foils required for the samples are gratefully acknowledged. We also wish to thank H. M. Feder for his valuable aid, criticism, and deep interest in this research.

(35) (a) International Union of Pure and Applied Chemistry, Information Bulletin Number 14B, Butterworth Scientific Publications, London, 1961; (b) See also *Chem. Eng. News*, **39**, No. 47, 43 (1961).

(36) F. D. Rossini, "Experimental Thermochemistry," F. D. Rossini, Ed., Interscience Publishers, Inc., New York, N. Y., 1956, Ch. 14, pp. 297-320.

(37) P. Gross, C. Hayman, and D. L. Levi, *XVIIth Intern. Congr. Pure and Appl. Chem., Abstr.*, **1**, 90 (1959). Communication from C. Hayman indicates that his previously reported value (−393.4) has been revised to −393.7 ± 0.1 kcal. mole^{-1}, but is not corrected for impurities in his iodide titanium sample.

(38) A. G. Turnbull, *J. Phys. Chem.*, **65**, 1652 (1961).

METAL COMPLEXING BY PHOSPHORUS COMPOUNDS. VI. ACIDITY CONSTANTS AND CALCIUM AND MAGNESIUM COMPLEXING BY MONO- AND POLYMETHYLENE DIPHOSPHONATES[1]

BY RIYAD R. IRANI AND KURT MOEDRITZER

Monsanto Chemical Company, Inorganic Division, Research Department, St. Louis 66, Missouri

Received February 14, 1962

The acidity constants of methylene and polymethylene diphosphonic acids $(HO)_2{-}\overset{\overset{O}{\|}}{P}{-}(CH_2)_n{-}\overset{\overset{O}{\|}}{P}{-}(OH)_2$ have been measured as a function of n, ionic strength, and temperature in the range 25–50°. It is shown that as n increases the effect of the two end phosphonate groups on one another decreases, and becomes negligible for n larger than 3. Calcium and magnesium complexing by the anions of these acids were measured nephelometrically in the presence of oxalate, and by the pH-lowering method as a function of ionic strength and temperature. Complexing drops off sharply as n increases and becomes negligible for $n = 10$. Comparison with other data suggests that in calcium and magnesium complexing by diphosphonates, the distance between the two phosphonate groups is critically important.

Introduction

In contrast with the salts of pyrophosphoric acid, $(HO)_2{-}\overset{\overset{O}{\|}}{P}{-}O{-}\overset{\overset{O}{\|}}{P}{-}(OH)_2$, or imidodiphosphoric acid, $(HO)_2{-}\overset{\overset{O}{\|}}{P}{-}\overset{\overset{H}{|}}{N}{-}\overset{\overset{O}{\|}}{P}{-}(OH)_2$, aqueous solutions containing methylene diphosphonic acid, $(HO)_2{-}\overset{\overset{O}{\|}}{P}{-}CH_2{-}\overset{\overset{O}{\|}}{P}{-}(OH)_2$, or its salts are extremely stable at room temperature against hydrolytic degradation, either in acidic or basic media. This is due to the high stability of P-C bonds relative to other bonds involving phosphorus.[2] In view of this, it is of interest to study the ability of the salts of methylene diphosphonic acid, $(HO)_2{-}\overset{\overset{O}{\|}}{P}{-}CH_2{-}\overset{\overset{O}{\|}}{P}{-}(OH)_2$, and polymethylene diphosphonic acids, $(HO)_2{-}\overset{\overset{O}{\|}}{P}{-}(CH_2)_n{-}\overset{\overset{O}{\|}}{P}{-}(OH)_2$, to complex metal ions. The results, coupled with the planned determination of phosphorus-to-phosphorus distances in these systems, will make it feasible to evaluate optimum separation of phosphorus atoms for the complexing of specific metal ions.

Schwarzenbach and Zurc[3] reported acidity constants for methylene-, trimethylene-, and tetramethylenediphosphonic acids. However, their work was done in the presence of alkali metal ions, which form complexes of their own with metal-complexing anions. Because of their inability to synthesize the member of the series with $n = 2$, wrong conclusions were drawn regarding the acidity constants of hypophosphoric acid, as will be discussed later. Limited data on calcium and magnesium complexing also have been reported.[4]

The synthesis and physical properties of mono- and polymethylene diphosphonic acids and esters in high purity were described elsewhere.[5] There, from the measurement of P^{31} n.m.r. chemical shifts as well as the infrared spectra, it was concluded that as n increases, the effect of the two end phosphorus atoms on one another decreases and becomes very small for values of n larger than three.

Experimental

Chemicals.—The 99.5+% pure methylene- and polymethylene diphosphonic acids were prepared and recrystallized as previously described.[5] When desired, the corresponding tetramethylammonium salts were prepared through neutralization with the proper amount of pre-standardized Eastman Kodak tetramethylammonium hydroxide. Boiled distilled water was used for solution makeup. All other chemicals were reagent grade.

Procedure.—All measurements were made in a nitrogen atmosphere, in the absence of extraneous cations, *e.g.*, alkali metal ions. Ionic strength was made up with tetramethylammonium bromide.

The acidity constants were determined using the titration procedure and IBM program previously described.[6]

The calcium complexing by methylene diphosphonate as a function of ionic strength and temperature was measured using the nephelometric procedure[7] with oxalate as the precipitating anion. The pH-lowering method[8] was used for measuring the magnesium complexing constants because of the absence of a well defined magnesium precipitate, as required in the nephelometric procedure.[7]

The pH-lowering method also was used for measuring the complexing of calcium and magnesium by polymethylene diphosphonates. Here, the nephelometric procedure with oxalate as a precipitate could not be used on calcium because of the poor competition for the calcium by the complexing anions.

Results and Discussion

Acidity Constants.—Stepwise titration curves with definite breaks for the weakest two hydrogens were obtained with all of the investigated methylene- and polymethylene diphosphonic acids. The remaining two hydrogens are too strongly acidic to show inflection points.

The acid–base titration data, obtained in duplicates at various constant temperatures and constant total ionic strengths, were fit to a least squares program of an IBM 704 computer, as

(1) Presented before the Division of Inorganic Chemistry, 141st National Meeting of the American Chemical Society, Washington, D. C., March, 1962.

(2) L. D. Freedman and G. O. Doak, *Chem. Rev.*, **57**, 479 (1957).

(3) G. Schwarzenbach and J. Zurc, *Monatsh. Chem.*, **81**, 202 (1950).

(4) G. Schwarzenbach, P. Ruckstuhl, and J. Zurc, *Helv. Chim. Acta*, **34**, 455 (1951).

(5) K. Moedritzer and R. R. Irani, *J. Inorg. Nucl. Chem.*, **22**, 297 (1962).

(6) R. R. Irani and C. F. Callis, *J. Phys. Chem.*, **65**, 934 (1961).

(7) R. R. Irani and C. F. Callis, *ibid.*, **64**, 1398 (1960).

(8) A. E. Martell and G. Schwarzenbach, *Helv. Chim. Acta*, **39**, 653 (1956).

previously described.[6] The resultant acid dissociation constants with the statistical 95% confidence limits are listed in Table I.

The various pK values refer to the equation

$$K_n = \frac{(H^+)(H_{n-1}L^{-(x-n+1)})}{(H_nL^{-(x-n)})} \qquad (1)$$

where parentheses indicate concentration. Constants in which the activity of the hydrogen ion is used can be obtained by multiplying K_n by the appropriate activity coefficients,[9] which, at 25°, are: 0.80, 0.78, 0.75, and 0.87 at ionic strengths of 0.1, 0.2, 0.3, and 1.0, respectively.

The dissociation of the weakest hydrogen corresponds to pK_1 and the strongest to pK_4. This is contrary to the convention of some other workers, who use pK_1 to denote the dissociation of the strongest hydrogen. The reason for the change is due to a simplification of the algebra involved, previously presented.[6]

The thermodynamic acid dissociation constants, pK_∞, also listed in Table I, were estimated by extrapolating the apparent dissociation constants at low ionic strength values to infinite dilution. Even though relatively few ionic strengths were investigated, the 95% confidence limits for pK_∞ are ±0.1 unit because of the use of previously established relationships for similar acids between apparent acid dissociation constants and ionic strength.[6,10]

The data in Table I for methylene diphosphonic acid show a small but measurable dependence of the pK values on temperature in the range 25–50° with the ΔH for dissociation of the weakest hydrogen being −3.9 ± 2.5 kcal./mole. With the polymethylene diphosphonic acids, the change in pK values with temperature was within experimental error. For the sake of brevity, only averages of the values at 25, 37, and 50° are reported in Table I.

The negative logarithm of our acidity constants at 25° and 0.1 ionic strength for methylene, trimethylene, and tetramethylene diphosphonic acids are higher than previously reported values.[3] This is expected because the previous data were obtained in the presence of alkali metal ions, which give lower apparent pK values due to complexing with the anion.

Effect of Linking Groups on Acidic Constants.—The extent of the effect of one phosphonate group on another in the same molecule can be ascertained semi-quantitatively by examining the trend of acidity constants of diphosphonic acids with change in the linking group. For polymethylene diphosphonic acids, $(HO)_2\overset{O}{\overset{\|}{P}}-(CH_2)_n-\overset{O}{\overset{\|}{P}}-(OH)_2$, the results in Table I show that the three weakest hydrogens, and probably all four, become more acidic as the number of $-CH_2-$ groups increases from one to six. Ignoring for the moment the data for $n = 10$, Fig. 1 shows that little change takes place in acidity constants for n values larger than three, and one would estimate that pK_1 and pK_2 approach the values of 8.5 and 7.9, respectively, as n approaches infinity. This is consistent with statistical considerations[3,11] that show the value of (pK_1 − pK_2) approaching 0.6 as the separation between acidic groups is increased to the point where intramolecular interaction is negligible. This also is confirmed by P^{31} n.m.r. studies[5] which showed that the shielding effect[12] of one phosphorus atom with respect to the other drops off rapidly with increasing number of $-CH_2-$ groups, n, between the two phosphorus atoms and becomes negligible for $n > 3$. Extensive investigations on

TABLE I

ACID DISSOCIATION CONSTANTS[a] FOR MONO- AND POLYMETHYLENE DIPHOSPHONIC ACIDS,

$(HO)_2\overset{O}{\overset{\|}{P}}-(CH_2)_n-\overset{O}{\overset{\|}{P}}-(OH)_2$

n	Temp., °C.	Ionic strength	pK_1	pK_2	pK_3	pK_4
1	25	0[b]	10.69	7.45	2.87	2.2
		0.1	10.42	7.33	2.75	1.7
		.2	10.31	7.28	2.70	1.5
		.3	10.22	7.25	2.65	1.5
		1.0	10.32	7.28	2.67	1.7
	37	0[b]	10.51	7.62	2.90	1.5
		.1	10.24	7.38	2.85	1.5
		.2	10.15	7.28	2.83	1.5
	50	0[b]	10.47	7.57	3.08	1.5
		0.1	10.25	7.40	2.88	1.5
		.2	10.16	7.33	2.80	1.5
		1.0	10.07	7.38	2.85	1.7
2	25–50	0[b]	9.28	7.62	3.18	1.5
		.1	9.08	7.50	2.96	1.5
		.2	9.00	7.45	2.87	1.5
		.3	8.96	7.44	2.71	1.5
		1.0	8.96	7.42	2.74	1.5
3	25–50	0[b]	8.63	7.65	3.06	1.6
		0.1	8.43	7.50	2.81	1.6
		.2	8.35	7.44	2.70	1.6
		1.0	8.33	7.41	2.69	1.7
4	25–50	0[b]	8.58	7.78	3.19	1.7
		.1	8.38	7.58	2.85	1.7
		.2	8.30	7.50	2.71	1.7
		1.0	8.30	7.47	2.70	1.7
6	25–50	0[b]	8.56	7.73	3.12	1.8
		0.1	8.34	7.65	3.07	1.8
		.2	8.25	7.62	3.05	1.8
		1.0	8.27	7.59	3.00	1.9
10	25–50	0[b]	8.94	7.93	3.27	2.1
		0.1	8.83	7.74	3.15	2.1
		.2	8.79	7.67	3.10	2.1
		1.0	8.73	7.68	3.06	2.0

[a] The 95% confidence limits for pK_1, pK_2, or pK_3 average ±0.07 unit and range between 0.05 and 0.09. The values of pK_4 are much more uncertain, with an estimated error of ±0.2 unit. [b] From extrapolation of the experimental data, as discussed in the text.

(9) H. S. Harned, A. S. Keston, and J. G. Donelson, *J. Am. Chem. Soc.*, **58**, 989 (1936).

(10) (a) M. M. Crutchfield and J. O. Edwards, *ibid.*, **82**, 3533 (1960); (b) A. E. Martell and M. Calvin, "Chemistry of the Metal Chelate Compounds," Prentice-Hall, Inc., New York, N. Y., 1952, p. 133.

(11) S. W. Benson, *J. Am. Chem. Soc.*, **80**, 5151 (1958).

(12) J. R. Van Wazer, C. F. Callis, J. N. Shoolery, and R. C. Jones, *ibid.*, **78**, 5715 (1956).

polyphosphoric acids and their salts also have shown[13] that many changes in physical and chemical properties with change in chain length become negligible for chain lengths larger than three.

But, why does pK_1 change direction and increase to 8.94 for decamethylene diphosphonic acids? One would expect polymethylene diphosphonic acids with large n values to act like alkyl phosphonic acids with half the number of $-CH_2-$ groups because of the small interaction between the two phosphonate groups. To eliminate statistical complications partially, the values of $(pK_1 + pK_2)/2$ and $(pK_3 + pK_4)/2$ for hexamethylene diphosphonic acid and decamethylene diphosphonic acid should be compared with the pK values for propyl and amyl phosphonic acids, respectively. The comparison is shown in Table II and looks amazingly close. Since the values for amyl phosphonic acids are not available, the constants for butyl and hexyl phosphonic acid are given. The pK values of alkyl phosphonic acids increase with an increase in the number of carbon atoms in the alkyl group and with the degree of branching of the carbon chain, probably due to the electron-repelling characteristics of the saturated carbon atom.[2]

TABLE II

APPARENT ACID DISSOCIATION CONSTANTS OF PHOSPHONIC ACIDS AT 0.1 IONIC STRENGTH

Acid	$\frac{1}{2}(pK_1 + pK_2)^a$ or pK_1^b	$\frac{1}{2}(pK_3 + pK_4)^a$ or pK_2^b
Hexamethylene diphosphonic acid	8.0	2.4
Propyl phosphonic[c] acid	8.1	2.5
Decamethylene diphosphonic acid	8.3	2.7
Butyl phosphonic[c] acid	8.2	2.6
Hexyl phosphonic[c] acid	8.2	2.6

[a] For diphosphonic acids. [b] For phosphonic acids. [c] From the compilation in reference 2.

In a previous paper of this series,[6] the effect of the linking groups $-CH_2-$, $-NH$, $-O-$, and $-O-O-$ on the acidity constants of diphosphonic acids, also shown in Fig. 1, was qualitatively explained on the basis of increasing electronegativities. Schwarzenbach and Zurc,[3] lacking data for dimethylene diphosphonic acid, attempted to fit hypophosphoric acid as a member of the polymethylene diphosphonic acids by claiming methylene diphosphonic acid to be an unusual member of the series due to structural effects. As clearly shown in Fig. 1, which includes the key data for dimethylene diphosphonic acid, hypophosphoric acid is no more part of the family of polymethylene diphosphonic acids than of the family of polyphosphoric acids.

Calcium Complexing.—All data represent two or more determinations. Table III gives the cc. of 8.86×10^{-2} M $Ca(NO_3)_2$ that had to be added at pH 12 to solutions containing tetramethylammonium oxalate and methylene diphosphonate to reach the point of incipient precipitation of $CaC_2O_4 \cdot H_2O$. Using previously described procedures,[7] it was found that the experimental data are best fit by assuming a 1:1 complex. Also, at this high pH value[14]

$$\frac{\beta_{CaL}}{K_{sp}} = \frac{\frac{C_1 A}{yz} - 1}{C_2} \qquad (2)$$

where β_{CaL} is the apparent dissociation constant of the complex, K_{sp} the solubility product of calcium oxalate at the appropriate ionic strength, A the volume of solution in cc., C_2 and C_1 the molar concentrations of oxalate and methylene phosphonate, respectively, and z and y are the molar concentration and cc. of calcium solution that had to be added to reach the nephelometric end point, respectively. At 25° the values for K_{sp} of $CaC_2O_4 \cdot H_2O$ are[7] 1.32×10^{-8}, 2.40×10^{-8}, and 7.80×10^{-8} at ionic strengths of 0.1, 0.5, and 1.0, respectively; at 50° the values are 4.32×10^{-8} and 2.45×10^{-7} at ionic strengths of 0.1 and 1.0, respectively. The results of the evaluation of the nephelometric data also are shown in Table III.

Extrapolation of the data in Table III to infinite dilution gives the following thermodynamic quantities at 25° for the reaction

$$\overset{+2}{Ca}\cdot(H_2O)_a + \overset{-4}{CH_2(PO_3)_2}\cdot(H_2O)_b \rightleftharpoons \overset{-2}{CaCH_2(PO_3)_2}\cdot(H_2O)_c + (a + b - c)H_2O \qquad (3)$$

$\Delta F^0 = -6.5 \pm 0.1$ kcal./mole, $\Delta H^0 = 0 \pm 2$ kcal./mole, and $\Delta S^0 = 22 \pm 7$ e.u., with the values having been corrected to refer to the absolute scale of a hypothetical unit mole fraction standard

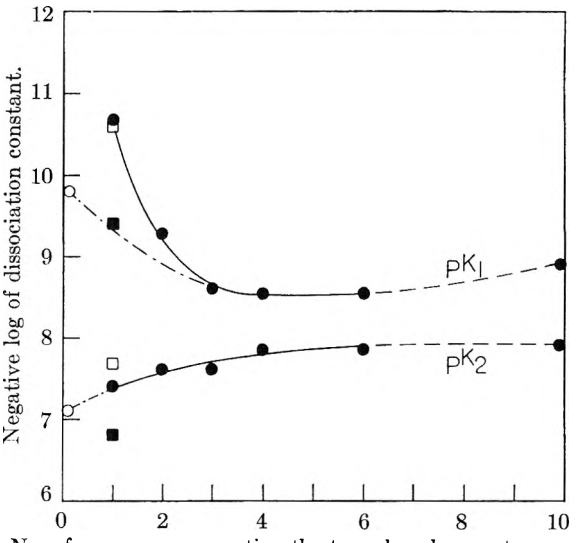

Fig. 1.—Thermodynamic acidity constants of diphosphonic acids: ●, $(HO)_2-\overset{O}{\overset{\|}{P}}-(CH_2)_n-\overset{O}{\overset{\|}{P}}-(OH)_2$, this work; ■, pyrophosphoric acid, ref. 6; ○, hypophosphoric acid, estimated from ref. 3 and 10a; □, imidodiphosphoric acid, ref. 6.

(13) J. R. Van Wazer, "Phosphorus and Its Compounds," Vol. I, Interscience Publ. Co., New York, N. Y., 1958.

(14) R. R. Irani and C. F. Callis *J. Phys. Chem.*, **64**, 1741 (1960).

TABLE III

NEPHELOMETRIC DATA FOR CALCIUM COMPLEXING BY METHYLENE DIPHOSPHONATE AT pH 12[a]

Temp., °C.	Ionic strength	Concn. of methylene diphosphonate (C_1) × 10^4, M	Concn. of oxalate (C_2) × 10^2, M	Cc. (y) of 8.86×10^{-3} M Ca soln. to nephelometric end point	Negative log of dissociation constant
25	0[b]	..	..	..	6.5 ± 0.1
	0.1	3.68	0.745	6.50	5.97
		3.68	1.49	5.20	6.06
		3.68	2.23	4.05	6.04
				Av.	6.02 ± 0.05
	1.0	3.68	0.745	3.00	4.95
		3.68	1.49	3.73	5.02
		3.68	2.23	2.80	5.02
		5.70	1.49	6.08	5.06
				Av.	5.01 ± 0.06
50	0.1	5.70	1.49	11.00	5.93
	1.0	5.70	1.49	7.90	4.77

[a] Total volume of solution was always 250 cc. [b] Extrapolated.

state.[15,16] These values indicate that complexing of calcium by methylene diphosphonate is more similar to polyphosphates than to imidodiphosphates in that the ΔH term is negligible. Also, a large positive entropy term, probably due to release of waters of hydration,[7] determines the magnitude of ΔF. The significant ΔH term with imidodiphosphates suggests some bonding between the calcium ion and nitrogen.

The complexing of calcium by methylene diphosphonate also could not be measured with the pH-lowering[4] method because of the rapid formation of a precipitate in solutions with the ratio of calcium to ligand concentration equal to or exceeding 1.0.

In Table IV the pH values are given after adding in the presence of calcium 0.5 and 1.5 equivalents of hydrogen ion per mole of dimethylene and decamethylene diphosphonate. The complete curve of acid–base titration in the presence of calcium showed stepwise complex formation. Utilizing the appropriate acidity constants in Table I, the dissociation constants for the calcium complexes were calculated using methods similar to those previously described by Lambert and Watters.[17] The results, also given in Table IV, show that the distance between the phosphonate groups is very critical in calcium complexing. This is shown in Table V, where the ligands are listed in an order of increasing distance between end phosphorus atoms. It is planned to determine these distances quantitatively with X-ray crystallographic techniques. Apparently, as long as there is a group separating the two end phosphonates, the smaller the size of the group the more stable is the calcium or magnesium complex, probably due to the release of more waters of hydration.

(15) A. W. Adamson, *J. Am. Chem. Soc.*, **76**, 1578 (1954).
(16) R. R. Irani and C. F. Callis, *J. Phys. Chem.*, **65**, 296 (1961).
(17) S. M. Lambert and J. I. Watters, *J. Am. Chem. Soc.*, **79**, 4262, 5606 (1957).

TABLE IV

COMPLEXING OF CALCIUM AND MAGNESIUM BY METHYLENE AND POLYMETHYLENE DIPHOSPHONATES

"a" is the number of equivalents of H^+ per mole of ligand, L. The total ligand concentration was always 2×10^{-3} M. C_m is the total concentration of either calcium or magnesium, with ML and MHL being the corresponding complexes. Total ionic strength was adjusted to 1.0 with tetramenthylammonium bromide.

"a"	pH	$C_m \times 10^3$, M	Neg. log of dissociation constant of ML	Neg. log of dissociation constant of MHL
	Calcium dimethylene diphosphonate, 25°			
0.50	9.08	0	..	..
0.50	8.97	2.20	2.80	..
1.50	7.54	0	..	..
1.50	7.34	2.20	..	2.60
	Calcium decamethylene diphosphonate, 25°			
0.50	8.85	0	..	..
0.50	8.83	2.50	Less than 1	..
1.50	7.80	0	..	..
1.50	7.77	2.50	..	Less than 1
	Magnesium methylene diphosphonate, 25°			
0.50	10.44	0	..	..
.50	9.02	2.00	4.79	..
.50	8.90	2.50	4.82	..
.50	8.88	2.50	4.85	..
			Av. 4.82 ± 0.03	
1.50	7.40	0	..	..
1.50	7.12	2.00	..	2.94
1.50	7.04	2.50	..	2.96
1.50	7.00	2.50	..	3.02
				Av. 2.97 ± 0.05
	Magnesium methylene diphosphonate, 50°			
0.50	10.19	0	..	..
0.50	8.65	2.50	5.07	..
1.50	7.40	..	..	..
1.50	6.88	2.50	..	3.33
	Magnesium dimethylene diphosphonate, 25°			
0.50	8.96	2.20	2.85	..
1.50	7.32	2.20	..	2.67
	Magnesium decamethylene diphosphonate, 25°			
0.50	8.85	2.50	Less than 1	..
1.50	7.84	2.50	..	Less than 1

TABLE V

CALCIUM AND MAGNESIUM COMPLEXES OF THE PHOSPHORUS-CONTAINING LIGANDS, 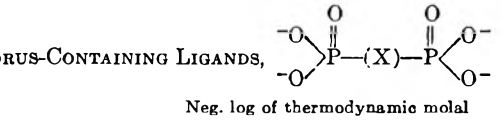

X	Neg. log of thermodynamic molal dissociation constant at 25° for Ca complex	Mg complex
None[a]	Less than 5	..
$-CH_2-$	6.5	6.3
$-NH-$	6.1	..
$-O-$	5.6	5.9[b]
$-(CH_2)_2-$	3.3[b]	3.4[b]
$-O-O-$[c]	..	3.8[b]
$-(CH_2)_3-$[d]	3.1[b]	3.3[b]
$-(CH_2)_4-$[d]	3.0[b]	3.2[b]
$-CH_2)_{10}-$	<1	<1

[a] From preliminary data, to be reported later. [b] Estimated by adding 0.5 unit to the apparent constant at 0.1 ionic strength. [c] Reference 10a. [d] Reference 4.

Magnesium Complexing.—Using the pH-lowering method, the complexing of magnesium by methylene-, dimethylene-, and decamethylene diphosphonate was measured. The results also are given in Tables IV and V. In Table V it is shown that similar to calcium complexing, the distance between phosphonate groups also is critical in magnesium complexing.

The temperature dependence data for methylene diphosphonate show that for the reaction corresponding to eq. 3, but with magnesium, $\Delta F^0 = -6.0$ kcal./mole, $\Delta H^0 = +4.4$ kcal./mole, and $\Delta S^0 = +34$ e.u. Therefore, complexing here is accompanied by a significant structural rearrangement, probably involving release of waters of hydration.[7]

The ΔH values for magnesium or calcium complexing by polymethylene diphosphonates are not reported. This is because of the large errors involved if the temperature dependence method is used with weak complexes. It is planned to measure these ΔH values as well as others directly, using calorimetry.

Our data were fit well assuming a 1:1 complex. However, we cannot preclude the existence of 2:1, 1:2, or higher complexes in systems containing a large excess of either ligand or metal ion.

Acknowledgment.—The authors thank Mr. William W. Morgenthaler for making some of the measurements.

NOTES

EFFECT OF DIMERIZATION UPON THE α-PHOSPHORESCENCE OF ACRIFLAVINE IN GLUCOSE GLASS

By Wen-Yang Wen and Robert Hsu

Department of Chemistry, DePaul University, Chicago, Ill.

Received August 16, 1961

Lewis, Lipkin, and Magel[1] have shown the correctness of the Jablonski–Lewis luminescence mechanism of a dye monomer by obtaining essentially identical energy separation between the lowest triplet and the excited singlet level by means of two different methods. One was the study of the temperature dependence of the α-phosphorescence decay time which gave the heat of activation for the process, and the other was simply the spectroscopic method of finding the energy levels of the states concerned. These methods, which have been successful for testing the mechanism of monomers, also may be useful in testing the current luminescence mechanism of dimers.[2-8] The acriflavine dye (I) was chosen for this purpose, since it gives rather long and strong α-phosphorescence at room temperatures.

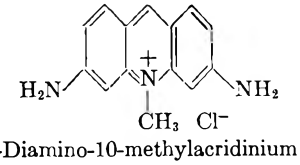

(I) 3,6-Diamino-10-methylacridinium chloride

(1) G. N. Lewis, D. Lipkin, and T. T. Magel, *J. Am. Chem. Soc.*, **63**, 3005 (1941).

(2) Th. Förster, *Naturwissenschaften*, **33**, 166 (1946).

(3) V. Zanker, *Z. physik. Chem.*, **199**, 225 (1951).

(4) G. S. Levinson, W. T. Simpson, and E. Curtis, *J. Am. Chem. Soc.*, **79**, 4314 (1957).

(5) J. Lavorel, *J. Phys. Chem.*, **61**, 1600 (1957).

(6) G. Weber and F. W. J. Teale, *Trans. Faraday Soc.*, **54**, 640 (1957).

(7) E. G. McRae and M. Kasha, *J. Chem. Phys.*, **28**, 721 (1958).

(8) D. W. Gregg and H. G. Drickamer, *ibid.*, **35**, 1780 (1961).

Experimental

Materials.—Acriflavine purchased from the National Aniline Division of the Allied Chemical Co. was purified twice by treating with freshly precipitated silver hydroxide to remove proflavine, and then recrystallized from absolute methanol. The sample was subjected to paper partition chromatography following the method of Lederer,[9] and was found to contain a minute amount of an unknown impurity which fluoresced at 440 mμ in water. This impurity emission was, however, easily removed in the experiments by suitable selection of filters and excitation wave lengths. The glucose was a Fisher certified reagent grade *d*-glucose. The glucose glass was prepared by evacuating an aqueous solution of glucose on an oil bath at 110° under a nitrogen atmosphere until the mole ratio of water to glucose dropped to about 2 to 1. The glass so prepared was quite rigid around room temperatures and its volume change was less than 5% for the largest temperature variation studied.

Instruments.—Phosphorescence spectra were obtained with a recording spectrophotometer in Dr. Lim's laboratory at Loyola University. Radiation from an Osram HBO 500-watt mercury arc lamp was passed through interference filters into a Pyrex sample tube in a dewar (with a band of unsilvered window) which held water or other cooling agents kept at the desired temperatures to within ±0.2°. The emissions were, in turn, passed through a Jarrell Ash 500-cm. scanning monochromator to a 1 P28 multiplier phototube. The output of the phototube was amplified by a Honeywell Accu Data III wide band amplifier and recorded on a Brown recorder. The decay curves of the α-phosphorescence were obtained with a flash tube (Sylvania R-4330) having a flash duration of about 2×10^{-4} sec. The emissions, observed at right angles to the exciting radiation, were focused on the cathode of a multiplier phototube. Filters were placed in the observation path to prevent exciting light from reaching the detector and to isolate the desired emission wave length. The output of the phototube was applied to the vertical deflection circuits of a Hewlett-Packard Model 130/B oscilloscope. The decay curve was displayed by letting the electron beam of the oscilloscope start its sweep at the firing of the flash tube. The oscilloscope sweep trace was photographed with a DuMont oscilloscope camera.

Results and Discussion

The α-phosphorescence spectra of 10^{-5} and 10^{-2} *M* acriflavine in glucose glass at 25° obtained with 440 mμ excitation are shown in Fig. 1. These

(9) M. Lederer, *Anal. Chem. Acta*, **6**, 267 (1952).

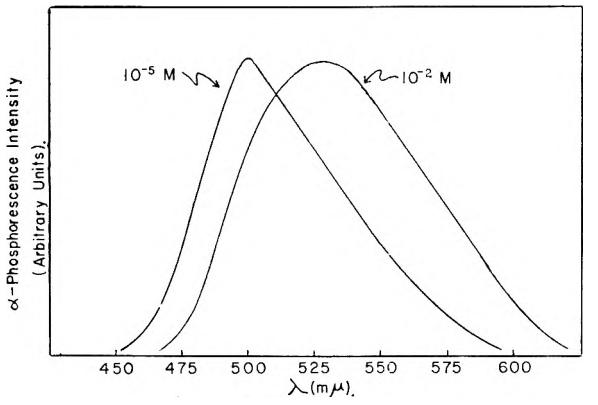

Fig. 1.—The α-phosphorescence spectra of 10^{-5} and 10^{-2} M acriflavine in glucose glass at 25° obtained with 440 mμ excitation.

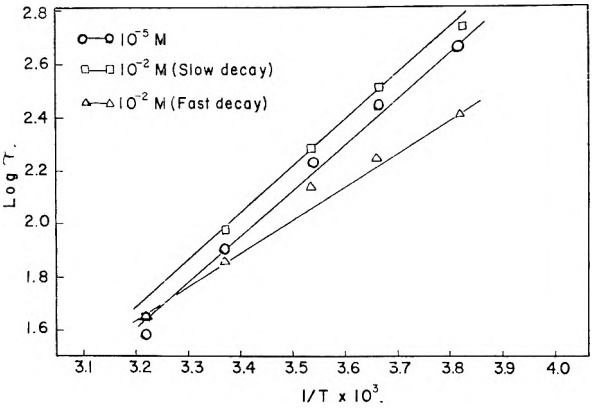

Fig. 2.—The plot of the logarithm of the α-phosphorescence decay mean-life *vs.* the reciprocal temperature for 10^{-5} and 10^{-2} M acriflavine in glucose glass.

spectra match closely, as they should, with the corresponding fluorescence spectra. The 10^{-2} M solution, which was found to contain a considerable amount of dimers from our absorption studies, gives an α-phosphorescence band that is relatively broad and red-shifted in comparison with the corresponding band of the solute monomer at 10^{-5} M. This is in accord with the mechanism of the splitting of the excited singlet level of the monomer upon dimerization. For the temperature range (−11 to 37.7°) studied, the α-phosphorescence of 10^{-5} M acriflavine decayed exponentially[10] with the mean-life given in Table I. The logarithm of the decay mean-life was plotted against the reciprocal of the absolute temperature in Fig. 2. The activation energy for the monomer is obtained from the slope and found to be 8.0 ± 0.5 kcal./mole. The decay of 10^{-2} M solution was, however, found to be an approximate superposition of two exponential decays; (one with a shorter mean-life to be called the fast decay, and the other with a longer mean-life to be called the slow decay hereafter). The obtained data for the fast and slow decays of 10^{-2} M solution at several temperatures are given in Table I and plotted separately in Fig. 2. Interestingly, the plot for slow decay gives almost identical activation energy with that for monomer, while the fast decay gives a smaller activation energy with a value of 5.5 ± 0.5 kcal./mole.

(10) Exponential decays at room temperature also were obtained by D. Yamamoto, *J. Chem. Soc. Japan*, **74**, 173 (1953).

TABLE I

THE DECAY MEAN-LIFE OF THE α-PHOSPHORESCENCE OF ACRIFLAVINE IN GLUCOSE GLASS AT VARIOUS TEMPERATURES

(Time in msec.)

	−11°	0°	10.2°	24.0°	37.7°
10^{-5} M	480	284	170	78	37
10^{-2} M (slow decay)	550	334	195	94	43
10^{-2} M (fast decay)	254	174	138	71	43

The fast decay is considered to be associated with the dimer emission from the following reason: The dimer excited singlet state is composed of two electronic energy levels, one above that of the monomer and the other below, in contrast to the fact that the dimer triplet state will remain essentially the same as that of the monomer. Consequently, the energy level difference between the triplet and the lower excited singlet of the dimer is smaller than the corresponding energy level difference between the triplet and the excited singlet of the monomer. In other words, the activation energy from the triplet to the excited singlet is smaller for the dimer than for the monomer. It is easy to see from an Arrhenius type equation, $1/\tau = Ae^{-\Delta E/RT}$, that a smaller activation energy ΔE will lead to a shorter decay mean-life, τ.

The α-phosphorescence peaks for 10^{-5} and 10^{-2} M solutions of acriflavine in glucose glass are 500 and 528 mμ, respectively. The β-phosphorescence peak is observed at 575 mμ for both solutions. On the assumption that the emission spectrum of 10^{-2} M solution is mainly of the dimers, while that of 10^{-5} M solution is of the monomers, we can calculate the activation energies from the respective peak separation of the α- and β-phosphorescence bands. The results are ΔE_M = 7.5 ± 0.5 kcal./mole for the monomer and ΔE_D = 5.0 ± 0.5 kcal./mole for the dimer.

The reasonable agreement between the values of ΔE_D obtained from the two different methods seems to give an experimental support to the luminescence mechanism of dimers.

Acknowledgment.—We are indebted to a grant support from the Research Corporation. Our thanks are due also for the technical assistance and many valuable suggestions of Dr. E. C. Lim of Loyola University.

THE DESTRUCTION OF THE ALUMINUM–CARBON BOND IN ALUMINUM ALKYLS BY CARBON TETRACHLORIDE

BY C. EDEN[1] AND H. FEILCHENFELD

The Petrochemical Laboratory of the National Council for Research and Development and of the Physical Chemistry Department, Hebrew University, Jerusalem, Israel

Received December 1, 1961

Alkali and alkali earth metal–carbon bonds in aluminum alkyls are instantaneously destroyed by carbon tetrachloride. Phenyllithium[2] at −70°

(1) Taken fron the Ph.D. Thesis of C. Eden.

(2) G. Wittig and H. Witt, *Ber.*, **74B**, 1474 (1941).

and methyllithium and butyllithium[3] at −60° react rapidly with CCl_4 even in dilute ether solutions. It was, therefore, surprising to find that triethylaluminum could be dissolved in CCl_4 at room temperature; except for a transient evolution of gas which on investigation proved to be due to impurities, no reaction could be observed. Even after standing for days, no further decomposition occurred.

This observation opened a field for the investigation of the use of carbon tetrachloride as a solvent in the polymerization of α-olefins in the presence of Ziegler catalysts. Ziegler in his patent[4] gave a long list of solvents; CCl_4 was not among them. On using CCl_4 as a solvent it could be shown[5] that the polymerization proceeded normally just as in *n*-heptane, except that after a period of about 1 hr. the pressure suddenly rose and polymerization stopped. This result was the starting point for the present investigation.

One hundred ml. of CCl_4 (analytical reagent) was introduced into a conical flask attached to a vacuum system. After outgassing, the temperature was adjusted to 30°, the liquid was stirred by a magnetic stirrer, and varying amounts of triethylaluminum were injected through a rubber gasket by means of a hypodermic syringe. If the CCl_4 was not pure, a slight reaction occurred. After achieving constant pressure, $TiCl_4$ was injected. In Fig. 1 the change of pressure with time for a constant volume system is shown graphically. At A triethylaluminum was added and the pressure rose to a constant value. At B $TiCl_4$ was added to the solution; a reaction occurred similar to that between triethylaluminum and $TiCl_4$ in the absence of CCl_4. In Table I the composition of the gas evolved during the reaction is given. At C the rate of decomposition suddenly increased spontaneously; in this "explosion" step CD all aluminum–carbon bonds were decomposed, for on addition of hydrochloric acid no hydrocarbons were liberated.

TABLE I

GASEOUS REACTION PRODUCTS (MOLE %)[a]

	1	2	3	4
H_2	4	..	..	..
CH_4	2	..	..	2.5
C_2H_6	79	84	10.2	25.5
C_2H_4	..	..	..	15.5
C_3H_8	..	..	6.6	..
n-C_4H_{10}	4	7.2	5.7	1.0
i-C_4H_{10}	8	2.3	39.2	..
i-C_5H_{12}	1	..	5.8	..
C_2H_5Cl	..	6.5	31.8	56.5

[a] Column (1) $Al(C_2H_5)_3$ + $TiCl_4$ (Al/Ti = 2); (2) 3.5 mmoles $Al(C_2H_5)_3$ + 1.8 mmoles $TiCl_4$ + 5 ml. CCl_4, stage BC of Fig. 1; (3) 3.5 mmoles $Al(C_2H_5)_3$ + 1.8 mmoles $TiCl_4$ + 5 ml. CCl_4, stage CD of Fig. 1; (4) $C_2H_5AlCl_2$ + CCl_4.

The reaction between triethylaluminum and $TiCl_3$ in CCl_4 also was investigated. (Since $TiCl_3$ is a solid it had to be introduced at the beginning.) In this case too the "explosion" occurred, though only after 4 hr. ($TiCl_4$, 3/4 hr.).

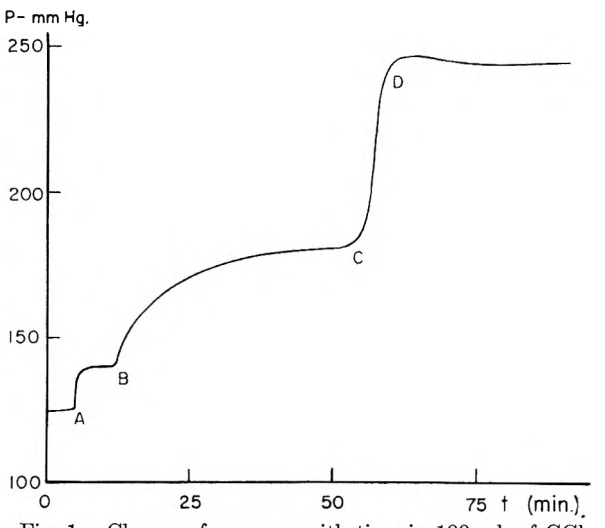

Fig. 1.—Change of pressure with time in 100 ml. of CCl_4 solution at 30°: at A addition of triethylaluminum; at B addition of titanium tetrachloride; at C beginning of "explosion"; at D end of decomposition.

The length of the induction period BC for the $TiCl_4$ depended on several factors.

(1) **Temperature.**—The induction period was increased by lowering the temperature. An induction period of 8 min. at 30° corresponded to one of more than 300 min. at 0°.

(2) **Concentration.**—The smaller the amount of CCl_4 used with triethylaluminum and $TiCl_4$ the shorter the induction period.

(3) **Ratio.**—Using greater excess of triethylaluminum over $TiCl_4$ lengthened the induction period.

It was surprising that the triethylaluminum had an inhibiting effect on its own decomposition. As a possible explanation it was considered that $AlCl_3$ acted as a catalyst for the decomposition. $AlCl_3$ is the final oxidation product from the action of $TiCl_4$ on triethylaluminum. It would be expected to appear only after no more triethylaluminum and diethylaluminum chloride were present. Excess of triethylaluminum therefore should increase the induction period. However, experiment showed that the mixture $AlCl_3$, triethylaluminum, carbon tetrachloride was stable (if the $AlCl_3$ was free from $FeCl_3$). $AlCl_3$ itself therefore did not cause the decomposition.

On the other hand when $AlCl_3$ and triethylaluminum first were heated together at 80° to give $C_2H_5AlCl_2$[6] and then, after cooling to room temperature, CCl_4 was added, instantaneous decomposition occurred. The decomposition therefore was due to the reaction between ethylaluminum dichloride and CCl_4 and occurred also in the absence of $TiCl_4$. This showed that the function of the $TiCl_4$ was only to oxidize the triethylaluminum to ethylaluminum dichloride. Obviously this reaction proceeded faster in more concentrated solutions (less CCl_4).

The gaseous decomposition products of the reaction $C_2H_5AlCl_2$ + CCl_4 are given in Table I.

(3) W. T. Miller, Jr., and C. S. Y. Kim, *J. Am. Chem. Soc.*, **81**, 5008 (1959).

(4) K. Ziegler, Israel Patent 8390.

(5) M. Jeselson, M. Sc. Thesis, Hebrew University of Jerusalem, 1959.

(6) A. V. Grosse and J. N. Mavity, *J. Org. Chem.*, **5**, 106 (1940).

They differ from those obtained during the decomposition stage CD of triethylaluminum in the presence of $TiCl_4$. This is due partly to the catalytic properties of the latter system.

The elucidation of the exact mechanism of the decomposition would need further study.[7] The analysis of the reaction products points to a carbonium ion mechanism. Were the reaction to pass through free ethyl radicals these would be trapped by the large excess of CCl_4 solvent and only C_2H_5Cl would be obtained. Furthermore a free radical decomposition would not explain the specificity of $C_2H_5AlCl_2$; just the opposite, it would be expected that the far more reactive triethylaluminum would react faster than ethylaluminum dichloride. The decomposition therefore must be ionic. Were the decomposition anionic, one would expect mainly the Wurtz reaction product, butane, from $Me-C_2H_5$ and the C_2H_5Cl which is present. Only 1% of butane was detected. Also the carbanionic decomposition product should yield $C_2H_5CCl_3$ rather than C_2H_5Cl.

Tentatively it may be suggested that an equilibrium passing through intermediate steps is set up

$$2CCl_4 + C_2H_5AlCl_2 \rightleftarrows 2CCl_3\cdot + C_2H_5{}^+AlCl_4{}^-$$

The equilibrium is displaced toward the right by recombination of the $CCl_3\cdot$ radicals giving C_2Cl_6; hexachloroethane could indeed be detected. It is reasonable to suppose that the ethylcarbonium will react further with both CCl_4 and $C_2H_5AlCl_2$

(a) $C_2H_5{}^+AlCl_4{}^- + CCl_4 \longrightarrow C_2H_5Cl + CCl_3{}^+AlCl_4{}^-$

$$\downarrow$$

$$CCl_4 + AlCl_3$$

(b) $C_2H_5{}^+AlCl_4{}^- + C_2H_5AlCl_2 \longrightarrow$

$$C_2H_6 + AlCl_4{}^-{}^+C_2H_4AlCl_2$$

$$\downarrow$$

$$C_2H_4 + 2AlCl_3$$

All the major reaction products stipulated actually have been found. However, the carbonium ion mechanism suggested in this case is in contrast with the carbanionic and free radical mechanisms established for the more normal decompositions of the metal–carbon bond.

(7) However, further work in this direction is not being undertaken.

OXIDATION OF PHOSPHOROUS ACID

By B. Silver and Z. Luz

Weizmann Institute of Science, Rehovoth, Israel

Received December 2, 1961

The oxidation of phosphorous acid by halogens has been the subject of previous studies. Mitchell[1] examined the kinetics of oxidation by iodine in dilute HCl and concluded that two mechanisms were operative, *viz.*, the attack of I_3^- ion on an "active" tautomer of phosphorous acid, and simultaneously a direct attack of molecular iodine on the "normal" form of the acid. He found that the over-all rate decreases with increasing acidity in the range 0.05 to 0.15 *N* HCl. Berthoud and Berger[2] studied the oxidation of H_3PO_3 by iodine in both acid and neutral solutions. On the basis of experiments carried out between 0.1 and 0.5 *N* HCl they conclude that the oxidation rate is acid independent and involves a direct attack of I_2 and I_3^- on phosphorous acid and its ions. In acetate buffer between ~pH 4.5 and 5.0 they found a decrease in rate with increasing acidity and, although they fail to analyze their experimental data, put forward a mechanism consisting of the attack of molecular iodine on the mono- or dianion of phosphorous acid, catalyzed by hydroxide ion. Griffith and McKeown[3] studied the oxidation up to 1.8 *M* acid using bromine and chlorine, and for the case of bromine were able to interpret their results as indicating the oxidation of the phosphite ions by molecular bromine, but unlike Mitchell they did not postulate the existence of tautomerism. The above works were reviewed by Yost and Russell,[4] whose conclusions are that tautomerism plays no part in the oxidation, and that all the results probably are explicable in terms of different reactivities of the two phosphite ions. Van Wazer[5] also comments on the obscurity of the mechanism of oxidation and suggests a chain reaction as one possible mechanism. Stranks and Wilkins[6] state that the absence of measurable deuterium exchange of the phosphorus-bonded hydrogen of H_3PO_3 rules out a tautomeric equilibrium prior to oxidation.

In 1959 Martin[7] showed that at high acidities such an exchange does in fact occur, but he did not discuss the relevance of this result to the oxidation reaction. The acid and base catalyzed oxidation of the dialkyl esters of phosphorous acid has been shown to follow the same rate law as that for exchange with deuterium of the phosphorus-bonded hydrogen.[8,9] On the basis of this result it was suggested that tautomerism precedes both exchange and oxidation.

Considering Martin's work and by analogy to the dialkylphosphonates it seems likely that tautomerism should play an important role in the oxidation of phosphorous acid in strong acid solutions. In the present work the oxidation and exchange reactions were re-investigated in the strong acid range (up to 4.0 *N*). The reaction also was studied at pH 8.6, where the dominant species of the phosphorous acid is the dianion HPO_3^{--}. In the acidic range the results suggest that tautomerism plays a role in the oxidation reaction. At acidities below ~1 *N* tautomerism takes no significant part in the oxidation reaction.

Experimental

Materials.—Normal and deuterated phosphorous acid were made from phosphorus trichloride and H_2O or D_2O, respectively.[10] The products were purified by crystallization

(1) A. D. Mitchell, *J. Chem. Soc.*, **123**, 2241 (1923).

(2) A. Berthoud and W. E. Berger, *J. chim. phys.*, **25**, 568 (1928).

(3) R. O. Griffith and A. McKeown, *Trans. Faraday Soc.*, **29**, 611 (1933).

(4) D. M. Yost and H. Russell, "Systematic Inorganic Chemistry," Prentice-Hall, Inc., New York, N. Y., 1946.

(5) J. R. Van Wazer, "Phosphorus and its Compounds," Interscience Publishers, Inc., New York, N. Y., 1958, Chap. 7.

(6) D. R. Stranks and R. D. Wilkins, *Chem. Revs.*, **57**, 743 (1957).

(7) R. B. Martin, *J. Am. Chem. Soc.*, **81**, 1574 (1959).

(8) Z. Luz and B. Silver, *ibid.*, **83**, 4518 (1961).

(9) B. Silver and Z. Luz, *ibid.*, **84**, 1091 (1962).

(10) D. Voigt and F. Gallais, "Inorganic Syntheses," ed., J. C. Bailar, Vol. IV, McGraw-Hill Book Co., New York, N. Y., 1953.

from H_2O or D_2O and subsequently dried under high vacuum. Na_2HPO_3 and Na_2DPO_3 were prepared by potentiometric titration of the corresponding acid with NaOH. All other materials were Analar reagent grade.

Kinetics. I. Exchange.—The exchange of the phosphorus-bonded hydrogen of H_3PO_3 with solvent D_2O could be observed only in strong acid and was studied by an n.m.r. technique previously described.[8] The decrease in intensity of the resonance line of the phosphorus-bonded hydrogen was measured using as an internal reference the methyl resonance of methanol which was present as 1% by volume.

II. Oxidation was followed by titration of iodine with standard sodium thiosulfate solution. At pH 8.6, where the oxidation is fast, aliquots of the reaction solution were quenched in sufficient dilute HCl to effectively stop the oxidation.

Results and Discussion

Strong Acid Range.—Martin's[7] observation of the acid-catalyzed exchange of the phosphorus-bonded hydrogen in H_3PO_3 was re-investigated at lower concentrations of H_3PO_3. The results are summarized in Table I, from which it may be seen that the exchange rate increases with DCl concentration. In view of these results and by analogy with the case of the dialky'phosphonates, the possibility arises that tautomerism plays a role in the oxidation of H_3PO_3 in acidic solutions. If tautomerism is the rate-determining step in oxidation, the oxidation reaction should show acid catalysis and, at sufficiently high iodine concentrations, should be independent of iodine concentration and have a comparable rate to the exchange reaction at the same acidity.

TABLE I

PSEUDO FIRST-ORDER RATE CONSTANT FOR EXCHANGE OF THE PHOSPHORUS-BONDED HYDROGEN OF A SOLUTION OF 2.4 *M* H_3PO_3 IN D_2O AS A FUNCTION OF [DCl]
Temp. 22°

DCl, mole l.$^{-1}$	$k \times 10$, hr.$^{-1}$
1.49	1.18
2.24	1.49
3.25	2.03
3.60	2.31
4.10	2.82

The oxidation of H_3PO_3 by iodine was studied at HCl concentrations of 1.0, 2.5, and 4.0 *N* HCl, the iodine concentration being varied at fixed acidity. The decrease in iodine concentration as a function of time was determined by titration with sodium thiosulfate solution. The results for 1.0 *N* HCl are shown in Fig. 1. Due to the fact that the decrease in titer is small compared to the total iodine titer, the accuracy of the runs is low and no attempt was made to make an exact kinetic interpretation. However, a number of qualitative observations can be made by plotting the initial slopes of the runs at different acidities and iodine concentrations against iodine concentration. The results are summarized in Table II and shown in Fig. 2. Two conclusions may be drawn from the results. First that the oxidation is acid-catalyzed and secondly that at 1.0 *N* HCl the initial rate is not linearly proportional to iodine concentration. As may be seen from the last run in Table II an appreciable kinetic isotope effect results from the substitution of deuterium for the phosphorus-bonded hydrogen of H_3PO_3. Martin observed a similar isotope effect in the case

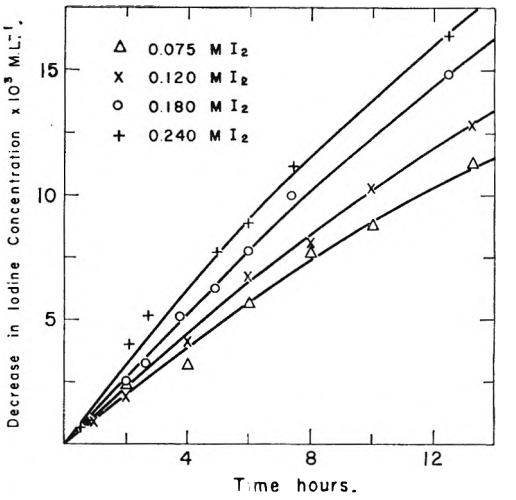

Fig. 1.—The decrease in iodine concentration as a function of time for the oxidation of phosphorous acid by iodine in 1.0 *N* HCl; temp. 22°. (Compositions of solutions are given in Table II.)

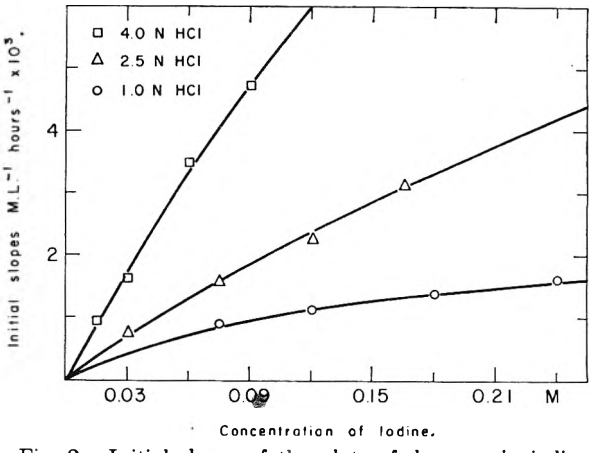

Fig. 2.—Initial slopes of the plots of decrease in iodine concentration for the oxidation of H_3PO_3 in various acid solutions; temp. 22°. (Compositions of solutions are given in Table II.)

TABLE II

INITIAL SLOPES OF THE PLOTS OF DECREASE IN IODINE CONCENTRATION FOR THE OXIDATION OF 0.05 *M* PHOSPHOROUS ACID

The ratio [KI]/[I_2] was 4.67 for all runs, temp. 22°.

HCl concn., *M*	Initial iodine concn., *M*	Initial slopes mole/hr. × 10³
1.0	0.075	0.90
	.120	1.13
	.180	1.38
	.240	1.62
2.5	0.030	0.75
	.075	1.58
	.120	2.25
	.165	3.13
4.0	0.015	0.95
	.030	1.63
	.060	3.50
	.090	4.75
1.0[a]	0.240	0.65

[a] This run is for 0.05 *M* D·OP(OH)$_2$.

of the exchange reaction of $H \cdot PO(OH)_2$ and $D \cdot PO(OH)_2$.

The prediction that the oxidation is acid-catalyzed is confirmed by the present results. Previous statements that the rate decreases with increasing acidity[1] or is independent of acidity[2] are explained by the limited range of acidity studied. The decrease of oxidation rate observed by Mitchell is explicable in terms of a corresponding decrease in the proportion of dissociated phosphorous acid to undissociated acid, since, as will be discussed later, the ions are oxidized much faster.

The expectation that the rate should approach a limiting value at high iodine concentrations is fulfilled by the results in 1.0 *N* HCl. For the reasons stated under Experimental it was not possible to study oxidation at higher ratios of iodine to phosphorous acid, at which we believe there would be complete independence of rate on iodine concentration. Above 1.0 *N* HCl the region of iodine-independent oxidation is presumably at still higher iodine concentration. The following mechanism is suggested to account for the acid-catalyzed exchange and oxidation. The scheme

$$H \cdot PO(OH)_2 + H^+ \rightleftharpoons H \cdot P(OH)_3^+ \rightleftharpoons \begin{cases} \xrightarrow{\text{Oxidation}} O \cdot P(OH)_3 \\ :P(OH)_3 \\ \xrightarrow{\text{Exchange}} D \cdot PO(OH)_2 \end{cases} \quad (I)$$

shows a reversible protonation of the phosphoryl group of H_3PO_3 followed by fission of the phosphorus–hydrogen bond to give a tricovalent form of phosphorous acid. This form is expected to be extremely reactive, undergoing oxidation in the presence of an oxidizing agent or accepting a proton (or deuteron) from the solvent to re-form the species $H \cdot PO(OH)_2$. In the presence of sufficient iodine the exchange reaction cannot compete with oxidation and the oxidation rate becomes independent of the concentration of oxidizing agent. Such an approach to independence at high iodine concentration may be seen from the results in 1.0 *N* HCl. From the initial slope of the run at the highest iodine concentration, a pseudo-first-order rate constant of approximately 0.3×10^{-1} hr.$^{-1}$ may be estimated for this run. This value is close to the asymptotic value for 1.0 *N* HCl, and is in fact of the same order as the pseudo-first-order rate constant for exchange at the same acidity, *i.e.*, 1.0×10^{-1} hr.$^{-1}$.

Oxidation of Phosphite Anions.—Phosphorous acid has two ionizable hydrogens with pK's of 1.29 and 6.74.[5] In order to isolate the oxidation reaction of the dianion the reaction was studied at pH 8.6 (borate buffer), where the dianion is the predominating species.

The experimental solutions contain a mixture of molecular iodine and triiodide ion. It was observed that KI depresses the reaction rate, which suggests that the main oxidizing agent is molecular iodine, since the addition of KI under the experimental conditions decreases the concentration of molecular iodine appreciably but hardly has any effect on the I_3^- concentration. In fact the kinetics could be interpreted in terms of a single significant reaction, *viz.*, the bimolecular attack of molecular I_2 on the dianion

$$\frac{d[I_2]}{dt} = -k_2[I_2][HPO_3^{--}] \quad (1)$$

Equation 1 may be integrated to give

$$kt = \frac{k_2}{K} t = R = \left[\left(\frac{\delta + 3a}{a - b}\right) \ln\left(\frac{a - x}{a}\right) - \left(\frac{\delta + 3b}{a - b}\right) \ln\left(\frac{b - x}{b}\right)\right] \quad (2)$$

where a and b are the initial concentrations of iodine and phosphorous acid, respectively, δ is the difference in initial concentration of potassium iodide and iodine, and x is the decrease in concentration of iodine up to time t, as determined by the thiosulfate titration. K is the equilibrium constant for the reaction $I_2 + I^- \rightleftarrows I_3^-$. It should be noted that the derivation of eq. 2 from eq. 1 rests on the assumption that, under the experimental conditions, the concentration of molecular I_2 is small compared to both δ and the concentration of I_3^-. This assumption follows from the large value[11] of K, 7.68×10^2 mole^{-1}.

Equation 2 implies that a plot of R against time should be linear, with a slope that is independent of δ. Such behavior is in fact followed over several half-lives, as may be seen from the experimental data plotted in Fig. 3. From the slope a value of 7.1×10^3 mole^{-1} min.$^{-1}$ was derived for k_2. The value of k_2 was unaffected, within experimental error, by doubling and tripling the buffer concentration.

The experimental results are consistent with a mechanism involving the attack of molecular iodine on phosphite ions. The possibility that hypoiodous acid (HIO) is the effective oxidizer is ruled out by an experiment carried out in NaOH. Under these conditions the hydrolysis of iodine to form HIO is practically complete and no measurable oxidation of H_3PO_3 was in fact observed.

In the case of the dialkylphosphonates a correlation was observed between the rate of oxidation in acetate buffer and the acetate ion-catalyzed exchange of the phosphorus-bonded hydrogen.[9] Such a correlation cannot be made in the case of phosphorous acid since we have observed that acetate buffer has no catalytic effect on oxidation and neither is there any measurable exchange of phosphorus-bonded hydrogen with deuterium in solutions of H_3PO_3 in acetate buffer at pH 5.3 at room temperature. The absence of base-catalyzed hydrogen exchange was confirmed by experiments in strong NaOH solution. Martin[7] and Brodskii[12] have noted the absence of exchange in solutions of Na_2HPO_3 and NaH_2PO_3. The negative charge on the anions of phosphorous acid thus appears to be sufficient to retard attack of a negatively charged base, such as occurs in the case of dialkyl phosphonates.

A further feature of the behavior of H_3PO_3 is the fact that an appreciable kinetic isotope effect was observed in the oxidation of the deuterated

(11) I. M. Kolthoff and R. Belcher, "Volumetric Analysis," Vol. III, Interscience Publishers, Inc., New York, N. Y., 1957, p. 202.

(12) A. I. Brodskii and L. V. Sulima, *Doklady Akad. Nauk S.S.S.R.*, **85**, 1277 (1952).

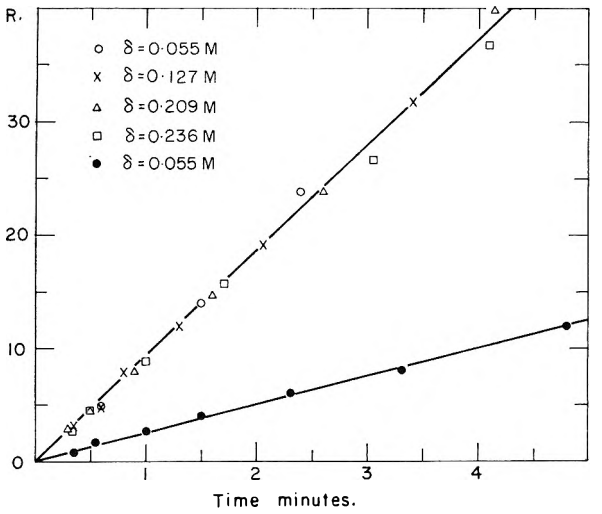

Fig. 3.—Oxidation of 0.01 M phosphorous acid in 0.1 M borate buffer at pH 8.6. Initial concentration of iodine 0.015 M; temp. 22°. R (as defined in eq. 2) is plotted *vs.* time, for different values of δ. The filled dots are for deuterated phosphorous acid, D·PO(OH)$_2$, under the same experimental conditions.

acid D·PO(OH)$_2$. In Fig. 3 the results of runs carried out with deuterated phosphorous acid are plotted together with the data for the normal form. The kinetic isotope effect $k_H/k_D \simeq 3.6$.

Some runs were carried out in acetate buffer at pH 4.4 and 5.3, the runs at pH 4.4 being slower than those at pH 5.3 and both sets being appreciably slower than those at pH 8.6. The decrease may be attributed to the decrease in concentration of the dianion, and the much lower oxidation rate of the monoanion. In principle it should be possible to derive a value for the bimolecular constant for the oxidation of the monoanion. However, such a derivation depends on an accurate knowledge of the dissociation constants of H_3PO_3 at the variety of ionic strengths obtaining under the experimental conditions. Such data are not available but a rough estimate gave an upper limit of $\sim$10 mole^{-1} min.$^{-1}$, and it is believed that the reaction of the monoanion is intermediate between that of the undissociated acid and the dianion.

Investigations were supported in part by a research grant (RG 5842) from the Division of Research Grants, U.S. Public Health Service. B. S. is the recipient of the Max and Rebecca Schrire Medical Research Grant.

THE INFLUENCE OF PRESSURE ON THE FORMATION OF MICELLES IN AQUEOUS SOLUTIONS OF SODIUM DODECYL SULFATE

By S. D. Hamann

Division of Physical Chemistry, Australian Commonwealth Scientific and Industrial Research Organization, Fishermen's Bend, Melbourne, Australia

Received December 18, 1961

Density measurements[1-6] have shown that the partial molar volumes of long-chain aliphatic salts, dissolved in water, are greater in the micellar state than in the free ionic state. It follows that an increase in hydrostatic pressure should generally inhibit the formation of micelles and so raise the critical micelle concentration (c.m.c.).

To test this prediction, some direct measurements have been made of the influence of pressure on the c.m.c. of solutions of sodium dodecyl sulfate.

Experimental

The c.m.c. was determined by measuring the specific conductivity of the solutions as a function of the molality of sodium dodecyl sulfate. At each pressure, the points lay on two straight lines whose intersection was taken to be the c.m.c.[7] (see Fig. 1).

The conductivity measurements were carried out in a Teflon cell[8,9] fitted with platinized platinum electrodes and mounted in a conventional steel pressure vessel.[10] The temperature of the cell was controlled to within ±0.01° and the pressure to within ±10 atm. The conductances of the solutions were measured by a Wayne-Kerr B221 Universal Transformer Bridge and were converted to specific conductivities by subtracting the measured conductance of water at the appropriate pressures and by applying cell constants corrected for the linear contraction of Teflon under pressure.[9,11] Two different samples of purified sodium dodecyl sulfate gave identical results.

Results

Conductivity measurements were made at eleven concentrations between 2×10^{-3} and 4×10^{-2} molal, at 25°, and at pressures of 1, 500, 1000, 1500, and 2000 atm.

Figure 1 shows the results of some of the measurements. For the sake of clarity in the diagram, the conductivity data at 500 and 1500 atm. have been omitted. The inset in Fig. 1 shows the variation of the c.m.c. with pressure. The measured value at 1 atm. (0.00827 mole/kg.) agrees well with values reported earlier by Goddard and Benson[7] (0.0084 mole/kg.) and by Flockhart and Ubbelohde[12] (0.0080 mole/kg.).

Discussion

The results show that the c.m.c. initially increases with increasing pressure in accordance with the general prediction made in the introduction.

On the basis of Stainsby and Alexander's[13] quasi-thermodynamic treatment of micelle formation, and its later refinement by Phillips,[14] we should expect the influence of pressure on the c.m.c. to be given by the relationship

$$\left(\frac{\partial \ln (\text{c.m.c.})}{\partial P}\right)_{T,m} = \frac{\Delta \bar{V}}{1.8\ \mathbf{R}T} \qquad (1)$$

where **R** is the gas constant, T is the absolute temperature, P is the pressure, and $\Delta \bar{V}$ denotes the change of partial molar volume when the salt passes

(1) D. G. Davies and C. R. Bury, *J. Chem. Soc.*, 2263 (1930).
(2) C. R. Bury and G. A. Parry, *ibid.*, 626 (1935).
(3) R. G. Paquette, E. C. Lingafelter, and H. V. Tartar, *J. Am. Chem. Soc.*, **65**, 686 (1943).
(4) R. J. Vetter, *J. Phys. Chem.*, **51**, 262 (1947).
(5) K. Hess, W. Philippoff, and H. Kiessig, *Kolloid Z.*, **88**, 40 (1939).
(6) K. A. Wright and H. V. Tartar, *J. Am. Chem. Soc.*, **61**, 544 (1939).
(7) E. D. Goddard and G. C. Benson, *Can. J. Chem.*, **35**, 986 (1951).
(8) J. C. Jamieson, *J. Chem. Phys.*, **21**, 1385 (1953).
(9) S. D. Hamann and W. Strauss, *Trans. Faraday Soc.*, **51**, 1684 (1955).
(10) J. Buchanan and S. D. Hamann, *ibid.*, **49**, 1425 (1953).
(11) C. E. Weir, *J. Research Natl. Bur. Standards*, **53**, 245 (1954).
(12) B. D. Flockhart and A. R. Ubbelohde, *J. Colloid Sci.*, **8**, 428 (1953).
(13) G. Stainsby and A. E. Alexander, *Trans. Faraday Soc.*, **46**, 587 (1950).
(14) J. N. Phillips, *ibid.*, **51**, 561 (1955).

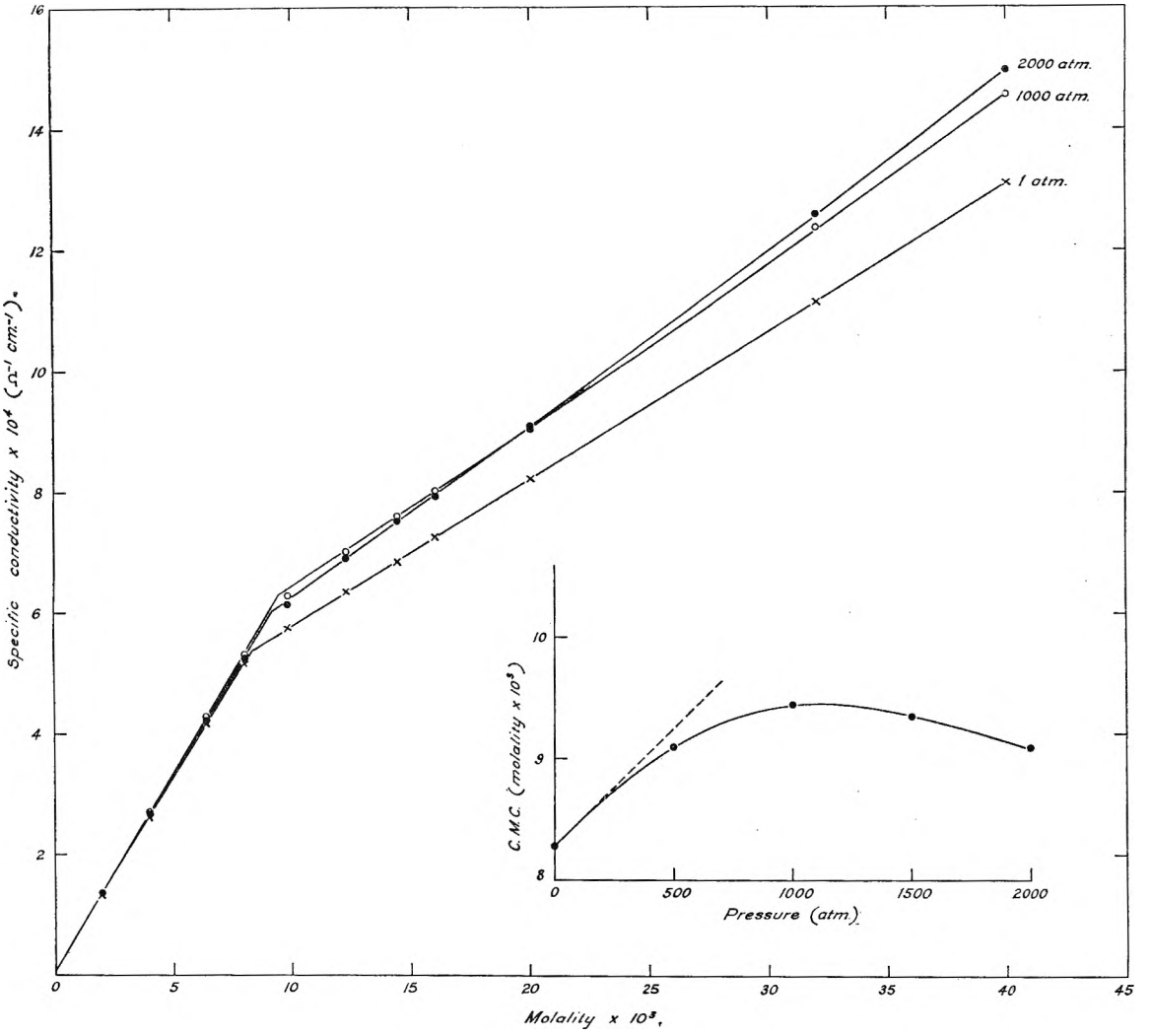

Fig. 1.—The specific conductivity of sodium dodecyl sulfate in aqueous solution at 25° and at 1, 1000, and 2000 atm. Inset: The variation of the c.m.c. with pressure.

from the free ionic state into the micellar state. The factor 1.8 allows for the influence of counterions associated with the micelles.[14]

Applying formula 1 to the present results we find that the initial rate of change of the c.m.c. with pressure (shown by the dotted line in Fig. 1) corresponds to a value: $\Delta\bar{V} = +11$ cm.^{3}/mole.

This agrees well with the value, $+10 \pm 3$ cm.^{3}/mole, given by Kushner, Duncan, and Hoffman's[15] density measurements on aqueous solutions of sodium dodecyl sulfate at 23°.

The reason for the expansion is not definitely known. Goddard, Hoeve, and Benson[16] have suggested that it might arise from the release of water molecules which had been tightly held as "icebergs" around the hydrocarbon chains of the free ions. To the author, it seems more likely that bound water is released from the solvation shells of the electrically charged terminal groups when the charges become partially neutralized by counterions associated with the micelles. A closely analogous expansion occurs when inorganic ions associate into ion pairs in aqueous solution.[17]

Considering the results at higher pressures, we see from Fig. 1 (inset) that the initial positive trend of the c.m.c. with increasing pressure reverses at about 1000 atm. If we accept the validity of eq. 1,[18] the reversal implies that $\Delta\bar{V}$ changes sign, which is a most unusual effect in a simple chemical system.

A change of this kind might occur if the interiors of the micelles became partially solidified under pressure. Bridgman[19] has shown that, at 25°, the normal hydrocarbons $C_{16}H_{34}$, $C_{12}H_{26}$, and $C_{10}H_{22}$ freeze at 410, 1650, and 2950 atm., respectively, and the present author has found that 1-dodecanol freezes at 700 atm. In each case the solidification

(15) L. M. Kushner, B. C. Duncan, and J. I. Hoffman, *J. Research Natl. Bur. Standards*, **49**, 85 (1952). (The author is grateful to the referee for drawing his attention to this paper.)

(16) E. D. Goddard, C. A. J. Hoeve, and G. C. Benson, *J. Phys. Chem.*, **61**, 593 (1957).

(17) Some unpublished experiments by Dr. F. H. Fisher have shown that the association

$$Mg^{2+} + SO_4^{2-} \longrightarrow (Mg^{+2}SO_4^{2-}) \text{ ion pairs}$$

in water, at 25°, involves an expansion of +7 cm.^{3}/mole.

(18) The validity of eq. 1 is questionable because the c.m.c., defined as the point of intersection of the two linear sections of the conductivity/molality plots (Fig. 1), may have no real thermodynamic meaning. As Goddard and Benson[7] remarked, there is actually a "smooth transition between the linear portions rather than the abrupt change in slope indicated."

(19) P. W. Bridgman, *Proc. Amer. Acad.*, **77**, 138 (1948–1949).

involves a contraction of about 10% (that is, 20 cm.^{3}/mole for dodecane) and this contraction would clearly outweigh the expansion which accompanies the formation of micelles of sodium dodecyl sulfate at low pressures (11 cm.^{3}/mole).

If this hypothesis is correct it should be possible to vary the freezing pressure, and hence the c.m.c. inversion pressure, by altering the temperature and the hydrocarbon chain length, and by dissolving short chain alcohols in the micelles. It is hoped to study the effects of some of these changes in future work.

RATE OF SPREADING AND EQUILIBRIUM SPREADING PRESSURE OF THE MONOLAYERS OF *n*-FATTY ALCOHOLS AND *n*-ALKOXY ETHANOLS

By A. V. Deo, S. B. Kulkarni, M. K. Gharpurey, and A. B. Biswas

Contribution No. 485 from the National Chemical Laboratory, Poona-8, India

Received December 19, 1961

In recent communications,[1,2] we reported the superior water evaporation retarding power of the alkoxy ethanols (glycolmonoalkyl ethers) to those of the commonly used cetyl and stearyl alcohols. With a view to understand this evaporation retardation behavior we have been studying their physico-chemical properties; and in what follows, preliminary results on the rate of spreading from the solid onto a clean water surface and on equilibrium spreading pressure at 25° are reported.

The Rate of Spreading.—For measuring this rate, the alcohol or the alkoxy ethanol sample was prepared by gently withdrawing a glass rod of uniform diameter from the melt of the substance kept 10° above its melting point. The rod then was left overnight at room temperature (~25°). The perimeter of the coated rod was measured with the help of a traveling microscope. It then was half-immersed vertically in a known area of clean water surface in a thermostated Langmuir trough fitted with a horizontal film pressure balance. The time required for the film pressure to rise to the low value of 1 dyne/cm. was noted. From such data and from the previously determined values of the area/molecule of the various substances at 1 dyne/cm., the rate of spreading in terms of the number of molecules entering the water surface from 1 cm. of the triple interface perimeter in 1 sec. was calculated. The values at 25° are given in Table I.

From the above it may be noticed that a modification of the terminal –OH group to $-OCH_2CH_2OH$ has considerably decreased the melting point and increased the rate of spreading. Again, in a homologous series the rate of spreading is decreased as the melting point is increased along with the chain length.

It is interesting to compare the log dN/dt *vs.* melting point curves for the two series as given in Fig. 1.

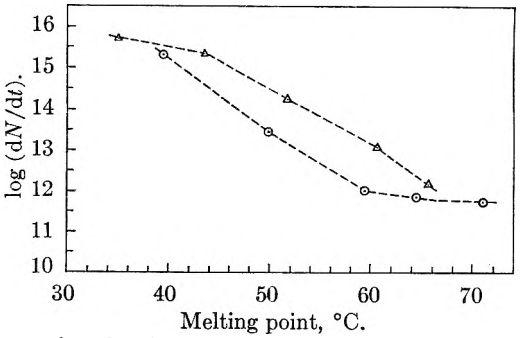

Fig. 1.—log dN/dt *vs.* melting point: ⊙, alcohols; △, alkoxy-ethanols.

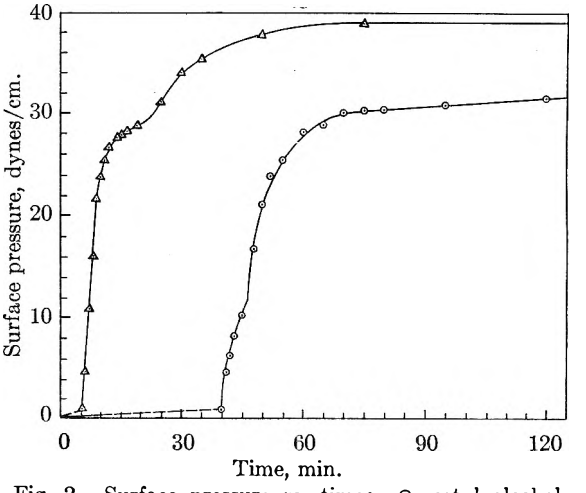

Fig. 2.—Surface pressure *vs.* time: ⊙, cetyl alcohol—A = 308.5 cm.^{2}; T = 25.3°; p = 2.12 cm. △, octadecoxyethanol—A = 308.5 cm.^{2}; T = 24.7°; p = 2.15 cm.

TABLE I

MELTING POINT, RATE OF SPREADING (dN/dt, NUMBER OF MOLECULES/CM./SEC.), AND EQUILIBRIUM SPREADING PRESSURE (DYNES/CM.)

	n-Fatty alcohols			*n*-Alkoxy ethanols		
	M.p., °C.	dN/dt	Π_e	M.p., °C.	dN/dt	Π_e
C_{14}	39.5	2.1×10^{15}	46.5	35.0	5.2×10^{15}	48.6
C_{16}	49.5	2.8×10^{13}	39.6	43.5	2.3×10^{15}	50.4
C_{18}	59.4	1.1×10^{12}	35.2	51.7	1.8×10^{14}	48.9
C_{20}	64.5	7.6×10^{11}	32.6	60.5[a]	1.2×10^{13}	49.0
C_{22}	71.0	6.0×10^{11}	27.6	65.6	1.5×10^{12}	47.2

[a] Compound not extremely pure.

In the intermediate range the curves run roughly parallel and here the rate of spreading of the *n*-alkoxy ethanol is about ten times higher than that of the *n*-alcohol. This may be attributed to the higher escaping tendency of the former compounds from the solid together with the enhanced interaction of the $-OCH_2CH_2OH$ group with the water subphase compared to the –OH.

The film pressure *vs.* time curves for the C_{16}-alcohol and the C_{18}-alkoxy ethanol at 25° are shown in Fig. 2. The points of discontinuity in the curves naturally correspond to those in the II-A curves and are a consequence of the sudden change in the film compressibility, and do not signify a sudden change in the rate of spreading at the corresponding pressure.

(1) A. V. Deo, N. R. Sanjana, S. B. Kulkarni, M. K. Gharpurey, and A. B. Biswas, *Nature*, **187**, 870 (1960).

(2) A. V. Deo, S. B. Kulkarni, M. K. Gharpurey, and A. B. Biswas, *ibid.*, **191**, 378 (1961).

The curves flatten at the higher pressures due to the balance between spreading and loss of molecules (by dissolution[3,4] and evaporation[5,6]). The steady-state spreading pressure value has been found to be a function of the perimeter/surface area ratio, the pressure tending to the equilibrium value for higher values of the ratio only, which is in agreement with the earlier work.[3] However, for the same perimeter–area ratio, a remarkably higher steady-state spreading pressure value of the C_{18}-alkoxy ethanol than that of the C_{16}-alcohol may be noted.

Equilibrium Spreading Pressure (e.s.p.).—The measurements were carried out by dropping a large number of solid specks of the pure compounds on a clean distilled water surface using a vertical film pressure balance. The e.s.p. at 25° of the fatty alcohols and the corresponding alkoxy ethanols are given in Table I.

It is seen that the alkoxy ethanols exhibit considerably higher pressure and that in this range the value does not fall as rapidly on increasing the chain length as in the case of the alcohols. The value for C_{14}-alkoxy ethanol may be lower than the true e.s.p., probably due to its higher rate of dissolution into the water. This also may be attributed to the greater escaping tendency of the alkoxy ethanol molecules from the solid state and to the increased interaction between their polar groups and the water surface.

The superior evaporation retardation[1] exhibited by the alkoxy ethanols thus could be attributed to their higher evaporation resistance[2] at high surface pressures and higher equilibrium pressure values as well as higher rates of spreading.

(3) A. Roylance and T. G. Jones, *J. Appl. Chem.*, **9**, 621 (1959).
(4) A. Roylance and T. G. Jones, 3rd Intern. Congr. of Surface Activity.
(5) W. W. Mansfield, *Australian J. Appl. Sci.*, **10**, 73 (1959).
(6) A. Roylance and T. G. Jones, *J. Appl. Chem.*, **11**, 329 (1961).

THE REACTIONS OF ACTIVE NITROGEN WITH $N^{15}O$ AND N_2^{15}

BY R. A. BACK AND J. Y. P. MUI[1]

Division of Pure Chemistry, National Research Council Laboratories, Ottawa, Canada[1a]

Received December 23, 1961

The reaction of active nitrogen with nitric oxide has been used in a number of laboratories in the last few years to estimate nitrogen atom concentration,[2-6] usually using the now-familiar gas-phase titration first described by Spealman and Rodebush.[7] The validity of this method depends upon two assumptions, first, that atomic nitrogen is the only species present which may react to consume nitric oxide, and secondly, that one nitrogen atom destroys one molecule of nitric oxide. There is almost no real evidence either to support or to contradict these assumptions, since the measurement of absolute atom concentrations by other means (mass spectrometry,[2,4,8] e.p.r.,[5] calorimetry,[9] Wrede gage[10]) has not been sufficiently accurate to indicate anything more than a very crude proportionality between atom concentration and nitric oxide consumption.[11] Despite this lack of evidence, many authors have assumed, usually tacitly, that these assumptions were well-proven facts. Verbeke and Winkler,[12] on the other hand, in order to account for the considerable discrepancy between nitric oxide consumption and hydrogen cyanide production from the reaction with ethylene, have suggested that nitric oxide might also be destroyed by reaction with excited nitrogen molecules present in active nitrogen. It was suggested that in addition to the simple atomic reaction

$$N + NO \longrightarrow N_2 + O \qquad (1)$$

there also occurred the process

$$N_2^* + NO \longrightarrow N_2 + N + O \qquad (2)$$

followed by reaction 1. If the velocity of reaction 2 were not much different from that of (1), then the occurrence of (2) would not have been detected in previous studies of the reaction.

The present work was undertaken to test this possibility by studying the reaction with $N^{15}O$ and examining the isotopic composition of the nitrogen produced. If the atomic reaction (1) is the only important one, then the nitrogen product should be all $N^{15}N^{14}$. If, however, reaction 2 occurs, free N^{15} atoms should be produced, which, with an excess of $N^{15}O$ present, should react by reaction 1 to give N_2^{15}.

The atomic exchange reactions

$$N^{14} + N^{15}O \longrightarrow N^{15} + N^{14}O \qquad (3)$$

and

$$N^{15} + N_2^{14} \longrightarrow N^{14} + N^{15}N^{14} \qquad (4)$$

could, if they occurred, cause some confusion, so these reactions also were investigated.

Experimental

Active nitrogen was generated in a fast-flow system with a condensed discharge operating at 60 discharges per second which, with a 5-liter ballast volume just before the pump, gave a steady, non-pulsating flow. The flow system between the discharge tube and the product traps was poisoned with 5% H_3PO_4 solution.

The reactions with nitric oxide and ethylene were studied in a cylindrical reaction vessel of 18 mm. o.d. Pyrex tubing about 30 cm. below the discharge tube, which could be heated to 300°. The reagent gases were admitted to the stream of active nitrogen through a cone-shaped axial nozzle designed to assure rapid mixing. The nitric oxide consumption was measured by the gas-phase titration method, while the hydrogen cyanide from the ethylene reaction was trapped at −196° and titrated with silver nitrate.

(1) Summer research assistant, 1961.
(1a) Issued as N. R. C. No. 6867.
(2) G. B. Kistiakowsky and G. G. Volpi, *J. Chem. Phys.*, **27**, 1141 (1957).
(3) P. Harteck, R. R. Reeves, and G. Mannella, *ibid.*, **29**, 608 (1958).
(4) J. T. Herron, J. L. Franklin, P. Bradt, and V. H. Dibeler, *ibid.*, **30**, 879 (1959).
(5) J. Kaplan, W. J. Schade, C. A. Barth, and A. F. Hildebrandt, *Can. J. Chem.*, **38**, 1688 (1960).
(6) M. A. A. Clyne and B. A. Thrush, *Proc. Roy. Soc.* (London), **A261**, 259 (1961).
(7) M. L. Spealman and W. H. Rodebush, *J. Am. Chem. Soc.*, **57**, 1474 (1935).
(8) D. Jackson and H. I. Schiff, *J. Chem. Phys.*, **23**, 2333 (1955).
(9) M. H. Saxe and N. N. Lichtin, Abstracts, 135th National Meeting, Am. Chem. Soc., 1959.
(10) R. A. Back and C. A. Winkler, unpublished results.
(11) K. R. Jennings, *Quart. Rev.* (London), **15**, 237 (1961).
(12) G. J. Verbeke and C. A. Winkler, *J. Phys. Chem.*, **64**, 319 (1960).

In the experiments with $N^{15}O$, the unreacted NO and the NO_2 product were removed by two traps cooled to −210°, leaving only nitrogen and oxygen in the gas stream. A small sample of this non-condensable gas was extracted from the flow system by a Toepler pump, for later analysis by mass spectrometer. Blank experiments with $N^{14}O$ showed that removal of nitric oxide in the traps was complete. In some experiments, the unreacted $N^{15}O$ remaining in the traps was distilled into a sample tube and its isotopic composition examined. In all experiments the $N^{15}O$ flow rate was in about twofold excess over the NO flow rate at the end-point of the gas-phase titration.

The exchange reaction with N_2^{15} was investigated from room temperature up to 1000° in cylindrical vessels of Pyrex or quartz surrounded by suitable furnaces. The N_2^{15} was admitted through an axial nozzle at one end of the vessel, and samples of non-condensable gas were extracted downstream for isotopic analysis as before. For temperatures above 400°, $Mg_3(PO_4)_2$ was used to poison the surface of the reaction vessel.[13]

Nitrogen, ethylene, and nitric oxide were obtained in cylinders from the usual sources. Nitrogen-15 compounds were obtained from Merck of Canada, Ltd. The $N^{15}O$ was stated to be 95.5% N^{15}, but was found to contain about 10% N_2O impurity, which must have confused the isotopic analysis. Upon separation from this impurity by careful distillation, the nitric oxide was found to contain 89% $N^{15}O$. The N_2^{15} contained about 8.5% $N^{15}N^{14}$. Appropriate corrections were made in all calculations to allow for N^{14} present in the reagents, and for natural N^{15} present in the active nitrogen, always assuming no isotope effect either in the generation of the active nitrogen or in its reactions.

Results and Discussion

Comparison of the Reactions of Active Nitrogen with Ethylene and Nitric Oxide.—The reaction with ethylene between 200 and 300° gave a yield of hydrogen cyanide which was independent of ethylene flow rate and temperature, shown in Table I. It is seen that the nitric oxide titration, done at the same pressures and operating conditions, indicated flow rates of nitrogen atoms higher by a factor of about 1.5 than the hydrogen cyanide yield, with no significant trend with pressure. Thus the discrepancy between the two systems is confirmed in approximate quantitative agreement with Verbeke and Winkler.[12]

The Reaction with $N^{15}O$.—In Table II are shown the results of the experiments with $N^{15}O$, done at both room temperature and 380°. It is immediately obvious that the yield of N_2^{15} is quite negligible, the highest yield being less than 0.5% of the $N^{15}N^{14}$ produced in the reaction. If reaction 2 were to account for the discrepancy between the nitric oxide and ethylene reactions, the yield of N_2^{15} should have been about 25% of the $N^{15}N^{14}$.

TABLE I

COMPARISON OF ETHYLENE AND NITRIC OXIDE REACTIONS[a]

Pressure (mm.)	HCN yield (μmole/sec.)	NO titration (μmole/sec.)	NO titration / HCN yield	% Dissociation measured by NO titration
1.01	4.3	6.6	1.54	6.5
1.51	7.2	10.8	1.50	5.3
2.02	7.0	10.4	1.49	3.2

[a] The data at each pressure represent averages of several experiments.

It also is seen from the last column of Table II that there is almost no change in the isotopic composition of the nitric oxide recovered from the reaction. Less than 0.2% of the $N^{15}O$ was converted to $N^{14}O$, while about 50% of the $N^{15}O$ was disappearing by reaction 1. Thus the exchange reaction (3) is at least 250 times slower than reaction 1, and has no effect in the present study.

TABLE II

ISOTOPIC ANALYSES FROM $N^{15}O$ REACTION

Pressure (mm.)	Non-condensable gas (mass 28 = 100) Mass 29	Mass 30	Cor.[a] mass 30	Nitric oxide (mass 31 = 100) Mass 30	Cor.[a] mass 30
1.02	14.02	0.097	+0.033	...	....
1.01	12.80	.110	+ .046	...	....
1.02	13.03	.097	+ .033	10.98	−0.10
1.49	12.10	.060	+ .006	...	....
1.50	11.83	.050	− .004	11.13	+ .03
1.50	11.59	.052	− .002	11.20	+ .10
1.50	12.14	.082	+ .028	11.30	+ .20
2.02	8.54	.060	+ .019	...	....
2.02	7.84	.050	+ .009	11.17	+ .07

[a] Corrected for mass 30 originally present.

One may also independently calculate the flow rate of nitrogen atoms from the yield of $N^{15}N^{14}$, assuming it all to arise by reaction 1, and in Table III these values are compared with those obtained by the nitric oxide titration, expressing each as a per cent dissociation of the nitrogen. (These data for the nitric oxide titration differ slightly from those in Table I because of slight changes in operating conditions between the two sets of experiments.) It is seen that there is reasonable agreement between the values of atom concentration determined by the two methods. This is in accord with the observations that both the nitric oxide destroyed, measured by chemical methods,[12] and the yield of oxygen atoms from the reaction[6,14] were equal to the nitric oxide flow rate at the end-point of the titration.

TABLE III

PER CENT DISSOCIATION MEASURED FROM $N^{15}N^{14}$ YIELD

Pressure (mm.)	% Dissociation of nitrogen: From $N^{15}N^{14}$	By titration	Ratio of two methods
1.02	6.96	6.71	1.04
1.01	6.36	6.71	0.93
1.02	6.46	6.71	0.96
1.49	6.01	5.64	1.07
1.50	5.87	5.64	1.04
1.50	5.75	5.64	1.02
1.50	6.02	5.64	1.07
2.02	4.19	3.49	1.20
2.02	3.83	3.49	1.10

In summary, we have shown that the $N^{15}O$ consumed in reaction with active nitrogen was quantitatively converted to $N^{15}N^{14}$, with almost no N_2^{15}, under conditions where a large discrepancy was observed between the nitric oxide consumed and the hydrogen cyanide produced by reaction with ethylene. Reaction 2, or any other reactions yielding free N^{15}, or N_2^{15}, may be ruled out as a cause of the discrepancy. It is still possible to envisage a reaction of an excited nitrogen molecule with $N^{15}O$ to give only $N^{15}N^{14}$, in the following manner

$$N_2^{14*} + N^{15}O \longrightarrow N^{14} + (N^{14}N^{15}O)^* \longrightarrow N^{14}N^{15} + O + N^{14}$$

(13) R. A. Back, W. Dutton, and C. A. Winkler, *Can. J. Chem.*, **37**, 2059 (1959).

(14) J. E. Morgan, L. Elias, and H. I. Schiff, *J. Chem. Phys.*, **33**, 930 (1960).

or perhaps through a four-center reaction

$$N_2^{14*} + N^{15}O \longrightarrow \begin{matrix} N^{14}\text{--}N^{14} \\ | \quad | \\ N^{15}\text{--}O \end{matrix} \longrightarrow N^{14}N^{15} + N^{14}O^* \longrightarrow N^{14} + O + N^{14}N^{15}$$

although these mechanisms seem rather unlikely. Thus the present results tend to support the validity of the nitric oxide titration, but by no means prove it. The discrepancy between the nitric oxide and ethylene reactions remains unexplained.

The Exchange Reaction with N_2^{15}.—The exchange reaction of isotopically-natural active nitrogen with N_2^{15} was examined at a number of temperatures from 30 to 1000°. No measurable exchange was detected in any of the experiments, and at 1000° an upper limit for the rate constant of reaction 4 may be calculated. Using a value of the nitrogen atom concentration based on the nitric oxide titration, $k_4 < 4 \times 10^8$ cc. mole.$^{-1}$ sec.$^{-1}$, and if one assumes a value between 10^{11} and 10^{14} cc. mole^{-1} sec.$^{-1}$ for the pre-exponential term in the Arrhenius equation, a lower limit for the activation energy lies between 14 and 31 kcal./mole. Thus the exchange reaction (4) is apparently much too slow to have had any effect in the experiments with $N^{15}O$. It might be argued that excited N_2, either formed by reaction 1 or originally present, might undergo more rapid exchange with nitrogen atoms than was observed for "thermal" N_2, but it still seems doubtful whether it would compete successfully with the very fast reaction 1.

It was calculated by Hirschfelder[15] that the activation energy of a simple atomic exchange reaction should be about 5.5% of the dissociation energy of the bond being broken. Nitrogen apparently resembles hydrogen[16] in having an activation energy somewhat higher than this prediction. The oxygen exchange reaction, on the other hand, appears to have an abnormally low activation energy, close to zero.[17] If this is attributed to the existence of ozone as a stable intermediate causing a completely attractive O–O_2 collision, then conversely the high activation energy for the nitrogen exchange reaction might be taken as evidence against the stability of N_3.

The authors wish to thank Mr. R. Pilon for making the mass spectrometric analyses for these experiments.

(15) J. O. Hirschfelder, *J. Chem. Phys.*, **9**, 645 (1941).

(16) A. F. Trotman-Dickenson, "Gas Kinetics," Butterworths Publications Ltd., London, 1955.

(17) R. A. Ogg, Jr., and W. T. Sutphen, *Discussions Faraday Soc.*, **17**, 47 (1954).

CHARGE AND CONFIGURATIONAL EFFECTS IN THE CONCENTRATION DEPENDENCE OF SEDIMENTATION OF SODIUM CARBOXYMETHYLCELLULOSE[1]

BY G. SITARAMAIAH, R. F. ROBERTSON, AND D. A. I. GORING

Chemistry Department, McGill University, and the Physical Chemistry Division, Pulp and Paper Research Institute of Canada, Montreal, Canada

Received December 26, 1961

During the course of a recent investigation of the hydrodynamic properties[2] of sodium carboxymethylcellulose (CMC), sedimentation constants were measured in aqueous sodium chloride at ionic strengths of 0.1 and 0.001 *M*. An unusually pronounced dependence of the sedimentation constant on the concentration of CMC was found, particularly in the low ionic strength solvent. In this note, an interpretation is attempted based on certain current theories of the effect of charge and molecular volume on the sedimentation constant.

Sedimentation measurements were made in a Spinco Model E ultracentrifuge at 260,000 *g* and 26 (±0.5)°. Single peaks were observed. The maximum-ordinate sedimentation constant, s_m, was obtained in the standard manner from the linear logarithmic plot of the boundary position *vs.* time. Dilutions were made isoionically with respect to the Na^+ cation.[2-5] Thus at all concentrations of CMC, the ionic strength, I_E, of Na^+ was held at either 0.1 or 0.001 *M*. Two fractions, H1 and L1, are considered. Fractions H1 and L1 had sedimentation-diffusion molecular weights of 350,000 and 90,000, degrees of substitution of 0.66 and 0.70, and neutralization equivalents of 3.07×10^{-3} and 3.21×10^{-3} equiv. g.$^{-1}$, respectively. Details of the preparation and characterization of the fractions of CMC are given in an earlier report.[2]

Results for the two fractions at ionic strengths of 0.1 and 0.001 *M* are given in Fig. 1 and 2, respectively. The data are plotted as $1/s_m$ *vs.* the concentration, *c*. For both H1 and L1 the solution of highest concentration shown in Fig. 2 contained no chloride ion. The CMC alone supplied sodium ion at an ionic strength of 0.001 *M*. At lower values of *c*, NaCl was added to maintain the Na^+ concentration constant at 0.001 *M*. In Fig. 2, the maximum *c* for H1 exceeded that for L1 because the effective ionization of H1 was determined viscometrically to be only 70% while that of L1 was 100 %. The lines shown in Fig. 1 and 2 are relationships of $1/s_m$ *vs.* *c* predicted theoretically from equations discussed in the following paragraphs.

The dependence on concentration of the sedimentation constant in dilute solutions of polyelectrolytes is influenced by two effects: (a) The effective hydrodynamic volume of the molecule in solution which determines the intermolecular hydrodynamic interaction; (b) The charge on the molecule which decreases the sedimentation constant due to the electric field produced in the cell of the ultracentrifuge.

The intermolecular hydrodynamic interaction in sedimentation has been considered by Wales and Van Holde in the case of uncharged polymer molecules.[6] These authors presented a derivation of the well known empirical equation

$$\frac{1}{s_m} = \left(\frac{1}{s_m}\right)_{c=0}(1 + k_e c) \qquad (1)$$

(1) Paper presented before the Wood, Cellulose and Fiber Chemistry Division at the 140th National Meeting of the American Chemical Society, Chicago, Ill., 1961.

(2) G. Sitaramaiah and D. A. I. Goring, *J. Polymer Sci.*, in press.

(3) D. F. T. Pals and J. J. Hermans, *Rec. trav. chim.*, **71**, 433 (1952).

(4) H. Terayama and F. T. Wall, *J. Polymer Sci.*, **16**, 357 (1955).

(5) A. Rezanowich and D. A. I. Goring, *J. Colloid Sci.*, **15**, 452 (1960).

(6) M. Wales and K. E. Van Holde, *J. Polymer Sci.*, **14**, 81 (1954).

in which c is the concentration of the macromolecular solute and the constant k_c is given by

$$k_c = \frac{\Lambda N[\eta]}{16{,}200\pi^2(\phi^{1/3}P^{-1})^3} \quad (2)$$

in which N is Avogadro's number, $[\eta]$ is the intrinsic viscosity, $(\phi^{1/3}P^{-1})$ is the universal polymer constant described by Mandelkern, *et al.*,[7] and Λ is a constant deduced by Burgers[8] to be equal to 55/8 for a dilute suspension of spheres. Wales and Van Holde found $k_c/[\eta]$ to be 1.6 ($\pm$0.26) for many vinyl polymers. This confirmed eq. 2 for $(\phi^{1/3}P^{-1})$ equal to 2.5×10^6. It is significant that the results for cellulose derivatives did not fit into the general trend. This is not surprising since the values of $(\phi^{1/3}P^{-1})$ reported for cellulose derivatives[2,9] are higher than 2.5×10^6.

Let us now consider the effect of the charge carried by the macro-ion on the concentration dependence of the sedimentation rate. Pedersen[10] distinguishes between two types of charge effect, the primary and the secondary. The former, which is the larger, arises from the differential sedimentation of the macro-ion and its "gegenion." The macro-ion sediments more quickly than the small counterions, builds up a charge at the base of the cell, and causes a decrease in the sedimentation rate by back electrophoresis of the sedimenting macro-ions. The secondary charge effect is due to the difference in the sedimentation rate of the positive and negative ions in the supporting electrolyte. In the present work, the secondary charge effect is not important because the added electrolyte is sodium chloride and the sedimentation constants of the Na^+ and Cl^- ions are essentially equal.[11]

The Tiselius[12] equation for the primary charge effect in sedimentation may be written

$$s_m = s_m^n\left(1 - \frac{UFN_e c}{100\kappa}\right) \quad (3)$$

in which s_m is the observed sedimentation constant of the macro-ion, s_m^n is the sedimentation constant in the absence of charge, U is the electrophoretic mobility, F is the Faraday constant, N_e is the equivalents per g. of macro-ion, c is the concentration in g./dl., and κ is the specific conductivity of the solution.

If hydrodynamic interaction effects are neglected in eq. 3, s_m^n can be replaced by $(s_m)_{c=0}$, provided that κ does not tend to zero as c tends to zero, *i.e.*, provided there is an added supporting electrolyte at zero concentration of the macro-ion. Thus eq. 3 can be inverted to give

$$\frac{1}{s_m} = \left(\frac{1}{s_m}\right)_{c=0}(1 + k_e c + k_e^2 c^2 + \ldots\ldots) \quad (4)$$

in which

$$k_e = \frac{UFN_e}{100\kappa} \quad (5)$$

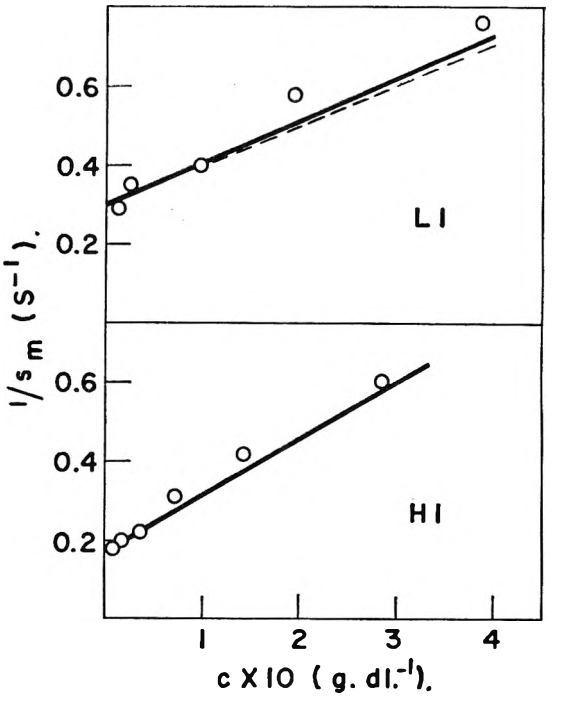

Fig. 1.—Graphs of $1/s_m$ *vs.* c for the high (H1) and low (L1) molecular weight fractions at $I_E = 0.1\ M$. The solid lines are derived by substituting appropriate values of k_c and k_e (Table I) into eq. 6. The dashed line corresponds to eq. 1. For H1, the two lines were almost coincident.

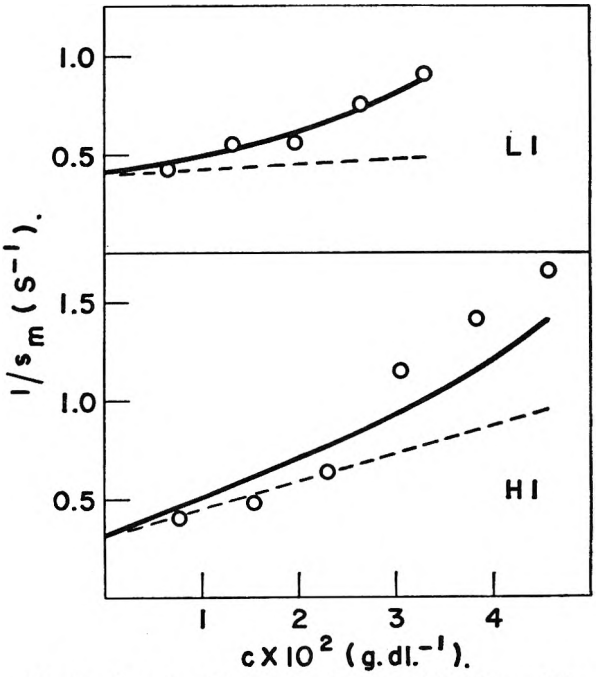

Fig. 2.—Graphs of $1/s_m$ *vs.* c for the high (H1) and low (L1) molecular weight fractions at $I_E = 0.001\ M$. The solid lines are derived by substituting appropriate values of k_c and k_e (Table I) into eq. 6. The dashed lines correspond to eq. 1.

To a first approximation at low concentration, the hydrodynamic intermolecular interaction and the primary charge effect may be considered to act independently of each other in increasing the fric-

(7) L. Mandelkern, W. R. Krigbaum, H. A. Scheraga, and P. J. Flory, *J. Chem. Phys.*, **20**, 1392 (1952).
(8) J. M. Burgers, *Proc. Acad. Sci. Amsterdam*, **45**, 9 (1942).
(9) R. St. John Manley, *Arkiv Kemi*, **9**, 519 (1956).
(10) K. O. Pedersen, "The Ultracentrifuge," Oxford University Press, 1940.
(11) K. O. Pedersen, *J. Phys. Chem.*, **62**, 1282 (1958).
(12) A. Tiselius, *Kolloid-Z.*, **59**, 306 (1932).

tional constant of the sedimenting molecule. Thus eq. 1 and 4 may be summed to give

$$\frac{1}{s_m} = \left(\frac{1}{s_m}\right)_{c=0} (1 + (k_c + k_e)c + k_e^2c^2 + \ldots\ldots) \quad (6)$$

in which k_c and k_e are given by eq. 2 and 5, respectively. Equation 6 would be expected to apply only when the configuration of and the charge on the polyelectrolyte are unaffected by the dilution process. This condition is effectively fulfilled by the isoionic dilution technique used in the present work.

Values of k_c and k_e were calculated by means of eq. 2 and 5, respectively, and are shown in Table I. In calculating k_c, $(\phi^{1/3}P^{-1})$ was taken to be 3.4×10^6. This is a mean of previously determined values[2] for CMC. The intrinsic viscosities used in computing k_c are given in Table I.

TABLE I

CALCULATED VALUES OF k_c AND k_e AT IONIC STRENGTHS OF 0.1 AND 0.001 M

k_e is given at concentrations of CMC equivalent to 0 and 0.001 M

Fraction	I_E	$[\eta]^a$ (g.$^{-1}$ dl.)	$(s_m)_{c=0}{}^a$ (S)	k_c (g.$^{-1}$ dl.)	k_e (g.$^{-1}$ dl.) 0	k_e (g.$^{-1}$ dl.) 0.001 M
H1	0.1	12.3	5.8	8.1	0.12	0.12
H1	.001	62.5	3.0	41.0	10.3	17.0
L1	.1	5.2	3.3	3.4	0.13	0.13
L1	.001	9.3	2.5	6.1	11.2	18.5

[a] Reported in an earlier paper[2] and included here for reference.

The coefficient, k_e, contains the quantities U and κ, which may themselves vary with the concentration of CMC. From the results of Napjus and Hermans[13] it is evident that the electrophoretic mobility of CMC is almost constant up to CMC concentrations of 0.05 g. dl.$^{-1}$. These authors also noted that U was essentially independent of the ionic strength and increased from 2.90×10^{-4} to 3.90×10^{-4} cm.^{2} volt^{-1} sec.$^{-1}$ for an increase in the neutralization equivalent of from 1.81×10^{-3} to 2.70×10^{-3} equiv. g.$^{-1}$. In the present work U was assumed to be independent of c and I_E. Values of 4.3×10^{-4} and 4.5×10^{-4} cm.^{2} volt^{-1} sec.$^{-1}$ corresponding to the neutralization equivalents of 3.07×10^{-3} and 3.21×10^{-3} equiv. g.$^{-1}$ were computed, respectively, for H1 and L1 by interpolation of the data of Napjus and Hermans.[13]

Napjus and Hermans[13] also showed that the experimentally determined specific conductivity of the solution increased with decreasing concentration of CMC. This is due to the large CMC anion being replaced by an equivalent number of the more mobile chloride ions on isoionic dilution. The effect is negligible at $I_E = 0.1$ M but must be allowed for at the ionic strength at 0.001 M when the chloride ion concentration changes from 0.001 M to zero as the equivalent concentration of CMC changes from zero to 0.001 M, *i.e.*, to the maximum values shown in Fig. 2. From the data of Hermans and Longsworth[14] an approximate value of 25 ohm^{-1} was derived for the equivalent conductance of a CMC macro-ion at $I_E = 0.001$ M. Specific conductivities then were computed at various concentrations of CMC from the equivalent conductances of 74 and 50 ohm^{-1} for the chloride and sodium ions, respectively. Thus κ increased from 75×10^{-6} to 124×10^{-6} ohm^{-1} cm.$^{-1}$ as the equivalent concentration of CMC fell from 0.001 M to zero. This change in κ produced an increase in k_e (eq. 5) with increasing concentration of CMC. The range of k_e is shown in Table I.

The solid lines in Fig. 1 and 2 give the variation of $1/s_m$ with c predicted from eq. 6. With the possible exception of the data for H1 at low ionic strength, the fit of the predicted curve with the experimental points is quite good. The dashed lines in Fig. 1 and 2 are derived by substituting into eq. 1 the k_c values given in Table I. Thus the dashed lines represent the expected contribution of the hydrodynamic interaction in the absence of the primary charge effect.

From Fig. 1, it is apparent that at $I_E = 0.1$ M the contribution of the charge effect is rather small. As shown in Fig. 2, the relative importance of the charge effect at 0.001 M is considerably greater than at 0.1 M but for H1 the major part of the concentration dependence is still due to hydrodynamic interaction. This is in contrast to the low molecular weight fraction at $I_E = 0.001$ M for which the primary charge effect is the dominating influence in the variation of $1/s_m$ *vs.* c. Such behavior is to be expected from the parameters in eq. 2, 5, and 6. At high ionic strength κ is large and thus k_e is negligible compared to k_c. However, κ decreases in almost direct proportion to I_E and thus the magnitude of the charge effect will increase by a hundredfold between 0.1 and 0.001 M. At the lower ionic strength, $[\eta]$ and therefore k_c also increase but considerably more slowly than k_e, as shown in Table I.

Some comment may be made concerning the upward curvature of the predicted $1/s_m$ *vs.* c lines at low ionic strength. This effect is due to the c^2 term in eq. 6 and appears to be supported experimentally, particularly for fraction L1. Such a result is in contrast to data reported for uncharged derivatives of cellulose in which the coefficient of c^2 is negative.[9,15] Differences in the curvature of the $1/s_m$ *vs.* c graphs have been reported by Schachman,[16] but no theoretical reason for the effect has yet been proposed.

In conclusion, the concentration dependence of the sedimentation coefficient of CMC on isoionic dilution at 0.1 and 0.001 M is in fair accord with an approximate combination of the Wales and Van Holde and the Tiselius equations. Also, the results support the theoretical prediction that the relative importance of the primary charge effect will increase at low ionic strength and low molecular weight.

(13) P. J. Napjus and J. J. Hermans, *J. Colloid Sci.*, **14**, 252 (1959).

(14) R. Longsworth and J. J. Hermans, *J. Polymer Sci.*, **26**, 47 (1957).

(15) S. Newman, L. Loeb, and C. M. Conrad, *J. Polymer Sci.*, **10**, 463 (1953).

(16) H. K. Schachman, "Ultracentrifugation in Biochemistry," Academic Press, New York, N. Y., 1959.

THE CALCULATION OF ζ-POTENTIAL FROM MOBILITY MEASUREMENTS

BY ROBERT J. HUNTER

C.S.I.R.O., Division of Soils, Canberra, Australia

Received December 26, 1961

The calculation of ζ-potential from mobility measurements is a simple matter only when κa is very large (≥ 100) or very small (≤ 0.1). For intermediate values, a correction must be applied for the retardation and relaxation effects. The resulting equation for the mobility, U, takes the form of a power series in ζ. Overbeek[1] has calculated the coefficients of this series up to terms in ζ^3, for both symmetrical and unsymmetrical electrolytes, while Booth[2] has calculated the coefficients up to ζ^4 for symmetrical electrolytes. Booth's equation takes the form

$$U = C_1\zeta + C_3\zeta^3 + C_4\zeta^4 \qquad (1)$$

since $C_2 = 0$ for a symmetrical electrolyte. The necessity of solving a quartic equation to determine ζ for any given U has led Stigter and Mysels[3] to rearrange eq. 1 to produce an expression for ζ as a power series in U

$$\zeta = \frac{U}{C_1} - \frac{C_3}{C_1}\left(\frac{U}{C_1}\right)^3\left[1 - \left(\frac{C_3}{C_1}\right)^3\left(\frac{U}{C_1}\right)^6 - \left(\frac{C_4}{C_1}\right)^3\left(\frac{U}{C_1}\right)^9 \cdots\cdots\right] - \frac{C_4}{C_1}\left(\frac{U}{C_1}\right)^4\left[1 - \left(\frac{C_3}{C_1}\right)^4\left(\frac{U}{C_1}\right)^8 - \left(\frac{C_4}{C_1}\right)^4\left(\frac{U}{C_1}\right)^{12} \cdots\cdots\right] \qquad (2)$$

These workers have not indicated the method they adopted but there are at least two possible procedures. First we may rearrange eq. 1 thus

$$\zeta = \frac{U}{C_1} - \frac{C_3}{C_1}\zeta^3 - \frac{C_4}{C_1}\zeta^4 \qquad (3)$$

and substitute $\zeta_1 = U/C_1$ in the r.h.s. of (3) to obtain ζ_2 and so on for ζ_3. We find

$$\zeta_3 = \frac{U}{C_1} - \frac{C_3}{C_1}\left(\frac{U}{C_1}\right)^3\left[1 - \frac{C_3}{C_1}\left(\frac{U}{C_1}\right)^2 - \frac{C_4}{C_1}\left(\frac{U}{C_1}\right)^3\right]^3 - \frac{C_4}{C_1}\left(\frac{U}{C_1}\right)^4\left[1 - \frac{C_3}{C_1}\left(\frac{U}{C_1}\right)^2 - \frac{C_4}{C_1}\left(\frac{U}{C_1}\right)^3\right]^4 \qquad (4)$$

Comparison of (4) with (2) suggests that the algebraic signs of the terms in the second series of eq. 2 are incorrect and that Stigter and Mysels have dropped the terms in U^5, U^6, U^7, U^8 and included terms which under some circumstances would be much less important. That these terms do not disappear in the higher approximations is shown by the second procedure. Writing

$$\zeta = aU + bU^2 + cU^3 + \cdots\cdots$$

and substituting in (1) we may evaluate $a,b,c\ldots$ by comparing coefficients of U. This procedure gives a result identical with the first method (*i.e.*, eq. 4) for powers of U up to and including U^6. Beyond this point the two methods should give identical results only when the first method is carried to higher approximations.

It is, however, readily shown that the higher terms are of no value for the calculation of ζ because of the inherent limitations of eq. 1. Booth's eq. 1 is actually an infinite series for which only coefficients up to C_4 have been evaluated. To estimate the influence of the remaining terms on ζ we may introduce into (1) the next term in the series ($C_5\zeta^5$); we then find, using the second procedure

$$\zeta = \frac{U}{C_1} - \frac{C_3}{C_1}\left(\frac{U}{C_1}\right)^3 - \frac{C_4}{C_1}\left(\frac{U}{C_1}\right)^4 + 3\left[\left(\frac{C_3}{C_1}\right)^2 - \frac{C_5}{C_1}\right]\left(\frac{U}{C_1}\right)^5 + 7\,\frac{C_3C_4}{C_1^2}\cdot\left(\frac{U}{C_1}\right)^6 + \cdots\cdots \qquad (5)$$

Now if we assume that eq. 1 gives an estimate of U accurate to within 5% for $\zeta \approx 50$ mv. and $\kappa a \approx 5$, we find that $C_5 \approx C_4$ (*i.e.*, assuming that the error in U is due solely to neglect of the term in ζ^3). The coefficient of U^5 in (5) then is dominated by the (unknown) value of C_5 and there is no point in continuing the expansion beyond U^4. Even if we assume that $C_5 << C_4$ (say $C_5 = 0.1C_4$) the uncertainty in the value of the coefficient of U^5 is about 25% so that the use of terms higher than U^4 is of doubtful value.

It would seem, then, that the final expression given by Stigter and Mysels is the most satisfactory power series expansion of ζ for most applications but that it is still somewhat limited.[4] Its accuracy in the region where $\kappa a \approx 5$ rests on the rather fortunate coincidence that each of the coefficients of $(U/C_1)^5$, $(U/C_1)^6$, $\ldots\ldots(U/C_1)^{10}$ is smaller, by a factor of about 3, than its predecessor. Since C_3 and C_4 are of opposite sign, these terms tend to cancel out for $U/C_1 \approx 3$.

The limitations of the power series expansion for ζ may be circumvented by evaluating ζ directly from eq. 1, using Horner's method of successive approximation.[5] In this way, we may obtain a value for ζ which is as accurate as eq. 1 permits. Applying Horner's method once, using $\zeta = U/C_1$ as a trial solution, and neglecting all save the linear term in ζ

$$\zeta = \frac{U}{C_1} - \left[\frac{C_3\left(\frac{U}{C_1}\right)^3 + C_4\left(\frac{U}{C_1}\right)^4}{C_1 + 3C_3\left(\frac{U}{C_1}\right)^2 + 4C_4\left(\frac{U}{C_1}\right)^3}\right] \qquad (6)$$

The value of ζ calculated from eq. 6 agrees with that obtained by complete solution of (1) to within an accuracy of 1% for $U \leq 4 \times 10^{-4}$ and to within 4% for $U = 5 \times 10^{-4}$ cm.^{2} v.$^{-1}$ sec.$^{-1}$. When transformed into dimensionless variables (see Stigter and Mysels (ref. 3)) this becomes

$$\Phi = \frac{u}{X_1^*} - \left[\frac{C_3'\left(\frac{u}{X_1^*}\right)^3 + C_4'\left(\frac{u}{X_1^*}\right)^4}{X_1^* + 3C_3'\left(\frac{u}{X_1^*}\right)^2 + 4C'_4\left(\frac{u}{X_1^*}\right)^3}\right] \qquad (7)$$

where

(1) J. Th. G. Overbeek, *Kolloid-Beih.*, **54**, 287 (1943).

(2) F. Booth, *Proc. Roy. Soc.* (London), **A203**, 514 (1950).

(3) D. Stigter and K. J. Mysels, *J. Phys. Chem.*, **59**, 45 (1955).

(4) It should be noted that Stigter and Mysels were well aware of the limitations of their equation. This discussion in no way invalidates the conclusions drawn in their paper.

(5) See H. W. Turnbull, "Theory of Equations," Oliver and Boyd, London, 1952, p. 30. The result may also be obtained using Newton's Approximation Method (above, p. 92). The very high accuracy obtained in this case results from the near linearity of $f(\zeta)$ in the neighborhood of the root.

$$C_3' = q_3(X_3^* + Y_3^*) + q_3^* Z_3^*$$
$$C_4' = q_4^* Z_4^*; \quad q_3 = \Sigma n_i z_i^4 / \Sigma n_i z_i^2$$
$$q_m^* = KkT\Sigma n_i \omega_i^{-1} z_i^{(m-1)} / \epsilon^2 \pi\eta \Sigma n_i z_i^2$$

where n_i, z_i are the concentration (ions/cc.) and valency, respectively.

The ionic mobility, ω_i, is the velocity per unit *force;* $\omega_i = 6.25 \times 10^{11} v_i$, where v_i is the ionic mobility in cm.^{2} volt^{-1} sec.$^{-1}$, without regard to sign.

$$q_3 = z^2; \quad q_3^* = 4 \times 10^{-4} (1/v_+ + 1/v_-)$$

and

$$q_4^* = 4 \times 10^{-4} |z| (1/v_+ - 1/v_-)$$

for a solution of a single symmetrical electrolyte.

X_1^* is a function of κa given by Henry.[6] Henry's Fig. 1, curve 1 shows $(^2/_3)X_1^*$ but his second expression for X_1^* (ref. 6, p. 124) is correct only for $\kappa a = 1$. The correct expression is given by Overbeek.[7] X_3^*, Y_3^*, Z_3^*, Z_4^* are also functions of κa, given by Booth,[2] and a few values of $q_3^*/_6$ are given by Overbeek[8] for different values of the ionic mobility. $\Phi = \epsilon\zeta/kT$ and $u = (6\pi\eta\epsilon/KkT)U$, where ϵ is electronic charge, k is Boltzmann's constant, T is absolute temperature, η is viscosity, and K is the permittivity.[9]

Acknowledgments.—The author wishes to thank Professor A. E. Alexander of the University of Sydney for his continued interest in this work and Professor A. Brown of the Australian National University, Mathematics Department, for valuable discussions.

(6) D. C. Henry, *Proc. Roy. Soc.* (London), **A133**, 106 (1931).
(7) J. Th. G. Overbeek, *Advan. Colloid Sci.*, **3**, 105 (1950).
(8) Reference 1, p. 316, Table 3, columns 4 and 5.
(9) See R. J. Hunter, *J. Colloid Sci.*, **16**, [2] 191 (1961).

KINETICS OF CHLORINE EXCHANGE BETWEEN CHLORIDE AND ETHYL CHLOROACETATE

By J. F. Hinton and F. J. Johnston

Department of Chemistry, University of Georgia, Athens, Ga.

Received December 26, 1961

The simultaneous reactions involving the hydrolysis of chloroacetic acid and the exchange of its chlorine with chloride ions have been previously reported.[1] In that system the hydrolysis reaction was satisfactorily described as a pseudo first-order process with the exchange reaction obeying a second-order rate law. The apparent activation energies for the two reactions were experimentally indistinguishable.

This note describes the results of a kinetic study of the corresponding exchange reaction involving ethyl chloroacetate and chloride ion in ethanol and in ethanol–water mixtures. Reaction rates were conveniently measurable above 70° in both solvent systems.

In pure ethanol, reaction rates for the process

$$CH_2ClCOOC_2H_5 + Cl^{-*} \rightleftharpoons CH_2Cl^*COOC_2H_5 + Cl^-$$

were evaluated in the usual manner from the equation

$$R_x(t) = -2.303 \frac{(a)(b)}{(a)+(b)} \frac{\log(1 - F_t)}{t} \qquad (1)$$

F_t represents the ratio of the specific activity of the ester at time t to that at exchange equilibrium, (a) and (b) refer to the concentrations of chloride and chloroacetic ester, $R_x(t)$ is the exchange reaction rate at t.

In ethanol–water mixtures some chloride production occurred due to reaction of the ester during the time for which our samples were heated. The extent of this hydrolysis, occurring during the exchange experiments, was too little, however, to allow the calculation of significant rate constants for the process. Rates of the exchange reactions in non-equilibrium systems of this type may be obtained from the expression[1,2]

$$\frac{d[\ln(1 - F_t)]}{dt} = -\frac{R_x(t)[(a)+(b)]}{[(a)+p(t)][(b)-p(t)]} \qquad (2)$$

(a) and (b) now refer to the initial concentrations of chloride and ester, respectively. $p(t)$ is the amount, in moles per liter, of ester which has undergone hydrolysis with the production of a corresponding amount of chloride.

In the event that the rate of the exchange reaction is first order with respect to each of the reacting species, eq. 1 and 2 reduce to

$$\ln(1 - F_t) = -k_x(a + b)t \qquad (3)$$

Experimental

The ethyl chloroacetate used was reagent grade, fractionally distilled with the middle third taken as the reactant material. The ester was stored in the dark in a desiccator containing phosphorus pentoxide. The ester prepared in this manner had a refractive index of 1.42135 and a corrected boiling point of 142.5°.

Sodium chloride-36 was made from the labeled acid, obtained from the Radioactive Isotope Sales Department at Oak Ridge National Laboratory, by titration with sodium hydroxide to a pH of 6. The solution then was evaporated to dryness.

Reaction cells were prepared by adding absolute ethyl alcohol or alcohol–water mixtures containing chloride-36 to ethyl chloroacetate in a 50-cc. volumetric flask. Eight-cc. aliquots were introduced into cleaned Pyrex cells, degassed *in vacuo*, and sealed off. If not reacted immediately, cells were stored in Dry Ice until used.

Reactions were carried out by immersing the cells in an oil thermostat at temperatures from 73.5 to 99.2°. Temperature control was within ±0.05°. Following reaction, the cells were cooled rapidly with Dry Ice, opened, and titrated potentiometrically with silver nitrate. The solution was placed in a 50-cc. flask, stoppered, and stored in the dark for a period of 12 hr. to aid filtration. The solution was filtered and diluted to a volume of 50 cc. Control experiments showed that no background exchange occurred during this procedure. A 1-cc. portion was placed in a planchet and counted with an end window Geiger Mueller tube of window thickness 1.4 mg./cm.^{2}. Observed counting rates for the ethyl chloroacetate portion of 16 to 918 c./min. above background were obtained. Five to ten different 1-cc. portions were counted, each for 5 min. In every case the net counting rate was characterized by a standard deviation of less than 2%.

The total counting rate for a cell was obtained by diluting an 8-cc. fraction of the original reactant mixture to 50 cc. and counting 1-cc. portions.

The fraction of equilibrium exchange at time t was obtained from

$$F_t = \frac{(\text{Specific Activity of } CH_2ClOOC_2H_5)_t}{(\text{Specific Activity of Total chlorine})_{t=\infty}}$$

(1) R. A. Kenney and F. J. Johnston, *J. Phys. Chem.*, **63**, 1426 (1959).

(2) C. P. Luehr, G. E. Challenger, and B. J. Masters, *J. Am. Chem. Soc.*, **78**, 1314 (1956).

TABLE I

DATA SUMMARY FOR EXPERIMENTS AT 99.2°K.

Time (hr.)	(Cl^-), mole $l.^{-1}$	$(CH_2Cl\text{-}COOC_2H_5)$, mole $l.^{-1}$	C/M (Ester)	F	k_x, l. $mole^{-1}$ $hr.^{-1}$
Set I (710 C/M total), 100% ethanol					
0	0.0135	0.0473	0	0	..
0.50			56	0.079	2.71
1.00			105	.148	2.63
1.50			164	.231	2.88
2.00			190	.267	2.56
2.50			212	.299	2.32
				Av.	2.62
Set II (1325 C/M total), 100% ethanol					
0	0.0165	0.0946	0	0	..
0.50			187	0.141	2.74
1.00			370	.279	2.94
1.50			478	.361	2.69
2.00			581	.438	2.50
2.50			608	.459	2.22
				Av.	2.68
Set III (754 C/M total), 100% ethanol					
0	0.0080	0.0189	0	0	..
0.75			35	0.046	2.36
1.50			71	.094	2.45
2.50			107	.142	2.28
3.00			124	.164	2.24
				Av.	2.33
Set IV (1091 C/M total), 100% ethanol					
0	0.0059	0.1418	0	0	..
0.52			183	0.168	2.42
0.75			258	.236	2.43
1.25			430	.394	2.71
1.75			488	.447	2.30
2.25			583	.534	2.30
				Av.	2.43
Set V (454 C/M total, 75% ethanol–25% water)					
0	0.0021	0.0473	0	0	..
2.00	.0024	.0470	87	0.201	2.28
3.25	.0026	.0468	130	.302	2.25
4.00	.0031	.0463	153	.360	2.26
8.00	.0036	.0458	242	.575	2.17
				Av.	2.24
Set VI (832 C/M total, 75% ethanol–25% water)					
0	0.0039	0.0946	0	0	..
3.00	.0051	.0934	356	0.451	2.03
4.00	.0056	.0929	454	.579	2.20
5.00	.0059	.0926	522	.667	2.23
Set VII (2020 C/M total, 50% ethanol–50% water)					
0	0.0096	0.0473	0	0	..
1.00	.0099	.0470	154	0.092	1.70
2.00	.0102	.0465	300	.181	1.76
5.00	.0115	.0450	580	.360	1.57
				Av.	1.68
Set VIII (1875 C/M total, 50% ethanol–50% water)					
0	0.0099	0.0946	0	0	..
1.80	.0103	.0942	453	0.268	1.66
3.00	.0110	.0934	656	.391	1.58
3.80	.0116	.0928	782	.470	1.60
5.00	.0124	.0921	918	.556	1.55
				Av.	1.60

Results and Discussion

Table I summarizes in detail the results of our experiments at 99.2°. In column 6 are listed reaction rate constants for the exchange calculated according to eq. 1 and 2. In Table II our complete results are summarized. The consistency of the reaction rate constants for exchange over wide ranges of reactant concentrations indicates that this process is first order with respect to the chloride concentration and to the ethyl chloroacetate concentration.

TABLE II

SUMMARY OF REACTION RATE CONSTANTS FOR THE CHLORIDE–ETHYL CHLOROACETATE EXCHANGE IN ETHANOL AND IN 50% ETHANOL–50% WATER

Temp., °C.	(Cl^-), mole $l.^{-1}$	$(CH_2ClCOOC_2H_5)$, mole $l.^{-1}$	k_x, l. $mole^{-1}$ $hr.^{-1}$
(A) Absolute ethanol			
99.2	0.0080	0.0189	2.33
	.0135	.0473	2.62
	.0058	.1418	2.43
	.0165	.0946	2.68
			Av. 2.51
89.4	0.0118	0.0473	1.07
	.0066	.0945	1.10
	.0047	.0189	1.23
			Av. 1.13
81.5	0.0046	0.0473	0.566
	.0089	.0945	.578
	.0067	.0189	.579
			Av. 0.574
73.5	0.0058	0.1418	0.239
	.0089	.1891	.226
	.0143	.0473	.236
			Av. 0.234
(B) 50% Ethanol–50% water			
99.2	0.0096	0.0473	1.68
	0.0099	0.0945	1.60
			Av. 1.64
89.4	0.0055	0.0473	0.633
	0.0061	0.0945	0.630
			Av. 0.632
81.5	0.0075	0.0473	0.315
	0.0064	0.0945	0.349
			Av. 0.332

Activation energies and frequency factors for the reactions in ethanol and in 50% ethanol–water were evaluated in the usual way from a plot of log k_x *vs.* $1/T$. Entropies of activation, as defined by the equation[3]

$$k_x = (kT/h) \exp[\Delta S^*/RT] \exp[-\Delta H^*/RT]$$

with $\Delta H^* = E_a - RT$, were calculated for 80°. The standard state is that corresponding to one mole per liter. The results of these calculations are summarized in Table III. Our experiments with the 75% ethanol–25% water system were not sufficiently extensive to allow a calculation of energies and entropies of activation.

(3) A. A. Frost and R. G. Pearson, "Kinetics and Mechanism," John Wiley and Sons, Inc., New York, N. Y., 1953, p. 96.

TABLE III

CONSTANTS FOR $CH_2ClCOOC_2H_5$–Cl^- EXCHANGE

System	*Ea*, cal. mole^{-1}	Frequency factor, l. mole^{-1} sec.$^{-1}$	ΔS^*, cal. mole^{-1} deg.$^{-1}$
C_2H_5OH	23,000 ± 900	0.221×10^{11}	−13 ± 3
50% C_2H_5OH–50% HOH	23,000 ± 900	0.136×10^{11}	−14 ± 3

Solubility limitations prevented our carrying out these experiments in solutions of higher water concentration than the 50% mixtures.

Our results indicate that the exchange takes place through a simple bimolecular displacement type reaction

$$Cl^{-*} + CH_2ClCOOC_2H_5 \rightleftarrows CH_2Cl^*COOC_2H_5 + Cl^-$$

A significant increase in water content of the solvent did not, within the limits of experimental error, change the activation energy. This suggests that the solvent effect is principally manifest in the frequency factor and thus in the apparent entropy of activation. The direction of this effect is consistent with the increased solvation of the chloride ion in the aqueous mixtures.

The difference in the solvent systems prevents our meaningfully comparing these results with those for the chloroacetic acid–chloride exchange.

This work was supported by A. E. C. Contract AT(40-1) 2826.

THE KINETICS OF HYDROGEN PEROXIDE FORMATION DURING THE DISSOLUTION OF POLYCRYSTALLINE COPPER

BY D. W. COLCLEUGH AND W. F. GRAYDON

Department of Chemical Engineering and Applied Chemistry, University of Toronto, Toronto 5, Canada

Received December 30, 1961

The basis for this work was the introductory work done by Lu and Graydon[1] on the dissolution of polycrystalline copper in dilute sulfuric acid solutions. This work[1] was extended to include the observed presence of hydrogen peroxide in the corroding solution.

A typical run consisted of rotating a sample of 11.4 cm.^{2} in 500 ml. of an air-saturated sulfuric acid solution of 0.1 *M* concentration at 25.8°. Samples were removed periodically for analysis of cupric ion and hydrogen peroxide.

Experimental

Apparatus.—The technique used in this work consisted of rotating a cylindrical sample of copper in a solution of sulfuric acid which was continually saturated by bubbling an oxygen:nitrogen mixture through it. The apparatus was described in full previously and no modifications were made.

Analysis.—A polarographic method of analysis was used for cupric ion and hydrogen peroxide determinations.

Solutions of inhibitor-free hydrogen peroxide in 0.1 *M* sulfuric acid were standardized by titration with potassium permanganate which previously was standardized with the primary standard sodium oxalate.

The cupric ion standardization was done with suitably prepared solutions of cupric sulfate pentahydrate in 0.1 *M* sulfuric acid.

The supporting electrolyte was 1 *M* sodium acetate and the maximum suppressor was a 0.01% gelatin solution. The capillary had "*m*" and "*t*" values of 3.24 mg./sec. and 3.19 sec., respectively.

(1) B. C.-Y. Lu and W. F. Graydon, *Can. J. Chem.*, **32**, 153 (1954).

Results and Discussion

Polarographic analysis at −0.9 volt *vs.* the saturated calomel electrode, in de-aerated samples, revealed the presence of hydrogen peroxide in the corroding solution. The data, when plotted as hydrogen peroxide to the one-half power *vs.* time (Fig. 1), yielded straight lines.

Thus

$$\frac{d[H_2O_2]}{dt} \propto [H_2O_2]^{1/2}$$

Rate Dependence on Oxygen Concentration.—The slopes of the straight lines in Fig. 1 were plotted against the corresponding partial pressure of oxygen in the gas phase to the one-half power, with which the corroding solution was equilibrated and a straight line obtained.

Thus

$$\frac{d[H_2O_2]}{dt} \propto (p_{O_2})^{1/2}$$

The concentration of oxygen dissolved in the corroding solution was found to be directly proportional to the partial pressure of oxygen in the gas phase.

$$[O_2] = 12.5 \times 10^{-4}(p_{O_2})$$

where

$[O_2]$ = concn. in solution in moles/l.
p_{O_2} = partial pressure in gas phase in atm.

The oxygen concentration in solution was obtained by polarographic analysis.

The experiments discussed above also indicated that there was a simple stoichiometric relationship between the cupric ion and the hydrogen peroxide in solution (Table I). There were two moles of cupric ion formed for every mole of hydrogen peroxide.

TABLE I

Partial pressure of oxygen in gas phase, atm.	Molar ratio[a] $\frac{[Cu^{++}]}{[H_2O_2]}$
0.0423	2.0
.0983	2.0
.210	1.8
.500	1.6
.698	2.1
1.00	1.8

[a] Each value listed was an average of 4 or 5 determinations made during a run.

Rate Dependence on Temperature.—The Arrhenius activation energy calculated from the slope of the straight line in Fig. 2 was found to be 11.5 kcal./g. mole.

The molar ratio of cupric ion concentration to hydrogen peroxide concentration at the temperatures studied was again about two (Table II).

TABLE II

Temp., °C.	Molar ratio $\frac{[Cu^{++}]}{[H_2O_2]}$
13.5	2.7
25.8	1.8
34.0	2.0
43.5	2.1

Rate Dependence on Acid Concentration.—To further test the stoichiometric relationship between cupric ion and hydrogen peroxide, and to determine the dependence of the rate of formation of hydrogen peroxide on acid concentration, a set of experiments varying acid concentration and no other variable was carried out.

The rate dependence was shown in Fig. 3 and the stoichiometric relationship in Table III.

TABLE III

Acid concn., moles/l.	Molar ratio $\frac{[Cu^{++}]}{[H_2O_2]}$
0.006	2.7
.03	2.2
.10	1.8
.23	2.2
.40	2.0

The consistency of the molar ratio as given in Table III indicated that the rate of cupric ion formation had a similar dependence.

Rate Dependence on R.p.m. of Sample.—From Table IV it was found that the rate of formation of hydrogen peroxide and the molar ratio were independent of the speed of rotation of the sample.

TABLE IV

$\frac{d[H_2O_2]^{1/2}}{dt} \times 10^4$	R.p.m. of sample	Molar ratio $\frac{[Cu^{++}]}{[H_2O_2]}$
6.9	0	2.1
7.4	78	2.1
7.0	880	2.0
6.2	2300	2.2

Thus the rate of formation of hydrogen peroxide, under these experimental conditions, was chemically controlled and not diffusion controlled.

It also was noted that the stoichiometric coefficient, two, was not affected by the wide variation in r.p.m. of sample.

Rate Dependence on Sample Area and Corroding Solution Volume.—A linear relationship between the rate of formation of hydrogen peroxide and the ratio of sample area to corroding solution volumes was found.

Thus

$$\frac{d[H_2O_2]}{dt} \propto \frac{A}{V}$$

From Table V it also was observed that changes in the A/V ratio did not affect the stoichiometry of the controlling reaction.

TABLE V

A/V, cm.^{2}-l.$^{-1}$	Molar ratio $\frac{[Cu^{++}]}{[H_2O_2]}$
11.4	2.2
14.3	1.9
22.8	1.8
28.6	2.1

Conclusion

Over the wide range of experimental conditions employed for reaction times up to 30 hr., or a hydrogen peroxide concentration of approximately 5×10^{-4} M, the molar ratio of cupric ion formed to hydrogen peroxide formed was found to be 2.0, with an average deviation in 31 runs of 0.2. This independence of the cupric ion, hydrogen peroxide concentration ratio on oxygen concentration, temperature, acid concentration, r.p.m. of sample,

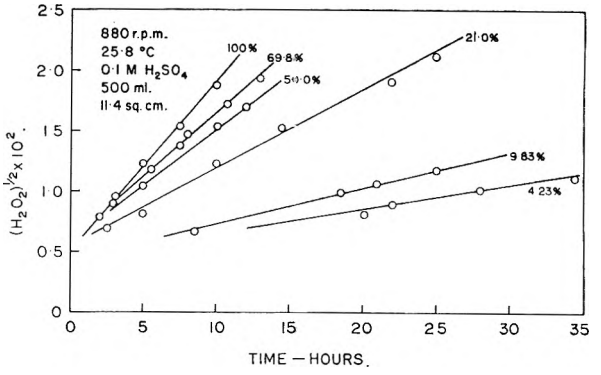

Fig. 1.—Concentration of hydrogen peroxide to one-half power in (moles/liter)$^{1/2}$ *vs.* reaction time in hours. Parameter is per cent oxygen in the gas phase.

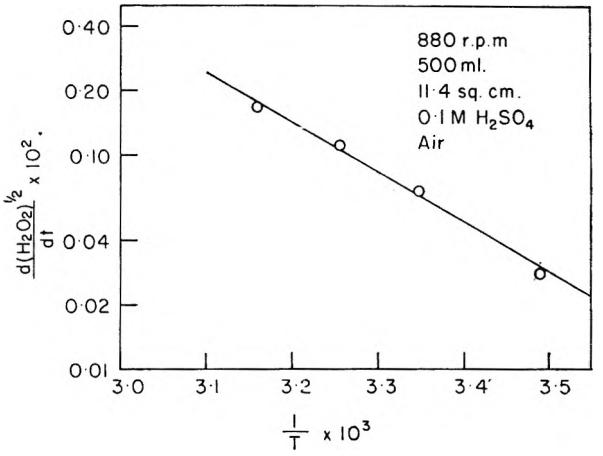

Fig. 2.—Slopes of plots of hydrogen peroxide concentration to one-half power *vs.* time in hours at various temperatures *vs.* the reciprocal of the corresponding absolute temperature.

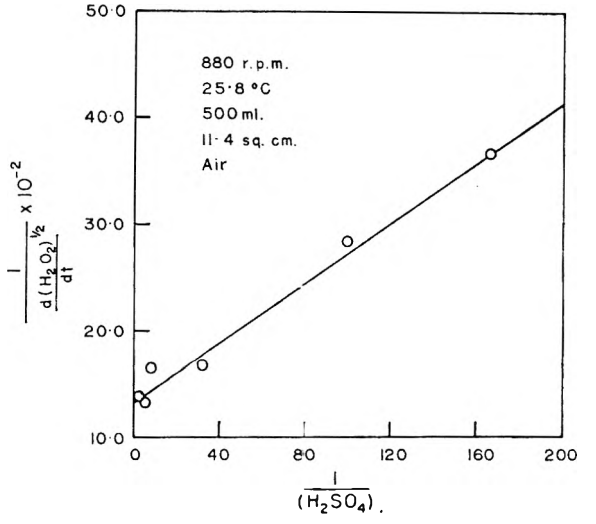

Fig. 3.—Reciprocal of slope of plot of hydrogen peroxide concentration to one-half power *vs.* time in hours at various acid concentrations *vs.* the reciprocal of the acid concentration measured in (moles/l.)$^{-1}$.

and A/V ratio indicated that the two substances were produced by a single reaction.

Empirical Equation and Range of Application.—The data discussed above may be summarized in the form of the following empirical equation at a constant temperature of 25.8°

$$\frac{d[H_2O_2]}{dt} = \frac{4.21 \times 10^{-3}[O_2]^{1/2}[H_2O_2]^{1/2} \times \frac{A}{V}[H_3O^+]}{1.97 \times 10^{-2} + [H_3O^+]}$$

Now over the range of experimental conditions employed the molar ratio of cupric ion to hydrogen peroxide was constant at the value two, or

$$2 \times \frac{d[H_2O_2]}{dt} = \frac{d[Cu^{++}]}{dt} = \frac{5.95 \times 10^{-3}[O_2]^{1/2}[Cu^{++}]^{1/2}[H_3O^+] \times \frac{A}{V}}{1.97 \times 10^{-2} + [H_3O^+]}$$

At a constant acid concentration of 0.2 M the equation above takes the form of the equation found by Lu and Graydon.[1]

$$2 \times \frac{d[H_2O_2]}{dt} = \frac{d[Cu^{++}]}{dt} = 5.44 \times 10^{-3}[O_2]^{1/2}[Cu^{++}]^{1/2}\frac{A}{V}$$

$A = 5.7-14.3$ cm.[2]
$V = 0.500-0.800$ l.
$[O_2] = 0.53 \times 10^{-4}-12.35 \times 10^{-4}\ M$
$[Cu^{++}] = 0-10 \times 10^{-4}\ M$
$[H_2O_2] = 0-5 \times 10^{-4}\ M$
$T = 298.8$°K.
$[H_3O^+] = 0.009-0.41\ M$

The value of the rate constant was actually $5.44 \times 10^{-3} \pm 0.48 \times 10^{-3}$ for 31 runs.

Proposed Mechanism.—The following reaction scheme, which is consistent with the constant molar ratio of cupric ion to hydrogen peroxide of two and the empirical dependence of the hydrogen peroxide rate on the variables examined, is suggested

$$Cu_i^+ + O_s \underset{k_{-1}}{\overset{k_1}{\rightleftharpoons}} Cu^+ \ldots O_s$$

$$Cu^+ \ldots O_s + H_3O^+ \xrightarrow{k_2} Cu_i^{++} + OH + H_2O$$

$$OH + OH \xrightarrow{k_3} H_2O_2$$

$$Cu_i^{++} + Cu \underset{}{\overset{K'}{\rightleftharpoons}} 2Cu_i^+ \text{ (equilibrium)}$$

$$O_{2i} \underset{}{\overset{K''}{\rightleftharpoons}} 2O_s \text{ (equilibrium)}$$

The symbol $Cu^+ \ldots O_s$ was meant to represent some transitory combination of cuprous ion and oxygen at the solution–metal interface which comes rapidly to a stationary concentration as does the hydroxyl free radical OH.

The subscripts i and s refer to interface and surface, respectively, and the letters k and K refer to rate constants and equilibrium constants, respectively.

Also

$$[Cu^{++}] = [Cu^{++}]_i$$
$$[O_2] = [O_2]_i$$

These assumptions combined with the reaction scheme given above result in equations of the same form as the empirically developed ones

$$\frac{d[Cu^{++}]}{dt} = 2 \times \frac{d[H_2O_2]}{dt} = \frac{k_2k_1K'^{1/2}K''^{1/2}[O_2]^{1/2}[Cu^{++}]^{1/2}[H_3O^+]}{k^{-1} + k_2[H_3O^+]}$$

ELECTRIC MOMENTS FROM EXTRAPOLATED MIXED SOLVENT DATA. IV. AMIDES AND THIOAMIDES[1,2]

BY GEORGE K. ESTOK AND SATYA P. SOOD

Chemical Laboratories of The Men's College, University of San Diego, San Diego, Calif.

Received January 29, 1962

This work represents the final part in the titled series.[3,4]

Because simple amides are known to associate strongly in benzene solution, this work was done to determine reliable moments for such compounds in this solvent. Previous work[5,6] on carboxylic acid amides has indicated considerable abnormal solvent effect (>0.15 D.) between moments obtained from benzene and dioxane solutions. However the known association in benzene solution puts considerable doubt on the reliability of extrapolation intercepts at infinite dilution.

No previous work has been noted on moments of thioamides in benzene solution, although some values in dioxane and CCl_4 solution have been reported (Table I).

Experimental

Preparation and Purification of Compounds.—Benzene and dioxane were purified by standard methods.[4]

Recrystallization details and melting points of Eastman Kodak Co. products were: **Propionamide**, thrice from benzene, and dried in a vacuum desiccator; 80°. ***n*-Butyramide**, from CCl_4–petroleum ether; 114–115°. **Acetanilide**, twice from water; 114°. **Thioacetanilide**, from water, dried in a vacuum desiccator; 75–76°. **Thiobenzanilide**, four times from methanol at Dry Ice temperature; 101.5–102.0°. **Thiourea** was purified as indicated in earlier work[7]; m.p. 180°.

Benzanilide, prepared in a standard manner, was recrystallized twice from methanol; m.p. 163°. **Thioacetamide**, a Matheson Coleman and Bell product, was recrystallized four times from benzene and stored over P_2O_5; m.p. 112–113°.

Measurements and Calculations.—These were made as reported earlier.[3,4] Figures 1 and 2 are plots of data where mixed solvent was required to obtain satisfactory intercepts at infinite dilution for benzene solution. The satisfactory solubility and non-cyclic association of the aromatic compounds obviated the need for mixed solvent work. Table I lists moments and related data.

Discussion of Results

A significant observation made possible by mixed solvent work is that the simple non-substituted carboxylic acid amides, whether aliphatic or aromatic, do not show any abnormal solvent effects in passing from benzene solution to dioxane solution. Table I indicates a difference of less than 0.15 D.

(1) This work was supported mostly by a Frederick Gardner Cottrell Grant from Research Corporation, New York, N. Y.

(2) Presented at the Pacific Southwest Regional Meeting of the American Chemical Society, San Diego, Calif., Dec. 1–2, 1961.

(3) G. K. Estok, S. P. Sood, and C. H. Stembridge, *J. Phys. Chem.*, **62**, 1464 (1958).

(4) G. K. Estok and S. P. Sood, *ibid.*, **61**, 1445 (1957).

(5) W. W. Bates and M. E. Hobbs, *J. Am. Chem. Soc.*, **73**, 2151 (1951).

(6) J. E. Worsham and M. E. Hobbs, *ibid.*, **76**, 206 (1954).

(7) W. D. Kumler and G. M. Fohlen, *ibid.*, **64**, 1944 (1942).

TABLE I

ELECTRIC MOMENTS AND RELATED DATA (25°)[a]

(Benzene: $\epsilon_1 = 2.2730$, $v_1 = 1.145$; Dioxane: $\epsilon_1 = 2.206$, $v_1 = 0.973$)

Solute	MR_D	v_2[b]	Solvent	α_∞	$P_{2\infty}$	μ	$\Delta\mu$	μ lit.
Propionamide	19.5[5]	1.002[c]	Benzene	20.7	306	3.73		$3.30_{30°}$[5]
							(0.14)	
			Dioxane	25.5	328	3.87		$3.85_{30°}$[5]
n-Butyramide	24.1[5]	1.037[c]	Benzene	17.9	320	3.78		$3.48_{30°}$[5]
							(0.07)	
			Dioxane	21.20	330	3.85		$3.86_{30°}$[5]
Acetanilide	40[8]	0.906[8]	Benzene	10.8	311	3.62		4.01,[8] 3.5_{CCl_4}[9]
							(0 35)	
			Dioxane	14.85	366	3.97		4.02[10]
Benzanilide	48.4[d]	0.860[c]	Benzene	7.70	336	3.66		$3.38_{30°}$[6]
							(0.28)	
			Dioxane	10.15	379	3.94		3.83[f]
Thioacetamide	25.5[g]	0.869[e]	Benzene	30.3	448	4.53		.....
							(0.27)	
			Dioxane	39.55	509	4.80		$4.77_{35°}$[h]
Thioacetanilide	47.9[d]	0.846[e]	Benzene	13.65	426	4.28		4.5_{CCl_4}[9]
							(0.36)	
			Dioxane	18.22	491	4.64		.....
Thiobenzanilide	67.4[d]	0.832[e]	Benzene	9.03	415	4.10		.....
							(0.43)	
			Dioxane	12.53	492	4.53		.....
Thiourea	24.0[7]	0.652[7]	Benzene[i]	36	534	5.0		.....
							(0.1)	
			Dioxane	42.8	552	5.07		4.89[7]

[a] Data at 25° unless otherwise indicated. [b] G. K. Estok, *J. Phys. Chem.*, 60, 1336 (1956). [c] Extrapolated from melt data in J. Timmermans "Physicochemical Constants." [d] From atomic refractions. [e] Based on solution densities. [f] A. Kotera, S. Shibata, and K. Sone, *J. Am. Chem. Soc.*, 77, 6183 (1955). [g] From solution refraction measurements. [h] S. Soundararajan, *Trans. Faraday Soc.*, 53, 159 (1957). [i] Hypothetical benzene solution.

for propionamide and *n*-butyramide. This also is true for benzamide (3.77, 3.88), reported previously.[4] These results are in contrast to larger effects indicated by other earlier work[5,6] in benzene and dioxane solutions only. The strong cyclic association in benzene solutions leads to unreliable extrapolation to infinite dilution in such cases. Moments in dioxane solution in Table I, however, are in good agreement with other work in dioxane solution.

Because of steric effects it is generally agreed that amides with aromatic groups on CO and on N exist essentially in the *s-trans* conformation, for which resonance structures may be written as

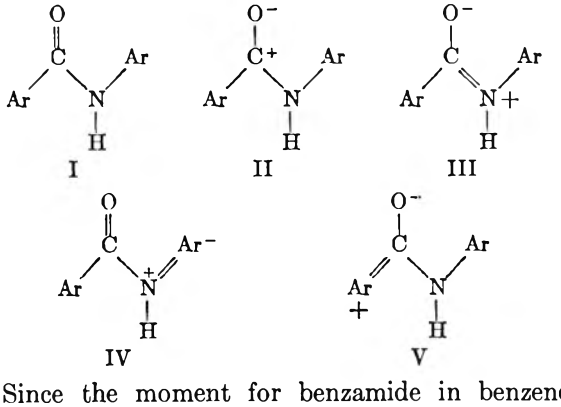

I II III

IV V

Since the moment for benzamide in benzene (3.77) is consistent with those for simple aliphatic amides (*ca.* 3.7–3.8) it is concluded that V contributes little to the over-all moment. It is generally conceded, however, that I, II, and III contribute significantly. The role of IV serves to reduce the over-all moment a little by reducing the contribution of III. Thus acetanilide (3.62) and benzanilide (3.66) have lower moments than the simple amides. The moment of acetanilide was redetermined because previously reported values[8,9] were not consistent. The value of 3.97 obtained in dioxane solution, however, is in satisfactory agreement with 4.02 reported earlier.[10]

There is a definite solvent effect with acetanilide and with benzanilide which may be attributed to hydrogen-bonding between dioxane and the aniline residue, a marked effect observed earlier with aniline itself, and with various substituted anilines.[11,12]

The behavior of the thioamides is somewhat comparable to that of the amides in that moments for thiobenzanilide (4.10) and thioacetanilide (4.28) are lower than for thioacetamide itself (4.53). However the latter does show some abnormal solvent effect.

The low solubility of thiourea in benzene and dioxane makes the moment values of 5.0 in benzene and 5.07 in dioxane too uncertain for a judgment

(8) C. G. LeFevre and R. J. W. LeFevre, *J. Chem. Soc.*, 1130 (1936).

(9) I. Suzuki, M. Tsuboi, T. Shimanouchi, and S. Mizushima, *Spectrochim. Acta*, **16**, 471 (1960).

(10) S. Nakakura and A. Kuboyama, *Chem. Abstr.*, **46**, 1315f (1952).

(11) A. V. Few and J. W. Smith, *J. Chem. Soc.*, 753 (1949).

(12) C. Curran and G. K. Estok, *J. Am. Chem. Soc.*, **72**, 4575 (1950).

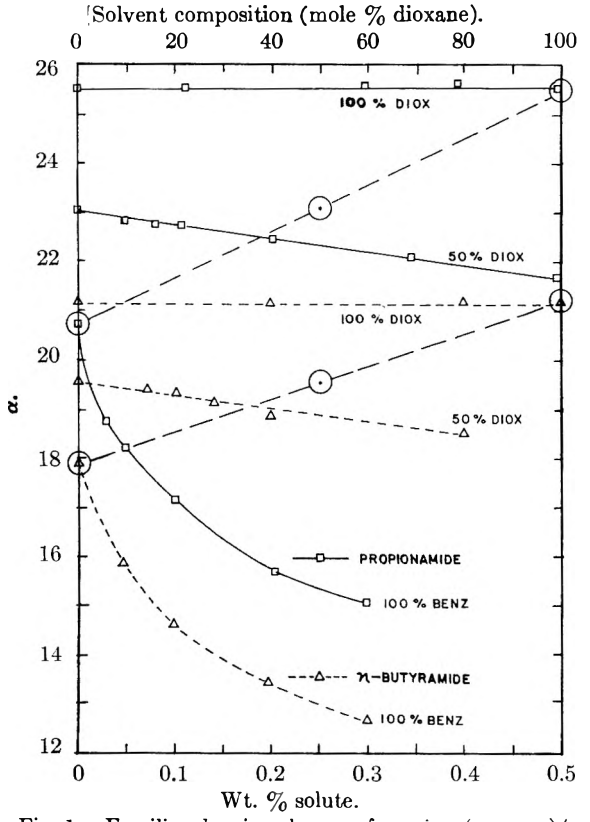

Fig. 1.—Families showing change of α: *i.e.*, $(\epsilon_{12} - \epsilon_1)/w_2$ *vs.* solute concentration in different benzene–dioxane environments. Large circles are plots of family ordinate intercepts *vs.* solvent composition.

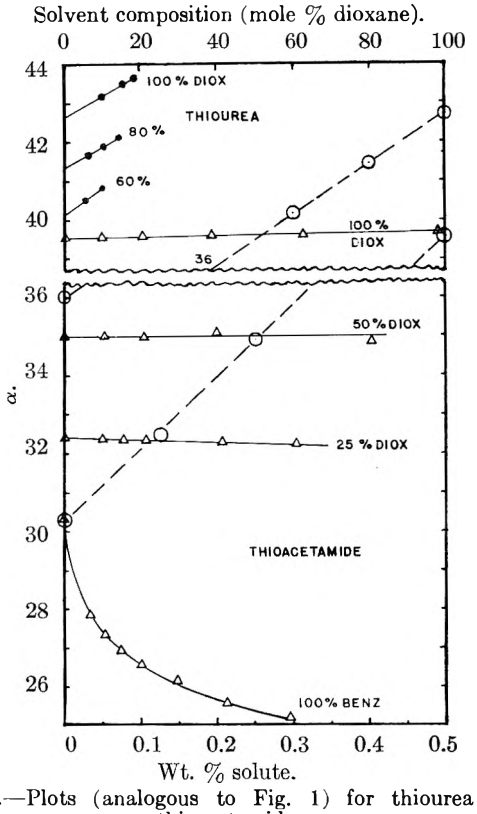

Fig. 2.—Plots (analogous to Fig. 1) for thiourea and thioacetamide.

of solvent effects. Such high moments, however, may be attributed to the large resonance effect due to equivalence of resonance structures. The steepness of the data plots for thiourea also indicates complex associations, probably both mutually and with the dioxane solvent.

The data plots for propionamide, *n*-butyramide, and thioacetamide, in benzene solutions, show considerable cyclic association of the solutes into dimers of zero moment. This association for thioacetamide is interesting because it represents a case of hydrogen-bonding involving sulfur (N–H · · · S). Evidently two such bonds are strong enough to yield a discrete cyclic dimer. The weaker nature of these bonds relative to N–H · · · O bonds, however, is evidenced by their disappearance in solvent with 25% dioxane, whereas amides still show some association at 50% dioxane.

The *s-trans* conformation of N-phenylated amides and thioamides prevents cyclic association. The rise in α with concentration for acetanilide (not plotted) indicates that some linear association occurs in benzene solution in the range 0.17 to 1.2 wt. % solute. However, thioacetanilide does not show any evidence of such linear association in benzene in the concentration range 0.05 to 0.30 wt. %. Evidently a single N–H · · · S bond is not strong enough to promote appreciable linear association.

COMMUNICATIONS TO THE EDITOR

THE STRUCTURE OF ACTIVE CENTERS IN NICKEL CATALYST

Sir:

On annealing cold-worked nickel, release of the stored energy and changes of the physical properties take place in two temperature ranges, *i.e.*, 200–300° (T_V) and ~400–700° (T_D).[1] They are attributed to the disappearance of vacancies and dislocations, respectively. As the concentration of lattice defects increases with the degree of cold-working, strong interactions among them lowers T_D, resulting in unavoidable overlapping of T_V and T_D.[1,2] On the other hand, T_D is elevated remarkably by the existence of non-metallic impurities; hence the difference among specimens is considerable.[3] One of us (I.U.) and his co-workers[4] estab-

(1) (a) L. M. Clarebrough, M. E. Hargreaves, and G. W. West, *Proc. Roy. Soc.*, **A232**, 252 (1955); *Phil. Mag.*, **1**, 528 (1956); (b) W. Boas, "Defects in Crystalline Solids," The Physical Society, 1955, p. 212.

(2) D. Mitchell and F. D. Haig, *Phil. Mag.*, **2**, 15 (1957).

(3) L. M. Clarebrough, M. E. Hargreaves, M. H. Loretto, and G. W. West, *Acta Met.*, **8**, 797 (1960).

(4) I. Uhara, S. Yanagimoto, K. Tani, and G. Adachi, *Nature*, **192**, 867 (1962).

lished experimentally that the ends of dislocations at the surface of copper catalyst are the active centers for the decomposition of diazonium salt. In this communication some experimental evidence concerning the structure of active centers in nickel catalyst is given.

Well annealed nickel wire containing 0.009% C, 0.011% Si, and 0.001% S, etc., was twisted or rolled, and annealed again in hydrogen at various temperatures for 1 hr., after which the catalytic activities were studied for the following reactions. Stepwise decrease of activities was observed at two temperature ranges, T_{A1} and T_{A2}, which coincide approximately with T_V and T_D, respectively, given in the literature. When the same specimen was employed for the measurements of both catalytic activity and changes of the physical properties, the coincidence was excellent.[5]

(A) Hydrogenation of $C_6H_5CH{:}CHCO_2H$ in ethanol at 25°. Measured volumetrically with Warburg's apparatus. Nickel wire (d = 0.50 mm.) rolled to plate, 0.11 mm. thick, was employed as catalyst, T_{A1} = 150–270°, T_{A2} = 400–600°.

(B) The reaction, $C_2H_5OH = CH_3CHO + H_2$, at 200°. The yield of aldehyde was determined colorimetrically. Specimen twisted after elongation was employed; T_{A1} = 200–300°, T_{A2} = 460–540°.

(C) Decomposition of H_2O_2 solution (30%) at 20°. Measured with Warburg's apparatus employing twisted nickel wire containing 0.023% C, 0.07% Si, and 0.006% P, (d = 0.514 mm., nd/l = 0.41, where n = number of turns, d = diameter, and l = gage length); T_{A1} = 300–400°, T_{A2} = 600–700°.

(D) Para–ortho hydrogen conversion. Studied at 150° with Pirani gage employing nickel wire (d = 0.50 mm.) rolled to plate, 0.13 mm. thick; T_{A1} = 200–300°, T_{A2} = 400–500°.

(E) Electrolytic generation of hydrogen at a nickel cathode. Hydrogen overvoltage (π_H) was measured at 25° in 0.12 N HCl and compared at a current density of 10^{-4} amp./cm.^{2}. Twisted nickel (nd/l = 0.217) was employed. Elevation of π_H due to annealing means decrease of catalytic activity for the evolution of H_2; T_{A1} = 220–300°, T_{A2} = 570–*ca.* 700°.

Change of the surface area due to annealing at T_V and T_D was shown to be quite small compared with decrease of activities even for ordinary reduced catalysts so long as they are non-porous.[4,6] Accordingly, we may conclude that the active centers annealed at T_{A1} are point defects at the surface which co-exist and vanish together with vacancies in the bulk metal, and those annealed at T_{A2} are the terminations of dislocations at the surface. According to Eckell,[7] rolled nickel (foil) lost most of the acitivity for the hydrogenation of ethylene on annealing at 275° and completely at 300°, suggesting that the active center is some kind of point defect at the surface. Contribution of the normal surface to the activity of nickel is almost negligible (at most only a few per cent) in any case so far studied.

(5) S. Kishimoto, to be published.

(6) S. Iijima, *Rev. Phys. Chem. Japan*, **14**, 128 (1940).

(7) J. Eckell, *Z. Elektrochem.*, **39**, 433 (1933).

With the increasing degree of cold-working, separation of T_V and T_D (hence that of T_{A1} and T_{A2}) becomes diffuse, resulting only in continuous decrease of activity with increasing temperature of annealing, as observed in the case of nickel foil for para–ortho hydrogen conversion (*ca.* 200–500°).[8] Ordinary catalysts which usually are prepared by chemical procedures and display much higher activity than cold-worked metals have only one continuous sintering temperature range (T_S = ~300–*ca.* 600°), as shown for the same reaction,[9] probably owing to the highly distorted structure, which often is proved by the X-ray method, and analogous to that of specimens extremely cold-worked as discussed above. Their active centers may be substantially the same as those generated at the surface of metals by cold-working, considering the approximate coincidence of T_S with T_{A1} (or T_V) and T_{A2} (or T_D), although the possibility cannot be denied that two or more lattice defects combine to form a complex active center with new functions when the concentration of defects is high.

(8) E. Cremer and R. Kerber, *Advan. Catalysis*, **7**, 82 (1955).

(9) G. Tammann, *Z. anorg. allgem. Chem.*, **224**, 25 (1935); E. Fajans, *Z. physik. Chem.*, **B28**, 252 (1935).

ITURO UHARA
CHEMISTRY DEPARTMENT TADASHI HIKINO
FACULTY OF SCIENCE YOSHIHIKO NUMATA
KOBE UNIVERSITY HIDEBUMI HAMADA
KOBE, JAPAN YŌICHI KAGEYAMA

RECEIVED MARCH 26, 1962

THE THERMODYNAMICS OF MICELLE FORMATION IN ASSOCIATION COLLOIDS

Sir:

In recent years, the thermodynamics of micellization has been based mainly on a two-phase theory.[1–7] The purpose of this communication is to point out some difficulties of this theory and to show that the mass-action approach is much more satisfactory.

According to the two-phase model the micelles form a separate phase with constant activity. The model, therefore, predicts an abrupt change in properties reflecting micellization at the critical micelle concentration (c.m.c.) and a constant activity of the monomer above the c.m.c. Careful measurements, however, invariably show a smooth continuous change of such properties near the c.m.c.[8–10] and dialysis experiments indicate that

(1) G. Stainshy and A. E. Alexander, *Trans. Faraday Soc.*, **46**, 527 (1950).

(2) E. Hutchinson, A. Inaba, and L. G. Bailey, *Z. physik. Chem.* (Frankfurt), **5**, 344 (1955).

(3) E. D. Goddard and G. C. Benson, *Can. J. Chem.*, **35**, 986 (1957).

(4) E. Matijević and B. A. Pethica, *Trans. Faraday Soc.*, **54**, 587 (1958).

(5) J. M. Corkill, J. F. Goodman, and R. H. Ottewill, *ibid.*, **57**, 1627 (1961).

(6) B. D. Flockhart, *J. Colloid Sci.*, **16**, 484 (1961).

(7) K. W. Herrmann, *J. Phys. Chem.*, **66**, 295 (1962).

(8) R. J. Williams, J. N. Phillips, and K. J. Mysels, *Trans. Faraday Soc.*, **51**, 728 (1955).

(9) E. D. Goddard, C. A. J. Hoeve, and G. C. Benson, *J. Phys. Chem.*, **61**, 593 (1957).

(10) P. Mukerjee, K. J. Mysels, and C. I. Dulin, *ibid.*, **62**, 1390 (1958).

monomer activity must increase with concentration above the c.m.c.[11] A further serious inconsistency of the two-phase model has developed from some recent work with non-ionic compounds. The standard free energy of micellization, ΔG, for the two-phase theory, is given by

$$\Delta G = RT \ln \text{c.m.c.} \qquad (1)$$

where R is the molar gas constant and T the absolute temperature. The $\Delta\Delta G$ for an increase in the chain length by two carbon atoms is given by $RT\Delta$ ln c.m.c., irrespective of the chosen standard state. For ionic compounds the c.m.c. is known to decrease by a factor of nearly four.[3,7] In several non-ionic series, the factor has been found to be about ten.[5,7,12] The difference in the resulting $\Delta\Delta G$ values is in pronounced disagreement with Traube's well known rule,[13] according to which its value should be about RT ln 3 for each methylene group and, therefore, about RT ln 9 for two.

For a simple formulation of the mass-action approach[14] we choose a typical anionic system NaL in the presence of an electrolyte with a common ion such as NaCl. If the equilibrium reaction is

$$n\mathrm{L}^- + (n - p)\mathrm{Na}^+ \rightleftharpoons \mathrm{M}^{-p} \qquad (2)$$

the equilibrium constant Km for forming micelles M^{-p} is given by

$$K_m = \frac{C_{\mathrm{M}^{-p}}}{(C_{\mathrm{L}^-})^n (C_{\mathrm{Na}^+})^{n-p}} \qquad (3)$$

If C_0, C_1, and C_2 be the concentrations of M^{-p}, L^-, and Na^+ at the c.m.c., we can write, neglecting activity coefficients

$$\frac{\Delta G'}{nRT} = \frac{-\ln C_0}{n} + \ln C_1 + \left(1 - \frac{p}{n}\right) \ln C_2 \qquad (4)$$

where $\Delta G'/n$ is the free energy change per monomer. Since n is large (50–100), the C_0 term is small and insensitive to large errors in the estimated C_0.[8] C_1 can be replaced by the c.m.c. with little error.[8] In the absence of added salt, C_2 equals the c.m.c. also, and the right hand side of eq. 4 can be written, to a good approximation, as $(2 - p/n)$ ln c.m.c. For non-ionic compounds, eq. 4 reduces essentially to eq. 1 since the C_2 term disappears.

For ionic compounds, the primary difficulty is in getting reliable estimates of p/n, which may be defined as the thermodynamic degree of dissociation, estimable, in principle, from equilibrium measurements. For sodium lauryl sulfate at 25°, idealized interpretation of turbidity data gives a value of about 0.16.[15] More detailed theories suggest upward revisions.[16] The electrophoretic value of p/n of about 0.36 gives an upper limit.[17] A value in the range 0.25–0.30 is thus likely and is supported by other equilibrium and kinetic measurements on a similar system.[18] On using such a value, the $\Delta\Delta G$ for ionic compounds becomes 1.7 RT ln 4, or about RT ln 11, which is in good agreement with the $\Delta\Delta G$ for non-ionic compounds and Traube's rule. The difference using any other value in the range quoted is not large and may be due to association below the c.m.c.,[10] which causes problems for all approaches.

From eq. 4 it is clear that for the heat of micellization, ΔH, the temperature variation of not only the c.m.c., as in the two-phase theory, but also p/n are important. The conductance below the c.m.c. for several systems[3] increases with temperature fairly proportionately to the fluidity, whereas that above the c.m.c. increases considerably faster. This suggests, in accordance with theoretical expectations and some recent light-scattering results,[19] that p/n increases with temperature. This factor makes ΔH more positive, which is in the right direction for explaining another discrepancy noted between a positive ΔH obtained from calorimetry and a negative one obtained by using the two-phase theory.[20]

(11) B. S. Harrap and I. J. O'Donnell, *J. Phys. Chem.*, **58**, 1097 (1954); H. B. Klevens and C. W. Carr, *ibid.*, **60**, 1245 (1956).

(12) K. Shinoda, T. Yamaguchi, and R. Hori, *Bull. Chem. Soc. Japan*, **34**, 237 (1961).

(13) R. H. Aranow and L. Witten, *J. Phys. Chem.*, **64**, 1643 (1960).

(14) (a) R. C. Murray, *Trans. Faraday Soc.*, **31**, 207 (1935); (b) J. N. Phillips, *ibid.*, **51**, 561 (1955); (c) K. J. Mysels, *J. Colloid Sci.*, **10**, 507 (1955).

(15) K. J. Mysels and L. H. Princen, *J. Phys. Chem.*, **63**, 1699 (1959).

(16) D. Stigter, *ibid.*, **64**, 842 (1960).

(17) D. Stigter and K. J. Mysels, *ibid.*, **59**, 45 (1955); recalculated, using molecular weights from ref. 15.

(18) I. M. Kolthoff and W. F. Johnston, *J. Am. Chem. Soc.*, **73**, 4563 (1951).

(19) K. Kuriyama, *Kolloid-Z.*, **180**, 55 (1962).

(20) P. White and G. C. Benson, *Trans. Faraday Soc.*, **55**, 1025 (1959).

DEPARTMENT OF PHYSICAL CHEMISTRY
INDIAN ASSOCIATION FOR THE CULTIVATION OF SCIENCE
JADAVPUR, CALCUTTA-32, INDIA PASUPATI MUKERJEE

RECEIVED APRIL 28, 1962